# Assessment of the immunological modulation following high intensity focused ultrasound treatment of soft tissue sarcoma and renal cell carcinoma


**Megan Lorna Bradbury**

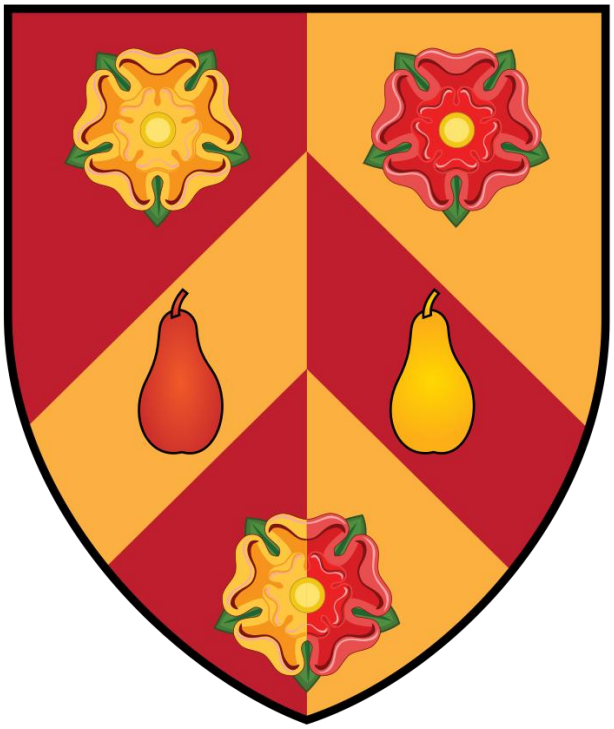

**Wolfson College**

**Nuffield Department of Surgical Sciences**

**University of Oxford**


**Hilary Term 2025**


**Supervisors:**

**Dr Paul Lyon**

**Professor Joanna Hester**

**Professor Robert Carlisle**

# Abstract

High intensity focused ultrasound (HIFU) is a treatment modality using ultrasound waves to thermally ablate tissues, including tumours. The coagulative necrosis caused has been hypothesised to increase anti-tumour immune response. This thesis investigated 'immune-cold' sarcoma tumours and 'immune-hot' renal cell carcinoma tumours to explore this effect.

Within this thesis an *in vivo* murine fibrosarcoma model was established to investigate local and systemic immune modulation with associated HIFU treatment (**Chapter 3**). The immune profile of untreated tumour highlighted a high proportion of CD4 T cells to be Tregs compared to the other tissues. In the first HIFU study a significant increase in the CD8 Tcm T cell memory population was seen in the dLN 24-hours after treatment. In subsequent studies, the treatment area was reduced due to welfare concerns. This showed that in the dLN there was a significantly increase in neutrophils 24-hours after HIFU therapy. When the treatment included aPD-L1 antibody therapy, there was an aPD-L1 associated significant reduction in the tumour growth 5-days post-treatment.

Clinical sarcomas have been reported to have varying immune infiltration based on subtype, which may be of interest in HIFU treatment of these tumours. Transcriptomic profiling of the immune populations within different sarcoma subtypes were assessed in **Chapter 4**. The transcriptomic profile of undifferentiated pleomorphic sarcoma (UPS) and leiomyosarcoma (LMS) showed that tumours that have been historically reported with 'high' immune infiltration (UPS) were characterised by increased antigen presentation and macrophages signature, whereas 'low' immune infiltration subtype (LMS), was shown to have high expression of structural genes.

Finally, the investigation of the immunological changes associated with HIFU treatment in subtypes of 'immune hot' renal cell carcinoma was conducted using spatial transcriptomics (**Chapter 5**). Interestingly, HIFU treatment increased interferon pathway (I and II) expression regardless of subtype and treatment specific macrophage and antigen presentation signatures in clear cell RCC (ccRCC), which in untreated patients, showed lower abundance of these signatures compared to the papillary RCC (pRCC) tumours.

# Acknowledgements

Firstly, my thanks go to my supervisors. Professor Joanna Hester, for all her support in the lab, helping me develop my skills and having faith in my abilities. Also, her positive output when things didn't go quite right. Professor Robert Carlisle, for his support with *in vivo* experiments, keen eye and drive for me to complete this thesis. Dr Paul Lyon, for believing in me throughout this DPhil, with support with the clinical aspects, experimental input and willingness to spend evenings and holidays to read through this work.

This work would not have been possible without the funding from the amazing people at Sarcoma UK, for funding the studentship, laboratory work and clinical trial. Further funding support was supplied by the Focused Ultrasound Foundation for the spatial transcriptomic portion of this work for sarcoma and renal tumours.

My additional thanks go to those across Translational Immunology Research Group (TRIG) and Biomedical Ultrasonics, Biotherapy and Biopharmaceuticals Laboratory (BUBBL). This included Dr Michael Gray, who's expertise with ultrasound was greatly appreciated and welcomed when it came to the *in vivo* experiments. Professor Fadi Issa, who always asked questions that got me to think more about the work and how to expand this further. Dr Amy Cross, who's coding support and chats over cups of tea were needed while completing my DPhil. Dr Matilde Maardalen for being my counterpart within the *in vivo* experiments, for running the ultrasound arrays while I did injections. Professor Constantin Coussios for support with this research, through funding and suggestions for improvements in the *in vivo* studies.

I would also like to thank Dr Hisashi Hashimoto, Mr Oliver McCallion, Dr Sarah Short, and Dr Helen Stark for their help with developing my lab skills and not laughing too hard when I

suggested crazy *in vivo* experiments. Especially to Sarah Short for being a great friend throughout and helping with experiments. Looking forward to seeing you in the Australian sunshine.

I would like to acknowledge OCHRe including David Maldonado-Perez and Elizabeth Latham for handling access to the human samples. And at NDS: Mr Tom Leslie, Mr Robert Ritchie, James Kennedy and Professor David Cranston who originally conducted the renal HIFU trials along with Professor Feng Wu.

Thank you to the Bradbury family, for their support through this endeavour, being a part of the family is so lovely. And to my friends, Taylor, Cloe, Flo, Aidan, Zak and Georgia for being there when I needed them and the understanding that life was busy during the DPhil but still being there at the end of it.

And last but not least, my husband Adam, for looking after our ever-expanding fluffy family when I was working late in the lab or busy writing this thesis. For all your mental support, grounding and not letting it all get to me when it felt like too much.

# Abbreviations

| | |
|---|---|
| AH | AML HIFU |
| AJ | Adjacent |
| AML | Angiomyolipoma |
| ANOVA | Analysis of Variance |
| APC(s) | Antigen presenting cells |
| aPD-L1 | Anti-programmed death-ligand 1 |
| ATP | Adenosine triphosphate |
| BS | Bone sarcoma |
| BSA | Bovine serum albumin |
| ccRCC | Clear cell renal cell carcinoma |
| CD | Cluster of differentiation |
| CC | Clear cell renal cell carcinoma control |
| CH | Clear cell renal cell carcinoma HIFU |
| cLN | Contralateral lymph node |
| CTLA-4 | Cytotoxic T lymphocyte associated antigen 4 |
| CTLs | Cytotoxic T lymphocytes |
| CK8 | Cytokeratin 8 |
| C monocytes | Conventional monocytes |
| DAMPs | Danger molecular signalling proteins |
| DC(s) | Dendritic Cells |
| DEG | Differentially expressed gene(s) |
| DGE | Differential gene expression |
| DI | Deionised |
| dLN | Draining lymph node |
| DPBS | Dulbecco's phosphate buffered saline |
| DPEC | Diethylpyrocarbonate |
| DSP | Digital spatial profiling |

| | |
|---|---|
| EDTA | Ethylenediaminetetraacetic acid |
| FCS/FBS | Foetal calf/bovine serum |
| FFPE | Formalin-fixed paraffin embedded |
| FMO | Fluorescent minus one |
| FUS | Focused Ultrasound |
| HIER | Heat-induced epitope retrieval |
| HIF | Hypoxia inducible factor |
| HMGB-1 | High mobility group box 1 protein |
| HSP | Heat shock protein |
| H&E | Hemotoxin & eosin |
| ICI | Immune checkpoint inhibitors |
| IF | Immunofluorescence |
| IFN- | Interferon- |
| IHC | Immunohistochemistry |
| IL- | Interleukin- |
| IM | Immune |
| LMS | Leiomyosarcoma |
| LN | Lymph node |
| LogFC | Log fold change |
| LR | Local recurrence |
| LRSM | Local recurrence and subsequent metastasis |
| MC | Mast cell |
| MHC-I/II | Major histocompatibility complex I/II |
| MoDCs | Monocyte derived dendritic cells |
| mRCC | Metastatic renal cell carcinoma |
| NBF | Neutral buffered formalin |
| NC monocytes | Non-conventional monocytes |
| NGS | Native goat serum |

| | |
|---|---|
| NK(s) | Natural Killer Cells |
| NTC | Non-tumour bearing control |
| OCHRe | Oxford centre for histopathology research |
| OS | Overall survival |
| ORB | Oxford Radcliffe Biobank |
| ORR | Objective response rate |
| p adj | Adjusted p value |
| PCA | Principal component analysis |
| PD-1 | Programmed cell death protein 1 |
| PD-L1 | Programmed cell death ligand 1 |
| PAM | Passive acoustic mapping |
| PC | Papillary cell renal cell carcinoma control |
| pDC | Plasmacytoid dendritic cell |
| PH | Papillary cell renal cell carcinoma HIFU |
| PT | Peritumour |
| pTreg | Peripheral T regulatory cells |
| pRCC | Papillary renal cell carcinoma |
| RCC | Renal cell carcinoma |
| ROI | Regions of interest |
| RT | Radiotherapy |
| SD | Standard deviation |
| STS | Soft tissue sarcoma |
| TAA | Tumour associated antigen |
| TB | Tumour border |
| TCGA | The Cancer Genome Atlas |
| Tcm | Central Memory T cells |
| Tconv | Conventional T cells |
| TCR | T cell receptor |

| | |
|---|---|
| Tem | Effector Memory T cells |
| TGF- | Transforming growth factor |
| TKI | Tyrosine kinase inhibitor |
| TLS | Tertiary Lymphoid structure |
| TMA | Tissue microarray |
| TME | Tumour microenvironment |
| Tnaïve | Naïve T cells |
| TNF- | Tumour necrosis factor |
| TSA | Tumour specific antigen |
| Tregs | Regulatory T cells |
| UPS | Undifferentiated pleomorphic sarcoma |
| US | Ultrasound |
| USS | Uncategorised spindle cell sarcoma |
| VEGF | Vascular endothelial growth factor |
| VHL | Von Hippel-Lindau disease |
| WGCNA | Weighted gene correlation analysis |

# Contents

# 1 Introduction

## 1.1 An overview of focused ultrasound

### 1.1.1 Introducing ultrasound treatments

Focused ultrasound (FUS) is a non-invasive, non-ionising treatment modality that has demonstrated clinical benefit including the treatment of cancer[1], fibroids[2] and tremors caused by Parkinson's disease[3] as well as opening the blood brain barrier for drug delivery[4]. Unlike imaging ultrasound, the ultrasound arrays for focused ultrasound are designed for a small point of focus using a concave or electrotonically controlled wave impedance with a high energy deliverance (typically $10^3$ – $10^4$ W/cm$^2$ with a frequency of 0.5 to 10MHz[5] for ablation compared to typically imaging ultrasound with an intensity of 100s of W/cm$^2$ with a similar frequency[6]). In addition to the treatment using focused ultrasound, a secondary method is typically used for imaging during treatment. This can be a standard diagnostic imaging probe, where the acoustic waves of ultrasound are recorded as they are reflected from the tissue. Recent updates in the technology have led to magnetic resonance imaging (MRI) techniques being employed for cross-sectional imaging within tissues during treatment.

### 1.1.2 Applications for different ultrasound modalities

There are multiple modalities for the therapeutic use of focused ultrasound including mechanical tissue destruction and histotripsy, thermal ablation and improvements in drug delivery using cavitation nuclei. To change the treatment modality the frequency, duty cycle (percentage of time that the ultrasound is on), and pressures can be altered, and cavitation nuclei can be generated in situ or administered intravenously.

Boiling histotripsy uses low frequency and large variations in pressure within the tumour to create and destroy bubbles formed within the tissue causing mechanical disruption to the tissue by a boiling vapour bubble and cavitation clouds[7]. There can be some tissue damage caused by the heating with this technique, but this much less than that of the mechanical action. The mechanical action can cause shockwaves in the tissue which leads to larger areas of the tissue being affected[7,8]. The benefit of this technique is that, compared to thermal ablation, this technique is thought to be more localised and due to higher tissue tolerances may spare vital structures such as bile ducts and nerves[9] minimising collateral damage. This is in comparison to thermal ablation which may be less localised due to heat dissipation and less specific due to lack of tissue property selection. Further, this technique has been shown to be immunogenic, causing increased activation markers on antigen presenting cells[10,11]. However, histotripsy was not the focus of the studies in this thesis and no clinically approved histotripsy device was available in Oxford at the time of study.

Cavitation focuses on the creation, expansion and destruction of air bubbles within the tissue. Exogenous cavitation nuclei are injectable particles that respond to ultrasound in a similar manner by oscillating (non-inertial cavitation) or collapsing (inertial cavitation). This has been assessed *in vivo* to impact tumour growth by increasing reactive oxygen species and increased drug delivery into tumour by sonoporation[12] which can sometimes include injection of cavitation nuclei which contain tumour treating drugs[13] or by co-injecting with cavitation nuclei. Intravenous chemotherapy has the undesired effect of off target toxicity which limits the dosage available for clinical benefit. Wang et al. have shown that in a study of gastric tumours clinically relevant chemotherapy can be delivered with subsequent injection of microbubbles and targeted ultrasound treatment with each patient received between 2 and 9 treatments of the tumour with few adverse events[14]. Within this study

patients had previously not responded to chemotherapy. Another effect of cavitation is apoptosis of cells, which is beneficial in cancer studies. Although this is a promising therapeutic approach it was not the primary focused ultrasound bioeffect investigated in this thesis.

Ultrasound-based thermal ablation techniques, often referred to as high intensity focused ultrasound (HIFU), cause heating of cells within the tissue by intense energy deposition at a small focus. This leads to a rapid increase in temperature (typically in excess of 60°C) which causes immunogenic cell death by coagulative necrosis[11]. This modality has been used to treat many cancer types in small studies including for the treatment of renal cell carcinoma[15,16], prostate[17–20], pancreas[21], sarcoma[22] and breast cancer[23–25]. The thesis focuses on the HIFU for treatment of cancers and, specifically, the downstream response of the immune system to the treatment for soft-tissue sarcoma (STS) and renal cell carcinoma (RCC). The investigation into the immune populations in sarcoma and RCC with HIFU therapy have previously been limited to *in vivo* studies.

### 1.1.3 How has thermally ablative focused ultrasound been used in cancer treatment

The clinical adoption of HIFU as an upcoming cancer treatment has taken time since its first clinical application in the 1960s but is now starting to accelerate. HIFU has been explored in several cancer types clinically. Ghai et al. conducted a whole ablation feasibility study in patients with prostate cancer, where of the 44 treated patients, only three had residual disease 5-months post treatment (7%)[19]. This was theorised to be caused by inadequate margins in 1/3 and heat dissipation by vessels in 2/3[19]. The side effects were minimal with no change in incidence of erectile dysfunction, incontinence or fistula formation, which are

well-recognised risks of prostatectomy and often seen with increasing cancer burden[19]. Chin at al. conducted a feasibility study with a 10% untreated margin[20]. The outcome of this study was reduced prostate specific antigen levels in the blood of the patients, a biochemical indication of treatment response. Biopsies showed remaining disease, 9/29 with significant disease and 16/29 having indications of remaining disease[20]. This study showed no changes in erectile function, and incontinence issues resolved within 1 year in all but 1 case [20]. These studies highlight the safety and feasibility of HIFU for the treatment of prostate cancer, however, whole ablation within this context was key.

A feasibility study of HIFU treatment of breast cancer was conducted by Wu et al., where post-treatment these tumours were resected, and histopathological assessment of the tissue was conducted. Tissue samples showed complete necrosis of the HIFU-exposed tumour tissue[24]. This study highlighted that the imaging technology was not always able to provide clear visualisation of the margins, so in this case large margins were created[24]. The study indicated no increased treatment side effects; however, only limited clinical follow-up was available.

Ritchie et al. have conducted two different studies on the treatment of renal cell carcinoma with ablative HIFU which has included laparoscopic and extracorporeal treatment approaches. The laparoscopic study was conducted to demonstrate the feasibility of treatment of RCC. The HIFU treatment was immediately followed by nephrectomy. Assessment of frozen tissue sections indicated that there was successful ablation of the tumour tissue [16]. There was no incidence of metastasis or local recurrent disease in the follow-up for these patients. The extracorporeal study indicated successful ablation in two thirds of patients[15]. This approach is favourable over the laparoscopic approach as it is

completely non-invasive and, if successful, avoids the need for invasive surgery and preserves kidney function. A mean tumour shrinkage of 30% was demonstrated, compared to the typical growth of 6 mm typically seen in these tumours if untreated over the same time[15].

Zhao et al. reported that HIFU treatment was feasible in combination with gemcitabine (chemotherapy) as a first line treatment for pancreatic cancer. In a feasibility study this study reported a median overall survival on the study as 16.5 months (8-28.5 months) with the treatment being well-tolerated and similar median overall survival (10.2-16.2) compared to historic published chemoradiotherapy treatments[21] suggesting treatment outcomes of chemotherapy with HIFU that were equivalent to chemoradiotherapy.

These studies represent a selection of some of the clinical applications for the treatment of solid cancers by thermal HIFU therapy. These studies have highlighted the benefits of HIFU treatment which included the ability to treat these patients with either low grade adverse events which resolved quickly or no side effects. Assessment of the immunological modulation of cancer patients treated with HIFU has also been a topic of discussion within more recent papers, although there remains a relative paucity in the literature. This modulation is discussed in section 1.2.2, below.

## 1.2 Cancer immune environment

### 1.2.1 Typical cancer immune environment

The tumour microenvironment (TME) is made up of stroma, cancer cells and immune cells. The immune cells within the tumours include T cells, B cells, natural killer (NK) cells, macrophages, monocytes and dendritic cells (DCs), as shown in Figure 1.1. The B cells,

macrophages, monocytes and DCs can all act as antigen presenting cells (APCs). The T cells, B cells, macrophages and NK cells can have functional effects within the tumour and draining lymphatics. It is of note that individual tumour subtypes have different tumour microenvironments, and this includes the infiltrating immune cell populations. For example, in the interest of this thesis, soft tissue sarcoma (STS) is often reported to have low immune abundance in the tumour tissue [26–28], whereas renal cell carcinoma (RCC) is often reported to have high immune infiltration [29–32].

Within the immune cell types, there are subsets of cells with specific functions. For example, T cells include CD8 T cells which are comprised of cytotoxic T cells. Also, CD8 T cells can be characterised by their memory phenotype: naïve (Tnaïve), effector (Tem), central memory (Tcm) and effector memory (Tem) T cells. Tnaïve cells acquire specific functions after encountering antigen presenting cells in the lymphatics, blood or tissues. The CD8 T cells that are antigen experienced acquire a Tcm or Tem phenotype. The Tcm types populate the lymphatics, whereas the Tem populate the vasculature[33]. Both produce cytotoxic responses (perforin) after antigen recognition, the Tcm also produces interleukin-2 (IL-2) and can subsequently differentiate into Tem. The Tem produce granzyme B[34] and FasL, which binds to cancer cells causing apoptosis, cytotoxic granules and interferon-γ (IFN-γ) for the further destruction of cancer cells[35].

The T cells also have the CD4 T cell subset which can be further characterised into conventional T cells (Tconv) and regulatory T cells (Tregs). Tconvs are antigen activated to cross-present by MHC-II on DCs and macrophages for the subsequent activation of CD8 T cells via MHC-I[36]. Tconv can also produce cytokines to such as IFN-γ in tumour tissue, which has been shown to recruit CD8 T cells into the tumour tissue[34]. On the other hand, Tregs

have been shown to inhibit the other immune cells such as the CD8 T cells or conventional CD4 T cells and are also antigen activated[37]. Often this cell type is highly abundant in tumour tissues because of selective self-antigen activation from the tumour in the draining lymphatics[38], leading to their highly active phenotype and abundance. These cells inhibit the function of the APCs by binding the costimulatory receptor CD80 with CTLA-4[39], effectively blocking antigen presentation to CD8 T cells. Also, Tregs can sequester IL-2, which is required by all CD4 T cells for survival[40,41] whilst producing regulatory interleukin-10 (IL-10) and transforming growth factor β (TGF- β)[41].

Macrophages within tumours can switch between a CD64+ anti-tumour phenotype (M1) and a CD163+ protumour phenotype (M2) depending on the cytokine secretion by CD4 populations and cancer cells in the environment. M1 types are induced by the expression of IFN-γ[42] whereas M2 are polarised by TGF- β[43]. M1 produce IL-1β, IL-6, IL-12, IL-23, IFN-β and TNF-α which in turn increases CD4 T cell and NK cell population abundances and can act as antigen-presenting cells[44]. M2 express IL-10, IL-1β, VEGF [45] and promote angiogenesis into tumours[46].

The environment of tumours can often have an anti-immunogenic phenotype, derived by the phenotype of the tumour, to evade recognition and downstream activation of immune cells which would otherwise lead to the eradication of the tumour tissue. The programmed cell death protein 1/programmed cell death ligand1 (PD-1/PD-L1) axis and downregulation of expression of MHC-I molecules are just some examples of how the tumour cells can act to avoid immune responses. The interaction of PD-L1 expressed by cancer cells[47] to PD-1 on T cells where it can reduce T cell receptor (TCR) mediated proliferation, cytokine secretion and

thus cell survival[48]. Cancer cells are known to reduce their MHC-I molecule expression, reducing the CD8 mediated control of tumours[49].

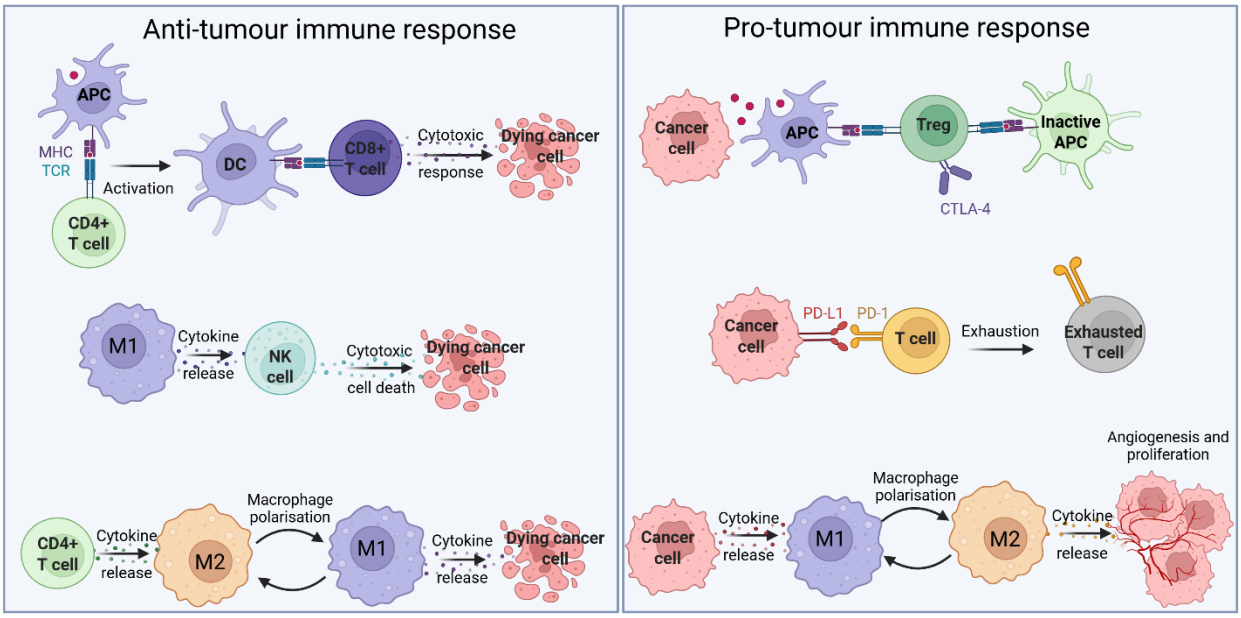


Figure 1.1: An overview of some of the predominant immune cells and their functions within tumours, created with BioRender.com.

### 1.2.2 Immunomodulatory responses to HIFU

HIFU initiates necrotic cell death in the treated area[11,24,50], which is an immunogenic cell death process[51,52]. Heat-shock proteins (HSP) are often expressed following necrosis[53] and HIFU. Specifically, HSP-70 has been shown to induce macrophage expression of TNF-α[54]. Assessment of other HSP by Basu et al. showed increased expression of cytokines (TNF-α, TNF-β, IL-12, and IL-1β) by macrophages following upregulation in the environment[53]. The HSPs were shown to increase DC maturation (in the form of upregulation of CD40 and MHC-II expression) in the same study[53]. The increase in HSP has also been reported in a prostate study by Su et al., where HSP70 and INF-γ was shown to be increased[17].

Other danger-associated molecular proteins (DAMPs) besides HSP have been shown to increase after thermal ablation. *In vitro,* Hu et al. showed that DCs and macrophages were

activated with the increased expression of ATP and HSP produced by colon adenocarcinoma (MC-38) that were treated with thermal ablation *in vitro*[55]. On the DCs, this was assessed expression of costimulatory molecules CD80 by median fluorescence intensity (128±12.4 vs 145±5, $p<0.05$). A ~2-fold increase in TNF-α expression by macrophages was also seen ($p<0.05$)[55]. Nam et al. showed an increase in HMGB-1 after thermal ablation of murine colon cancer CT26[10]. Within this study they also saw increased activation markers (CD40 and CD80) on CD11c+ cells and increased ratio of pro-inflammatory M1macrophages compared to pro-tumour M2 macrophages[10].

Along with the increase in HSP eliciting an immunogenic response, the HIFU increases tumour antigen within the environment, which has led to increased recognition by antigen recognition pathways. Antigen responses caused the CD4 and CD8 TCR repertoire to increase. Chavez et al. demonstrated in a melanoma (B16-OVA and B16-F10) *in vivo* model, there was increased TCR diversity in mice treated with thermal ablation and immunotherapy (Toll-like receptor adjuvants) compared to immunotherapy alone[56]. The expanded clonotypes were shared in the tumour and blood tissues, suggesting a global immune response [56].

Cells of interest that have been reported to be upregulated in thermally ablated tumours include CD4 and CD8 T cells, macrophages and DCs. As described above, CD4 T cells and APCs can cross-present for the activation of cytotoxic CD8 T cells. In an *in vivo* study conducted by Hu et al. showed a 3.4-fold increase in CD11c+ cells (DCs) in the tumour in a colon adenocarcinoma murine model treated with thermal ablation[57]. In a study conducted by Su et al. in an *in vivo* study of prostate cancer (a typically 'immune-cold' tumour) treated with thermal ablation showed increased prostate specific CD4 and CD8 T cell expression

increases after treatment[17]. Zhu et al. were able to show a significant increase (~2-fold, $p<0.001$) in the proportion of lymphocytes that expressed cytotoxic markers within the axillary lymph nodes of patients treated with thermal ablation[58].

There has been lots of previous work that has focused on antigen presentation after HIFU, with overviews of T cell populations also described, as above. Most studies have been conducted in *in vivo* models. Further assessments in human tissues are required to further the understanding of the immune response to HIFU treatments with a view to optimising the potential clinical benefits. Also, different subtypes of tumours have different tumour microenvironments with various immune populations which remain to be explored clinically in depth.

## 1.3 Soft tissue sarcoma

### 1.3.1 An overview of sarcomas and typical treatments

Soft tissue sarcomas (STS) are heterogenic mesenchymal malignancies with the literature reporting between 50 and 100 of known sarcoma subtypes[59–64]. STS affects between 1-2% of adults and 7% of children who have cancer[65,66]. These tumours invade adjacent tissues such as muscle, fat, nerves, and vessels. Alternatively, sarcoma tumours can be found in bone (bone sarcoma, BS) in the cases of osteosarcoma and chondrosarcoma, however, this thesis will focus on STS. STSs are relatively rare tumours but confer a poor prognosis at diagnosis of recurrent disease[67]. Fifty percent of patients have tumour metastasis within 5 years (depending on site, grade and subtype)[62,68] with a 5-year survival rate of 16% given distant metastasis[69]. Tumour progression can typically be aggressive, often with diagnosis made in late stages due to non-specific symptoms, reducing effectiveness in treatment and

life expectancy[70]. Median overall survival (OS) for stage 4 STS has between reported from 18-24 months[71] or 12 to 18 months[72].

Patients with STS require specialist care which is best coordinated by a multidisciplinary team of healthcare providers, in line with current UK guidance. Brennan et al (2014) suggested that "the two of the most important predictors of outcome are histology/histologic subtype and grade" with other factors such as size and depth being known factors that will affect prognosis[62]. The mainstay treatment of STS is typically total resection with clear margins, or limb salvaging surgery with neoadjuvant treatment[72]. The issue with traditional cancer treatments on this type of cancer is that due to the heterogeneric condition and environment of the tumour the treatments required need to be individualised for an improved outcome. Due to the large number of possible STS subtypes and the relative rarity of sarcoma, many chemotherapy agents and combination treatments have not been tested to full statistical power meaning that the success rate of each therapy specific to STS subtype is still limited[73].

Combination chemotherapy is typically used to treat STS patients; this includes doxorubicin and ifosfamide treatment[74]. A significant improvement in the median progression-free survival has been reported for individuals on the combined treatment, although this comes at the cost of increased toxicities[75]. A study conducted by Cesne et al. investigated trabectedin as secondary treatment in a feasibility study as either continuous or interruption treatment. The most common further treatments after trabectedin were gemcitabine (three patients in each group), gemcitabine plus dacarbazine (two in the continuation group and four in the interruption group), or dacarbazine alone (three in the continuation group). The median progression free survival for the continuation group who completed cycles was significantly higher, although still only a modest improvement, at 10.5 months compared to

5.3 months ($p<0.01$) in the interruption group. The continued trabectedin was also associated with significant improvement in progression-free survival[75]. Median overall survival in the continuation group was 27.9 month compared to 16.5 months in the interruption group [75]. The survival statistics were higher in this study than previous studies[75], thus highlighting the importance of tailored treatment strategy for individual STS patients.

Neoadjuvant or adjuvant radiotherapy (RT) is well-established in the STS treatment pathway, and there is a wealth of research relating to optimal RT treatment protocols. RT is used in combination with other treatments, notably surgical resection, either after the tumour has been shrunk by radiotherapy or to reduce the chance of tumour recurrence after surgery. Initial research in this area investigated extremity sarcoma and the efficacy of limb sparing surgeries with RT compared to amputation alone. Both treatment arms provided similar overall survival rates[76], however whilst function and quality of life is significantly improved, it was found that there was local recurrence with the limb sparing surgery, regardless of tumour subtype. This study has paved the way for limb saving surgeries to date with a view to minimising functional loss where possible.

Saxby et al. found that individuals who have surgical resection without RT are significantly more likely to have local recurrence, irrespective of margin size compared to RT patients at various follow up intervals, and that adjuvant (post-operative) RT is less effective than neoadjuvant (pre-operative) RT[77]. Other findings suggested that surgery without RT had a higher incidence in recurrence in older patients compared to the younger patients[77]. Myxofibrosarcoma was found to have a significantly higher recurrence rate (36%), compared to the next most commonly recurrent type: pleomorphic sarcoma (7%).

Recent research has assessed the use of lower doses of radiation to improve wound healing while maintaining a response to treatment, one such study focused on myxoid liposarcoma. The findings concluded that a safe reduction in radiation provided comparable overall survival up to 24 months after treatment[78]. The lower dose of RT used in this study is likely to have led to a reduction in the number of post-RT complications and possibly allows for eligibility to further treatments that may otherwise have been contra-indicated due to the collateral damage that higher doses of radiation may have caused. This is of relevance given the growing range of treatments available to STS patients in recent years. In the long term, and especially in metastatic STS patients, systemic treatments including chemotherapy become more relevant.

A study conducted by Hasan et al. (2021) retrospectively analysed patients with STSs and BS after surgical treatment for curative intent regarding surgical margins and the incidence of local recurrence (LR) and subsequent metastasis (LRSM)[79]. Current surgical practices aim to retain limb function (to ameliorate the reduction to quality of life) which may be detrimental to OS; informing surgeons on the cost/benefits of the chosen margin. However, the results show that this is not the case, the incidence of LR had little correlation with LRSM but more so the type of tumour. The study was conducted at a single site and included paediatric patients; 63 ± 23 for LR only and then a further population analysis including patients 58 ± 22, and 67 ± 26 years for LRSM and LR respectively. The study did not define the negative margin of the sarcoma, which limits the comparison of the few LR which had LRSM to those which did not.

Immunotherapy for the treatment of STS is now emerging as a treatment. Immune checkpoint therapies act to alter invading tumour growth through CD8+ cytotoxic T cell activation causing an anti-tumour response, in the cases of programmed cell death protein-

1/programmed cell death ligand-1 (PD-1/PD-L1) therapies. STS tumours seem to downregulate CD8 T cell activation which allows for rapidly growing invasive tumours to form, reducing survival.

A study conducted by D'Angelo et al. (2019) analysed nivolumab monotherapy and nivolumab and ipilimumab combination therapy in a unblinded double arm study in both BS and STS to determine disease progression and toxicity[59]. This therapy aimed to control immune checkpoint blockade by PD-L1 and the activation of effector T cells by cytotoxic T-lymphocyte-associated protein 4 (CTLA-4). The monotherapy had very little lasting response compared to current treatment modalities for sarcomas, whereas the combined therapy had promise as a second line therapy with an objective response rate (ORR) of 16% and a median OS of 14.3 months[59]. The current US food and drug administration (FDA) approved doxorubicin and olaratumab combined therapy has an OS of 24 months for patients of a similar cohort[59]. The benefit of the monotherapy was individuals tended to be more tolerant with fewer adverse events compared to the combined therapy[59].

Further studies by the same group have used bempegaldesleukin in combination with nivolumab to treat STS[80]. The study analysed the clinical outcomes of the patients as well as tumour samples before and after treatment. The study found that the combination was safe with few side effects and adverse reactions although there was one severe reaction which may have resulted in death. PD-1 expression at baseline was associated with ORR and CD8 and PD-1 are associated with ORR suggesting the treatment influenced the tumour microenvironment for those who had a response. A positive response was seen with changes in the PD-1+ population. RNA analysis was able to cluster the samples into three distinct immunological types were dependent on CD8+ and neutrophils.

Pembrolizumab (aPD-L1) has been evaluated as a monotherapy for STS and BS[81]. The study by Tawbi found a median PFS of 18 weeks with variability based on subtype. Undifferentiated pleomorphic sarcoma (UPS) had the highest response to the treatment with a median PFS of 30 weeks; this is often reported as an immune 'hot' tumour. The study suggested that the sarcoma subtype influenced the success of the treatment but due to the small cohort size of each sample, this was not significant. The study reported no expression of PD-L1 on biopsies, except in only a subset of UPS tumours (3 out of the 70 evaluable tissues).

### 1.3.2 Immune environments of soft tissue sarcoma

STS tumours have classically been thought of as immunogenically 'cold' tumours having very little interaction with the immune system. However, recent literature has demonstrated variation in the response that the immune system produces in STS dependent on the type of tumour and location[26,81]. In addition, some tumours produce an immunosuppressive tumour microenvironment caused by downregulation of cytotoxic cells or dysregulation and exhaustion (likely by PD-1 expression)[82]. There has been a reduction in response to immunotherapy effectiveness in some STS, specifically those that are immunogenically 'cold' compared to immunologically 'hot'[81] as suggested by Tawbi et al.

Much of the immunological research in sarcoma has focused on immune checkpoint inhibitor molecules. A study conducted by Smolle et al. assessed the clinical staging, demographics and outcome data compared to tumour infiltrating immune cells analysed using IHC. The data assessed many individuals and subtypes. The study showed large variation in population numbers of key cells including T cells, and subsets and the expression of PD-1 or PD-L1[27]. The study showed statistically significant differences in T cells and subsets (CD4, CD8, cytotoxic CD8 and Tregs) between the various STS types[27].

Myxofibrosarcoma and UPS tended to have the highest proportion of T cells, while leiomyosarcoma had low T cell population abundance. Correlations between immune cells, checkpoint markers and clinical demographics was conducted and found that there was a strong positive correlation assessed by spearman's Rho correlation with PD-1 + cells and FoxP3+ cells (0.737), with a weak positive correlation of PD-L1 and Tregs (0.311)[27]. Also indicated that increased age had a positive influence on the PD-1+PD-L1+ and PD-L1+ ($p<0.05$) cells[27]. The prognostic factor analysis found that these immune and checkpoint markers had no effect on metastasis but advanced age ($p < 0.001$), high CD3-PD-L1+ ($p < 0.05$) and low FoxP3 cells ($p < 0.05$) were associated with worse overall survival. There was also a trend towards increased risk of LR with higher levels of PD-1+ Tregs, PD-L1+PD-1+ cells, and CD3−PD-1+ cells (all $p>0.05$) [27].

D'Angelo et al. conducted a similar study. However, this study showed that low CD3+ and CD4+ infiltration correlated with an improved OS of individuals by immunohistochemistry (IHC) and clinical data[83]. The study focused on immune cell infiltrates in sarcoma tissues including CD3, CD4, CD8, and FOXP3 stains with subsequent PD-L1 staining. The results showed that tumours that were larger ($p<0.05$) or metastasised (7/11, 64%, $p<0.05$) tended to have a higher proportion of CD8+ T cells. Tumours that express PD-1 were highly infiltrated with CD3+ ($p<0.001$) or CD8+ ($p<0.01$)[83] T cells. PD-L1 expressing tumours were associated with high CD8 T cell abundance ($p<0.05$) and PD-L1 positive immune cells were associated with high CD8 T cell abundance ($p<0.05$). The issue with this study and many studies is the large variation in sarcoma subtype and low abundance of cases which leads to small groups of each with very little statistical power for deconvolution of all factors[83]. The differences in the findings between the two studies could be explained by immune differences of individual tumours within the same subtype as suggested by Smolle et al.

Another key cell type noted in the sarcoma TME was macrophage populations. Dancsok et al. assessed FFPE tissue microarrays from various STS and BS using IHC to quantify tumour-associated macrophages. The study found that there was more of the M2 type macrophages than the M1 type[84]. M1 have been associated with a better outcome linked to the immune-promoting mediation whereas M2 have been associated with a worse prognosis with a link to the immune-suppressing mediation[84], as previously discussed in section 1.2. This suggested that the immune environment is pro-tumour within these cancer types.

The importance of the B cell lineage has been highlighted as a prognostic indicator using RNA sequencing from The Cancer Genome Atlas (TCGA) data and sarcoma tissue. Petitperez et al. were able to classify tumours into "sarcoma immune classifications (SIC)" from low (A) microenvironment immune cell composition to high (E)[26]. For example, UPS and dedifferentiated liposarcoma mostly clustered into the 'hot' immune type, while leiomyosarcoma was mainly associated with the immune 'cold' cluster. The immune profiles found in the immunogenic environment were T cell lineage cells, including CD8 T cells and Tregs. Other immune cell types included monocytes and myeloid dendritic cells expression profiles reduced in the 'cold' clusters compared to the 'hot' cluster. The data suggested ($p>0.05$) that high B cell infiltration into STS resulted in poorer outcomes. CD8 T cell infiltration differences did not correlate with outcome in this study.

Smolle et al. have assessed the sarcoma immune profile from immunohistochemistry (IHC), supported by TCGA data[85]. The immune cells identified by the IHC showed variability both within and between the sarcoma subtypes. This was corroborated by the TCGA data. Immune abundances with higher amounts of CD68+ macrophages ($p< 0.005$) and CD20+ B cells ($p <0.05$) were significantly associated with increased risk of LR[85]. The increased

expression of these antigen presenting cell types being associated with worse prognosis is indeed contrary to the expected function of these cells. The B cell abundance corroborated the previous analyses by Petitprez as discussed. Also, high cytotoxic memory CD8 T cell abundance above the median was associated with worse OS ($p < 0.05$)[85]. Regulatory immune cells (Tregs or M2 macrophages) were not highlighted or assessed within this data, yet are cell types whose abundance is expected to have an impact.

On the flip side, B cells have also been found to be important in a study by Sorbye et al. as a positive prognostic factor. CD20 B cells were found to be highly localised in the tumour tissue of patients that had improved survival which was correlated ($p<0.01$) with disease-specific survival (DSS)[86]. This was along with higher CD4 ($p<0.01$) T cells assessed by univariate analysis. When assessed by multivariate analysis, the significant improvement of DSS with B cells was associated with wide tumour margins ($p<0.01$) which differs for the assessment by Petitprez and Smolle. Also, there were more tumour types assessed by Sorbye, which most likely covered a larger variation in immune populations and phenotypes.

## 1.4 Renal cell carcinoma

### 1.4.1 An overview of renal cell carcinomas and typical treatments

Renal cell carcinomas (RCC) arise from the epithelial tissue within the kidney. RCC accounts for 3% of female cancer and 5% of male cancers worldwide[87]. These tumours are characterised into three subtypes: chromophobe (chRCC), clear cell (ccRCC) and papillary (pRCC) renal cell carcinomas[88]. The most common subtype is ccRCC, with an incidence of around 75-92% of diagnosed RCC tumours, followed in incidence by pRCC at around 7-17%,

and chRCC has an incidence of 2-6% in resected tumours[89,90]. With the advent of increasing cross-sectional imaging, RCC is becoming more commonly incidentally diagnosed.

The gold standard treatment strategy for non-metastatic RCC is partial or whole surgical resection of the kidney (nephrectomy) in surgical candidates. Leibovich et al. reported retrospective outcomes from partial and whole nephrectomy of RCC from 1980 to 2010. In ccRCC, at 5 years there was a 74% (73-76%) PFS maintained at 60% (57-62%) at 15-years following resection. For pRCC PFS was 91% (89–93%) at 5 years and 86% (83–90%) at 15 years[90]. This demonstrated that resection is a very good treatment strategy for those tumours that had not metastasised, but nephrectomy comes at the cost of loss of kidney function, and this may impact quality of life post-resection. Imaging surveillance or thermal ablation of smaller RCC tumours are options, typically used in poor surgical candidates. For solitary or metastatic RCC (mRCC), traditional cancer treatments including radiotherapy and chemotherapy are not typically indicated due to chemo- and radio-resistance[91].

Typically, RCC are locally advancing and/or metastatic[87]. Common locations of metastasis include lung, lymph nodes, bone and liver[89]. In the case of locally advancing and metastatic disease, patients are often treated with cytoreductive nephrectomy to reduce tumour burden with or without additional treatment interventions.

Even though radiotherapy is not a mainstay treatment of RCC, a feasibility study was conducted by Tang et al. has shown the response of oligometastatic ccRCC to radiotherapy after nephrectomy. One-year progression-free survival was 64%[91] suggesting the possible future use of this treatment. However, this treatment again relies upon nephrectomy as the first line of treatment.

A systematic review conducted by Dahm et al. was able to show that interferon or sunitinib (tyrosine-kinase inhibitor, TKI) was likely to increase progression-free survival in metastatic RCC cases, with the caveat that treatment with TKI before surgery increased survival compared to TKI after surgery[92]. This led to clinical approval of sunitinib for first line treatment of mRCC in 2006. Although these studies were able to show that there is improvement in progression-free survival for those with metastatic disease, none of these studies were curable or able to save the kidney.

Treatment strategies for mRCC also include immunotherapy, mainly interferon and interleukin-2 treatments due to the high response rates to these treatments[93–95]. This may be owing to the immune cell infiltration in these tumours, and the association of expression of immunomodulators including immune-checkpoint inhibitors and stimulatory molecules owing their responsiveness to immunotherapy treatments[29]. An overview of the immune populations in RCC is discussed in the subsequent section. Nivolumab (PD-1 inhibitor) with ipilimumab (CTLA-4) has been shown to produce better treatment outcomes than sunitinib (TKI) in patients with advanced RCC after nephrectomy. A study by Tannir et al. showed that progression-free survival at 90 months was increased in patients where it was intended to treat the disease. For Nivolumab + ipilimumab this was 22.8% compared to sunitinib alone which was 10.8%[96].

Choueiri et al. have investigated the response of advanced ccRCC to adjuvant Pembrolizumab (PD-1 inhibitor) following partial or radical nephrectomy (and any, non-brain metastatic lesions negative surgical margins) in a double-blind study[97]. The risk of death was calculated to be 38% lower in the pembrolizumab compared to placebo group with significant improvements in survival ($p<0.005$). Choueiri et al. have also assessed immune

checkpoint and antiangiogenic therapies in a randomised control experiment of patients that had previously had immunotherapy. Patients were treated with either belzutifan (HIF2α) or everolimus (mTOR inhibitor). The objective response rate to belzutifan treatment was 21.9% (17.8 26.5%) compared to 3.5% (1.9 to 5.9%) in the everolimus group (P<0.001, partial response)[98].

Typically, in poor surgical candidates, multifocal RCC or oligometastatic disease, RCC may also be treated with locoregional therapies, including microwave ablation, cryo-ablation as standard of care, and therapeutic ultrasound-based therapies including HIFU and histotripsy are under investigation. These all have the advantage of being minimally or non-invasive and are nephron-sparing. With thermally ablative treatment of any tumour, not least RCC by any modality, unlike resection, tumour debris remains in situ[99–101] (the so called 'in situ cancer vaccine'). Thus, it is anticipated that the immune response mounted to the primary treated tumour would provide extra-beneficial effects in metastatic disease.

RCC can occur in transplant kidneys as an unfavourable outcome of the transplant[102]. Typically, the kidney is resected in this case. These transplants are required as lifesaving therapy for the loss of kidney function in many disease settings. Being able to treat the tumour without removal of the kidney would be an ideal outcome from HIFU treatment.

### 1.4.2 Immune environment of renal cell carcinoma

As previously discussed, RCC tumours are regarded as highly infiltrated tumour types[103]. The TME and immune infiltration of the RCC subtypes are vastly different from each other. Many single cell analyses have assessed the immune populations within the tumours.

Zhang et al. conducted a large study of the immune populations in the RCC subtypes from TCGA data (2018). This study reported that a high proportion of the immune cells within the

RCC types were macrophages (35%) with CD8 T cells being the second most abundant immune cell type. The macrophages were further subcategorised into the resting macrophages (M0), and M1 and M2 types previously discussed in section 1.2.1. The pro-tumour M2 macrophages were most prevalent in the pRCC tumours and was associated with worse prognosis in this tumour subtype[29]. The assessment of T cells showed that naïve CD4 T cells were the most common T cell in pRCC and chRCC, whereas CD8 T cells were the most common subtype in ccRCC, with CD8 T cells having positive prognostic indication in chRCC and a very small negative indication in both pRCC and ccRCC[29]. Whereas the CD4 T cells were split into multiple subtypes, the regulatory T cells were highly associated with negative outcomes in ccRCC but far less so in pRCC and chRCC. Activated memory CD4 T cells were associated with positive outcomes in pRCC, but negative outcomes in chRCC and ccRCC. Zhang et al. were also able to assess the prognostic indications of immune modulators. This assessment found that there were differences in the prognostic indications based on tumour subtype. Expression of CTLA-4, LAG3, and TIGIT showed shorter OS. With pRCC, the expression of LAG3, IDO1 and PD-L1 was associated with shorter OS[29]. For both subtypes, high TIM-3 expression was associated with higher OS survival[29].

Ricketts et al. also assessed the RCC phenotype from the TCGA. In their assessment of the immune populations within RCC dependent on subtype, they found upregulation of almost all immune genes in ccRCC compared to pRCC and chRCC apart from Th17 and CD56$^{bright}$ and IL-8 genes[104]. This agrees with other studies findings that ccRCCs are more immunogenic than the other RCC types. However, this study did not subcategorise the macrophages or T cells as Zhang et al. did, meaning that the subtle differences in subpopulations were not identified within this study. Although there is a difference between the individual tumours in each subtype, TCR signalling also seemed to be detected at a

similar level across all RCC types[104], suggesting that there is a similar ability of the T cells to respond to antigen within the tissue.

Single cell analyses by Zhang et al. of RCC tumours compared to healthy control tissues. The study focused on the assessment of the myeloid populations in ccRCC. The study found that there was a higher frequency of macrophage populations in the ccRCC compared to healthy control tissues [103]. Also, that the monocyte population smaller in the ccRCC samples [103].

A study by Clark et al. assessed the TME of treatment naïve ccRCC patients and found that CD8 T cell infiltration was related to poorer OS[105]. Further investigation highlighted that CD8 T cell abundance correlated with higher INF-γ expression which was hypothesised to lead to increased immune evasion markers such as PD-L1 and CTLA-4[105]. On the other hand, reduced VEGF (angiogenesis) expression was associated with lower CD8 T cells and increased myeloid lineage, which may in turn produce a poorer outcome with pro-tumour macrophage abundance[105]. This may suggest that the increased CD8 T cell abundance is associated with increased angiogenesis and poorer outcomes.

Tertiary lymphoid structures (TLS) have been noted as important in RCC studies. In a study by Meylan et al., the immune populations in the TME of tumours with and without association of TLS were compared by transcriptomic profiling. This found that B cell, T cell, monocyte and fibroblast genes were upregulated in areas associated with TLS of the TME[106]. This was then validated across TLS+ and TLS- tumours where the B cell signatures were seen to be expressed in areas surrounding TLS. The study suggested links to macrophage presence and cell killing by CD68+ macrophages[106] (M1) within these tumours. TLS have been associated with improved prognosis in many tumours besides RCC, including pancreas and hepatocellular carcinoma[107,108].

Taken together, these studies suggest variability in the immune cells of the TME based on subtype of RCC. The immune environment has been linked to effects on survival outcomes, and they have an effect on the immune response to immune modulating HIFU therapy.

## 1.5 Conclusion

HIFU has been demonstrated to be clinically safe and feasible for thermal ablation of many different solid benign and cancerous tumours in a non-invasive manner. The coagulative necrosis cell death mechanism of thermal ablation has been reported as immunogenic by the increase of DAMPs including HSPs, HMGB-1 and ATP within the environment that leads to increased activation of APCs. The technique also increases tumour antigen within the environment, which can be recognised by the APCs such as DCs and macrophages to activate cytotoxic T cells.

STS have a large variety of subtypes which arise in various soft tissues and locations throughout the body with great heterogeneity. Within the sarcoma environment, the immune infiltration into tumours is lower than that of other cancer types. The reason for this is not well understood. However, it does mean that the use of immunotherapies for the treatment of these tumours has been limited with relatively poor outcomes in the past, and treatment personalised to the tumour genetics will become increasingly important. Further investigation into the immune environment of sarcomas is warranted. The investigation of the use of HIFU therapy may be able to provide information on the mechanisms for this low infiltration as well as provide a treatment strategy for these patients potentially in combination with immunotherapy.

There is a desperate clinical need for improved outcomes in metastatic STS for which there are otherwise very limited treatment options over local control with surgery and radiotherapy

and palliation. Thus, there is a great precedence to further investigate STS immunology and immunomodulatory effects of HIFU. The activation of the immune populations by HIFU treatment may be able to improve immune infiltration into the sarcoma tumours which can have further anti-tumour effects. Alternatively, the abundance anti-tumour subpopulations may become more frequent.

In the case of RCC, nephron-sparing locoregional therapies such as HIFU and cryoablation are of great clinical value not least due to preservation of renal function. Also, the success of HIFU treatment and the possible immunological effects may be of benefit in the treatment of metastatic disease. The STS and RCC subtypes have markedly different immune phenotypes, thus the investigation of their modulation with HIFU treatment is of interest as a basic science question. These differences are of interest for future studies as well as having translational importance in terms of personalised immunotherapies and potentially combination therapies which may become transformative for advanced cancers.

## 1.6 Hypothesis

The tumour microenvironment, encompassing tumour, stroma and immune cells, differs by tumour subtype, affecting the type and activation status of tumour infiltrating immune populations including T cell subpopulations and antigen presenting cells (APCs).

In this thesis, I will focus on the 'immune-cold' sarcoma tumours and 'immune-hot' renal cell carcinoma tumours, exploring the effects of HIFU treatment on the immune response to the tumour.

I am hypothesising that the HIFU treatment will increase immune infiltration into immune 'cold' sarcoma tumours combined with increased activation of antigen presenting cells in secondary lymphoid organs and subsequent activation of T cells and increased memory T cell populations. This will be assessed in a murine sarcoma *in vivo* model, in chapter 3.

Sarcomas have different subtypes which have different immune profiles. The transcriptomic profile of the immune cells and the tumour surrounding these cells will indicate the difference in the immune infiltrations. I am hypothesising that in the lower infiltrated leiomyosarcoma (LMS) the abundance and activity of cytotoxic CD8 T cells will be less pronounced than that of the highly infiltrated undifferentiated pleomorphic sarcoma (UPS). This will be investigated in chapter 4.

Finally, I am hypothesising that the immune populations infiltrating the of RCC tumours following HIFU treatment will be different depending on the subtype of RCC because of the inherent, tumour type specific pre-treatment differences. Specifically, I will focus on relative abundance and distribution of antigen presenting cells and cytotoxic T cells in two types of RCC, papillary RCC (pRCC) and clear cell RCC (ccRCC), without HIFU treatment as well as

post HIFU. I will test the hypothesis that HIFU treatment will increase CD8 T cell abundance and activity. These hypotheses will be tested in chapter 5.

## 1.7 Thesis Aims

**i.** Development of a pre-clinical sarcoma model to investigate immune modulation with HIFU treatment **(Chapter 3)**.

**ii.** Assessment of the transcriptomic profile of immune populations associated with soft tissue sarcoma to determine mechanisms for low immune abundances in sarcoma subtypes **(Chapter 4)**.

**iii.** Investigate the immunological changes associated with HIFU treatment in renal cell carcinoma and investigate differences based on subtype **(Chapter 5)**.

# 2 Methodology

## 2.1 Cell culture of MCA205 cell line

All cell culture work was conducted in a lamina flow category 2 biological hood. MCA205 is a mouse fibrosarcoma cell line and was purchased from Millipore (SCC173) and was grown under recommended conditions from Millipore.

Briefly, cells were expanded in expansion media comprised of RPMI-1640 (R0883), supplemented with 2 mM L-glutamine (Sigma-Aldrich, G7513), 1 mM sodium pyruvate (S8636), heat-inactivated 10% foetal bovine serum (FBS, Gibco, 10270-098), 1x non-essential amino acids (Sigma-Aldrich, M7145), 100U/mL penicillin- 100 µg/mL streptomycin (Sigma-Aldrich, P433), and 1x β-mercaptoethanol (Gibco, 21985023) in a T75 flask with vent cap (Corning, 430641U). Cells were incubated at 37°C with 5% supplemental $CO_2$ for 3 to 4 days, to 80% confluency (checked by visual inspection under 20x magnification) before being passaged.

At passage, cells were washed with 1x DPBS (no Mg++ or Ca++, Gibco, 14190094) followed by an incubation with 0.05% trypsin-EDTA (Gibco, 15400054) diluted in DPBS at room temperature (RT) for 5 minutes. Cells were centrifuged at 300 RCF for 5 minutes at RT and the supernatant was discarded. Cells were seeded at 1 x $10^6$ cells per new T75 flask in 25 mL media. A minimum of 2 passages was completed from frozen before cells were implanted.

## 2.2 *In vivo* model

Female C57BL/6NCrl mice were obtained from Envigo by the Biomedical Services at the John Radcliffe Hospital (Oxford, United Kingdom) for initial growth studies. Subsequently

mice were obtained from Charles River by the Biomedical Services at the Radiobiology Research Institute (Oxford, United Kingdom). Mice were housed in individually ventilated cages, in groups of up to 6 individuals. Housing conditions were in line with Home Office (HO) Legislation. All procedures were performed under a HO approved project licence (PCB113E8E) and all people involved had appropriate HO personal license and training.

### 2.2.1 Induction and monitoring of fibrosarcoma tumours

Typically, under 2% isoflurane (obtained through Biomedical Sciences) anaesthesia with a 2 L/min flow rate, 2x $10^5$ MCA205 cells in RPMI-1640 (with no FCS), unless specified, were injected into the mouse flank above the left leg. Care was taken to achieve implantation to the left of the centre line so that draining lymph nodes could be compared to contralateral lymph nodes. Tumours were treated when they were palpable, typically 8 to 11 days post implantation. Once implanted, the mouse was shaved for improved visibility of the tumour. Tumours were measured using callipers, typically every other day. Volume was calculated by:

$$\frac{abc}{2}$$

Where a, b and c represent width, height and length.

### 2.2.2 HIFU Equipment

Ultrasound was generated within a water-bath filled with pre-heated (37°C) degasses distilled water (see schematic in Figure 2.1). The transducer was a single element spherically focused (Sonic Concept, H107C) with a focal length of 63 mm. The ultrasound was generated by a signal amplifier (EMI model 3100LA RF) which was attached to the wave form

generator (Agilent, 33220A) and oscilloscope (Teledyne Lecroy, wavesurfer 3014z). This enabled output voltage to be assessed throughout experiments. Typically, a pressure of 4.3 MPa (peak negative peak), with a duty cycle of 100%, and frequency of 1.6 MHz was utilised, unless otherwise stated. A second, unused transducer was mounted at 90° to the transducer in use. These transducers had linear arrays (GE, L11-5v) mounted within a rectangle cut out, which were each connected to a Verasonics research system (Verasonics Vantage 256) for alignment and mapping of cavitation effects.

During treatment, B mode ultrasound was recoded and assessed with a custom algorithm, written by Dr Micheal Gray to assess cavitation events occurring outside the aligned tumour area during treatment, whilst also ensuring maintenance of alignment of the ultrasound exposure and the tumour during treatment. Post-experimental analysis of recorded passive acoustic mapping (PAM) data was assessed by a custom algorithm, written by Dr Micheal Gray to compare cavitation energy delivered to individual mice.

### 2.2.3 *In vivo* HIFU Treatment

These treatments focused on a partial ablation model to explore the mechanisms of immune modulation caused by the treatment. This was partly due to welfare concerns with the alignment and treatment of these tumours, as well as maintaining an unablated margin of tissue surrounding the ablation area to determine the local immune response caused by the treatment of these tumours. Complete ablation may not preserve a non-ablated margin of viable tumour. Partial ablation preserved this to allow for the assessment of the surrounding tissue for the subsequent immune modulation by histology or flow cytometry.

Mice bearing MCA205 fibrosarcoma tumours were treated with one dose of HIFU under anaesthetic.

Whilst positioned and mounted in a specialised mouse holder, the remaining hair on the tumour was removed with depilation cream (VEET, Reckitt Benckiser) before being placed in a 37°C warmed water-bath. The HIFU array was aligned using B-mode ultrasound, as shown in Figure 2.1. Control mice were anesthetised, placed in the water-bath and recovered after 3 minutes to simulate the alignment time. Mice were recovered in a warming box before being return to their home cage.

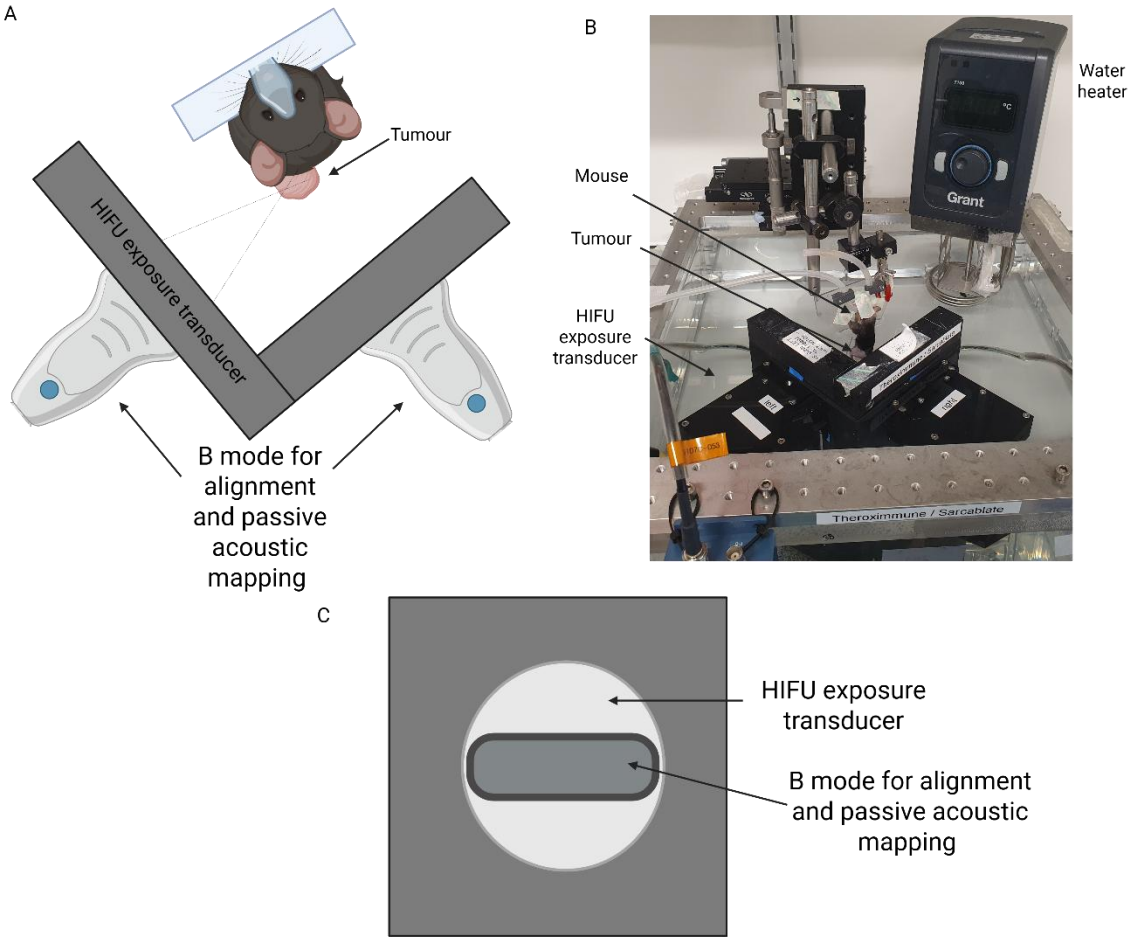


Figure 2.1: (A) Schematic top-down overview of the set up and alignment for the HIFU treatment of fibrosarcoma in an in vivo setting, with (B) a photo of the experimental set-up, (C) Schematic of front on view of ultrasound treatment transducer array with B mode and passive acoustic mapping (PAM) ultrasound array. Created with BioRender.com

### 2.2.4 *In vivo* immunotherapy treatment

Mice were treated with αPD-L1 therapy in combination with HIFU or sham treatment (ie placement in the water bath but no exposure to HIFU). A PD-L1 blocking antibody was purchased from BioXCell: InVivoMAb Rat IgG2b, anti-Mouse PD-L1 (10F.9G2, BE0101). Isotype control was also purchased from BioXCell: InVivoMAb Rat IgG2b, anti-Mouse keyhole limpet hemocyanin (LTF-2, BE0090). Immunotherapy was administered via the tail vein at a dose of 200 µg diluted in PBS, immediately prior to HIFU. For the survival study, subsequent injections via the tail vein were administered 5- and 10-days after HIFU treatment.

### 2.2.5 Blood sampling and processing

Blood was taken from the inferior vena cava after culling. 50 µL of blood was diluted in 100 U/mL heparin (obtained through Biomedical Sciences) as an anti-coagulant. Red blood cells were lysed using Pharmalyse buffer (BD Biosciences, 555899) for 10 minutes at RT before the addition of PBS. Samples were centrifuges at 500 RCF for 5 minutes at RT. The supernatant was discarded, and the samples were resuspended in PBS before subsequent analysis.

### 2.2.6 Lymphoid tissue harvesting and processing

The inguinal and brachial lymph nodes were harvested after culling. The draining and contralateral lymph nodes and spleen were harvested and stored separately in PBS (Gibco, 10010-023) at 4°C before processing. Tissues were processed within 6 hours of harvesting.

Spleen, contralateral lymph nodes (cLN, comprised of inguinal and brachial LNs), and draining lymph nodes (dLN, comprised of inguinal and brachial LNs) were processed by

mashing through a 70 µm sieve (VWR International Ltd, 732-2758) with PBS. Once homogenised, samples were spun at 500 RCF for 5 minutes before resuspension. Red blood cells from homogenised spleen were lysed in Pharmalyse buffer for 10 minutes at RT, before subsequent dilution in PBS. Samples were centrifuged at 500 RCF for 5 minutes. LNs were immediately resuspended in PBS after the first centrifugation. Spleens and lymph nodes were not taken for histological evaluation due to difficulty in maintaining vasculature and orientation post-harvest, and workflow constraints.

### 2.2.7 Tumour harvesting

The tumour was harvested, the skin and surrounding connective tissue was removed, depending on subsequent processing the tumour was then placed in neutral buffered formalin (NBF, Sigma-Aldrich, HT5012) or PBS. Tumours for embedding were transferred from NBF to 70% ethanol (Merck Life Science UK, 32221-M), 24 hours after excision.

### 2.2.8 Cell suspensions from tumour tissue

Tumours were weighed before being cut to break open the tumour capsid. Tumours were incubated in digestion mix. Digestion mix was comprised of RPMI-1640 supplemented with 1 mg/mL DNAse (PanReac AppliChem, A3778.0100), 1 mg/mL collagenase IV (Merck, C4-28), and 1 mg/mL hyaluronidase (MP Biomedicals, 0210074080). Subsequently, samples were diluted in RPMI-1640 before being mashed through 70 µm sieve with RPMI-1640. Once homogenised, samples were spun at 500 RCF for 5 minutes before resuspension. Red blood cells from homogenised tumours were lysed in Pharmalyse buffer for 5 minutes, before subsequent dilution in PBS and centrifugation at 500 RCF for 5 minutes.

## 2.3 Ethical approval for the use of human tissue

Sarcoma and renal tumour tissues for transcriptomic analysis were obtained from Oxford Radcliffe Biobank (OCB), through The Oxford Centre from Histopathology Research (OCHRe). Ethical approval and patient consent checking for the use of tissue was obtained through OCHRe research tissue bank ethics reference 19/SC/0173 for renal tissue (24/A082, Supplementary Figure 2.1) and sarcoma tissue (22/A020, Supplementary Figure 2.2) with the ethics letter from OCHRe (Supplementary Figure 2.3).

## 2.4 Histological based assays

### 2.4.1 Tissue embedding

*In vivo* study tissues were embedded at the Botnar Research Centre (Oxford, United Kingdom). The tumours were processed on an automated Leica ASP300S (Leica Biosystems), the samples were dehydrated in increasing ethanol concentration followed by incubation in xylene and then incubation in paraffin wax. Tissues were embedded in paraffin wax (Sigma-Aldrich, 76242) using a Leica EG1140H and Leica EG1140C (Leica Biosystems). Blocks were intended to be embedded with the skin facing side at the front of the block.

All *in vivo* tumours were cut on a Leica HistoCore BIOCUT (Leica Biosystems) at 5 µm before being air dried at RT for 1 hour and overnight baking at 70°C.

All human slides (STS and RCC) were cut by technicians at OCHRe using RNase clean conditions (deionised water in the waterbath and cleaning with RNAaway, Thermo Scientific, 7002) followed by drying at RT.

### 2.4.2 Haematoxylin and Eosin staining

For mouse *in vivo* and human sarcoma tumour samples, 5 µm tissue slides were deparaffinised in xylenes (Sigma-Aldrich, 214736), a subsequently rehydrated in decreasing ethanol concentration at 2 minutes per step, diluted in deionised (DI) water (100%, 100%, 90%, 70%, 0%). Slides were immersed in Harris haematoxylin solution (Sigma-Aldrich, HHS32) for 2 seconds before being rinsed in running water. This was followed by subsequent immersion in Eosin Y salt (Sigma, E-4382) dissolved in 80% ethanol, pH 8, corrected with the addition of acetic acid (BDH, 270133V) for 30 seconds. Slides were washed in DI water and dehydrated by increasing concentration of ethanol at for 2 minutes per step (70%, 90%, 100%, 100%). Slides were immersed in xylenes before being mounted in EcoMount (BIOCARE medical, EM897L) and applying coverslip.

### 2.4.3 Manual immunohistochemistry staining

For the manual staining of *in vivo* and human sarcoma tumours, markers of interest as outlined in Table 2.1 were used. The baked 5 µm tissue slides were deparaffinised in xylenes (Sigma-Aldrich, 214736), a subsequently rehydrated in decreasing ethanol concentration at 2 minutes per step, diluted in DI water (100%, 100%, 90%, 70%, 0%). Heat-induced antigen retrieval (HIER) was completed by immersion in DI water prior to the appropriate antigen retrieval solution (outlined in Table 2.1), both heated in a steamer (Russel Hobbs, 21140) to 99°C. Either 1x citrate antigen retrieval buffer (Insight Biotechnology, GTX30936) was used to achieve pH6 or 1x eBiosciences IHC Antigen Retrieval Solution - High pH (Invitrogen, 00-4956-58), was used to achieve pH9. Slides were incubated for 25 minutes before being immersed in RT PBS. In the case of CK8 staining, slides were then immersed in 1 µg/mL

proteinase K (Invitrogen, AM2546) diluted in 1x PBS, at 37°C for 15 minutes then washed in 1xPBS for 5 minutes.

Endogenous peroxidase activity was blocked by incubating slides for 10 minutes in 3% hydrogen peroxide (Fisher Scientific UK Ltd, 10687022) followed by washing in PBS. Non-specific protein binding was blocked by incubation with 1% bovine serum albumin (BSA, Sigma-Aldrich, A7906) for 30 minutes. Slides were washed in PBS and as much liquid as possible was removed before staining with primary antibody, diluted in 1% BSA, for 1 hour as outlined in Table 2.1. The slides were washed thrice with PBS. The subsequent corresponding secondary antibody for detection (polymer conjugated horseradish peroxidase goat IgG) as outlined in Table 2.1, was incubated with the slides for 30 minutes before slides were washed thrice with PBS. Slides were then incubated with 3,3'diaminobenzidine (DAB) substrate (abcam, ab64238) for 2 minutes for chromatic detection before washing in PBS. Slides were subsequently dehydrated and mounted as outlined in Section 2.4.2.

Table 2.1: Table of antibodies used in manual immunohistochemistry staining.

| Target | Use | Raised in | HEIR | Concentration µg/ml | Clone | Cat # |
|---|---|---|---|---|---|---|
| Vimentin | RCC, *in vivo* | Mouse | pH9 | 0.4 | E-5 | sc-373717 |
| CD68 | Sarcoma | Mouse | pH6 | 0.4 | KP1 | sc-20060 |
| CD8 | Sarcoma | Rabbit | pH6 | 1 | CAL66 | ab237709 |
| CD8 | *In vivo* | Rabbit | pH9 | 1 | CAL66 | ab237709 |
| CD45 | Sarcoma | Mouse | pH6 | 1 | HI30 | 555480 |
| CD45 | *In vivo* | Rat | pH6 | 1 | 30-f11 | 103101 |
| FoxP3 | *In vivo* | Rabbit | pH6 | 1.1 | EPR15038-69 | ab191416 |
| CK8 | *RCC* | Mouse | pH6 | 0.5 | CAM5.2 | 452M-94 |
| mouse IgG | Sarcoma, *in vivo, RCC* | Goat | N/A | N/A | N/A | ab214879 |
| rabbit IgG | Sarcoma, *in vivo* | Goat | N/A | N/A | N/A | ab214880 |
| rat IgG | Sarcoma, *in vivo* | Goat | N/A | N/A | N/A | ab214882 |

### 2.4.4 Automated immunohistochemistry staining

The clinical sarcoma samples obtained from OCHRe were stained using the LeicaBOND system (Leica Biosystems) for the detection of CD45 cells. The baked 5 µm tissue slides were automatically stained for CD45 (HI30, BD biotechnology) at a dilution of 1:500. Briefly, the LeicaBOND was set to use a IHC protocol with a 30-minute bake and dewax protocol, with a 20-minute HIER step. Epitope retrieval solution 2 (Leica Biosystems, AR9640) was used to achieve pH9 HIER. Slides were subsequently dehydrated and mounted as outlined in section 2.4.2.

### 2.4.5 Slide scanning and image processing

For slides involved in *in vivo* and sarcoma data analysis, slides were scanned on Zeiss Axioscan 7 (Zeiss Group) at the Kennedy Institute of Rheumatology (Oxford, United Kingdom) under 20x magnification. Slides were processed using QPath 0.5.1 for white balance and cell

counting. Cell counts were conducted on areas of tumour with connective tissue excluded. Default settings were retained, except for:

- Reduction of the minimum area to 0.04 $\mu m^2$
- Reduction of maximum area to 200 $\mu m^2$
- Intensity parameters threshold was set to 0.05
- Cell expansion parameter was set to 4 µm
- Intensity threshold was set for each stain type, between 0.2 to 0.4

The RCC H&E slides were requested from ORB and subsequently scanned at 40x magnification by OCHRe.

## 2.5 Flow cytometry-based protocols

Flow cytometry data were acquired by Attune NxT flow cytometer (Thermo Fisher) and analysed by FlowJo software v10 (BD Biosciences). All antibodies used within their respective panels is outlined in Table 2.2. Where possible, 50 µL of blood, 1 LN, 1/10 of the spleen and 1/4 of the tumour was stained for each panel.

### 2.5.1 Live dead cell differentiation staining

All cells were washed in PBS prior to live dead differentiation dye staining. Cells were resuspended in diluted zombie aqua fixable viability kit (Biolegend, 423101) diluted 1:1000 in PBS for all flow panels. This was incubated at RT for 15 minutes at 4°C in the dark before being centrifuged at 500 RCF for 5 minutes. The supernatant was discarded, and the cells were washed in PBS. The stock solution was created by diluting a vial of the zombie aqua

fixable viability kit in 100 µL of DMSO, followed by through mixing and storage in aliquots at -20°C before use.

### 2.5.2 Cell surface staining

Following live/dead staining, cells were resuspended in antibody mix, diluted in FACs (PBS supplemented with 1% FBS) for each experiment as outlined in Table 2.2. Cells were incubated for 1 hour at 4°C in the dark. Cells were washed in FACs buffer, followed by centrifugation at 500 RCF for 5 minutes. The supernatant was discarded. Cells were washed in FACs buffer prior to fixation in buffer from eBioscience Foxp3/Transcription Factor Staining Buffer Set (Invitrogen, 00-5523-00). The fixation buffer was diluted 1:3 in the fixation diluent immediately before use. Stained cells were fixed for 45 minutes before washing in FACs buffer by centrifugation at 500 RPM for 5 minutes at RT.

Table 2.2: Table containing antibodies for the assessment of immune populations within the *in vivo* models, (PB) Pacific Blue, (BV) Brilliant Violet, (AF) Alexa Fluor, (PerCP) Peridinin-Chlorophyll-Protein, and (Cy) Cyanine.

**Higher Seeding Density**

**CD4 Subsets**

| Target | Fluorophore | Concentration mg/ml | Clone | Cat # |
|---|---|---|---|---|
| CD45 | eFluor 450 | 0.001 | 30-F11 | 48-0451-82 |
| CD44 | BV605 | 0.001 | IM7 | 103047 |
| Tim-3 | BV711 | 0.001 | RMT3-23 | 119727 |
| CD3 | BV785 | 0.001 | 17A2 | 100231 |
| PD-1 | FITC | 0.001 | 29F.1A12 | 135213 |
| CD4 | PerCP-eFluor710 | 0.001 | RM4-5 | 46-0042-82 |
| CTLA-4 | PE | 0.001 | UC10-4B9 | 106305 |
| CD25 | PE/Dazzle 594 | 0.001 | PC61 | 102047 |
| FoxP3 | APC | 0.001 | FJK-16S | 17-5773-82 |
| CD8a | AF700 | 0.001 | 53-6.7 | 56-0081-82 |

**CD8 Memory**

| Target | Fluorophore | Concentration mg/ml | Clone | Cat # |
|---|---|---|---|---|
| CD45 | eFluor 450 | 0.001 | 30-F11 | 48-0451-82 |
| CD3 | BV605 | 0.001 | 17A2 | 100237 |
| Tim-3 | BV711 | 0.001 | RMT3-23 | 119727 |
| ICOS | BV785 | 0.001 | C398.4A | 313533 |
| CD44 | FITC | 0.001 | IM7 | 103021 |
| CD4 | PerCP-eFluor710 | 0.001 | RM4-5 | 46-0042-82 |
| PD-1 | PE | 0.001 | 29F.1A12 | 135205 |
| CD8a | AF700 | 0.001 | 53-6.7 | 56-0081-82 |
| CD62L | APC-eFluor780 | 0.001 | MEL-14 | 47-0621-82 |

**Lower Seeding Density**

**CD4 Subsets**

| Target | Fluorophore | Concentration mg/ml | Clone | Cat # |
|---|---|---|---|---|
| CD45 | BV421 | 0.001 | 30-F11 | 48-0451-82 |
| CD4 | BV650 | 0.001 | RM4-5 | 100547 |
| CD3 | BV786 | 0.001 | 17A2 | 100231 |
| Ki67 | FITC | 0.001 | 16A8 | 652409 |
| CD25 | PE | 0.001 | PC61.5 | 12-0251-82 |
| CD19 | PE/Dazzle 594 | 0.001 | 6D5 | 115553 |
| FOXP3 | APC | 0.001 | FJK-16S | 17-5773-82 |
| CD8a | APC-Cy7 | 0.001 | 53-6.7 | 100713 |

**CD8 Memory**

| Target | Fluorophore | Concentration mg/ml | Clone | Cat # |
|---|---|---|---|---|
| CD45 | eFluor 450 | 0.001 | 30-F11 | 48-0451-82 |
| CD4 | BV650 | 0.001 | RM4-5 | 100547 |
| TIM-3 | BV711 | 0.001 | RMT3-23 | 119727 |
| CD3 | BV786 | 0.001 | 17A2 | 100231 |
| CD44 | FITC | 0.001 | IM7 | 103021 |
| CD62L | PE | 0.001 | W18021D | 161203 |
| PD-1 | PE-Cy7 | 0.001 | 29F.1A12 | 135215 |
| CD69 | APC | 0.001 | H1.2F3 | 17-0691-82 |
| CD8a | AF700 | 0.001 | 53-6.7 | 56-0081-82 |

**Development of the Ablation Profile**

**CD4 Subsets**

| Target | Fluorophore | Concentration mg/ml | Clone | Cat # |
|---|---|---|---|---|
| CD8a | PB | 0.001 | 53-6.7 | 48-0081-82 |
| CD4 | BV650 | 0.001 | RM4-5 | 100547 |
| CD3 | BV786 | 0.0025 | 17A2 | 100231 |
| Ki67 | FITC | 0.001 | 16A8 | 652409 |
| CD25 | PE | 0.001 | PC61.5 | 12-0251-82 |
| CD19 | PE/Dazzle 594 | 0.001 | 6D5 | 115553 |
| FOXP3 | APC | 0.001 | FJK-16S | 17-5773-82 |
| CD45 | AF700 | 0.001 | 30-F11 | 56-0451-82 |

**CD8 Memory**

| Target | Fluorophore | Concentration mg/ml | Clone | Cat # |
|---|---|---|---|---|
| CD8a | PB | 0.001 | 53-6.7 | 48-0081-82 |
| CD4 | BV650 | 0.001 | RM4-5 | 100547 |
| CD3 | BV786 | 0.0025 | 17A2 | 100231 |
| CD44 | FITC | 0.001 | IM7 | 103021 |
| CD62L | PE | 0.001 | W18021D | 161203 |
| PD-1 | PE-Cy7 | 0.001 | 29F.1A12 | 135215 |
| CD45 | AF700 | 0.001 | 30-F11 | 56-0451-82 |

**Optimisation of the Ablation Profile**

**Treg**

| Target | Fluorophore | Concentration mg/ml | Clone | Cat # |
|---|---|---|---|---|
| CD45 | BV421 | 0.001 | 30-F11 | 48-0451-82 |
| CD4 | BV650 | 0.001 | RM4-5 | 100547 |
| CD3 | BV786 | 0.0025 | 17A2 | 100231 |
| Ki67 | FITC | 0.001 | 16A8 | 652409 |
| CD25 | PE | 0.001 | PC61.5 | 12-0251-82 |
| CD19 | PE/Dazzle 594 | 0.001 | 6D5 | 115553 |
| FOXP3 | APC | 0.001 | FJK-16S | 17-5773-82 |
| CD8a | APC-Cy7 | 0.001 | 53-6.7 | 56-0451-82 |

**Myeloid**

| Target | Fluorophore | Concentration mg/ml | Clone | Cat # |
|---|---|---|---|---|
| CD45 | eFluor 450 | 0.001 | 30-F11 | 48-0451-82 |
| CD14 | BV605 | 0.001 | SA14-2 | 123335 |
| CD3 | BV786 | 0.0025 | 17A2 | 100231 |
| CD11c | FITC | 0.001 | N418 | 11-0114-82 |
| F4/80 | PE | 0.004 | BM8 | 123109 |
| Ly6C | PE-Cy7 | 0.001 | AL21 | 560593 |
| Gr1 | APC | 0.001 | RB-8C5 | 17-5931-82 |
| CD11b | APC-Cy7 | 0.001 | PK136 | 101255 |

**CD8 Memory**

| Target | Fluorophore | Concentration mg/ml | Clone | Cat # |
|---|---|---|---|---|
| CD45 | eFluor 450 | 0.001 | 30-F11 | 48-0451-82 |
| CD4 | BV650 | 0.001 | RM4-5 | 100547 |
| CD3 | BV786 | 0.0025 | 17A2 | 100231 |
| CD44 | FITC | 0.001 | IM7 | 103021 |
| CD62L | PE | 0.001 | W18021D | 161203 |
| PD-1 | PE-Cy7 | 0.001 | 29F.1A12 | 135215 |
| CD8a | APC-Cy7 | 0.001 | 53-6.7 | 56-0451-82 |

**HIFU with Immunotherapy**

**Tcell**

| Target | Fluorophore | Concentration mg/ml | Clone | Cat # |
|---|---|---|---|---|
| CD45 | eFluor 450 | 0.001 | 30-F11 | 48-0451-82 |
| CD44 | BV605 | 0.001 | IM7 | 103047 |
| CD4 | BV711 | 0.001 | RM4-5 | 100549 |
| CD3 | BV786 | 0.0025 | 17A2 | 100231 |
| CD8a | FITC | 0.001 | 53-6.7 | 11-0081-82 |
| Ki67 | PerCP-Cy5.5 | 0.001 | 11F6 | 151221 |
| PD-1 | PE | 0.002 | J43 | 12-9985-82 |
| CD25 | PE/Dazzle 594 | 0.001 | PC61.5 | 102047 |
| CD62L | PE-Cy7 | 0.001 | SAL4-2 | 47-0621-82 |
| FOXP3 | APC | 0.001 | FJK-16S | 17-5773-82 |

**Myeloid**

| Target | Fluorophore | Concentration mg/ml | Clone | Cat # |
|---|---|---|---|---|
| CD45 | eFluor 450 | 0.001 | 30-F11 | 48-0451-82 |
| CD3 | BV605 | 0.001 | 17A2 | 100237 |
| CD11c | PerCP-cy5.5 | 0.001 | N418 | 117327 |
| F4/80 | PE | 0.001 | BM8 | 123109 |
| CD11b | PE/Dazzle 594 | 0.001 | M1/70 | 101255 |
| Ly6C | pe-cy7 | 0.001 | AL21 | 560593 |
| Ly6G | APC | 0.001 | S19018G | 164505 |
| MHC-II | AF700 | 0.0025 | M5/114.15.2 | 107621 |

**PD-L1**

| Target | Fluorophore | Concentration mg/ml | Clone | Cat # |
|---|---|---|---|---|
| CD45 | eFluor 450 | 0.001 | 30-F11 | 48-0451-82 |
| CD3 | BV786 | 0.0025 | 17A2 | 100237 |
| CD29 | PE | 0.001 | HMβ1-1 | 130-102-994 |
| PD-L1 | APC | 0.001 | 10F.9G2 | 124311 |

### 2.5.3 Intracellular staining

Cells that were stained for FoxP3 or Ki67 (as outlined in Table 2.2) were washed in permeabilisation buffer from eBioscience Foxp3/Transcription Factor Staining Buffer Set (Invitrogen, 00-5523-00) diluted 1:9 in DI water, twice by centrifugation at 500 RCF. Cells were stained with antibodies diluted in permeabilisation buffer for 1 hour at 4°C in the dark. Cells were washed in FACs and centrifuged at 500 RPM for 5 minutes. The supernatant was discarded, cells from lymph node, spleen and blood were resuspended in FACs buffer, cells from tumours were resuspended in MACs buffer. MACs buffer comprised of PBS, 1% FBS and 1nM ethylenediaminetetraacetic acid (EDTA, Invitrogen, 15575020) before acquisition.

## 2.6 Spatial transcriptomic analysis of clinical samples by Nanostring GeoMx Digital Spatial Profiler

### 2.6.1 Preparation of slides for spatial profiling

Sarcoma and renal tumour samples were sectioned by OCHRe in clean conditions as outlined in Section 2.4.1. These slides were baked for 3 hours before subsequent protocol steps. The protocol developed by Nanostring (Bruker) for Manual slide preparation of Whole Human Transcriptome RNA assessment with Illumina sequencing was followed. An overview of the protocol is described below. RNA clean techniques were adopted, mainly the use of RNAaway to clean surfaces and equipment.

The baked 5 µm slides were deparaffinised in 3 washes of Xylene for 5 minutes, followed by rehydration of the tissue in decreasing concentrations of ethanol for 5 minutes (100%, 100% and 95%). Slides were washed in autoclaved 1x PBS (Oxoid, BR014G) made from

diethylpyrocarbonate (DPEC, Invitrogen, AM9915G) treated deionised water. HEIR was conducted using pH9 antigen retrieval solution, diluted in DPEC-treated DI water, for 20 minutes. Slides were washed in 1x PBS for 5 minutes, then immersed in 1 µg/mL proteinase K diluted in 1x PBS, at 37°C for 15 minutes then washed in 1x PBS for 5 minutes. Within a lamina flow hood, slides were incubated in 10% NBF for 5 minutes and then twice in NBF stop buffer for 5 minutes each. NBF stop buffer consisted of 1x PBS, 0.1 M tris (BDH, 103156X), 0.1 M glycine (Sigma, G8898). Slides were washed in 1x PBS for 5 minutes.

Next, slides were incubated with probes. The GeoMx Human Whole Transcriptome Atlas starter kit (Bruker, 999063) and collection plates (Bruker, 100473) were purchased from Nanostring (Bruker). These kits contained all reagents required from Nanostring. For the assessment of the renal tumours, an additional Sequencing Code Pack was purchased (Bruker, 121400202). The Human Whole Transcriptome Atlas Probes were diluted in buffer R at recommended dilution ratios. Each slide was incubated with 180 µL of total diluted stock, (made up of 18µL of mixed and spun down probes, 18µL of DPEC DI water, and 144 µL of buffer R). These slides were incubated at 37°C for a minimum of 16 hours and a maximum of 18 hours, in the dark with a hybridisation coverslip (Grace Bio-Labs, GBL716024).

Following incubation, slides were washed in 2x SSC (Sigma-Aldrich, S6639), diluted in DPEC treated DI water to remove the coverslip and immersed in two consecutive stringent wash steps for 25 minutes each. The stringent wash was comprised equal parts 2x SSC and formamide (Sigma-Aldrich, F9037). Slides were then washed twice in 2x SSC for 2 minutes each.

Immunofluorescent staining was utilised to identify cells of interest in the tissue. First, unwanted protein binding to antibodies was blocked by incubation with blocking solution for

30 minutes. Blocking solution comprised of 5% native goat serum (NGS, abcam, ab7481) diluted in the buffer 'W' provided in the kit from Bruker. Fluorescent staining was conducted in three parts for both the sarcoma and renal tumour slides as outlined in Table 2.3. Between each staining step, slides were washed thrice in 2x SSC. Slides were washed trice in 2x SSC before loading onto the Nanostring GeoMx digital spatial profiling (DSP) machine following the Nanostring protocol.

Table 2.3: Overview of the antibodies for the immunofluorescent staining of the tissues in the sarcoma and RCC transcriptomic profiling. Asterisk denotes antibody provided by Nanostring, where the concentration was not provided.

| | Sarcoma | | | | | |
|---|---|---|---|---|---|---|
| **Staining step** | **Target** | **Species** | **Fluorophore** | **Concentration µg/ml** | **Clone** | **Cat #** |
| **Primary** | CD8 | Rabbit | unconjugated | 1 | CAL66 | ab237709 |
| | Vimentin | Mouse | unconjugated | 0.4 | E-5 | sc-373717 |
| **Secondary** | mouse IgG | Goat | Cy-3 | 1 | N/A | ab97035 |
| | rabbit IgG | Goat | AF647 | 0.4 | N/A | ab150083 |
| **Tertiary** | CD45 | Mouse | AF594 | * | PD7/26+2B11 | N/A |
| | Nucleus | N/A | SYTO 13 | * | N/A | N/A |

| | RCC | | | | | |
|---|---|---|---|---|---|---|
| **Staining step** | **Target** | **Species** | **Fluorophore** | **Concentration µg/ml** | **Clone** | **Cat #** |
| **Primary** | CD45 | Mouse | unconjugated | 1 | 2D1 | 65082-1-IG |
| | CD45 | Mouse | unconjugated | 1.6 | PD7/26+2B11 | ab781 |
| | CD8 | Rabbit | unconjugated | 1 | CAL66 | ab237709 |
| **Secondary** | mouse IgG | Goat | TR | 0.4 | N/A | ab6787 |
| | rabbit IgG | Goat | AF647 | 0.4 | N/A | ab150083 |
| **Tertiary** | PanCk | Mouse | AF532 | * | AE1+AE3 | N/A |
| | Nucleus | N/A | SYTO 13 | * | N/A | N/A |

## 2.6.2 Region of interest selection

Fluorescence intensity thresholds for cells of interest were selected on an individual tissue basis. From this, regions of interest (ROIs) were selected based on parameters outlined within the subsequent relevant chapters.

Following ROI selection, the RNA oligoprobes were photocleaved within the machine within the ROI selected. The oligoprobes were collected within the machine in individual wells of a 96 well plate. Following collection, the oligoprobes within the plate were frozen at -20°C until subsequent library preparation for sequencing.

### 2.6.3 Library preparation for Illumina sequencing

Library preparation for Illumina sequencing was conducted based on the manufacture's protocol from Nanostring. The plates were defrosted and dried on a thermocycler for 2 hours, until all liquid evaporated. Plates were covered with a permeable seal (AeraSeal film, Merck, A9224). Each well was resuspended in nuclease-free water (Invitrogen, AM9932). The plate was sealed, allowed to resolubilise for 10 minutes before pipette mixing and centrifugation at 500 RCF for 2 minutes. For each well of sample, 4 µL of primer from the centrifuged Sequencing Code Primer Mix, 2 µL of Master Mix, and 4 µL of DSP aspirate were added to a clean 96 well plate for each DSP plate produced by experiments. The Primer Mix and Master Mix were part of the kit from Nanostring. Wells were mixed by pipetting before being pulse centrifuged at 3000 RCF. Plates were incubated in a thermocycler with the program outlined in Table 2.4.

Following PCR, 4 µL of product from each well of the plate was pooled. Each pool was then individually cleaned before quality checking by Bioanalyser. Briefly, following the Nanostring protocol, 1.2x AMPure XP bead (Beckman Coulter, A63880) volume was added to the pool volume and pipette mixed. This was incubated for 5 minutes before the samples were placed on a magnet and incubated until the SPRI beads pelleted. Once pelleted, the supernatant was discarded. The beads were washed twice with 80% ethanol before being air dried and eluted off the magnet in 50 µL of elution buffer for 5 minutes. Elution buffer was PBS with 10

mM pH 8.0 Tris-HCl and 0.05% Tween-20. A subsequent AMPure XP clean was conducted following the same protocol. At this step plates were eluted at 0.5 µL per well.

The cleaned PCR product was quantified and assessed for purity using Agilent Bioanalyser (Agilent) with High Sensitivity DNA Kit (Agilent, 5067-4626) following manufacturer's protocol before sequencing.

Table 2.4: Thermocycler program for the amplification of oligoprobes.

| Step | Temp | Time | Cycles |
|---|---|---|---|
| UDG Incubation | 37°C | 30 mins | 1 |
| UDG Deactivation | 50°C | 10 mins | 1 |
| Initial denaturation | 95°C | 3 mins | 1 |
| Denaturation | 95°C | 15 secs | 18 |
| Anneal | 65°C | 60 secs | |
| Extend | 68°C | 30 secs | |
| Final Extension | 68°C | 5 mins | 1 |
| Hold | 4°C | Infinite | 1 |

### 2.6.4 Illumina sequencing

Libraries were shipped to Novagene for sequencing. The Sarcoma study library was sequenced on a NovaSeq machine as a partial lane. The RCC study library was pooled based on a ratio of the ROI size for each plate, as recommended within the Nanostring protocol. This was then sequenced as a partial lane on a NovaSeq X Plus. Concentration was based on recommendations from Nanostring.

## 2.7 Data processing from digital spatial profiling

### 2.7.1 Data pre-processing

After sequencing, the data was kindly deconvoluted and converted from fastq to digital compact cassette (DCC) by Dr Oliver McCallion following instructions from Nanostring using the Biomedical Research Computing Cluster at the University of Oxford.

Following deconvolution, the data was processed through the DSP pipeline to produce an initial dataset for downstream analysis which was conducted in R. Base R version 4.4.2[109], along with the dplyr[110], openxlsx[111] and tidyverse[112] packages were used throughout.

Firstly, the sequencing depth, nuclei count, and area of the ROIs were assessed. Any ROIs that contained fewer than 50 nuclei were discounted (none in either experiment). The ROI area was viewed to assess any variation in the normalisation.

The limit of detection was based on the geometric mean of the negative probes in the wells. A study of the distribution of the geometric mean of the negative was used to threshold the limit of detection, a minimum of 25 replicated reads of each gene was required to pass the threshold in both studies. The distribution of the data was normalised using quantile normalisation in R.

Post-normalised data was assessed by principal components analysis based on the variables within the data. FactoMineR[113] package was used to calculate PCA and foctoextra[114] was used to generate the PCA plots.

### 2.7.2 Cellular deconvolution of the data

Estimates of cell abundances within ROIs based on expression profiles were generated using the SpatialDecon analysis with the ImmuneTumor_safeTME reference model[115]. Data

within the model was generated from normalised TCGA data[116]. Heatmaps were generated using ComplexHeatmap[117] with RcolorBrewer package[118].

### 2.7.3 Differential gene expression analysis

Differential gene expression analysis was performed using the Limma package[119]. For the Limma analysis, the Voom model was used with an adjusted p value of 0.05 for the pCutOff and a log fold change of 0.5 was used to identify significant differences in gene expression across both analyses. A correction was made for the use of more than one ROI selected per patient sample within the model by calculating the correlation of the samples and accounting for that as part of the model as part of the Limma code. Volcano plots were generated using EnhancedVolcano[120]. Gene pathway analysis was generated using clusterProfiler[121] (KEGG-based pathway assessment) with the mapping of gene names using org.Hs.eg.db[122]. Redundant pathways were removed using the simplify function before manual correction to remove replicated pathways with similar context.

### 2.7.4 Unbiased gene expression analysis

An unbiased approach to assess the differential gene expression analysis was conducted using weighted gene correlation network analysis (WGCNA[123] with the circularize package[124]) using a signed hybrid model with the kind help of Dr Amy Cross.

Soft threshold was used to assess the shared genes between modules and a power that should be used for the WGCNA analysis as shown in Figure 2.2. For the sarcoma analysis, the threshold of 0.9 was not achieved, thus a power threshold of 5 was selected as to conduct a descriptive analysis to support the differential gene expression analysis. For the RCC analysis, the power of 7 was over the 0.9 threshold. Minimum genes to generate a

module was set to 30. Pathways were assessed in the same manner as the differential gene expression analysis in section 2.7.3.

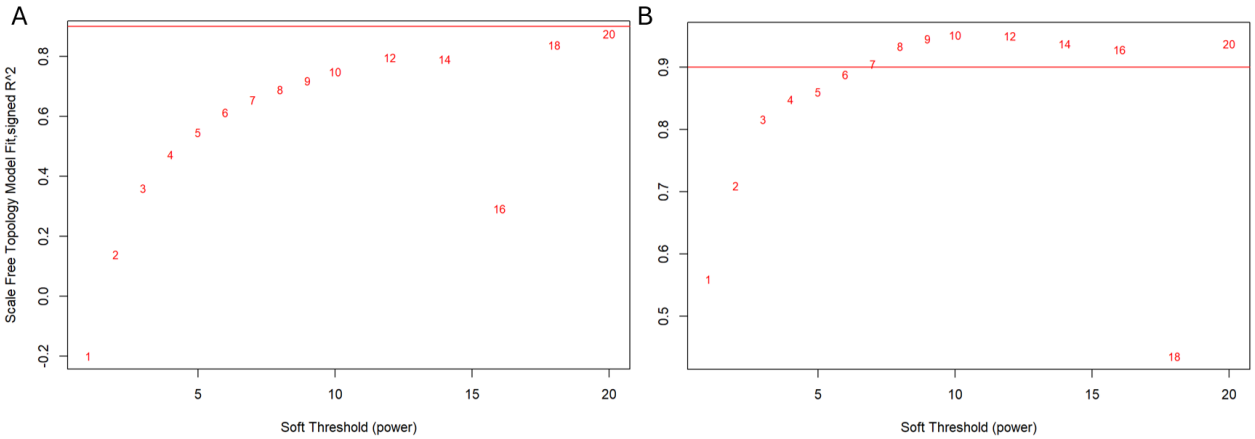


Figure 2.2: Scale of independence analysis for selection of power threshold WGCNA analysis using soft threshold analysis of (A) sarcoma and (B) RCC transcriptomic studies. Scale free topology network correlations with resulting network for each threshold. Red line indicated threshold of 0.9.

## 2.8 Statistics and graph generation

Generation of graphs and statistical analysis of tumour volume changes and tumour growth data was performed in Prism (GraphPad, Dotmatics). ANOVA, and grouped analysis with Tukey's post-hoc test was performed. For statistical analysis of populations identified by flow cytometry, ANOVA with Tukey's post-hoc test was performed in R version 4.4.2[109]. Generation of the different graphical representations using ggplot2[125] package. Analysis of digital spatial profiling data and subsequent statistical analysis were performed in R. Packages are outlined in the previous Section 2.7.

# 3. Assessment of Immunological Modulation of Sarcoma After HIFU Treatment in an *in vivo* Model

## 3.1 Chapter Introduction

The literature surrounding HIFU treatment suggests that thermal ablation may increase available tumour associated and tumour specific antigen (TAA and TSA). This is caused by the necrotic nature of the cell death produced by the treatment. The literature from previous studies in multiple tumour types also suggests that thermally ablative HIFU can drive infiltration by antigen presenting cells (APCs)[126] as well as cytotoxic T cells (CTLs) with improved function into the tumour[127]. HIFU is thought to increase circulating antigens which are recognised by DCs and cross presented to CTLs[128,129]. Furthermore, it has been reported that HIFU can increase circulating danger associated molecular patterns (DAMPs) [25,127] which can increase the response of APCs[55,127,130]. Increased lymphocytic infiltration has been seen *in vivo* before in a sarcoma model treated with HIFU ablation[131], specifically mice implanted with Ascitic sarcoma 180 cells and exposed to 10 W/cm$^2$ at 3MHz for 10 seconds of HIFU. This showed around 300-fold ($p<0.001$) increase in TRAP+ cells (macrophage and DCs) and a 400-fold and 600-fold increase in CD4 and CD8 T cells respectively in tumours as measured by immunohistochemistry staining. However, this model appeared as immune 'cold' which is not representative of all sarcomas and detailed assessment of the CD4 and CD8 T cell subtypes, as well as individual APCs was lacking. This study did not go on to assess the possible mechanism for recruitment nor did they include immunotherapy to try to improve outcomes.

Soft tissue sarcomas are regarded as minimally immune infiltrated tumour types[132], but with variation in the immune milieu often being reported between subtypes[26,85] or individual tumours[133,134]. The rationale for using HIFU therapy within these minimally immune infiltrated tumours would be to improve the immune infiltration to increase tumour clearance whilst also possibly improving response to metastatic lesions by bolstering antigen-specific immune responses.

HIFU treatment has been the focus of many clinical cancer trials. Most focus has been on prostate[19,20], pancreatic[21,135], RCC[15] and breast cancer[24]. To date sarcoma has not received the same attention with only pre-clinical studies reported. The aim of this chapter was to evaluate the potential treatment efficacy of HIFU and investigate immune modulation within sarcoma to develop an *in vivo* sarcoma model where survival and tumour growth could be evaluated. A subcutaneous fibrosarcoma cell line model was adopted using the MCA205 cell line, which was originally developed as a 3-methylcholanthrene-induced fibrosarcoma in C57BL/6 mice. This cell line was first established by serial cell implantation followed by in vitro culture. The use of a subcutaneous model allowed for the evaluation of tumour size and access to the tumour for HIFU treatment. It is also possible to observe potential local side effects caused by the treatment such as skin damage and bruising. The cell line MCA205 was used within these studies as there was previous literature on the cell line which suggested, that although it is a relatively poorly infiltrated tumour, it is not immune desert[136–138].

## 3.2 Chapter Hypothesis and Aims

### Hypothesis

The model of fibrosarcoma will show limited immune infiltration which will be increased by the HIFU treatment (with further effects on peripheral organs such as the spleen and lymph nodes), caused by increased recognition of the tumour, which will be synergistic with immunotherapy,

### Aims

i. Use a murine model to evaluate the immune infiltration of fibrosarcoma tumours and peripheral tissues, focusing on T cell and myeloid populations
ii. Assess the impact of HIFU treatment on this fibrosarcoma model
iii. Evaluate the difference in immune infiltration of these tumours after HIFU treatment vs sham treatment
iv. Assess the change in infiltration of these tumours after immunotherapy bolstered with HIFU compared to single or sham treatments.

## 3.3 Development and profiling of the tumour model

Initial studies aimed to confirm the previously reported immune landscape of subcutaneous implanted fibrosarcoma using the MCA205 cell line[139]. It was pertinent that the tumours were not completely immune deserted after implantation. It was hypothesised that there would be low level infiltration of CD8 and CD4 T cells within the tumour. Subsets of these cell types are of interest in the profiling of the immune function within this tumour model. This analysis would also provide insight into the possible targetable populations for future work.

### 3.3.1 Implanting a high seeding density of cells led to large variation of tumour growth and a high incidence of ulceration

To identify the conditions needed for a reliable, reproducible and fast-growing tumour model from the implantation of fibrosarcoma cell line MCA205, a high seeding density of MCA205 cells (5 x $10^5$) was evaluated (Figure 3.1). Tumours were palpable and measurable 9 days after implantation. Ulceration incidence was high within these tumours, indicated in Figure 3.1B. There was also large variation in the growth of these tumours between day 8 and day 11. There seems to be a reduction in the spread after this timepoint, but this may be an artefact of the sample size decreasing, caused by the loss (and exclusion of data) due to ulceration.

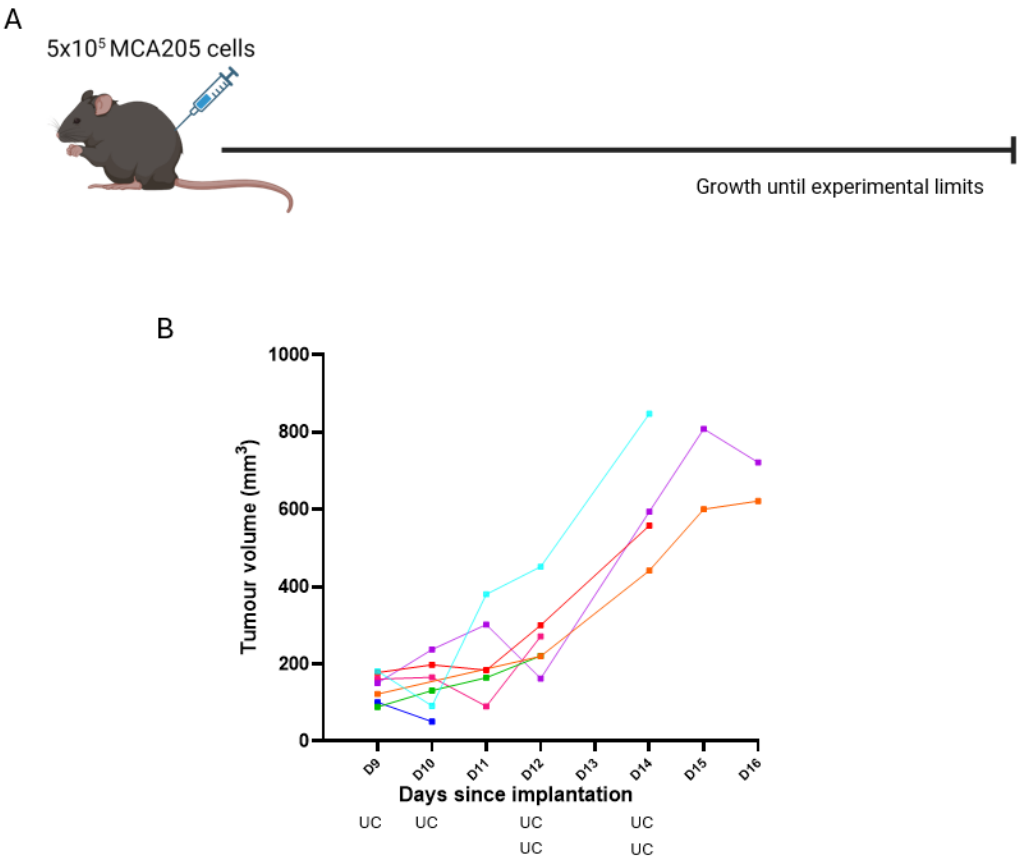


Figure 3.1: (A) Schematic overview of in vivo study to assess the growth of MCA205 fibrosarcoma in C57/Bl6 mice. Created with BioRender.com (B) The growth profile of individual tumours within the study, each line represented a tumour, n = 7. The UC annotation represents when a mouse was culled due to ulceration of the tumour.

Regarding the immunological analysis, CD8 subpopulations were assessed across the tissues using flow cytometry (Supplementary Figure 3.1). The naïve (Tnaïve), central memory (Tcm), effector memory (Tem), and CD44-CD62L- populations are shown in Figure 3.2. This showed a larger proportion of the CD8 cells belonged to the Tnaïve subset within the lymph nodes, and to a lesser extent, the spleen (Figure 3.2). These tissues support APC migration from the peripheral tissues and expansion of the Tcm populations[140]. However, the expected expansion of the memory populations within the dLN was not seen in this study when compared to the cLN as a control. This suggests some nuances within the antigen recognition and adaptive immune response that were missed.

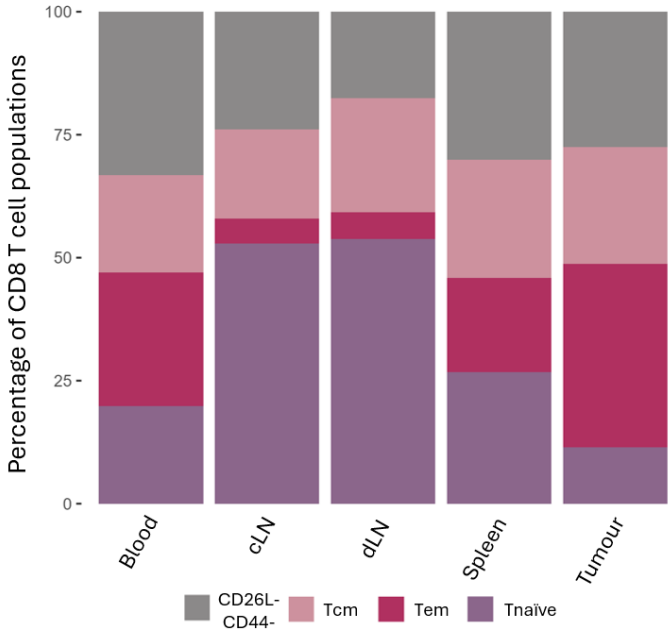


Figure 3.2: Representation of proportion of CD8 subpopulations as a percentage of total CD8 T cells detected by flow cytometry analysis of blood (n = 6), contralateral lymph nodes (cLN, n = 8), draining lymph nodes (dLN, n = 8), spleen, and the tumour (n = 7) from MCA205 growth pilot with 5 x $10^5$ cell seeding density experiment. Blood had reduced replicates due to CD3 stain being poor in 2 samples, tumour had reduced replicates due to issue with sample acquisition. Grey represents CD8+CD62L-CD44- T cells, light pink represents CD8+ T effector cells (Tem, CD62L-CD44+), dark pink represents CD8+ T central memory cells (Tcm, CD62L+CD44+), and purple represents CD8+ naïve T cells (Tnaive, CD62L+CD44-).

The tumour tissue was also evaluated and showed to have a higher proportion of Tem compared to the other tissues (37.3±9.2% in tumour compared to 5.5±2.6% in dLN, 24.0±12.0% and blood 19.8±7.6%, $p>0.05$) This raised infiltration has previously been linked

to improved outcomes with immune checkpoint treatments[141], for example Principe et al showed that in vivo, mice with increased frequency of Tem showed better response to CTLA-4 and PD-L1 therapy. This has been relevant for studies reported later in this chapter. This may be a tumour-specific effect of an increased adaptive immune response due to antigen recognition in the tumour. However, the assessment of the origin of this population by TCR clonotyping was beyond the scope of this work. There was variation in the proportions of T cell populations between individuals in all tissues as indicated in Supplementary Figure 3.2. For example, in the tumour, the Tcm population varied from 8.4 to 37.8% of the CD8 population. The range within the CD4 subpopulations was far less variable. For example, the Tconvs in the dLN covered 88 to 89.6% of the CD4 population.

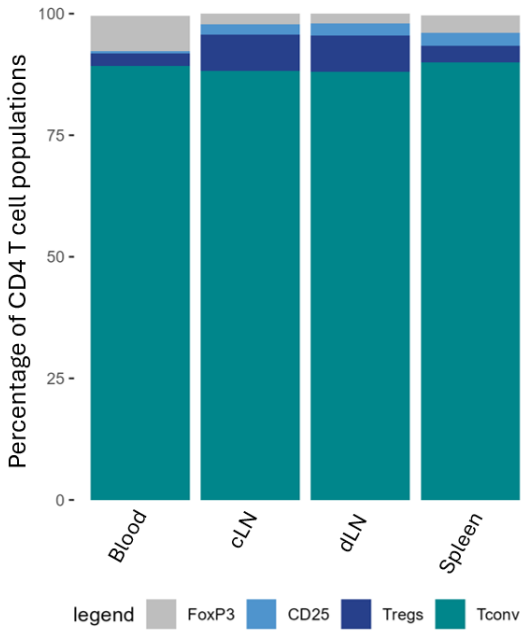


Figure 3.3: Representation of proportion of CD4 subpopulations as a percentage of CD4 T cells from flow cytometry analysis of blood (n = 8), contralateral lymph nodes (cLN, n = 8), draining lymph nodes (dLN, n = 8), and spleen (n = 7) from MCA205 growth pilot with 5 x $10^5$ cell seeding density experiment. Spleen had reduced replicates due to issue with acquisition. Grey represents CD4+CD25-FoxP3+ T cells, light blue represents CD4+CD25+FoxP3- T cells, dark blue represents CD4+ regulatory T cells (Tregs, CD4+CD25+FoxP3+), and teal represents conventional CD4 T cells (Tconvs, CD4+CD25-FoxP3-).

CD4 populations were also evaluated by flow cytometry (Supplementary Figure 3.1). These data (Figure 3.3), showed the most abundant CD4 type within all tissues was conventional T cells (Tconvs), with a higher proportion of Tregs in the lymph nodes (7.5±1% in the dLN vs 2.6±1.5%in the blood, $p>0.05$). It is known that Tregs move into the dLN after differentiation before entering the tumour[38,142]. However, the evaluation of CD4 populations within the tumour to further dissect this was not possible due to issues with the acquisition of the flow cytometry. The blood samples had a proportion of cells that were CD4+CD25-FoxP3+ which is negligible in the other tissues, this role of this population has been the source of debate[143]. These cells could be a differentiated Treg pool that can be primed to the CD25+ activated pool after homeostatic signalling[144]. Alternatively, these cells could be alternative Treg precursors, that will become peripheral Tregs (pTregs). pTregs have been demonstrated to play a crucial role in tumour progression[145]. pTregs encounter cognate antigens in the periphery to become terminally differentiated before entering the tissue[145], hence why they may be present in the blood and these precursor populations (CD4+CD25-FoxP3+[146] and CD4+CD25+FoxP3-[144]) were in low abundance in the lymph nodes.

### 3.3.2 Using a seeding density of 2 x $10^5$ MCA205 cells gave a plateauing growth rate at 11 to 13 days post implantation for HIFU treatment

To try and reduce the variability within the tumour growth profiles and the incidence of ulceration, the seeding density was reduced. It was hypothesised that the rate of tumour growth may affect the immune populations within the tissues. To assess this, 2 different seeding densities, reduced from the first study were compared. A seeding density of 1 x $10^5$ and 2 x $10^5$ MCA205 cells in a small pilot study, as outlined in Figure 3.4A. Mice were sacrificed when tumour volumes were thought to exceed the welfare threshold (1000 $mm^3$)

before the following measurement, for ulceration or other welfare concerns. Assessing the growth profiles of these tumours (Figure 3.4B and C) it is noted that implanting 2 x $10^5$ MCA205 cells produced a tighter growth curve, with standard deviations of 12.4, 80.8 and 98.0 at days 9, 10 and 11 vs 52.3, 99.7 and 117.1, respectively. The tumours produced reached a threshold that would allow for HIFU treatment after a shorter post-implantation duration than 1 x $10^5$. These tumours also reach a growth plateau at 11 days post implantation. This was pertinent for the future studies as it provided a window to treat these tumours at similar volumes.

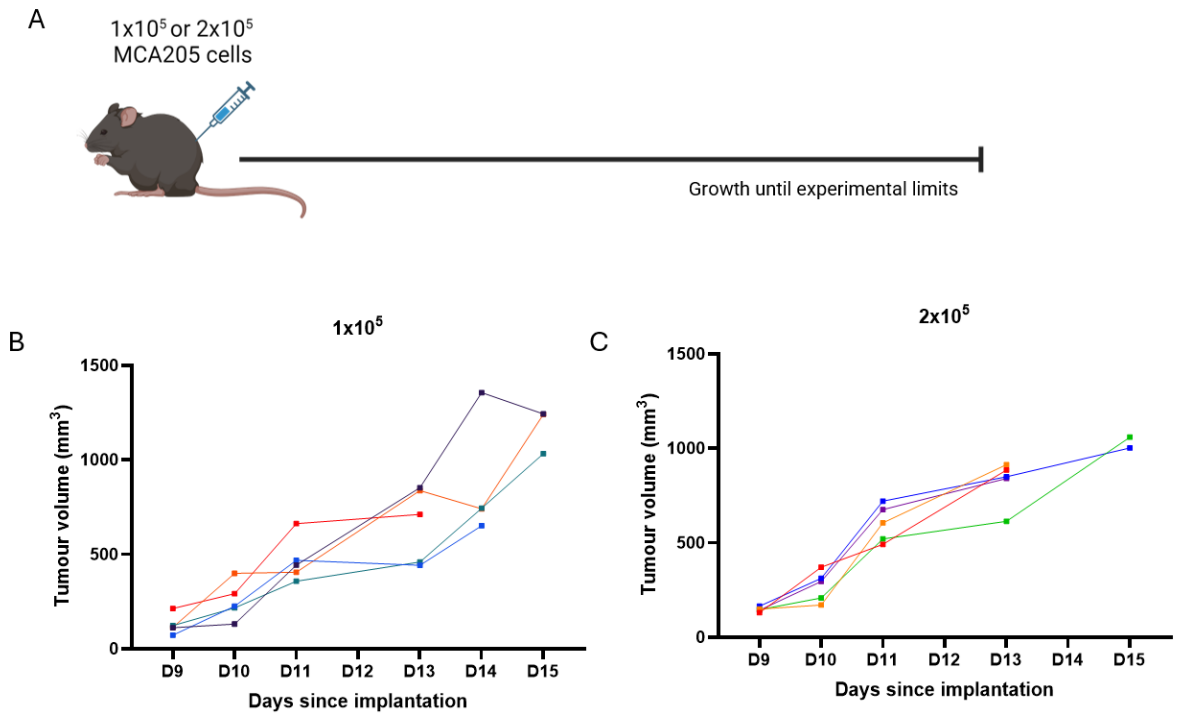


Figure 3.4: (A) Schematic overview of in vivo study to assess the growth of MCA205 fibrosarcoma in C57/Bl6 mice for the assessment of various immune cell populations. Created with BioRender.com (B) The growth profile of individual tumours after subcutaneous implantation of 1 x $10^5$ cells, each line represents a tumour (n = 5). (C) The growth profile of individual tumours after subcutaneous induction of 2 x $10^5$, each line represents a tumour (n = 5).

Assessment of the CD8 subpopulations across tissues (gating strategy outlined in Supplementary Figure 3.3) highlighted that there were very similar proportions of the Tcm, Tem, and Tnaïve cells across the groups within the dLN (Figure 3.5A), where Tnaive was the

most abundant cell type (77±11.4% for 1 x $10^5$ cells group and 77±8.2% for 2 x $10^5$ cells group, p>0.05). Within the spleens (Figure 3.5B), a trend of a higher proportion of Tnaive and Tem cells across the groups when compared to the dLNs was observed. However, these groups are small, so drawing definitive conclusions was not possible. Due to issues with compensation, CD8 T cells subpopulations in the blood and tumour could not be assessed. The trends dependent on tissue type were like those seen in the previous assessment in section 3.3.1.

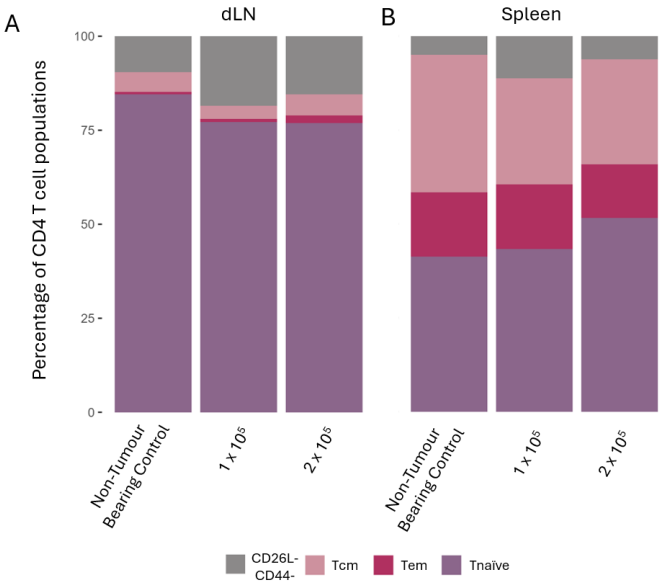


Figure 3.5: Representation of proportion of CD8 subpopulations as a percentage of CD8 T cells from flow cytometry analysis of (A) draining lymph nodes (dLN), and (B) spleen of MCA205 growth pilot with lower cell seeding density experiment. Groups included non-tumour bearing control (n = 2), 1 x $10^5$ cells (n = 5), 2 x $10^5$ cells (n = 5). Grey represents CD8+CD62LCD44- T cells, light pink represents CD8+ T effector cells (Tem, CD62L-CD44+), dark pink represents CD8+ T central memory cells (Tcm, CD62L+CD44+), and purple represents CD8+ naïve T cells (Tnaive, CD62L+CD44-).

The assessment of CD4 populations (Figure 3.6) showed that Tconvs were the more abundant CD4 T cell across the groups in spleen, blood, dLNs and cLN, as expected, regardless of the cell number implanted. The same ratios of CD25+FoxP3-CD4+ T cells, CD25-FoxP3+CD4+ T cells, and Tregs were observed across the 1 x and 2 x $10^5$ cell implantation groups. The assessment of the blood did not show the same increase in CD25-FoxP3+CD4+ T cells as seen following implantation of 5 x $10^5$ cancer cells in the previous

study in Section 2.3.1. This could be related to a difference in the cell numbers implanted although, slight variations in the flow cytometry panel and set up may be the cause of this difference. However, the CD25-FoxP3+CD4+ T cell population was increased in the spleen compared to the other tissues for both seeding densities. For example, in the spleen the frequency was 7.0±1.6% and 5.0±2% vs in the dLN the frequency was 1.8±0.2% and 2.0±0.4%, $p>0.05$ for the 1 x $10^5$ and 2 x $10^5$ cell groups respectively. This population difference was also observed in the previous experiment outlined in Section 3.3.1.

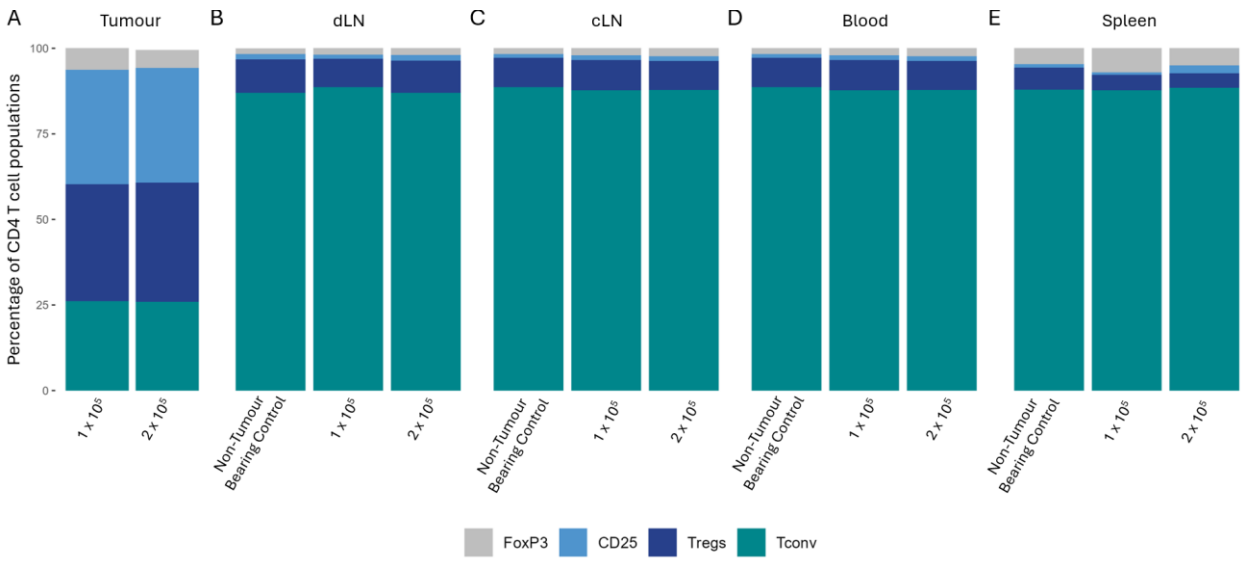


Figure 3.6: Representation of proportion of CD4 subpopulations as a percentage of CD4 T cells from flow cytometry analysis of (A) Tumour, (B) draining lymph nodes (dLN), (C) contralateral lymph nodes (cLN), (D) blood and (E) spleen from MCA205 growth pilot study with lower cell seeding density experiment. Groups included non-tumour bearing control (n = 2), 1 x $10^5$ cells (n = 5), 2 x $10^5$ cells (n = 5). Grey represents CD4+CD25-FoxP3+ T cells, light blue represents CD4+CD25+FoxP3- T cells, dark blue represents CD4+ regulatory T cells (Tregs, CD4+CD25+FoxP3+), and teal represents conventional CD4 T cells (Tconvs, CD4+CD25-FoxP3-). ANOVA with Tukey's post hoc test was performed (* $p<0.05$).

The main point of interest in this study was the drastically larger Treg and CD25+FoxP3-CD4+ T cell population in the tumour compared to the other tissues. For the Treg populations this included the dLNs (34.1±7.9% and 34.9±15.4% vs 8.3±1.3% and 9.4 ±1.4%, $p<0.01$ for the 1 x $10^5$ and 2 x $10^5$ cells groups respectively) (Figure 3.6).

The Tregs implicate a highly regulatory environment in cancers[145,147], including sarcoma[27,66,85,148]. This will be pertinent to the study how this population changes after HIFU treatment and decreased Treg abundance within the tumour would have clinical benefit[27,145,149,150]. Also, an increase in CD8+ T cells within the tissue has been seen in other tumour types to associate with survival outcomes[151] and treatment efficacy[141,152]. Previous research evaluating immune profiles after HIFU have only assessed CD8 and CD4 populations as a whole and found increased abundance[23,153]. For example, a ~4-fold increase in CD3+ cells were found after HIFU treatment in an *in vivo* hepatocellular carcinoma (H22) study[153]. However, these studies did not evaluate the subpopulations highlighted in this chapter. This study also found an increase in the CD25+FoxP3-CD4+ T cells in the tumour vs the dLN (33.4 ±10.1 and 33.4 ±13.0 vs 1.2±0.3 and 1.6±0.1%, p 0.001, for the 1 x $10^5$ and 2 x $10^5$ cells groups respectively), regardless of seeding density. These could have been exhausted Tregs[154] or Treg precursors[144]. Either way, these cells have been previously correlated with survival in ovarian cancer studies[155,156]. This may be related to the loss of regulatory function caused by constant antigen recognition by these pathways[154]. When assessing the Treg to CD8 ratio, the tumour had the highest ratio, suggesting that there is a more regulatory environment in the tumour compared to other tissues, strengthening this finding (Figure 3.7).

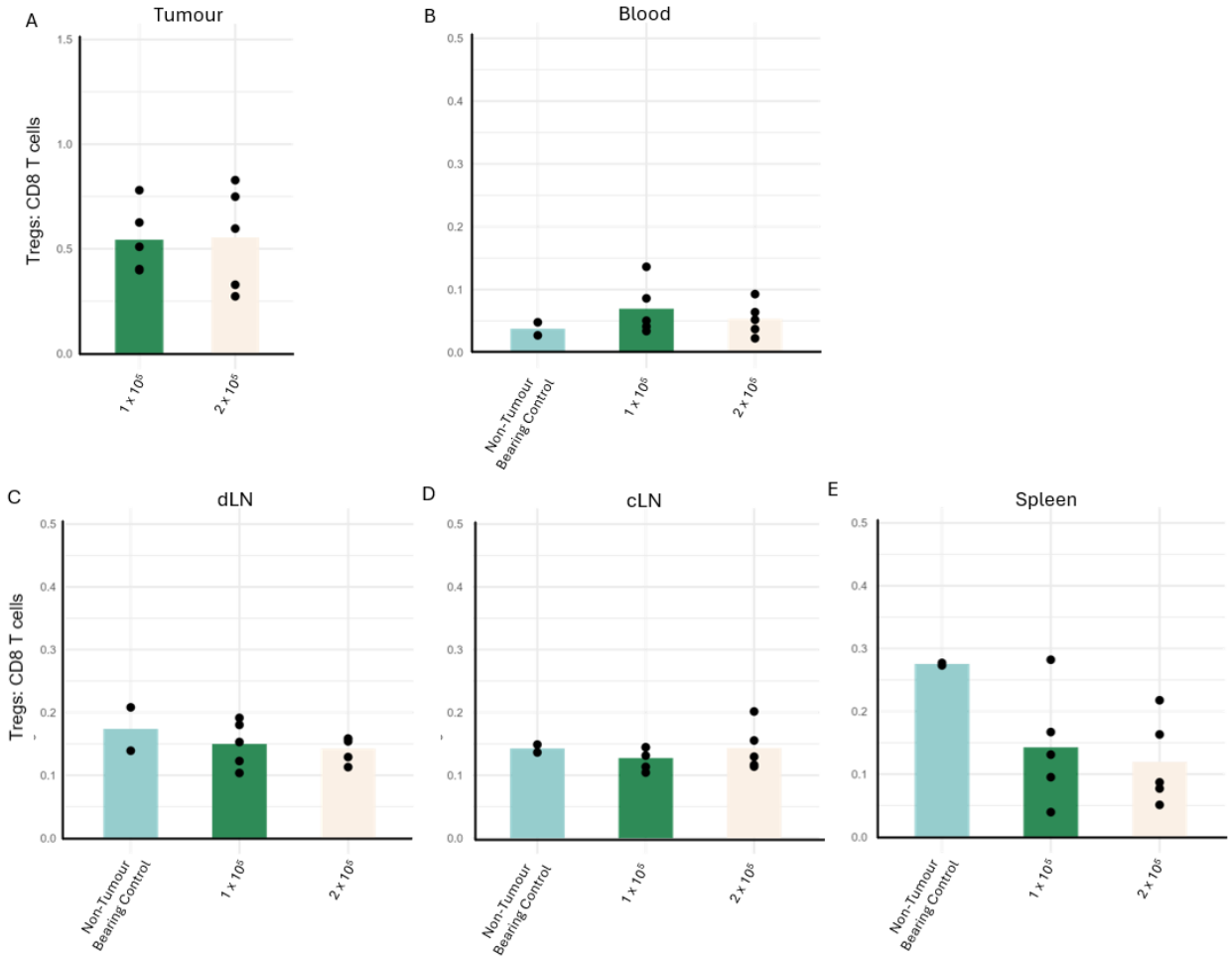


Figure 3.7: Flow cytometry analysis of Treg to CD8 T cell ratio of (A) Tumour, (B) blood, (C) draining lymph nodes (dLN), (D) contralateral lymph nodes (cLN), and (E) spleen from MCA205 growth pilot with lower cell seeding density experiment. Light blue represents the non-tumour bearing mice (n=2), green represents mice injected with 1 x $10^5$ cells (n = 5), cream represents mice injected with 2 x $10^5$ cells (n=5).

It was unexpected to see an increase in Treg population within the tumour to this extent and not see a substantial increase in this population in the dLNs[38,142]. However, compared to the spleen and blood, a trending increase across the groups was observed with a mean Treg frequency in the dLN of 1.4±0.2% vs 8.4±1.8% for spleen and 2.4±1.3% vs blood ($p>0.05$). The increase in the Treg population in the dLN was mirrored by the cLN. The placement of the tumour on the flank of the mouse may have meant that the cLN was also antigen experienced. However, the abundance of Tregs in the blood and spleen of non-tumour

bearing control mice showed no differences in expression. This was corroborated by the Treg/CD8 ratio (Figure 3.7).

When comparing the abundance of the CD4 and CD8 subsets based on seeding density, there was no variability in population abundance. This was assessed in the tumour, lymph node and blood. This again suggested that in future studies, tumours harvested at a range of volumes will still be comparable.

### 3.3.3 Summary of findings

These studies indicated a stable growth profile for the predictions of growth to be used in future studies. Along with the baseline immune profiles of these tumours to compare to future studies for confidence in findings. The data suggested a high proportion of Tregs and CD8 Tem populations within the tumour. Previous studies have shown that the CD4 and CD8 T cell populations are modulated following exposure to thermally ablative HIFU treatment so continued assessment of these populations was paramount. The Tregs would be exerting a regulatory phenotype within the tumour which will need to be overcome in the future studies. Importantly, although seeding density could be used to regulate tumour growth rate and reproducibility, it did not alter immune profile, giving confidence that slight differences in tumour size or day of cull should not prove confounding when looking at the impact of HIFU.

## 3.4 Development of the ablation profile model

It was hypothesised that the thermal ablation caused by HIFU will produce an immunogenic response involving the upregulation of CD8 T cells and affect the CD4 T cell population. The effect on the regulatory subpopulations of CD4 T cells with ablation may be affected, and as discussed may have clinical benefit. Previous studies in the literature have highlighted that

Tcm are more tumour reactive than Tem[157], which may be promoted by the HIFU treatment. It was believed that there would be increased antigen recognition after treatment, and this would involve the tumour dLNs. A peripheral response in mice treated with HIFU caused by antigen release through the vasculature into the blood by treatment, may also be expected.

Ten tumour-bearing mice were treated with various doses of thermally ablative ultrasound within the tumour. This was alongside controls: untreated tumour-bearing mice and non-tumour bearing mice for immunological investigation. The mice were separated into treatment groups with the intention of achieving compatible mean tumour volumes in each group. The mice were treated when the tumour volume was palpable and treatable, the volume for the tumours in each group at treatment is outlined in Figure 3.8. Although the process did achieve groups with no statistically significant difference in mean size at treatment ($p>0.05$) between the groups by ANOVA, the 'Sham-group' did have the smallest mean size due to calculation error. This also meant that 4 tumours were below the desired 25mm$^3$ threshold outlined (high HIFU n = 1/5, low HIFU n=1/5, HIFU-Sham n = 2/4).

A

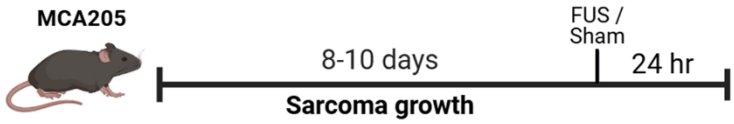


B

| Treatment | N | Mean Tumour Volume (mm$^3$) | SD Tumour Volume (mm$^3$) | Percentage of Tumour Ablated |
|---|---|---|---|---|
| High (15 secs) | 5 | 48.91 | 19.06 | 43.5 |
| Low (10 secs) | 5 | 39.46 | 16.96 | 33.9 |
| Sham (0 secs) | 4 | 29.10 | 15.03 | N/A |
| NTC (0 secs) | 4 | N/A | N/A | N/A |

Figure 3.8: (A) Schematic overview for the pilot in vivo study to assess immune response to various HIFU exposures of MCA205 fibrosarcoma in C57/Bl6 mice. Created with BioRender.com. Tumours were induced into mice, tumour growth was monitored for 8 to 10-days until size threshold (25mm$^3$) was reached, followed by treatment and culling for harvest 24-hours after treatment. (B) The mean volume, standard deviation (SD) and predicted percentage of tumours treated with HIFU for each group within the study.

A single-source ultrasound array (as described in methods section 2.3.3) was used for these treatments. Based on previous work with support by Dr Michael Gray, treatment parameters were 4.3 MPa peak-to-peak, 100% duty cycle, with a frequency of 1.6MHz. To allow for variation in the treatment parameters, 10-seconds and 15-seconds of HIFU exposure was assessed to determine a treatment regime for partial ablation of the MCA-205 induced fibrosarcoma tumours. The volume of the cylindrical ablation zone was calculated for the 10 and 15 second exposures as 10.1$mm^3$ and 17.8$mm^3$ respectively. The ablation volume was predicted by Professor Mike Grey using CEM43 contour plots from data produced in a water tank using a calibrated 200 μm needle hydrophone. The assessed dimensions of the 10- and 15-second treatment was a spot diameter of 1.8 mm and 2 mm with a depth of 7 mm and 8.5 mm, respectively. The use of partial ablation of the tumour volume rather than attempted coverage of the entire volume was rationalised based on enabling sufficient access to immune cells[131].

Adjustment of exposure duration allowed avoidance of possible off-target effects of the HIFU. Notably, although the small proportion of the mice did not recover post treatment was in-line with expectations for periods of anaesthesia of this duration, a small proportion also appeared weak and unwell over the 24 hours following treatment but recovered in response to increased welfare checks and interventions (e.g. enhanced feeding, heating and hydration) along with skin burns. It was felt that the duration of treatment with continuous wave was at upper limits of welfare for these animals, thus subsequent treatments would require lower duration of sonication for reduced treatment volume.

### 3.4.1 There was histological evidence of thermal ablation in these tumours.

As discussed, it was hypothesised that there would be increased infiltration of CD8 and CD4 T cells into tumours after treatment, and that this infiltration would be more concentrated around the treatment area of the partial ablations.

H&E staining showed tumours in the treatment group with pyknosis (condensation of chromatin in the nucleus)[16,24], represented by darker eosin staining in an area of the tumour[18] (Figure 3.9), as reported as evidence of thermal ablation in previous literature with thermal HIFU treatment. This could not be evidenced in all tumour sections due to technical issues with embedding and cutting of some samples. This study assessed the expression of vimentin, a canonical marker for sarcoma in the tissue (as shown in representative images in Figure 3.10A-F). When the expression of vimentin (Figure 3.10) was compared to the location of the pyknosis, overlap of these stains was observed, for both high- (15 sec) and low- (10sec) HIFU exposure, which suggests that there was thermal ablation in the areas of tumour.

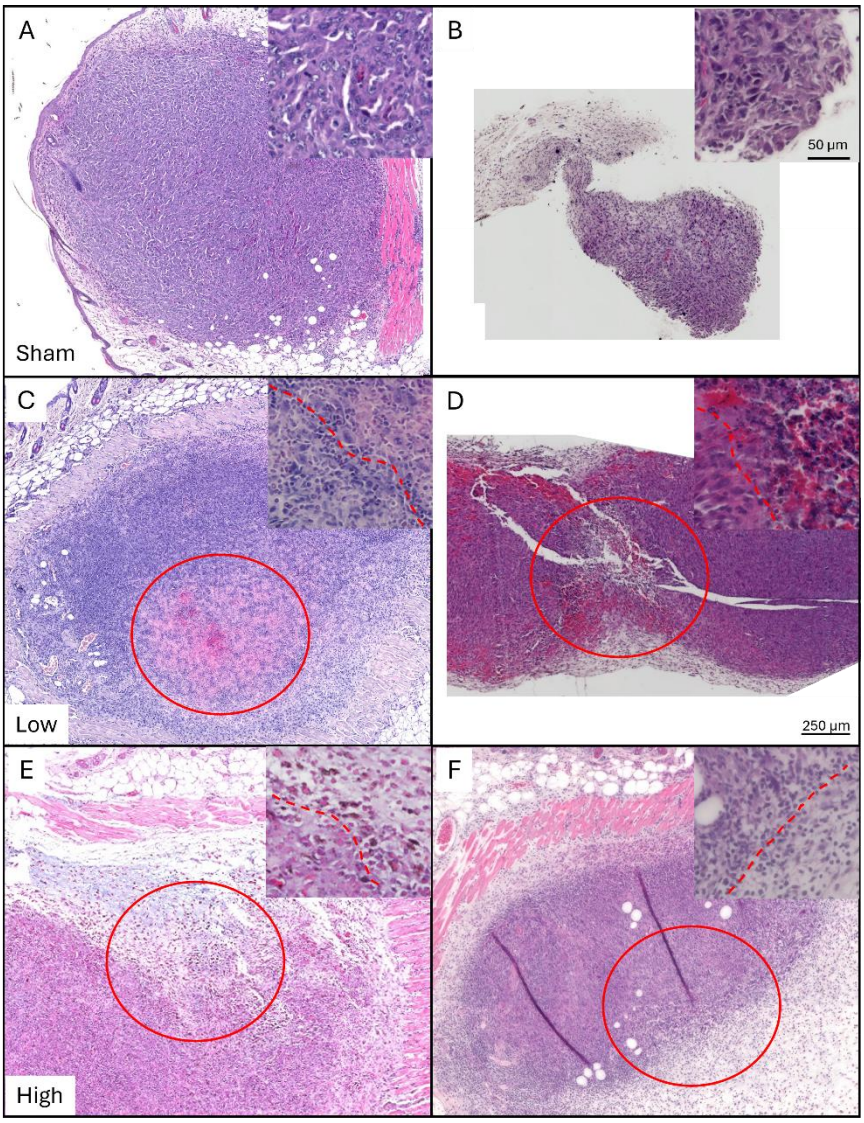


Figure 3.9: Examples of haematoxylin and eosin (H&E) slides (5µm thick) of tumours within groups treated with (A-B) Sham HIFU, (C-D) low dose HIFU, (E-F) high dose HIFU. Red ring used to highlight areas of pyknosis (recognisable as increased eosin stain uptake), a sign of thermal ablation of tissue. Image of increased magnification included with red dotted line indicating border of ablation (pyknosis).

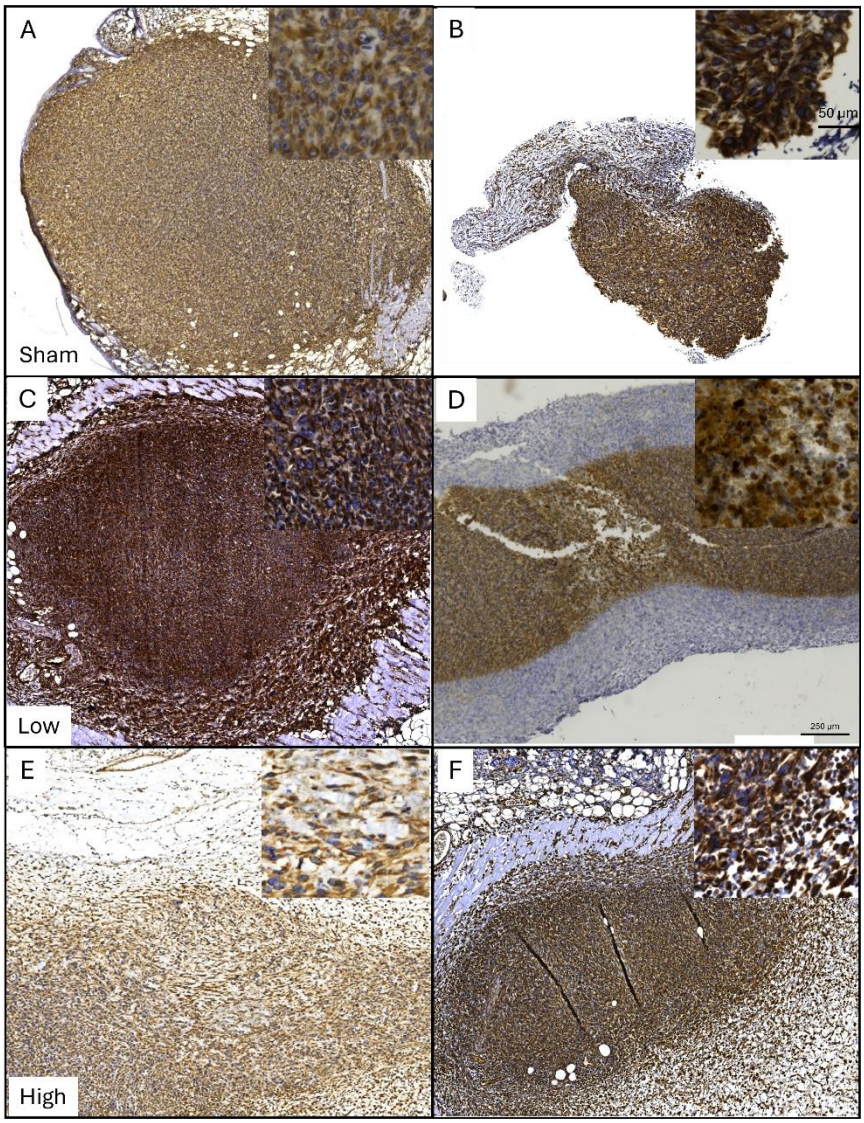


Figure 3.10: Examples of slides stained for vimentin (5µm thick) of tumours within groups treated with (A-B) Sham HIFU, (C-D) low dose HIFU, (E-F) high dose HIFU. Vimentin stain (DAB, brown) for mesenchymal tissue to select areas of fibrosarcoma tumour.

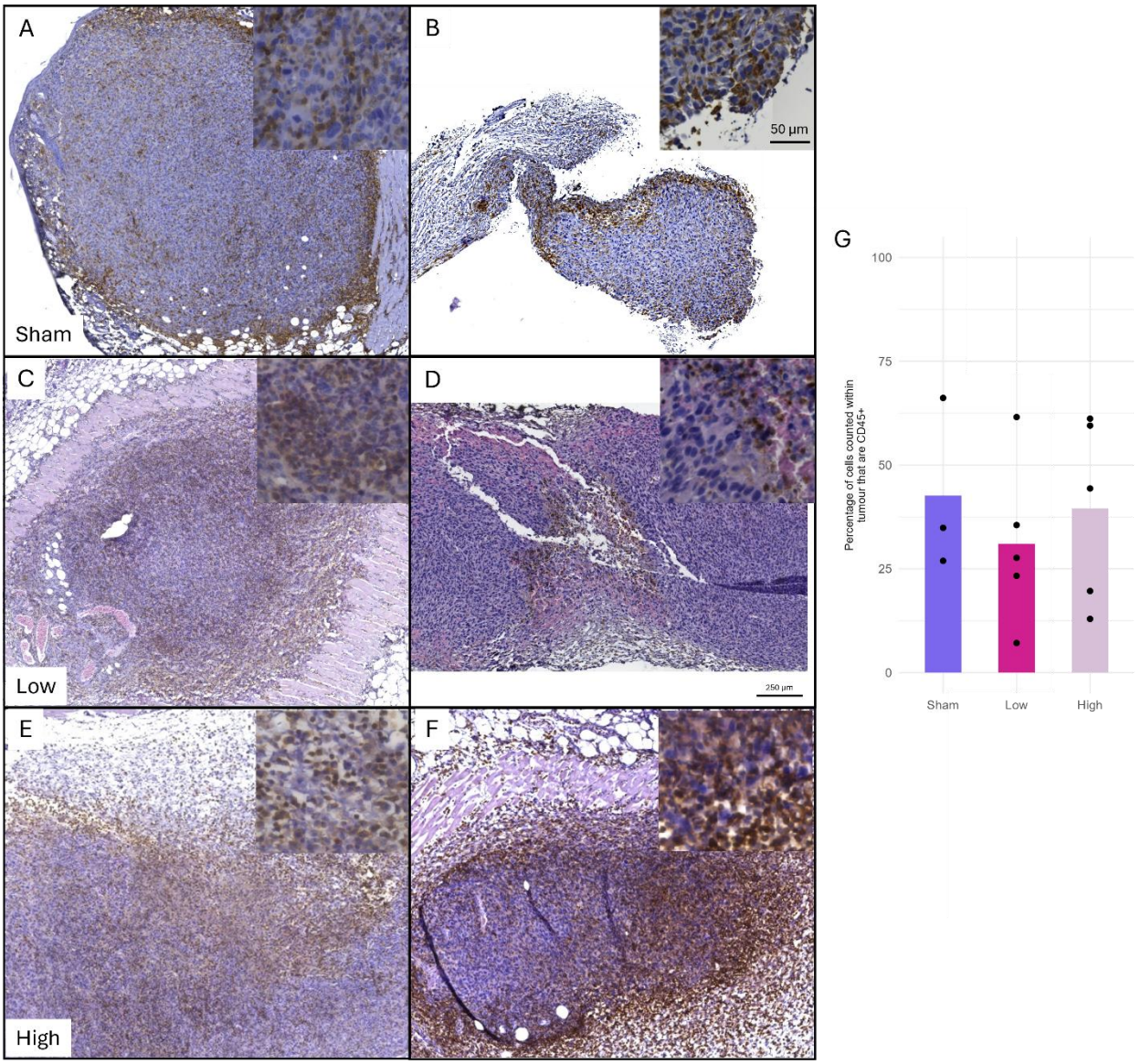


Figure 3.11: Examples of slides stained for CD45 (5µm thick) of tumours within groups treated with (A-B) Sham HIFU, (C-D) low dose HIFU, (E-F) high dose HIFU. CD45 stain (DAB, brown) for leukocyte cell infiltration within the fibrosarcoma tumour. (G) Quantification of CD45 stain as a percentage of haematoxylin positive (blue) nucleated cells within the tumour area (see section 2.4.5 for methodology).

Quantification of the expression of CD45+ cells (Figure 3.11G) within these tumours did not show a trend towards increased infiltration into treated tumours, nor did these cells associate to the tumour-to-normal tissue border or tumour-to-HIFU area border or within the area of HIFU. Indeed, Figure 3.11 showed that the infiltration of these tumours is very variable between the groups meaning firm conclusions are hard to make. For example, Figure 3.11C shows infiltration throughout the tumour, whereas when compared to Figure

3.11D, there is little infiltration throughout the tissue. It is believed that this is due to the nature of tumours having variable biology[158]. The example images did not show concentrated infiltration of the HIFU treated tumour area regardless of the HIFU duration, although it may be that 24 hours after treatment there was also an inflammatory response, which may have convoluted the immune assessment of these tissues. At 24-hours after tissue damage, there is a typical neutrophil influx[159] and priming of DCs for migration to dLNs[160]. Within the literature, there have been reports of release of immune modulating cytokines and chemokines[161,162] for the attraction of these neutrophils to the areas of thermal damage[159].

### 3.4.2 Immunological assessment of peripheral tissues suggested an increased proportion of the CD8 T cells were Tcm with the lower ablation, whilst this is lost with higher ablation

To assess the possible mechanisms leading to infiltration into the tumour, the immune composition of the dLNs and the spleen was also profiled for a peripheral immune response assessed by flow cytometry (Supplementary Figure 3.4). This assessment focused on CD4 and CD8 subpopulations, to align with the assessment of the HIFU treatment naïve tumours in section 3.3.

A reduction in absolute numbers of CD8 and CD4 T cells within both the dLN and spleen was seen within the **high-HIFU (15 sec)** treatment compared to **low-HIFU (10 sec)** in Figure 3.12. For the dLN, this difference was significant (9833±9141 vs 57456±8334, $p<0.05$). There was also a reduction in the percentage proportion of CD8 T cells from CD3 T cells in the spleen

within the high-HIFU (15 sec) treatment compared to low-HIFU (10 sec): 20712±11060 vs 262340±178626 ($p<0.05$). This trend was not seen in the dLN (Figure 3.13A).

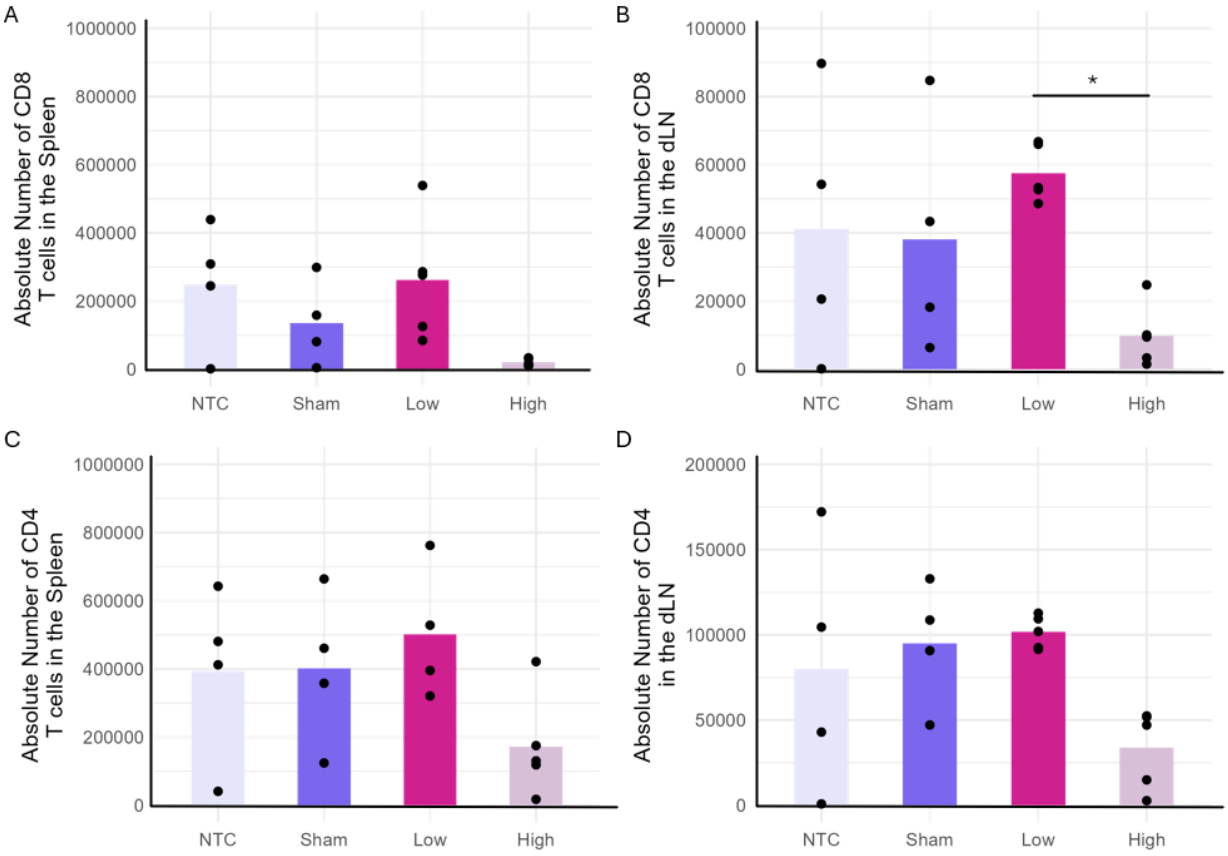


Figure 3.12: Absolute number of CD8 (A-B) and CD4 (C-D) T cell populations from flow cytometry analysis of spleen in (A, C) and draining lymph nodes (dLN, B, D) from mice that are non-tumour bearing controls (NTC, n = 4, lilac), tumour-bearing Sham-HIFU controls (Sham, n = 4, purple), low dose HIFU-treated (low, n= 5, vibrant pink), and high dose HIFU-treated (high, n= 5, light pink). Bar height represents mean value, dots individual replicates. ANOVA with Tukey's post hoc test was performed (* $p<0.05$).

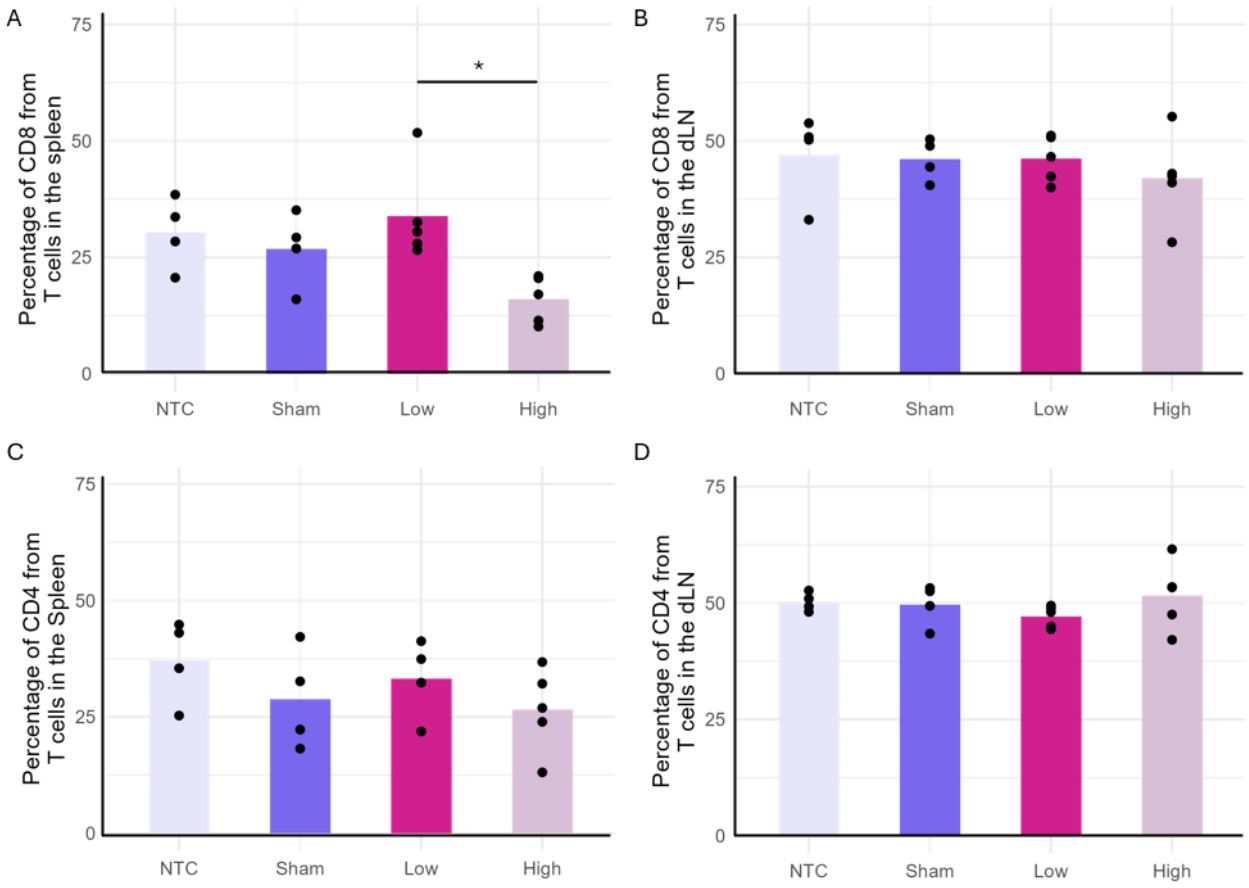


Figure 3.13: The percentage of CD8 (A-B) and CD4 (C-D) T cell populations from flow cytometry analysis of CD45+CD3+ T cells in the spleen in (A, C) and draining lymph nodes (dLN, B, D) from mice that are non-tumour bearing controls (NTC, n = 4, lilac), tumour-bearing Sham-HIFU controls (Sham, n = 4, purple), low dose HIFU-treated (low, n= 5, vibrant pink), and high dose HIFU-treated (high, n= 5, light pink). Bar height represents mean value, dots individual replicates. ANOVA with Tukey's post hoc test was performed (* $p<0.05$).

The differences in absolute number CD4 T cells were not significant (Figure 3.13B-D), nor was the percentage of CD3 T cells. This could be because of the treatment leading to sequestering of immune response into the tumour. However, the tumour samples could not be examined by flow cytometry as the tissue had been prioritised for histology. Infiltration of CD45 cells assessed by the histology and was not found to be decreased in the high-HFIU group vs the low-HIFU group as discussed in section 3.4.1. It was also notable that the non-tumour bearing mice had a large CD4 and CD8 population within the lymph nodes, however there was a large variation in this between individuals.

This study assessed the memory subpopulations of the immune populations in the control LNs, (brachial and ipsilateral LNs taken from the left-side of the mouse to replicate the dLNs) without antigen stimulation by a tumour, i.e. in a **non-tumour bearing control mouse** (**NTC**). This provided a baseline for comparison to the tumour-bearing mice, and subsequently tumours treated with HIFU (Figure 3.14). It was hoped that this would address whether the Tcm and Tem populations were affected by the tumour and whether the HIFU treatment was able to improve response to tumour antigen. This showed the main cell type of NTC group was Tnaive. This population reduced in **Sham-HIFU** mice, with the CD62L-CD44- population becoming abundant. These groups had large variation in population abundances (Figure 3.14B). This again may be related to biological variations in these tumours. The **low-HIFU** (10 sec) ablation group retained a large Tnaive population (Figure 3.14A), larger than the NTC mice while also having a significantly increased abundance of Tcm with low variability compared to the Sham-HIFU and high-HIFU mice (21.1±5.6% vs 6.3±6.4% vs 9.2±5.0% respectively with $p<0.01$ and $p<0.05$ respectively).

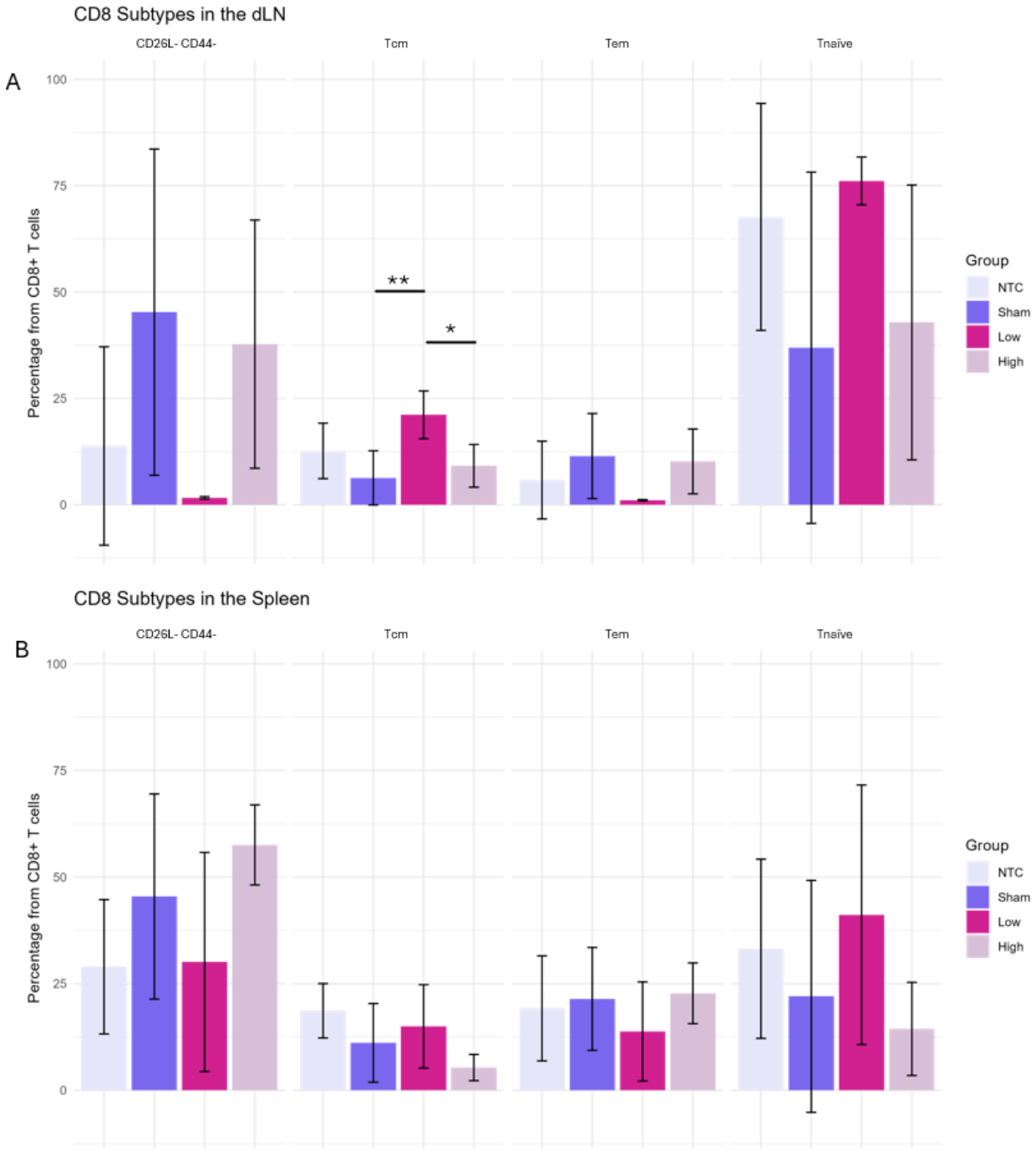


Figure 3.14: Representation of the CD8 subpopulations from flow cytometry analysis of tissues from mice treated with HIFU. Representation of proportion of CD8 subpopulations as a percentage of CD8 T cells from (A) draining lymph nodes (dLN), and (B) the spleen from mice that are non-tumour bearing controls (NTC, n = 4, lilac), tumour-bearing Sham-HIFU controls (Sham, n = 4, purple), low dose HIFU-treated (low, n= 5, vibrant pink), and high dose HIFU-treated (high, n= 5, light pink). The CD8 subpopulations with error bars representing the standard deviation. ANOVA with Tukey's post hoc test was performed (* $p<0.05$, ** $p<0.01$).

When treated with the **high-HIFU**, the CD8 subpopulations in the dLN had a similar proportion of Tcm and Tem to the **Sham-HIFU and NTC groups.** Tcm in the high-HIFU, NTC,

Sham-HIFU was 9.1±5%, 12.7±6.5% and 6.3±6.4% respectively, whereas Tem was 10.2±7.6%, 5.8±9.1% and 11.5±10% respectively. This may reflect HIFU induced destruction of the release antigen or prevention of access to antigen, which would make generation of response to such antigen challenging. The phenotype of the high-HIFU treated group is like that of the HIFU-Sham group. It could be that tumour-derived suppressive factors halt the further differentiation of Tcm cells into effectors[163], with other studies suggesting that increased Tcm presence[164] as well as abundance in dLN before entering tumour correlates with an improved future outcome[157]. Previous research has also shown that after immunotherapy treatment, Tnaive remain a predominant cell within the dLN, with Tcm being more abundant than Tem, as expected for lymphatic tissue[141,165], thus supporting this finding.

Comparatively, in the spleen there were minimal differences between the NTC, Sham-HIFU, low-HIFU and high-HIFU groups (Figure 3.14B). The CD62L-CD44- population was the most abundant, followed by Tnaïve. There was large variability within the groups as highlighted in Figure 3.14B which has made the interpretation of these data difficult. There was no increase in memory populations, although as this is not tumour specific, so changes within the spleen may not be expected. However, a larger Tem population was seen within the spleen of all tumour-bearing groups when compared to the dLN. This could be related to the low levels of persistent antigen presentation by the tumour leading to a slight increase in this population within the peripheral lymphatic tissue. Within these tissues, the 24-hour time point may have been too early to assess a robust memory response to HIFU treatment.

When assessing the CD4 responses to treatment an increase in the overall population had previously been reported in the literature in both *in vivo*[11,131] and a clinical study[23]. It was

hypothesised that there would be modulation of the regulatory phenotype of the tumour after HIFU treatment as antigen presenting pathways were affected, thus affecting the Treg population. These data shown in Figure 3.15 suggested that the Tconv population was the most prevalent CD4 T cell type within both the spleen and dLN across all treatments as expected by the literature and the previous work conducted here. There was a trend increase in the Treg abundance in dLN in the HIFU treatment groups (Figure 3.15A and C) when compared to the LN from NTC mice or dLN from Sham-HIFU mice. This could be related to antigen activated Treg induction, which is often seen in cancer studies[38,166,167]. Within the dLN the ratio of Treg to CD8 T cells also follows this trend, with a slight increase in the ratio. This suggested that the systemic environment is becoming more regulatory rather than cytotoxic after HIFU treatment.

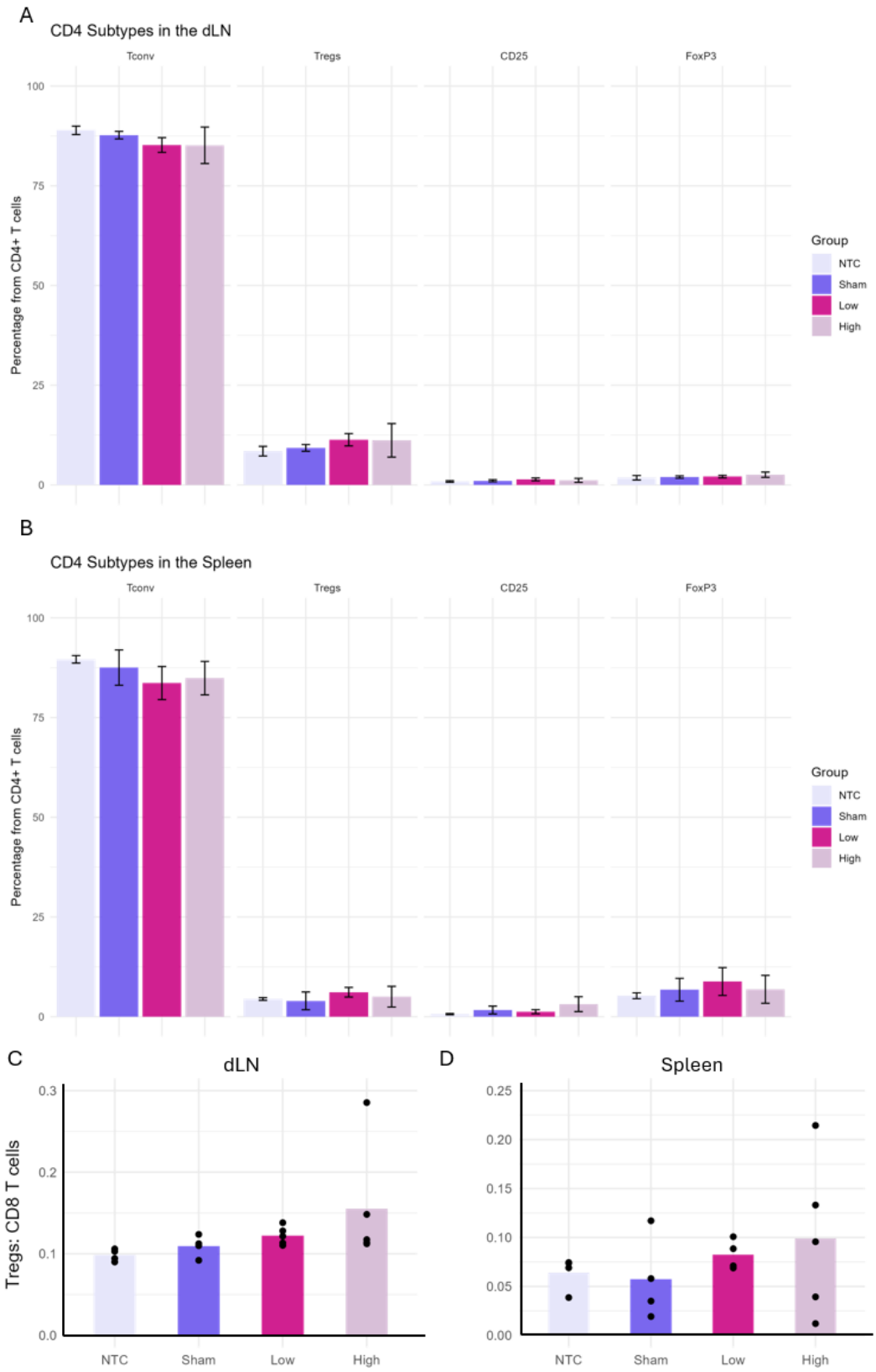


Figure 3.15: Representation of the CD4 subpopulations from flow cytometry analysis of tissues from mice treated with HIFU. Representation of proportion of CD4 subpopulations as a percentage of CD4 T cells from (A) draining lymph nodes (dLN), and (B) the spleen with error bars showing the standard deviation. Treg to CD8 T cell ratio of (C) draining lymph nodes (dLN), and (D) spleen from mice that are non-tumour bearing controls (NTC, n = 4, lilac), tumour-bearing Sham HIFU controls (Sham, n = 4, purple), low dose HIFU-treated (low, n= 5, vibrant pink), and high dose HIFU-treated (high, n= 5, rosy pink ). ANOVA with Tukey's post hoc test was performed.

### 3.4.3 Implications

In summary, this study evidenced indications of an ablation zone in a subset of tumours, which was believed to be caused by exposure to thermally ablative HIFU. Following this, the assessment of the subpopulations of CD8 and CD4 T cells suggested an increase in the CD8+ Tcm and Tregs after low-HIFU (10 second) treatment which was not seen with the high-HIFU (15 second) treatment. However, these findings did not show statistical significance. A more apparent and robust effect may have been detected had samples been taken at more extended durations post-exposure than the 24 hours used here.

To further assess the hypothesis that the activity of antigen presenting cells increases after HIFU treatment, future studies set out to assess the myeloid populations within the tumours, along with the assessment of the circulating blood and associated lymphatics to identify the effect of the treatment on antigen recognition of the tumour.

## 3.5 Optimisation of ablation profiles

As discussed in section 3.4, when treating with ablative HIFU, there can be some off target effects which impede the efficacy and assessment of the treatment. To try to mitigate these issues, we assessed a shorter HIFU treatment time. The results of which will be discussed in the following section. As before, a single-source ultrasound array (as described in methods section 2.2.3, and section 3.4) was used for these treatments. To avoid unwanted effects of the treatment for the extended assessment of immune populations HIFU exposure was conducted for 5-seconds for partial ablation of the MCA-205 induced fibrosarcoma tumours. The treatment volume was calculated to be 0.9mm$^3$. The small treatment volume may mean that the treatment may have limited impacts on the tumour microenvironment

and subsequent immune infiltration and activation. However, a balance of unwanted effects and immune modulation had to be kept.

Section 3.4.2 showed an increase in the proportion of Treg and Tcm within respective T cell populations in the dLN after low-HIFU treatment of the tumour. As discussed, it was thought that this increased Treg and Tcm abundance was due to increased activation after HIFU treatment, possibly caused by antigen presentation. The study showed stable CD4 and CD8 T cell populations within the dLN and spleen of the low-HIFU treatment group, which may suggest this activation of the immune populations rather than recruitment.

To try to assess that antigen presentation responses were affected by the HIFU treatment, myeloid populations which may have mediated this were assessed. It was hypothesised that there would be more APCs in the dLN after treatment. The populations selected for analysis in this study include dendritic cells (DCs), neutrophils, monocytes and macrophages. Circulating monocytes have been linked to increased tumour DCs for the development of a regulatory environment[168], whereas macrophage number within the tumour is often explored due to antigen recognition[131] and downstream responses as well as association to prognosis and treatment outcomes[169] meaning these populations are important to assess.

The previous study suggested that 24 hours after treatment may be too soon to see a robust T cell response, hence this study also assessed 5 days post treatment. Activation and memory states of the CD8 T cells was inconclusive within the previous study, again possibly related to the sampling time.

A

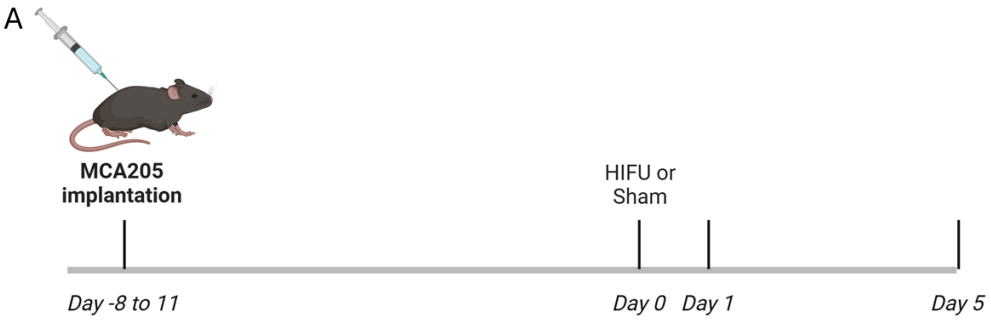


B

| Treatment | Group | N | Mean Tumour Volume ($mm^3$) | SD Tumour Volume ($mm^3$) | Mean Percentage of Tumour Ablation |
|---|---|---|---|---|---|
| HIFU | 24-hour | 5 | 119.68 | 53.86 | 0.99 |
| | 5-days | 4 | 34.58 | 11.39 | 2.87 |
| Sham | 24-hour | 3 | 60.30 | 60.48 | N/A |
| | 5-days | 5 | 41.12 | 28.97 | N/A |

C

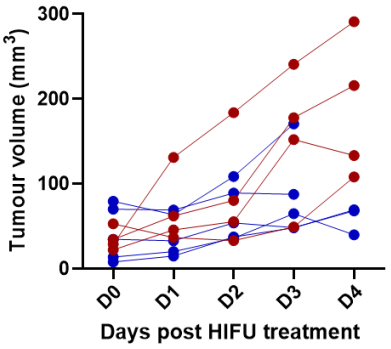


D

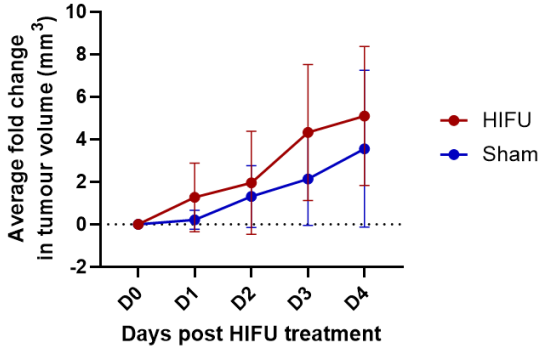


Figure 3.16: (A) Schematic overview for the pilot in vivo study to assess immune response to HIFU treatment of MCA205 fibrosarcoma in C57/Bl6 mice at an extended time. Created with BioRender.com. Tumours were induced into mice, tumour growth was monitored for 8- to 11-days until required size threshold (50$mm^3$) was reached, followed by treatment and culling for harvest 24-hours or 5-days after treatment. (B) The mean volume, standard deviation (SD) and predicted percentage of tumours treated with HIFU for each group within the study. (C) Tumour growth volume of tumours treated as HIFU-Sham (blue, n = 5 on days 0 to 3, n = 3 on day 4) or with HIFU (red, n = 4 on days 0 to 4). (D) Mean of the volume fold change of volume from day of treatment with standard deviation of mice treated with HIFU-Sham (blue, n = 5 on days 0 to 3, n = 3 on day 4) and HIFU treated (red, n = 4 on days 0 to 4) tumours.

This study was planned to assess APC myeloid populations, CD8, and CD4 subpopulations 24-hours and 5-days post-HIFU treatment as outlined in Figure 3.16A. There were 5 mice per group which were intended to have similar tumour volumes at the time of treatment. Due to data processing issues, the tumour volumes for the groups were not as similar as intended and the intended treatment volume was not observed as intended and as such the

percentage of treated tumour between the timepoints varied, as shown in Figure 3.16B. The study allowed for assessment of immune populations in peripheral tissues, 24-hours and 5-days after treatment. The assessment of the tumour volume saw no difference in the tumour volume (Figure 3.16C) or growth rate (Figure 3.16D) after 4 days (data for day 5 was not recorded in error). After 3 days the data for 2 of the Sham-HIFU mice was not available which may have skewed the data.

### 3.5.1 There was histological evidence of effective HIFU treatment, however spatially related immune response to treatment was not observed

The histological assessment of the HIFU treated tumours compared to non-treated 'Sham-HIFU' tumours showed evidence of ablation, as in the previous study in section 3.4.1. This included pyknosis (Figure 3.17A-D, in comparison to Figure 3.17E-H) which indicates an effective partial treatment in these tumours. Vimentin staining (Figure 3.18) was used to confirm the pyknosis was within the area of the tumour.

When assessing the abundance of particular immune populations, quantification of important markers including CD45 (Figure 3.20), CD8 (Figure 3.21) and FoxP3 (Figure 3.22) was used to profile levels of leukocyte, cytotoxic T cell and Treg abundances, respectively. No correlation between HIFU treatment and infiltration of cells with these markers was observed (Figure 3.19). The assessment of these populations did not show the expected trend in change with the treatment. This may be because histology is an imperfect way of assessment of these tissues. The approach taken lacks the ability to assess the whole tumour as a 3D object, thus information on only a portion of the tumour is attained. As discussed in section 3.4, this was a partial ablation study, which creates the risk of the small, modified area being missed in analysis.

Many factors will then impact on the ability of the mouse to raise a response to the increased antigen and necrotic factors released because of HIFU treatment. These include the availability of the antigen to reach the vasculature to leave the tumour and be recognised. Also, immune cells require functional vasculature to then enter the tumour after antigen recognition. With a small ablation zone, there may not be available vasculature within the vicinity of the treatment area. The ablation can disrupt vasculature which may also affect the ability of the cells to enter the tumour after treatment.

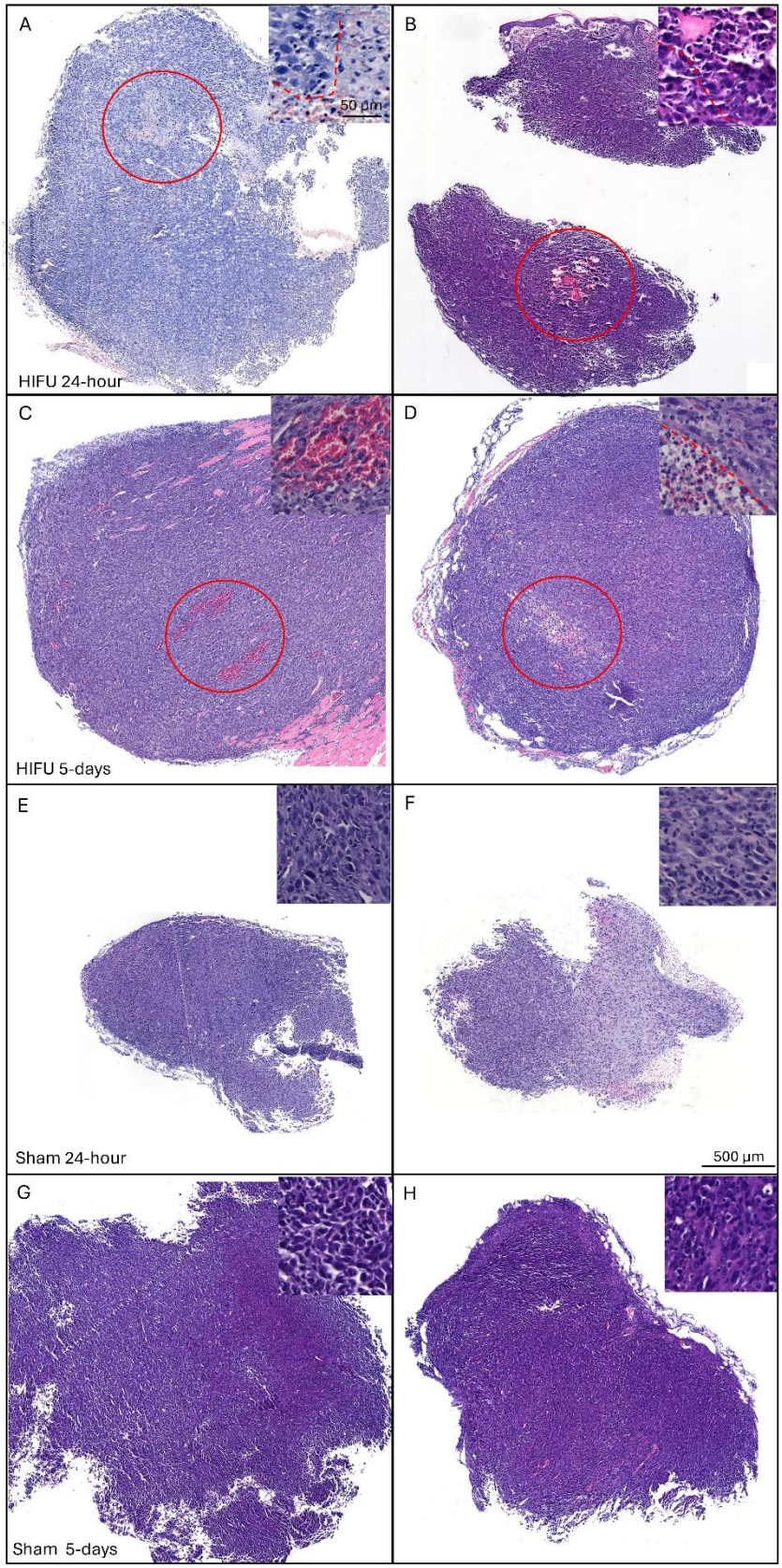


Figure 3.17: Example haematoxylin and eosin (H&E) slides (5µm thick) of tumours within groups treated with (A-B) HIFU at 24-hours, (C-D) HIFU at 5-days, (E-F) Sham-HIFU at 24-hours and (G-H) Sham-HIFU at 5-days. Red arrows used to highlight areas of pyknosis (recognisable as increased eosin stain uptake), a sign of thermal ablation of tissue.

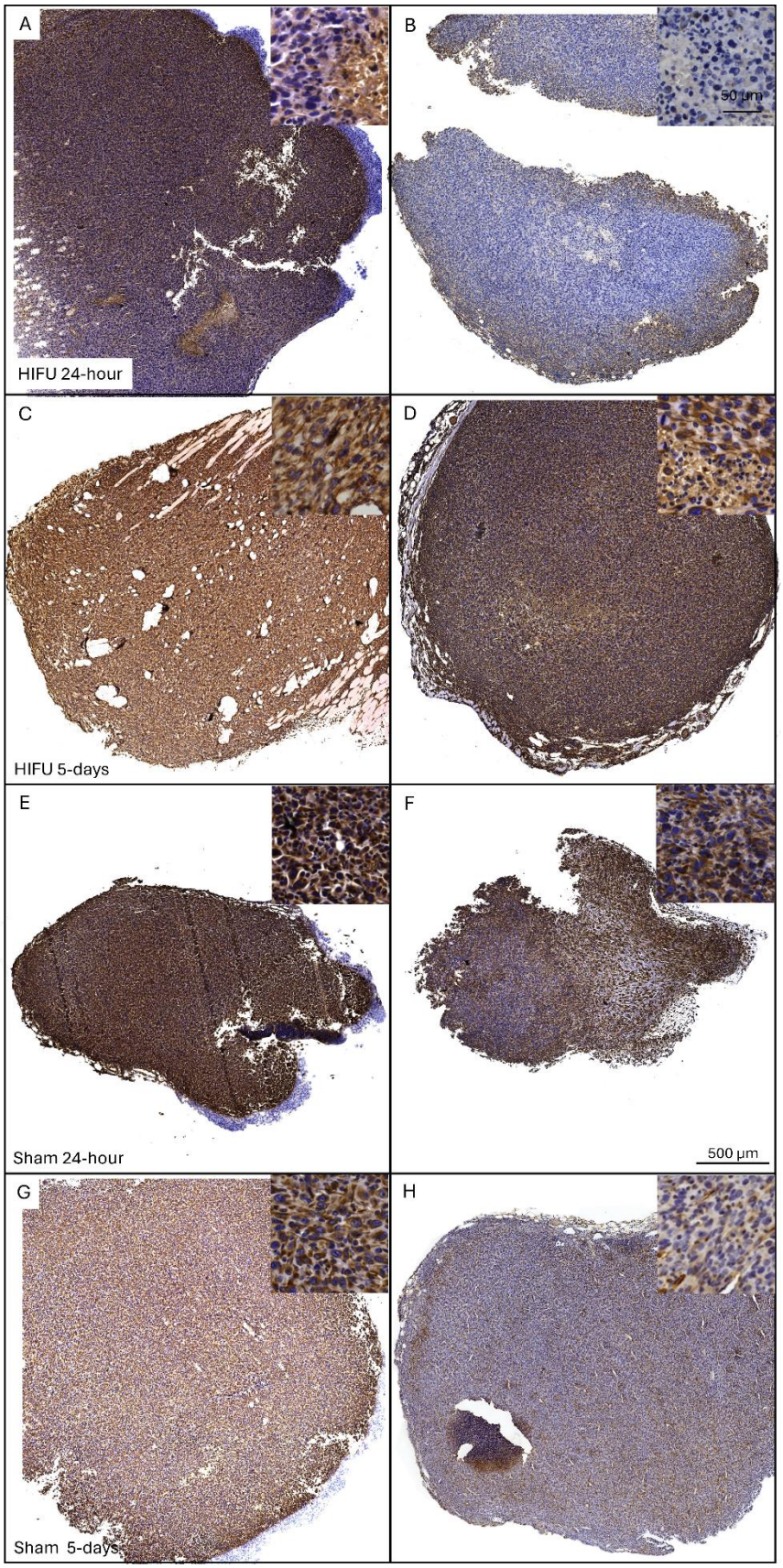


Figure 3.18: Example vimentin slides (5µm thick) of tumours within groups treated with (A-B) HIFU at 24-hours, (C-D) HIFU at 5-days, (E-F) Sham-HIFU at 24-hours and (G-H) Sham-HIFU at 5-days. Vimentin stain (DAB, brown) for mesenchymal tissue to select areas of fibrosarcoma tumour.

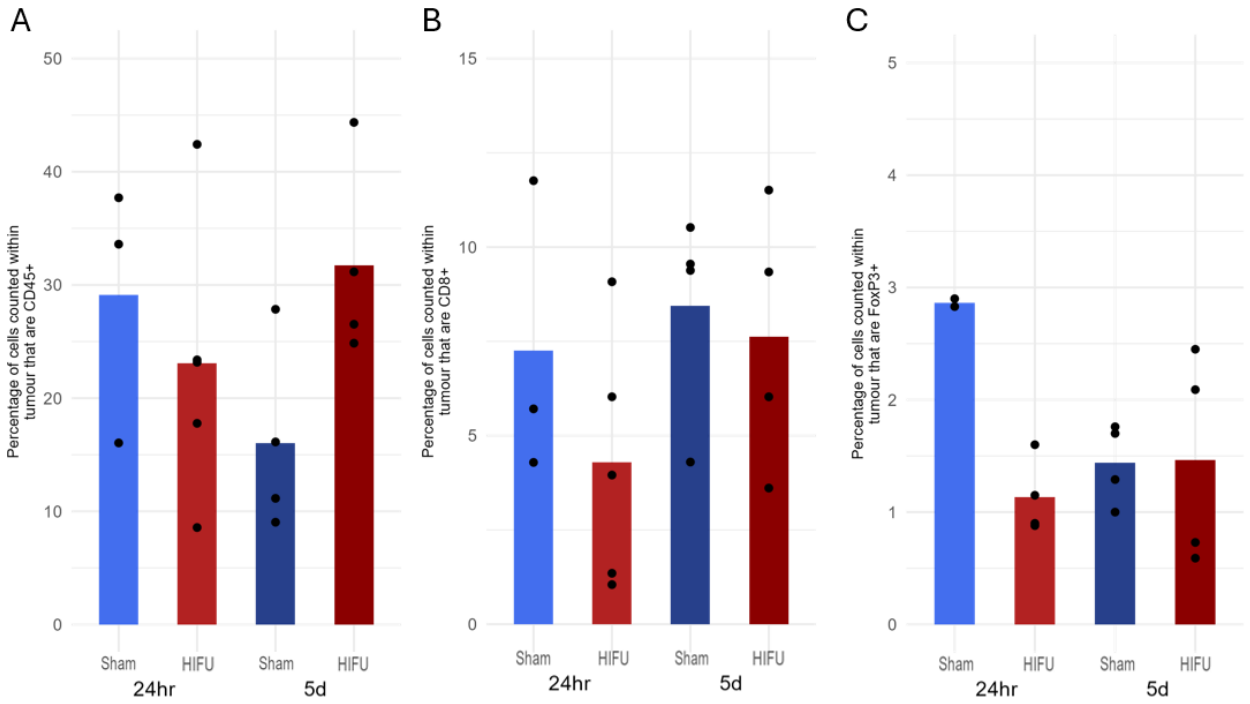


Figure 3.19: Quantification of histological stains as a percentage of haematoxylin positive nucleated cells within the tumour area. Represented cell types include (A) CD45 (Sham 24-hour N = 3, HIFU 24-hour N = 4, Sham 5-days N = 4, HIFU 5-days N = 4), (B) CD8 (Sham 24-hour N = 3, HIFU 24-hour N = 4, Sham 5-days N = 4, HIFU 5-days N = 5), (C) FoxP3 (Sham 24-hour N = 2, HIFU 24-hour N = 4, Sham 5-days N = 4, HIFU 5-days N = 4) percentage positive cells. Quantification of immunohistochemistry stains as a percentage of haematoxylin positive (blue) nucleated cells within the whole tumour area (see section 2.4.5 for methodology).

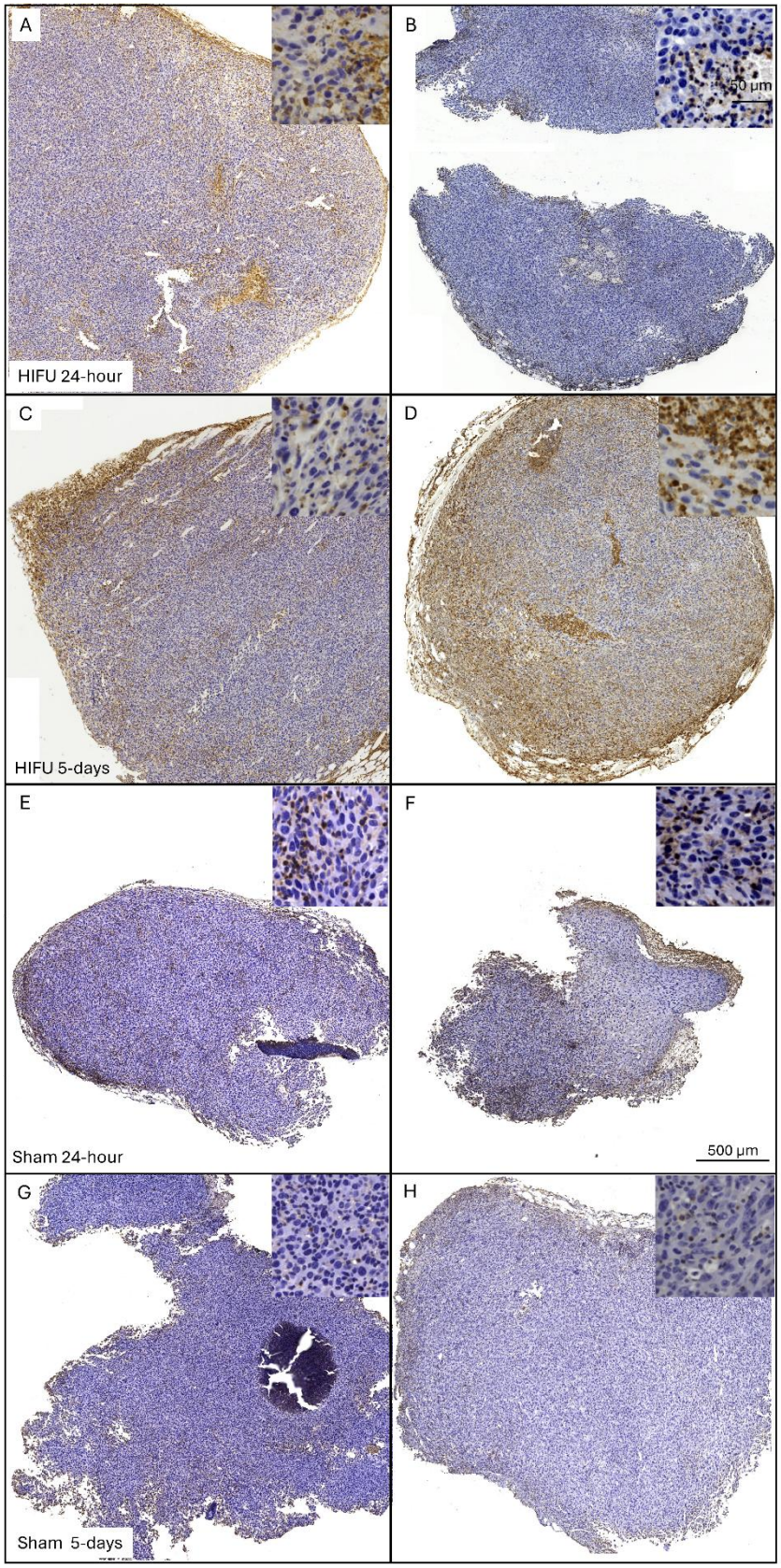


Figure 3.20: Representative CD45 slides (5µm thick) of tumours within groups treated with (A-B) HIFU at 24-hours, (C-D) HIFU at 5-days, (E-F) Sham-HIFU at 24-hours and (G-H) Sham-HIFU at 5-days. CD45 stain (DAB, brown) for leukocyte cell infiltration within the fibrosarcoma tumour.

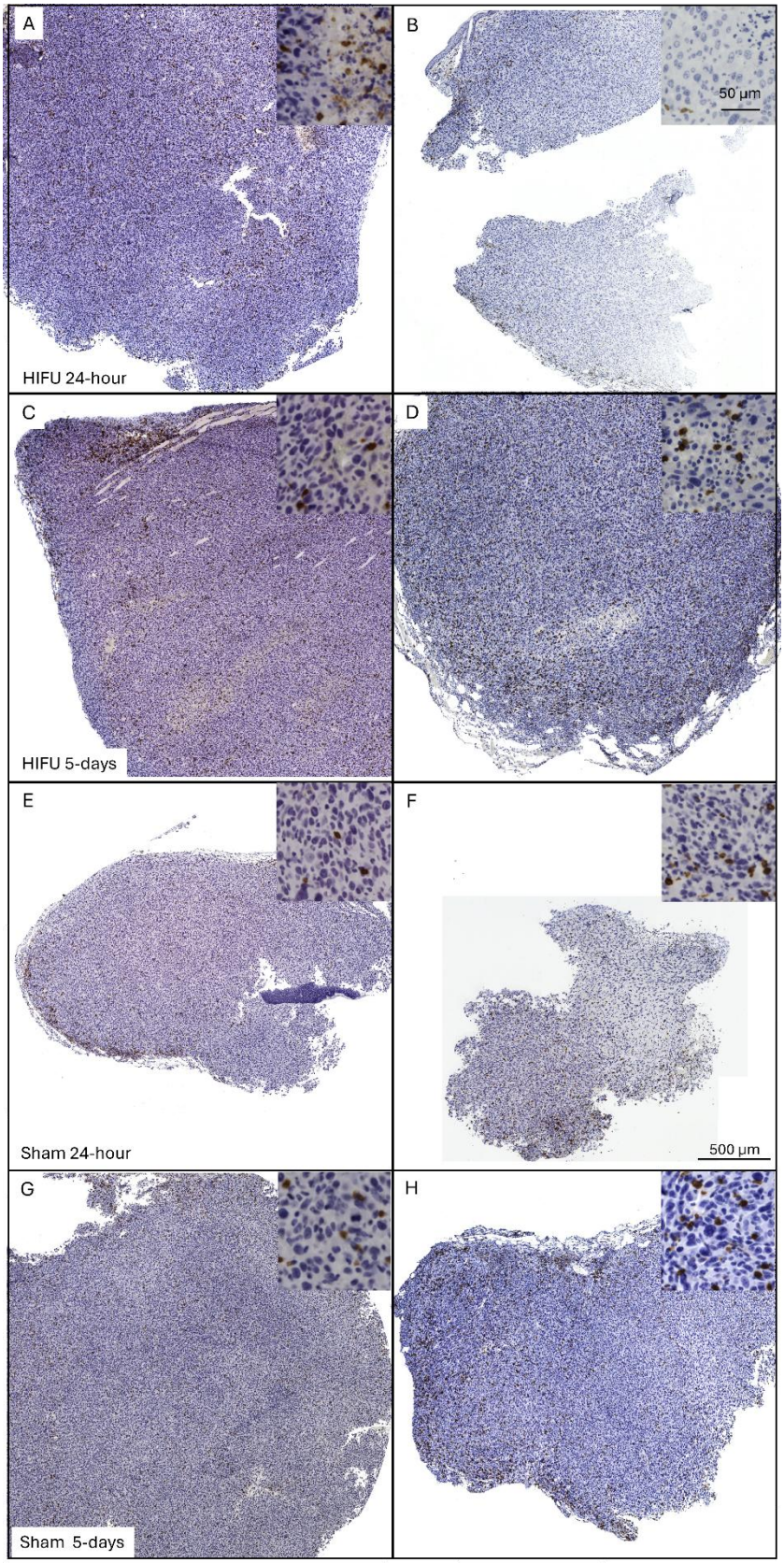


Figure 3.21: Representative CD8 slides (5µm thick) of tumours within groups treated with (A-B) HIFU at 24-hours, (C-D) HIFU at 5-days, (E-F) Sham-HIFU at 24-hours and (G-H) Sham-HIFU at 5-days. CD8 stain (DAB, brown) for CD8+ T cell infiltration within the fibrosarcoma tumour.

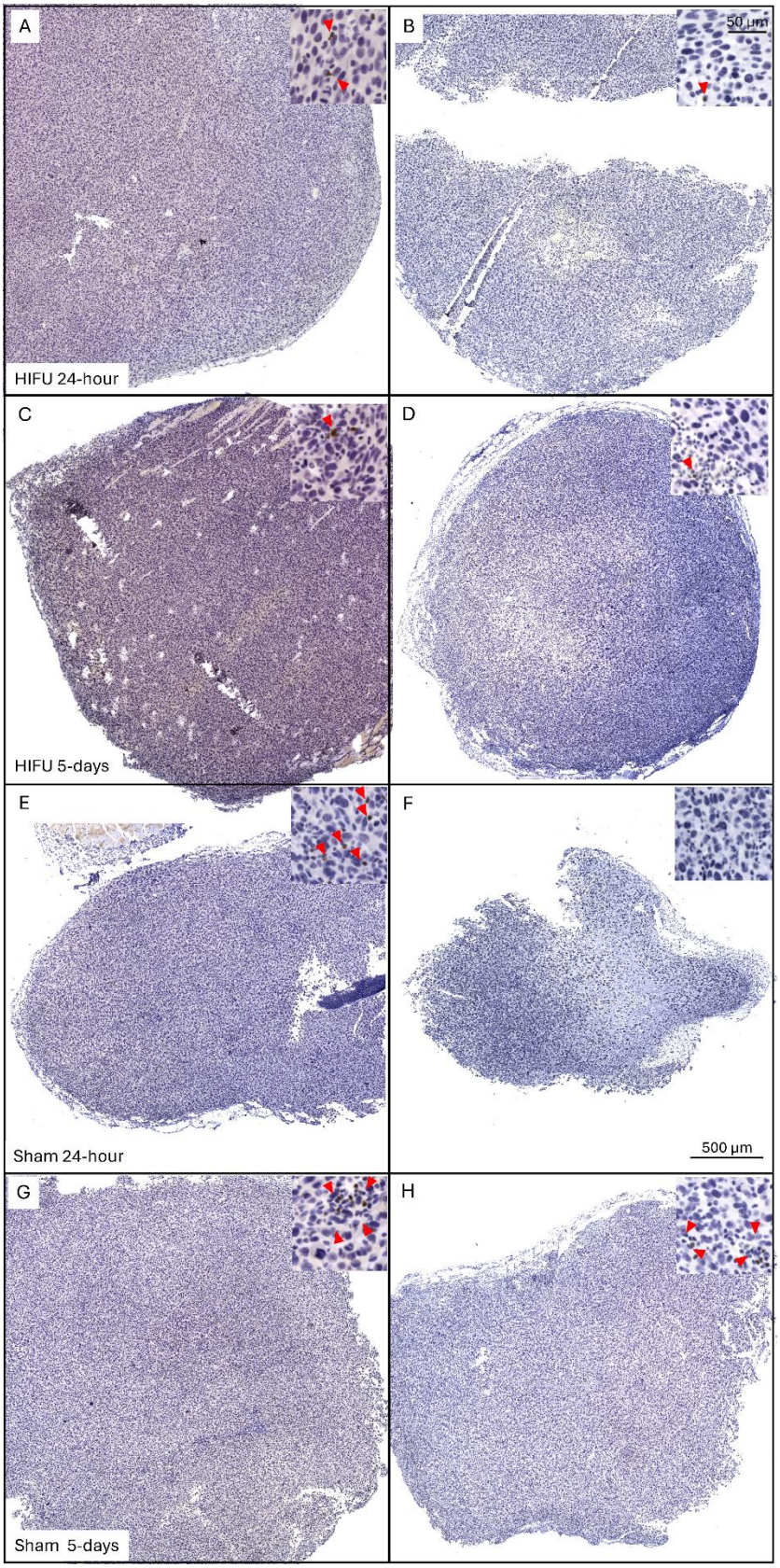


Figure 3.22: : Representative FoxP3 slides (5µm thick) of tumours within groups treated with (A-B) HIFU at 24-hours, (C-D) HIFU at 5-days, (E-F) Sham-HIFU at 24-hours and (G-H) Sham-HIFU at 5-days. FoxP3 stain (DAB, brown) for regulatory T cell infiltration within the fibrosarcoma tumour. Higher magnification representations of the tissue are shown in the inset, red arrows used to highlight positively stained cells.

### 3.5.2 There was modulation of monocyte abundances five days after HIFU treatment with increased macrophage abundances

It was hypothesised that there would be changes in the APC populations after HIFU treatment. It was believed to be related to the increased levels of necrotic tissue which in turn leads to increased circulating antigen, and DAMPs. To address this, the distribution of myeloid derived APCs in the dLNs was assessed using flow cytometry 24-hours and 5-days after treatment. These populations were compared to non-treatment control tissues and the cLNs. The treatment may have abscopal effects because of the antigen recognition which may affect the periphery.

Previously, high abundance of neutrophils has been associated with tumour progression but also the polarisation of macrophages to an M1 phenotype[170], hence the interest in their expression within this work. A significant increase in the neutrophil abundance 24-hours after treatment was seen in the **HIFU** group when compared to **Sham-HIFU** control at the same timepoint (0.29±0.02% vs 0.080±0.03%, $p<0.01$). This resolved by 5-days, comparing the **HIFU** treatment to the same timepoint **Sham-HIFU** control (0.13±0.05% vs 0.13±0.07%, $p>0.05$). Neutrophil are known to increase following necrotic cell death [171], which was the intended mechanism of this HIFU treatment, and the effectors of the cell death may be circulating through the lymphatics after treatment. This may have led to the recruitment of macrophages specifically to the tumour, through the lymphatic system. This population seemed to specifically be associated to the tumour as neutrophils were a stable population within the cLN.

In the dLN, there was a trend for an increase in monocyte (1.08±0.25% vs 0.71±0.22%, $p>0.05$) and macrophage (0.18±0.04% vs 0.08±0.02%, $p>0.05$) populations in the **HIFU**

treatment group at 5 days  post treatment compared to **Sham-HIFU** at the same timepoint (Figure 3.23A), which may be related to HIFU treatment.

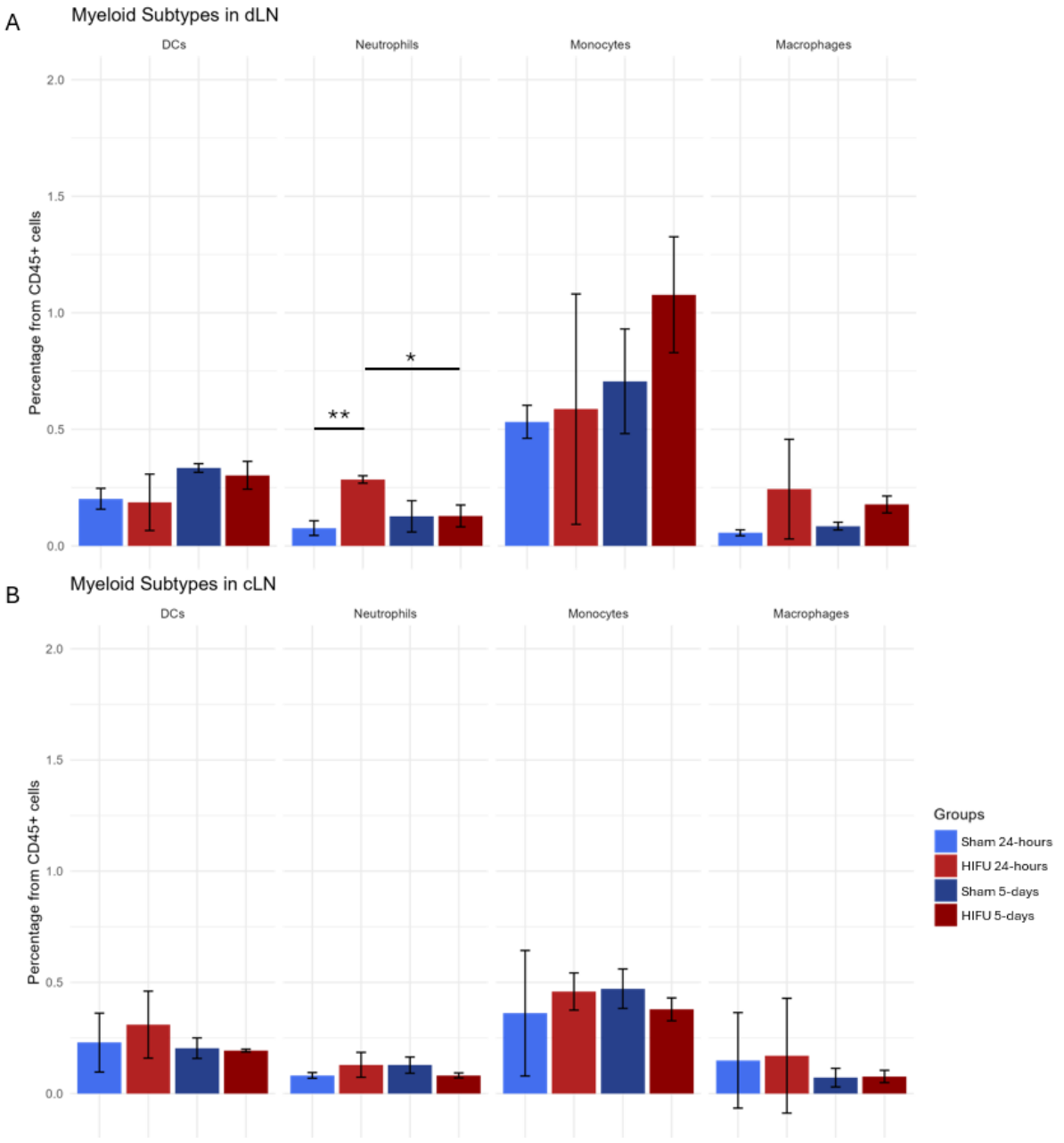


Figure 3.23: Representative plots of myeloid populations including dendritic cells (DCs, CD45+CD3-CD11b-CD11c+) neutrophils (CD45+CD3-CD11b+CD11c-Gr1+), monocytes (CD45+CD3-CD11b+CD11c-Gr1-Ly6C+F4/80-), and macrophages (CD45+CD3-CD11b+CD11c-Gr1-Ly6C+F4/80+) as percentage of CD45+ leukocytes with error bars to show standard deviation from flow cytometry analysis of populations in (A) draining lymph nodes (dLN, Sham 24-hours n = 2, HIFU 24-hours = 3, Sham 5-days n = 3, HIFU 5-days n= 3), and (B) contralateral lymph node (cLN, Sham 24-hours n = 3, HIFU 24-hours = 5, Sham 5-days n = 5, HIFU 5-days n= 4), of mice treated with Sham HIFU or HIFU at 24-hours and 5-days post treatment. ANOVA with Tukey's post hoc test was performed, (* $p<0.05$, ** $p<0.01$). Reduced replicates due to issues with the flow cytometry staining and sample acquisition.

An increase in the DC population abundance was expected, but this was not the case. It is known that monocyte populations become abundant in response to cell death[130]. Along with this, there has been evidence in the literature to show that monocyte derived DCs (MoDCs) from dLNs are required for the priming of cytotoxic CD8 function within tumours[172,173]. Increased cytotoxic T cell activity through DC mediated antigen presentation was the hypothesised pathway after HIFU treatment. However, it seems that the phenotype was pushed towards the accumulation of macrophages within the dLN. This is suggested by the persistent low level of DCs but small increase in macrophage abundance (Figure 3.23A). These macrophage populations can either have a pro-tumour[169] or anti-tumour response[42,174] with antigen presentation functions[131,175] but the assessment of this was beyond the scope of the study.

This analysis uncovered that DC, monocyte and macrophage populations were stable within the cLN (Figure 3.23B), although there was some variability based on the group. This is to be expected in an experiment of this type with small groups.

### 3.5.3 Indications of an increased proportion of Tregs within the dLN after HIFU treatment may be indicative of an antigen initiated regulatory T cell response

It was hypothesised that an increase in T cell populations would be seen within the dLN 5 days after HIFU treatment. Assessment of the Treg population was pertinent after modulation of this population was seen within the previous studies as discussed in sections 3.3.2. Limitation on tissue availability meant that the memory population could only be assessed in the periphery. However, modulation of circulating CD8 T cell memory populations may be seen. To assess this, flow cytometry of the dLNs was performed, with

cLN as internal controls. Peripheral results were also of interest as CD8 abundances, and CD8:Treg ratios have previously been clinically relevant[176–178].

Firstly, assessment of the overall B cell, T cell, CD4 and CD8 T cell populations was conducted in dLN, cLN and blood (Figure 3.24). This showed a significant decrease in T cell populations in the dLN with **HIFU**, 24-hours after treatment compared to the **Sham-HIFU** group (71.2±11.6% vs 45.3±10.2%, $p<0.05$, as shown in Figure 3.24A). Such decreases were not observed in the cLN (Figure 3.24B) or blood samples (Figure 3.24C). A significant reduction in the CD8 T cell population was seen 24-hours after treatment in the **HIFU** treated group compared to **Sham-HIFU** at the same timepoint (30.6±2.5% vs 17.3±5.0%, $p<0.01$). Also, there was a significant reduction in the CD8 population when comparing the **5-day** Sham-HIFU group to the **24-hour** Sham-HIFU group (20.0±5.2% vs 30.6±2.5%, $p<0.05$). This may suggest that these cells are leaving the dLN and bloodstream to infiltrate into the tumour, however, the tumour histology was inconclusive so did not confirm this. Furthermore, it should be noted that the population frequency at 24-hours compared to 5-days is marginal within the **HIFU** group and the abundance within the Sham-HIFU group at 24-hour may be misleading. The T cell population in the Sham-HIFU group at 5-days was significantly lower than 24-hours (71.2±11.6% vs 48.2±10.6%, $p<0.05$), when it would be expected to be similar as there was no treatment given to these mice. However, the tumour size was larger at baseline in the 24-hours which may have affected the T cell responses to the untreated HIFU-Sham tumours.

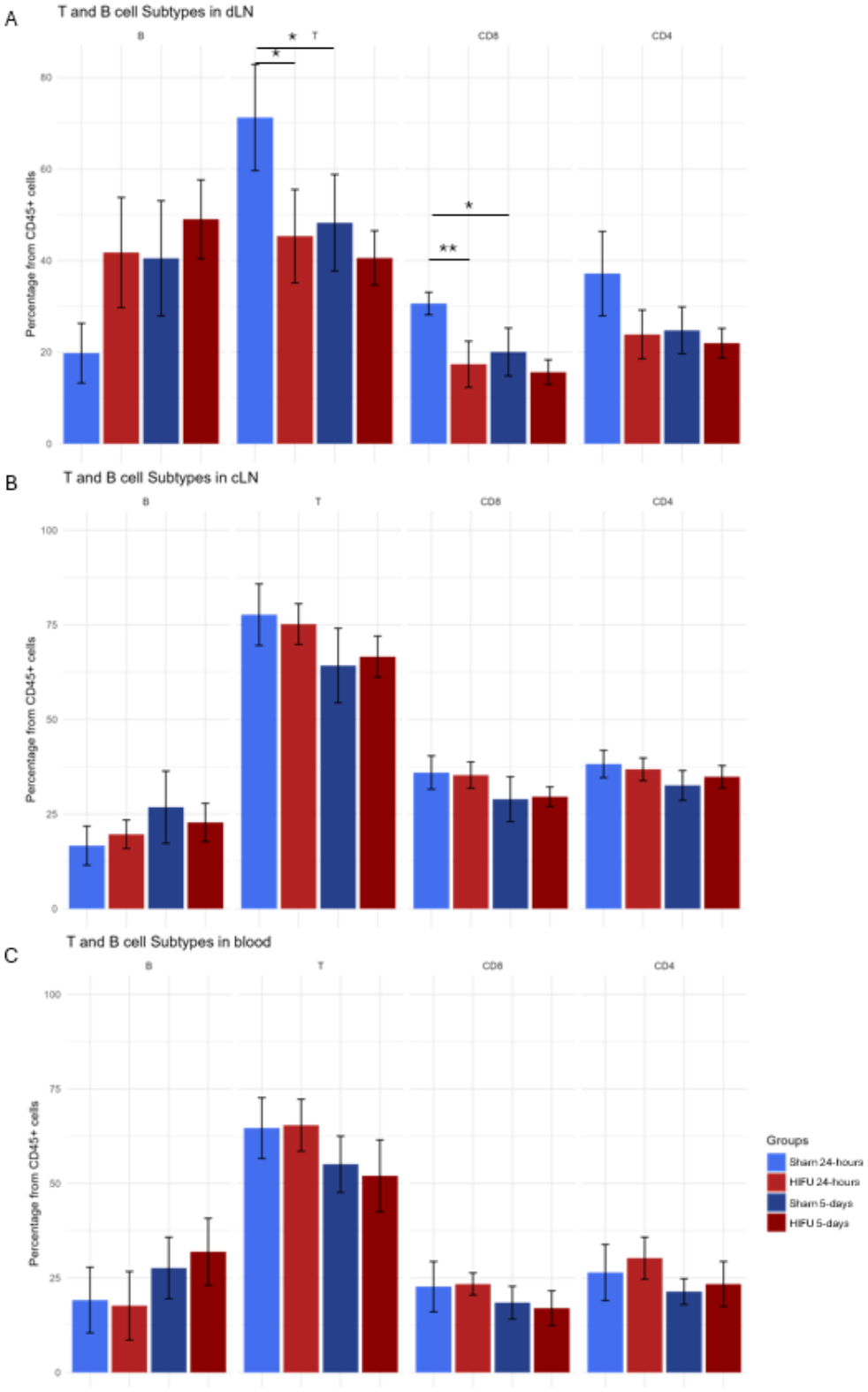


Figure 3.24: Representative plots for proportion of B cell, T cell, CD8 T cell and CD4 T cell populations as percentage of CD45+ leukocytes from flow cytometry analysis of populations with error bars to show standard deviation in (A) draining lymph node (dLN, Sham 24-hours n= 3, HIFU 24-hours = 5, Sham 5-days n = 5, HIFU 5-days n= 3), (B) contralateral lymph node (cLN, Sham 24-hours n= 3, HIFU 24-hours = 5, Sham 5-days n = 5, HIFU 5-days n= 4 and (C) blood (Sham 24-hours n= 3, HIFU 24-hours = 5, Sham 5-days n = 5, HIFU 5-days n= 4) of mice treated with Sham HIFU or HIFU at 24-hours and 5-days post treatment. ANOVA with Tukey's post hoc test was performed (* $p<0.05$, ** $p<0.01$). HIFU 5-day dLN had removed replicate due to flow cytometry staining issue.

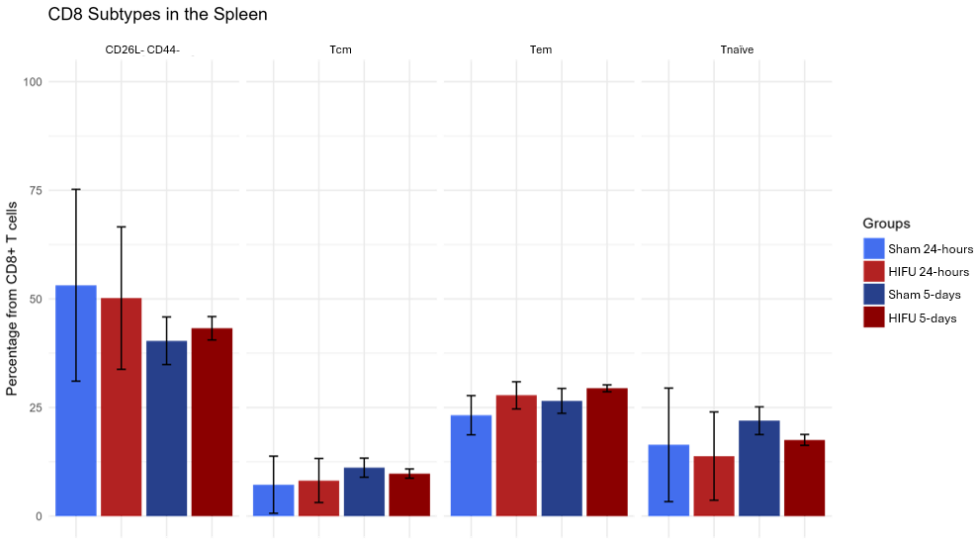


Figure 3.25: Representative plots of CD8 subpopulations as percentage of CD8 T cells from flow cytometry analysis of populations Spleen (Sham 24-hours n= 3, HIFU 24-hours = 5, Sham 5-days n = 5, HIFU 5-days n= 4), of mice treated with Sham HIFU or HIFU at 24-hours and 5-days post treatment. In detailed view of the proportion of the CD8 subpopulations with error bars. ANOVA with Tukey's post hoc test was performed, there were no significant differences. Reduced replicates in the blood analysis due to tissue availability and flow cytometry acquisition recording issues.

Within the HIFU-treated group, there was a not-significant increased abundance of B cells in the dLN 24-hours (41.7±12.0% vs 19.8±6.5%, $p>0.05$) and 5-days (49.0±8.6% vs 40.5±12.6%, $p>0.05$) after treatment (Figure 3.24). This may have been related to antigen recognition caused by treatment. As B-cells are known to be prevalent in sarcoma[26], and there were limitations on what could be provided by the techniques used, this was not investigated any further.

The analysis of the CD8 subpopulations by flow cytometry (gating strategy in Supplementary Figure 3.5) was able to explore memory populations within the spleen (Figure 3.25). Due to tissue availability and limitations of the techniques the other tissues were prioritised to assess the myeloid and CD4 T cell lineages. The spleen showed a stable CD8 populations, that did not vary with treatment. CD44-CD62L- cells were the most abundant subpopulation. The Tem population was abundant within all groups, with Tcm and Tnaïve cells also present at lower abundance. This may suggest a response to the tumour, but the treatment may not influence these splenic populations.

The assessment of CD4 T cell populations in the dLN (gating strategy in Supplementary Figure 3.5) showed Tregs made up a slightly higher frequency of the CD4 T cell population 5-days after **HIFU** treatment when compared to the **Sham-HIFU** at 5-days (10.34±0.5% vs 7.8 ±2.45%, $p>0.05$), as well as the **HIFU** treated group at 24-hours (10.34±0.5% vs 5.0±2.3%, $p<0.05$, Figure 3.26A). This was supported by the Treg/CD8 ratio which increased in the dLN of HIFU treated mice at **5-days** post treatment when compared to the **24-hour** treatment group (Figure 3.26G). These finding did not reach statistical significance because of the large variability in this data. If this Treg population increase was also indicative of levels within the tumour after the HIFU treatment, then this could explain why the expected decrease in tumour growth and improved survival was not achieved. It may have been that the tumour environment and signalling pathways may skew antigen presentation responses towards bolstering the regulatory response which is known to be the phenotype tumours with an MHC-II response. As previously suggested, the dLN are involved in the antigen response for the generation of Tregs into tumours[38,142]. In the dLN, a subtle decrease in Tconv frequency was seen as the Treg population became more dominant, when comparing the **HIFU** treated groups to **Sham-HIFU** groups at both 24-hours (88.9±2.8% in Sham-HIFU vs 86.9±2.8% in HIFU, $p>0.05$) and 5-days (85.5±1.7 in Sham-HIFU vs 83.9±0.4% in HIFU) post treatment. The increase in Treg frequency was compared to CD8 T cell abundance. This indicated a slight increase in the Treg/CD8 ratio in the HIFU group compared to HIFU-Sham, 5-days after treatment but there was large population variability, so it is difficult to specifically determine any differences.

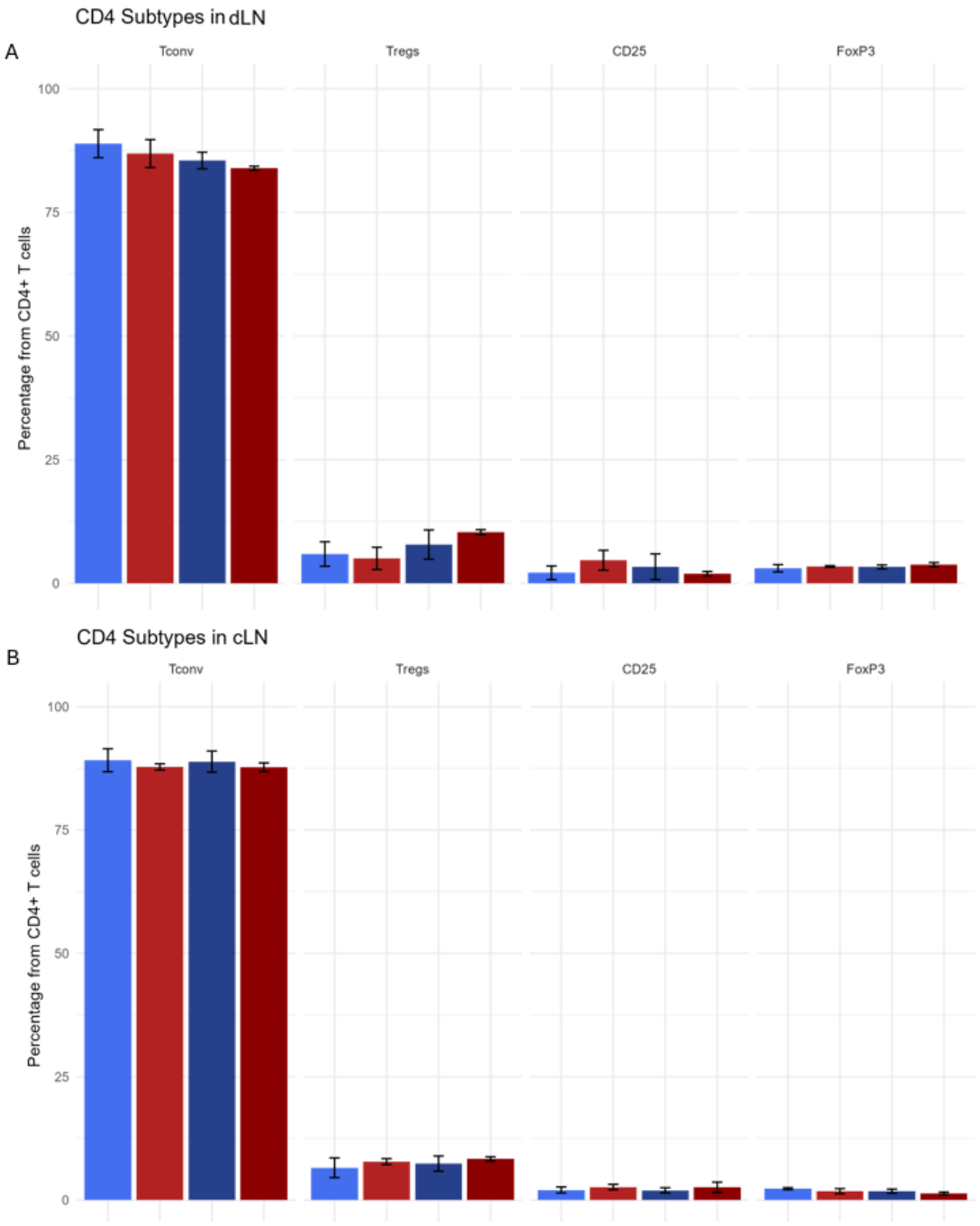
A
CD4 Subtypes in dLN
Tconv
Tregs
CD25
FoxP3
Percentage from CD4+ T cells
100
75
50
25
0
B
CD4 Subtypes in cLN
Tconv
Tregs
CD25
FoxP3
Percentage from CD4+ T cells
100
75
50
25
0

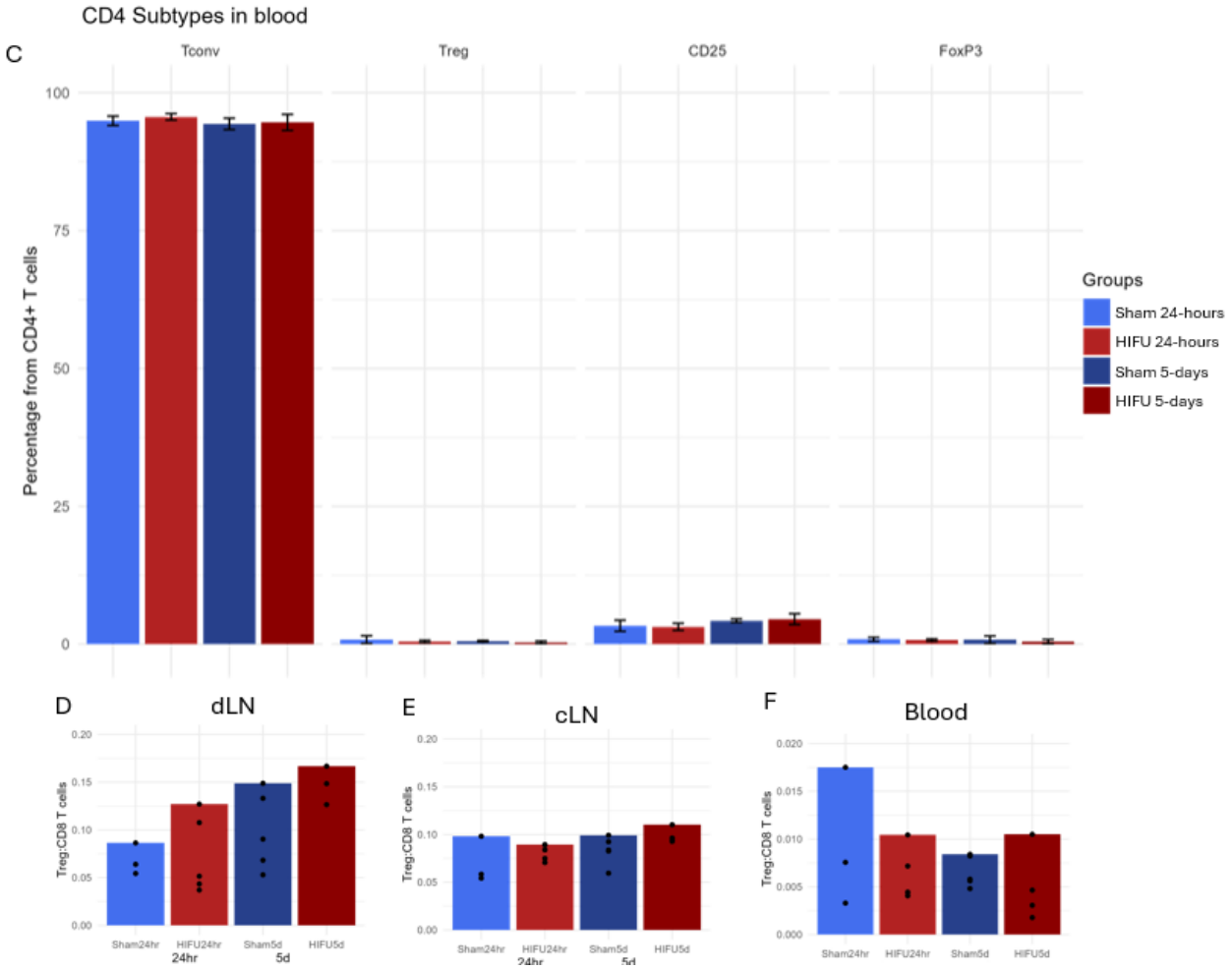


Figure 3.26: Representation of proportion of CD4 subpopulations as a percentage of CD4 T cells from flow cytometry analysis of (A) draining lymph nodes (dLN, Sham 24-hours n = 3, HIFU 24-hours n= 5, Sham 5-days n = 5, HIFU 5-days n = 3 ), (B) contralateral lymph nodes (cLN, Sham 24-hours n = 3, HIFU 24-hours n= 5, Sham 5-days n = 5, HIFU 5-days n = 4), and (C) blood (Sham 24-hours n = 3, HIFU 24-hours n= 5, Sham 5-days n = 5, HIFU 5-days n = 4) of mice treated with Sham HIFU or HIFU at 24-hours and 5-days post treatment. ANOVA with Tukey's post hoc test was performed, there were no significant differences. (A, B, and C) Detailed view of the proportion of the CD4 subpopulations with error bars to show SD. Treg to CD8 T cell ratio of (D) draining lymph nodes (dLN), (E) contralateral lymph nodes (cLN), and (F) blood. ANOVA with Tukey's post hoc test was performed.

These data showed a stable proportion of Tconvs and Tregs, within the cLN, and blood for all groups, regardless of treatment (Figure 3.26B and C). This was as well as a stable Treg/CD8 ratio in the cLN (Figure 3.26E and F). There was large variability in the Treg/CD8 ratio within the blood of the 24-hour Sham group, but overall there seemed to be little difference in this between the Sham-HIFU and HIFU treated groups (Figure 3.26I). This suggests that the modulation of the CD4 subtypes was a HIFU treatment response, specifically to the tumour.

### 3.5.4 Summary of findings

Assessment of the myeloid, T cell and B cell populations within the dLN, cLN, and blood samples of mice treated with HIFU after 24-hours and 5-days indicated an increase in the proportion of neutrophils in the dLNs 24-hours after **HIFU** treatment, when compared to Sham control tumour bearing mice. An increased proportion of monocytes, macrophages and Tregs were identified in the dLN 5-days after **HIFU** treatment. This study suggested that there was modulation of APC populations within the lymphatic system associated with the tumour with subtle suggestion that the Treg populations are also modulated in the dLN requiring further analysis within the tumour itself.

## 3.6 HIFU ablation with immunotherapy

In the literature, tumour growth of sarcoma (S180) has been reduced after partial thermal ablation[131]. However, within Section 3.5, a reduced growth was not seen. Assessment of an extended period after treatment to investigate the treatment outcome in terms of tumour growth control was pertinent. The previous data suggested modulation of myeloid derived APC such as monocytes and macrophages as well as neutrophils and Treg populations was occurring.

Within this chapter, it was of interest to determine how HIFU treatment may be able to improve suboptimal (for sarcoma) immunotherapies for treatment. Treatment with aPD-L1 antibody therapies have had limited impact on sarcoma patient survival. It was noted in the literature that PD-L1 expression was reported to be low within primary and metastatic sarcoma tumours[83,150,169,179] with variability dependent on type. However, when it was present the expression of PD-L1 was often associated with poorer clinical outcomes [83,150,179].

It seemed pertinent to the studies reported here, that the use of aPD-L1 blocking antibodies has been reported in the literature to influence the specific cell types profiled in response to HIFU in sections 3.4.2, 3.5.2 and 3.5.3. Specifically, Huang et al have reported an increase tumour specific-reactive CD8 memory T cells within the dLN in response to antigen following anti-PD-L1 treatment in a melanoma model (B16-F10)[180]. It was thought that this can improve the intended response to produce a CD8 T cell specific response, as has previously been seen in neuroblastoma *in vivo* study[127]. Also noted in the previous studies was a decrease in the Treg population with a combination therapy of aPD-L1 and aTGFβ in the LNs of a metastatic MCA205 model[137]. This seemed relevant with the previous studies outlined in this work suggesting an increase in the Treg population (section 3.4.2 and 3.5.3).

Clinically, aPD-L1 in the form of Avelumad, Atezolizumab, and Durvalumab, have been used in the treatment of sarcoma in phase I/II clinical trials as a part of a combination therapy approach. Avelumad for advanced liposarcoma and leiomyosarcoma has been used in combination with trabectedin (chemotherapeutic) which showed a progression free survival of 6-months of 52%, with improved median progression free survival of 8.3 months compared to studies of trabectedin alone, where the progression free survival has been reported at 4.2, 5.1 and 5.6 months[181]. This suggested that the treatment had some improved effect on the cohort. Avelumad has also been assessed with gemcitabine (chemotherapeutic). This was a phase II study conducted on patients with leiomyosarcoma which showed an overall response rate of 20% with the better outcomes being associated with higher immune infiltration[182].

These findings and the increase in CD4 and CD8 populations reported after HIFU treatment, in the studies in this chapter (sections 3.4 and 3.5), help build the rationale for the use of

HIFU in combination with ICI. The treatment of adolescent alveolar soft-part sarcoma in a phase II trial using Atezolizumab showed a response rate of 37% (complete and partial response)[183] further emphasises the potential of ICI for improving treatment of sarcoma indications. Durvalumab has been used with Tremelimumab (aCTLA-4) and radiotherapy for the treatment of high-grade soft tissue sarcomas with stable disease or partial response being achieved in most patients, suggesting its use in combination treatment as favourable, but still with room for improvement[184]. Durvalumab with Trabectedin as a combination therapy in a phase Ib study has shown less favourable outcomes, with just 43% of patients showing tumour shrinkage[185]. Again, providing some encouragement that the mechanistic action of ICI is supported, but that there is still room for improvement of the treatment.

It was therefore hypothesised that the combination of HIFU and aPD-L1 antibody would synergise to provide better outcomes when compared to each approach in isolation or a control no-treatment regimen. aPD-L1 therapies provide better treatment outcomes with increased immune infiltration, which may be provided by the HIFU ablations. Previous work had shown aPD-L1 antibodies to have a limited effect on the ability to effectively treat MCA205[186,187], hence there is scope for HIFU to provide enhancement in this model.

In terms of measurable outputs from the combination of HIFU and aPD-L1, assessment of the immune milieu may be expected to reveal an increase APC and T cell activation. Indeed, previously it was hypothesised that DCs will be a main APCs, which migrate to the dLN and increase CD8 T cell activity towards the tumour. However, data (section 3.5.2) suggested that neutrophils an Mice were harvested at 24-hours and 5-days d macrophages may be the main cell type impacted which may then influence the T cell population activity. The modulation of the Treg population within the tumour was also seen, (section 3.5.3), which

may be linked. The previous reliance on histological assessment of these tumours may not have been the optimal approach for assessing the infiltration into the tumours. Thus, this study will focus on the assessment of immune population modulation after treatment in the periphery, lymphatics and tumour using flow cytometry.

The focus of this study was to provide immunotherapy on the day of tumour ablation by HIFU, with additional injections at 5- and 10-days post HIFU treatment for the combination therapy group as outlined in Figure 3.27A. Typical human trials treat with 10mg/kg of aPD-L1 drug which equates to 200µg of antibody for the mouse. An antibody control matching the Isotype of the aPD-L1, as discussed in methods section 2.2.4 was used as a control, along with HIFU Sham treatment as described in methods section 2.2.2. Mice were therefore treated in one of the following ways: aPD-L1 + HIFU (PD-L1 HIFU), aPD-L1 + HIFU Sham (PD-L1 Sham), Isotype control + HIFU (Iso HIFU), and Isotype control + HIFU Sham (Iso Sham) as outlined in Figure 3.27B. The treatment volume was calculated to be 0.9mm$^3$. The percentage of the tumour that was treated is shown in Figure 3.27B. The treatment volume may mean that the treatment may have limited impacts on the tumour microenvironment and subsequent immune infiltration and activation. However, due to welfare concerns in the previous study, a balance had to be considered for practicality.

Flow cytometry analysis was conducted on the tumour, dLN, and cLN, the gating strategy was outlined in Supplementary Figure 3.6. Mice were harvested at 24-hours and 5-days after HIFU and aPD-L1 treatment. Mice were assigned to groups to achieve equivalent mean tumour volumes per group before treatment (Figure 3.27B). These tumours were larger at the time of treatment than previous studies to account for vascularisation requirements of aPD-L1 antibody delivery within the tumour.

A

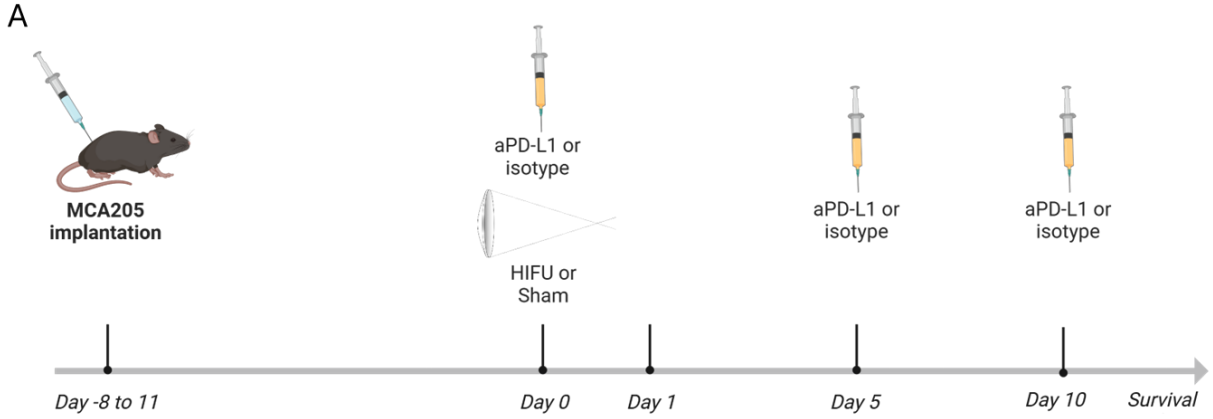


B

| Treatment | Timepoint | Number of mice | Mean Tumour Volume ($mm^3$) | SD Tumour Volume ($mm^3$) | Mean Percentage of Tumour Ablation |
|---|---|---|---|---|---|
| Iso Sham | 24-hours | 5 | 90.49 | 15.69 | N/A |
| | 5-days | 5 | 80.68 | 35.10 | N/A |
| | Survival | 6 | 112.66 | 14.53 | N/A |
| Iso HIFU | 24-hours | 5 | 97.37 | 14.12 | 0.95 |
| | 5-days | 5 | 102.32 | 39.59 | 1.09 |
| | Survival | 5 | 106.61 | 35.84 | 0.95 |
| PD-L1 Sham | 24-hours | 5 | 98.88 | 8.74 | N/A |
| | 5-days | 5 | 102.00 | 31.96 | N/A |
| | Survival | 5 | 83.32 | 8.74 | N/A |
| PD-L1 HIFU | 24-hours | 5 | 93.91 | 16.32 | 0.99 |
| | 5-days | 5 | 85.79 | 13.94 | 1.08 |
| | Survival | 5 | 97.64 | 36.90 | 1.04 |

Figure 3.27: A) Schematic overview for the pilot in vivo study to assess immune response to HIFU treatment with aPD-L1 immunotherapy of MCA205 fibrosarcoma in C57/Bl6. Created with BioRender.com. Tumours were induced into mice, tumour growth was monitored for 8- to 11-days until required size threshold (>60$mm^3$) was reached, followed by treatment and culling for harvest 24-hours, 5-days, or in a survival study after treatment. (B) The mean volume, standard deviation (SD) and predicted percentage of tumours treated with HIFU for each group within the study.

### 3.6.1 There was successful reduction of PD-L1 expression on tumour cells, and significant downregulation of its expression on leukocytes

The assessment of PD-L1 expression on cancer and CD45 immune compartment was conducted by flow cytometry. Previous research has shown that the MCA205 cell line does express PD-L1[137]. Furthermore, the immune milieu in the tumour, vasculature and lymphatics may also be affected by the treatment. The hypothesis was that using the same antibody clone for flow cytometry would indicate the binding of the anti-PD-L1 within the tissue. It was believed that the relative abundance of PD-L1+ cells at 24-hours after treatment would be lower in the mice treated with the aPD-L1 antibody compared the isotype control mice. It was also hypothesised that the additional aPD-L1 antibody would be required at 5-days as the relative abundance of PD-L1+ cells would increase again at 5-days post-injection.

Firstly, the staining and identification of MCA205 cells by flow cytometry was optimised in vitro. The expression of CD45, CD29 and PD-L1 were profiled on cells collected from monolayer culture. Figure 3.28 shows the MCA205 tumours express CD29 (an integrin receptor) (Figure 3.28A) and PD-L1 (Figure 3.28A), both indicated, compared to the FMO population. CD29 is associated with cancer stem cells, EMT and other sarcoma types in human studies[188]. These cells did not express CD45 or CD3. This was used as the basis for of flow cytometry protocols to discern tumour cells from immune cells from whole tumour samples rescued from the study.

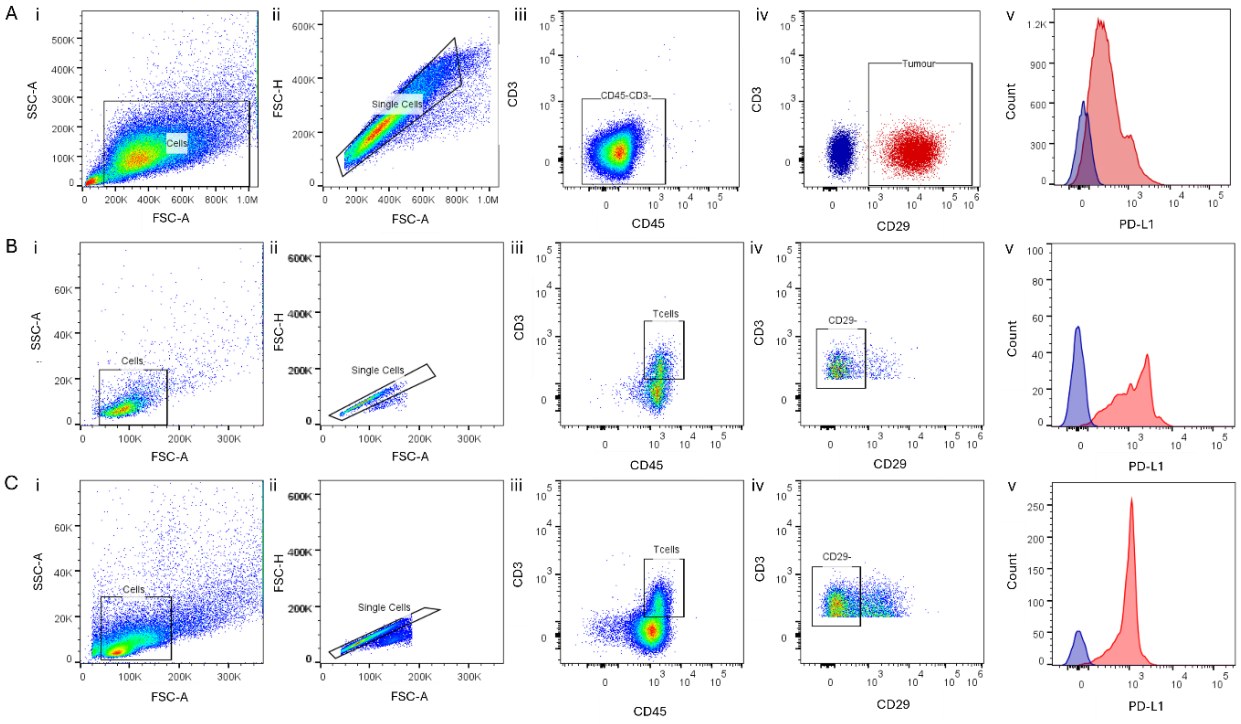


Figure 3.28: Gating strategy for identifying MCA205 tumour cells used to identify the expression of PD-L1. (A) Gating on MCA205 cells from culture at passage 7, (i) forward and side scatter for size selection of cells, (ii) single cell selection, (iii) identifying CD45-CD3- cells, (iv) CD29 expression on MCA205 cells (red) compared to fluorescence-minus-one (FMO, blue), (v) PD-L1+ MCA205 cells (red) in comparison to fluorescence-minus-one (FMO, blue). Gating strategy on cells from lymph node (B) and spleen (C). (i) forward and side scatter for size selection of cells, (ii) single cell selection, (iii) identifying CD45+CD3+ T cells for interest, (iv) CD29 expression for interest, (v) PD-L1+ T cells (red) in comparison to fluorescence-minus-one (FMO, blue).

Such analysis of disaggregated suspensions from tumours showed reduced expression of PD-L1 in tumour treated with anti-PD-L1 at 24-hours post-treatment within both the MCA205 induced cancer population and CD45 immune when assessed compared to fluorescence minus one (FMO). These data are shown in Figure 3.29A and B, respectively. The expression of PD-L1 is also paramount as there have been previous studies that show many immune populations express PD-L1 including DCs, macrophages and T cells[189–191]. The reduction in PD-L1 expression was assessed by ANOVA with Tukey's post-hoc test. Twenty-four-hours post treatment, there was a significant decrease in the PD-L1 expression on CD45 cells for the aPD-L1 + Sham ($p<0.001$) and aPD-L1 + HIFU ($p<0.01$) groups relative to respective controls (Figure 3.29). Five-days post treatment there was a maintained reduction in the expression of the PD-L1 expression on the CD45 population (Figure 3.29D). Also, there was

a significant reduction in the PD-L1 expression ($p<0.01$) of the CD29+ selected tumour cells comparing the aPD-L1 + HIFU group to its respective Iso + HIFU control (Figure 3.29B). There is a large variability in the Isotype + HIFU group which could be related to the biology of those tumours. This may suggest that the aPD-L1 is having more of an impact on the immune population expression than that of the cancer cells. This may be related to the dosing of the drug within the tumour and requirement of vasculature of delivery throughout the tissue. Assessment of the tumours from the previous studies did not indicate high vascularisation which may be hindering the dosing of the antibody.

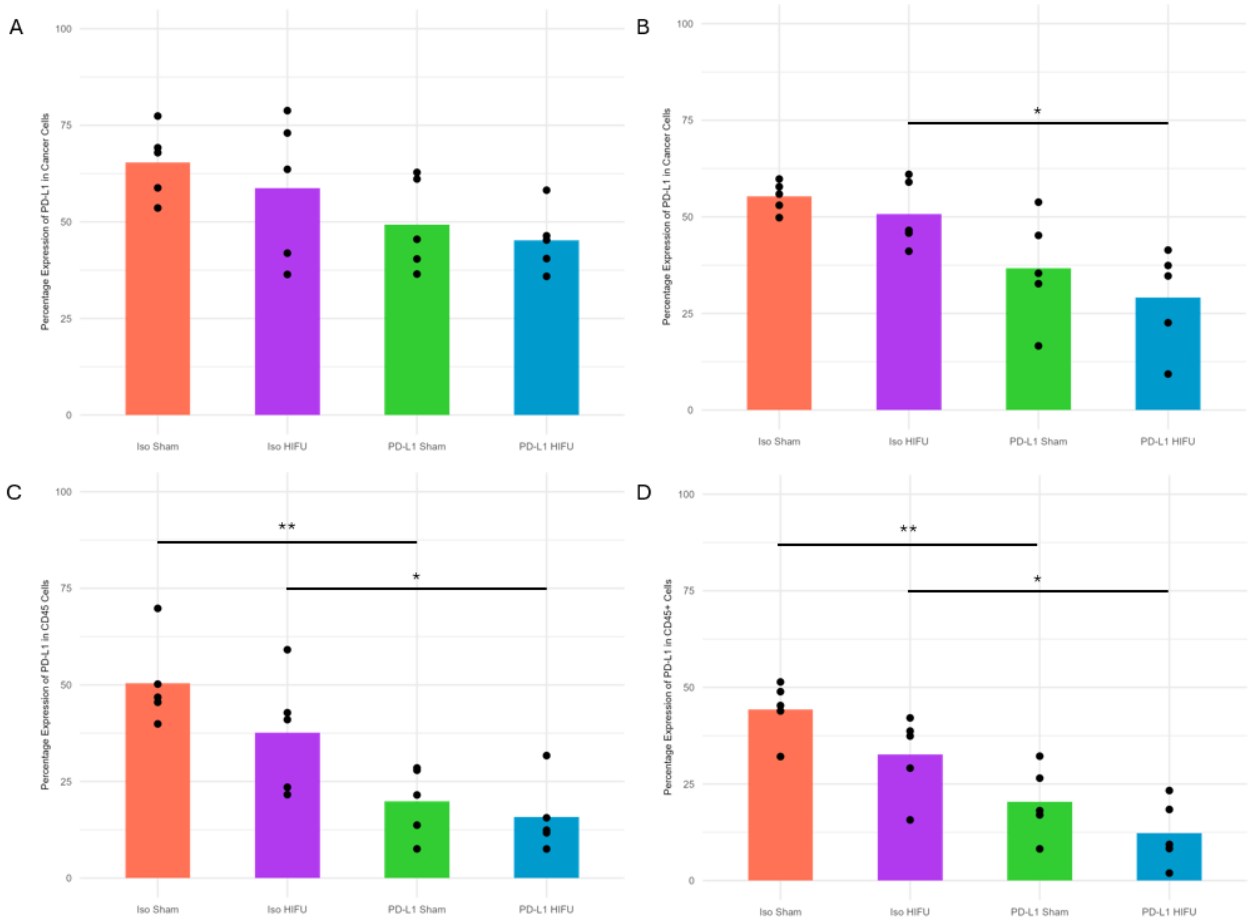


Figure 3.29: Representation of proportion of PD-L1+ cells from flow cytometry analysis as a percentage of (A and B) CD45-CD29+ cancer cells, or (C and D) CD45+ leukocytes when investigating the immune modulation of HIFU treatment combined with aPD-L1 immunotherapy 24-hours (A, C) and 5-days (B, D) post-treatment. Groups represented were Isotype Sham (Iso Sham, red, n= 6), Isotype HIFU (Iso HIFU, purple, n = 5), PD-L1 Sham (green, n = 5) and PD-L1 HIFU (blue, n = 5). ANOVA with Tukey's post hoc (adjusted P value) showed a significant reduction in PD-L1 expression 24-hours and 5-days after treatment in CD45 leukocytes in PD-L1 Sham ($p<0.01$) and PD-L1 HIFU ($p<0.05$) compared to respective Isotype controls. PD-L1 expression was significantly reduced 5-days after treatment in cancer cells in PD-L1 HIFU ($p<0.05$) compared to respective Isotype control.

To confirm ablation of these tumours, a representative sample was taken for histology to confirm the presence of thermal ablation indicators. This showed evidence of pyknosis as outlined in Figure 3.30A-B, which was not present in historic control (Figure 3.30C). Also, representative plots for the passive acoustic mapping which showed similar profiles of delivered cavitation energy between the two HIFU treated groups (Figure 3.30D).

A significant reduction ($p<0.01$) in the tumour volume fold change was seen 5-days after HIFU treatment in the 5-day treatment group in tumours treated with aPD-L1 antibody, was observed which was marginally improved by HIFU treatment (Figure 3.31A). Within the survival arm data, there was reduced tumour volume fold-change in the tumours that were treated with HIFU + aPD-L1 3-days after HIFU treatment (Figure 3.31B). There was not an increased incidence of ulceration with HIFU treatment (Figure 3.31C).

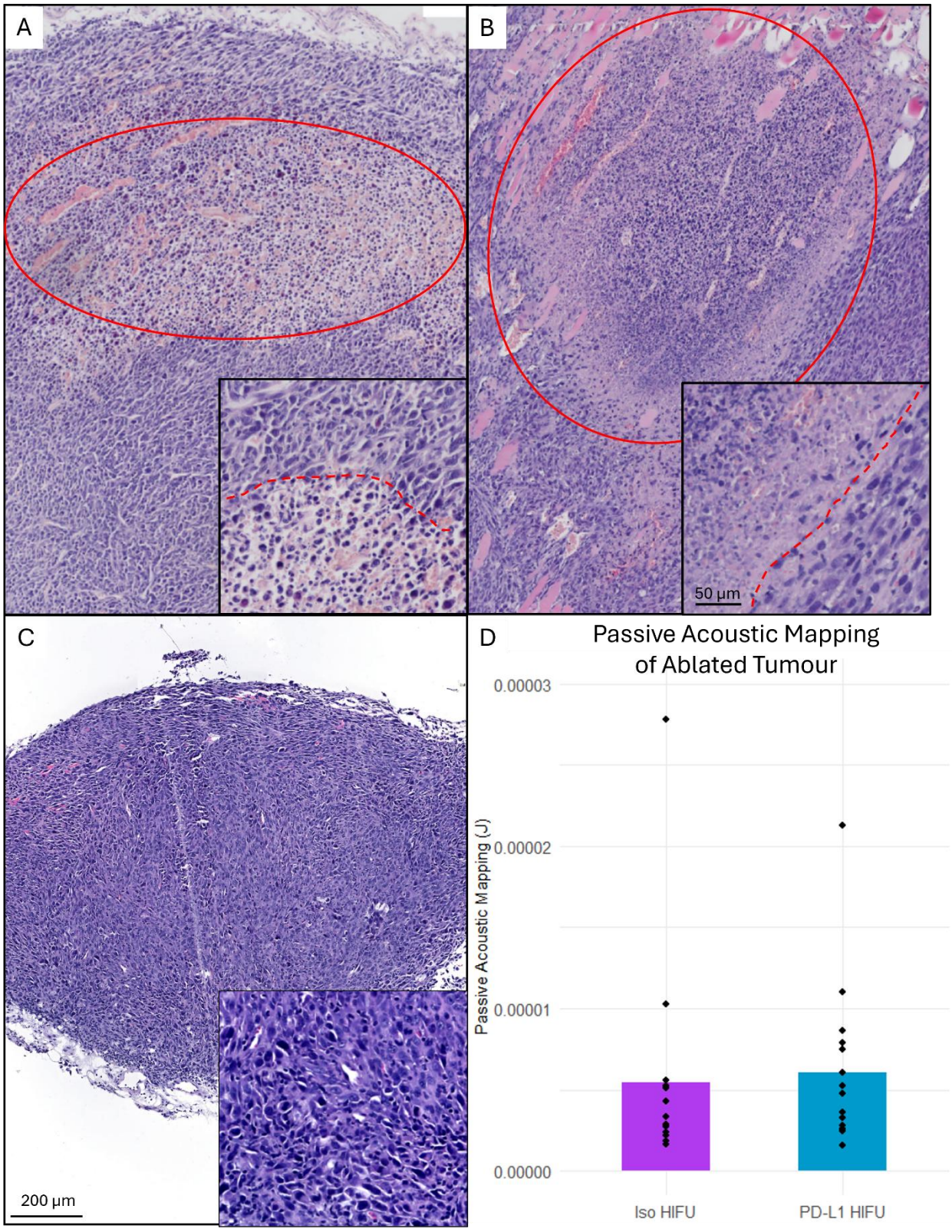


Figure 3.30: Representative haematoxylin and eosin (H&E) slides (5µm thick) of tumours (A-B) treated with HIFU parameters used within set-up and (C) historic control, culled at 24-hours. (D) Passive acoustic mapping energy determined by B-mode for assessment of cavitation energy delivered into the tumour, measured in joules (J) for the mice treated with HIFU in groups Isotype HIFU (Iso HIFU, purple, n = 15) and PD-L1 HIFU (blue, n = 15). Dotted red line indicates border of HIFU therapy.

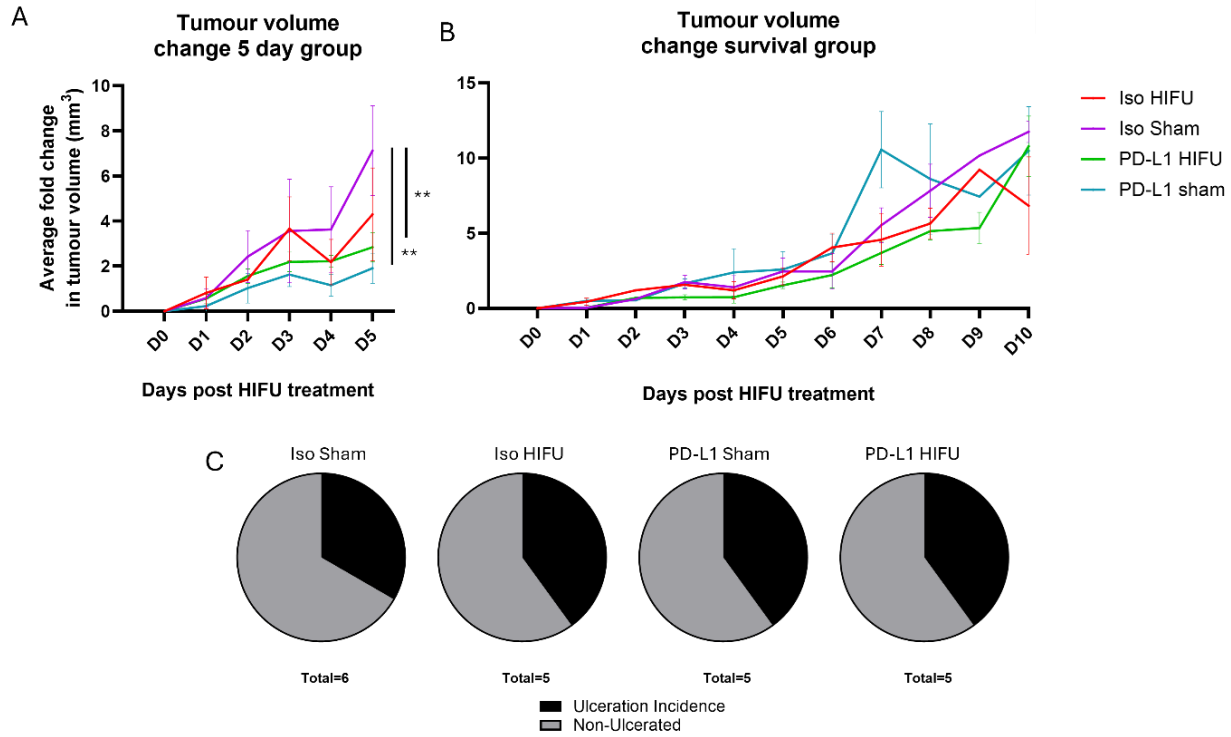


Figure 3.31: (A) Mean of the fold change of tumour volume from day of treatment with standard deviation of mice in the 5-day treatment arm. (B) Mean of the volume fold change of volume from day of treatment with standard deviation of mice treated of the survival arm, Isotype Sham (Iso Sham n = 6), Isotype HIFU (Iso HIFU n = 5), PD-L1 Sham (n = 5) and PD-L1 HIFU (n= 5). Two-way ANOVA with multiple comparisons (Tukey's post hoc test), the Sham PD-L1 and HIFU PD-L1 treatment showed significant (adjusted p value <0.01) decrease in the fold change 5-days after treatment in the 5-day treatment arm. (C) Representation of the incidence of tumour ulceration within the survival groups.

### 3.6.2 aPD-L1 reduced MHC-II expression on DCs, while dual treatment may have increased macrophage accumulation within the tumour

There was histological evidence of the impact of ultrasound treatment with the HIFU parameters applied (see Figure 3.30). This study aimed to assess the modulation of immunological populations in the tumour and lymph nodes at 24-hours and 5-days post-HIFU treatment. It was hypothesised that an increase would be triggered in myeloid populations and APCs within the tumours treated with HIFU. In addition, improvements in the level and antigen reactivity of CD8 T cell populations may be expected to be bolstered by aPD-L1 treatment, which would result in a robust immune response. An increase in APCs

within the dLN was expected with possible peripheral effects noticed within the blood. Previous research suggested a possible bottle neck to the treatment being the upregulation of the proportion of Tregs in the CD4 population (section 3.4.2 and 3.5.3). To assess the implications for antigen presentation to CD4 T cells, MHC-II expression was assessed on the APC within these tissues.

Firstly, the absolute number of myeloid populations, and proportion of MHC-II expression on APCs were assessed within the tumour (Figure 3.32). At 24-hours post HIFU-treatment, the monocyte population was increased in the aPD-L1 + Sham treatment group and the macrophage population showed increased number within the aPD-L1 + HIFU group, as shown in Figure 3.32D. These findings were not significant, however the previous study by Chida et al. reported increased TRAP+ cells (macrophages and DCs) in a sarcoma *in vivo* study after HIFU ablation[131]. The lack of statistical significance could be related to the variation in the abundance of this population within all treatment groups. Regardless it is suggested that antigen recognition and immune response priming was occuring[175]. These data also suggested an increased monocyte population within the tumours treated with aPD-L1 + Sham (Figure 3.32C). This could again suggest activation of the immune response, with monocytes primed to become APCs such as DCs and macrophages [172,192]. There was no pattern of modulation seen in the neutrophil population (Figure 3.32B) unlike previous HIFU treatments set out in section 3.4 and 3.5.

When assessing the immune response 5-days post treatment in the tumour (Figure 3.32H-N), there was no difference in the populations based on treatment group. When compared to the data from the 24-hour groups, there was a decrease in DCs and monocyte absolute numbers. There was not an increased number of macrophages (Figure 3.32H, J and K

respectively) in any of the groups. The comparison of the 24-hour and 5-days group suggested that there may have been an immune response to the isotype control antibody, which resolved after 5-days (Figure 3.32A-D compared to H-K). There was no modulation of the neutrophil population 5-days post-treatment (Figure 3.32I).

Assessment of the proportion of cells expressing MHC-II, a marker for antigen presentation, on APCs was conducted. This showed a significant ($p<0.05$) decrease in expression on DCs in tumours of mice that were treated with aPD-L1 when compared to those treated with isotype control, regardless of HIFU treatment at 24-hours (Figure 3.32I). Decreased MHC-II on DCs has been noted in tumour environments rich with IL-10[193] which may be a downstream response to the immunotherapy. Previous work in myeloma has reported dose dependent decreased MHC-II expression after aPD-L1 therapy[194] , which may be occurring here. Expression of MHC-II remained stable within other myeloid populations, regardless of treatment at 24-hours and 5-days post-treatment (Figure 3.32J-K, M-N). The exception being the aPD-L1 + Sham group which showed a slight but not significant continued reduction of MHC-II expression on DCs 5-days post treatment (Figure 3.32L).

Although there was a reduction in the DC MHC-II expression at 24-hours, there was no decrease in the total DC population within the tumour when compared between groups (Figure 3.32A and D). The change to the MHC-II expression in the DC population was not maintained 5-days post-treatment, suggesting a transient response to the treatment. This may be related to the migration of these APCs into the lymphatics. Assessment of the dLN myeloid populations was investigated to decipher this. However, it may be that the treatment only provided a brief immune response caused by the partial ablation, the antigen released was not sufficient to provide a sustained response.

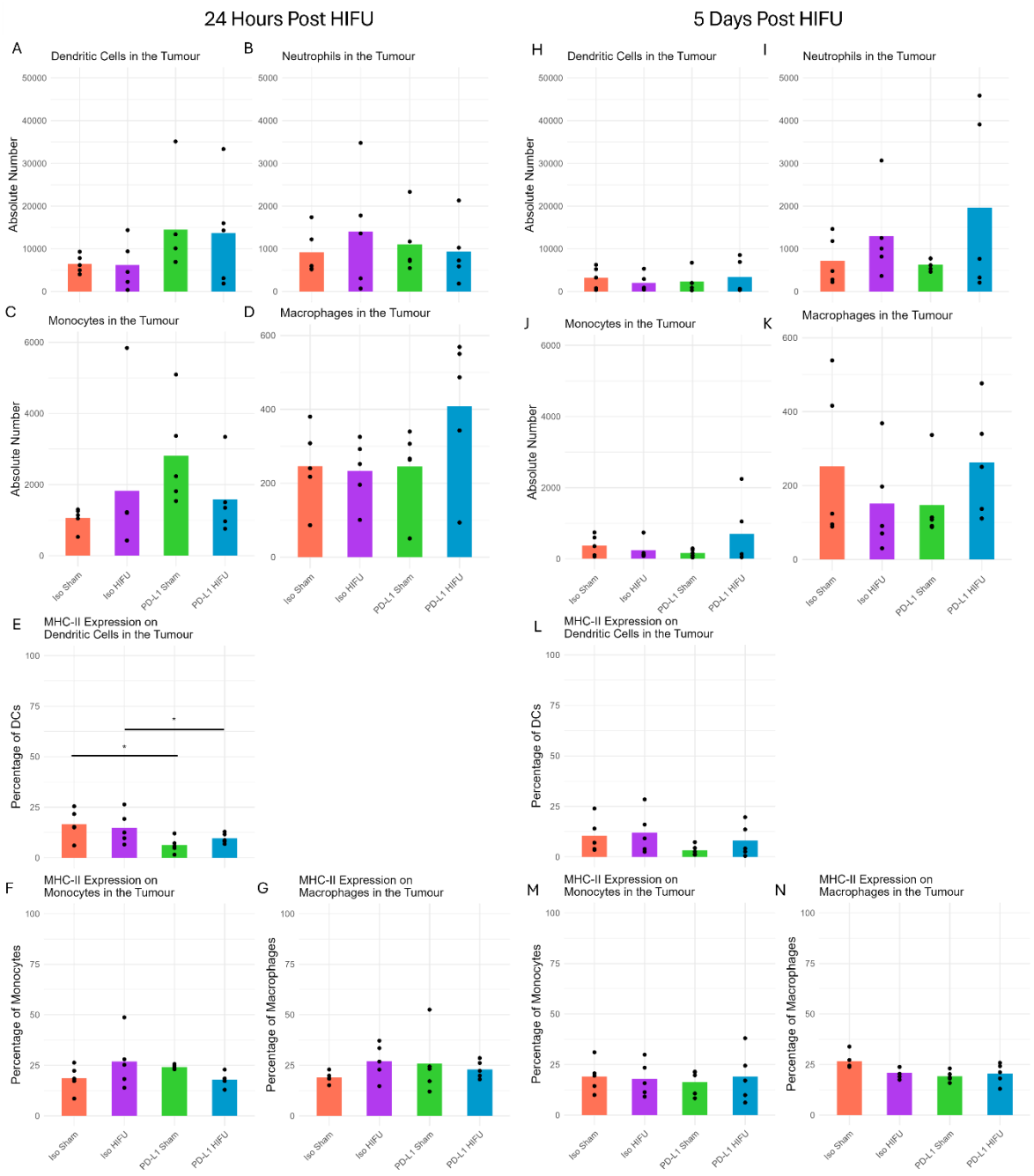


Figure 3.32: Representative plots of myeloid populations identified by flow cytometry in tumour of treatment groups for both timepoints were Isotype Sham (Iso Sham, red, n= 5), Isotype HIFU (Iso HIFU, purple, n = 5), PD-L1 Sham (green, n = 5) and PD-L1 HIFU (blue, n = 5) at 24-hours (A-G) and 5-days post-treatment (H-N). ANOVA with Tukey's post hoc test showed no significant differences in absolute population numbers. Included populations were assessed as absolute numbers dendritic cells (DCs, CD45+CD3-CD11b-CD11c+ in A and H) neutrophils (CD45+CD3-CD11b+CD11c-Ly6G+ in B and I), monocytes (CD45+CD3-CD11b+CD11c-Gr1-Ly6C+F4/80- in C and J), and macrophages (CD45+CD3-CD11b+CD11c-Gr1-Ly6C+F4/80+ in D and K) and percentages of these populations that expressed MHC-II included the DCs (E and L), monocytes (F and M), and macrophages (G and N). ANOVA with Tukey's post hoc test showed significant reduction in MHC-II expression on DCs at 24-hours post treatment in PD-L1 Sham (<0.05) and PD-L1 HIFU (<0.05) compared to respective controls.

### 3.6.3 There was suggested modulation of antigen presenting cells within the draining lymph node

The myeloid populations including macrophages and monocytes within the tumour showed a transient response to treatment. It was hypothesised that the myeloid populations may have migrated to the lymph nodes, causing an increase in the dLNs and thus the dLN was assessed by flow cytometry (gating strategy in Supplementary Figure 3.6) as shown in Figure 3.33. Along with this, the cLNs were assessed as internal controls for tumour specific immune responses as shown in Figure 3.34.

Assessment of the myeloid populations within the dLN showed an increase (2-fold) in DCs 24-hours after treatment within the aPD-L1 + HIFU group compared to Isotype + Sham in Figure 3.33A. Along with this, a higher proportion of the tumours treated with Isotype + HIFU had a higher abundance of DCs within the dLN (Figure 3.33A). However, these findings did not reach statistical significance. A larger proportion of the mice showed a higher abundance of macrophage and monocytes (Figure 3.33C and D) within these groups (Isotype + HIFU and aPD-L1 + HIFU) in the dLN. This would suggest an increased immune response favouring antigen recognition and presentation 24-hours after treatment with HIFU therapy. However, these data did not suggest that there is an improvement in these immune responses with the addition of aPD-L1 to HIFU.

The data suggested that 5-days after treatment (Figure 3.33H-K), these groups (Isotype + HIFU and aPD-L1 + HIFU) had a higher proportion of mice with lower DC populations within the dLN (Figure 3.33H). Assessment of the MHC-II expression on the DCs, macrophages and monocytes 5-days after treatment showed a slight decrease in abundance of MHC-II+ DCs (Figure 3.33L) in the aPD-L1 + HIFU therapy group which was not seen within this group at

the 24-hour time point. The abundance of this population decreased in the tumours of the aPD-L1 + Sham treated mice and the combination groups at 24-hours (Figure 3.33E). Hence the abundance of the DC population in the tumour and dLN could be related, but the absence of a reduction in this population in the dLN of the aPD-L1 + Sham group does not align with this interpretation. This may suggest that there is a transient response in the myeloid populations which may have affected the T cell populations. This made it pertinent to assess the T cell populations within the tumour and dLN.

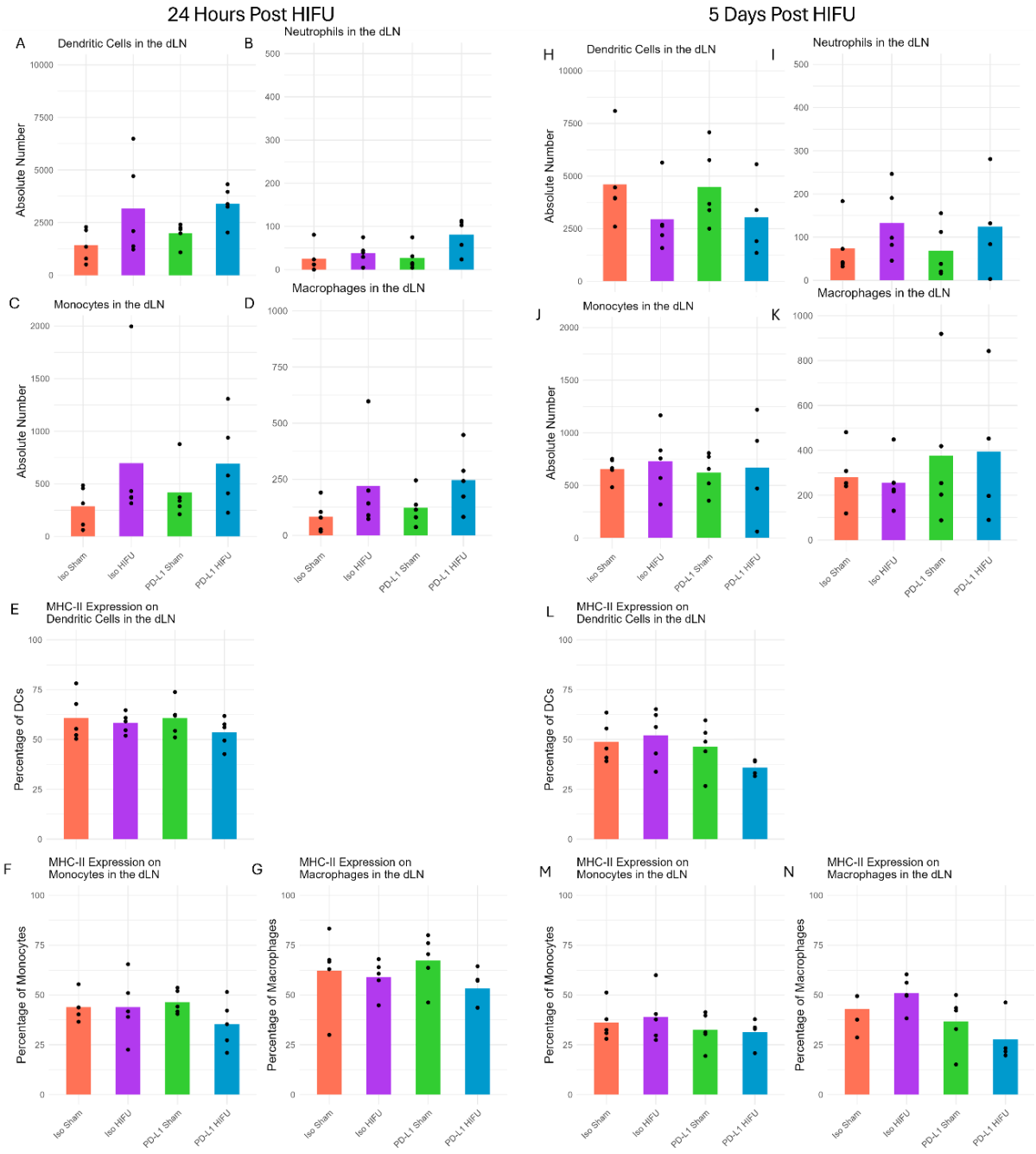


Figure 3.33: Representative plots of myeloid populations identified by flow cytometry in draining lymph nodes (dLN) of treatment groups for both timepoints were Isotype Sham (Iso Sham, red, n= 5), Isotype HIFU (Iso HIFU, purple, n = 5), aPD-L1 Sham (green, n = 5) and aPD-L1 HIFU (blue, 24-hr n = 5, 5-day n = 4 due to issue with flow cytometry staining) at 24-hours (A-G) and 5-days post-treatment (H-N). ANOVA with Tukey's post hoc test showed no significant differences in absolute population numbers. Included populations were assessed as absolute numbers dendritic cells (DCs, CD45+CD3-CD11b-CD11c+ in A and H) neutrophils (CD45+CD3-CD11b+CD11c-Ly6G+ in B and I), monocytes (CD45+CD3-CD11b+CD11c-Ly6G-Ly6C+F4/80- in C and J), and macrophages (CD45+CD3-CD11b+CD11c-Ly6G-Ly6C+F4/80+ in D and K) and percentages of these populations that expressed MHC-II included the DCs (E and L), monocytes (F and M), and macrophages (G and N). ANOVA with Tukey's post hoc test showed no significant differences between the groups.

When assessing the cLN as the internal control this study it was observed that these myeloid populations were vastly reduced when compared to the dLN (Figure 3.34). This suggests that there was antigen recognition of the tumours which involved activation of the myeloid populations within the dLN, which was to be expected. The data also suggested that there was a higher proportion of the mice with higher DC and macrophage populations within the cLN in the aPD-L1 + HIFU group at 24-hours compared (Figure 3.33A, D) to 5-days (Figure 3.33H, K), which may suggest an abscopal effect of the treatment caused by increased circulation of the antigen through the lymphatics and blood. Five-days after treatment there were no differences in the populations between the groups (Figure 3.33H-K). This supports the finding that there was a transient response to the tumour. The proportion of the DC, monocyte and macrophages which expressed MHC-II was variable within all groups, but there was no trend to suggest that there was a treatment related effect.

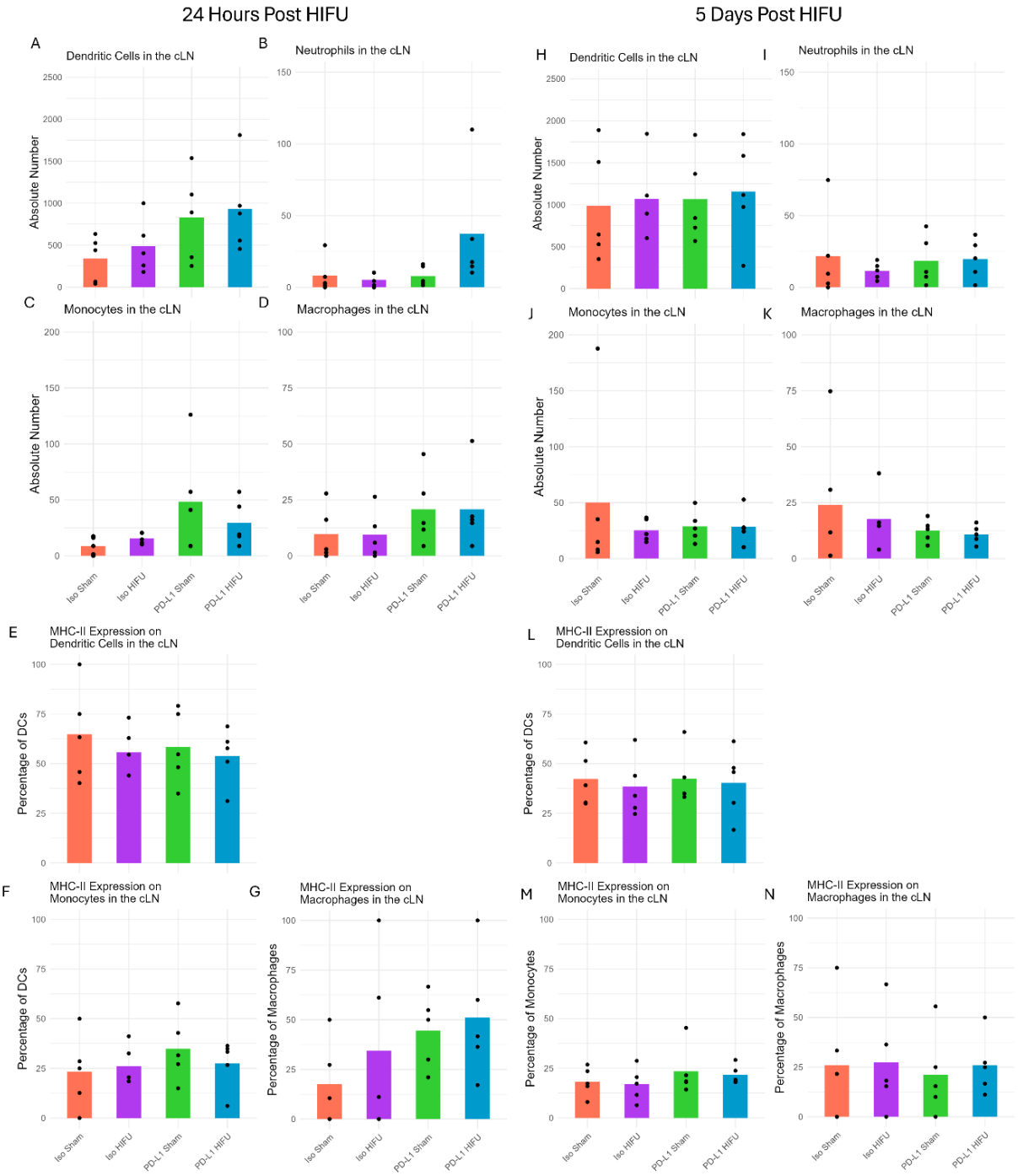


Figure 3.34: Representative plots of myeloid populations identified by flow cytometry in contralateral lymph nodes (cLN) of treatment groups for both timepoints were Isotype Sham (Iso Sham, red, n= 5), Isotype HIFU (Iso HIFU, purple, n = 5), PD-L1 Sham (green, n = 5) and PD-L1 HIFU (blue, 24-hr n = 5) at 24-hours (A-G) and 5-days post-treatment (H-N). ANOVA with Tukey's post hoc test showed no significant differences in absolute population numbers. Included populations were assessed as absolute numbers dendritic cells (DCs, CD45+CD3-CD11b-CD11c+ in A and H) neutrophils (CD45+CD3-CD11b+CD11c-Ly6G+ in B and I), monocytes (CD45+CD3-CD11b+CD11c-Ly6G-Ly6C+F4/80- in C and J), and macrophages (CD45+CD3-CD11b+CD11c-Ly6G-Ly6C+F4/80+ in D and K) and percentages of these populations that expressed MHC-II included the DCs (E and L), monocytes (F and M), and macrophages (G and N). ANOVA with Tukey's post hoc test showed no significant differences between the groups.

### 3.6.4 Assessment of the CD4 T cell populations did not show a robust change with HIFU or combination therapy in the tumour

To address the suggestion of upregulation of Treg populations within the dLN within previous studies in sections 3.4.2 and 3.5.3, it seemed pertinent to assess these populations within the tumour within this study. The suggestion was that the increase in Treg abundance within the dLN could be related to an increase in this population within the tumour, likely linked to antigen presentation. Although the latter point was not confirmed from the assessment of antigen presentation marker MHC-II within myeloid populations assessed in section 3.6.4, it was decided that it was still pertinent to phenotype the T cells populations from the treated tumour. The suggestion being that the addition of aPD-L1 therapy, would enable the CD8 population to have a less exhausted phenotype, and possibly expand. This may skew the Treg/CD8 ratio, reducing the regulatory phenotype.

Within the tumour, there was a large **proportion** of the CD4 cells that that were CD25+ or Tregs in the 24-hour group regardless of treatment as shown in Figure 3.35A. The data suggests stable populations, which is different to what was previously seen within the dLNs in section 3.5.3. 5-days after treatment, the Treg population was reduced regardless of treatment when compared to the frequencies in the 24-hour groups.

Assessment of absolute number of Tregs and CD4+CD25+ T cells within tumours suggested similar Treg populations 24-hours and 5-days after treatment across all the groups (Figure 3.35B, C, E, F), with a larger variability in these populations within all groups besides the Isotype + HIFU group. However, there was a propensity towards a lower absolute number of Treg and CD4+CD25+ cells within the Isotype + HIFU treated tumours compared to other groups at both 24-hours and 5-days but this was not significant. These populations were

marginally larger within the aPD-L1 + HIFU treated group at 24-hours, and larger again, 5-days after treatment. When CD4 population abundances within the tumour were assessed 5-days after treatment, the data presented in Figure 3.35D compared to Figure 3.35A suggested that there was a higher proportion of cells that were CD25+ at 5-days than at 24-hours post-treatment regardless of treatment. This may suggest a variability in the FoxP3 staining between the timepoints, which may have been due to the amount of tumour stained in each incidence. The absolute number of this population was also assessed as previously discussed. This may suggest an increase in Treg precursors which may suggest a regulatory phenotype. However, this could also be related to insufficient flow cytometry staining. Definitive conclusions are difficult to make about this data due to large within group variability.

CD8 populations were also assessed at 24-hours (Figure 3.35D-H) and 5-days (Figure 3.35L-P) after treatment in the tumour. With antigen presentation, regardless of Treg abundance, it was expected that there would be an increase in the overall CD8 infiltration into the tumour, with a skew in the population towards the Tcm phenotype as previously discussed (section 3.3.1 and 3.4.1). The data showed an increase in the absolute number of CD8 T cells in the aPD-L1 + HIFU treatment compared to all other groups 5-days post treatment. A mean of 20348±6782% in aPD-L1 + HIFU vs 10599±9045% in Isotype + Sham and 6631±8052% in Isotype + HIFU (Figure 3.35L). However, due to the spread of the data, this was not significant when tested by ANOVA. The proportion of the CD8 subpopulations did not show modulation within the tumour, regardless of treatment or timepoint (Figure 3.35E and M).

24 Hours Post HIFU

5 Days Post HIFU

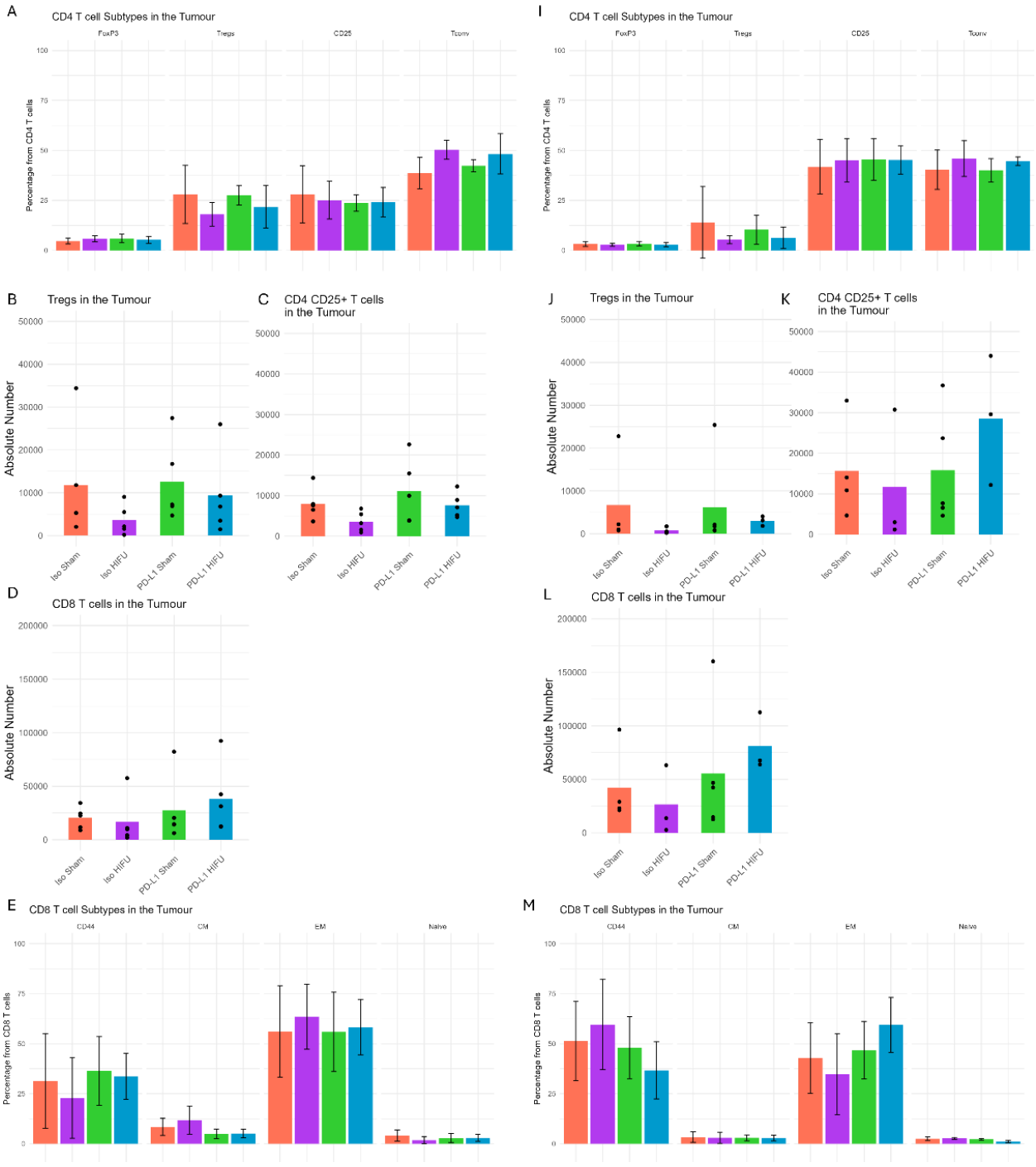

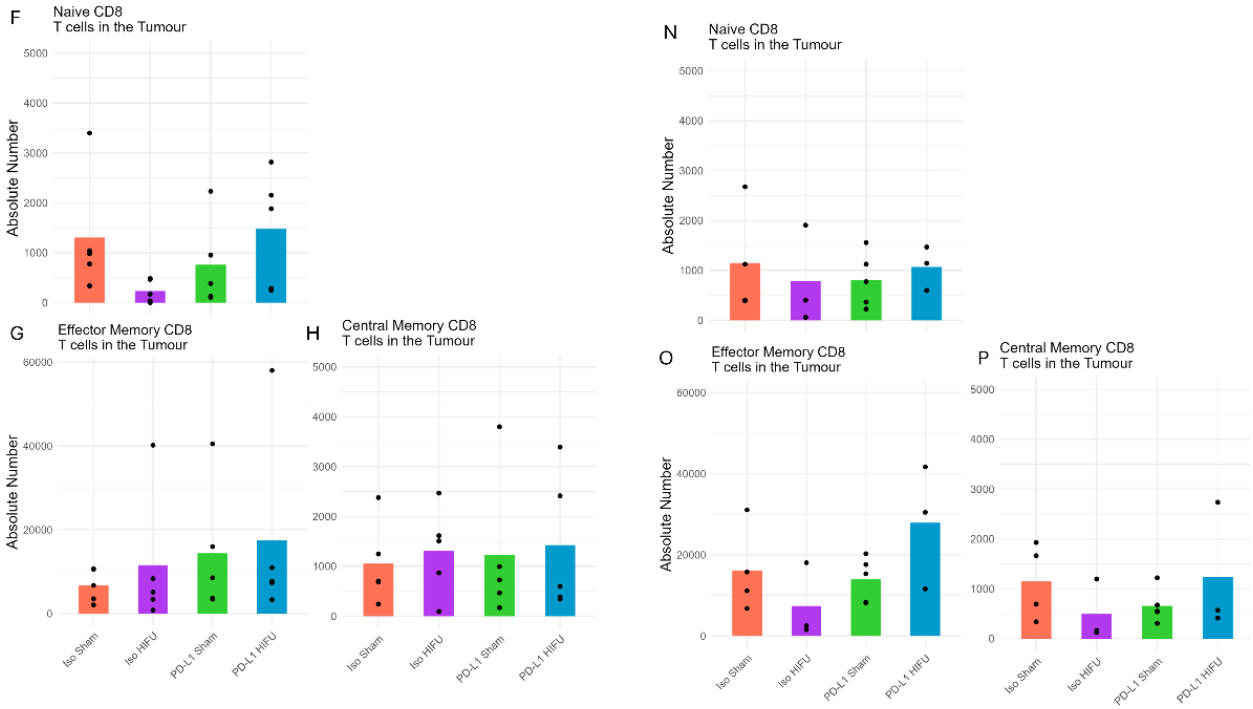


Figure 3.35: Representative plots of T cell subpopulations identified by flow cytometry in tumour of treatment groups at 24-hours (A-H) including Isotype Sham (Iso Sham, red, n= 5), Isotype HIFU (Iso HIFU, purple, n = 5), PD-L1 Sham (green, n = 5) and aPD-L1 HIFU (blue, 24-hr n = 5) and 5-days post-treatment (I-P) including Isotype Sham (Iso Sham, red, n= 4), Isotype HIFU (Iso HIFU, purple, n = 3), aPD-L1 Sham (green, n = 5) and aPD-L1 HIFU (blue, 24-hr n = 4), with reduced replicates at 5-days due to flow cytometry staining issue. ANOVA with Tukey's post hoc test showed no significant differences in absolute population numbers. The proportion of CD4 subpopulations were assessed at 24-hours (A) and 5-days (I), along with the absolute number CD4+ Tregs and CD4+CD25 T cells at 24-hours (B, C) and 5-days (J, K). CD8 absolute number was assessed based for both timepoints in D and L respectively, with proportions of subpopulations assessed in E and M respectively. The absolute number of the CD8 subpopulations were also assessed. These included Naïve CD8 T cells (Tnaive, CD62L+CD44- in F and N), effector memory CD8 T cells (Tem, CD62L-CD44+ in G and O), and central memory (Tcm, CD62L+CD44+, H and P). ANOVA with Tukey's post hoc test showed no significant differences between the groups.

Assessment of the absolute number of these populations suggested there was an increase in the Tem population 5-days post-treatment for the combination group for 2 of the 3 tumours assessed, in comparison to all other groups but this was not significant (Figure 3.35O). The Isotype + HIFU and PD-L1 + Sham groups did not show a partial response. This suggested that the HIFU treatment alone is not producing enough damage in this model to trigger an immune response. This may be because HIFU induced damage did not produce sustained antigen or because the DAMP theorised to be produced are not sufficient to overcome the exhausted and regulatory phenotype. It is perhaps only with the addition of the aPD-L1, which can reverse the exhaustion phenotype, that the HIFU treatment can have

the desired effect of an increased cytotoxic function. However, as shown by the growth data Figure 3.31, there is a slight response to the treatment in the form of stunted tumour growth. This stunted growth was observed in the aPD-L1 + HIFU treatment to possibly coincide with this increase in Tem, suggesting that the two findings may be linked and giving weight to each other.

### 3.6.5 Lack of distinct changes in lymph node T cell subsets upon treatment

The effects of the possible increased antigen presentation, indicated by the myeloid population changes, on the function of T cells previously assessed within **tumours** of these mice, was assessed by evaluating the T cell populations within the **dLN and cLN** from mice treated as previously described. The data shown in Figure 3.36 and Figure 3.37 outlines the modulation of CD4 and CD8 T cell populations for these treatment groups in the dLN with the cLN as an internal control. It was hypothesised that a similar CD4 phenotype, with increased Treg abundance would be seen within the dLN as in the tumour from mice whose tumour was treated with HIFU, as was described in the previous studies outlined in sections 3.4 and 3.5. It was further proposed that the addition of aPD-L1 treatment would reduce the regulatory environment of these tumours[150], as previously discussed. This effect on the Treg population was expected to be mirrored in the dLN, with reduced antigen activation of Tregs within the dLN being presented by a reduction in their numbers. PD-L1 has also been previously shown to affect the function of Treg migration into tumours via lymphatic migration[195].

Within the dLN there were no substantial changes in the proportion of the Treg population within the CD4 T cell population, 24-hours after treatment (Figure 3.36A). A slight, not

significant decrease in the Treg population at 5-days post-treatment was observed in the aPD-L1 + HIFU group compared to the Isotype + Sham and Isotype + HIFU groups (8.9±1.9% vs 12.5±3.2% vs 13.6±3.7%, $p>0.05$), as shown in (Figure 3.35I). However, there was no increase in the absolute number of Tregs within the treatment groups at either timepoint (Figure 3.35B and J). There was a large variability in the aPD-L1 + HIFU group, but this does not seem to account for there being no difference in the absolute number of cells.

When assessing the CD8 T cell population the absolute number was not affected by the treatment at either timepoint (Figure 3.35D and L). Assessment of the CD8 subpopulations showed large variation in the proportions of these cell types (Figure 3.35E and M). The absolute number of Tem and Tcm slightly increased 24-hours after treatment in aPD-L1 + Sham treated mice compared to the Isotype + Sham control, but this was not seen in the aPD-L1 + HIFU group (Figure 3.35G-H). This resolved by 5-days post treatment and the variability within the groups was large (Figure 3.35O and P). In the cLN there was no variability in the proportions of the CD4 and CD8 T cell subsets between the groups as shown in Figure 3.37. This argues that the small variations in these populations within the dLN were real effects and treatment related.

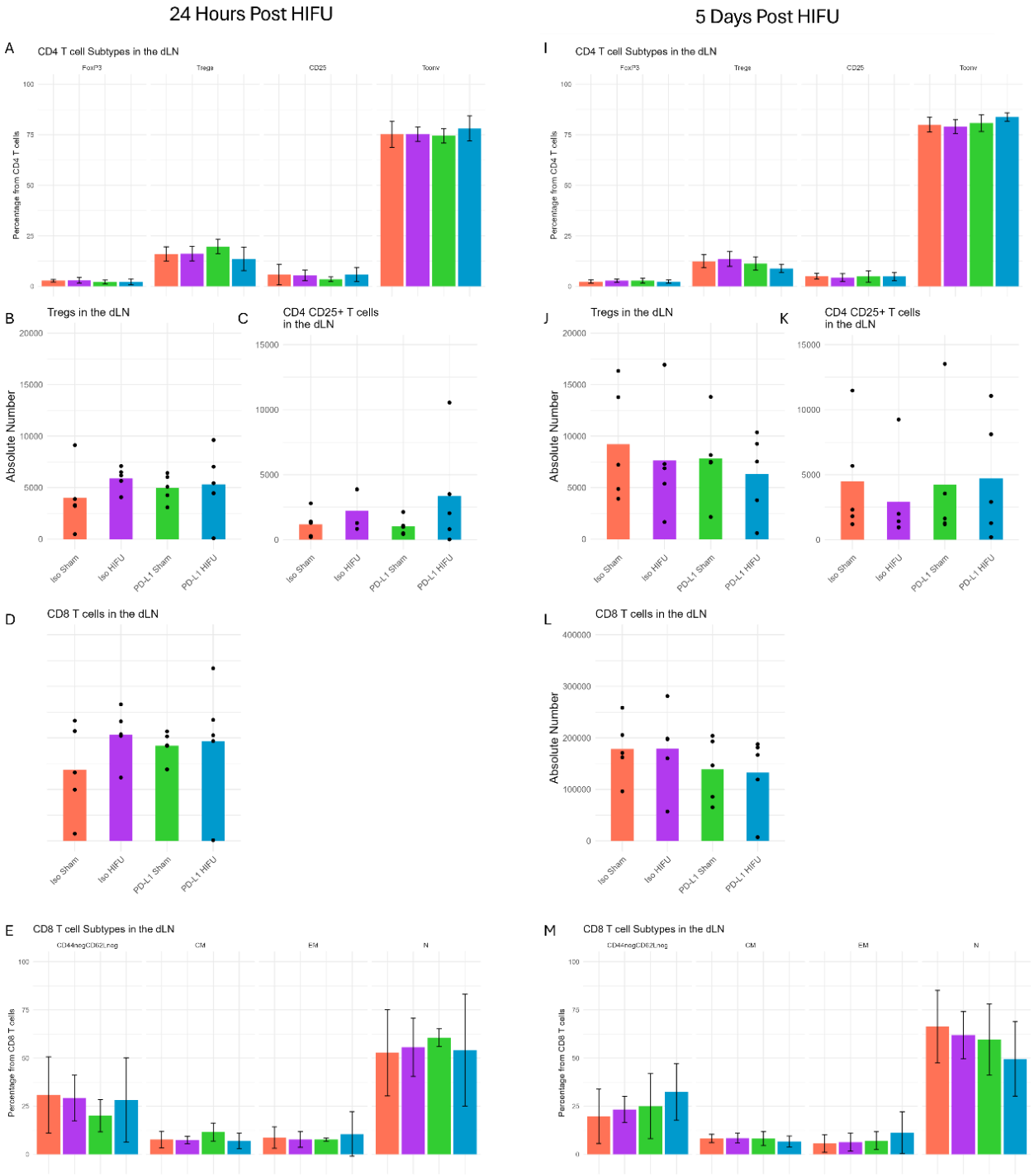
24 Hours Post HIFU
5 Days Post HIFU
A
CD4 T cell Subtypes in the dLN
FoxP3
Tregs
CD25
Tconv
Percentage from CD4 T cells
B
Tregs in the dLN
Absolute Number
C
CD4 CD25+ T cells in the dLN
D
CD8 T cells in the dLN
E
CD8 T cell Subtypes in the dLN
CD44negCD62Lneg
CM
EM
N
Percentage from CD8 T cells
I
J
K
L
M
Iso Sham
Iso HIFU
PD-L1 Sham
PD-L1 HIFU

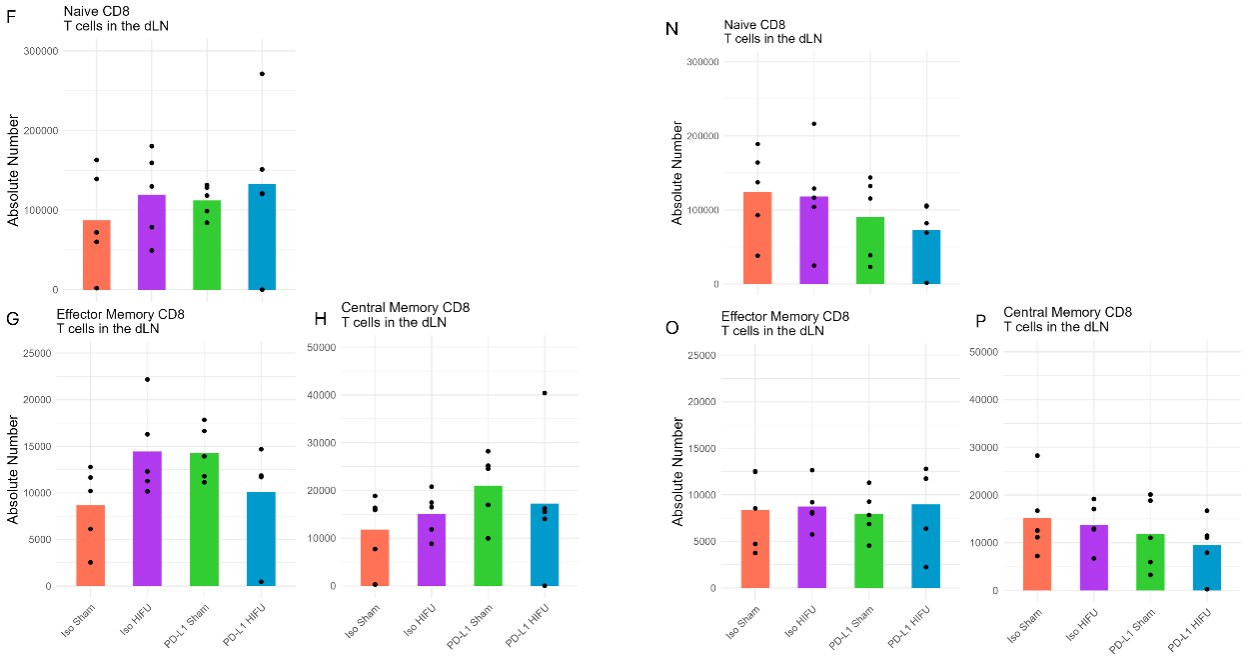


Figure 3.36: Representative plots of T cell subpopulations identified by flow cytometry in the draining lymph nodes (dLN) of treatment groups at 24-hours (A-H) and 5-days post-treatment (I-P). Groups included Isotype Sham (Iso Sham, red, n= 5), Isotype HIFU (Iso HIFU, purple, n = 5), PD-L1 Sham (green, n = 5) and PD-L1 HIFU (blue, 24-hr n = 5) and 5-days post-treatment ANOVA with Tukey's post hoc test showed no significant differences in absolute population numbers. The proportion of CD4 subpopulations were assessed at 24-hours (A) and 5-days (I), along with the absolute number CD4+ Tregs and CD4+CD25 T cells at 24-hours (B, C) and 5-days (J, K). CD8 absolute number was assessed based for both timepoints in D and L respectively, with proportions of subpopulations assessed in E and M respectively. The absolute number of the CD8 subpopulations were also assessed. These included Naïve CD8 T cells (Tnaive, CD62L+CD44- in F and N), effector memory CD8 T cells (Tem, CD62L-CD44+ in G and O), and central memory (Tcm, CD62L+CD44+, H and P). ANOVA with Tukey's post hoc test showed no significant differences between the groups.

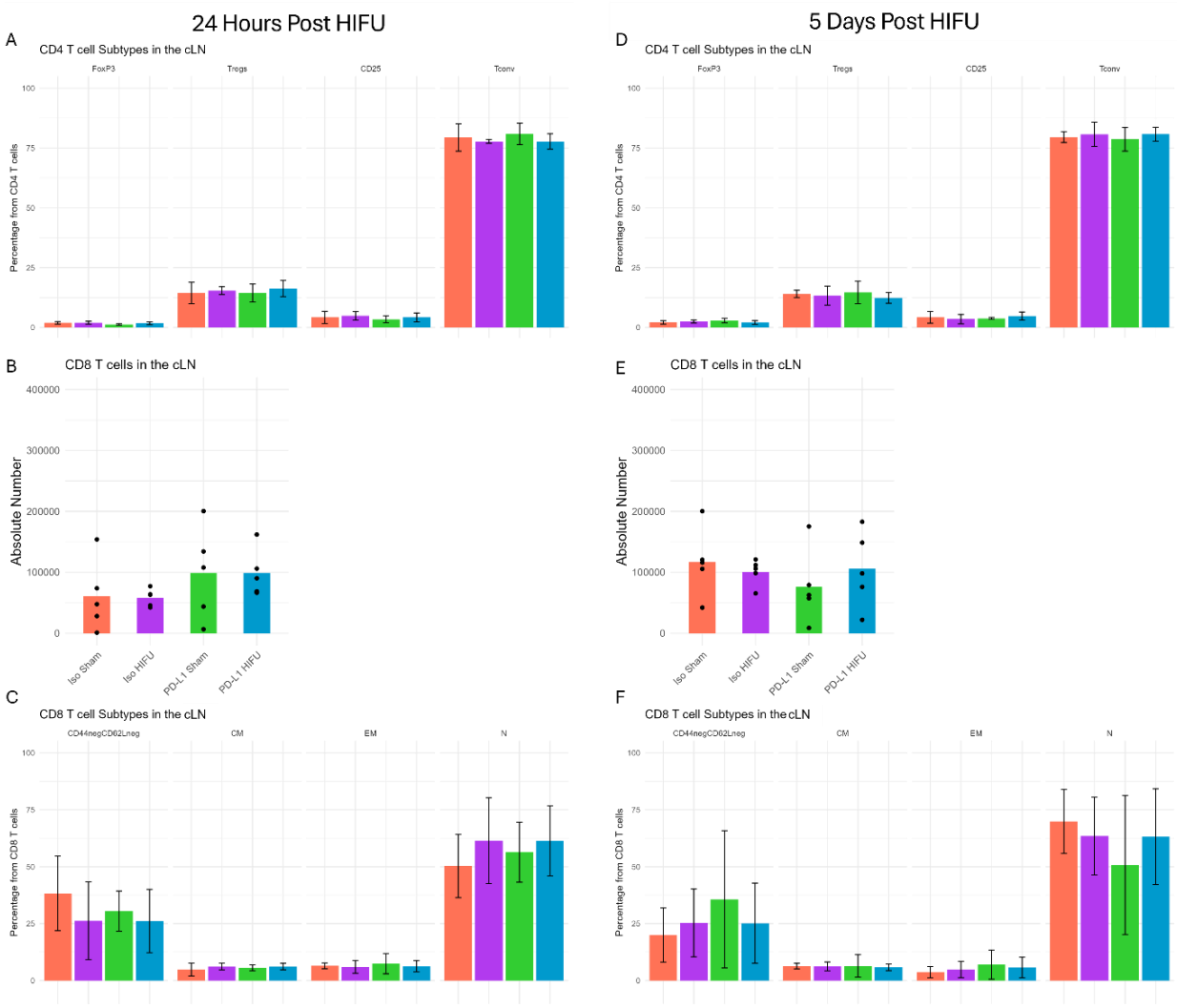


Figure 3.37: Representative plots of T cell subpopulations identified by flow cytometry in the contralateral lymph nodes (cLN) of treatment groups at 24-hours (A-C) and 5-days post-treatment (D-F). Groups included Isotype Sham (Iso Sham, red, n= 5), Isotype HIFU (Iso HIFU, purple, n = 5), PD-L1 Sham (green, n = 5) and PD-L1 HIFU (blue, 24-hr n = 5) and 5-days post-treatment ANOVA with Tukey's post hoc test showed no significant differences in absolute population numbers. The proportion of CD4 subpopulations were assessed at 24-hours (A) and 5-days (D). CD8 absolute number was assessed based for both timepoints in B and E respectively, with proportions of subpopulations assessed in C and F respectively. Error bars represent the standard deviation. ANOVA with Tukey's post hoc test showed no significant differences between the groups.

### 3.6.6 Summary of findings when treating murine fibrosarcoma with HIFU and or aPD-L1 immunotherapy

Changes in expression of MHC-II on APC populations within the tumour suggested that there was possible modulation in antigen presentation by tumour infiltrating DCs 24-hours post-treatment which resolved before 5-days post-treatment. There was evidence of modulation of the macrophage populations in the aPD-L1 + HIFU group, with the monocytes being

affected in the PD-L1 + Sham therapy group. MHC-II expression on other cell types was consistent between the groups. There was evidence of transient responses within the tumours, which suggested the need for repeated HIFU treatment as well as repeated aPD-L1 dosing. The Treg population within the tumour was not modulated in this study as it was in the previous studies which could have been related to the size of the tumours at treatment. This indicates that this treatment modality may have limited effect dependent on the size of the tumour and the area within the tumour that is treated.

A transient effect on the CD8 populations was observed within the dLN within this study which suggested that there was a transient effect on the antigen presentation and response to the tumour. There was not modulation of the Treg populations as previously seen (sections 3.4.2 and 3.5.3), so confirming that that the antigen activation of this population within the dLN was not confirmed.

The results were different to those of the previous experiments outlined in sections 3.4 and 3.5 which may relate to the starting size of the tumour affecting the outcome of the treatments. With larger tumour size there is a smaller proportion of the tumour being treated and theoretically more of a suppressive phenotype from the tumour which suppresses immune cell activation and proliferation such as PD-L1 expression[83,190]. Also, the vasculature will be supplying a much larger tumour volume, and the immune populations may be unable to infiltrate to the same proportion of the tumour cells.

## 3.7 Chapter discussion

In this chapter, an *in vivo* murine fibrosarcoma model was used to assess the ability of HIFU treatment to modulate the immune system and tumour growth. This was intended to provide information for future studies and to ultimately contribute to improved clinical outcomes.

Typically, after tissue damage, there is an inflammatory response which is followed by an adaptive immune response. Higher infiltration of CD45 cells are typically seen up to 5-days after injury of damage[196], with reports suggesting this inflammatory phenotype can continue until 3-days after injury[197], which leads into an immune response. Chemokines such as CCL2/CCR2 and CXCL12 are involved in the recruitment of immune cells into the area of damage[160]. The cell types that are typically first recruited are neutrophils. Following this, monocytes and macrophages[198] are recruited or monocytes mature into macrophages[162]. Dendritic cells migrate from the tissue into the dLNs[198], where they encounter and activate T cell populations for the immune response to tissue damage[160]. T cells are seen to peak at around 3 to 5-days post injury[196].

Typically, in an injury scenario the response of the migrating and activated immune cells would be aimed towards wound healing[196]. However, in the case of HIFU treated tumours where DAMPs and neoantigens (also referred to as tumour associated and tumour specific antigens) are released, previously reported, there are cytotoxic responses with increased CD8 T cell numbers and active function[23]. The DCs in this case are likely to be more mature with increased markers such as CD80/CD86 and MHC-II for improved recognition and downstream activation of the T cells in, linking the antigen presenting cells to the adaptive immune response within the dLNs.

Within these sets of experiments, it was possible to assess the CD4 subpopulations in MCA205 induced fibrosarcoma tumours. A high proportion (~34-35%) of the CD4 T cells within the tumour were identifies as Tregs. Also, upon HIFU treatment the proportion of Tregs within the dLNs increased in three of the treatment regimens used (see Figure 3.15 and Figure 3.26). However, this finding was not recapitulated in the follow-on experiment where the Isotype control + HIFU group showed no modulation of Treg abundance. This lack of internal consistency may relate to the different biological variations in tumours which occur with their development, and thus size for lack of a better way to quantify this.

Notably, when aPD-L1 was added to the HIFU regimen, a decrease in Treg was seen. When assessing the myeloid population within later experiments, there were increases in monocyte, macrophage and neutrophil populations 5-days after HIFU treatment, suggestingan inflammatory response. These data also suggested that increasing the ablation above a threshold may destroy the released antigen, limiting the potential for immune modulation. Assessing the MHC-II expression on the DC, monocyte and macrophage populations to try to address the modulation in Treg population, there was a decrease in the proportion of DCs expressing MHC-II after HIFU alone and in combination with aPD-L1 at 24-hours.

Assessment of the CD8 populations within these tumours highlighted that the most prevalent subpopulation within the tumour was Tem and within the dLN was Tcm. The proportions of the cells post-HIFU suggested increased abundance of Tcm within the dLN within initial studies suggesting an immune response 5-days after treatment, however the data from the follow-on study did not provide a clear picture of the modulation of these CD8 subpopulations.

In summary, the culmination of in vivo experiments led to the assessment of HIFU treatment in combination with aPD-L1 immunotherapy. This suggested that there was a trend to an increase in macrophage, DC, monocyte, Treg, and Tcm populations following treatment with HIFU alone which was not recapitulated when HIFU treatment was combined with aPD-L1, however, aPD-L1 therapy was able to reduce the tumour growth rate regardless of HIFU treatment. The limited response could have been related to the small ablation zone and regulatory phenotype of the tumour.

The **limitations** of this study were partly due to the tumour model:

- This model was aggressive and fast growing which meant that the number of mice required to maintain statistically significant results whilst balancing the welfare needs was difficult.
- There was large variability in the populations assessed which may have been resolved or better understood with the n number as initially planned rather than the number available after exclusion of mice with too large or too small tumours.
- Conducting this as a larger trial with larger model such as a rabbit, may provide better treatment opportunities which reduce the off-target side effects seen within the mice treated. A larger model may have allowed for whole tumour ablations or a larger proportion of the tumour to be treated without the issue of skin damage or ablation of normal tissue under the tumour.
- The assessment of the immune populations within the tumour by histology only provided a partial picture of the effects that the treatment had within the tumour.
- The partial ablation meant the histological slices produced did not always provide the clearest representation of the areas within tumours which were targeted for ablation.

Lost within this is the 3D structure of the tumour which includes the vasculature within and surrounding the tumour, along with the involvement of the lymphatic vessels which are interlinked to the lymph nodes.

- Tertiary lymphoid structures were not seen within the histological analysis but have a large role within the immune response to tumours.

**Future work** to further the assessment of the immune cell populations involved would be useful to include the NK cell interactions within these tumours as they may also provide insight into the immunological modulation caused by HIFU. Another avenue would be to assess the activation markers such as CD28 on the CD4 and CD8 populations along with CCR7, for lymph node migration potential assessment and Granzyme B for cytotoxic function. Further investigations into the expression of MHC-I and activation marker CD80 with robust testing of MHC-II on the myeloid cells over a wider timeframe may have provided information on when the antigen presentation was at its peak post-HIFU ablation to inform the timing of a potential secondary HIFU treatment and PD-L1 dosing. The immunotherapy could be expanded to include a blocking antibody for Treg abundance/activity within the tumours and bolster the cytotoxic function of CD8 T cells. The assessment of the TCR clones in blood, tumour dLNs and tumours for Tregs and CD8 populations would be of interest as a possible way to track the antigen release caused by the HIFU treatments. As discussed in section 3.4, it may have been pTregs that were within the tumour as well as thymic-derived Tregs.

# 4. Assessment of Immune Populations within Clinical Sarcoma Samples

## 4.1 Chapter Introduction

Chapter 3 described experiments which defined the impact of HIFU application to a sarcoma tumour model in mice. Tumour size and the infiltration of immune cells before and after treatment, were assessed. In these typically immune cold tumours[132,199] HIFU-driven increased macrophage and Treg infiltration into the tumour.

To relate these findings to the clinical situation, in this chapter, a transcriptomic assessment of differently infiltrated regions of clinical sarcoma samples was performed. Immune infiltrates and tissue surrounding these regions were sampled to investigate the effects that sarcoma tissue may have on the immune component. Also, it was postulated the study may provide information regarding the immunoregulatory phenotype within human sarcomas[68].

A range of immune infiltration is found in all types of cancer. It is well-recognised that the immune profile of tumours can influence the outcome of cancer treatment, including in sarcoma[80,200]. Main indicators include the Treg to CD8 ratio, CD8 infiltration and Treg infiltration into tumours has been linked to differences in treatment outcomes in various cancer types[147,151], including sarcoma[27,201]. Differences in the tumour microenvironment (TME) including vascularisation, suppressive signalling and regulatory pathways may mediate the changes in immune infiltration.

Sarcomas are typically associated with poor immune infiltration, however there is variation seen within this. Subtype categorisation of sarcoma is typically aligned with the levels of infiltration with T cells, B cells, and macrophages, although the relationships have yet to be

fully defined or agreed on. With consideration of the raft of new immunotherapy options (both drug and device based), understanding the differences between these subtypes may provide more informed choice of treatment options and ultimately improved outcomes.

For this study, **undifferentiated pleomorphic sarcoma** (**UPS**), which is typically identified by presence of spindle shaped cells and undifferentiated cells[202], was assessed. This subtype represents approximately 10% of all soft tissue sarcomas[203,204]. This tumour subtype is typically well infiltrated, particularly with CD8 T cells when compared to other sarcoma subtypes[26,61,148]. For comparison, **leiomyosarcoma (LMS)** was assessed, which has an incidence of 15-25% of soft tissue sarcomas[203,204]. The LMS type has been reported to have lower T cell, B cell and macrophage infiltration than UPS by Smolle et al[85]. These tumours have been reported to have variable immune infiltration but have previously also been associated with an 'immune desert' phenotype[26] with low levels of CD8 T cell infiltration[26,83]. One study did however find that a small subset (18.4%) of LMS samples within their cohort had an immune hot phenotype[205], and Dancsok et al reported high level of macrophage infiltration in their study[174]. Both UPS and LMS tumour subtypes typically present in areas near muscle. Also included within the study is an **uncategorised spindle cell sarcoma (USS),** which when assessed by immunohistochemistry (Section 4.4) had low immune infiltration. Its inclusion allows for the assessment of differences in tumour structure and infiltration, with this sample showing very low infiltration.

To date, most of the sarcoma research has been conducted on single cell analyses of large quantities of data from single cell databases. One such study was conducted by Petitprez et al. in 2020 whom used The Cancer Genome Atlas (TCGA) data to categorise sarcoma based on infiltration and vascularisation status. They indicated association of these groups with

sarcoma subtype[26]. Although this work focused on B cells, it demonstrated that higher infiltration was associated with poorer progression free survival and tumour volume reductions with treatment. The analysis is however limited by lack of spatial correlation, which may influence the understanding of mechanisms affecting the infiltration.

On the other hand, interesting histological studies have been conducted to probe macrophage infiltration and polarisation. Dancsok et al. (2020) assessed the effects these factors have on survival in 1242 sarcoma patients. The effects of regulatory macrophages and proinflammatory macrophages was highlighted. These cells infiltrate to different levels depending on tumour subtypes and influence outcomes[174]. Macrophage polarisation has been linked to the downstream activation of lymphocytes in other studies[68]. These studies use tissue microarrays (TMAs) which lack the spatial context and may not be as accurately representative of the tumour microenvironment. Although the study by Dancsok looked to evaluate resulting differences within the tumour, it is limited to including M1 and M2 macrophages but neglecting all other immune cell types. Within this work, proportions of macrophages within immune cells were identified based on H&E rather than a CD45 stain.

Spatial transcriptomic platforms allow for biobanked formalin fixed paraffin embedded (FFPE) samples to be evaluated. The technique employs and combines tissue morphology and RNA assessment. Here, Nanostring GeoMx Digital Spatial Profiling platform has been used, which allows for specific areas of tissue to be targeted and the transcriptome to be evaluated[206–208]. In the case of this study, GeoMx-based spatial tissue analysis allowed comparison of different compartments of sarcoma tumours to be performed. This includes the peritumour, tumour border and central tumour locations across several subtypes. As detailed above there is a tenuous consensus on the link between subtype and immune

infiltration. Thus, the analysis sought to determine if and to what level infiltration as well as sampled location within the tumour correlates to cancer subtype.

## 4.2 Chapter Hypothesis and Aims

### Hypothesis

Tumour heterogeneity aside, soft tissue sarcoma tumours have varying immune infiltration based on their subtype and thus will have different transcriptomic landscapes. The differences in immune abundance will be associated with the expression profiles of the subtype of sarcoma tumour tissues. The lowly immune infiltrated LMS tumour type will have lower or spatially distinct expression of cytotoxic CD8 T cell genes, and the reduced cytotoxic effects of the immune cell types will be indicated in the transcriptome of these tissues and with additional knock on effects to the transcriptome.

### Aims

i. Assess transcriptomic profiles of immune infiltrated areas, comparing sarcoma types, and locations within tumours to identify factors which may correlate to variations in immune abundance.
ii. Investigate the immune populations and immediate surrounding tumour microenvironment transcriptome for regulatory and activation phenotypes.
iii. Investigate the mode of action for cells moving into the tumour tissue including signalling, vascularisation, and migration-associated pathways.

## 4.3 Overview of Samples

The table below (Table 4.1) outlined the 6 clinical sarcoma samples that were used in this spatial transcriptomics study. Samples were obtained from Oxford Radcliffe Biobank (ORC) via Oxford Centre for Histopathology Research (OCHRe). Patients mean age was 62 with samples obtained from both male and female patients. There was a range of treatment within the LMS samples including recent radiotherapy, chemotherapy and treatment naive. The USS tumour was treated with radiotherapy. The single UPS tumour analysed was treatment naïve.

Table 4.1: Patient characteristic of clinical sarcoma samples. The tumour grade in accordance with FNCLCC guidelines with tumour type reported by pathologist. Treatment as reported as described above.

| ID | Gender | Age | Tumour Type | Grade | Location | Previous treatment and date |
|---|---|---|---|---|---|---|
| H201064 | Male | 47 | Undifferentiated Pleomorphic Sarcoma | 3 | Right thigh | Naïve |
| H202415 | Female | 58 | Leiomyosarcoma | 2 | Retroperitoneum | Naïve |
| H203557 | Male | 80 | Leiomyosarcoma | 2 | Right medial thigh | Neoadjuvant radiotherapy 50Gy in 25 cycle, 1 month prior |
| 10481/21 | Female | 44 | Leiomyosarcoma | High | Pelvic mass | Previous and current chemotherapy |
| H210024 | Female | 72 | Uncategorised Spindle Cell Sarcoma | High | Left posterior thigh | Neoadjuvant radiotherapy 50Gy in 25 cycles, 2 months prior |
| H214439 | Female | 69 | Leiomyosarcoma | High | Left abdominal wall | Naïve |

## 4.4 Identification of CD45 and CD8 clusters within these tissues

It was possible to do a limited histological assessment of select immune populations within the sarcoma tissue. Firstly, to review the tissue architecture of the sarcoma samples, a haematoxylin and eosin (H&E) stain. Histological assessment demonstrated stark differences in the structure of the tumour and tumour capsid between individual tumours and subtypes. Figure 4.1A was a section taken from the UPS tumour. The structure of the tumour shows close contact of the cells which demonstrate similar morphology. In comparison, the USS section (Figure 4.1B) shows sparse cells with varying morphology. Within the LMS type, the H&E sections (Figure 4.1C to F), there are elongated, striated cells (top right of Figure 4.1C, see arrow) akin to resemblance of smooth muscle, there was some variation in these structures, this may be related to the plane on which the tissue was cut or the location from which the tumour was resected. Sample 1048121 (Figure 4.1E) was reported as an abdominal mass, thus it may have not been embedded within the muscle itself.

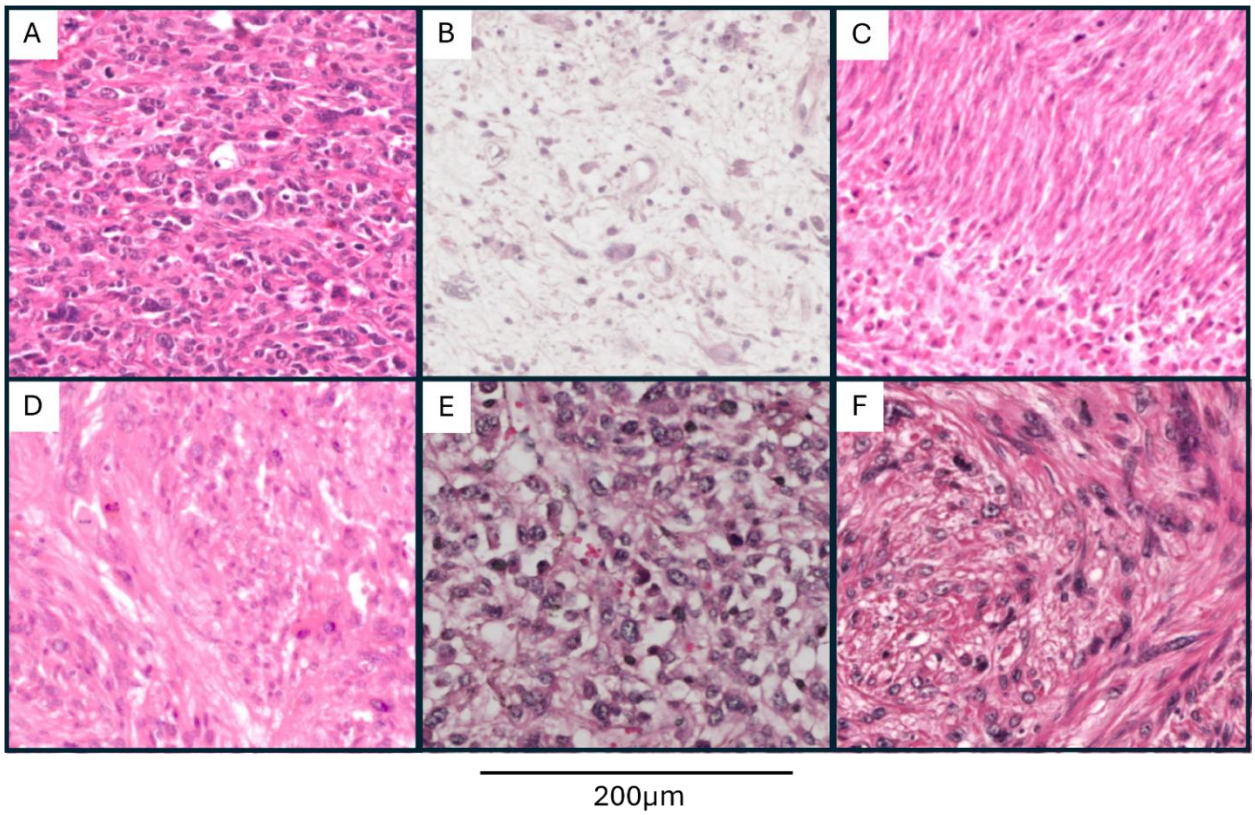


Figure 4.1: Haematoxylin and eosin (H&E) staining of sarcoma tissue (A) H201064 (UPS), (B) H210024 (USS), (C) H202415 (LMS), (D) H214439 (LMS), (E) 1048121 (LMS), (F) H203557 (LMS).

Immunohistochemistry staining (IHC) (see methods Section 2.4) was used to identify immune infiltration into the tumours. Clusters of CD45 cells are shown in Figure 4.2. Within these tissues it was possible to see clusters of these cells ranging in their abundance. As can be seen in Figure 4.2 A and B, the USS had quite dense clusters of these CD45 cells when compared to some of the LMS samples shown in Figure 4.2 D to F. The LMS samples seem to have varied infiltration of CD45 positive cells within the same tissue. Figure 4.2 C showed a large cluster of cells, within an area that has a much lower density whilst 4.2 E, appears to lack this density. Evaluation of the CD8 infiltration (Figure 4.3) indicated a similar variation in the abundance of these cells within each of the LMS tumours. CD8 cells (Figure 4.3) were represented throughput the tissue in all tumours, but with some areas showing intense clustered staining and other areas showing more widely spread and diffuse staining (e.g.

panel E vs panel F). Analysis of CD68+ macrophages was not possible due to unspecific peroxidase staining (Figure 4.4).

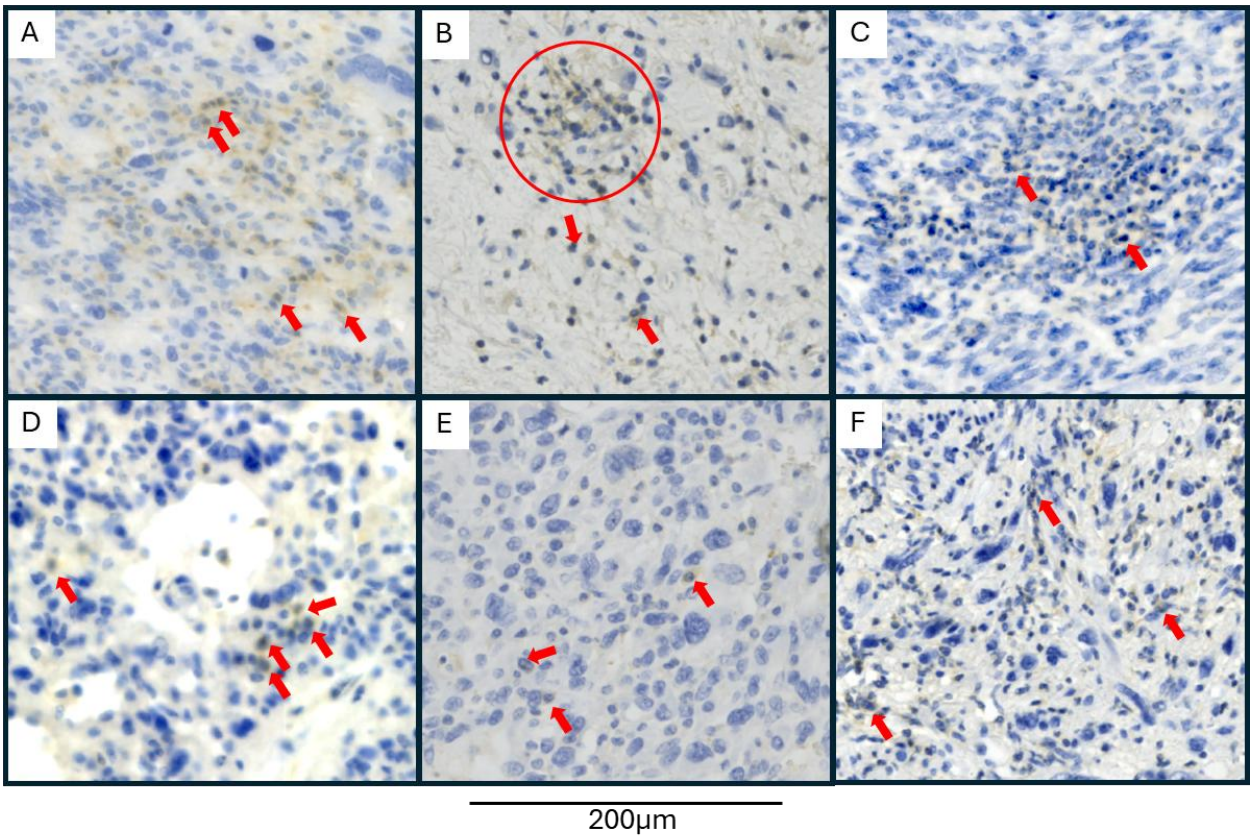


Figure 4.2: Immunohistochemistry staining of CD45 with DAB (brown) with hemotoxin nuclei stain (blue) of sarcoma tissue (A) H201064 (UPS), (B) H210024 (USS), (C) H202415 (LMS), (D) H214439 (LMS), (E) 1048121 (LMS), (F) H203557 (LMS). The red arrows and red circle indicate representative positive CD45+ staining (brown) for each tumour, indicative of leukocytes.

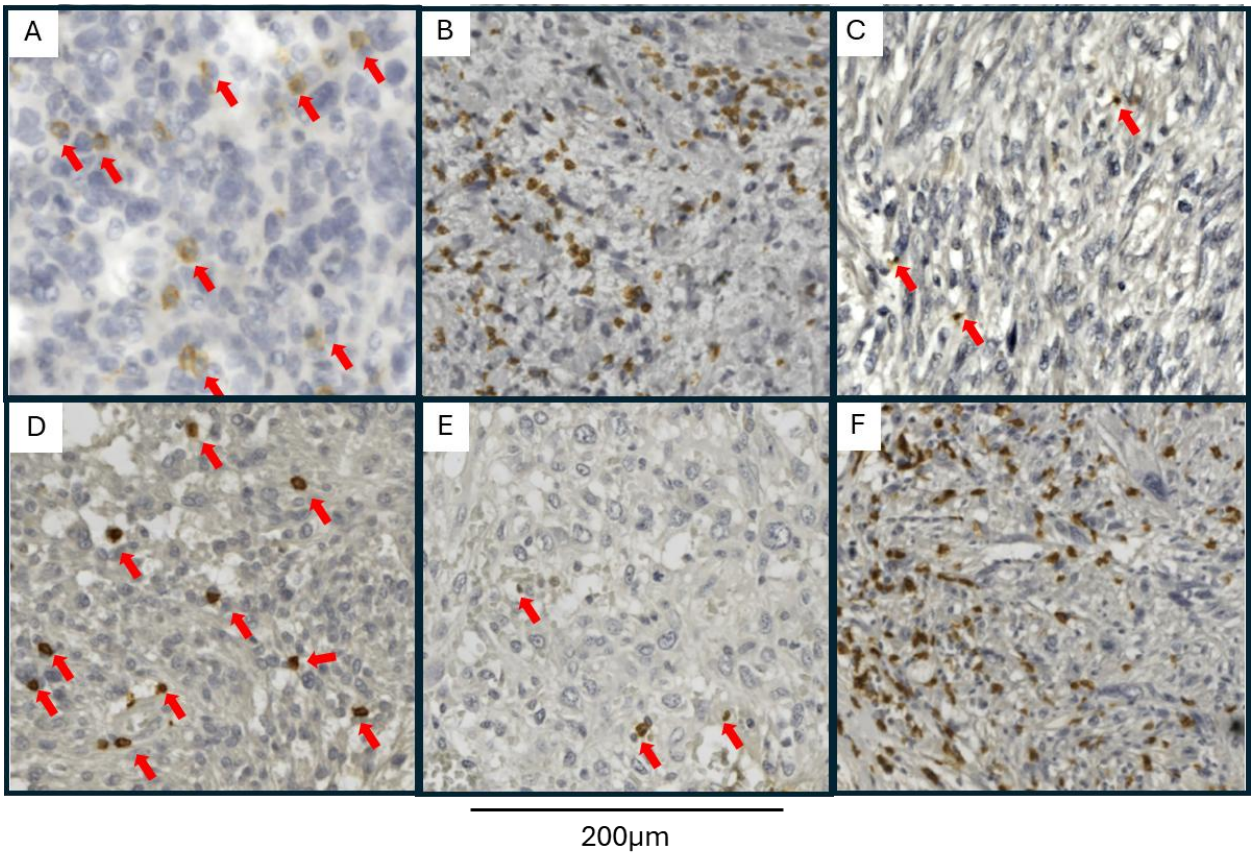


Figure 4.3: Immunohistochemistry staining of CD8 with DAB (brown) with hemotoxin nuclei stain (blue) of sarcoma tissue. (A) H201064 (UPS), (B) H210024 (USS), (C) H202415 (LMS), (D) H214439 (LMS), (E) 1048121 (LMS), (F) H203557 (LMS). The red arrows indicate representative positive CD8+ staining for each tumour, indicative of CD8+ T cells.

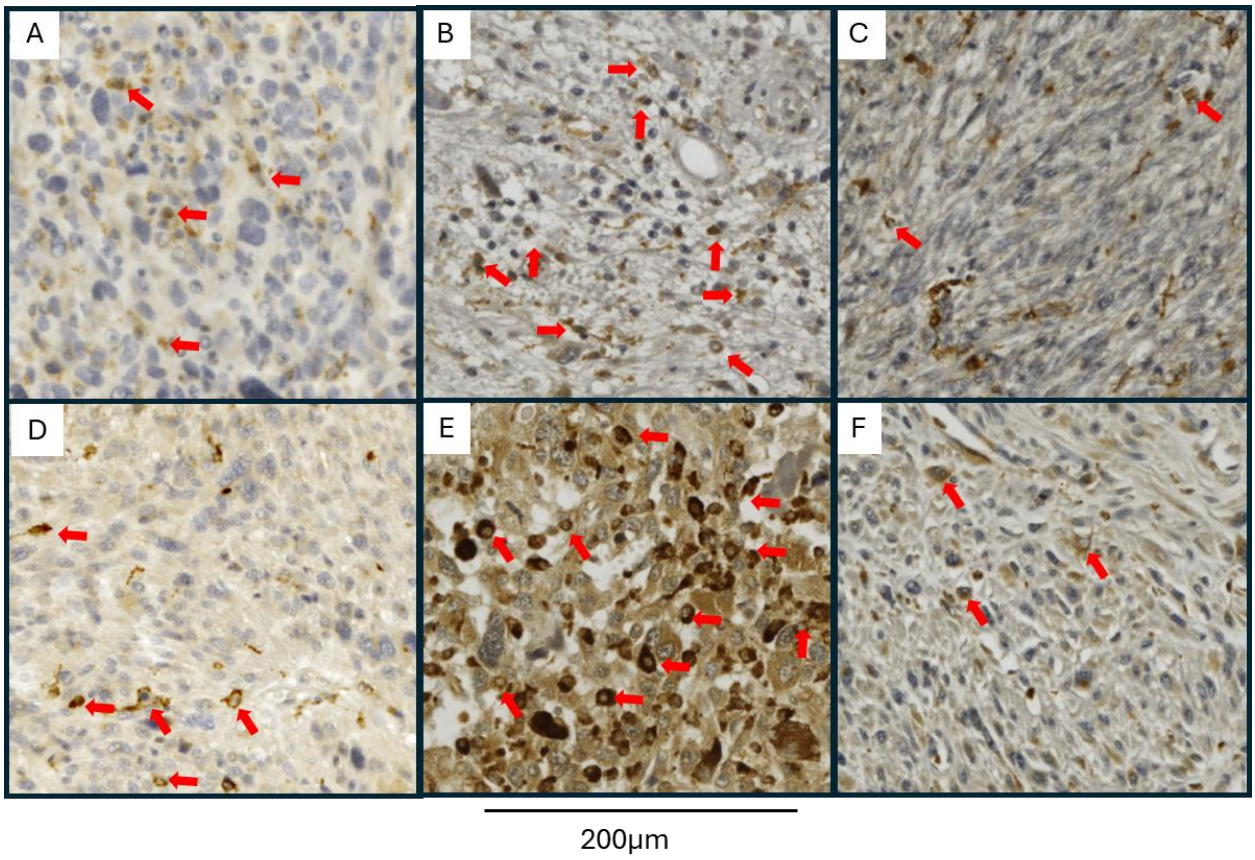


Figure 4.4: Immunohistochemistry staining of CD68 with DAB (brown) with hemotoxin nuclei stain (blue) of sarcoma tissue. (A) H201064 (UPS), (B) H210024 (USS), (C) H202415 (LMS), (D) H214439 (LMS), (E) 1048121 (LMS), (F) H203557 (LMS). The red arrows indicate representative positive CD68+ staining for each tumour, indicative of a macrophage population. Some unspecific staining prevalent in all tissues, E has strong unspecific staining.

This descriptive analysis confirmed that CD45+ leukocyte and CD8+ T cell populations are present to some degree within all the analysed tumour subtypes. These IHC studies suggest that there were differences in the immune infiltration between sarcoma subtypes, within the same subtype, and within the same tumour as shown in Figure 4.3 and Figure 4.4. There are extensive reports in the literature profiling multiple immune cells in sarcoma[27,83,86]. T cell populations in STS tumours have been identified as key factors in prognosis[134,201]. Recent studies are focusing on the structures of tissues surrounding CD8+ T cells and the effect this has on the function of these infiltrates[209–211]. The analyses discussed in this chapter will focus on CD8+ T cells as the primary infiltrate of interest. The rationale being that CD45 expression was shared among all leukocyte populations. CD8+ T cells have less

heterogeneous populations, in contrast to CD4+ T cells with Tregs and T helper cells, or macrophages with their M1 and M2 phenotypes. CD8+ T cells implicitly have an antitumour function[61,151,209] which makes their transcriptomic profile, and that of the surrounding tissue, of interest.

Investigating the transcriptomic profile of the immediately adjacent microenvironment of these immune cells within this UPS tumour and to compare to the 'non-immunogenic' LMS samples was thought to give information on the difference in the mechanisms behind their infiltration and function which may be used in future treatments.

Analysis of resected sarcoma was performed using a bulk transcriptomic approach (GeoMx DSP, Nanostring) as outlined in section 2.6. An overview of the tissue sections selected for this analysis stained using immunofluorescence (IF) can be seen in Figure 4.5. Regions of interest (ROIs) were selected along the tumour border, central tumour or peritumour where available. Areas were selected based on the CD45 and CD8 IF staining. Immune infiltration stratification into high and low was decided based on IF staining when ROI selection was completed and reviewed before analysis. The rationale for selection was shown in Figure 4.6, demonstrating a selection of the ROIs with their labels. The organisation tree (Figure 4.7) outlines how the tumours were sampled and allow for these areas to be compared within the same tissue and across the tissues.

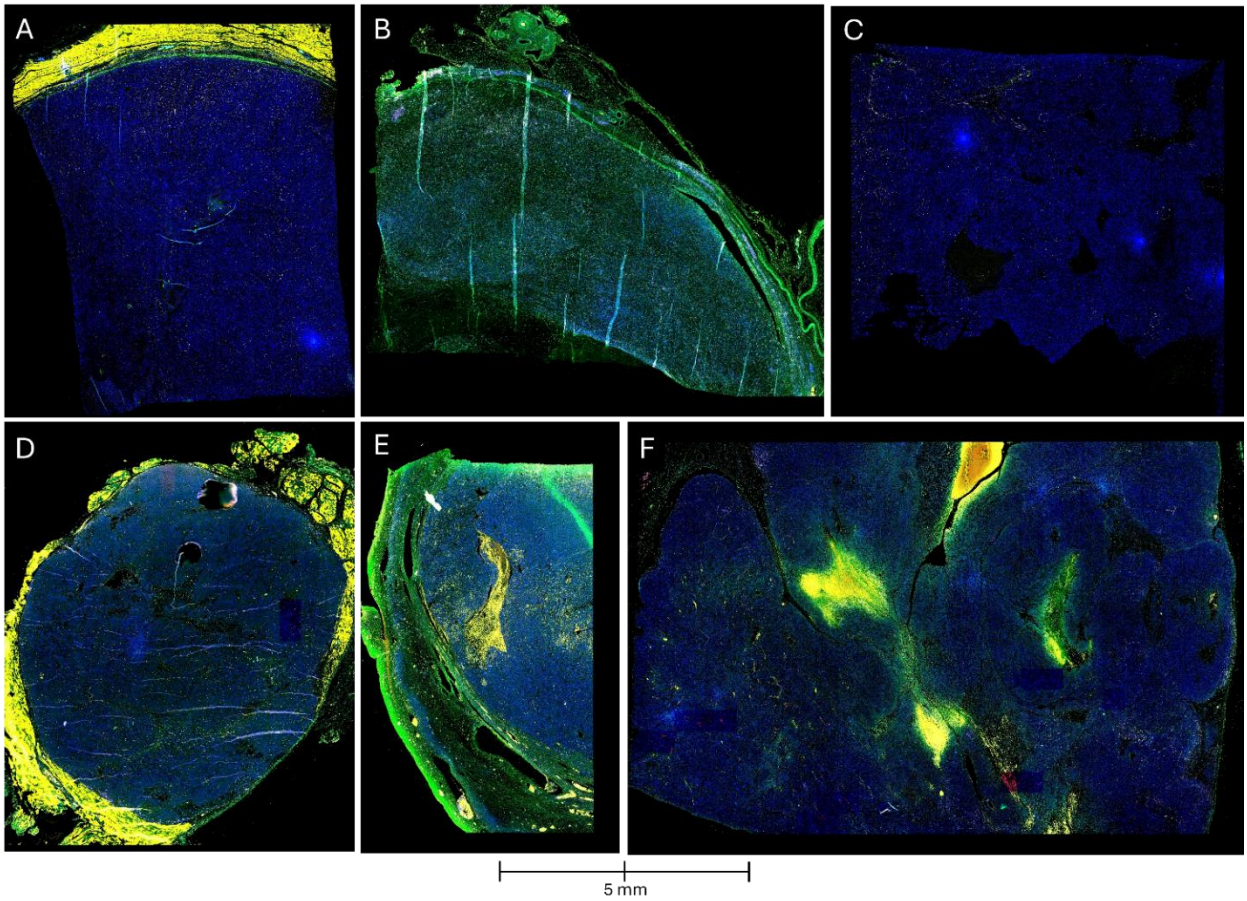


Figure 4.5: Overview of the four-colour fluorescent staining used to identify CD45 (red), CD8 (yellow), vimentin (green) and SYTO 13 (blue) for identification of nucleated cells and immune cells for targeted transcriptomic analysis in the digital spatial analysis on six sarcoma samples. (A) H201064 (UPS), (B) H210024 (USS), (C) H202415 (LMS), (D) H214439 (LMS), (E) 1048121 (LMS), (F) H203557 (LMS).

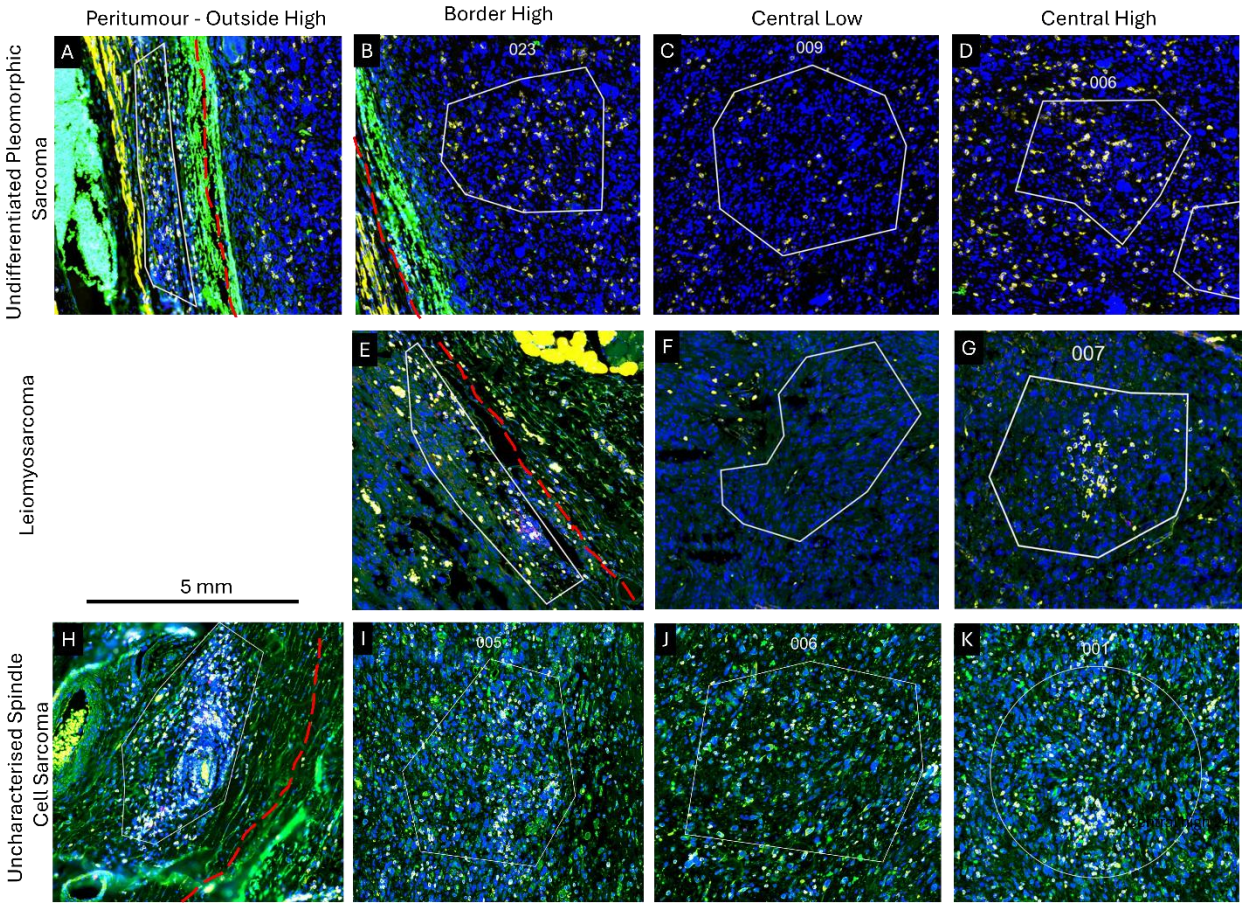


Figure 4.6: Examples of ROIs selected from four-colour fluorescent staining used to identify overlapping CD45 (red), and CD8 (yellow) immune cell markers and SYTO 13 (blue) included to identify nucleated cells. Vimentin (green) included to identify other cells, example images of the three sarcoma subtypes. (A-D) undifferentiated pleomorphic sarcoma (UPS) ROIs, (E-G) Leiomyosarcoma (LMS) ROIs, and (H-K) uncharacterised spindle cell sarcoma (USS) ROIs. ROI types included (A and H) peritumour - outside the tumour ROIs, (B, E and I) high immune infiltrated tumour border ROIs, (C, F and J) lowly infiltrated central tumour ROIs, and (D, G and K) highly infiltrated central ROIs. Red dotted line indicates the tumour border.

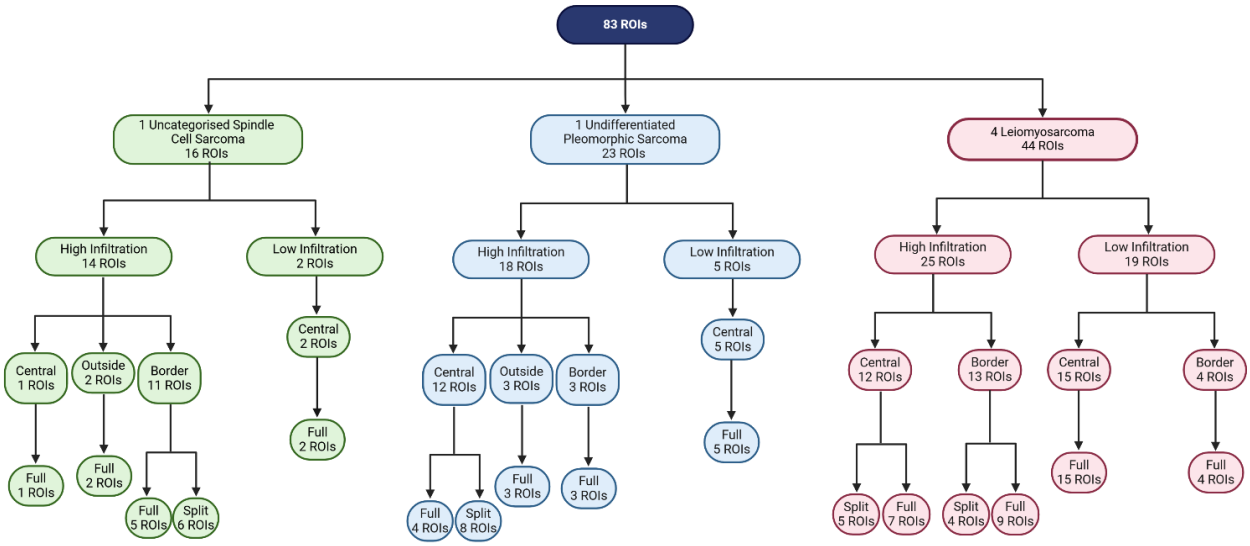


Figure 4.7: Decision tree for selection of the regions of interest (ROI) within this transcriptomic study of sarcoma samples for the 83 ROIs selected. Created with BioRender.com.

## 4.5 Identifying biological differences between tumours by principal component analysis

To assess the possible factors that were affecting the distribution of data a principal component analysis was conducted using the factoextra package within R[114]. This dimensionality reduction methodology was used to create a simplified output with the patterns and trends included from this large dataset. The scree plot (Figure 4.8) outlines how each component contributes to the factors of difference, the first component in the analysis accounts for 14.1% of the variation in the principal component analysis (PCA), with the second, third and fourth accounting for 6.9%, 5.4% and 4.1% respectively. This covers 30.5% of the difference in this dataset.

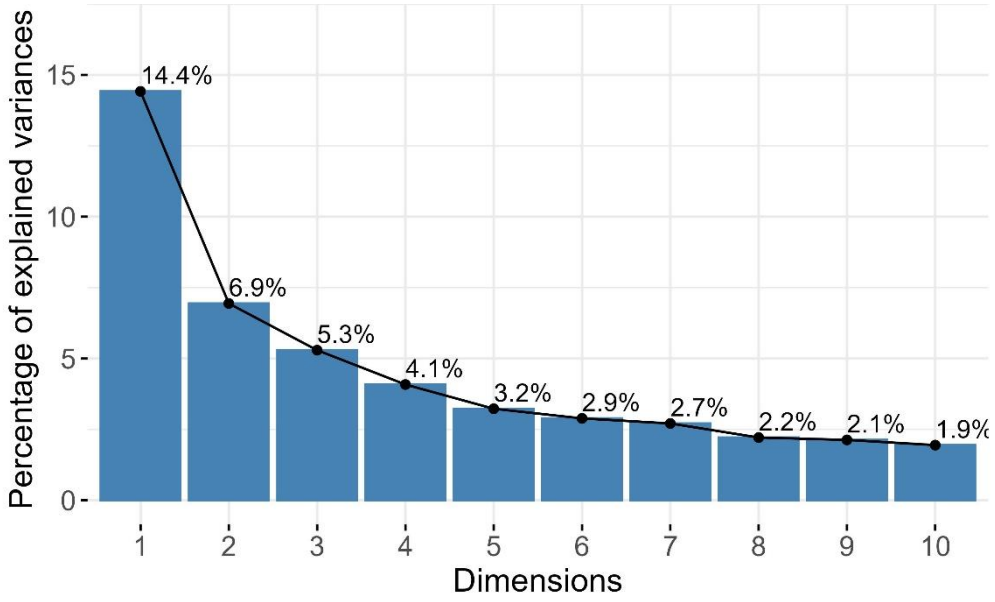


Figure 4.8: Scree plot outlining the dimensions of variance from the PCA analysis.

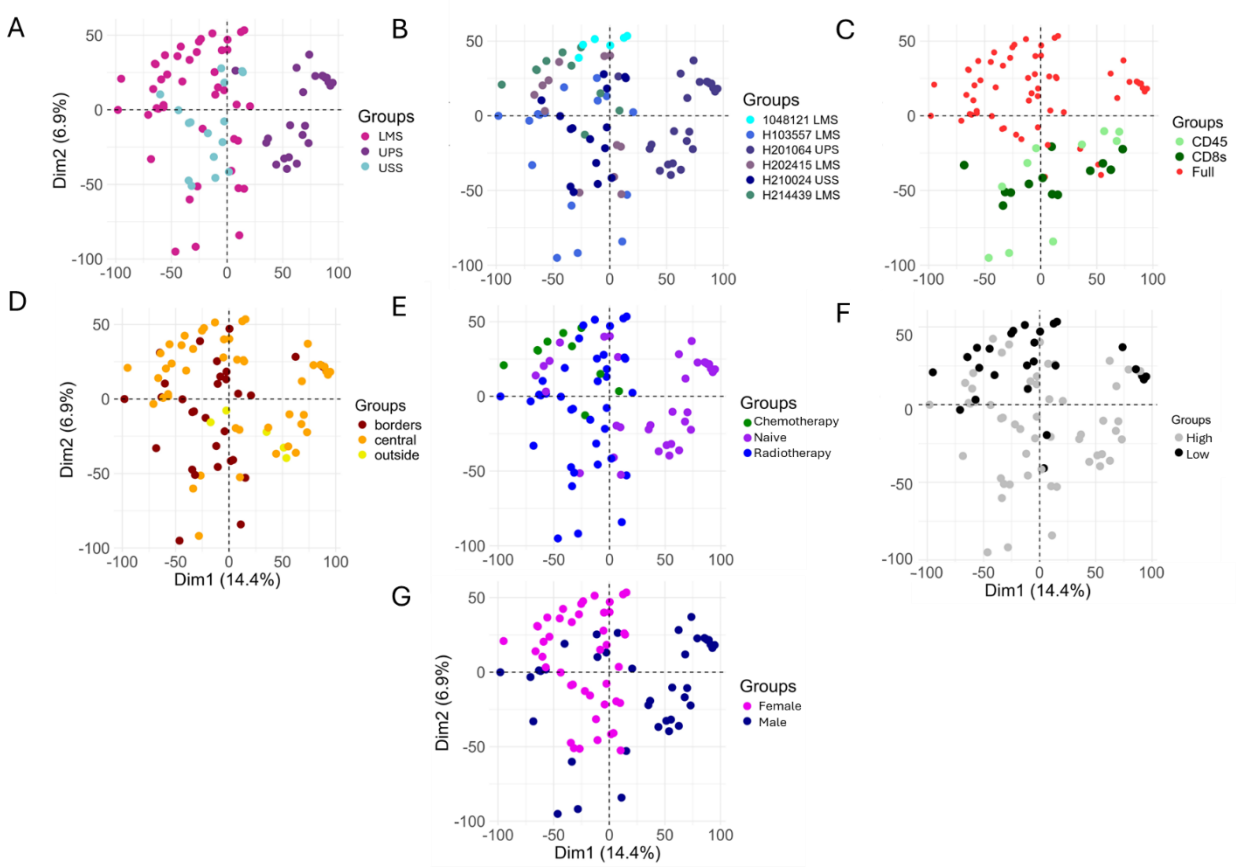


Figure 4.9: Visualisation of the first and second dimensions in the principal components analysis of the transcriptomic data of the 6 sarcoma samples assessing multiple factors within the study to investigate each factor's effect represented for (A) tumour type, (B) individual tumours, (C) segmentation strategy, (D) location within the tumour, (E) previous treatment, (F) immune abundance, and (G) gender.

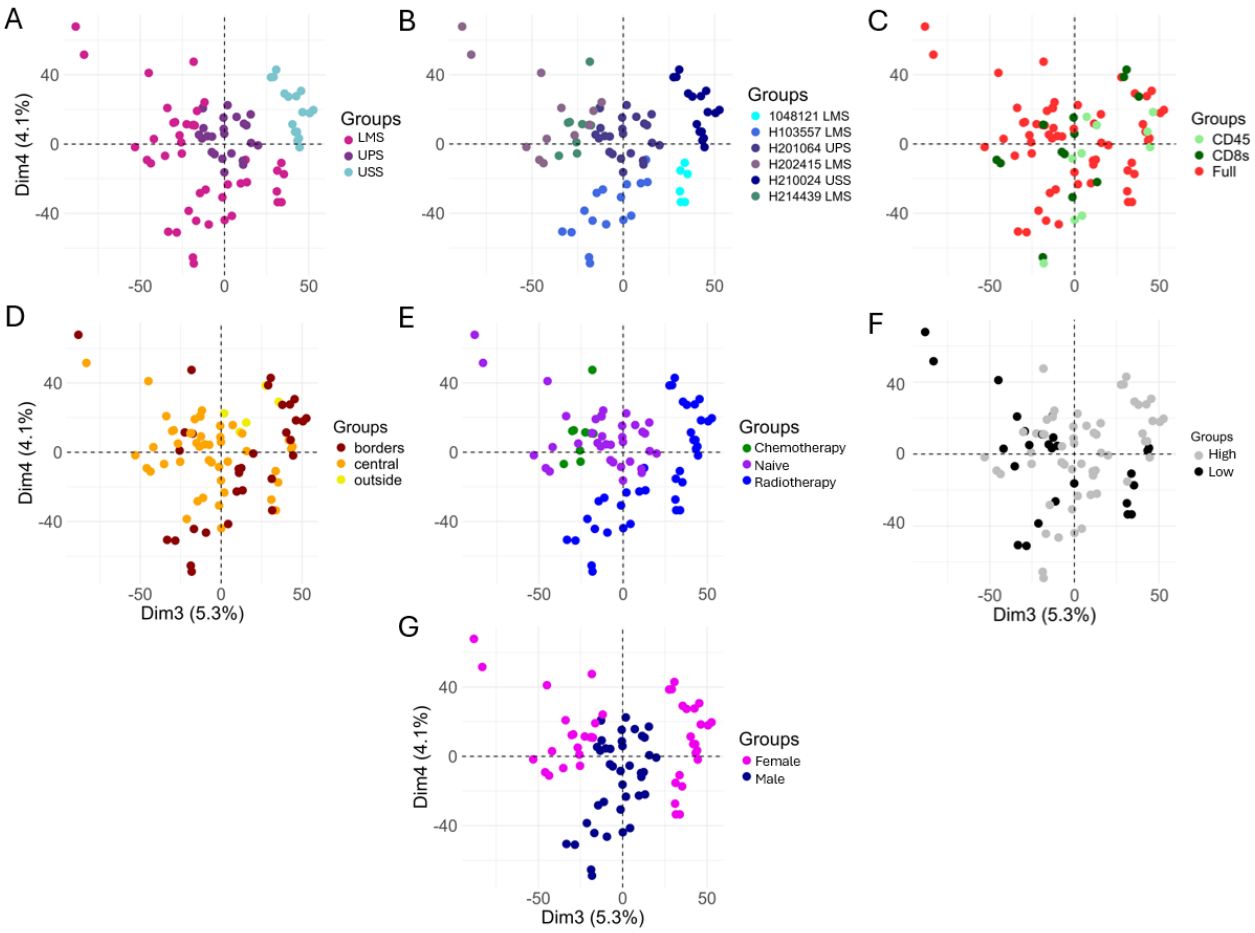


Figure 4.10: Visualisation of the third and fourth dimensions in the principal components analysis of the transcriptomic data of the 6 sarcoma samples assessing multiple factors within the study to investigate each factor's effect represented for (A) tumour type, (B) individual tumours, (C) segmentation strategy, (D) location within the tumour, (E) previous treatment, (F) immune abundance, and (G) gender.

Comparison of the tumours based on their pathologically diagnosed subtype, mapped to the first dimension influencing the difference in the data, separating the UPS from the LMS and USS within the first dimension (Figure 4.9 A). The individual tumours showed a different clustering pattern elucidating the factor influencing the third, and forth dimensions (Figure 4.10 B). This suggests an intrinsic heterogeneity in the profiles of these tumours. This highlights the inherent heterogeneity of tumours, even within tumour subtype.

The second and third dimension looked to be resolved by the USS tumour, which was different from the LMS and UPS tumours (Figure 4.9A and Figure 4.10A). Due to the nature of Nanostring's GeoMx technology, multiple tissue samples can be processed on the same

slide, in accordance with the differences observed being the consequence of real differences in the tumour biology, rather than resulting from a technical issue. This lends into the idea that even tumours of the same subtype (e.g. LMS) from different patients may be markedly different from each other due to genetic differences. The LMS subtype does share some similarity suggested by the clustering in the first and second dimension.

Analysing the PCA based on ROI segmentation strategy seemed to resolve the second component of difference, as shown in Figure 4.9C. ROIs segmented by CD45 and CD8 (CD45+CD8- or CD45+CD8+) immunofluorescence staining separated from ROIs that were not segmented. The data demonstrated that the transcriptome of immune cells alone is, as expected, vastly different from cancers cells with some infiltration. Investigation of other experimental and clinical factors indicates that previous treatment (chemotherapy, or radiotherapy) before the resection seems to have small impacts along the third dimension. However, this finding was intertwined with the tumour subtype and individual tumour differences. The classification of low or high immune infiltration, and gender did not have a separating effect on these first four components on the PCA.

## 4.6 Differential gene expression and pathway analysis of sarcoma transcriptomic data

Differential gene expression was conducted using the Limma package in R[119] discussed in section 2.7.3. The analysis was used to compare factors such as tumour subtype, infiltration abundance and infiltration type based on location of the area sampled within the tumour Figure 4.11-Figure 4.16. For all analyses volcano plots were created using the EnhancedVolcano[120] package in R with a p adjusted threshold of 0.05 (p adj. = 0.05), and

log-fold change of 0.5 (LogFC = 0.5). Pathways were identified from these genes using the clusterProfiler[212] package in R. Pathways with a p and q significance of 0.05 were assessed.

### 4.6.1 Comparing immune infiltration between sarcoma subtypes highlighted structural differences of the tumour tissue

The first aim of the differential gene analysis was to compare the immune infiltration in the UPS to the LMS tumours. As discussed, this focused on CD8 T cells and surrounding tumour tissue as it was hypothesised that there was a reduction in the function of these immune cells within sarcomas, despite their high abundance in some instances. This analysis was therefore used to evaluate difference in abundance of these cytotoxic immune cells between the different subtypes and evaluate variations in the expression profiles of these populations. The analysis also sought to explore differences in the tumour tissue adjacent to CD8+ T cells.

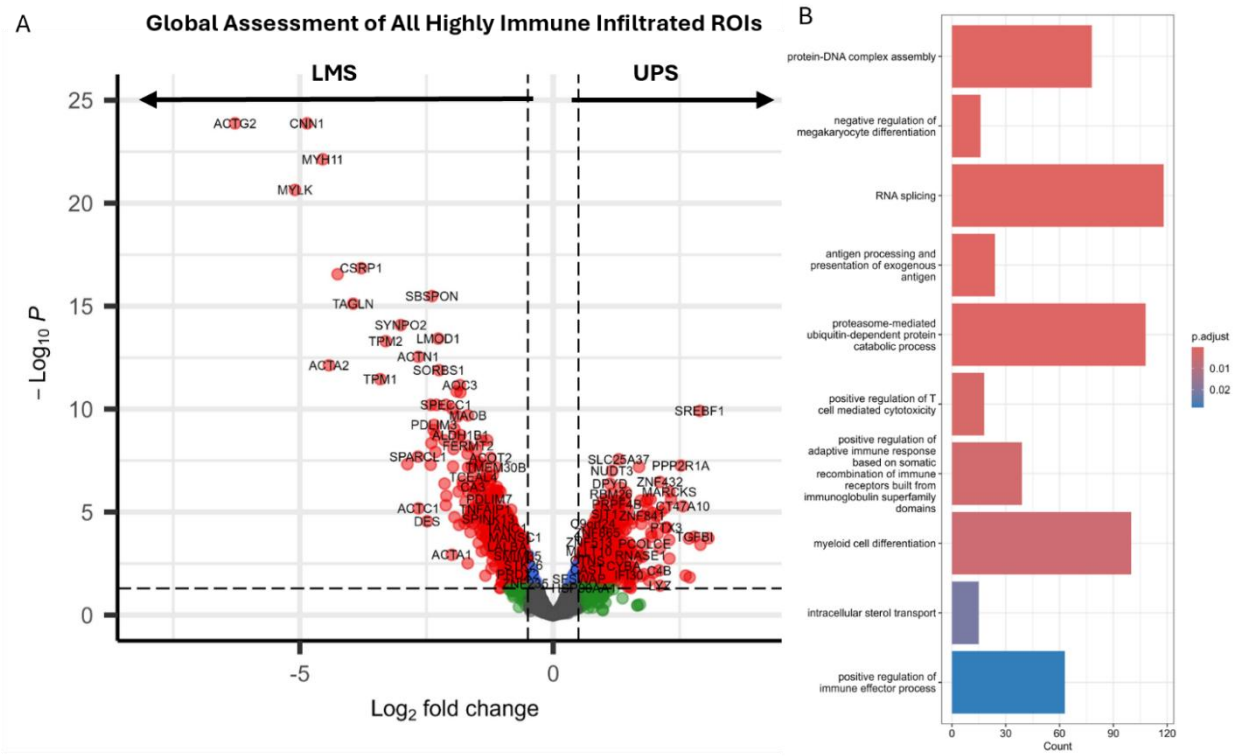


Figure 4.11: Comparing areas of high infiltration assessed by immunofluorescence during ROI selection between tumour types. (A) Volcano plots showing differential expressed genes within highly infiltrated ROIs between (left) LMS and (right) UPS with log2 FC indicates the relative expression level changes for each gene compared to each other with P adj = 0.05 significance level. Points in red represent gene that were expressed significantly over both thresholds, blue were significantly over the adjusted p value, green points were above the fold change threshold but were not above the Padj value and genes represented in black were not statistically different between the variables being described. (B) Pathway analyses of differentially expressed genes from UPS samples in highly infiltrated ROIs with a Padj value of 0.05.

Firstly, in a global overview of the tissue, comparisons of the highly infiltrated, non-segmented ROIs of these subtypes were made (Figure 4.11 A). There were 3240 DEG differentially expressed genes (DEG, p adj. = 0.05). Within the **LMS ROIs**, there was upregulation of smooth muscle and actin genes: CNN1, ACTG2, MYH11, MYLK, CSPR1, TAGLN, ACTN1, ACTAC2, COL6A2 (Figure 4.11 A), and PDLIM3, and PALLD (Supplementary Figure 4.1). This was in accordance with these tumours arising within smooth muscle, with these tumour cells retaining aspects of muscle-like phenotype. Other functions of these genes to note are that CNN1 has further associations with reduced T cell differentiation and mature tumours[213]. CNN1 may be a factor in the reduced CD8 infiltration and function within these tumours. Whereas PDLIM3 expression has been associated with increased

immune infiltration[214]. ACTN1 has been linked to increased proliferation and metastasis in many tumours[215,216], with association to fibroblasts in the tumour tissue which leads to increased escape and metastasis of tumours[216]. CSRP1 is also associated with tumours that have a large proportion of the TME being made up of stroma and fibroblasts[217]. CSRP1 is associated with epithelial mesenchymal transition[217], as is ACTG2 and ACTAC2[218]. MYLK depletion (suggested by the upregulation in LMS over UPS) is implicated in influencing the migration of the tumour microenvironment through ICAM-1, IL-1α, IL-6 and IL-8[219] which might indicate why the UPS sample was inherently more infiltrated (see Figure 4.5and Figure 4.6). Along the same lines, TAGLN (TGFβ inducible gene) is associated with reduced hMSC cell proliferation and increased cell migration[220]. With the differences in EMT which will affect the tissue structure and CNN1 that is involved in reduced T cell differentiation it was possible to theorise that immune cells within these tumours do not migrate through the tissue, nor become activated and cannot therefore instigate the desired beneficial anti-tumour response. This may be contradicted by the increase in PDLIM3 which is a signalling gene for immune infiltration. However, it is possible that this rise relates to an increase in suppressive regulatory cells, assessment of Treg or M2-like macrophage abundances would be needed to resolve this question. COL6A1-2 are genes encoding collagen, collagen abundance has been associated with reduced function of CD8+ T cells[210], and raised fibroblast levels within the tumour which increases a regulatory phenotype[221], and creates a dense ECM barrier

Next, the genes upregulated in the **UPS ROIs** are discussed. There was higher expression of CRIP1, CRIP2, CFD, and TNXB (Supplementary Figure 4.1). These genes are involved in cell migration with downstream links to epithelial-mesenchymal transition (EMT)[222–224]. CRIP1 has been reportedly involved in tumour invasion and metastasis[222,225]. Whilst CRIP2 is

associated with angiogenesis[226] which could lead to increased infiltration. CFD is linked to the alternative complement pathways[227] which in turn has been linked to collagen type I expression[224] which may be involved in the oncogenesis of the UPS tumour. CFD is also associated with fibroblast cell migration[224] which might be involved in the infiltration in these tumours and the links to collagen expression. Other associated immune-related genes include LAIR1 and CD40 (Supplementary Figure 4.1), which are involved in antigen recognition and response. LAIR1 is involved in MHC-I independent mediated NK cell regulation[228]. NK cell abundance is typically negatively correlated with T cells which could be caused by the expression of this regulatory signal[200]. The upregulation of CD40 might suggest antigen presentation on DCs within the tumour due to CD40 being required to activate DCs[229]. RASSF4 (Supplementary Figure 4.1) was also higher in the UPS samples and has been shown to be associated with Ras-dependent apoptosis[230] and dysregulation of the Hippo pathway in sarcoma. This pathway has been shown to lead to sarcoma cell growth and proliferation[231].

From the differential expression comparing UPS to LMS, the top 10 differentially expressed pathways in the **UPS ROIs** are shown in Figure 4.11B. Upregulated immunological pathways include those driving antigen processing and presentation of exogenous peptide antigen along with positive regulation of adaptive immune response based on immunoglobulins, positive regulation of T cell cytotoxicity and myeloid cell differentiation all pointing towards a functional immune response to the UPS tumours. Taken together these pathways suggest immune recognition of the tumour and a higher involvement of the immune compartment within the UPS tumours compared to the LMS tumours.

Overall, these findings showed that when assessing the global transcriptomic profiles, there were many relevant differentially expressed genes which included structural, and immunological genes, between these sarcoma tumour subtypes. The question of whether different regions within the same tumour might show differences in immune profile was worthy of further study. As the transformed cells within a tumour remodel their surroundings the profile of the regions surrounding tumour tissue was also of interest.

### 4.6.2 Investigation of the differences in immune populations at the tumour border showed similar immune population differences between the tumour subtypes as the global analysis

It was hypothesised that immune infiltration into the tumour can come from adjacent tissues and vasculature. It was of interest to determine if there were differences in the immune cell profiles entering the LMS tumours compared to the UPS tumour. Notably, infiltration was increased in UPS, when assessed by histology and subsequent IF used in the DSP workflow (Figure 4.5). It was thought that the differences in TME structure and morphology of the tumours may influence the infiltration of immune cells. With increased pro-infiltration signalling being an additional or alternative explanation. The analysis showed 331 DEG (p adj. = 0.05) within the tumour border ROIs in UPS vs LMS (Figure 4.12A).

Many of the genes seen on the previous differential analysis which compared all ROIs across the LMS and UPS samples (Figure 4.11 A) were upregulated in these **LMS border ROIs**. These genes included ACTG2, MYH11, TAGLN, CNN1, ACTN1, MYLK, and PDLIM3 (Figure 4.12 and Supplementary Figure 4.2) as previously discussed, along with TPM1, TPM2 (Figure 4.12) and CALD1, FBXO32, and FHL1 (Supplementary Figure 4.2). These genes are associated with the tissue architecture[232–235]. There are some secondary associations to the immune infiltration

as previously discussed. Involvement of structural genes could be differentially expressed due to sarcoma types typically arising in muscle tissues. SPARCL1 is also upregulated, its expression has been associated with suppressed metastasis in mesenchymal cancer types as well as recruitment of macrophages[236]. Fibroblast associated genes MYL9 and CALD1 were also upregulated. The former is implicated in MHC-II formation and fibroblast presence in the tumour[237], the expression of the latter is associated with high fibroblast density in tumours along with M2 macrophages and a reduced CD8+ T cells in the tumour[238]. These structural and regulatory cells are of interest to this study. For greater precision the involvement of macrophages and fibroblasts in these tumours will be looked at using cellular deconvolution in section 4.7.

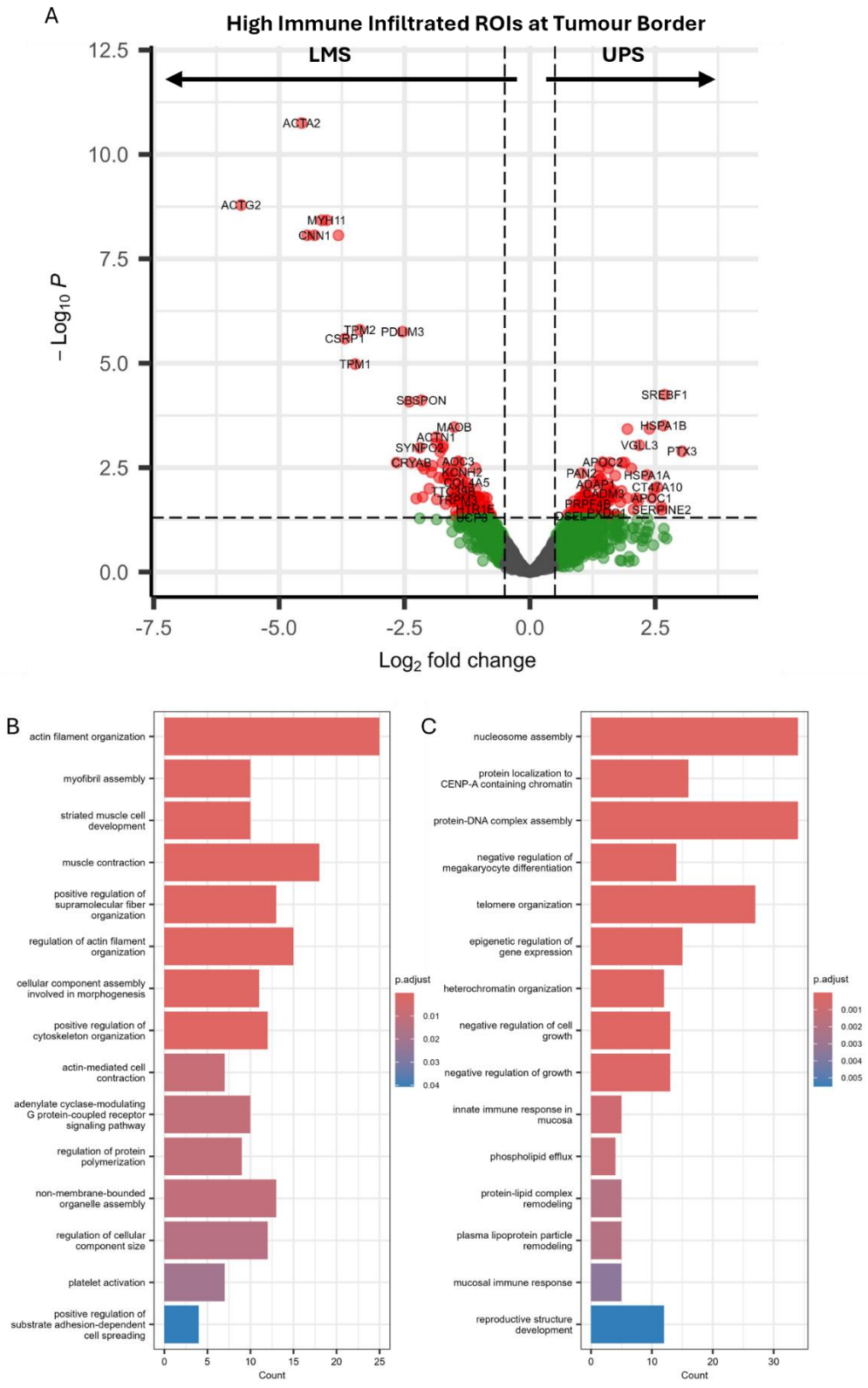


Figure 4.12: Comparing highly infiltrated areas of the tumour border between tumour types assessed by IF during ROI selection. (A) Volcano plots showing differential expressed genes within highly infiltrated ROIs from the border of the tumour between (left) LMS and (right) PMS with log2 FC indicates the relative expression level changes for each gene compared to each other with P adj = 0.05 significance level. (B) Pathway analyses upregulated differentially expressed genes from LMS samples, and (C) pathway analyses upregulated differentially expressed genes from UPS samples from highly infiltrated ROIs from the border, and with a Padj value of 0.5. Points in red represent gene that were expressed significantly over both thresholds, blue were significantly over the adjusted p value, green points were above the fold

change threshold but were not above the Padj value and genes represented in black were not statistically different between the variables being described.

When investigating the genes upregulated in the **UPS border ROIs** (Figure 4.12 and Supplementary Figure 4.2) genes of interest include RASSF3 and RASSF4, which induces Ras-dependent apoptosis[230], sarcoma cell growth and proliferation[231]), CRIP1, TNXB (both linked to cell migration[222,223]), and CFD (complement pathway[224]). Other immune associated genes of interest include PTX3, and MAFK. PTX3 can acts as a chemoattractant for inflammatory cells in cancers, through the complement pathway and implicated in M2 polarisation and fibroblast gowth[239]. M2 macrophages are associated with a regulatory environment[169] and fibroblasts are known to affect the cytotoxic ability of CD8+ T cells[152,240]. MAFK is associated with increases NF-κB activity which affects immune inflammatory responses, apoptosis, and survival[241]. NCOA3 and AHR (Supplementary Figure 4.2) are associated with dedifferentiated sarcoma phenotypes[242,243]. The function of many of the upregulated genes might be expected to aid the development and growth of the tumour.

When assessing upregulated pathways of the **UPS border ROIs** (Figure 4.12C) pathways involved were like those identified in whole tissue analysis. These included protein localisation to CENP-A, and negative regulation of megakaryocyte growth. Associated pathways included innate immunity in the mucosa which suggests a tissue resident immune element to the transcriptomic profile.

Also investigated, was the significantly upregulated pathways from the **LMS border ROIs** (Figure 4.12B). These pathways were markedly different from UPS tumour border regions in that they were predominantly involved in muscle development, cytoskeleton organisation, and actin function which is indicative of the environment that makes up these tumours.

When compared to the increases in dedifferentiation genes in the UPS type, this may suggest that the structure of the LMS subtype has a tighter matrix where immune cells cannot move into the tissue which is a factor leading to reduced infiltration. This has previously been reported in dense stroma of pancreatic cancer[244] and dense breast cancer[245].

Taken all together, we have observed significant differences between both tumour types, both on a gene and pathway level, reflecting their different dedifferentiation levels, cellular composition and leukocyte infiltration levels and composition; similarly to differences observed in chapter 4.6.1.

### 4.6.3 The central tumour UPS ROIs express more collagen genes which may be associated with fibroblasts when compared to LMS

By comparing the immune infiltration of the central parts of the tumour between the UPS and LMS subtypes, it was thought that different routes of entry into the central tumour region could be identified. It was also thought that differences between signalling pathways in cells from the tumour subtypes would results in the differences in infiltration. Figure 4.13 A compares the central tumour regions of the two subtypes. There were 4087 DEG (p adj. = 0.05), many of which were described in the previous analyses shown in Figure 4.11 and Figure 4.12.

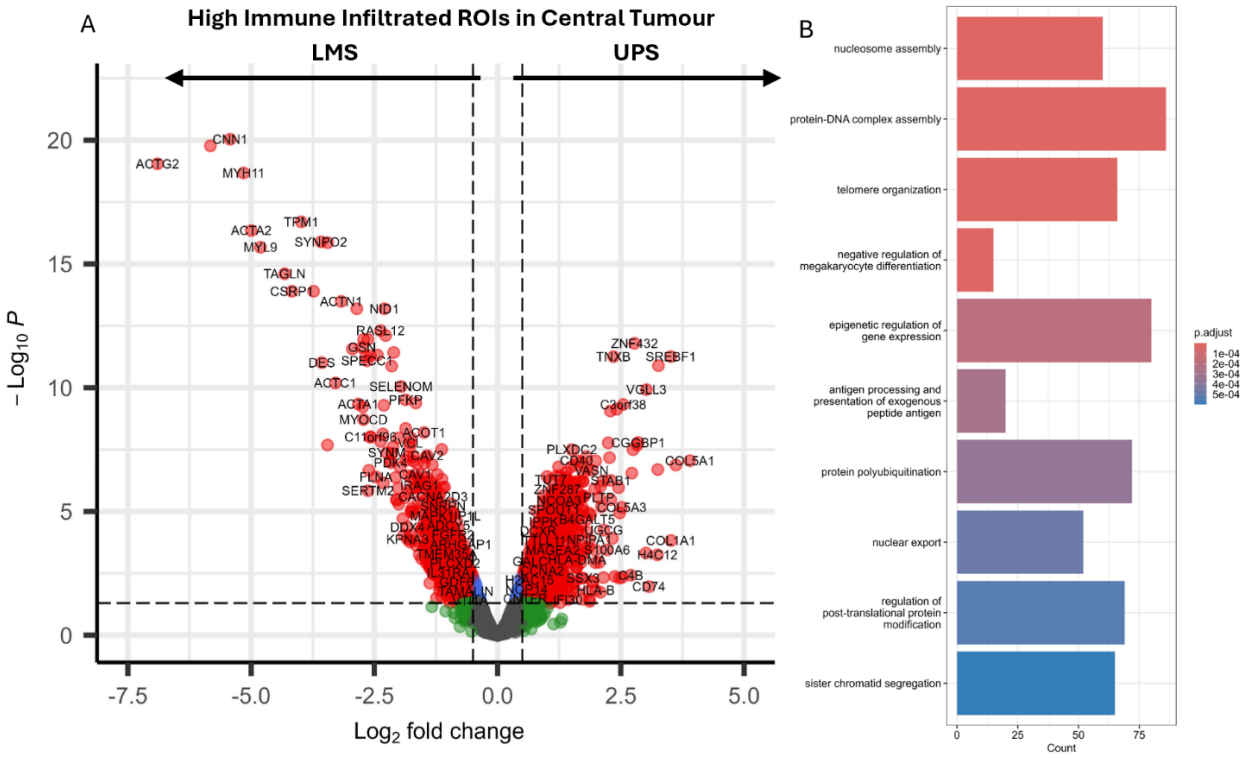


Figure 4.13: Comparing areas of high infiltration between tumour types assessed by immunofluorescence during ROI selection. (A) Volcano plots showing differential expressed genes within highly infiltrated ROIs between (left) LMS and (right) UPS, with log2 FC indicates the relative expression level changes for each gene compared to each other with P adj = 0.05 significance level. (B) Pathways analyses upregulated differentially expressed genes from UPS samples from highly infiltrated ROIs from the central of the tumour with a Padj value of 0.5. Points in red represent gene that were expressed significantly over both thresholds, blue were significantly over the adjusted p value, green points were above the fold change threshold but were not above the Padj value and genes represented in black were not statistically different between the variables being described.

Focusing on the genes upregulated in **central LMS ROIs**, genes included tissue organisation genes. These included MYL9, ACTN1, ACTA2, TPM2, PDLIM3, PALLD, MYLK, SPARCL1, TPM2, ACTG2, TPM2, CNN1 as mentioned in the previous Sections 4.5.1 and 4.5.2. Genes that were not previously highlighted in the differential analysis included NID1 (Figure 4.13), and MCAM (Supplementary Figure 4.3). These genes are involved in collagen and laminin linking and associated with expression typically occurring with mesenchymal genes with some links to reduced proliferation and migration of tumours[246], as well as vessel maturation. MCAM is associated with the apoptosis protection and metastatic potential[247]. This suggests that the LMS central tumour had similar structural gene expression profiles to the tumour border.

CD40, TNXB, MAFK, RASSF4, CFD, PTX3, AHR continued to be upregulated in the **UPS ROIs** as shown in Figure 4.13 and Supplementary Figure 4.3. Comparatively, in the central tumour many collagen genes were upregulated, including, COL1A1, COL5A1, and COL5A3 (Figure 4.13). These may be highlighted due to a high stromal content in these tumours. Fibroblasts express high amounts of these collagen genes due to their structural role and have been implicated in dampening CD8 T cells cytotoxic functions in the surrounding environment[210]. Along with upregulation of NOTCH3 (Supplementary Figure 4.3), which is associated with lower infiltration of activated CD8 T cells but increases in regulatory cells such as M2 macrophages[248] and NOTCH3 expression by cancer-associated fibroblasts has been associated with angiogenesis in other tumour types[249]. This may improve immune infiltration in tumours. Also, the expression of Notch signalling by non-cancerous cells within tumours has previously been associated with tumour growth in **UPS** tumours[250].

These data suggest that the immune cells within these UPS tumours may recognise tumour associated antigens more effectively than immune cells in the LMS type which might have led to the increased infiltration. This is further evidenced by the upregulation of MHC genes HLA-B and HLA-DMA. This covers both type I and type II MHC pathways implicating both T cells and myeloid lineage antigen recognition[251,252]. CXCL1 was also upregulated in the **central UPS** tumour region (Supplementary Figure 4.3). This is involved in neutrophil recruitment and points towards there being different immune population between subtypes[253]. There are no other differentially expressed chemokines or cytokines in this analysis. This suggested that there are similar signalling pathways in the central regions of both tumour subtypes. From this, the ability of immune cells to enter the tissue from local vasculature or movement through the tissue should be similar between the tumour types. However, the IF (Figure 4.5) and literature[26,83] suggests otherwise, which suggest a different

mechanism at play, such as the difference in structural genes as described in the **tumour border of the LMS** or different composition of extracellular matrix components like collagen genes highlighted above, affecting the movement into the tumour.

When investigating the differentially expressed pathways centrally in these tumours, the pathways upregulated in **UPS ROIs** (Figure 4.13B) included antigen recognition pathways, for example 'antigen processing and presentation of exogenous peptide antigen'. This suggested that the immune cells are upregulating these pathways in the **UPS** when compared to the **LMS** tumours. Cancer cells also present MHC molecules: it is possible that the upregulation of this pathway is influenced by expression on **UPS tumours** when compared to the **LMS tumours**. This in turn can influence the immune system to produce an antigen driven immune response. However, recent studies suggest that rare clonotypes can be presented by these tumours which are not recognised and do not provide the desired response within UPS tumours[251]. On the flip side, MHC-I expression can be downregulated within tumours to reduce the antigen driven response[254,255]. This may be occurring within the LMS tumours.

The immune cell abundance could be affected by increased infiltration, proliferation or differentiation to immune cells within the tumour tissue. However, this analysis does not provide an insight into which cells these might be, therefore the use of a cellular deconvolution approach is required to elucidate this (Chapter 4.7).

### 4.6.4 LMS tumours exhibit higher expression of immunoactivity but not cytotoxic genes in the higher infiltrated regions

Defining the differences in distribution of immune cells within the same tumour subtype, was a study aim of this chapter. Therefore, comparisons were performed between areas that

had higher infiltration than others. It was of interest if the cells were entering the tissue and becoming functional and proliferative. To probe this, the transcriptomic profiles of areas with higher infiltration were compared to those with lower infiltration (as assessed by IF staining and outlined in Figure 4.6), with interesting output metrics being the activation and function of the cytotoxic T cells within the tissue. It is also of interest as to whether the environment was regulatory or immunogenic, so this aspect was also studied.

Firstly, Figure 4.14A contains the assessment of the differential expression analysis of **regions of higher and lower infiltration in LMS**. There were 46 genes (p adj. = 0.05) that were differentially expressed in LMS high infiltration compared to LMS low infiltration ROI. There were no significantly upregulated genes when assessing the lower infiltrated regions of LMS. In contrast, T cell signatures (such as TRBC1, CD3E), immunoglobulin genes (IGKC, IGHG1, IGHG3, and IGHG4), MHC-II genes (HLA-DQB1, HLA-DPB1, HLA- DQA1, and HLA-DPB1), and MHC-I genes (HLA-E, TAP2, Supplementary Figure 4.4), were upregulated in high infiltration ROI. These data confirm the correct selection of the CD8 T cell dense areas, as well as provide the expected result of significantly raised expression of T cell-related genes in the highly infiltrated ROIs. The immunoglobulin genes may suggest an increase in B cells[256] within these areas which is plausible with the increase in immune cells being selected. B cells and IGHG genes (IgG plasmablasts), have been associated with better outcomes in some cancer types[257,258], although the assessment of human sarcoma samples is mixed, with some studies suggesting a positive outcome[86], while others associated a negative outcome[26,85]. Upregulation of canonical B cell signatures such as CD19 in this dataset was not seen, only the Ig constant region gene (IGKC) was raised. There is evidence that IgG+CD19- plasmablasts can be found in chronically inflamed tissue, with intact function[259]. This could explain the findings in these LMS samples.

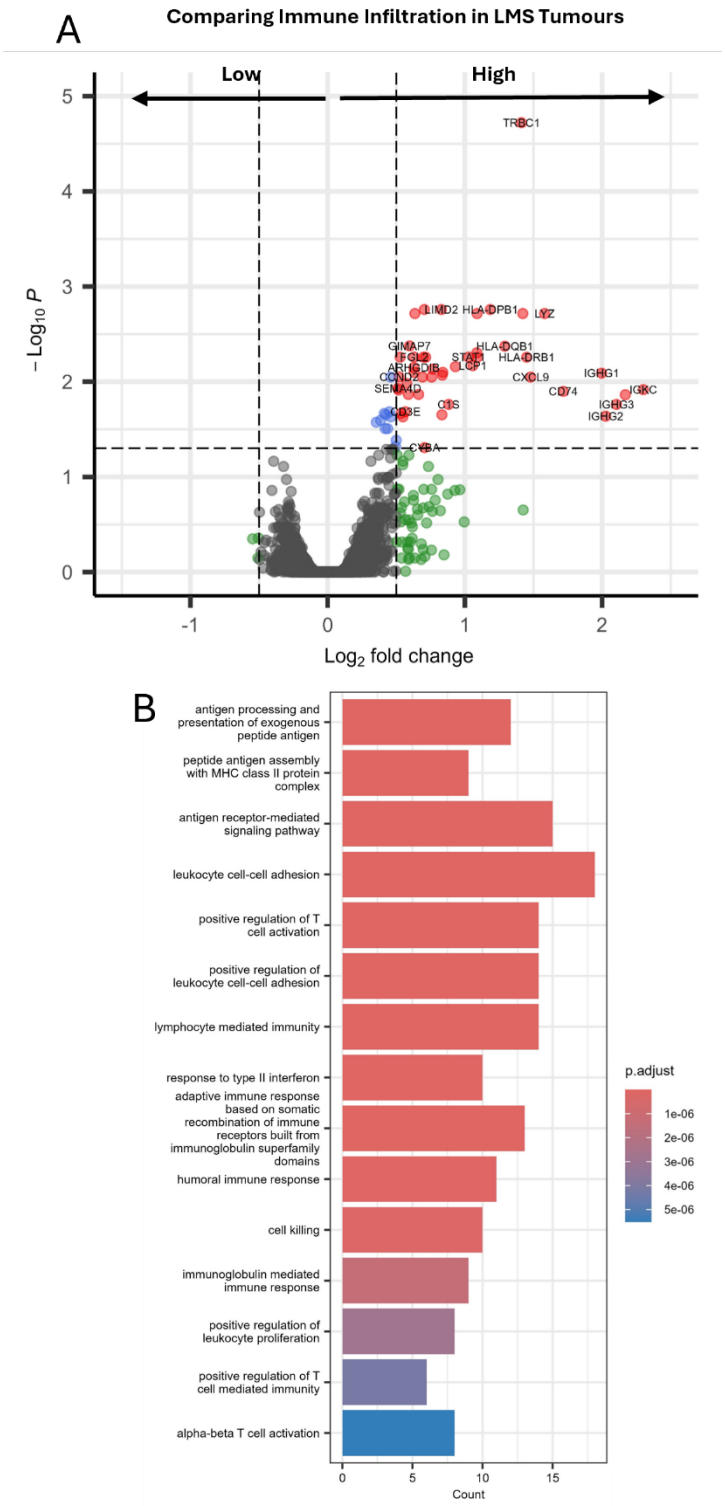


Figure 4.14: Comparing areas of different infiltration within the LMS tumours assessed by immunofluorescence during ROI selection. Volcano plots showing differential expressed genes within (A) the LMS tumours, comparing (left) low infiltration and (right) high infiltration with log2 FC indicates the relative expression level changes for each gene compared to each other with P adj = 0.05 significance level. Pathway analyses upregulated differentially expressed genes from (B) highly infiltrated LMS ROIs, Padj value of 0.5. Points in red represent gene that were expressed to a level which exceeds the fold-change and significance level thresholds, blue were significantly over the adjusted p value but with a small magnitude of change, green points were above the fold change threshold but were not above the Padj value and genes represented in black were not statistically different between the variables being described.

The upregulation of antigen presentation genes including MHCI, MHC-II and TAP2 genes could suggest that there is increased recognition or response to antigen within these ROIs[252,260–262]. This could be related to the increase in density of T cells along with other CD45 immune cells. Interestingly, the upregulation of MHC-II related genes may suggest activation of CD4 T cells, rather than CD8 T cells. This may lead to the activation of Tregs which would suggest a regulatory environment. However, the upregulation of TAP2 gene still supports the activation of the CD8 T cells that this study focused on. Alternatively, the downregulation of TAP genes is one of the drivers in the downregulation of MHC-I on cancer cells[255]. This may be causing areas in the tumour to be immune sparse. However, the mechanism influencing this in some areas of the tumour over others was not elucidated.

This comparison also showed an upregulation of STAT1, CCL5, CXCL9, FYB1, and FGL2 in these more highly infiltrated regions. CCL5 (Supplementary Figure 4.4) is linked to infiltration of tumour suppressive immune cells in multiple tumour types[263,264] but is also associated with CD8 T cell infiltration[265], which is more likely when CD8 T cells were targeted in this study. FGL2 is a regulatory T cell effector protein which is linked to reduced T cell activation[266]. FYB1 is associated with IL-2 cytokine production[267], IL-2 is required by T cells to maintain function[34]. Tregs require IL-2 for their suppressive function but in this case, the study focused on areas of CD8 T cells, likely accounting for this. CXCL9 is often associated with inflammation and immune biomarkers including CTLA4, GZMB, LAG3, PD-1 and PD-L1[268]. Although the expression of these markers has mixed downstream indications. However, its expression has been shown to improve immunotherapy outcomes *in vivo*[263]. High immune cell infiltration areas correlating with immune activation, antigen processing and presentation (both genes and pathways), i.e. local immune response are present and likely activated, but some features of immune regulation are present (CCL5, FGL2, and the

double-sided action of IL-2). That is normal for a developing immune response, effective immune response will require activation mechanisms to prevail.

Assessing these immune rich areas compared to immune low regions suggested in the LMS tumours showed that some T cells (and B cells) were able to infiltrate and get activated but might not be able to mount effective immune response. However, interestingly differences in checkpoint inhibitor expression was not observed.

Upregulated pathways in the **LMS highly infiltrated ROIs** (Figure 4.14B) included MHC-II antigen processing and presentation, and adaptive immune response from immunoglobulins. This suggested there was recognition of antigen within the tumour and B cells activity within the tissues. B cell abundances have been found in studies previously conducted and may play a role in the recognition of the tumour much like the MHCs[26]. Also, within the differential pathways there was positive regulation of leukocyte activation, αβ T cell activation, and positive regulation of T cell activation pathways in the highly infiltrated ROIs (Figure 4.14B). This suggested that there are some mechanistic reasons behind the difference in the abundance of immune cells within these immune clusters. There was upregulation of cell killing so these cells may still be having a cytotoxic response. Response to Type II interferon pathway was upregulated. There are multiple mechanisms driven by INF-γ. These include MHC-I presentation on macrophages[269], activation of M1 macrophages. However, INF-γ has been reported to induce apoptosis of tumour-reactive $CD8^+$ T cells and reducing effector memory responses in vivo[270]. Within a colorectal cancer model, one report showed that INF-γ can inhibit release of cytotoxic granzyme B release from CD8 T cells[271]. These differentially expressed pathways therefore suggested a presence of

mechanisms both promoting and inhibiting the cytotoxic response, making the interpretation more complicated.

When assessing difference in gene expression profiles of **UPS ROI with high vs low immune infiltration** there were no differential expressed genes as shown in Supplementary Figure 4.5.

The analysis of ROIs with different immune infiltration from the LMS tissues showed genes and pathways linked to upregulated antigen presentation, increased macrophages with cytokines and chemokines that suggest infiltration of immune cells but possibly not adequate activation. Unfortunately, the cell types which express these regulatory and suppressive genes could not be elucidated. There were no proliferation inducing genes which can account for the areas of higher immune abundance. It could be that the regulatory and suppressive genes were shown to be upregulated in the more highly infiltrated genes because of the general raised abundance of immune cells per-se. Also, there are no genes specifically associated with cytotoxic cells within these highly infiltrated regions unlike the broad T cell and B cell signatures which also suggests that there is little anti-tumour immune activity in LMS, regardless of the level of infiltration. Genes associated with cytotoxicity were expected to be upregulated in the higher infiltrated regions, however this was not the case. The level of immune infiltration does not necessarily relate to level of anti-tumour activity.

### 4.6.5 The peritumour areas showed upregulation of immune signatures compared to the tumour border.

The transcriptomic differences of the immune populations throughout the tumour were sampled and compared to peritumoral ‘normal’ areas around foci of infiltrate from the same tumour type. It was thought that the cells outside of the tumour would not be under the same

regulatory environment as within the tumour. This may lead to the tumour having low immune abundance. It was believed pertinent to the study as these findings may also be seen when comparing tumour subtypes.

It was possible to compare the transcriptomic profiles of areas on high immune abundance of the **tumour border** vs the **peritumour** tissue of a **UPS** tumour (Figure 4.15). It was not possible to sample the peritumour areas of LMS tumours as the peritumour tissue was not included in the sections. For the UPS tumour, perivascular peritumoral areas were included in the analysis. These areas were selected as it was hypothesised that the immune cells infiltrating from these vessels will then enter the tumour. It was also possible to compare the **immune border** to the **central tumour** for both the **LMS and UPS** to evaluate the difference between these ROI as well.

This differential expression analysis showed 1942 significant DEG (Figure 4.15A). FOS, EGR1, SFRP4, and CD96 were shown to be significantly upregulated in the **UPS peritumour ROIs** (Supplementary Figure 4.6). FOS is implicated in immune regulation in cancer[272] so this could be a factor towards explaining why this tumour is not being infiltrated from the surrounding healthy tissue and vasculature. EGR1 is known for regulation of TGFβ1, PTEN, p53, and fibronectin. TGFβ1 is associated with macrophage polarisation towards a M2 phenotype[43,273]. These genes are implicated in the growth of tumours, and this suggests that the tumour receiving signals to advance into the peritumour[274]. CD96 is expressed on both T and NK cells[275]. *In vivo* studies have shown reduced INFγ production from NK cells bound to CD96 ligand and suggested that upregulation of CD96 increased susceptibility to MCA-induced fibrosarcoma formation[276]. With this being prevalent in the peritumour tissue, this might be a factor in reduced effective anti-tumour response.

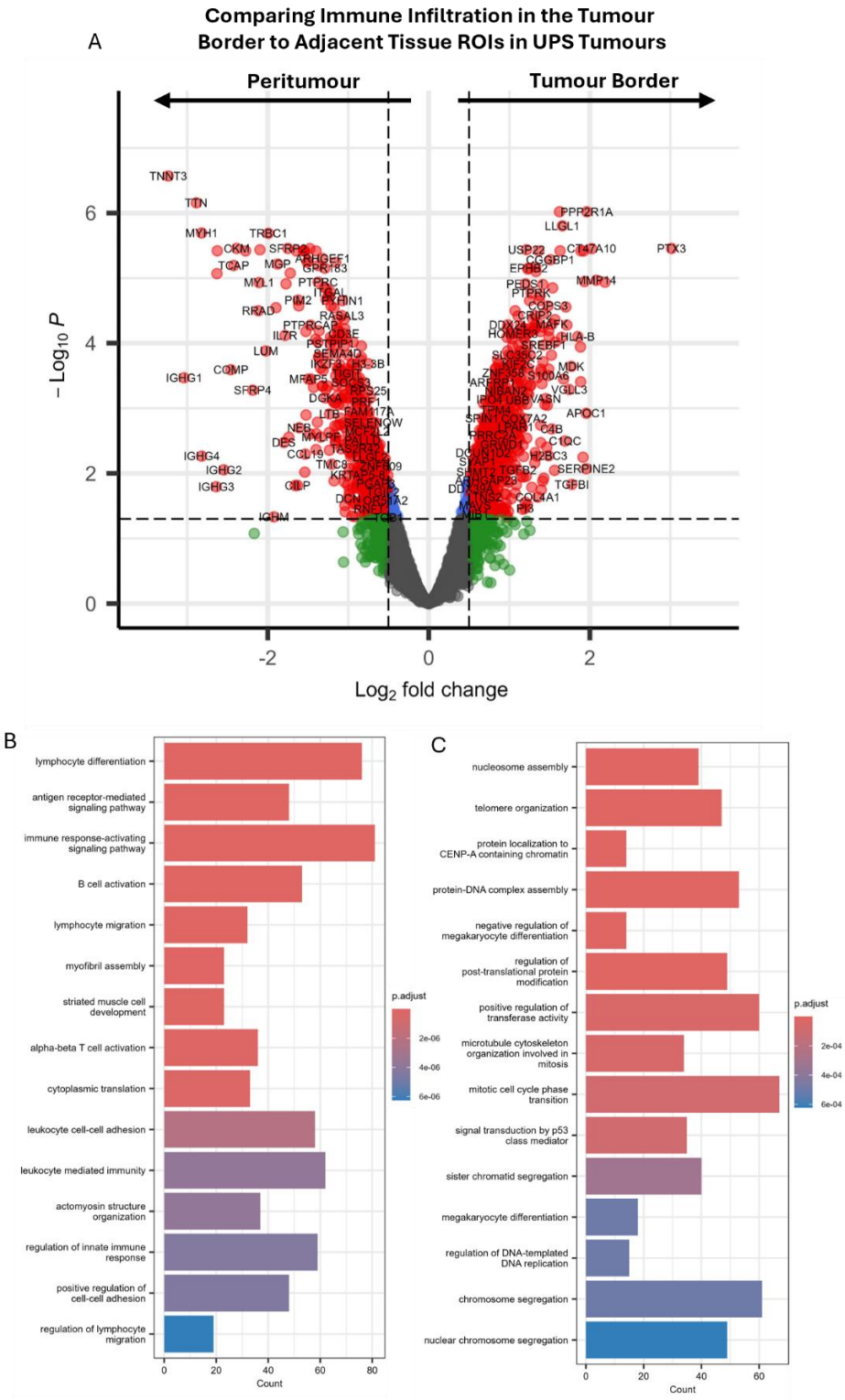


Figure 4.15: Comparing the transcriptomic profile of highly infiltrated regions at the tumour border to areas peritumour areas in the UPS tumour type assessed by immunofluorescence during ROI selection. (A) Volcano plots showing differential expressed genes comparing (left) peritumour and (right) the tumour border, log2 FC indicates the relative expression level changes for each gene compared to each other with P adj = 0.5 significance level. (B) Pathway analyses of upregulated differentially expressed genes from peritumour when compared to regions tumour border, and (C) pathway analyses of upregulated differentially expressed genes from tumour border compared to peritumour with a Padj value of 0.5. Points in red represent gene that were expressed significantly over both thresholds, blue were significantly over the adjusted p value, green points were above the fold change threshold but were not above the Padj value and genes represented in black were not statistically different between the variables being described.

Also upregulated in the **UPS peritumour** vs the **UPS tumour border** were immune markers IGHG1-4, and SFRP4 (Figure 4.15) along with CD3E, CD69, MZB1 (Supplementary Figure 4.6) suggesting more immune cells outside of the tumour than within it. MZB1 is involved in T cell immune responses and the differentiation of plasma cells[277], suggesting that the function of T cells outside of the tumour may be improved and that plasma cells are more frequent outside of the tumour environment. The increase in B cells is supported by the increase in immunoglobulin genes (IGHG1-4) outside the tumour. The expression of CD3E in the peritumour increases the confidence that the abundance of immune cells within the tumour is much lower than healthy tissue. With CD69 expression being higher outside the tumour, it suggests that there is increased activation of the cells as well as abundance outside the tumour. SFRP4 expression has been shown to correlate with TfH, Treg and macrophage infiltration in a cancer study[278]. There is not a clear result as to whether the environment outside the tumour is regulatory or not. Signalling genes upregulated in the peritumour include CCL19, IL7R, (Figure 4.15) CCL18, CXCR4 (Supplementary Figure 4.6). IL7R is required for T cell development[279] and survival and CCL19 is associated with T cell activation and homing of CCR7 expressing naïve T cells[280], comparatively CCL18 is produced by M2 macrophages[281] which are immunoregulatory in nature and is a ligand for CCR8, frequently expressed on activated Tregs. This provides a mixed message as to whether the environment outside the tumour is regulatory or not. This may reflect the temporal and spatial resolution limitations of the analysis technique or the genuine complexity of the balance in tumour immunity.

When comparing the **tumour border** ROIs to the **peritumour** ROIs, TNXB, PTX3, NCOA5, CRIP2, and MAFK were previously reported as differentially expressed in the **UPS tumour border ROI** compared to the LMS border and when compared to UPS central tumour (Figure

4.11 to Figure 4.14) and were also upregulated in this assessment. Interestingly, there were also increases in C1QC, and TGFB, (Figure 4.15) as well as CXCL1, and HLA-B genes (Supplementary Figure 4.6). C1QB is a complement related gene[282] but also has prognostic implications independent of the (innate immunity) complement system in a cancer study[283]. This may suggest the involvement of complement in the tumour but there is mixed evidence to support this. TGFBI is associated with tumour metastasis and proliferation but also tumour associated fibroblasts[284] which may relate back to the increase in collagen genes within the UPS central tumour[221]. CXCL1 expression is implicated in the recruitment of neutrophils[253] and stromal cells suggesting its possible impact on the tumour progression. HLA-B can be presented on the cancer cells themselves as well as most nucleated cells. With the other immune signatures being downregulated in the cancer border when compared to the peritumour, the expression of HLA-E on immune cells seems unlikely. HLA-E was most likely expressed on the cancer cells. MHC-I expression is common in sarcoma; however, sarcoma cells are not typically recognised by the immune system[251], so MHC-I may be present but internalised into the cell where it is no longer available to for immune activation[285]. Spatial proteomic analysis may help un-pick this complexity. Many of the other DEG are non-immune related and so will not be discussed here.

Pathways upregulated in the **UPS peritumour ROIs**, compared to the **UPS tumour border ROIs** there were many implicated immune pathways, again suggesting more immune prevalence outside of the tumour. These include leukocyte homeostasis, immune response-activating cell surface receptor signalling pathway, antigen response, αβ T cell activation, also with leukocyte chemotaxis, suggesting that the prevalence of immune cells within the tumour is much lower than in healthy tissue. This is expected as these tumours are reported

to be minimally infiltrated tissues[83,85,132,199]. In comparison, in the tumour border there was a distinct lack of immune pathways (Figure 4.15C).

The peritumour regions surrounded vasculature around the tumour. The similarities in the immune cells at the tumour border to these peritumour perivascular regions were compared to determine how different these regions were. There seems to be a lack of similarity in the environment and immune cell composition and activity. This suggests that there is a vast difference between the immune populations outside the tumour compared to inside the tumour. This supports our hypothesis that there are suppressive or regulatory effects within the tumour tissue.

### 4.6.6 The tumour border of the UPS sample showed upregulation of antigen presenting genes compared to the central tumour

When comparing the **border tissue** of the UPS to the **central tumour** areas there were 179 DEG (Figure 4.16). The most prominent of these were IGF2, IGHG1-4, IGKC, IGLL5, HLA-DQA1, B2M, and C1QC shown in Figure 4.16A. HLA-DRA, HLA-DRB1, HLA-B, CD4 were also upregulated (Supplementary Figure 4.7). IGF2 has been the focus of studies where its expression has been seen in some undifferentiated sarcoma types[286]. It has also been linked to poorer outcomes and is a treatment target[287]. The differential expression of this gene at the tumour border may have implications for future treatment of sarcoma, especially if vascularisation is required for dosing and is also variable within the tumour. IGHG1-4 genes, with IGKC, and IGLL5 which are all immunoglobulin genes that can be associated with an increase in B cells at the tumour border. As previously discussed in section 4.6.4, B cells and IgG plasmablasts (highlighted by IGHG1-4) are associated with improved

prognosis and antigen recognition[26]. This pairs well with the upregulation of MHC-I and MHC-II expression.

Upregulated HLA-II and CD4 genes suggest antigen presentation to CD4 cells. This implies antigen presentation by professional APCs such as DCs and macrophages[252,262]. However, it could be that CD4 Tregs may be involved. These cells can reduce the cytotoxic function of CD8 T cells without reducing the abundance of the population[149]. On the other hand, there was also upregulation of HLA-I and B2M suggesting possible upregulation of CD8 T cell responses[288]. Indeed, B2M has been associated with improved outcomes in some sarcoma types[289]. These factors could influence the observed increased infiltration into the **UPS tumours.** Cell deconvolution will be employed in Chapter 4.7 to further explore these findings.

The pathways that were upregulated in the **border tissue** support these findings (Figure 4.16B). This included the upregulation of MHC-II antigen presentation, activation of the immune system and activation of T and B cells. This more active phenotype in border areas was supported by upregulation of the cell killing pathway being upregulated, cell proliferation and IFN-II response. However, as discussed in section 4.6.4, increased type II interferon can also have a regulatory function leading to the reduced function of the CD8 T cells[270,271]. This may be one of the driving factors for increased immune activity outside of the tumour compared to at the tumour border. Cell-cell adhesion pathways were also observed, and this might be linked to the movement of cells into the tumour.

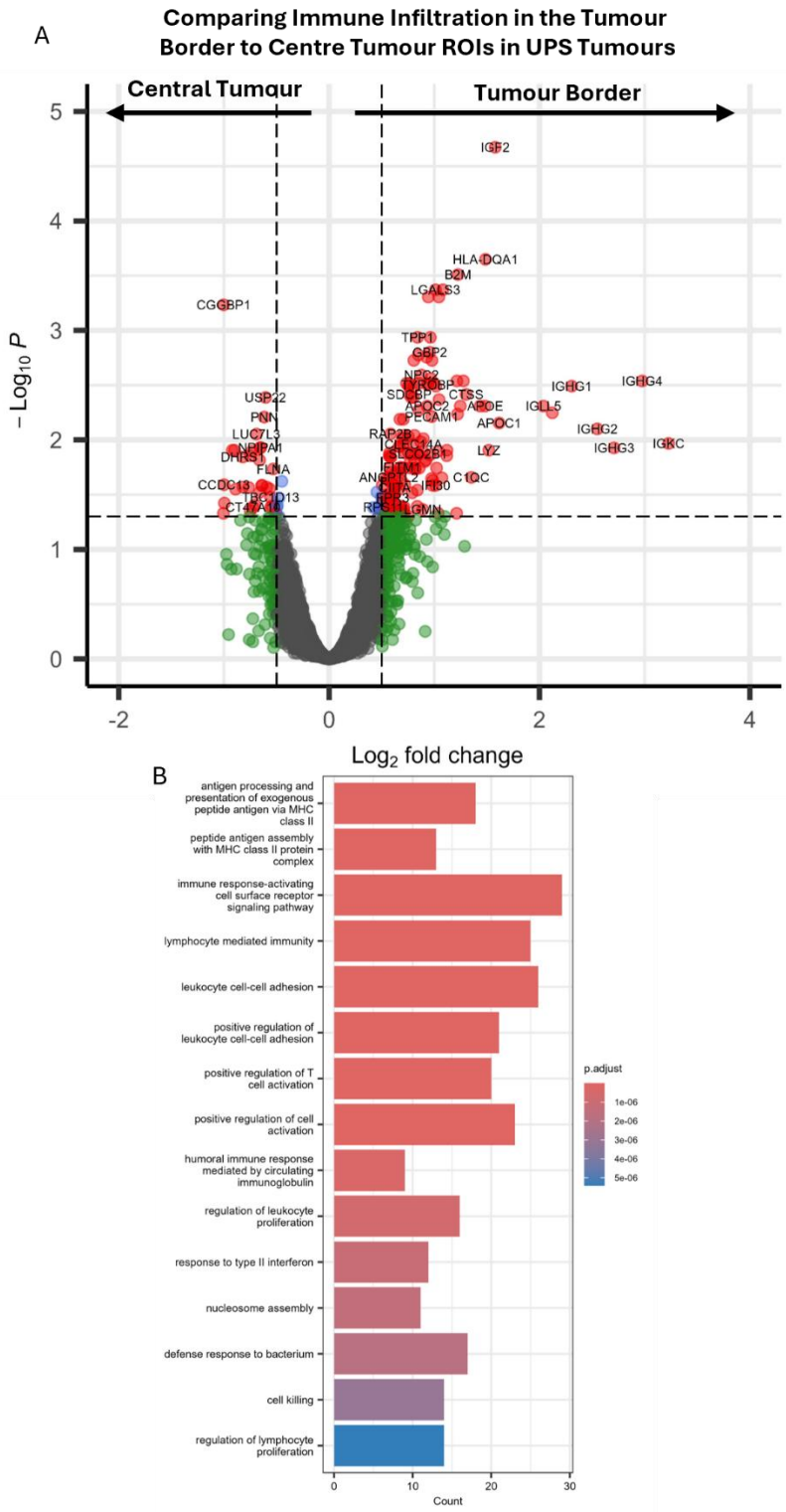


Figure 4.16: Comparing the transcriptomic profile of highly infiltrated ROIs at the tumour border to central tumour in the UPS tumour type assessed by immunofluorescence during ROI selection. (A) Volcano plots showing differential expressed genes comparing (left) central tumour and (right) the tumour border, log2 FC indicates the relative expression level changes for each gene compared to each other with P adj = 0.5 significance level. (B) pathway analyses of upregulated differentially expressed genes from regions inside the tumour border when compared to central tumour, with a Padj value of 0.5. Points in red represent gene that were expressed significantly over both thresholds, blue were significantly over the adjusted p value, green points were above the fold change threshold but were not above the Padj value and genes represented in black were not statistically different between the variables being described.

There were no significantly DEG within the same comparison (i.e. border vs central tumour) of the LMS tumour types (Supplementary Figure 4.8).

These data suggested higher antigen recognition at the UPS tumour border compared to the central tumour. This suggested differences in infiltration between the locations within this UPS tumour. The lack of DEG in the LMS tumours may be that having a binary difference associated with location within the tumour was not specific enough to assess the differences. Analysis by weighted gene correlation network analysis (WGCNA) may provide more detail.

### 4.6.7 There was upregulation of CD8A expression within the central tumour

Next, the transcriptomic assessment of CD8 T cells was assessed in different regions of the tumour, using a segmentation tool during the ROI selection on GeoMx platform. This was to specifically assess the transcriptomic profile of this cell type, identified using IF staining of cell surface receptors. Expression profiles **of CD45+CD8+ T cells in LMS tumour border ROI** were compared to the **central tumour**. There were 58 DEG (p adj. = 0.05, Figure 4.17A). CD8A, IGHG3, and IGHG1 were upregulated within the central tumour (Supplementary Figure 4.9). CD8A expression suggests that the areas selected were more infiltrated with CD8 T cells. This finding goes against the hypothesis that there would be more immune cells at the tumour border with closer proximity to healthy vasculature which would allow for infiltration. IGHG3, and IGHG1 are immunoglobulin genes. In the **tumour border ROIs,** there was upregulation of HLA-DRB1 (as previously discussed in sections 4.6.4-4.6.6) and CXCL9, the expression of which is associated with increased immune infiltration in breast cancer[263,268]. CXCL9 is also shown to drive interferon mediated immune cell infiltration[263]. This showed that there were mechanisms for cells to enter the tissue at the tumour border

but interestingly the central tumour shows higher immune signatures. The assessment by the SpatialDecon and WGCNA packages, discussed in chapter 4.7, may provide more insight into the mechanism driving this. However, because the GeoMx technique has an inherent bias, the selection and annotation of the ROIs may be influenced by the relative immune abundance within each individual tumour.

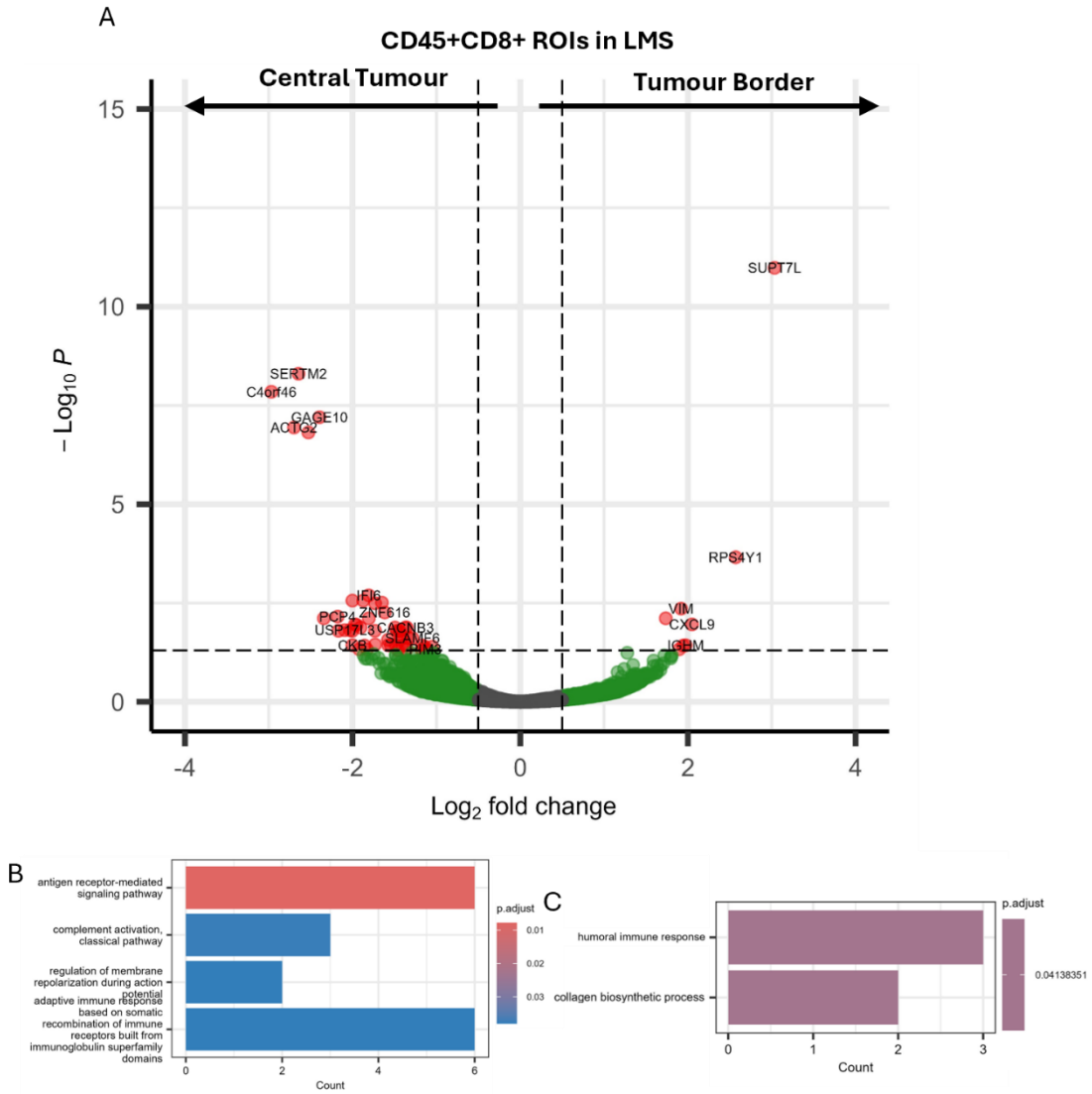


Figure 4.17: Comparing the transcriptomic profile of segmented ROIs in LMS. (A) Volcano plots showing differential expressed genes of CD45+CD8+ segmented ROIs in the central tumour (left) to the tumour border (right) in the same tumour type. Cut off points at log2 FC indicates the relative expression level changes for each gene compared to each other with Padj = 0.05 significance level. Pathway upregulated in (B) CD45+CD8+ segmented border ROIs in the LMS tumour when compared to the central tumour, (C) CD45+CD8+ segmented central ROIs in the LMS tumour when compared to the tumour border. Padj value of 0.05. Points in red represent gene that were expressed significantly over both thresholds, blue were significantly over the adjusted p value, green points were above the fold change threshold but were not above the Padj value and genes represented in black were not statistically different between the variables being described.

Pathways of interest in the **central tumour tissue of the LMS samples** (Figure 4.17B) included antigen receptor-mediated signalling pathways, and adaptive immune response based on immunoglobulins. Along with this there is the complement activation pathway. This all suggests there are immune cells at work in the central tumour but not enough to overcome the tumour or drive an 'immune hot' phenotype. Upregulated genes in the **border LMS ROI** (Figure 4.17C) include humoral immune response from upregulated immunoglobulin genes. B cell responses have been implicated in sarcomas before[86] making this reassuring to find within the tissue. This is contrary to what is seen in the UPS tumours, specifically increased immunoglobulin and MHC genes in the tumour border.

It was not possible to compare CD45+CD8+ profiles in the UPS samples as there were too few regions selected for comparison.

## 4.7 Investigating immune cell infiltration by transcriptomic deconvolution

Many DEG were identified depending on the tumour subtype, immune abundance, and/or location within the tumour. However, canonical immune markers, for example CD8A, were not typically differentially expressed (except in the targeted segmentation analysis). This suggested that the distribution of immune cells may not be as variable between tumours and in relation to the tumour border as the previous literature would suggest. Cell populations hypothesised to be present from this data included macrophages, Tregs and fibroblasts. However, the cell types involved were not confirmed by DGE analysis. It therefore seemed pertinent to attempt to identify the cells involved using cellular deconvolution. The SpatialDecon[115] package in R was used to estimate the cell types and abundance within the ROIs based on a reference dataset (ImmuneTumor_safeTME[115]).

The intention was to investigate which immune populations could be causing upregulation in antigen presentation and whether the factors believed to be contributing to differences in the phenotype were having an effect. It was hypothesised that there would be more antigen presenting cells in the UPS border compared to the central tissue. The inverse was hypothesised for the LMS tumours. It was also hypothesised that the USS tissue would show variations in immune populations across different regions, whereas fibroblasts abundance was hypothesised to differ between the tumour types.

### 4.7.1 Increased fibroblast presence in the tumours may be reducing immune abundance and function whereas CCR7 expression on Tregs could be linked to higher infiltration

Firstly, the populations of all non-segmented ROIs were investigated. Figure 4.18 A shows a relative estimate of abundance of immune and stromal populations comparative to each of the cell types in the ROIs. These data suggests that the immune infiltrates within the different LMS tumours are similar, whereas there was more variation in these populations in the single UPS and single USS tumours. The location of the ROI within the tumour did not seem to show differences. This could possibly suggest that the cells within these have very similar immune populations throughout these tissues.

The most highly abundant immune cell type across these tumour tissues was theorised to be macrophages based on relative expression of macrophage markers. These were the highest proportion in the USS and UPS tumours when compared to the LMS tumours. Macrophages can be proinflammatory, having anti-tumour effects or pro-tumourigenic, depending upon the polarisation of the population. This can be determined by the expression profile of the macrophage. Looking at the top genes that are associated to the

cell type of macrophage in Figure 4.18 B, both CD68 (pro-immunogenic) and CD163 (pro-tumour)[174] are expressed and seen within the heatmap. These markers do not associate to one type of tumour, so it is unclear if there are differences in these populations. The expression pattern of FN1 is intriguing. FN1+ macrophages have been linked to an increasingly suppressive environment in other cancer studies[290]. So, although the LMS ROIs show lower abundance of macrophages, it is suggested that the macrophages present have a more regulatory function[290].

There was higher expression of HLA-II class genes, including HLA-DPA1, HLA-DRA, HLA-DPB1, and HLA-DQB1 within the ROIs selected from the **border** of the **USS** and **UPS** ROIs (Figure 4.18B) which agrees with the DGE analysis. These data could suggest increased antigen recognition by macrophage populations in the border tissues of UPS and USS tumours. Also, within the **border UPS** and **USS** ROIs there was high expression of complement genes C1QA, C1QB and C1QC[282], when compared to the central ROIs and LMS ROIs (Figure 4.18B). The C1Q genes are often expressed by tissue resident macrophages found within tumours[291] and C1QC has been linked to fibroblast associated macrophages in UPS samples[283,291]. Reports suggest that macrophages can bind to fibroblasts within UPS tumour types increasing cancer cell escape[202]. With both cell types being estimated to make up a high proportion of the tumour microenvironment this is important to consider. However, C1QA, C1QB and C1QC expression has also been reported on T follicular helper cells, memory B cells and CD8 T cells in an analysis of human osteosarcoma samples and has been associated with infiltration into those tumours[282]. This ubiquity of expression by several cell types and the non-cell type selective nature of the whole transcriptome analysis of a large ROI means it is not possible to confirm the expression of these C1Q genes is by the macrophages.

A

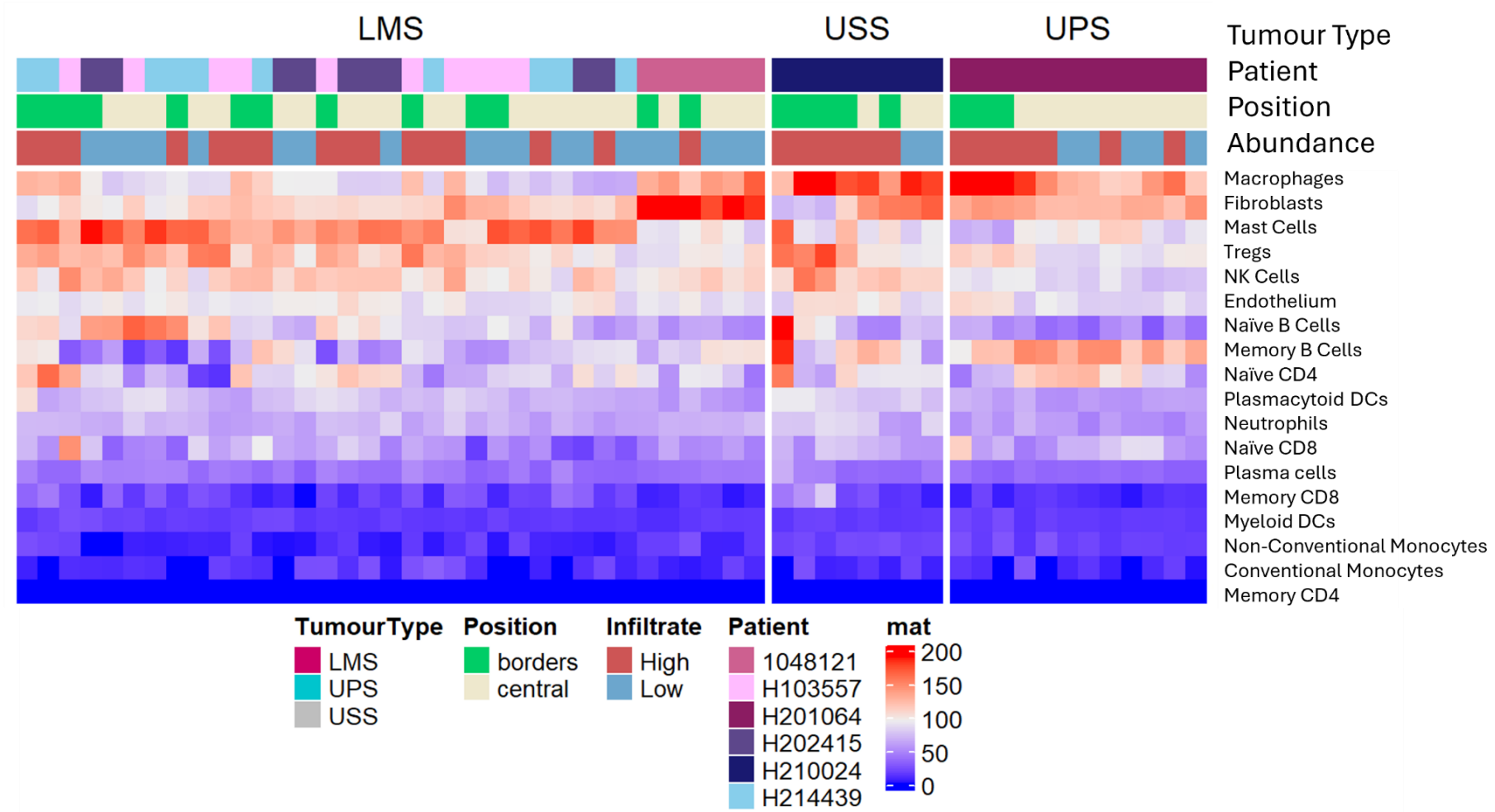
LMS
USS
UPS
Tumour Type
Patient
Position
Abundance
Macrophages
Fibroblasts
Mast Cells
Tregs
NK Cells
Endothelium
Naïve B Cells
Memory B Cells
Naïve CD4
Plasmacytoid DCs
Neutrophils
Naïve CD8
Plasma cells
Memory CD8
Myeloid DCs
Non-Conventional Monocytes
Conventional Monocytes
Memory CD4
TumourType
LMS
UPS
USS
Position
borders
central
Infiltrate
High
Low
Patient
1048121
H103557
H201064
H202415
H210024
H214439
mat
200
150
100
50
0

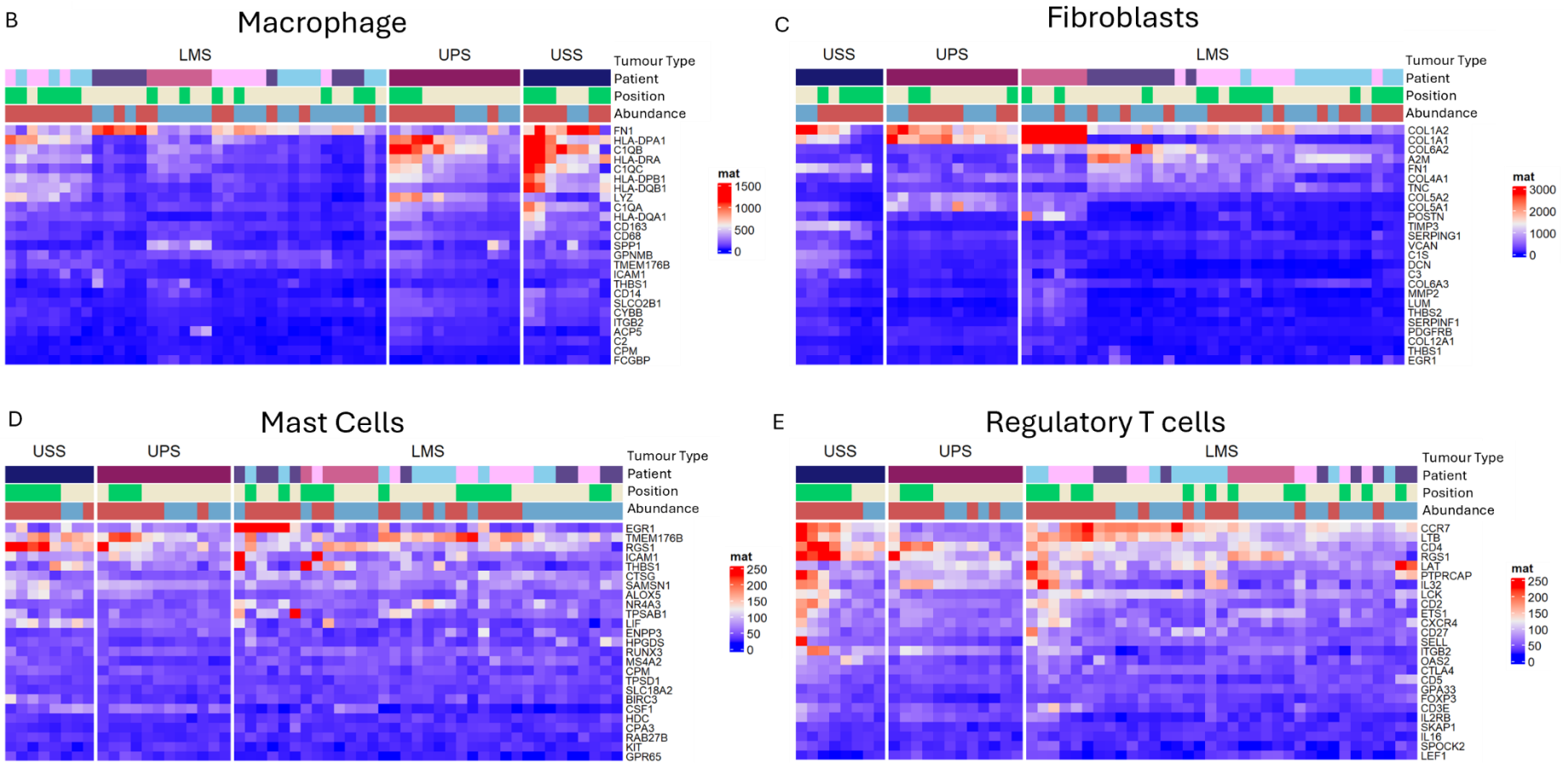


Figure 4.18: A heatmap representations for the abundance of cell types identified from cell deconvolution evaluation from transcriptomic analysis of sarcoma digital spatial profiling. The expression profiles of genes from cells of interest. (A) is the cell deconvolution for the whole, unsegmented ROIs with the top annotations including the tumour type with LMS (teal), USS (grey) and UPS (raspberry), tumour location with border (green) and central (cream), and infiltrate abundance being high (brown) or low (blue). The individual patients are also included with H103557 (plum), 1048121 (hot pink), H214439 (sky blue), H201064 (maroon), H202415 (purple), H210024 (midnight blue). Expression profiles of the reference set for cell types of interest including (B) macrophages, (C) fibroblasts, (D) mast cells, and (E) regulatory T cells for each ROI. The matrix scale (mat) is the cell abundance estimate (beta) produced by the SpatialDecon analysis. This was based on expression of genes associated to a cell type within the selected ROIs, relative and normalised across the dataset.

In the *in vivo* sarcoma HIFU study outlined in chapter 3, increases in macrophage infiltration were demonstrated post-HIFU (Section 3.5.2). The data from the SpatialDecon analysis suggests that the more infiltrated sarcomas had a higher infiltration of macrophages. This aligns the two analyses and implicates macrophage populations as being a prevalent immune population.

Fibroblast related genes are highly expressed across all three of the sarcoma tumour subtypes analysed. These cells are implicated to be important in tumour development, by helping shape the tumour microenvironment including the infiltration of immune cells and the extracellular matrix composition, although there does not seem to be a direct link in the abundance of fibroblasts with survival[292]. There have been studies to suggest that the types of fibroblasts affect the ability of immune cells to contact cancer cells leading to reduced infiltration into the deeper tissue[293]. Within this study, levels of fibroblasts do not correlate with the immune abundance or location within the tumour. However, there is literature to suggest that fibroblasts vary between sarcoma subtypes, with LMS estimated to have higher fibroblast composition. Due to sarcomas being from a mesenchymal origin, many of the genes used for the identification of fibroblasts may be expressed by the cancer cells which could be very abundant within these whole ROI selected samples. Notably, collagen genes including COL1A2 and COL1A1 are raised within a subset of patients (Figure 4.18C). There have been studies that describe an increase in collagen formation due to tumour-associated fibroblast presence within tumours[210]. This has consequently led to high collagen density within tumours and can lead to weaker T cell responses[210], while maintaining their abundance.

When focusing on the mast cell (MC) population, as shown in Figure 4.18A, a higher infiltration of MCs was seen in LMS ROIs. This is a shared trait across most of the patients (3 out of 4 tumours). Typically, MCs are involved in the distribution and release of secretory granules which can contain histamine as well as other modulators including cytokines[294,295]. Not unlike the aforementioned macrophages, the MCs can either have both a pro-inflammatory or pro-tumourigenic phenotype dependent upon the signals that are being produced by the cell[187,296]. Unfortunately, the MC type could not be elucidated from the expression profiles produced (Figure 4.18D). However, EGR1 was associated with a subgroup of the LMS tumours, which have varied factors associated with them. Expression of EGR1 is associated with TNF release by MCs[297]. These TNF producing MCs have been shown to be associated with antigen activation[297,298]. It is plausible to suggest that this did not provide a strong enough response for downstream activation of effector cells.

Regulatory T cells (Tregs) were featured at high levels across tumour types, independent of position within the tumour and immune abundance. This is shown in Figure 4.18A. Tregs are involved in immune tolerance, impacting on regulation of differentiation and activation of other immune cell types[150]. High infiltration of Tregs has been previously reported to be associated with poorer outcomes in many tumours[27,299], including sarcomas[150]. When assessing the expression of Treg genes (Figure 4.18E) there did not seem to be a correlation between any of the factors within this analysis. Tregs seem to be here a particularly homogeneous population, however CCR7 expression was upregulated in some ROIs, mostly favouring the LMS and USS ROIs. Tregs require CCR7 to migrate into lymph nodes where they encounter APC and proliferate[37] before entering tissues. In cancer studies, CCR7+ Tregs are correlated with poorer outcomes[37]. The expression of CCR7 seems to correlate with

immune abundance so it may be that these areas of denser infiltration are caused by infiltration of the CCR7+ Tregs into tissue.

Within Chapter 3, within the tumour a high proportion of the CD4 T cells were Tregs (Section 3.3.2). Along with this, the data suggested that the HIFU treatment given to the sarcoma tumours caused an increase in this Treg phenotype within the draining lymph node (Sections 3.4.2 and 3.5.3), which may have been related to the antigen presentation caused by the treatment. This suggest that Tregs are quite prevalent within sarcomas, as also suggested in Figure 4.18 A.

NK cell genes were expressed across the samples as seen in Figure 4.18 A. NK signatures were more highly expressed compared to CD8 T cell genes. Previous literature suggest that infiltration of NK cells is inversely proportional to T cells[200]. This phenomenon can also be seen in this study. It is noted that metastasis free survival of sarcoma is associated with a specific subset of NK cells[5], however this requires the single cell resolution that is not available within this study.

When evaluating B cell populations, the SpatialDecon package associated two types of B cells to the expression data. Naïve B cell signatures were more highly expressed in the LMS samples. Memory B cell genes were more highly expressed in the UPS samples. Both types were expressed across the USS ROIs. This suggests that B cells in the UPS samples might have been activated in the tumours. Typically, 'immune-hot' tumours like melanoma have higher memory B cell populations within the tumour microenvironment[300].

Within this analysis, macrophages, mast cells, and B cell subsets had different proportions in the different tumour subtypes analysed. This gave an indication that the tumour subtypes have different tumour microenvironments. The different abundance of different cells may

have influenced previous work that only focused on one cell type that some tumour subtypes were globally more infiltrated than another. Regardless of the tumour type, Tregs and fibroblasts were similarly abundant across subtypes. The regulatory cells would likely reduce infiltration and activation of other cells which may account for the lack of cytotoxic cell signal in these tumours. This includes the prevalence of FN+ macrophages in LMS and SSS tumours, as well as the collagen genes in fibroblasts in the UPS. The immune cell profile may account for varied response to immunomodulatory therapies based on tumour subtypes as previously reported[59,73,75,81]. Ideally, future systemic treatments including immunotherapies would be personalised not only for subtypes but for individual tumours based on general infiltration types.

### 4.7.2 Transcriptomic profiling of segmented immune infiltrates identified naïve CD8+ T cells and macrophages as the predominant populations

Next, the segmented immune regions of interest were investigated. This allowed for the transcriptomic profile from specific cells to be sampled based on their immunofluorescence. The segmentation works sequentially so that the CD45+CD8+ T cells are first selected, and this is followed by CD45+CD8- leukocyte cells.

CD45+CD8+ ROIs expression profiles were evaluated in Figure 4.19A and naïve CD8 cells were identified as a highly expressed cell type. This suggests that these CD8 T cells are not antigen experienced[118], however cancer studies have shown these types do continue to be cytotoxic in the tumour and are more resistant to TGF-β-induced apoptosis. This may be a causative factor for this being the most prevalent CD8 T cell type. Hence the ROI selected do not have a strong cytotoxic signal. Data presented here show that that the ROIs from the USS tumour border had both a memory and naïve CD8 phenotype (Figure 4.19A).

Noteworthy, the SpatialDecon estimation shows presence of other cell types as well as CD8+ T cells. This suggested that the probes from other cell types were also sampled during the segmentation. It is possible the segmentation strategy acts more as an enrichment analysis rather than a strict isolation of the cell type of interest. This was demonstrated by the macrophage, mast cell, NK cell and Treg cells shown to be variably detected within these ROIs (Figure 4.19A).

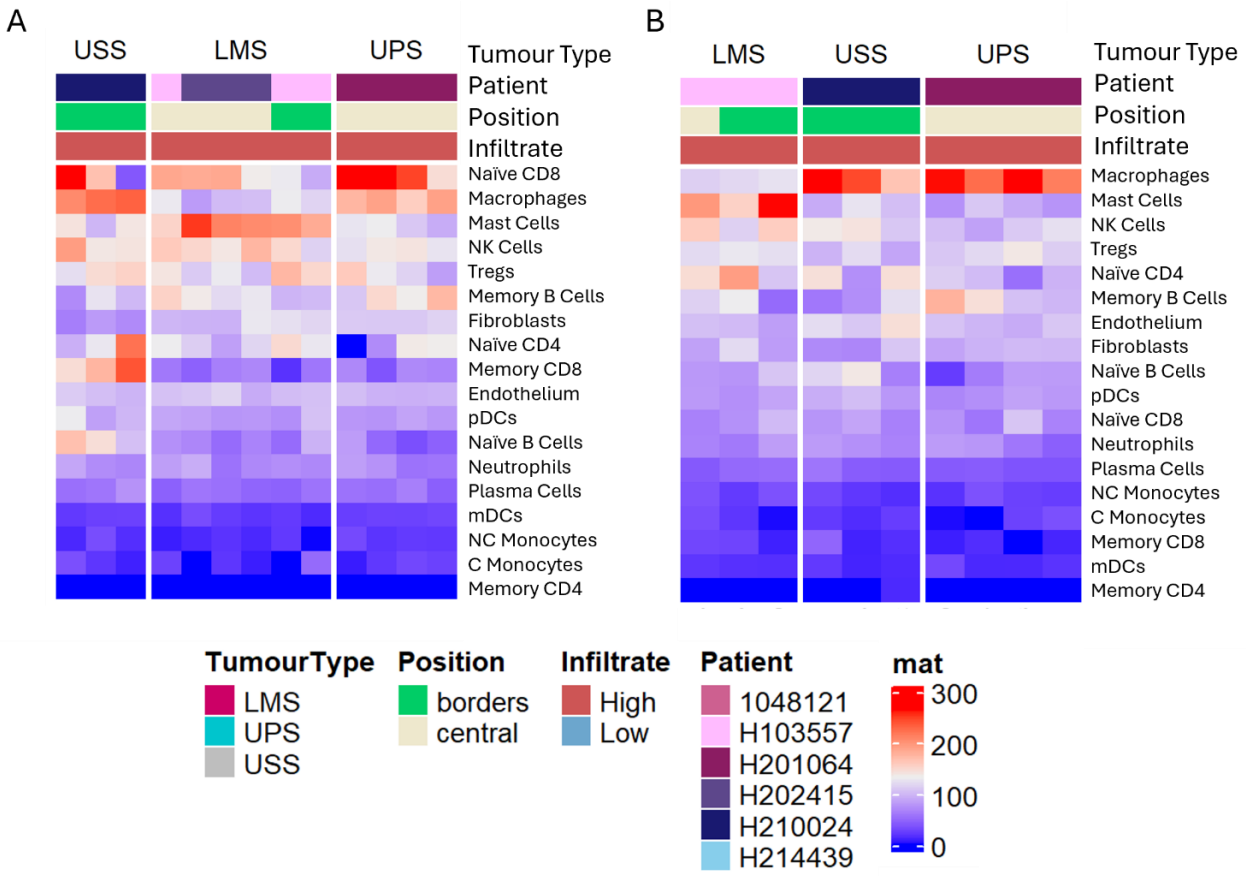


Figure 4.19: A heatmap representations for the abundance of cell types identified from cell deconvolution evaluation from the transcriptomic analysis for (A) the cell deconvolution for the CD45+CD8+ ROIs and (B) CD45+CD8- ROIs with the top annotations including the tumour type with LMS (pink), UPS (purple), and USS (grey), tumour location with border (green) and central (cream) and infiltrate abundance being high (red) or low (blue). The individual patients are also included with H103557 (plum), 1048121 (hot pink), H214439 (sky blue), H201064 (maroon), H202415 (purple), H210024 (midnight blue).

Following this, the CD8+ T cell excluded CD45+ immune cells were specifically assessed. When the CD45+CD8- segmented ROIs were assessed (Figure 4.19 B), the detection of CD8+ cells was almost non-existent which suggests that the initial selection of CD8 T cells based on IF was adequate. There was a difference in estimated macrophage abundance

between subtypes. Macrophages are a predominant immune cell in the UPS tumours[174], which was reflected in this analysis. Macrophages were also demonstrated to be an abundant cell within the USS ROIs, whereas mast cells are more prevalent within the LMS tumour ROIs than UPS. This finding reflected the whole ROI comparisons in section 4.7.1 and suggests that macrophages are the predominant immune cell within the **UPS** and **USS** samples but not the **LMS ROIs**.

### 4.7.3 Interpretation from SpatialDecon analysis

It is important to note that the majority if the CD45 IF stain seemed to colocalise with the CD8 IF staining within all tumours as outlined in Figure 4.6. This possibly suggested by IF alone that the predominant immune cell population was CD8 T cells. However, the transcriptomic analysis suggested a larger proportion of the cell types were macrophages. This is of note because previous research investigating the infiltration of these tumours has been conducted by immunohistochemistry alone which may have lower sensitivity for immune cells. The work presented here therefore highlights that the true picture of immune cell infiltration may be underrepresented without the power of spatial transcriptomics, and thus the notion that some soft tissue sarcomas are immunologically 'dessert' may be somewhat inaccurate. This idea is supported in a few recent studies[61,169]. This strengthens the hypothesis that differences in immune cell types are seen between different sarcoma subtypes. This may have influence on treatment outcomes and direct relevance to future treatment strategies including immunotherapies for sarcoma.

## 4.8 Unbiased gene network analysis

It was hypothesised that these three tumour subtypes (LMS, UPS, USS) have vastly different TME. The DGE analysis (Figure 4.11-Figure 4.17) and cellular deconvolution (Figure 4.18-Figure 4.19) aimed to identify the factors that are contributing to the distinct infiltration of these tumour types. These analyses gave insight into the localisation of antigen recognition, structural differences between the subtypes, differences in different immune cell abundances and levels of regulatory cells, based on locations in the tumour and subtypes. However, thus far the ability to definitively determine these cell types, and the mechanisms truly involved in the infiltration differences has not been established.

To this end, an unbiased analysis was conducted to determine if these factors are separate or interlinked. There may have been factors that the analysis was biased by (such as immune abundance within ROI) that has led to the important differences between the data being missed. It was thought that gene network analysis could help identify such biases. Further information on the different cell types that have been identified as being important in analyses in sections 4.6 and 4.7 may also be provided.

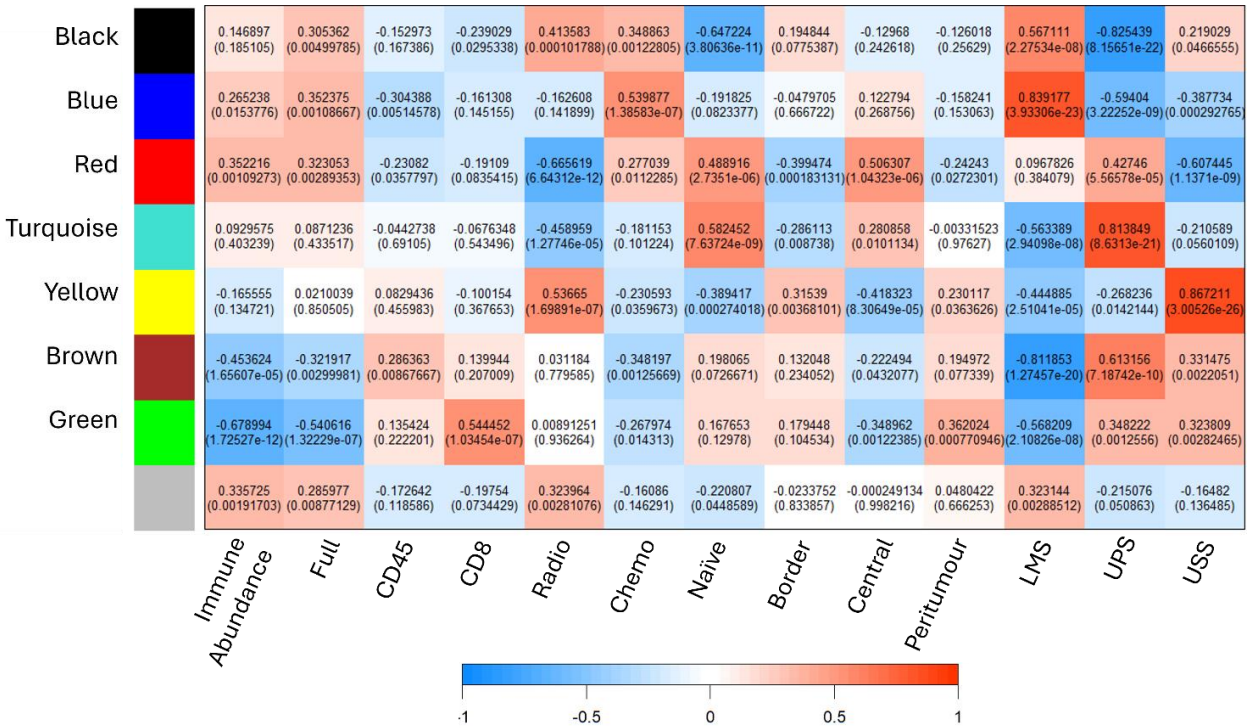


Figure 4.20: Study and clinical factors association with modules identified by weighted gene correlation network analysis. Pearson's correlation coefficient matrix with the module trait correlation and p adjusted expression in brackets.

A weighted gene correlation network analysis[123,301] (WGCNA) was performed (as outlined in methods section 2.7.4). This was used to develop a network of genes based on clinical or workflow factors within the study (for example tumour subtype, ROI location relative to the tumour border, previous treatment, and segmentation strategy). It was hypothesised that a global analysis of the data may elucidate the most important mechanisms driving differences in infiltration. The correlation of factors in the study associated to modules are shown in Figure 4.20. There were 7 modules identified, with genes that were not associated to a module in Grey. A detailed assessment of association of each individual ROI to the modules are shown in Figure 4.21. To assess and understand these modules, pathway analyses was conducted on the modules using the clusterProfiler package in R[121]. Six of the 7 modules had significant pathways (P adj < 0.05, q value cut off at 0.1). The black module did not have any pathways associated that were above this threshold. These findings are discussed below.

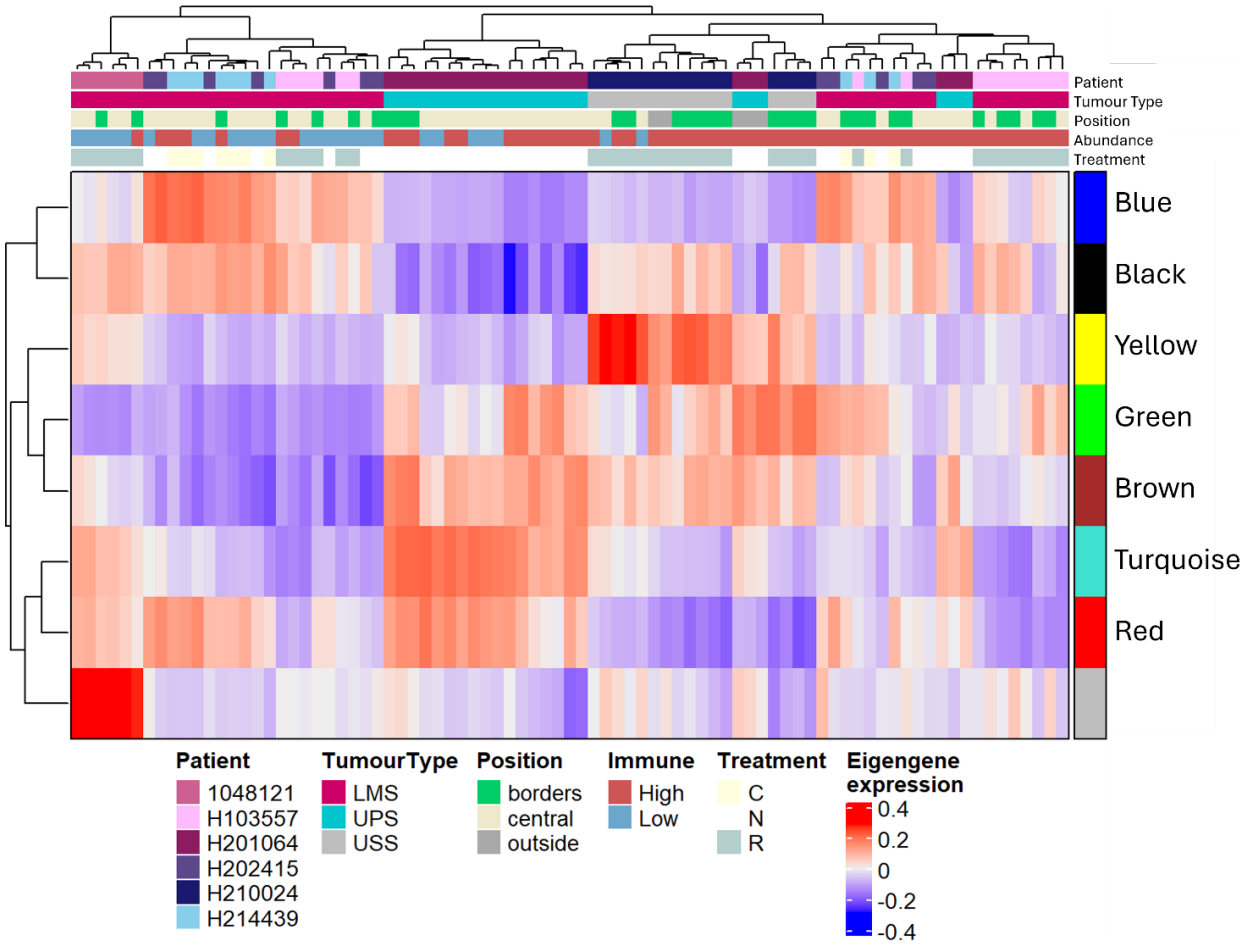


Figure 4.21: Hierarchical clustering dendrogram with samples and the expression of the genes within each module for each ROI with the top annotation including annotations for tumour type with LMS (pink), UPS (teal) and USS (grey). The position of ROI in the tumour, either border (green), central (cream) or outside the tumour (grey), the immune infiltration either high (red) or low (blue). The individual patients are also included with H103557 (plum), 1048121 (hot pink), H214439 (sky blue), H201064 (maroon), H202415 (purple), H210024 (midnight blue).

### 4.8.1 The unbiased assessment of the transcriptomic profiles of the LMS and UPS tumour support the findings of the differential expression analysis

The blue module was primarily correlated with LMS ROIs (0.838. p<4e-23), secondarily correlating with chemotherapy treatment (0.540. p<2e-07) as shown in Figure 4.20. There were inter-LMS patient differences in the strength of the association indicating biological tumour individuality (Figure 4.21). The position and immune abundance of the ROI did not seem to affect the correlation of the tumour to this module. The pathways implicated by the genes in this module (Figure 4.22A) were muscle and structural related, with many of the

genes being highlighted in the differential expression when comparing the LMS type to the UPS type in sections 4.6.1 to 4.6.3, supporting the validity of these findings. Muscle genes included are MYOC, MYOCD, MYLK, MYL9, ATCN, ACTC1, with collagen genes COL6A1, COL6A3, COL14A1 also within this module. On pathway analysis, some of these genes were shown to be shared while others are limited only to that individual pathway as shown in Figure 4.21A. The involvement in these muscle pathways is likely linked to the LMS being a smooth muscle tumour with this being a strong driver of the highly expressed genes within these tumours. Muscle related genes are often reported higher in LMS tumours when compared to UPS tumours[302–304]. There has also been work that shows upregulation of these muscle genes is correlated with a reduction in immune infiltration[305]. As discussed, collagen meshes in the tumour can reduce T cell functions by impairing their cytotoxic function. It could be that muscle fibres throughout the tumour are increasing this phenomenon.

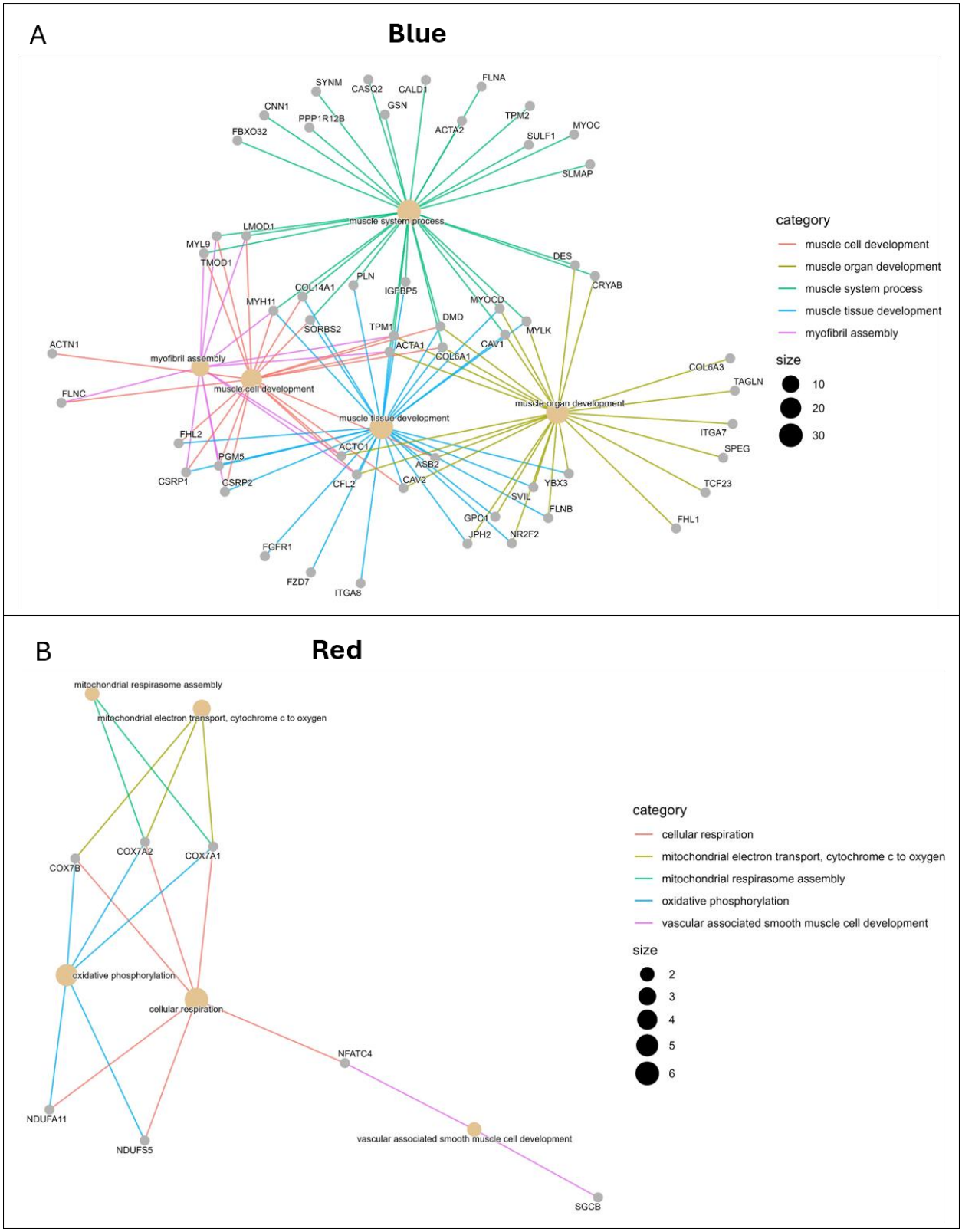
A
Blue
SYNM
CASQ2
CALD1
FLNA
CNN1
GSN
PPP1R12B
TPM2
FBXO32
ACTA2
MYOC
SULF1
SLMAP
muscle system process
LMOD1
MYL9
TMOD1
DES
CRYAB
PLN
COL14A1
IGFBP5
MYH11
MYOCD
SORBS2
TPM1
DMD
MYLK
ACTN1
ACTA1
CAV1
COL6A1
myofibril assembly
COL6A3
TAGLN
FLNC
muscle cell development
muscle organ development
muscle tissue development
ITGA7
FHL2
ACTC1
SPEG
PGM5
ASB2
CSRP1
CSRP2
CFL2
CAV2
YBX3
TCF23
SVIL
FLNB
FHL1
GPC1
JPH2
NR2F2
FGFR1
FZD7
ITGA8
category
muscle cell development
muscle organ development
muscle system process
muscle tissue development
myofibril assembly
size
10
20
30
B
Red
mitochondrial respirasome assembly
mitochondrial electron transport, cytochrome c to oxygen
COX7A2
COX7A1
COX7B
oxidative phosphorylation
cellular respiration
NFATC4
NDUFA11
NDUFS5
vascular associated smooth muscle cell development
SGCB
category
cellular respiration
mitochondrial electron transport, cytochrome c to oxygen
mitochondrial respirasome assembly
oxidative phosphorylation
vascular associated smooth muscle cell development
size
2
3
4
5
6

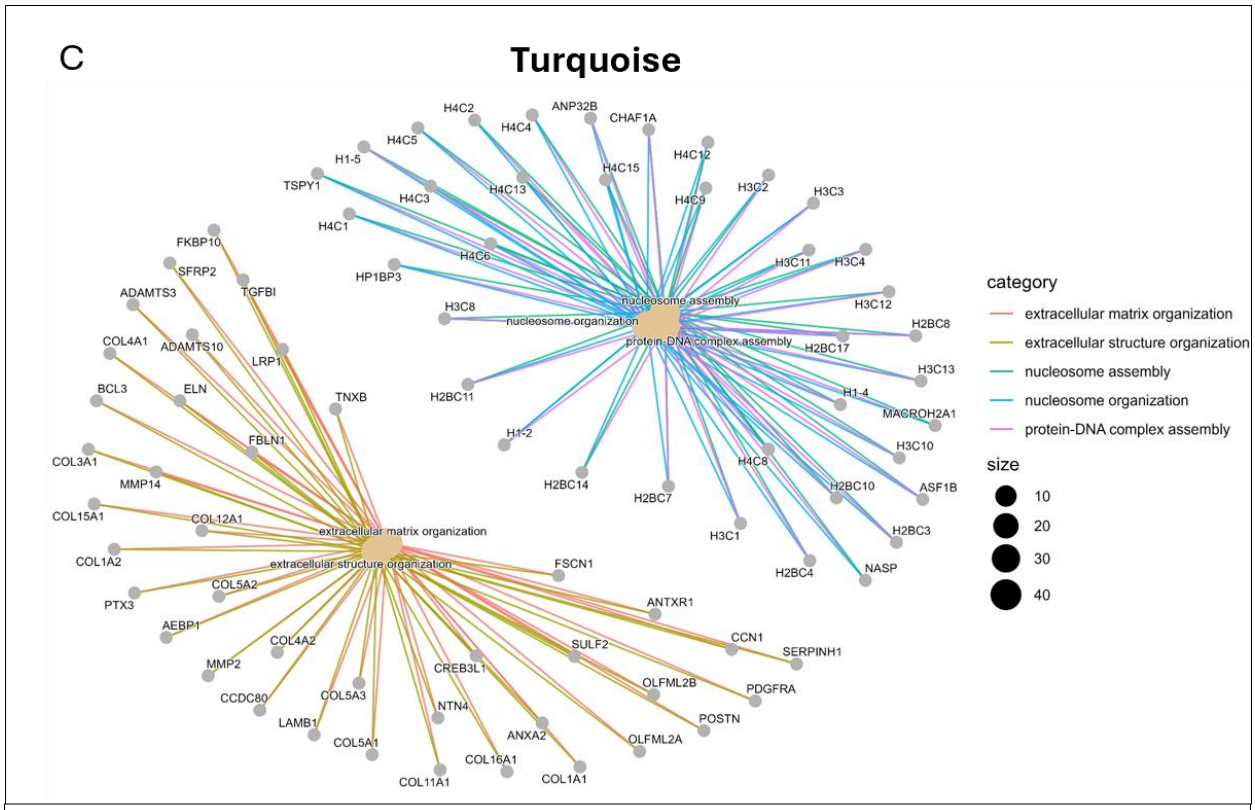
C
Turquoise
H4C2
ANP32B
CHAF1A
H4C4
H4C5
H4C12
H1-5
H4C15
TSPY1
H4C13
H3C2
H3C3
H4C3
H4C9
H4C1
FKBP10
H4C6
SFRP2
HP1BP3
H3C11
H3C4
ADAMTS3
TGFBI
nucleosome assembly
H3C12
H3C8
nucleosome organization
H2BC8
COL4A1
ADAMTS10
protein-DNA complex assembly
H2BC17
LRP1
H3C13
BCL3
ELN
TNXB
H2BC11
H1-4
MACROH2A1
FBLN1
H1-2
H3C10
COL3A1
H4C8
MMP14
H2BC14
H2BC7
H2BC10
ASF1B
COL15A1
COL12A1
H3C1
H2BC3
extracellular matrix organization
COL1A2
extracellular structure organization
FSCN1
H2BC4
NASP
COL5A2
PTX3
ANTXR1
AEBP1
CCN1
COL4A2
SULF2
SERPINH1
MMP2
CREB3L1
OLFML2B
PDGFRA
CCDC80
COL5A3
NTN4
POSTN
LAMB1
ANXA2
OLFML2A
COL5A1
COL16A1
COL11A1
COL1A1
category
extracellular matrix organization
extracellular structure organization
nucleosome assembly
nucleosome organization
protein-DNA complex assembly
size
10
20
30
40

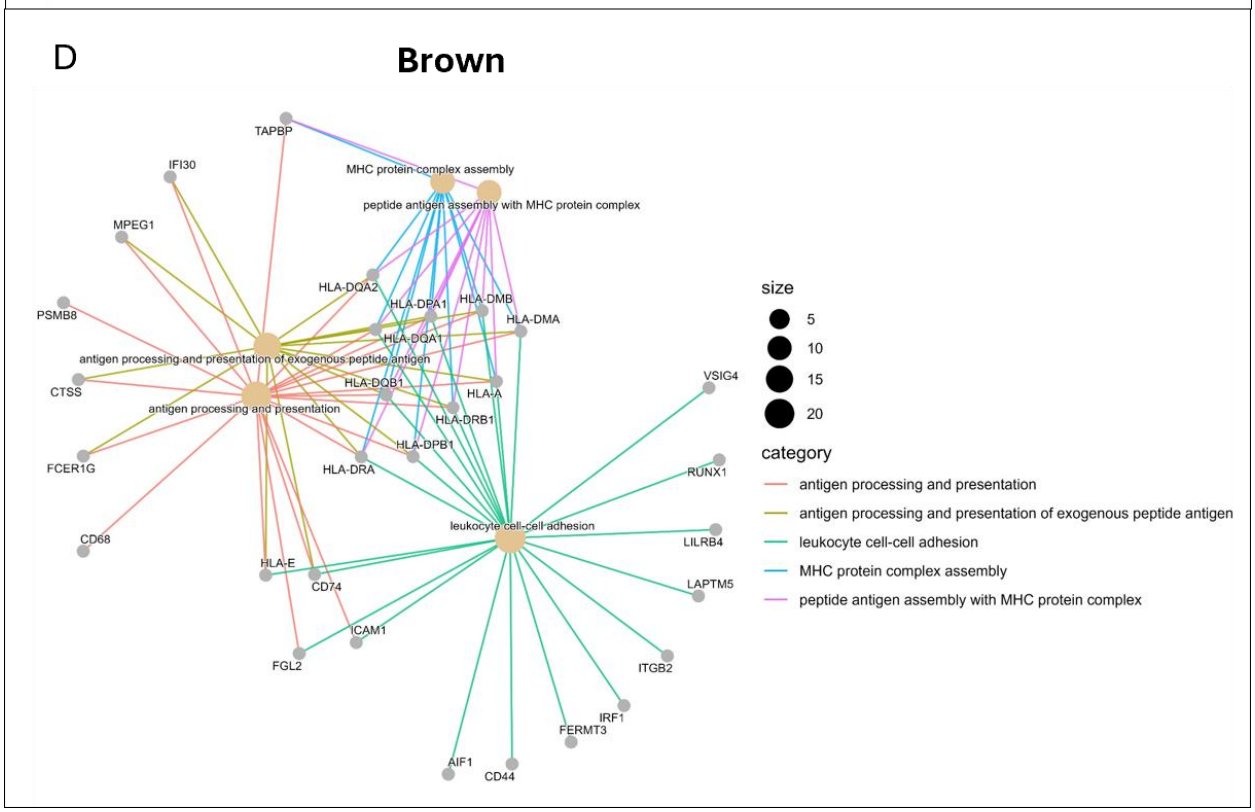
D
Brown
TAPBP
IFI30
MHC protein complex assembly
peptide antigen assembly with MHC protein complex
MPEG1
HLA-DQA2
PSMB8
HLA-DPA1
HLA-DMB
HLA-DMA
HLA-DQA1
antigen processing and presentation of exogenous peptide antigen
HLA-DQB1
VSIG4
CTSS
HLA-A
antigen processing and presentation
HLA-DRB1
HLA-DPB1
FCER1G
HLA-DRA
RUNX1
leukocyte cell-cell adhesion
CD68
LILRB4
HLA-E
CD74
LAPTM5
ICAM1
FGL2
ITGB2
IRF1
FERMT3
AIF1
CD44
size
5
10
15
20
category
antigen processing and presentation
antigen processing and presentation of exogenous peptide antigen
leukocyte cell-cell adhesion
MHC protein complex assembly
peptide antigen assembly with MHC protein complex

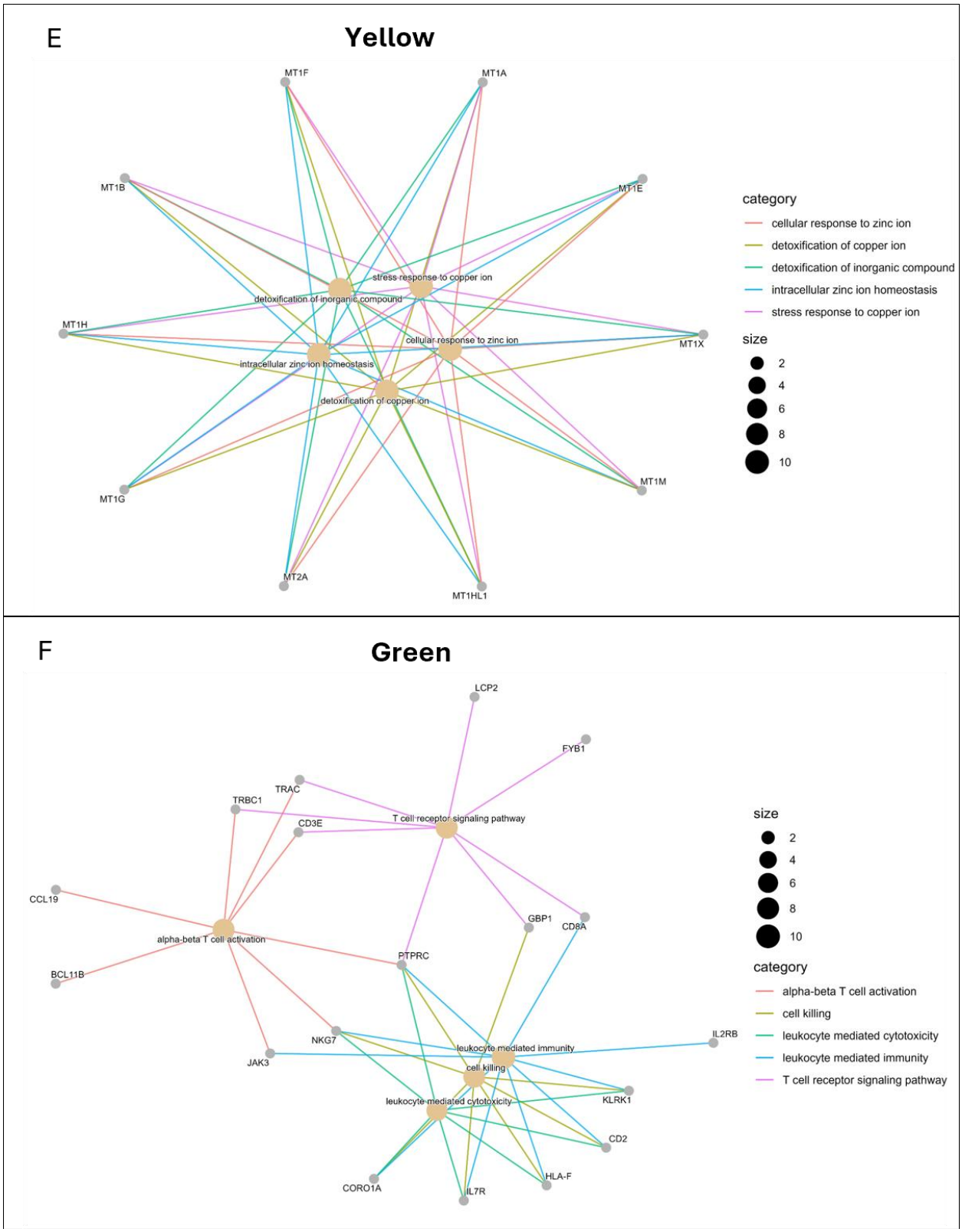


Figure 4.22: The pathway analysis of the modules identified in the weighted gene correlation network analysis represented as dotplots of genes and pathways within six of the modules including the (A) Blue, (B) Red, (C) Turquoise, (D) Brown, (E) Yellow, and (F) Green. Each line represents a link of a gene to a pathway with the different colours within the same module representing a different pathway with the bubble size representing the gene ratio from the pathway assessment.

The red module correlated primarily with treatment naïve samples (0.489. p<3e-06) and central tumour (0.506. p<2e-06), with a lower correlation to UPS tumours (0.427. p<6e-05) as shown in Figure 4.20. Although not apparent of the summed LMS data, an association with the red module was also seen to a subset of the LMS ROIs (Figure 4.21). The significant pathways from this analysis (Figure 4.22B) included respiration-based pathways, notably mitochondrial genes. Sarcomas are known to have high glycolytic rates and most cells use oxidative phosphorylation[306] as identified in this study. This is in accordance with previous studies using in vitro cell lines which show differences in the metabolic profiles based on sarcoma subtype. However, the associations seem to be differently expressed within subsets[307]. COX genes are associated with increased apoptosis within other tumour types[152]. The implicated importance in this subset of the data is not clear. The genes within this small network are highly interlinked and not much weight can be placed on these findings.

Investigating the turquoise module, the genes seem to be strongly expressed in a UPS tumour type (0.814. p<9e-21) and treatment naïve tumours (0.582. p<8e-09) as shown in Figure 4.20, although the UPS tumour is a naïve tumour which could be influencing this Figure 4.21. When interpreting the pathway analysis (Figure 4.22C), there were 2 distinct clusters of pathways that did not interact. The first of which contained structural genes that may be influencing the pathways highlighted. The matrix included many collagen genes (COL3A1, COL1A2, COL15A1, COL4A2, etc.), matrix metalloproteases genes (MMP14, MMP2, ADAMTS10, ADAMTS), and structural functional genes (TNXB, CREB3L1). The collagen genes were also highlighted in the SpatialDecon analysis when assessing the fibroblast abundances in section 4.7. This again brings into account the recent research which has been conducted on the relevance of collagen within the tumour and its effect on

the interactions T cells and cancer cells which affects the ability of further infiltration[210]. Within the turquoise module there were genes associated with nucleosome assembly, nucleosome organisation and protein-DNA assembly. These pathways have also been implicated in the previous differential gene expression analyses in sections 4.6.1 to 4.6.3 when assessing differences between the tumour types based on the tumour location. This may be implicated in increased cell proliferation or transcription. As discussed in section 4.6.3, this may be related to tumour mutational burden, however sarcomas are thought to have relatively low mutational burden[26,61,308].

The yellow module is highly associated with the USS ROIs (0.867, p<4e-26) and ROIs from tumours treated with radiotherapy (0.537, p<2e-07) as shown in Figure 4.20. These genes are associated with pathways involved in metal ions within cells and are typically upregulated after radiotherapy treatment[309]. This suggests that these genes are upregulated likely due to the treatment.

The brown module had primary association to UPS ROIs (0.613. p<8e-10) followed by the CD45 segmented regions (0.286. p<0.009) as shown in Figure 4.20. However, upon further investigation Figure 4.21 shows association to all UPS ROIs. Figure 4.22D outlines immunological pathways identified from the identified genes. Included in this analysis was multiple HLA genes spanning MHC-I and MHC-II molecules which are associated with antigen processing and presentation pathways with a response to exogenous protein. Further associations include leukocyte cell-cell adhesion, it suggested that the uptake of antigen and activation of immune cells, which likely led to the increase in filtration. The genes that are associated with these pathways include immune related genes such as HLA-II genes, CD68, CD74, CD44, and ICAM. This points towards MHC-II APC recognition by M1

macrophages. With this finding being more closely related to the segmented ROIs it is more likely that the expression of the HLA molecules is by immune cells rather than cancer cells. This improves our confidence in the hypothesis that some sarcoma subtypes have different immune phenotypes as the brown module was strongly associated to UPS ROIs. This may be due to increased recognition of the tumour.

The green module was associated (Figure 4.20) to the CD45+CD8+ segmented ROIs (0.544. p<2e-07). The pathways identified (Figure 4.22E) included αβT cell activation with TCRs, cell killing, leukocyte mediated cytotoxicity and leukocyte mediated immunity. These findings were reassuring as there was enriched for the CD8 T cell populations through segmentation. This module also associated with both the UPS and USS tumour subtypes. This assessment suggested the increased CD8 T cell infiltration in these types and provided more insight into the function of the T cells. The analysis suggested that there is a cell killing response from these cytotoxic cells. T cell genes associated with these pathways include IL2RB (CD122), CD8A, PTPRC, and CD3E. These suggest activated CD8 cells were sampled due to the inclusion of IL2RB expression (CD122) CD8 T cells have previously been associated with poorer survival in a pancreatic study[310]. In addition, the expression of CD122 on CD8 T cells has been associated with TCR mediated antitumour immunity[311]. However, it was not possible to assess these cells further within this study. NKG7 was detected within this analysis, suggesting cytotoxic function and involvement of the NK cells in these segmented ROIs[312,313]. Also implicated was BCL11B, which has previously been associated with TCR signalling in CD8 cells[314]. However, this only suggest that there was some cytotoxic function remaining in the tissue and does not answer the questions posed as to why the cytotoxic activity is not more prominent.

### 4.8.2 Summary of the WGCNA analysis

The WGCNA analysis showed an unbiased approach to assessing the transcriptomic data which agrees with many of the findings from the DEG analysis with some links to the findings in the cellular deconvolution analysis. Modules associated with structural genes were associated with different tumour subtypes. The **LMS tumours** showed **muscle** related genes and pathways whereas the **UPS tumour** showed **collagen** related genes which could be influenced by fibroblasts within the TME. Again, this highlighted the vast differences within subtypes and may implicate differences in the infiltration into these tumours. Of note, an **immunogenic phenotype** associated with **UPS** tumours by the WGCNA and cellular deconvolution showed antigen presentation associated with macrophages being implicated as the prevalent APC. There were T cell antigen recognition and infiltration signatures in the border tissue when assessing the differential gene expression analysis which supported the original hypothesis. The cytotoxic phenotype of CD8 T cells was associated with UPS and USS tumours. This may link into the antigen recognition and infiltration, but the data is too limited to be certain. Previous assessments of the data did not show differential expression of these genes (Figure 4.11), so it helps conclude that there is some but probably not a strong cytotoxic response in these tumours. There was no correlation of the antigen presenting pathways to the central LMS tumours in the WGCNA in contrast to the differential expression analysis (Figure 4.13), which implied a minor effect. This discrepancy may suggest the DEG analysis can be misleading, and that the expression of these genes was lower in the LMS compared to the UPS and USS. It may be that the structures of the tumours affect immune responses as discussed in the DGE analysis in Section 4.6.2.

## 4.9 Chapter Discussion

Within this chapter it was possible to assess the RNA transcriptome of three different sarcoma subtypes across 6 patient samples. The UPS and LMS subtypes are historically reported to have differing immune infiltrations. These differences in the infiltration have previously been highlighted due to the correlation with response to radiotherapy[315].

Table 4.2 presents an overall summary of the differential expression in different tumour regions using spatial characterisation. This study suggested that there were increased **T cell immune** cell signatures and antigen recognition and response within the samples from the UPS tumour transcriptome when compared to the LMS tumours. A deeper investigation into this highlighted that antigen presentation was variable across the ROI within these two tumour types, with **upregulation** being found in the **UPS border** and **LMS tumour centre**.

These analyses showed broad lymphocyte and leukocyte pathways in both tumour types. Specifically, this included B cells and myeloid lineage cells such as macrophages. There have been previous reports of a difference in macrophage infiltration based on sarcoma subtype, in studies which used IHC to profile tumours[169,174]. However, this study implicates macrophages as the main APC within the UPS tumour. Although there seems to be increases in T cell markers in the **UPS** subtype, there was also upregulation of collagen genes within the ROIs which can be linked to fibroblasts within the TME. The **increase in fibroblasts** within the TME has been linked to **reduced CD8 T cell** cytotoxicity. This could be causing a reduction in cytotoxic activity of these cells. The level of immune infiltration does not necessarily relate to level of anti-tumour activity, as shown within the WGCNA analysis (Figure 4.21 and Figure 4.22).

Comparatively, the analysis of the LMS tumours indicated more structural, regulatory and suppressive genes which may influence the infiltration and function of immune cells into these tumours, including an increase in MCs, although these cells can have multiple functions within tumours, both pro and anti-tumourogensis[294,296,298]. It follows that the common distinction of 'hot' and 'cold' subtypes in sarcoma is an oversimplification. The immune cell infiltration into these tumours might have been underrepresented without the power of spatial transcriptomics. However, Nanostring's digital spatial profiling platform has an inherent bias within the data collection. Regions of interest are selected based on IF of selected cell populations, CD45+ and CD8+ immune populations in the case of this study which will have produce a bias within the transcriptomic data that is produced. In many cases of this chapter, the bias was wanted.

Overall, there was increased expression of regulatory immune cells with Treg and macrophage genes being present all tumours (Figure 4.18). There were only a few chemotactic pathways upregulated within these tumours which suggested that these immune cells may be limited in their movement into or through the tissue.

Table 4.2: Concatenation of the findings for the spatial transcriptomic analysis of the UPS, LMS and USS samples

| Focus | Analysis | Expression | Significance |
|---|---|---|---|
| | LMS (vs. UPS) | ACTG2, ACTAC2, ACTN1, CNN1, TAGLN, etc. | Upregulation of structurally related genes within the LMS suggested reduced ability for the function of immune cells |
| | UPS (vs. LMS) | CRIP1/2, CFD, TNXB | Cell migration and EMT genes which may be related to improved mobility of cells within the UPS tissue |
| Border | LMS (vs. UPS) | ACTG2, ACTAC2, ACTN1, CNN1, TAGLN, etc. | Upregulation of structurally related genes within the LMS suggested reduced ability for the function of immune cells |
| Border | UPS (vs. LMS) | NCOA3, AHR | Dedifferentiation genes, associated with ability for cells to move through tissue |
| Central | LMS (vs. UPS) | ACTG2, ACTAC2, ACTN1, CNN1, TAGLN, etc. | Upregulation of structurally related genes within the LMS |
| Central | UPS (vs. LMS) | COL1A1, COL5A1, and COL5A3 | Association of fibroblasts into the central tumour compared to the tumour border and LMS central tumour |
| LMS | High (vs. Low Immune Infiltration) | IGHG1-4, IGKC, HLA-II and HLA-I related genes, INF-y activating pathways | More involvement of MHC-II genes which may lead to unwanted activation of Tregs from antigen presentation pathways |
| UPS | High (vs. Low Immune Infiltration) | No significant differences | Suggested similar immune infiltration throughout the tumour |
| UPS | Peritumour (vs. Border) | FOS, EGR1, SFRP4, CD96 CD3E, IGHG1-4, SFRP4, CD69, MZB1 | Implications for immune cell migration, activation, and vascularisation<br>Suggested immune cell accumulation outside the tumour |
| LMS | Peritumour (vs. Border) | Not able to assess | N/A |
| UPS | UPS (vs. LMS) | IGF2, IGHG1-4, IGKC, IGLL5, HLA-DQA1, B2M, C1QC | More involvement of MHC-II genes which may lead to unwanted activation of Tregs from antigen presentation pathways<br>More B cell at the PMS tumour border |
| UPS | Central (vs. Border) | No significant differences | Higher immune infiltration within the PMS tumour border |
| UPS | Border (vs. Central) | IGF2, IGHG1-4, IGKC, IGLL5, HLA-DQA1, B2M, C1QC | Similar findings to the UPS tumour border suggesting similar immune populations through the UPS tumour |

| | | | |
|---|---|---|---|
| USS | SpatialDecon | Macrophage, fibroblast and Treg abundance | There may be an increased regulatory phenotype within this tumour |
| UPS | SpatialDecon | Macrophage, Treg and fibroblast abundance | There may be increased Treg abundance associated to the upregulation of MHC-I genes |
| LMS | SpatialDecon | Fibroblast, Tregs and MC abundance | Fibroblasts may be intertwined with the structural genes upregulated in the LMS tumours<br>Expression of cytokines by MCs may be influencing the structure and infiltration of the tumours |
| LMS | WGCNA | MYOC, MYOCD, MYLK, MYL9, ATCN, ACTC1, COL6A1, COL6A3, COL14A1 | Tumour development within the muscle, with fibroblasts within the tumour stroma |
| UPS | WGCNA | COL3A1, COL1A2, COL15A1, COL4A2, MMP14, MMP2, ADAMTS10, ADAMTS, TNXB, CREB3L1<br>MHC-I and MHC-II genes<br>CD68, CD74, CD44, and ICAM | Related to fibroblasts within the stroma<br>Variations seen in tumours with high tumour mutational burden<br>Antigen presentation to both CD8 and CD4 T cells<br>Higher immune cell abundance in the UPS tumours |
| Segmented CD8 T cell | WGCNA | IL2RB, CD8A, PTPRC, and CD3E | Although there is higher CD8 T cell populations within these tumours, they may lack cytotoxic function |

The **limitations** of this spatial transcriptomics sarcoma characterisation study are as follows:

(A) A small number of samples across only three subtypes, some having recent radiotherapy – this is largely due to rarity and accessibility of samples, together with the costs of spatial transcriptomics.

(B) The resolution of the technology is low, as it is bulk sequencing but of an enriched area. The gene expression profile and identity of each individual cell is not confirmed. For example, it is possible to conclude that there seems to be more antigen recognition and presentation on MHC class I and II but it was not possible to confirm which cell type expression was taking place on. The increase in collagen within the

UPS ROIs suggests that there is increased fibroblast involvement in the tumour. However, it was not possible to confirm that the collagen is indeed expressed on fibroblasts - it was not possible to confirm that there were fibroblasts present by IHC due to the mesenchymal nature of sarcoma tumours, which shares expression profiles with fibroblasts.

(C) The RNA transcriptome does not always reflect what is expressed at a protein level. Particularly with the MHC genes being expressed. Often in cancer MHC is internalised and this can be misleading.

**Future work** with this dataset could be to stratify the immune high and low groups and compare based on quantified counts from the IF images or the transcript reads for the immune cells of interest. An alternative would be to conduct a single cell approach to this work. This would provide more clarity on the cell subtypes involved in antigen presentation, immunoglobulin and collagen production. It would be of interest to determine the cells of origin for the observed regulatory and suppressive genes expression. Following this it would be of interest to probe if these findings are representative of all the individual tumours of these subtypes. This would be pertinent to identify a treatment plan to improve immunotherapies for individuals of this type.

# 5 Assessment of the impact of HIFU on the immune transcriptome of renal cell carcinoma

## 5.1 Chapter Introduction

Multiple studies have been conducted within the Oxford University NHS Foundation Trust to assess the feasibility of treatment of Renal cell carcinoma (RCC) with ablative HIFU therapy[1,16]. Subsequently, some patients underwent resection for their tumours following the HIFU intervention. Samples were stored by ORC and accessed via OCHRe. Like sarcoma, RCC has a range of reported immune infiltration based on subtype and the assessment of intratumoural immunomodulation by HIFU is of great clinical interest due to potential for exploitation. Also, the changes seen within this highly immune infiltrated tumour type may provide insight into strategies for bolstering immune response in tumours with sparse immune infiltration such as sarcoma.

The subtypes of RCC include papillary (pRCC) and clear cell (ccRCC), each having immunogenically distinct signatures. CD8 T cells have been demonstrated to be higher in ccRCC tumours compared to normal kidney tissue in a single cell analysis[31]. Also, Rooney et al. reported that ccRCC are more cytolytic than pRCC, defined by raised granzyme A (GZMA) and perforin 1 (PRF1) based on TCGA data[316]. This may improve the response to HIFU treatment as an increase in cytotoxic CD8 T cell population within the tissue has been associated with improved 10-year cancer specific survival outcomes by 21% in a breast cancer study[151]. However, CD4 T cells and MHC-II genes were also present in ccRCC tumours within this single cell analysis[31]. The increase in CD4 T cells following HIFU may lead to an increase in Tregs as shown in the *in vivo* treatment of fibrosarcoma in Chapter 3.

In contrast to ccRCC, the immune phenotype of pRCC has been reported to show lower CD8 and higher macrophage content, according to the CIBERSORT dataset[29]. Macrophages were skewed towards M0 and M2 type, suggestive of a regulatory phenotype. A study by de Vries-Brilland investigating pRCC within The Cancer Genome Atlas noted individual tumour variation within the pRCC subtype[32]. These baseline immune phenotypes will directly impact the influence that HIFU has on immune upregulation.

This chapter is focused on the transcriptomic profiling of tissue from RCC tumours treated with HIFU compared to non-HIFU treated resected controls. In addition, a small number of radiologically diagnosed RCC treated with HIFU but subsequently histologically demonstrated to be benign renal angiomyolipoma (AML) were also profiled post-resection.

The purpose of this characterisation was to assess the immune modulation after thermally ablative HIFU treatment and the impact that the theorised baseline regulatory phenotype of these tumours has on response to treatment. AML is often well vascularised and thus the immune infiltration following HIFU may also be altered[317]. Also to consider, it is theorised that the immune modulation after HIFU therapy is caused by increased self-antigen from the tumour, the immunologically modulatory phenotypes of malignant tumours affect the ability to respond to presented antigen by variation in MHC-I expression[49], which may not be seen in the benign AML tumours.

In renal AML tumours, very little has been reported on the immune profile of the tumours. A study by Puccetti et al. reported the production of cytokines was much reduced in CD4 T cell clones from AML compared to RCC[318] which may be indicative of higher Treg function within the malignant RCC tumours and thus a difference in HIFU response. In accordance, the same study reported cytolytic function against autologous tumour cells was higher in the

AML compared to RCC tumours[318], which may suggest that the benign tumours have less of a suppressive function on immune populations compared to RCC. This might provide insight regarding the immunomodulatory response to HIFU therapy.

In summary, the comparison of immune populations of post-HIFU RCC to untreated RCC may help elucidate variation in the immune populations and immunomodulatory mechanisms. Also, this analysis may provide insight into the signalling mechanisms of tissue surrounding immune populations, which may reduce infiltration and raise the regulatory phenotype, and whether this is modified after HIFU treatment. This may have implications of future immunotherapy strategies, which may be bolstered by partial HIFU treatment of one or more metastases in the setting of stage IV RCC.

## 5.2 Chapter Hypothesis and Aims

### Hypothesis:

Cytotoxic CD8 T cells and CD4 Tregs are key immune cells whose relative balance influences the progression and response to treatment in cancers. The subtypes of RCC will have differing proportions of these, ccRCC will have these cell types highly present, whereas in pRCC these will be reduced. This difference in the immune landscape based on subtype will relate to the immune changes seen in response to HIFU treatment. Also, the immune infiltration into HIFU treated tumours would be different in malignant kidney tumours (RCC) compared to benign tumours (AML), with the RCC tumour tissue having more tolerogenic phenotype.

## Aims:

(i) Assess the differences in immune populations between RCC subtypes with differences in immune infiltration at baseline.

(ii) Compare the immune landscape of RCC tumours which did not receive HIFU to HIFU treated RCC.

(iii) Compare immune populations between malignant (RCC) and benign tumours (AML) and to determine differences in the immune response to HIFU.

## 5.3 Overview of Samples

The table below (Table 5.1) outlines the 13 clinical resected renal tumours assessed by transcriptomic profiling (6 HIFU-treated RCC patients including VHL, 3 HIFU-treated AML patients and 4 control RCC patients). The samples were obtained from Oxford Radcliffe Biobank (ORB) via Oxford Centre for Histopathology Research (OCHRe). HIFU treated samples were resected between October 2011 and January 2013, control counterparts were resected between January 2013 and January 2024. There is a disparity in the age of the samples which would require assessment during the normalisation of the data to confirm that degradation of RNA over time did not affect the experimental outcomes. HIFU treated samples included papillary renal cell carcinoma (pRCC), clear cell renal cell carcinoma (ccRCC), Von Hippel-Lindau disease (VHL) associated RCC, and renal angiomyolipoma (AML). Patients were treated by JC200 (Haifu Medical Ltd) at 1MHz with 100% duty cycle with a power ramp until B-mode indication of treatment (typically between 200 and 360W). Control tissues available included pRCC and ccRCC for comparison. RCC subtype for VHL

samples was not reported in pathology notes, and subsequent secondary assessment could not identify subtype.

At the time of HIFU, the average age of patients was 63 (36 to 75) years. Confounding factors included previous non-renal cancer diagnosis in 2 of the 3 AML patients and 1 of the 3 ccRCC samples was within a kidney transplant, which may affect the immune profile of these samples. From the notes, it was also not possible to definitively confirm the tumour that was resected was the HIFU treated tumour. However, histological analysis (i.e. evidence of pyknosis) was supportive of HIFU exposure and there may be some abscopal immune impacts expected regardless. There was no report of immunotherapy, radiotherapy or chemotherapy given to any patients for treatment of RCC and information on immunosuppression for the transplant patient was not available for this study. In one of the patients, the ccRCC had concurrent prostate cancer and one of the control pRCC had concurrent chronic myelogenous leukaemia. Two of the samples (35227/11 and 5527/12) had two sample blocks (containing the same tumour, resected at the same time) both available from ORB that showed evidence of HIFU treatment (tissue damage and pyknosis), both blocks were sampled.

Table 5.1: Patient characteristics of high intensity focused ultrasound treated renal tumours and treatment naive clinical comparisons. pRCC is papillary renal cell carcinoma, ccRCC is clear cell renal cell carcinoma, AML is angiomyolipoma, VHL is renal cell carcinoma associated with Von Hippel-Lindau disease.

| Patient ID | Slide ID | Tumour Subtype | HIFU Treatment | Previous Treatments e.g. Radiotherapy | Comorbities | HIFU date | Surgery Date | Staging | Grade | Patient Age | Patient Gender | Pathologist Review Notes | CK8 Stain Review |
|---|---|---|---|---|---|---|---|---|---|---|---|---|---|
| 5022/12 | 3F | ccRCC | HIFU | Prior left partial nephrectomy, new lower pole anterior mass | HCC liver treated with chemoemoblisation | 31/08/2011 | 08/02/2012 | pT3b | | 75 | M | No evidence of HIFU | Slight loss of stain close to tumour border |
| 20177/12 | D | ccRCC | HIFU | Prior prostatectomy | Prostate cancer | 27/10/2011 | 08/06/2012 | pT1a | | 68 | M | Some dead tissue | Low staining |
| 4835/12 | 2C | pRCC | HIFU | Prior right nephrectomy | Chronic kidney disease | 14/12/2011 | 01/02/2012 | pT1a | | 60 | M | Some dead tissue | Tissue lifting |
| 784/13 | 1E | ccRCC | HIFU | | Transplant Kidney | 02/10/2012 | 08/01/2013 | pT1a | Grade 2 | 56 | M | ccRCC, some HIFU evidence | Stain varying throughout tissue |
| 35227/11 | 2P, 2X | VLH | HIFU | | Recent cryotherapy treatment, mulitple lung resections | 29/09/2011 | 11/10/2011 | | | 36 | F | Dead tumour core, live border | Stain varying throughout tissue |
| 34432/11 | 4G | VHL | HIFU | | Chronic kidney disease | 04/07/2011 | 01/10/2011 | | | 36 | M | Live and dead tissue, 3 small tumours | Stain varying throughout tissue |
| 5527/12 | A, D | AML | HIFU | | Adenocarcinoma in lung | 09/01/2012 | 14/02/2012 | n/a | n/a | 68 | F | Dead tumour core, live border | Stain ineffective |
| 13387/12 | B | AML | HIFU | | Basal cell carcinoma | 07/03/2012 | 17/04/2012 | n/a | n/a | 69 | F | HIFU with heat fixed nuclei | Stain ineffective |
| 37481/11 | A | AML | HIFU | | | 31/08/2011 | | n/a | n/a | 70 | F | Dead tumour core, live border | Stain ineffective |
| 176/24 | J | ccRCC | Control | | | n/a | 30/12/2023 | pT1b | Grade 3 | 75 | M | | Stain varying throughout tissue |
| 2998/24 | F | pRCC | Control | | | n/a | 17/01/2024 | pT1a | Grade 3 | 73 | M | | Stain varying throughout tissue |
| 51621/23 | I | ccRCC | Control | | High risk prostate cancer | n/a | 18/11/2023 | pT1a | Grade 2 | 74 | M | | Stain varying throughout tissue |
| 7729/13 | B | pRCC | Control | Right radical and left partial nephrectomy | Papillary adenomas and chronic lymphatic leukaemia | n/a | 26/02/2013 | pT1a | | 57 | M | | Stain varying throughout tissue |

### 5.3.1 Histological assessment of selected samples for transcriptomic analysis highlighted structural variability within the samples selected

Archival H&E slides were assessed by Dr Jennifer Brown from histopathology at the Nuffield Orthopaedic Hospital to assess for the presence of HIFU damage within the slides. Select H&E slides are presented in Figure 5.1 to illustrate the different tumour types within the study. Information on the indicators of HIFU by pathologist can be found in Table 5.1. The typical morphology of ccRCC tumour is demonstrated in Figure 5.1A with clear lipid-laden cytoplasm, and Figure 5.1B shows the morphology of pRCC with structured papillary cells. Within Figure 5.1B, and E, haemorrhage within the tumour can be identified by large areas of eosin accumulation (dark pink) by red blood cells (blue arrows), and areas of plasma accumulation which may have been caused by HIFU or may result from surgical resection. Figure 5.1F demonstrates retained typical characteristics of AML with large adipocytes. Of note, there was ablative change centrally within the tumour but not peripherally. Cellular damage (and haemorrhage) was also identified in the HIFU treated VHL sample in Figure 5.1E.

Cytokeratin 8 (CK8) staining using clone CAM5.2 has been reported within the literature to be instantaneously lost in tissue after thermal ablation treatment[18,319], including in cancer cells developed from papillary areas of the kidney the RCC tissue[320]. Figure 5.2 shows the assessment of the CK8 stain in an example of each tissue in each group, an overview of the samples is outlined in Table 5.1. Figure 5.2A and C showed weaker stain in the ccRCC compared to the control pRCC in Figure 5.2B. This may suggest that the stain is not as strong with the ccRCC compared to pRCC, regardless of treatment. The CK8 staining was not possible in the pRCC as the tissue was damaged during the staining process. For the AML

tissue, no CK8 staining was evident within the tumour, but the papillary cells of the surrounding kidney stained well (Figure 5.2F). The expected staining was shown within the VHL RCC samples, as outlined by the positive staining closer to the periphery compared to the central tumour as shown in Figure 5.2D.

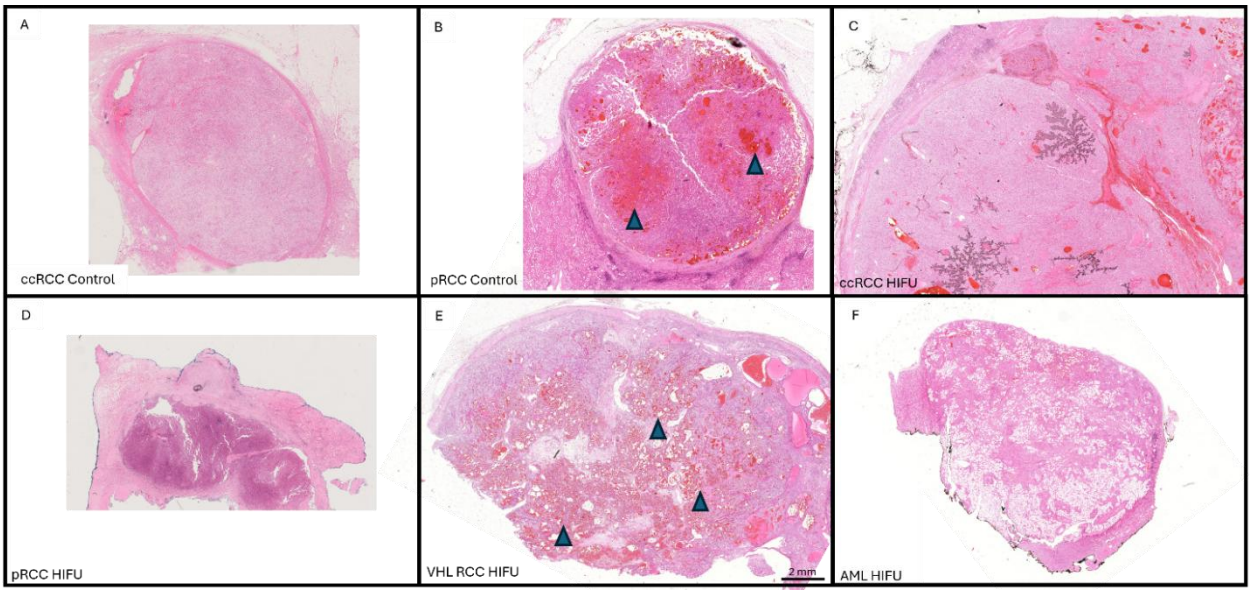


Figure 5.1: Haematoxylin and eosin (H&E) staining of one of each type of tumour including (A) control no HIFU clear cell renal cell carcinoma (ccRCC), (B) control no HIFU papillary renal cell carcinoma (pRCC), (C) HIFU treated clear cell renal cell carcinoma (ccRCC) where air was trapped when mounted (black/brown artefact), (D) HIFU treated papillary renal cell carcinoma (pRCC), (E) HIFU treated Von Hippel-Lindau renal cell carcinoma (VHL), (F) HIFU treated angiomyolipoma (AML). Red arrows indicate areas of haemorrhage.

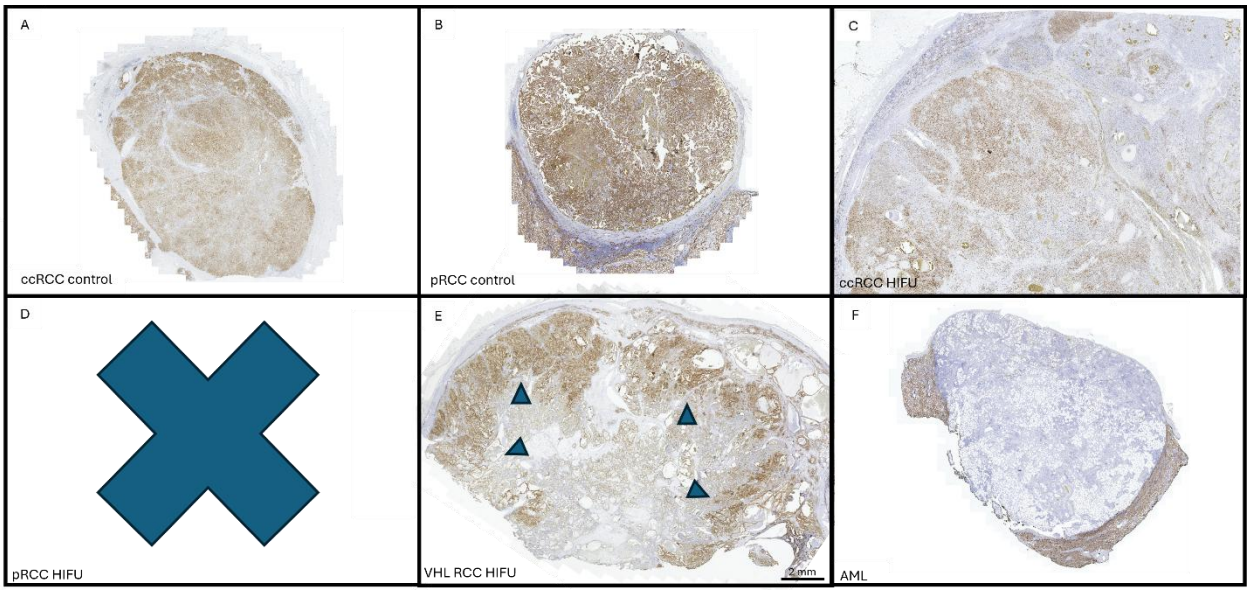


Figure 5.2: Correlating to Figure 5.1 sections, Cytokeratin 8 (CK8, CAM5.2) staining (brown) of one of each type of tumour for possible identification of thermally ablated tissue including (A) control no HIFU clear cell renal cell carcinoma (ccRCC), (B) control no HIFU papillary renal cell carcinoma (pRCC), (C) HIFU treated clear cell renal cell carcinoma (ccRCC) where air was trapped when mounted (black/brown artefact), (D) HIFU treated papillary renal cell carcinoma (pRCC) – the tissue was completely damaged, lifted off the slide and could not be presented, (E) HIFU treated Von Hippel-Lindau renal cell carcinoma (VHL), (F) HIFU treated angiomyolipoma (AML). Blue arrows indicate areas of darker CK8 stain indicative of heathy tissue at the tumour border.

### 5.3.2 Selection of regions for transcriptomic profiling

The transcriptomic assessment of these tissues focused on the immune populations within the RCC and benign AML tumours that had been exposed to HIFU compared to untreated (non-HIFU) controls. The wider immune population within the tumours was of interest so staining for CD45+ lymphocytes was performed. CD8 T cells were also stained for as they are a focus of the study and are reported to be variable between the RCC subtypes. Also, from the literature CD8 T cell were highly abundant within the ccRCC tumours, and less abundant in pRCC[29]. CD8 T cells have been hypothesised to be a key immune cell type modulated by HIFU treatment, with an increased cytotoxic T cell function caused by the release of antigen and DAMPs post-treatment.

The slides were stained to focus on these cells using the method as outlined in Section 2.6.1. Tissues were stained by immunofluorescence (IF) to identify foci of CD45 leukocytes (in red)

and CD8 T cells (in yellow). Then the tumour border was identified with a pan-cytokeratin stain (in green), which allowed for the healthy kidney tissue margin to be identified. These low magnification images demonstrated the high level of heterogeneity in the samples in terms of structure and composition.

The overview of this selection is outlined in Figure 5.4, which outlines the regions of interest (ROIs) selected in this analysis. Examples of the tissue sections are shown in Figure 5.5. The ROIs selected were stratified into four different region types as outlined in Figure 5.5O. These included areas within the renal tumours such as **immune** infiltrated (**IM**, Figure 5.5A-D), **tumour border** (**TB**, Figure 5.5E-H), and not targeted adjacent tumour (**AJ**, Figure 5.5M). Within the tissue adjacent to the tumours **peritumour** ROIs (**PT**, Figure 5.5I-L) were also selected.

The immune ROIs showed a range of immune abundance by IF, and were distributed throughout the tissue, whereas the tumour border ROI were along the tumour border with immune infiltration. Within one of the ccRCC samples there was an adjacent tumour that did not show signs of HIFU treatment; thus, it was sampled for the possibility of assessment in comparison to the treated tumour.

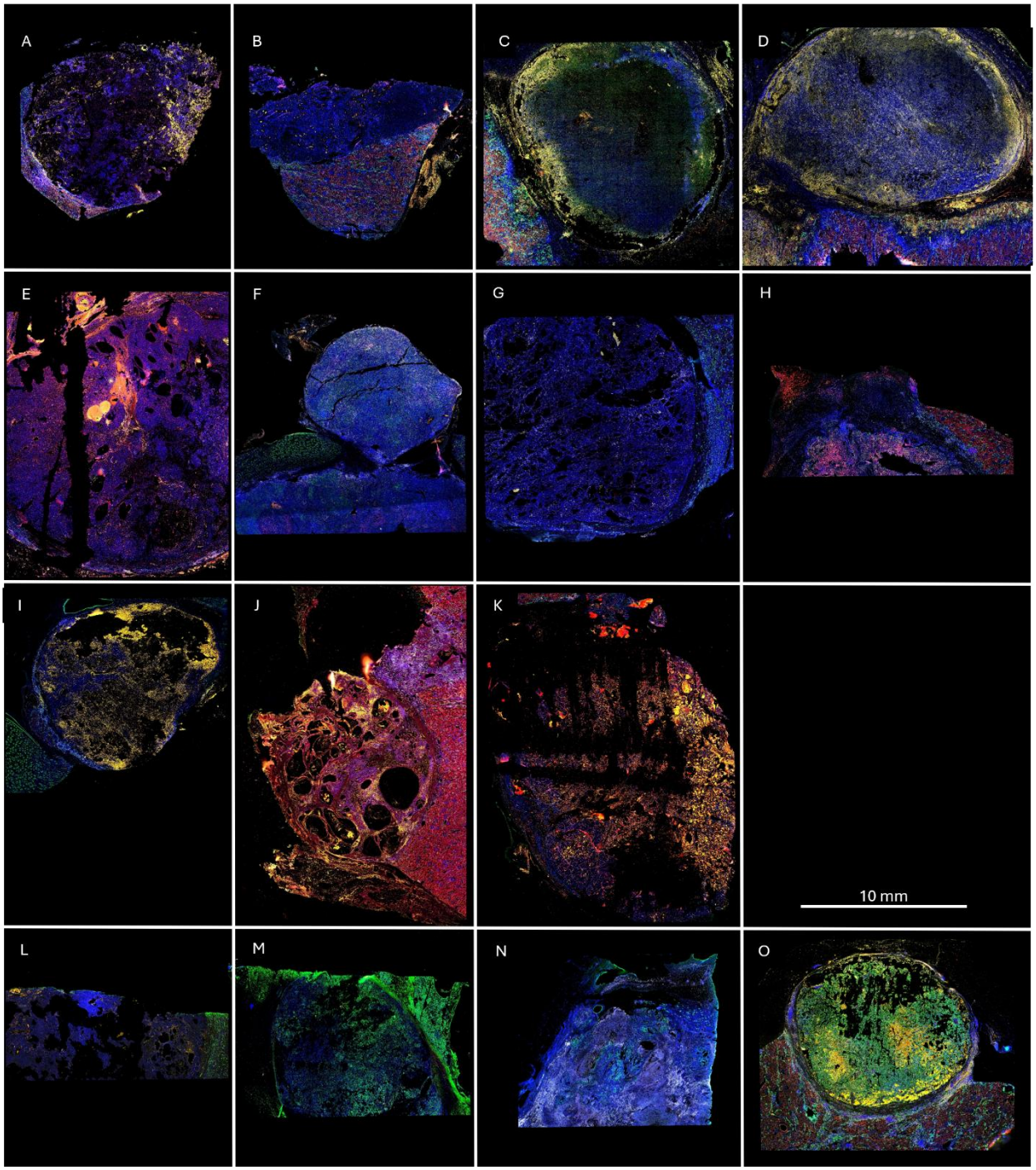


Figure 5.3: Overview of the four-colour fluorescent staining used to identify CD45 (red), CD8 (yellow), pan-cytokeratin (green) and SYTO 13 (blue, nuclear stain). All HIFU tissues are represented including AML samples (A) 13387/12 B, (B) 37481/11 A, (C) 5527/12 D, (D) 5527/12 A. RCC tumours including ccRCC tumours (E) 20177/12 D, (F) 5022/12 3F, (G) 784/13 1E, and pRCC tumour (H) 4835/12 2C, and VHL RCC tumours (I) 35227/11 2X, (J) 34432/11 4G, (K) 35227/11 2P. Control no HIFU samples included control ccRCC tumours (L) 51621/23 I (M) 176/24 J and control pRCC tumours (N) 2998/24 F and (O) 7729/13 B.

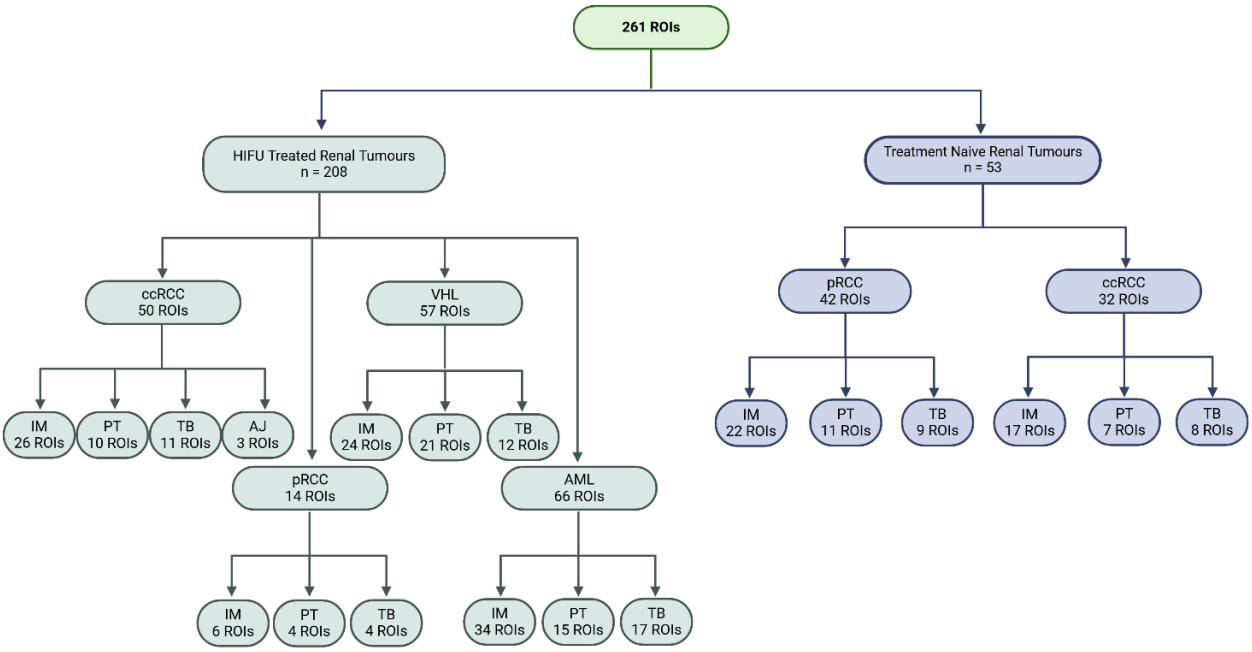


Figure 5.4: Decision tree for selection of the regions of interest (ROI) within this transcriptomic study of renal cell carcinoma samples of the 261 originally selected ROIs. ROIs selected included immune variable (IM), peritumour (PT), tumour border (TB) and in a case of ccRCC, an adjacent, non-treated tumour (AJ). Created with BioRender.com.

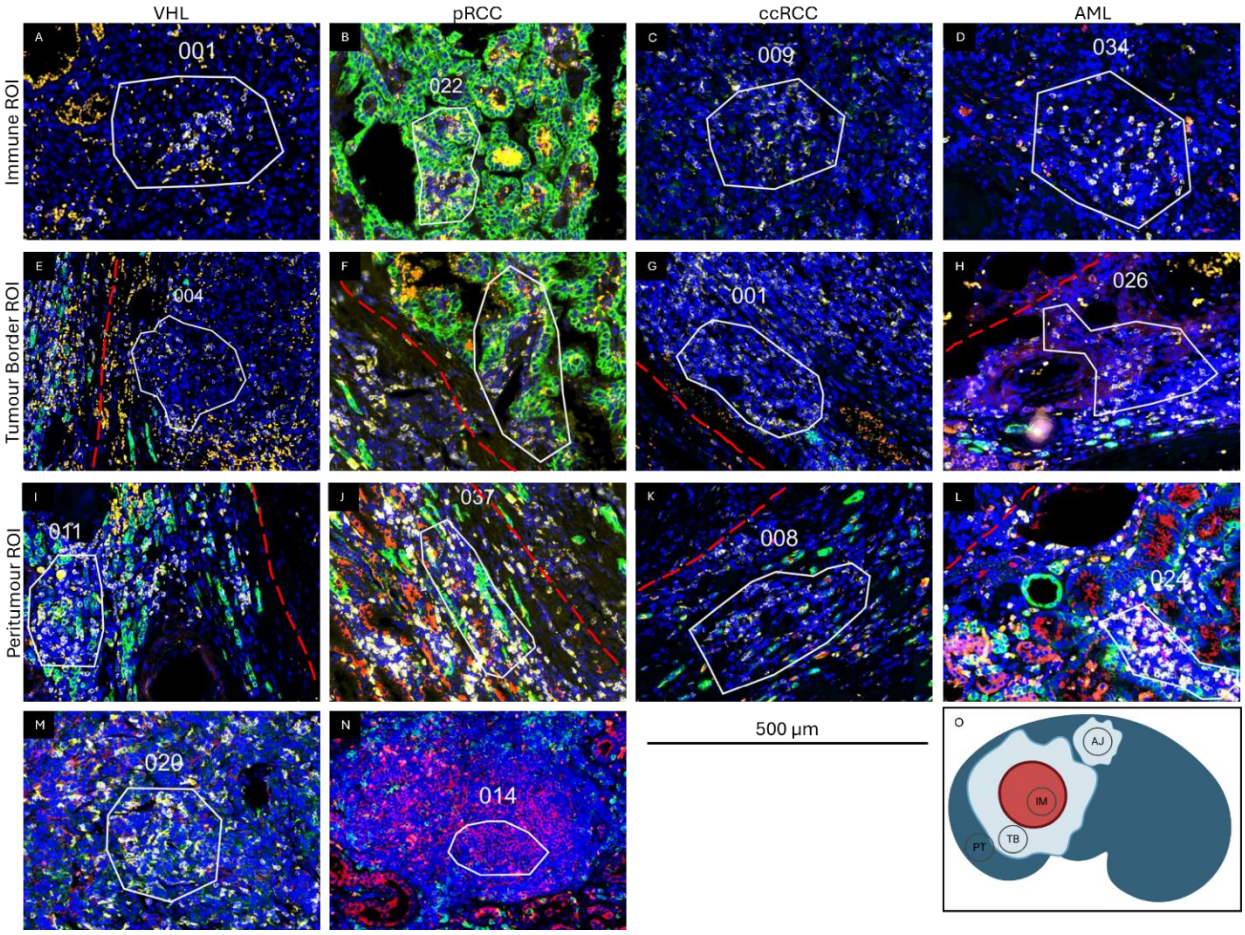


Figure 5.5: Example four-colour fluorescent staining used to identify different immune infiltration within the tissue using CD45 (red), and CD8 (yellow) cells and the tumour border using pan-cytokeratin (green) and SYTO 13 (blue). ROI stratification examples including (A-D) immune ROIs, (E-H) tumour border ROIs, (I-L) peritumour ROIs, and the (M) Adjacent ROIs from ccRCC. Possible TLS ROIs which were assessed as peritumour (N) from (A, E, I) VHL, (B, F, J) pRCC, (C, G, K) ccRCC and AML (D, H, L). Schematic of locations included (O) where the red represents the ablation zone, light blue represents the tumour, and dark blue represents the kidney created with BioRender.com. Peritumour (PT), tumour border (TB), immune (IM) and adjacent (AJ) ROI locations are shown. Red dashed line indicates the tumour border, identified by sparse nuclei and cell shape identified as connective tissue.

### 5.3.3 Summary of the samples and ROI selection for transcriptomic profiling

Assessment of the clinical features of the tissues selected for transcriptomic profiling indicated that there may have been confounding factors that needed to be considered during analysis. For examples, see section 5.4, with the PCA analysis showing the main factors that affected variability within the data. The assessment by the pathologist and CK8 staining

indicated that the samples selected had some evidence supporting the HIFU treatment of the samples. The tissues showed ablation in the centre of the tumour, with many tissues having 'healthier' tissue towards the tumour border.

Due to there being many different tumour types, different ROI types and including HIFU control tissues, analysis of the data using the WGCNA approach was suggested to provide a manageable workflow for analysis of the data generated. This can be followed up by more targeted differential gene expression analysis.

## 5.4 Identifying the contribution of factors within the study to variability within the data

Within this transcriptomic assessment, there are some confounding experimental factors which needed to be accounted for. The acquisition of the data was conducted over 3 different temporally separate runs of slides, which could affect the quality of data collection, thus the assessment of data factoring in this variable was conducted. The control samples were stored for a shorter timeframe compared to the historically stored HIFU samples, thus the affect the treatment has on the samples required assessment.

To assess these as potential contributors of differences within this transcriptomic assessment, aside from individual tumour biology, a principal components analysis was conducted. The assessment of the factors influencing the variability included the data acquisitions run, HIFU treatment vs. control (non-HIFU) regardless of tumour type, the ROI category, the tumour subtype with treatment, the biological difference within individual tumours, and patient gender. The first (12.8% of variability) and second (4.1% of variability)

dimensions were evaluated in Figure 5.6 and the assessment of factors influencing the third (3.5% of variability) and fourth (2.5% of variability) dimensions were evaluated in Figure 5.7. These plots showed that acquiring the data over multiple runs had little effect any dimension (first to fourth) tested (Figure 5.6A and Figure 5.7A). Also, the slide containing 2998/24 F was assessed over 2 runs, the points on across all dimensions are tightly fitting, suggesting no difference caused by batch. Thus, the data will not be batch corrected to account for run variability as it can affect the quality of the data output.

Focusing on whether other factors helped resolve the first- to fourth-dimensions of differences, the treatment type (Figure 5.6B and Figure 5.7B) did not resolve along these factors, even when accounting for tumour (Figure 5.6C and Figure 5.7C), nor did the different ROI types (Figure 5.6D and Figure 5.7D).

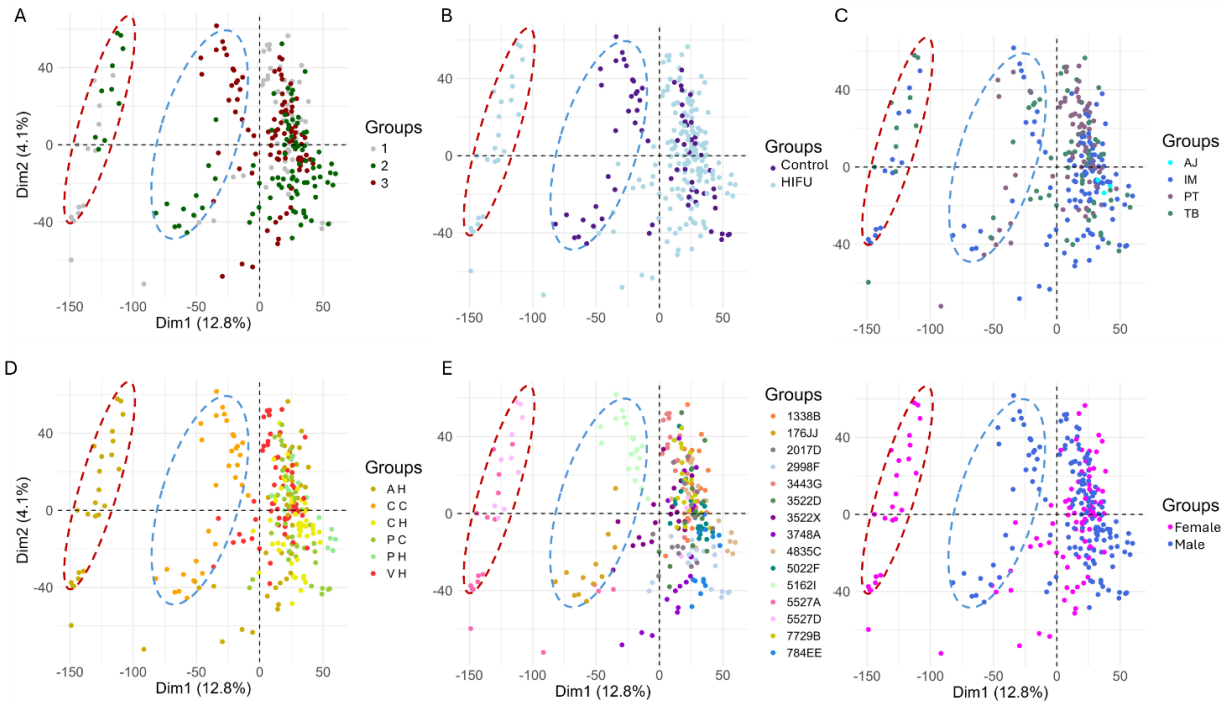


Figure 5.6: Visualisation of the first and second dimensions in the principal components analysis of the transcriptomic data of the 15 renal tumour samples (261 ROIs) assessed against multiple factors within the study to investigate each factor's effect represented for (A) run, (B) treatment, (C) ROI category, (D) tumour type and treatment, (E) individual tumour, (F) gender. ROI category includes adjacent (AJ), immune (IM), paratumour (PT) and tumour border (TB) ROIs. Tumour type included AML HIFU (AH), ccRCC control (CC), ccRCC HIFU (CH), pRCC control (PC), pRCC HIFU (PH) and VLH RCC HIFU (VH). Ellipses used to identify clusters of interest.

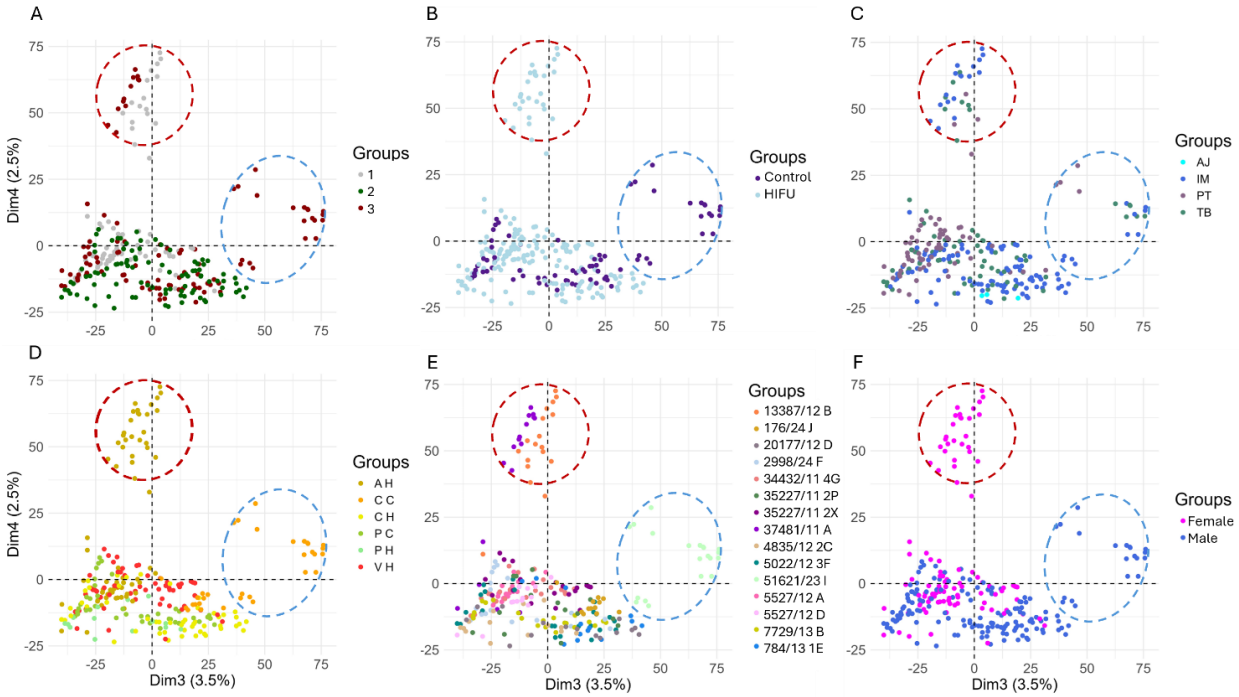


Figure 5.7: Visualisation of the third and fourth dimensions in the principal components analysis of the transcriptomic data of the 15 renal tumour samples (261 ROIs) assessing multiple factors within the study to investigate each factor's effect represented for (A) run, (B) treatment, (C) ROI category, (D) tumour type and treatment, (E) individual tumour, (F) gender. ROI category includes adjacent (AJ), immune (IM), paratumour (PT) and tumour border (TB) ROIs. Tumour type included AML HIFU (AH), ccRCC control (CC), ccRCC HIFU (CH), pRCC control (PC), pRCC HIFU (PH) and VLH RCC HIFU (VH). Ellipses used to identify clusters of interest.

The first dimension was resolved by a patient, 2 of the 4 AML slides separated from the rest of the data along the first dimension, see red ellipse (Figure 5.6E). This patient's tumour was sampled twice (two sample blocks, resected at the same time and showed evidence of HIFU treatment) and ROIs from both samples from this same tumour clustered together away from the rest of the ROIs (see ellipse in Figure 5.6E). This may suggest that they clustered because they were most like each other. This phenomenon was not seen for the VHL tumour that was sampled twice (two sample blocks, resected at the same time and showed evidence of HIFU treatment), suggesting this specific AML tumour was more biologically different from the other sampled AML HIFU treated tumours and all other renal tumours. Along the fourth dimension, the ROIs of two of the four AML tumour separated from all other ROIs (red ellipses in Figure 5.7). These are not the same 2 AML tumour samples from the

same tumour (Figure 5.6) identified in the first and second PCA analysis. This suggested the transcriptional profile of the AML tumours were vastly different from the RCC tumours (as expected). However, it also showed that there were inherent biological differences between these tumour samples. It was noted that the ROIs of two other tumours (both control ccRCCs) clustered together along the first and second dimension (blue ellipses). In the third dimension, the ROIs of 1 of the 2 control ccRCC samples (51621/23 I) identified in the first and second dimension (Figure 5.6E), separated from the ROIs from the other samples (see blue ellipse in Figure 5.7E).

From the principal components analysis (PCA) assessment, it was possible to conclude that the biological differences between individual tumours had a large influence on the distribution of the data. When assessing the transcriptomic analysis, it may be that specific tumours sampled relate to changes seen. The data analysis and interpretation will need to take this into account.

## 5.5 Cellular Deconvolution of ROIs selected from samples

ROI selection focused on sampling areas of renal tumours with a range in abundance of immune cells. To this end, CD45+ and CD45+CD8+ cell populations were analysed by IF. Immune population modulation within RCC tumours treated with HIFU compared to benign AML and untreated RCC samples were of particular interest.

Previous work by Hu et al. on murine colon adenocarcinoma (MC-36) and Xia et al. on murine hepatocellular carcinoma (H22) showed antigen release after HIFU treatment had a downstream effect on the modulation CD8 cells[50,321]. This chapter set out to explore the extent of this clinically desirable cytotoxic effect caused by HIFU therapy in human RCC. This

is because a continued CD8 T cell response after ablative HIFU treatment would theoretically allow the immune system to destroy any residual untreated tumour cells, with improved patient outcomes. Within Chapter 4, the sarcoma subtype ROIs were described as immune high or immune low, however the assessment by the IF did not always align with the SpatialDecon assessment, thus the assessment within this Chapter does not stratify the ROIs based on a quantification analysis. The comparison of the cellular deconvolution before the differential gene expression (DGE) analysis may shed more insight into subsequent findings. Assessments of the abundance of other immune cells within each ROI was also of interest with the SpatialDecon assessment (outlined in Section 2.7.3), which will be outlined in this section. This assessment will also estimate the abundance of other immune populations within the selected ROIs (Figure 5.8).

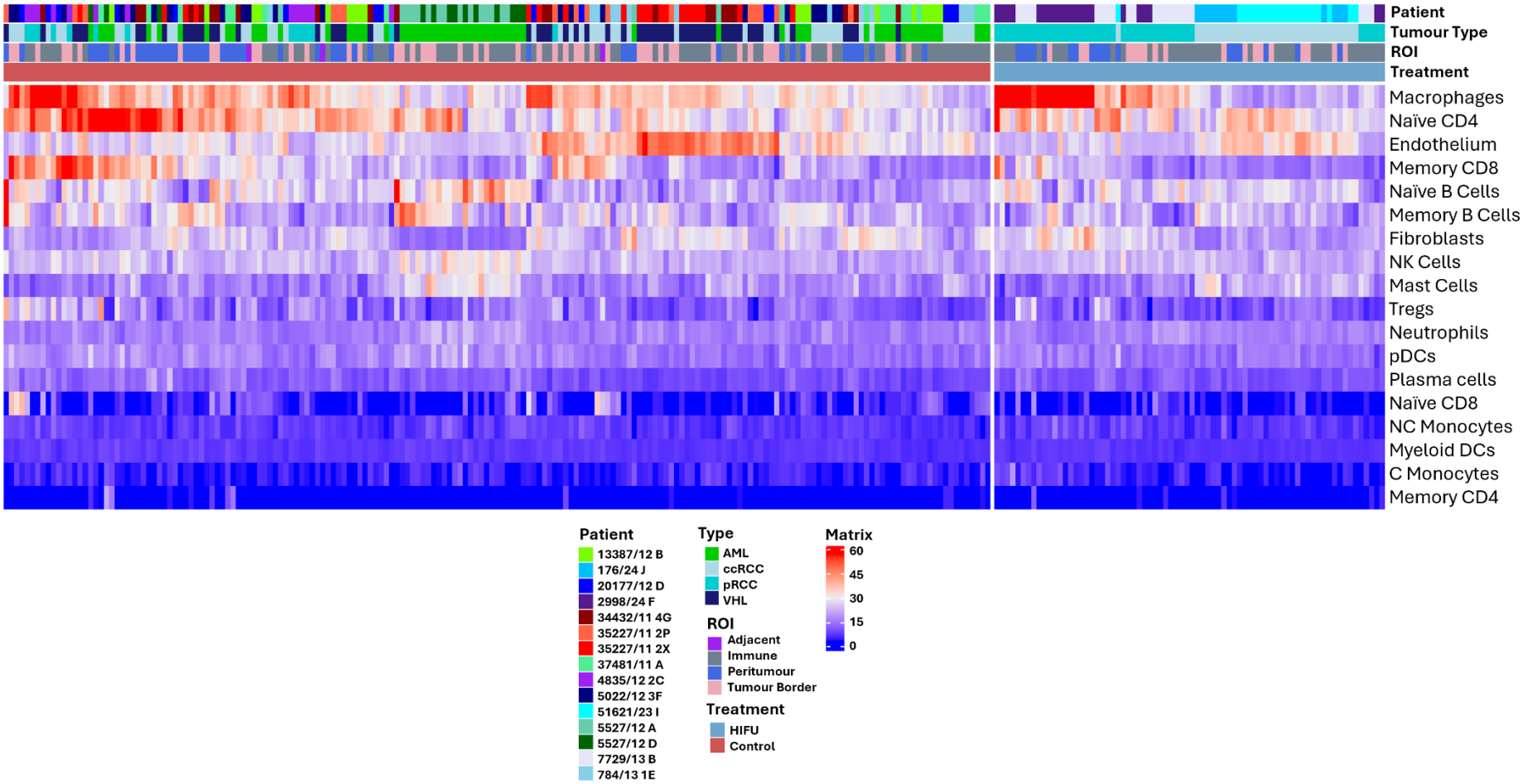


Figure 5.8: A heatmap representation for the abundance of cell types identified within the ROIs of renal tumours and adjacent tissue from cell deconvolution evaluation of bulk RNA transcriptomics and the expression profiles of genes from cells of interest. Cell annotations included: natural killer cells (NK cells), regulatory T cells (Tregs), plasmacytoid dendritic cells (pDC), non-conventional monocytes (NC monocytes), and conventional monocytes (C monocytes). The top annotations including the tumour type including AML (A, green), ccRCC (C, light blue), pRCC (P, teal), and VHL (dark blue). The ROI type including adjacent tumour (purple), immune (grey), peritumour (royal blue) and tumour border (pink). Patient 13387/12 B (yellow green), 176/24 J (sky blue), 20177/12 D (blue), 2998/24 F (purple), 34432/11 4G (dark red), 35227/11 2P (orange), 35227/11 2X (red), 37481/11 A (sea green), 4835/12 2C (light purple), 5022/12 3F (dark blue), 51621/23 I (cyan), 5527/12 A (aquamarine), 5527/12 D (dark green), 7729/13 B (lavender), 784/13 1E (light blue). Treatment groups were HIFU (maroon) and control (powder blue).

### 5.5.1 Assessment of the tumour microenvironment identified macrophages as a highly abundant immune type, as well as high endothelial genes expression

Assessment of the **immune** and **tumour border** ROIs by SpatialDecon of all renal tissues sampled showed variable macrophage abundance between ROIs (Figure 5.8). The **pRCC** showed high macrophage abundance in all ROIs in both HIFU treated and control groups. There was no discernible increase in macrophage content demonstrated in the HIFU treated pRCC, which was expected because of the high macrophage abundance within baseline pRCC tumours. The **ccRCC** seemed to have higher abundance of macrophages in the HIFU-treated samples compared to the control. However, the ccRCC tumours within the transplant kidney, did not show increased macrophage abundance. As mentioned in Section 5.3, this may have been a HIFU adjacent tumour, rather than a HIFU treated tumour, or this patient may have been treated with immunosuppression for their transplant. There was no record of immunosuppression provided. A similar distribution was seen within the **peritumour** ROIs of the different ccRCC tumour samples, with lower abundance than the immune and tumour border. The **AML** ROIs showed lower macrophage content in all **immune**, **tumour border** and **peritumour** ROIs when compared to all pRCC and HIFU treated ccRCC ROIs. The increase in macrophages seen in ccRCC tumours following HIFU may be a ccRCC or malignant tumour-related response after HIFU treatment.

The transcriptional profile of the CD4 T cell population were separated into naïve, memory and Treg populations for this analysis. Interestingly, naïve CD4 T cells were the most abundant CD4 T cell type. This population was more abundant than CD8 T cells in a higher proportion of **immune** ROIs (46/129 ROIs vs 15/129 ROIs) for all tissues. CD8 T cells were

one of the cell types of interest in this study, regardless of tumour type or treatment (Figure 5.8). The relative frequency of the naïve CD4 T cells was variable throughout the immune group. More **immune** ROIs had a high naïve CD4 population in the HIFU treated RCC (regardless of subtype) ROIs than the non-HIFU treated RCC ROIs, or the HIFU AML ROIs. This is the opposite of what was expected, which was an increase in tumour antigen presentation and recognition because of HIFU treatment which may be expected to the decrease the level of naïve CD4 T cells and increase the level of memory, cytotoxic CD8 T cells, as seen in the study of human breast cancer[23].

However, within the **tumour border** ROIs (Figure 5.8), the naïve CD4 T cells were lower within the control pRCC ROIs compared to pRCC HIFU ROIs. The highest naive CD4 T cell abundance was within a subset of HIFU treated non-VHL RCC ROIs. There has been previous work on liver and breast cancer which suggests that the naïve CD4 T cells may have a regulatory function within tumours, which may also be linked to macrophage accumulation within the tumour[322,323]. However, macrophage and naïve CD4 T cell accumulation does not always align in this study, which is limited by sampling only single slice snapshots of 5 µm thick piece of tissue. Macrophage – CD4 T cell interactions occurring in a 3D space may not be captured by these slender cross-sections.

Assessment of the **peritumour** ROIs demonstrated abundance of the macrophage and naïve CD4 T cells populations throughout the samples (Figure 5.8), indeed demonstrating high levels of immune activity in the peritumour in the all tumour types regardless of HIFU. This contradicts previous research which has suggested that RCC tumours are more immunogenic than healthy tissue[29], but this is possibly explained by the **peritumour** ROIs

selected being very close to the tumour border (around 1 mm) so the cells may be migrating towards the tumour or from tertiary lymphoid structures.

Endothelial related genes showed raised levels within all ccRCC tumours and some VHL tumours (suggesting that they are of ccRCC subtype) regardless of ROI type (Figure 5.8). This is in accordance with their endothelial origin[103,324]. Endothelial related expression may also be linked to the level of vascularisation within the tumour. These tumours have been reported to be highly vascular[325], which may also be linked to the immune abundance (possibly by enabling immune cell transport). A study conducted by Aziz reported that the level of vasculature within ccRCC tumours is higher than pRCC tumours[326]. This aligns with the raised endothelial signature reported here.

CD8 T cells are classified into naïve and memory cells within this analysis. The memory cells were more abundant than the naïve CD8 T cells (Figure 5.8). This is expected within a tumour setting[30], with tissue resident memory cells being common. The memory cell population did not become more abundant after the HIFU therapy. However, in Chapter 3, when assessing the CD8 T cell populations within the murine sarcoma *in vivo* study, there was subtle variability in the CD8 T cell memory subpopulations, which was significant in the dLNs, but only in the 10 second treatment group. It may be that the treatment increased the function of the existing CD8 T cells present within the HIFU exposed tumours, rather than modulating the absolute or relative levels in particular subpopulations. Alternatively, the high abundance of macrophages within the analysis may be hiding the change in abundance of this population within this heatmap. Also, macrophages have been shown to lead to an increase exhausted CD8 T cell phenotypes in RCC samples[327], which may mitigate any

response. Further investigation by WGCNA analysis may elucidate any variations in this population that were not detected within this analysis.

Notable differences in naïve and memory B cell populations were also observed. These populations were sporadically higher in different ROI types and tumour types. The ROIs with highest B cell populations were obtained from 2 of the 4 AML tumour samples, both of which came from the same patient. This may resolve the difference seen in the first- and second-dimensional analysis by PCA as many of the other tumours have a much lower B cell content. B cells can have an antigen response function, unfortunately the study was not able to include control no HIFU AML samples, but the other 2 out of 4 AML samples did not show similar B cell abundances. It may be that this B cell abundance is related to other factors. For example, this patient had co-existing lung adenocarcinoma which may affect the biology and responses in this tumour. Alternatively, this may relate to tertiary lymphoid structures (TLS). Assessment of the **peritumour** by IF suggested that some areas may have contained TLSs (Figure 5.5M). These areas were sampled and are included in the **peritumour** ROIs. The increase in the naïve and memory B cells strongly suggest that these ROIs were within TLS[106,328]. TLS have been indicated as important structures within various tumours for improved prognosis by supplying bolstered immunity[107,108].

Notably, NK cells were more abundant in a subset of ROIs in a subset of AML tumours, but these are not modulated between HIFU treatment and controls in RCC tumours. Also, Tregs and DC subtypes were not modulated between treatment groups. The stable DC population aligns with the murine *in vivo* assessment of sarcoma treated with HIFU in chapter 3. These cell populations may be stable in the tissues because of the delayed timeframe of resection after treatment (2 weeks to 8 months, much later than for the *in vivo* sarcoma – 1 or 5 days),

or their modulation was subtle and obscured by the change in macrophage population. The Treg variability was small within the *in vivo* study in Chapter 3, this may be identified in the WGCNA assessment conducted on these murine samples but not seen in the human samples in this chapter.

### 5.5.2 Summary of the SpatialDecon analysis

This chapter focuses on characterisation of the immune populations within the HIFU-treated and control renal tumours. An estimate of different cell types for the ROIs selected was produced. This showed that macrophages were highly prevalent within these tumours, along with naïve CD4 T cells. The function of these cells was convoluted and not well described within this analysis.

Although the expected modulation of the immune populations by HIFU did not demonstrate the desired population abundance changes (there was no increase in cytotoxic CD8 T cells), it was still pertinent to assess the possible functional modulation of the immune populations within these tumours. Although this analysis may have missed the window to assess the immediate and early differences in population abundance, there may have been lasting effects to the modulation of function of these cells. The previous Chapter (Chapter 4) assessed the contributing factors that classified the abundance of cells in each ROI. This was helpful in the smaller study, but the quantity of data within this renal cancer study made the comparison unmanageable. Instead, the WGCNA analysis allows for global transcriptomic differences to be assessed and the factors that associate to changes to be identified and evaluated.

## 5.6 Unbiased assessment of the RNA-expression of immune related regions selected from renal tumours

As discussed briefly in section 5.5, some of the subtle changes in cell populations may not be elucidated by the SpatialDecon analysis because of the differences in immune cell abundances within the areas selected. In addition, cell types like macrophages and memory CD8 T cells which have further subtypes with specific suppressive or activating functions could not be identified. Thus, the global and unbiased analysis (unlike differential gene expression analyses) of the data by the WGCNA analysis (Section 2.7.4) was pertinent. The long-term clinical follow-up data for the samples within this study was not available, thus discovery of expression profiles that correlate with outcome was not assessed.

The analysis approach was to assess the transcriptomic profile of the HIFU-treated RCC subtypes (pRCC, ccRCC, VHL-RCC), compared to control RCC (ccRCC and pRCC), and HIFU treated benign renal AML tumours. The aim of this assessment was to identify changes in the immune profile, specifically function of CD8 T cells and macrophages (identified by SpatialDecon in Section 5.5.1) of RCC tumours after HIFU treatment. Within the analysis, 13 modules were identified by WGCNA analysis (Figure 5.9, y-axis), with the grey containing genes that are not associated to a module. Correlation and statistical significance of experimental factors to the WGCNA modules are represented in Figure 5.11 From these 13 modules, 5 had significant and immunologically relevant pathways represented as barplots (P adj > 0.05, q value cut off at 0.1, Figure 5.11).

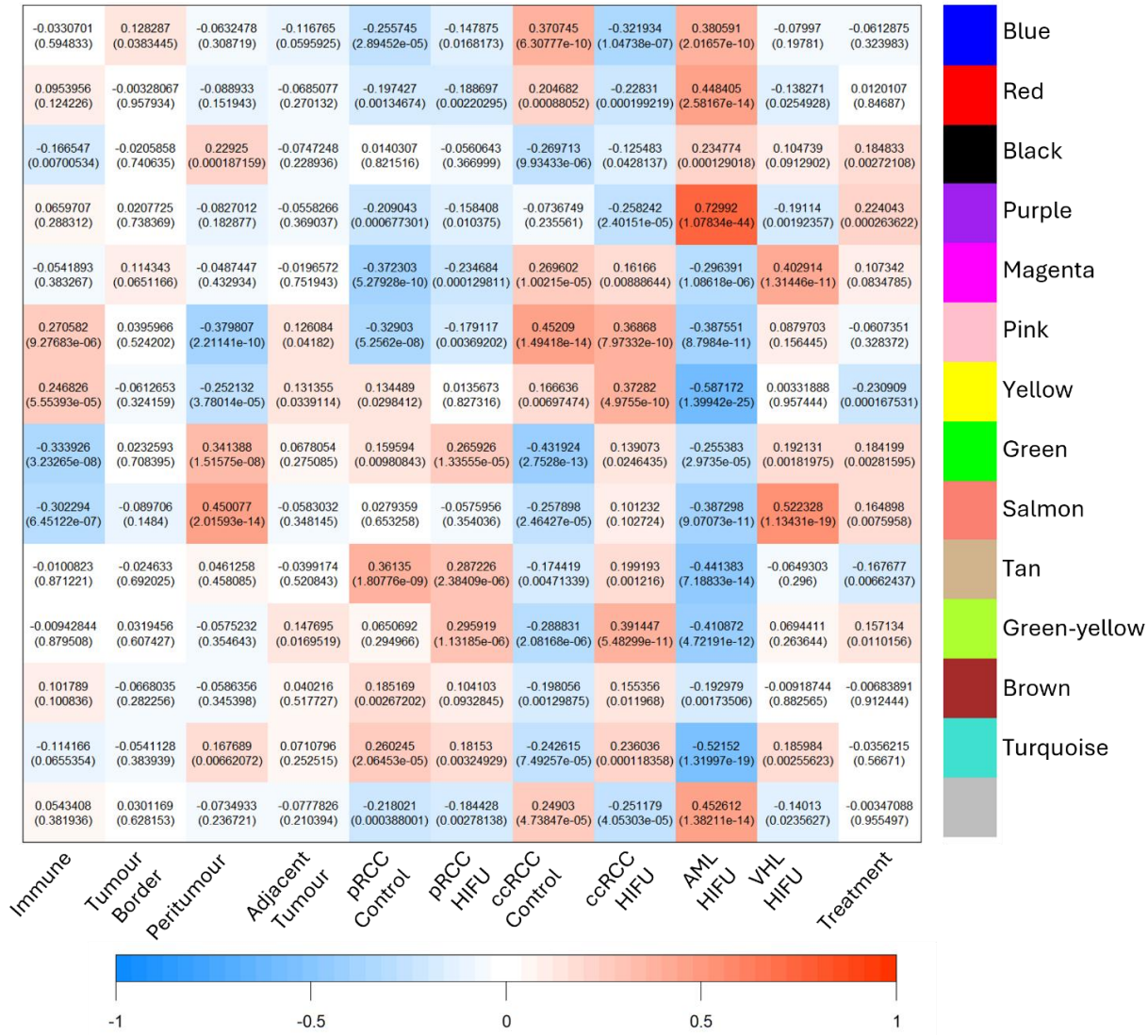


Figure 5.9: Clinical and study factors association with modules identified by weighted gene correlation network analysis assessed for the 15 renal tumours within this HIFU study grouped by ROI location, subtype and HIFU vs. non-HIFU. Pearson's correlation coefficient matrix with the module trait correlation level and p adjusted significance in brackets. The 13 modules are represented on y axis by coloured blocks, the grey represents genes that were not associated into a module. Factors within the study that potentially impacted the clustering of genes into modules along the x-axis. Scale for the correlation of factors to modules.

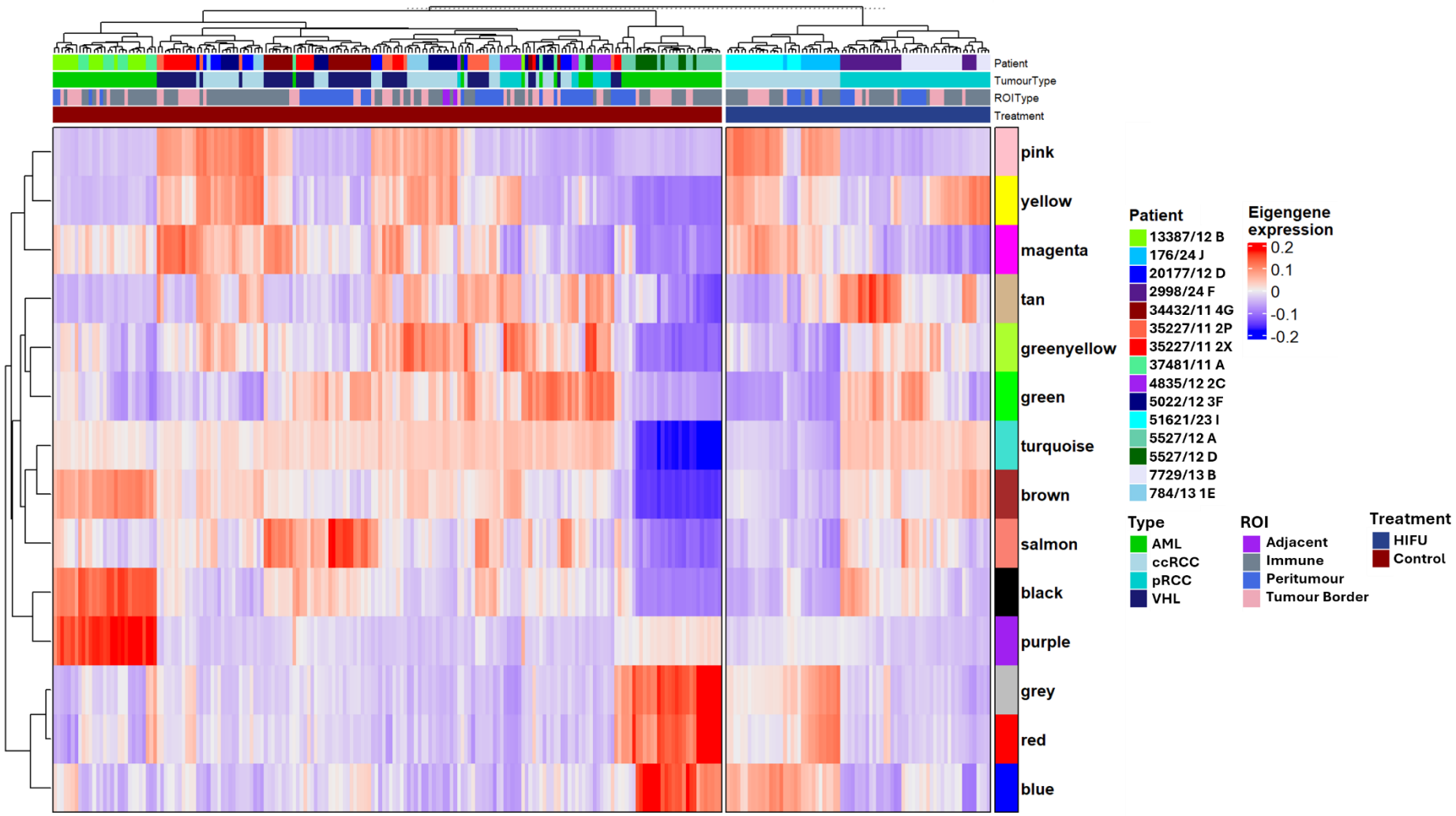


Figure 5.10: Hierarchical clustering dendrogram with samples and the expression of the genes within each module for each ROI with the 13 modules represented on y axis by coloured blocks, the grey represents genes that were not associated into a module. The top annotation including annotations for tumour type with patient: 13387/12 B (yellow green), 176/24 J (sky blue), 20177/12 D (blue), 2998/24 F (purple), 34432/11 4G (dark red), 35227/11 2P (orange), 35227/11 2X (red), 37481/11 A (sea green), 4835/12 2C (light purple), 5022/12 3F (dark blue), 51621/23 I (cyan), 5527/12 A (aquamarine), 5527/12 D (dark green), 7729/13 B (lavender), 784/13 1E (light blue). Tumour type: AML (Green), ccRCC (blue), pRCC (teal), VHL (dark blue), ROI type: Adjacent (purple), Immune (grey), Peritumour (blue) and Tumour Border (pink). Heatmap is split by treatment: HIFU (Maroon) and Control (Royal Blue). Eigengene expression, the relative expression of the genes within the module in each ROI.

### 5.6.1 Non-treatment related expression profiles were associated with tissue structure and hypoxia signalling

The tissue structure and endothelium (Magenta) module was positively associated with **HIFU VHL RCC** tumours (0.403. p<2e-11), **control ccRCC** tumours (0.270. p<2e-05) and **HIFU ccRCC** tumours (0.162. p<0.009), as shown in Figure 5.9. The assessment of expression of module genes in individual ROIs agreed with these findings (Figure 5.10) suggesting that this is linked to RCC tumour, rather than ROI or treatment specific differences. The pathways that were identified from the genes in this module (shown in Figure 5.11A) included tissue structure formation pathways such as bicellular tight junction assembly, basement cell organisation. This may be linked to the formation, development and growth of these tumours. Additionally, there were many pathways involved in vascularisation including vasculogenesis, blood vessel endothelial cell migration, and Notch signalling pathway[249,329,330]. Notch signalling is common in RCC[331]. To an extent, the tissue structure pathways may be involved in this vascularisation, along with tissue remodelling and response to transforming growth factor-beta (TGF-β)[332]. Genes relevant to glomerulus development are expected within normal kidney tissue[333], hence may still be expressed in the tumour cells, although many of these genes are shared with vascularisation (CD34, JAG1, NOTCH3, data not shown).

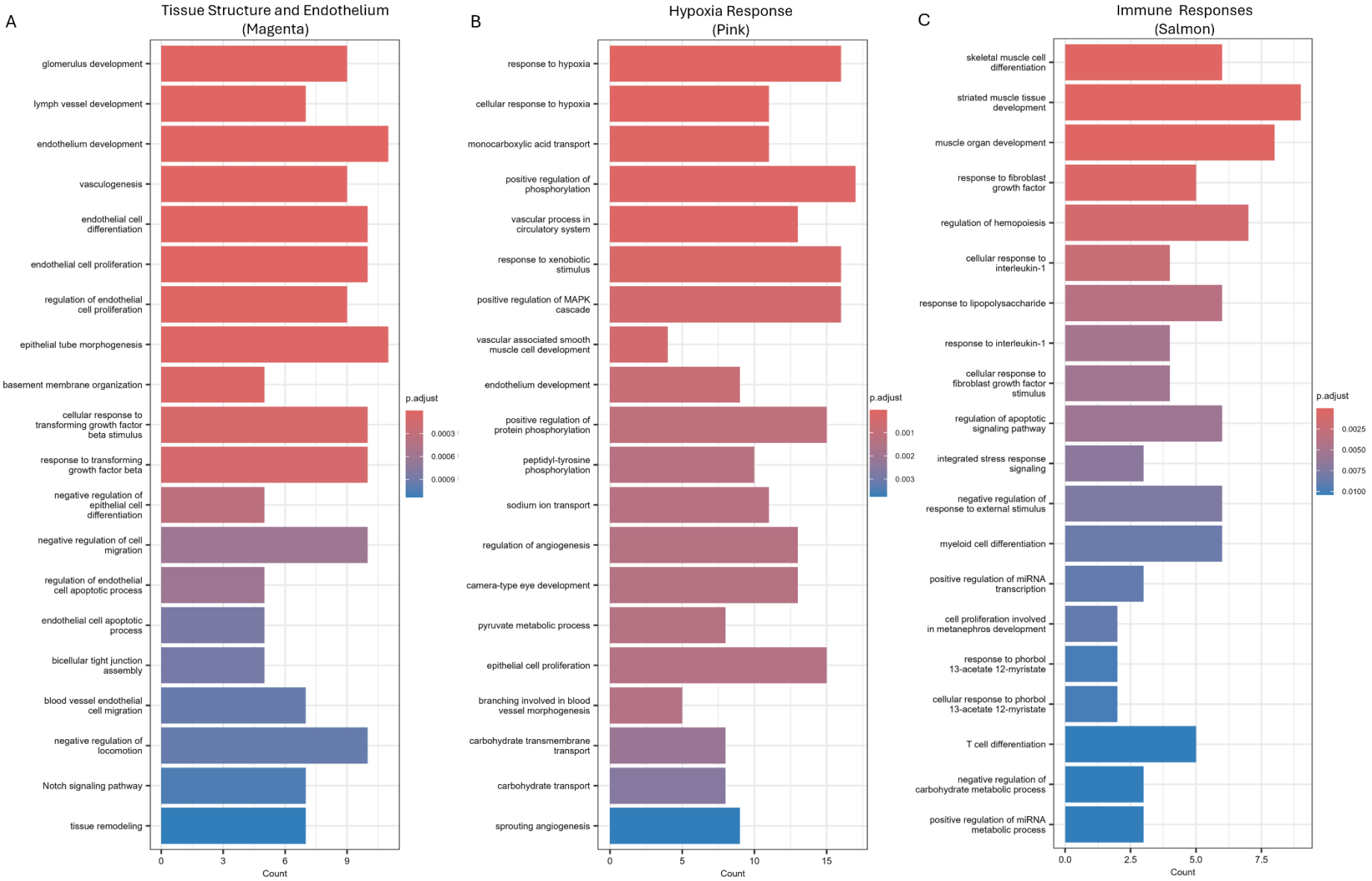
A
Tissue Structure and Endothelium
(Magenta)
glomerulus development
lymph vessel development
endothelium development
vasculogenesis
endothelial cell
differentiation
endothelial cell proliferation
regulation of endothelial
cell proliferation
epithelial tube morphogenesis
basement membrane organization
cellular response to
transforming growth factor
beta stimulus
response to transforming
growth factor beta
negative regulation of
epithelial cell
differentiation
negative regulation of cell
migration
regulation of endothelial
cell apoptotic process
endothelial cell apoptotic
process
bicellular tight junction
assembly
blood vessel endothelial
cell migration
negative regulation of
locomotion
Notch signaling pathway
tissue remodeling
0
3
6
9
Count
p.adjust
0.0003
0.0006
0.0009
B
Hypoxia Response
(Pink)
response to hypoxia
cellular response to hypoxia
monocarboxylic acid transport
positive regulation of
phosphorylation
vascular process in
circulatory system
response to xenobiotic
stimulus
positive regulation of MAPK
cascade
vascular associated smooth
muscle cell development
endothelium development
positive regulation of
protein phosphorylation
peptidyl-tyrosine
phosphorylation
sodium ion transport
regulation of angiogenesis
camera-type eye development
pyruvate metabolic process
epithelial cell proliferation
branching involved in blood
vessel morphogenesis
carbohydrate transmembrane
transport
carbohydrate transport
sprouting angiogenesis
0
5
10
15
Count
p.adjust
0.001
0.002
0.003
C
Immune Responses
(Salmon)
skeletal muscle cell
differentiation
striated muscle tissue
development
muscle organ development
response to fibroblast
growth factor
regulation of hemopoiesis
cellular response to
interleukin-1
response to lipopolysaccharide
response to interleukin-1
cellular response to
fibroblast growth factor
stimulus
regulation of apoptotic
signaling pathway
integrated stress response
signaling
negative regulation of
response to external stimulus
myeloid cell differentiation
positive regulation of miRNA
transcription
cell proliferation involved
in metanephros development
response to phorbol
13-acetate 12-myristate
cellular response to phorbol
13-acetate 12-myristate
T cell differentiation
negative regulation of
carbohydrate metabolic process
positive regulation of miRNA
metabolic process
0.0
2.5
5.0
7.5
Count
p.adjust
0.0025
0.0050
0.0075
0.0100

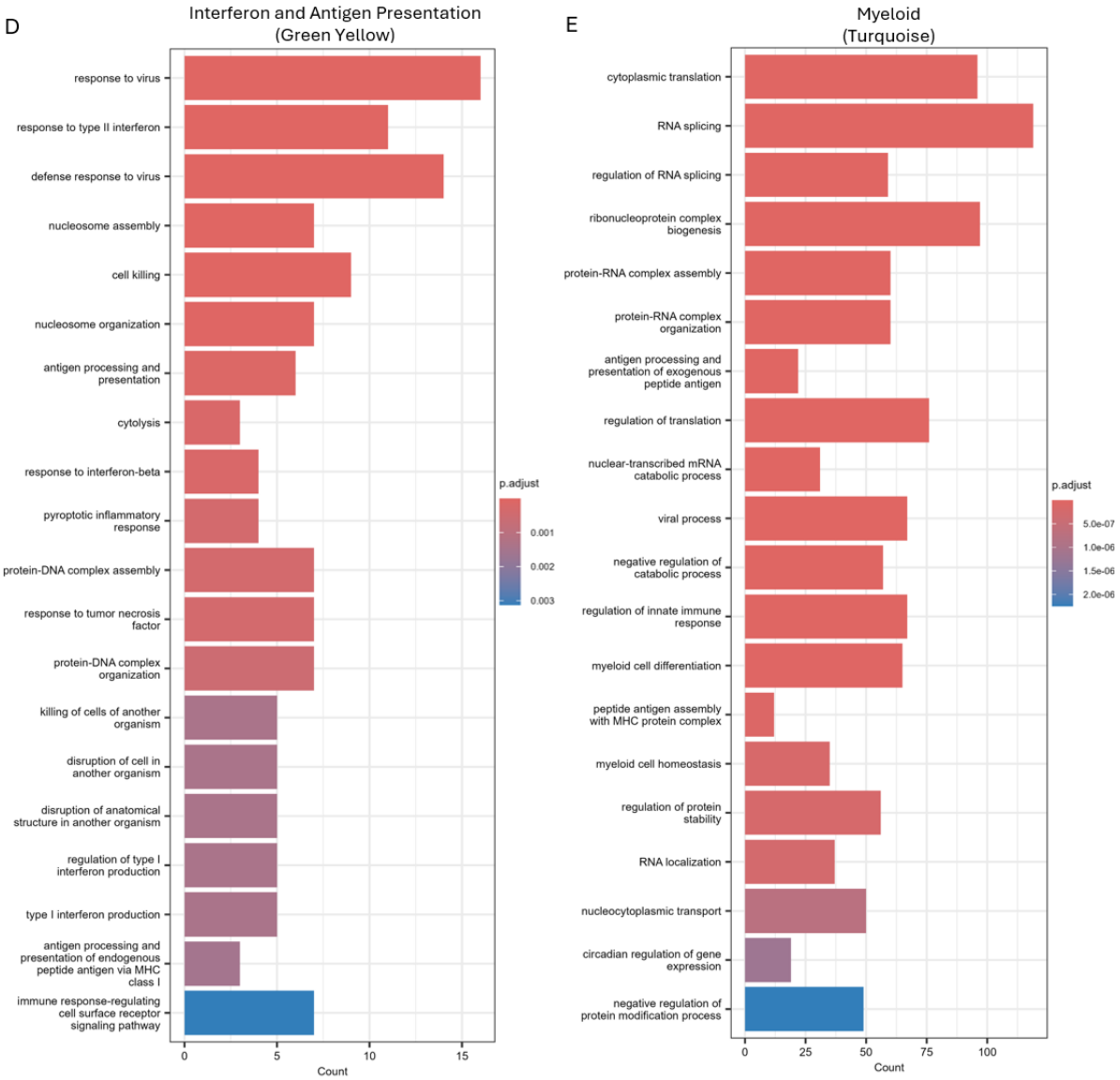


Figure 5.11: Pathway analysis of 5 of the 13 modules identified in weighted gene correlation network analysis including the (A) Tissue Structure and Metabolism (Magenta), (B) Hypoxia Response (Pink), (C) Immune Response (Salmon), (D) Antigen Presentation (Green-yellow), and (E) Myeloid (Turquoise).

Next, the hypoxia response (Pink) module was positively associated with **control ccRCC** (0.452. p<2e-14), **HIFU ccRCC** (0.369. p<8e-10), **immune** ROIs (0.271. p<1e-07), and **peritumour** ROIs (0.12, p<0.05) as shown in Figure 5.9. Assessment of the expression of module genes in individual ROIs (Figure 5.10) concurred with the correlation matrix, with the addition of the **VHL tissues** (2 of which were from the same patient) and some of the **tumour border** ROIs. This suggests a RCC subtype association to this module, rather than a treatment associated difference. The main pathways associated with this module (shown in Figure 5.11B), were hypoxia and metabolism responses which could be linked to hypoxia. For the former, this included response to hypoxia, cellular response to hypoxia and response to xenobiotic stimulus[334]. Hypoxia inducible factor (HIF)-2α (part of the hypoxia pathway) has been shown to promote proliferation of cancer cells in RCC tumours[335]. Also, the loss of the VHL gene in ccRCC contributes to the expression of HIF genes within these tumours[336]. This may suggest that the VHL tumours are of a ccRCC type. Of interest to this study, Zhang et al. have shown that expression of hypoxia related genes is associated with immunomodulatory immune phenotypes[337]. Also within this module was positive regulation of MAPK cascade[338], branching of blood vessel morphogenesis, sprouting angiogenesis, vascular process in circulatory system, endothelium development, and to extent the epithelial cell proliferation (genes for endothelium and epithelium can be shared within these pathways) which points towards vascularisation of the tissue. This complicated milieu of signals and functions within these tumours may demonstrate a drive to vascularisation, which is the expected consequence of hypoxia induced HIF activation. When considered in the context of the SpatialDecon analysis from Figure 5.8, it is likely also related to the high endothelial proportion of the RCC tumours.

The Immune Reponses (Salmon) module was positively associated with the **VHL tumours** (0.522. p<2e-19), and the **peritumour** ROIs (0.450. p<3e-14) as shown in Figure 5.9. Analysis of the expression of module genes in individual ROIs suggested that there was expression of the genes within this module in ROIs throughout the cohort (Figure 5.10). The highest expression was seen in the peritumour ROIs from a VHL patient. This may suggest that this module is linked to individual biology of this tumour. The pathways associated with this module (Figure 5.11C) broadly included muscle related, signalling response (interleukin-1, fibroblast growth factor, and lipopolysaccharide), apoptotic signalling and immune (myeloid and T cell lineage) pathways.

### 5.6.2 Treatment related expression profiles included interferon responses regardless of RCC subtype

The interferon and antigen presentation (Green-yellow) module was positively associated with **HIFU ccRCC** (0.391. p<6e-11), and **HIFU pRCC** (0.296. p<3e-06), with correlation to **treatment** group (0.157. p<0.02) as well (Figure 5.9). This points towards this module being associated specifically with the treatment, which was of interest to the aims of this chapter. Assessment of the expression of module genes in individual ROIs suggested that these pathways were upregulated in **HIFU treated RCCs**, including **VHL RCC** tumours, however there was low expression of the genes within the module in **control pRCC** (Figure 5.10) which may have been related to high macrophage abundance in baseline pRCC tumours. The relatively low statistical significance to treatment (p<0.02) would be a consequence of AML tumours also being within this 'HIFU treatment' group, the genes in this module were not highly expressed in the benign AML tumours (Figure 5.10) which suggested that this is a cancer-type specific response. The HIFU mediated changes to expression were evident in

fewer of the peritumour ROIs which lends confidence to the fact that the genes involved in the module were modulated inside the tumour, the area targeted by the HIFU treatment. The expression was seen variably within ROIs from patient 784/13 1E, the ccRCC within the transplant kidney, which may be related to off target immune responses to tumours, related to HIFU, or the tumour sampled was the HIFU treated tumour, as suggested by the pathologist's review of the H&E slide. The patient may have been treated with immunosuppression which may have altered the immune response to HIFU treatment, however there was no record of immunosuppression given.

Pathways upregulated were associated with interferon responses, these included response to type II interferon, response to interferon-β (IFN-β), along with regulation of type-I interferon production (IFN-α and IFN-β). To an extent, defence response to virus and response to virus pathways are IFN related. Analysis of the genes associated with both pathways (data not included) showed expression of CD40, CXCL9, IFI44L (interferon induced protein ligand 44[339]), IFIT3 (interferon induced protein with tetratricopeptide[340]) and STAT1. This suggested both type I and II responses to treatment. It has been suggested in previous literature that the upregulation of interferon response can be caused by DNA damage[341], which is seen with HIFU treatment[342]. IFN pathways have often been targeted in the treatment of RCC[343], making the therapeutic consequences of the HIFU treatment of clinical relevance.

Type II interferon (IFN-γ) has been shown to be produced by CD8 T cells[344,345], and within an *in vivo* melanoma model (B16), the expression of IFN-γ by CD8 T cells has been linked to cell cycle arrest of cancers cells instead of a tumour cell killing cytotoxic response[346]. When assessed with the SpatialDecon analysis, this data would suggest an increased expression

of IFN-γ by already present CD8 T cells, instead of a raised accumulation of CD8 T cells after HIFU treatment. Another benefit of increased INF-γ within the environment is a skewed polarisation of macrophages away from tumour promoting M2 like phenotype[347], which is beneficial in the TME.

IFN-β has also been shown to be important in maintaining an M1 phenotype in an *in vivo* setting[348]. With a high abundance of macrophages within these tumours, this may be the case. However, macrophage polarisation was not evaluated by the SpatialDecon analysis. IFN-β expression has been associated with HIF gene expression within RCC samples[349]. HIF response pathways was identified in the hypoxia response module pathway analysis (Figure 5.11B), and the expression may relate to the upregulation of these genes in the tissues as discussed in section 5.6.1. Functionally, IFN-β can be produced CD4 T helper cells and stimulate DCs for the development of CD8 cytotoxic T cell function, as shown from human samples taken from multiple head and neck cancers and colorectal carcinoma[350]. This may provide supporting evidence for immune stimulation following HIFU treatment in RCC.

*In vitro*, macrophages have been shown to increase INF-α secretion when cultured with supernatants from thermally ablated MC-36 cells (murine colon adenocarcinoma)[50]. With high macrophage abundance being estimated in the HIFU treated RCC tumours by the SpatialDecon analysis, the macrophages may be the source of INF-α expression, and hence the response pathways being upregulated. Hashimoto et al. showed INF-α has been associated with decreased Treg cell levels and increased CD8 T cell levels within a murine colorectal (CT26) *in vivo* model[351] while Cao, showed similar CD8 T cell effects in murine colorectal (MC38) and melanoma (B16) models[352]. This would be a desirable clinical outcome after HIFU ablation. INF-α is often associated with maturation of DCs within

tumours[351]. However, the SpatialDecon did not show modulation of the DC populations within the HIFU treated RCC tumours compared to control (Figure 5.8). As suggested in Section 5.5, the macrophage population was very abundant in these RCC tumours, this may be why the DC populations could not be reported on due to the high and over-riding abundance of macrophage signatures; however, they may still have an influence in the TME.

Also, within this module, was response to antigen as antigen processing and presentation, antigen processing and presentation of endogenous peptide antigen via MHC class I (suggesting antigen presentation by DCs for CD8 activation) and immune response-regulating cell surface receptor signalling pathways with cell killing (which featured antigen response genes HLA-C and TAP2[260], data not shown) and cytolysis. This suggests an antigen recognition and cell killing process that is associated with treatment of these tumours. It may be that the antigen recognition is by the high macrophage population[175] identified in the SpatialDecon analysis (Figure 5.8). With the prevalence of macrophages in this module, and the known high expression in pRCC at baseline, it is thought that the inclusion of some of the control pRCC ROIs was related to high macrophage content, supported by the literature[32] and SpatialDecon analysis (Figure 5.8).

Pyroptotic inflammatory response, which can be a response to danger associated molecular patterns (DAMPs)[353] was upregulated in this module. With the treatment, it was expected to have an increase in DAMPs[127]. It may be that the upregulation of the type-II interferon pathways was linked to the response to pyroptotic responses. This has been previously reported in a hepatic cellular carcinoma xenograft model following radiofrequency ablations[354]. It is interesting to see this expressed, along with antigen presentation pathways linked to CD8 T cell antigenic activation (by MHC-I). Unfortunately, this data did

not provide information on differences dependent on cancer subtype. A differential gene expression (DGE) analysis can be used as a targeted analysis required to elucidate this. This analysis was discussed in a future section.

### 5.6.3 Antigen recognition and myeloid cell abundance increases specifically in ccRCC and VHL RCC tumours

The myeloid (turquoise) module was associated with **HIFU ccRCC** (0.236. p<0.0002), **control pRCC** (0.260. p<3e-05), **HIFU pRCC** (0.182. p<0.004), and **HIFU VHL RCC** (0.186. p<0.003) as shown in Figure 5.9 indicating this was a treatment specific phenotype in ccRCC, and VHL (where the phenotype may be ccRCC). The analysis of the expression of the genes in individual ROIs (Figure 5.10) aligned with this assessment and showed that there was an association with most ROIs, (excluding the two control ccRCC tumours and two of the four AML samples: samples from the same patient tumour).

The pathways associated with this module (Figure 5.11) included antigen processing and presentation (including assembly of MHC molecules) as well as myeloid cell homeostasis, myeloid cell differentiation and regulation of innate immune response. The pathways did not describe which myeloid cells were upregulated. DCs and macrophages are assumed due to the increase in antigen presentation pathways within this module. Neutrophils have also been shown to be prevalent after HIFU therapy[171], but this cell type could not be assessed, much like the DCs because of the large macrophage population present within these tissues.

However, the genes associated with macrophages are shared with antigen presentation on macrophages (data not shown), so either of these functions may have increased after HIFU-induced necrosis, specifically in the ccRCC tumours where these cells were previously not

abundant. It may have been caused by increase DAMPs in the tissue, caused by necrosis[50]. The limitations of the dataset make it difficult to confidently determine which of the mechanisms this was or the function following treatment. Without having paired pretreatment tumour samples from the same patients, it was difficult to tease this apart. Increased macrophage abundance, activation and antigen presentation may be related to the interferon module as discussed in section 5.6.2.

This module could be related to the findings of the SpatialDecon analysis (Figure 5.8), where high macrophage abundance was seen in the HIFU ccRCC, pRCC, VHL and 2 out of the 4 AML tumours, along with the control pRCC but not the 2 control ccRCC tumours. The pRCC type has high abundance of macrophages within the TME at baseline compared to ccRCC tumours, which has previously been reported by Zhang et al.[29].

### 5.6.4 Summary of the WGCNA assessment

This section included the transcriptomic profiling of renal tumours assessed by RNA-expression profiles to try to understand the biological response to HIFU treatment in RCC. It was suggested that interferon responses were upregulated which may be associated with DNA damage and DAMP release following HIFU treatment. DGE analysis may elucidate the mechanisms and cell types in which the interferon responses are occurring in within the tumour environments after treatment, if there are genes upregulated together. Also, the assessment of the different RCC types may show tumour subtype intricacies that are lost within the large amount of data. The ccRCC had a specific response to HIFU (that was not seen in pRCC), with increased myeloid populations, whereas myeloid populations were already abundant in the pRCC tumours. The interferon responses in these tumours may be linked to the myeloid population changes seen.

These data also suggested that the immune populations in the AML samples were very heterogeneous. The data demonstrated differences between malignant (RCC) and benign (AML) response to HIFU treatment, with association to different modules in the WGCNA being assessed in Figure 5.9. Upon closer investigation, the modules associated with specific tumours within the AML subtype, this meant that the biological differences between individual tumours masked differences between the tumour types (AML vs RCC).

## 5.7 Differential gene expression analysis of renal tumours for assessment of immune modulation after HIFU treatment

The previous section on the WGCNA assessment of the HIFU treated RCC samples compared to untreated controls and benign tumours exposed to HIFU suggested an interferon signalling and antigen presentation response to HIFU treatment. The assessment was unable to determine which cells this related to or confirm that antigen recognition and presentation was associated with treatment due to variability with immune populations in the TME based on cancer subtype.

The specific DGE analysis of the data was employed to assess these differences based on specific factors within the data. The aims were to lend confidence to the differences seen in antigenic and interferon responses and identified within the data (Figure 5.11E). Also, the assessment may provide more information about the immune profiles of the tumour subtypes, as well as the cell expression profiles to assess differences in response to treatment between the two RCC subtypes. The macrophage related genes were upregulated in the ccRCC tumours after HIFU treatment, but this population was highly abundant in pRCC regardless of treatment.

DGE analysis was conducted using the Limma package in R[119] discussed in Section 2.7.2, with a p adjusted threshold of 0.05 (p adj. = 0.05), and log-fold change of 0.5 (LogFC = 0.5). Pathways were identified from these genes using the clusterProfiler[212] package in R. Pathways with a p and q significance of 0.05 were assessed. Within these analyses, the HIFU treated ccRCC sample was from a transplant kidney (784/13 1E) was excluded from assessment as it may have masked the immune response caused by HIFU.

### 5.7.1 Differential gene expression analysis of immune ROIs showed expression of antigen presentation genes and interferon response pathways

The comparison of **immune ROIs of HIFU treated RCC to control RCC** identified 57 DEG (Figure 5.12A). Within the HIFU treated tumours the DEG included HLA-G, HLA-DQA2, HLA-DPA1, HLA-DQB1, C1QB, C1QC, CXCL9, TAP1, STAT1, IL6ST, CXCL13, CD8A. This supports a conclusion that there was an antigenic response in the form of MHC-I and -II upregulation. This suggests cross-presentation to CD8 T cells, with likely involvement of CD4 T cells. This would cause activation of these cell types, which is seen within the pathway analysis (Figure 5.12B). The antigen presentation related genes may have been upregulated because of the increased macrophage abundance after treatment. MHC-II genes are often expressed by macrophages[291] and with the inclusion of the C1QB and C1QC this was most likely the abundant antigen presenting cell type[291]. The expression of CXCL13 and IL6ST suggested that the macrophages may be polarised towards an M2 protumour phenotype[355,356]. However, there was increased T cell activation within the pathway analysis (Figure 5.12B) in the **HIFU RCC** group, making this difficult to untangle.

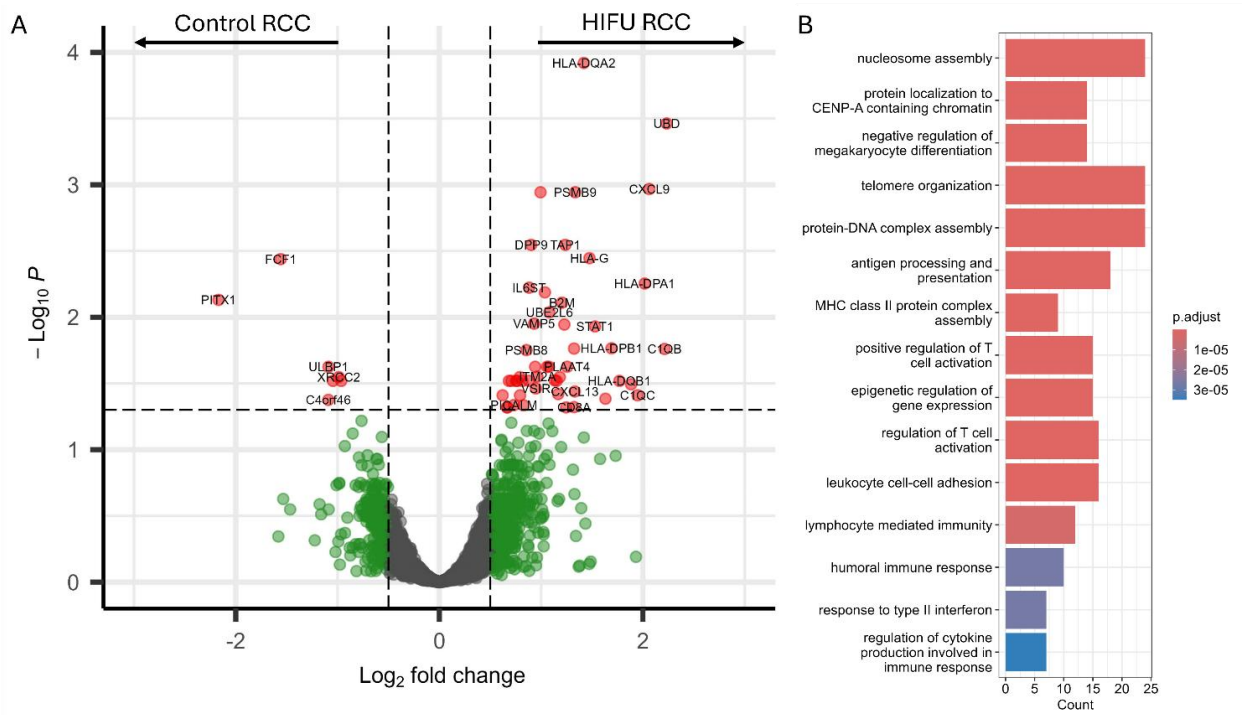


Figure 5.12: Comparing the transcriptomic profile of the immune ROIs in renal cell carcinoma after HIFU to control tumours, with a focus on immune populations assessed by immunofluorescence during ROI selection. (A) Volcano plots showing differential expressed genes within highly infiltrated ROIs between (left) control RCC and (right) HIFU treated RCC with log2 FC indicates the relative expression level changes for each gene compared to each other with P adj = 0.05 significance level. Points in red represent gene that are expressed significantly over both thresholds, blue are significantly over the adjusted p value, green points were above the fold change threshold but were not above the Padj value and genes represented in black are not statistically different between the variables being described. (B) Pathway analyses of differentially expressed genes from high intensity focused ultrasound treated tumours compared to control tumours with a Padj value of 0.05.

Additionally, CXCL9[265,345] and STAT[357] are genes associated with IFN responses, and were upregulated in the **HIFU RCC**. CXCL9 is IFN inducible cytokine and has been shown lead to CD8 T cell activation in human epithelia ovarian carcinoma[265]. This may be the downstream result of the antigen activation pathways also seen here and in the WGCNA (Figure 5.11D). This may explain why there is an increase in the macrophages after HIFU treatment. It will be of interest to assess this in the subtype analysis. These findings further support and extend the findings within the IFN and antigen presentation module (Figure 5.11D) from the WGCNA analysis.

As previously mentioned, pathway analysis showed increased antigen presentation and T cell activation responses in the **HIFU RCC** immune ROIs (Figure 5.12B). As discussed, the

antigen presentation can also be linked to the complement genes upregulated in the DGE analysis by relation to the abundance of macrophages within the TME as outlined in detail in Section 5.6.3. The cell-cell adhesion pathways may relate to the infiltration of immune cells into these tumours or the activation of immune cells by binding with macrophages. However, there was not enough detail from this analysis to confirm which. A humoral based immune response was also observed within the pathway analysis, which would suggest the involvement of B cell immune responses within the **HIFU RCC** tumours compared to **control RCC**. The pathway analysis showed increased responses to IFN-II and regulation of cytokine production which supports the findings from the WGCNA analysis.

### 5.7.2 Tumour border DEG analysis suggested increased CD8 activation in the HIFU treated RCC

The comparison of **tumour border** of **HIFU RCC** to **control RCC**, identified 40 DEG (Figure 5.13A). The profile of genes that were upregulated was like the immune ROIs (Figure 5.12A). In this analysis CD8A and NKG7 (cytotoxic gene expressed by NK and CD8 T cells[312,313]) were more significantly upregulated within the **tumour border HIFU RCC** (Figure 5.13A). This indicated that the **tumour border of HIFU RCC** had increased cytotoxic function of the CD8 T cell and possibly NK cell abundance compared to the **control RCC tumour border,** suggesting possible increase cytotoxic function in HIFU treated tissues compared to control tissues. The study aimed to focus on the CD8 T cell population, which aligns this finding with the chapter aims. This may be related to the IFN expression, which was noted as the IFN-γ pathway (Figure 5.13B). As previously discussed, CD8 T cells express INF-γ (section 5.6.2), so the increased IFN-γ expression could be related to CD8 T cell activation or abundance.

Genes additionally upregulated included CCL5, IL2RB, and CD27. CCL5 expression is known to be influenced by increased expression of IFN in a cancer setting[358]. CCL5 has been associated with increased CD8 T cell infiltration in solid tumours[265], which would be a beneficial outcome of the HIFU and aligns with the hypothesis. This DGE study saw upregulation of IL2RB, also known as CD122. Studies have associated CD122 expression on CD8 T cells as a marker for memory populations[359] and is required for responses to IL2 within the environment of CD8 T cell activation[311]. CD27 is associated with maintaining T cell immune responses[360] which has also been seen in *in vivo* tumours studies[361]. The selection of CD8 related genes can be associated to the CD8 T cells that were selected using IF in this study. This targeted strategy has possibly helped elucidated these targeted responses this study aimed to understand. This has suggested infiltration of memory CD8 T cells.

The pathways upregulated in the HIFU treated RCC compared to control RCC (Figure 5.13B) included MHC class II protein complex assembly, antigen processing and presentation, and inflammatory response to antigenic stimulation which suggests an antigen response to treatment by macrophages or an increase in macrophage abundance, (Figure 5.8) which has been discussed. Lymphocyte mediated response including T and NK cell responses strongly suggests an immune response in the RCC tumours treated with HIFU that was not seen in the untreated controls.

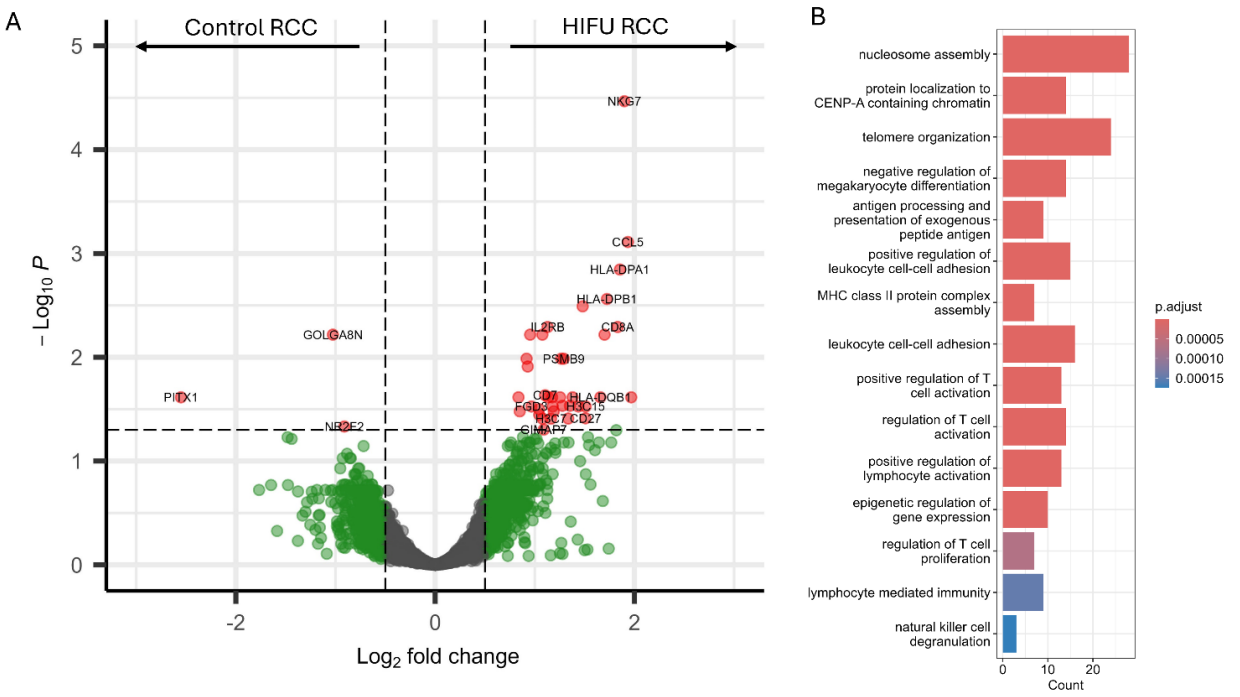


Figure 5.13: Comparing the transcriptomic profile of the border tissue of renal cell carcinoma after HIFU to control tumours, with a focus on immune populations assessed by immunofluorescence during ROI selection. (A) Volcano plots showing differential expressed genes between (left) control RCC and (right) HIFU treated RCC with log2 FC indicates the relative expression level changes for each gene compared to each other with P adj = 0.05 significance level. Points in red represent gene that are expressed significantly over both thresholds, blue are significantly over the adjusted p value, green points were above the fold change threshold but were not above the Padj value and genes represented in black are not statistically different between the variables being described. (B) Pathway analyses of differentially expressed genes from HIFU treated tumours compared to control tumours with a Padj value of 0.05.

## 5.7.3 Analysis of the different RCC subtypes indicated HIF response differences when comparing HIFU treated ccRCC to pRCC

The comparison of **immune ROIs** of HIFU treated **ccRCC** to **immune ROIs** of HIFU treated **pRCC** identified 26 DEG. Genes upregulated in HIFU treated pRCC tumours compared to HIFU treated ccRCC tumours included ANGPTL4, HILPDA, and FLT1. ANGPTL4 has been associated with controlling inflammatory responses by macrophages in high fat environments[362] and is hypoxia inducible[363]. HILPDA is a hypoxia inducible gene in macrophages that responds to environmental lipids[364], much like ANGPTL4. FLT1 is a member of the vascular endothelial growth factor receptor genes. These genes are associated with angiogenesis[365]. There was no upregulation of immune genes within this

DGE analysis which suggested that the immune profiles of the pRCC and ccRCC following treatment were similar, unlike what is known of baseline RCC from the literature and SpatialDecon analysis discussed in Section 5.5.

The pathways upregulated in pRCC from the DEG analysis included response to hypoxia, likely related to the expression of ANGPTL4, HILPDA, as already discussed. Other pathways included vasculogenesis, vessel formation and angiogenesis pathways, likely related to expression of FLT1. It was discussed in Section 5.6.1 that these pathways were a subtype specific differences which is unaffected by the HIFU treatment. However, it is seen in the other tumour type than the WGCNA which is peculiar. The inclusion of renal system processes was likely because these tumours are within the renal tissue and will retain some of the genes for the functions in the kidney.

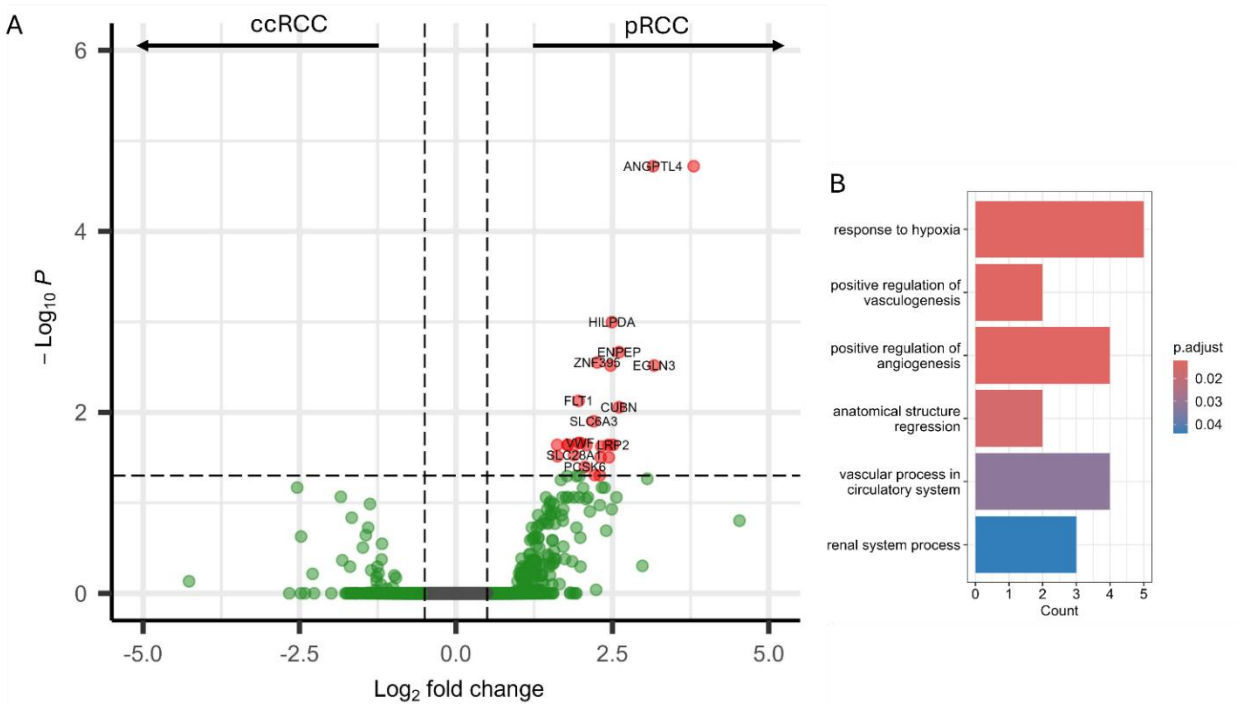


Figure 5.14: Comparing the transcriptomic profile of the immune related ROIs of the two renal cell carcinoma subtypes papillary (pRCC) and clear cell renal cell carcinoma (ccRCC) after HIFU treatment, with a focus on immune populations assessed by immunofluorescence during ROI selection. (A) Volcano plots show differential expressed genes between (left) ccRCC HIFU and (right) pRCC HIFU treated tumours with log2 FC indicated the relative expression level changes for each gene compared to each other with Padj = 0.05 significance level. Points in red represent gene that are expressed significantly over both thresholds, blue are significantly over the adjusted p value, green points were above the fold change threshold but were not above the Padj value and genes represented in black are not statistically different between the variables being described. (B) Pathway analyses of differentially expressed genes from HIFU treated pRCC tumours compared to ccRCC tumours with a Padj value of 0.05.

### 5.7.4 Conclusions of the differential gene expression analysis

The DGE analysis identified antigen presentation and IFN genes and pathways (Figure 5.12 and Figure 5.13) that were seen within the WCGNA analysis (Figure 5.11) which may have related to macrophage populations identified in the SpatialDecon cellular deconvolution (Figure 5.8). The DGE suggested that there was increased genes associated with cytotoxic T cell function in HIFU treated RCC when compared to the control RCC (Sections 5.7.1 and 5.7.2). There was a limited subtype specific change in the gene expression after HIFU when comparing pRCC to ccRCC. The genes related to hypoxia response and vessel formation. This may be important for immune infiltration, but also in the growth of the tumour. There

were no immune genes upregulated in the subtype DGE comparison suggesting similar immune profiles in the HIFU treated RCC subtypes.

## 5.8 Chapter Discussion

This chapter covered the transcriptomic assessment of the immune phenotype of HIFU RCC against untreated control RCC and benign tumours (AML), to evaluate the immune modulation caused by HIFU treatment. The results of this chapter are summarised in Table 5.2. In summary, the SpatialDecon analysis was used to determine immune population abundances from the RNA expression profiles of the ROIs selected within the tumours. This identified **macrophage** and **naïve CD4 T cell** populations as some of the main cells within the tissue. The macrophage population showed indication of increased abundance in **HIFU ccRCC** tumours compared to **control ccRCC**.

Assessment of the transcriptomic profile of the tissues by WGCNA analysis identified increased interferon signalling in the tissues in **HIFU RCC** tumours, not seen **control RCC** (Figure 5.11). This was identified as the upregulation of response pathways to both type I and II interferon signalling. It was hypothesised that the expression of interferon may be by the macrophage and CD8 T cell populations. The mechanism for the increased abundance of macrophages in HIFU treated ccRCC was not elucidated by WGCNA but is likely to result from increased cellular debris. **HIFU AML** tumours showed heterogeneity in their immune populations, whether this was a HIFU related difference could not be commented on as **control AML** was not assessed.

The WGCNA analysis identified increased antigen recognition and response pathways in **HIFU ccRCC** tumours compared to **control ccRCC** tumours, whilst the expression of these

pathways was constant in pRCC, regardless of HIFU treatment. It was thought that this was because macrophages are known to be highly abundant in treatment naïve pRCC. Although the CD8 population did not show evidence of increased abundance after HIFU treatment in the WGCNA analysis, there was evidence of activation of T-cell pathways.

The DGE analysis of the **HIFU RCC** compared to **control RCC** showed upregulation of MHC class I and II genes, complement genes and CD8A expression, within the **immune** and **tumour border** ROIs. The DEG analysis suggested that M2 macrophages were abundant in **HIFU RCC** tumours compared to **control RCC** with expression of IL6ST and CXCL13 in the immune ROIs, whilst the tumour border had upregulation of CCL5, IL2RB and CD27 which have all been associated with CD8 T cell activation and memory phenotype, aligning with the hypothesis. The DGE analysis of the RCC subtypes did not identify any differences in immune populations after HIFU treatment, when comparing **ccRCC** to **pRCC** which suggested similar immune profiles in these subtypes after treatment. The literature suggests that the tumours are vastly different when treatment naïve making this an interesting finding.

Table 5.2: concatenation of the results comparing HIFU treated RCC subtypes to untreated RCC controls and benign AML tumours exposed to HIFU.

| Focus | Analysis | Expression | Significance |
|---|---|---|---|
| ccRCC | SpatialDecon | Macrophage abundance | There was high macrophage abundance in HIFU treated ccRCC samples which was not seen in control ccRCC |
| pRCC | SpatialDecon | Macrophage abundance | High macrophage abundance was seen in all pRCC samples suggesting that this was not HIFU related |
| ccRCC | SpatialDecon | Endothelium abundance | ccRCC tumours had higher endothelium, some VHL tumours also had high endothelium which may sub classify them |
| ccRCC | WGCNA | Vascularisation | The ccRCC tumours had upregulation of vessel forming related pathways, suggesting higher vascularisation of this tumour type |
| ccRCC | WGCNA | Hypoxia and vascularisation | Hypoxia and vascularisation were upregulated in this subtype which are unusual to be expressed together |
| VHL | WGCNA | Immune responses and signalling pathways | There was suggestion of a strong immune response outside of one of the tumours |
| HIFU treated RCC | WGCNA | Interferon and antigen presentation response | There was increased antigen recognition pathways associated with the HIFU treated RCC tumours<br>Interferon responses may have increased because of increased DNA damage within the environment caused by HIFU |
| HIFU treated RCC | WGCNA | Myeloid cells and antigen presentation and response | Increased antigen recognition pathways may be associated with increased macrophage abundance |
| HIFU treated RCC IM ROIs | DEG | Upregulated HLA-DQA2, HLA-DPA1, C1QB, CXCL9, TAP1, STAT1, CXCL13 and IL6ST expression | Suggested antigen presentation to both CD4 and CD8 T cells in HIFU treated RCC and response to cancer antigen caused by treatment with the knock-on effects on interferon signalling |
| HIFU treated RCC TB ROIs | DEG | Similar profile as IM ROIs NKG7, CCL5 and IL2RB expression | At the tumour border of HIFU treated RCC there was upregulation of CD8A and cytotoxic genes compared to control tissues |
| pRCC | DEG | ANGPTL4, HILPDA and FLT1 | The subtype of tumour has little effect on the immune population response to HIFU treatment other than |
| ccRCC | DEG SpatialDecon | N/A | The immune profile of the ccRCC tumours after HIFU had no significant differences from pRCC unlike the phenotype of control tissue described in the SpatialDecon assessment, suggesting the immune phenotypes are modulated to be similar after HIFU treatment |

The **limitations** of the study are similar to those outlined in Chapter 4, these include:

(A) The resolution of the technology is poor and does not aim to individually identify cells which can lead to the estimation by the SpatialDecon may be incorrect if a gene is expressed by multiple cell types. For example, the increased antigen presentation genes accounted for the increased macrophage abundance within the selected ROIs. It is not possible to guarantee expression is on the cell population suggested by any of the workflows for data analysis of DSP data.

(B) The clinical subtype of VHL tumours (ccRCC or pRCC) was not available. Previous work, specifically with hypoxia induced pathways, had been linked to VHL gene variation. However, the pathways found did not associate with both VHL patients. This suggested that there was no specific upregulation based on this gene abnormality but there was the suggestion that one of the tumours was a ccRCC based on expression profiles, but this was not confirmed.

(C) The clinical response to treatment and outcomes were not available for this analysis. This may have given confidence to the findings as it would have confirmed that the assumption that there was an immune modulation after successful treatment.

**Future work** would be to quantify the CD8 T cell abundance by IF within the slide scans from the DSP workflow to compare different areas of infiltration abundance between the samples. Also, it may be possible to obtain further tissue sections to confirm the abundance of macrophage populations, along with the polarisation and expression profiles within the ccRCC to confirm that HIFU polarisation of the macrophages or if the treatment increased

the activity of the macrophages. Additionally, it may be possible to confirm the expression profiles of the identified naïve CD4 T cells and target CD8 T cells.

# 6 Discussion

## 6.1 Introduction

Thermal ablation caused by high intensity focused ultrasound has previously been assessed in feasibility studies as a localised treatment modality for carcinomas[16,20,21,24,135,366] including pancreatic, prostate, breast, renal cell cancer, and also sarcomas[366]. The technique is known to have immunogenic outcomes which have the potential improve treatment outcomes[10,55,56,127].

However, immune populations have complicated effects within tumour cells with subsets and activation markers often being associated with differences in tumour progression and survival statistics[27,86,151,367], which also often varies with tumours and their subtypes. For instance, CD8 T cells are expected to provide a cytotoxic response in tissues, however much research has associated high CD8 T cell infiltration with poorer outcomes[105]. To try to examine the function of this population in these tumour microenvironments (TMEs) and associated immune cells may elucidate fundamental biological questions whilst also highlighting potential treatment strategies for these cancers. Macrophages are another cell type of interest described by the literature and this thesis, which can assert an antigen presentation response[175], but can also be polarised to produce pro-inflammatory cytokines or pro-tumorigenic cytokines[44,368,369].

Understanding the role and functions of immune populations within soft tissue sarcoma (STS) is an active area of both pre-clinical and clinical research[26,83,85,174]. These tumours do not typically respond well to immunotherapies relative to more immunogenic tumour types including renal cell cancer, melanoma and lung cancers where immunotherapy is becoming

standard of care for advanced disease[370–372]. STS patients generally have poor prognosis with high metastatic potential from diagnosis[370]. Understanding the baseline immune populations within STS subtypes along with the ability of HIFU to generate an immune response within these tumours would be of great value in informing next generation treatments in this underserved patient cohort.

In the case of renal cell carcinoma, the modulation of the immune populations of the tumour after HIFU treatment had not been explored in detail previously. Of interest, much like STS, RCC has differences in the tumour immune environment based on tumour subtype. The key cells of interest to this thesis were the macrophages (which can be polarised) and the T cell subsets (including cytotoxic T cells and Tregs). Assessment of the abundant populations after treatment was of interest. The influence of signalling causing the change in immune populations may be translational to treatment strategies given in combination with HIFU therapy for the modulation of immune populations in future studies.

## 6.2 Summary of experimental results

### 6.2.1 Chapter 3

Chapter 3 outlined the *in vivo* assessment of the immune modulation in a fibrosarcoma murine model (MCA205) treated with HIFU therapy. Fibrosarcoma is an aggressive form of STS which has a varied immune infiltration and would greatly benefit from this treatment, whilst being a known model for investigating immune populations in sarcoma via *in vivo* methods without being immune ‘desert’ nor highly immune infiltrated, making it a good candidate to be representative to assess immune modulation following HIFU treatment in STSs that are currently not indicated for immunotherapy.

This chapter focused on assessment of T cell subsets and antigen presenting cells (APCs) of myeloid origin by flow cytometry in the peripheral lymphatics, blood and tumour. There was also histological assessment of immune populations within the tumour after HIFU. These populations included the subsets of CD4 T cells (Tconv, Treg and Treg precursors) and CD8 T cell memory subsets (Tnaïve, Tcm and Tem). The assessment of the CD4 populations within the tissues of mice with fibrosarcoma (MCA205) identified that Tregs were at a significantly higher frequency in the tumour compared to the other tissues and made up a large proportion of the CD4 T cell subsets (Figure 3.6). Theoretically, these cells exhibit a regulatory phenotype within the tumour, leading to the other immune populations being affected functionally[30,38,167]. For the other tissues the T conventional cells were the most abundant cell type.

With the HIFU treated tumours, there was evidence of pyknosis within the tissue, which is associated with the thermal damage and coagulative necrosis caused by HIFU treatment (Figure 3.9, Figure 3.17 and Figure 3.30). However, the assessment of immune populations in the tumour by immunohistochemistry (IHC) in pilot studies did not provide robust results (Figure 3.10, Figure 3.11, Figure 3.18 to Figure 3.22). Therefore, assessment of the immune populations in the harvested homogenised tumours were subsequently assessed by flow cytometry in the final study.

The immunological assessment of the lymphatics from mice whose tumours were treated with HIFU in pilot studies assessing different lengths of treatment (for differences in ablation). The low (shorter) HIFU treatment showed significantly increased central memory CD8 T cell (Tcm, $p<0.01$) abundance in from the draining lymph nodes (dLNs) of the tumour (Figure 3.14). When applying high (longer) HIFU treatment, the data pointed towards

sequestering of the immune populations from the dLNs (Figure 3.12 and Figure 3.13) with assessment of the CD8 and CD4 populations from the draining lymph nodes and spleen after high HIFU treatments.

When the HIFU treatment time was lowered in the interests of reducing adverse effects including skin damage (from 15 and 10 seconds to 5 seconds), the difference in abundance of the Tcm population in the spleen decreased between treatment groups, and significance was lost (Figure 3.25). The assessment of CD4 T cell subsets in mice whose tumours were treated with HIFU demonstrated a slight increase in the frequency of Treg populations within the dLN at 24-hours and 5-days post HIFU treatment (Figure 3.26).

Investigation of APCs in the dLNs from individuals whose tumours were treated with the HIFU treatment identified significantly increase neutrophils 24-hours after HIFU treatment compared to sham-control tissues, which normalised within 5-days (Figure 3.23), this was thought to be linked to an inflammatory response caused by tissue damage. In a typical inflammation response, macrophages were shown to be increased within dLNs 24-hours and 5-days after HIFU, while monocytes were more abundant 5-days after treatment, within the same context (Figure 3.23). This was theorised to be associated with the inflammation associated neutrophil abundance caused by HIFU induced tissue damage.

Next the growth of the tumours and distribution of the APCs and T cells were assessed in the context of HIFU treatment combined with aPD-L1 therapy. Within the 5-day groups tumour growth was significantly reduced ($p<0.01$) in mice treated with aPD-L1 regardless of HIFU treatment when compared to isotype + sham HIFU control treated mice. The modulation of immune populations did not strictly align with previous findings. Within the tumour, the absolute number of macrophages were higher in tumours treated with aPD-L1 + HIFU 24-

hours after treatment (Figure 3.32). There was a significant decrease in the expression of MHC-II on dendritic cells in tumour treated with aPD-L1 regardless of HIFU ($p<0.05$), which had previously been reported in the literature (Figure 3.32). The absolute number of dendritic cells were increased with aPD-L1 + HIFU treatment compared to untreated (Isotype + Sham) controls in the dLN (Figure 3.33). There was a hint of modulation of macrophages and monocytes as well.

Assessment of the T cell subsets in the tumour in the aPD-L1 + HIFU group demonstrated that the Treg population was smaller in the Isotype + HIFU treated group and stable with aPD-L1 regardless of HIFU treatment, when compared to the untreated group (Isotype + Sham). Within the dLN the CD4 subsets were stable, regardless of treatment. Modulation of the CD8 memory populations was not demonstrated within the tumour or dLNs with aPD-L1 or HIFU treatment.

These studies were able to identify that HIFU increased abundance of CD8 Tcm, and to an extent Tregs within the dLN of tumours treated with HIFU. This suggested the immune system can be stimulated in an STS model, likely by antigen presenting myeloid populations supported by the increased abundance of monocytes, macrophages, DCs, and neutrophils within the dLN. A potential drawback of HIFU therapy for STS may be stimulation of Treg populations, which consequently inhibited antitumour immunity. Future studies may be able to explore this further. The value of intratumour immune analysis was limited due to variability in the tumour sizes used within experiments because of the erratic growth of the MCA205 tumour cells. This is along with histology only being able to provide a snapshot of a small section of a much larger and complicated tumour.

### 6.2.2 Chapter 4

Digital spatial profiling with transcriptomic assessment of clinical STS samples was conducted with a focus on intratumour and peritumour immune populations to assess the landscape of this tumour type. This was with a view to elucidate key immune pathways in the TME differences seen with STS subtype. Further to this, it was thought to potentially inform future immunotherapy treatments in combination with HIFU treatment-induced immune modulation.

CD8 T cells are commonly noted in survival statistics studies and are a cell type of interest for HIFU immune modulation while CD45+ cells were assessed to capture the transcriptomic profile of all leukocyte populations. Given STS is known for being 'immune-cold', there is a potential role of regional therapy, such as HIFU, to activate the immune system as a positive effect along-side thermal ablation.

It is understood that STS subtypes demonstrate different immune profiles. The immune populations within different STS subtypes were analysed to characterise these differences and, in an attempt, to investigate the potential underlying mechanisms for the differences. This involved assessing the transcriptomic profile of areas of tumours with higher or lower immune abundance by stratification of the immune infiltration based on immunofluorescence of target immune populations to reveal any genes or pathways that were shared between analyses. The study also aimed to assess how immune cells enter and travel through the TME (chemotaxis) by assessing immune populations in different part of the tumour. Tumour types selected for this study were selected based on the literature and included the classically lower immune infiltrated leiomyosarcoma (LMS) and more highly infiltrated undifferentiated pleomorphic sarcoma (UPS), along with an uncategorised

spindle cell sarcoma (USS), which showed low immune infiltration based on histological assessment.

Comparison of the LMS tumour to UPS tumour by differential gene expression (DGE) analysis showed differences in the structures of the tumours (Figure 4.11 to Figure 4.13), with LMS having many muscle-related genes upregulated regardless of the location of the ROI. There was also high fibroblast abundance in all tumours, including LMS, when assessed by cellular deconvolution.

The assessment of the UPS tumour by DGE analysis compared to LMS suggested increased antigen presentation genes including MHC-II and antigen presentation pathways when assessed globally, then when compared at the tumour border and the central tumour (Figure 4.11 to Figure 4.13). The cellular deconvolution showed increased macrophage abundance in the ROIs of the UPS tumours which expressed almost exclusively MHC-II markers.

Comparing the highly infiltrated ROIs in LMS to lower infiltrated ROIs identified T cell, B cell, MHC-I and MHC-II genes (Figure 4.14). Pathway analysis identified T cell activation, MHC-II antigen presentation and INF-γ. This suggested that antigen presentation led to increased T cell activation in highly infiltrated areas, but this did not elucidate the mechanism for difference in immune abundance. Comparing the same in UPS did not have any significant genes or pathways (supplementary figure 4.5).

Although suppressive and regulatory functions were not noted within the DEG, Tregs were highly abundant in all tumours, but more so in the highly infiltrated ROIs. The assessment of the expression profiles of the Tregs indicated that CCR7 was upregulated in some of the ROIs, mostly within the LMS and USS tumours, indicating involvement of lymph node activation. Fibroblasts were an abundant immune cell type throughout the ROIs but were

higher in UPS ROIs and associated with poorer CD8 cytotoxic function. The fibroblasts which were identified in the cellular deconvolution were possibly identified by collagen genes identified in LMS tumours in the DEG and WGCNA and may be related to reduced CD8 T cell functions.

The comparison of the peritumour to the tumour border of the UPS tumours showed that the immune cells just outside the tumours were more abundant than at the border of the UPS tumours. These included T cell, and B cell markers and activation markers CD69 (Figure 4.15) which suggested a more active immune function outside of the tumour.

However, regulatory and suppressive functions were not demonstrated within the tumour, thus the mechanism was not elucidated. The UPS tumour border compared to central tumour had higher expression of B cells, CD4, MHC-I and -II and C1QC genes with pathways including MHC-II antigen presentation and INF-II response (Figure 4.16). This again suggested that there is increased antigen presentation leading to increased immune cell activation in different areas of the tumour, like the differences seen with immune abundance but the mechanism for this change was not devolved. There was no DEG for LMS of the same comparison (supplementary figure 4.8).

The WGCNA analysis agreed with the findings of the DEG, briefly, there was a module containing antigen processing, and a module containing immune activation marker, both were associated with UPS ROIs more than LMS ROIs. There was a module containing structural genes which associated with LMS ROIs.

### 6.2.3 Chapter 5

Renal cell carcinoma (RCC) is reported as being highly immunogenic and immunotherapy responsive overall, in contrast to the characteristics of STS. In RCC, immunomodulatory

effects and mechanisms due to HIFU have not previously been clinically explored. The subtypes of RCC have also been shown to have differing immune phenotypes, which therefore may directly influence HIFU immune modulation. Assessment compared untreated RCC to HIFU treated RCC, both covering papillary (pRCC) and clear cell RCC (ccRCC), as well as benign renal tumours (angiomyolipoma, AML) treated with HIFU.

Resection of RCC was on the order of weeks to months post-HIFU exposure in line with the clinical study pathway. Transcriptomic assessment of subtypes of clinical RCC treated with HIFU focused on CD45 and CD8 immune cells with the same rationale as the STS assessment. WGCNA and cellular deconvolution were used to assess the immune populations within the ROIs selected within these tumours. The rationale being that the DGE and WCGNA analysis provided similar results in Chapter 4 and the soft thresholding passed the typically used 0.9 threshold for WGCNA analysis (unlike in the STS analysis). Also, there were many clinical factors to assess and the WGCNA could identify the most important factors to further assess by DGE analysis from the multitude of factors in the study.

The WGCNA identified complement, myeloid and antigen presentation pathways was correlated specifically with **HIFU treated ccRCC** tumours but was present in pRCC regardless of treatment (Figure 5.11). The antigen presentation genes were mainly MHC-II genes, and along with the compliment genes, this was related back to the high abundance of macrophages seen in the cellular deconvolution (Figure 5.8) within the pRCC tumours regardless of treatment, but which seemed to increase in abundance after HIFU treatment in ccRCC tumours. It was suggested that this was related to the increased response to antigen within the environment after treatment. The DEG analysis showed increased

expression of signalling markers associated with M2 macrophages in the **HIFU treated RCC** compared to **control RCC** (Figure 5.12 and Figure 5.13).

Also identified by WGCNA was increased interferon-I and -II (IFN) response and pyroptotic cell death pathways in **HIFU treated RCC** compared to **control RCC** (Figure 5.11). Metastatic RCC is known to respond well to IFN treatment making this a promising finding. There are many functions that IFN can have, although genes and pathways associated with both pathways were upregulated suggesting a large cytokine response to the treatment. IFN has been associated with alterations to macrophage abundance and the polarisation with antigen presentation function of these immune cells in the past. The DGE analysis suggested that there was an upregulation of cytotoxic genes in the **HIFU treated RCC** tumours compared to the **non-HIFU RCC** tumours (Figure 5.12 and 5.13). Pyroptotic cell death is a typical immunogenic cell death, which was related to the HIFU treatment.

There were no differences seen in immune populations between the pRCC and ccRCC after HIFU treatment. Also of note was that the **HIFU AML** tumours were heterogenous with their immune populations, so unfortunately comparisons to the **HIFU RCC** tumours were complex and difficult to decipher.

## 6.3 Overarching discussion and conclusions

The aims of the thesis have been in understanding the immune system in response to poorly immune recognised tumour of STS. To understand how these tumours avoid immune activation but also have differences in their immune milieu, both murine and clinical STSs were assessed. Further to this, the *in vivo* study aimed to 'kick start' the immune recognition of these tumours with an immunogenic treatment modality – HIFU.

The assessment of a **murine fibrosarcoma** model provided described the steady state immune phenotype of different tissues in response to the tumour within the environment, including blood, spleen, lymph nodes and tumour tissue. This work described the role that the lymph nodes have in development of an immune in response to these tumours. Further to this, the response that the immune system had on the STS after it was treated with the immunogenic HIFU treatment was investigated. The study revealed that the dLNs had a vital role in the response with Tcm and Tregs being implicated.

The transcriptomic assessment of **clinical STS** was able to assess these populations in human samples and aimed to determine the variability that can be seen with STS subtypes at baseline. As highlighted within this thesis, there are many STS subtypes and their TME with immune cells vary both by type as well as between individuals increasing the heterogeneity. This assessment showed that macrophages were prevalent in the clinical samples. These have previously been modulated in the **murine HIFU model**, making this of interest for future work.

The fibroblasts were also of high importance within the **clinical STS samples**. These were highly abundant and were thought to affect the responses of the CD8 T cells. This may have limited the response of CD8 populations within the tumour of the murine model, although not assessed. Treg antigen activation was suggested by the modulation of this population in the dLNs of the murine model. Within the clinical STS, the identified Tregs expressed CCR7, a marker for lymph node migration suggesting the importance of antigen presentation for increased Treg abundance in STS. Although these findings were not conclusive, it would suggest that Tregs play a role in the reduced immune response in STS.

The immune populations of **HIFU treated clinical RCC** subtypes were then assessed to initially investigate the immunological changes in RCC following HIFU treatment. This assessment allowed for investigation of how tumour subtype differences, with the known differences of TME, can affect the immune responses following treatment. This may relate back to the STS tumour if HIFU treatment became available for these patients. The chapter briefly mentioned TLS, seen within the peritumour of an untreated pRCC, which may have been present in other ROIs. These have been associated with better prognosis in **RCC**, but they have also been associated with poor prognosis in STS. In any case they have been shown to affect the immune populations of tumours. Similar signatures from the RCC were seen in the STS, which demonstrated their prevalence in tumours.

Within the analysis of **clinical samples**, IFN, macrophages and antigen presentation were seen in both the **STS** and **RCC** transcriptomic profiles in different contexts. In ccRCC tumours a lower antigen presentation phenotype (MHC-I and MHC-II) and macrophages abundance than pRCC. After treatment, the antigen presentation and macrophage genes were comparable between the two subtypes. The antigen presentation and macrophage genes were variable in the STS based on subtype. This finding may be recreated in the clinical STS subtypes, which was supported by the *in vivo* work with the increase in macrophages with higher HIFU treatment parameters. The difficulties of the murine fibrosarcoma model and the delicate balance between producing treatments that had minimal side effects and enough HIFU for response, meant that meaningful responses were minimal when HIFU was combined with additional immunotherapy was given (aPD-L1).

Understanding that immune population in different subtypes of STS and RCCs and in the case of RCC how they would respond to HIFU, was important in a basic science setting as well as to inform future immunotherapy treatment strategies.

## 6.4 Future work

Perhaps the most clinically relevant future work would be to determine macrophage polarisation after HIFU treatment to confirm the phenotype due to their abundance in the clinical samples from both the sarcoma and RCC samples. This may also help determine the mechanisms that are the strongest drivers. Another factor to consider is the expression of activation markers in the sarcoma in both the *in vivo* and clinical setting. Histological or in-depth single cell analysis of the tumours would allow for the extent and expression profiles of these cells to be specifically assessed. These finding may not only be important for future treatments using HIFU in solitary or metastatic RCC, but also for other tumour treatments.

The assessment of Treg and CD8 T cell receptor (TCR) repertoire in STS could assess the tumours and lymph nodes from the murine fibrosarcoma model and human patients at steady state and after HIFU therapy. This would be used to determine which cell type is expanding more and the extent of the involvement of the lymph nodes, especially for the Treg populations. This would be invaluable in being able to adjust immunotherapy strategies to provide more effective treatment options for patients.

For advanced and metastatic cancers, despite the advances in immunotherapy, response remains limited to a small minority of patients with only transient responses. It is hoped that future personalised immunotherapies combined with targeted therapies (such as HIFU,

cryotherapy or microwave ablation) bolster treatment responses effects and improve patient prognosis. Further clinical studies will be required to continue to elucidate key immune pathways and the extent that individualised treatment is required.

# References

1. Wu, F., Wang, Z. B., Chen, W. Z., Zou, J. Z., Bai, J., Zhu, H., Li, K. Q., Xie, F. L., Jin, C. B., Su, H. B., & Gao, G. W. (2004). Extracorporeal focused ultrasound surgery for treatment of human solid carcinomas: Early Chinese clinical experience. *Ultrasound in Medicine and Biology*, *30*(2), 245–260. https://doi.org/10.1016/j.ultrasmedbio.2003.10.010

2. Zhou, Y., Chen, P., Ji, X., Sun, T., Li, Y., Yuan, J., Chen, Y., Xiong, Y., & Wang, Y. (2024). Long-term Efficacy of Fibroid Devascularization with Ultrasound-Guided High-Intensity Focused Ultrasound. *Academic Radiology*, *31*(5), 1931–1939. https://doi.org/10.1016/j.acra.2023.10.045

3. Bond, A. E., Shah, B. B., Huss, D. S., Dallapiazza, R. F., Warren, A., Harrison, M. B., Sperling, S. A., Wang, X. Q., Gwinn, R., Witt, J., Ro, S., & Elias, W. J. (2017). Safety and efficacy of focused ultrasound thalamotomy for patients with medication-refractory, tremor-dominant Parkinson disease a randomized Clinical trial. *JAMA Neurology*, *74*(12), 1412–1418. https://doi.org/10.1001/jamaneurol.2017.3098

4. Rezai, A. R., D'Haese, P.-F., Finomore, V., Carpenter, J., Ranjan, M., Wilhelmsen, K., Mehta, R. I., Wang, P., Najib, U., Vieira Ligo Teixeira, C., Arsiwala, T., Tarabishy, A., Tirumalai, P., Claassen, D. O., Hodder, S., & Haut, M. W. (2024). Ultrasound Blood–Brain Barrier Opening and Aducanumab in Alzheimer's Disease. *New England Journal of Medicine*, *390*(1), 55–62. https://doi.org/10.1056/nejmoa2308719

5. Clement, G. T. (2004). Perspectives in clinical uses of high-intensity focused ultrasound. *Ultrasonics*, *42*(10), 1087–1093. https://doi.org/10.1016/j.ultras.2004.04.003

6. Turner, B., & Cranston, D. (2024). A Review of High-Intensity Focused Ultrasound. *International Journal of Translational Medicine*, *4*(1), 197–207. https://doi.org/10.3390/ijtm4010011

7. Pahk, K. J., Lee, S., Gélat, P., de Andrade, M. O., & Saffari, N. (2021). The interaction of shockwaves with a vapour bubble in boiling histotripsy: The shock scattering effect. *Ultrasonics Sonochemistry*, *70*. https://doi.org/10.1016/j.ultsonch.2020.105312

8. Khokhlova, T. D., Canney, M. S., Khokhlova, V. A., Sapozhnikov, O. A., Crum, L. A., & Bailey, M. R. (2011). Controlled tissue emulsification produced by high intensity focused ultrasound shock waves and millisecond boiling. *The Journal of the Acoustical Society of America*, *130*(5), 3498–3510. https://doi.org/10.1121/1.3626152

9. Xu, Z., Hall, T. L., Vlaisavljevich, E., & Lee, F. T. (2021). Histotripsy: the first noninvasive, non-ionizing, non-thermal ablation technique based on ultrasound. In *International Journal of Hyperthermia* (Vol. 38, Issue 1, pp. 561–575). Taylor and Francis Ltd. https://doi.org/10.1080/02656736.2021.1905189

10. Nam, G. H., Pahk, K. J., Jeon, S., Park, H. J., Kim, G. B., Oh, S. J., Kim, K., Kim, H., & Yang, Y. (2020). Investigation of the Potential Immunological Effects of Boiling Histotripsy for Cancer Treatment. *Advanced Therapeutics*, *3*(8). https://doi.org/10.1002/adtp.201900214

11. van den Bijgaart, R. J. E., Eikelenboom, D. C., Hoogenboom, M., Fütterer, J. J., den Brok, M. H., & Adema, G. J. (2017). Thermal and mechanical high-intensity focused ultrasound: perspectives on tumor ablation, immune effects and combination strategies. *Cancer Immunology, Immunotherapy*, *66*(2), 247–258. https://doi.org/10.1007/s00262-016-1891-9

12. Browning, R. J., Able, S., Ruan, J. L., Bau, L., Allen, P. D., Kersemans, V., Wallington, S., Kinchesh, P., Smart, S., Kartsonaki, C., Kamila, S., Logan, K., Taylor, M. A., McHale, A. P., Callan, J. F., Stride, E., & Vallis, K. A. (2021). Combining sonodynamic therapy with chemoradiation for the treatment of pancreatic cancer. *Journal of Controlled Release*, *337*, 371–377. https://doi.org/10.1016/j.jconrel.2021.07.020

13. Kobzev, D., Semenova, O., Aviel-Ronen, S., Kulyk, O., Carmieli, R., Mirzabekov, T., Gellerman, G., & Patsenker, L. (2024). Sonodynamic Therapy for HER2+ Breast Cancer with Iodinated Heptamethine Cyanine–Trastuzumab Conjugate. *International Journal of Molecular Sciences*, *25*(18). https://doi.org/10.3390/ijms251810137

14. Wang, Y., Li, Y., Yan, K., Shen, L., Yang, W., Gong, J., & Ding, K. (2018). Clinical study of ultrasound and microbubbles for enhancing chemotherapeutic sensitivity of malignant tumors in digestive system. *Chinese Journal of Cancer Research*, *30*(5), 553–563. https://doi.org/10.21147/j.issn.1000-9604.2018.05.09

15. Ritchie, R. W., Leslie, T., Phillips, R., Wu, F., Illing, R., Ter Haar, G., Protheroe, A., & Cranston, D. (2010). Extracorporeal high intensity focused ultrasound for renal tumours: A 3-year follow-up. *BJU International*, *106*(7), 1004–1009. https://doi.org/10.1111/j.1464-410X.2010.09289.x

16. Ritchie, R. W., Leslie, T. A., Turner, G. D. H., Roberts, I. S. D., D'Urso, L., Collura, D., Demarchi, A., Muto, G., & Sullivan, M. E. (2011). Laparoscopic high-intensity focused ultrasound for renal tumours: A proof of concept study. *BJU International*, *107*(8), 1290–1296. https://doi.org/10.1111/j.1464-410X.2010.09620.x

17. Su, S., Wang, Y., Lo, E. M., Tamukong, P., & Kim, H. L. (2025). High-intensity focused ultrasound ablation to increase tumor-specific lymphocytes in prostate cancer. *Translational Oncology*, *53*. https://doi.org/10.1016/j.tranon.2025.102293

18. Anttinen, M., Yli-Pietilä, E., Suomi, V., Mäkelä, P., Sainio, T., Saunavaara, J., Eklund, L., Blanco Sequeiros, R., Taimen, P., & Boström, P. J. (2019). Histopathological evaluation of prostate specimens after thermal ablation may be confounded by the presence of

thermally-fixed cells. *International Journal of Hyperthermia*, *36*(1), 915–925. https://doi.org/10.1080/02656736.2019.1652773

19. Ghai, S., Finelli, A., Corr, K., Chan, R., Jokhu, S., Li, X., McCluskey, S., Konukhova, A., Hlasny, E., van der Kwast, T. H., Incze, P. F., Zlotta, A. R., Hamilton, R. J., Haider, M. A., Kucharczyk, W., & Perlis, N. (2021). MRI-guided Focused ultrasound ablation for localized intermediate-risk prostate cancer: Early results of a phase II trial. *Radiology*, *298*(3), 695–703. https://doi.org/10.1148/radiol.2021202717

20. Chin, J. L., Billia, M., Relle, J., Roethke, M. C., Popeneciu, I. V., Kuru, T. H., Hatiboglu, G., Mueller-Wolf, M. B., Motsch, J., Romagnoli, C., Kassam, Z., Harle, C. C., Hafron, J., Nandalur, K. R., Chronik, B. A., Burtnyk, M., Schlemmer, H. P., & Pahernik, S. (2016). Magnetic Resonance Imaging–Guided Transurethral Ultrasound Ablation of Prostate Tissue in Patients with Localized Prostate Cancer: A Prospective Phase 1 Clinical Trial. *European Urology*, *70*(3), 447–455. https://doi.org/10.1016/j.eururo.2015.12.029

21. Zhao, H., Yang, G., Wang, D., Yu, X., Zhang, Y., Zhu, J., Ji, Y., Zhong, B., Zhao, W., Yang, Z., & Aziz, F. (2010). Concurrent gemcitabine and high-intensity focused ultrasound therapy in patients with locally advanced pancreatic cancer. *Anti-Cancer Drugs*, *21*(4), 447–452. https://doi.org/10.1097/CAD.0b013e32833641a7

22. Yu, W., Tang, L., Lin, F., Jiang, L., & Shen, Z. (2019). Significance of HIFU in local unresectable recurrence of soft tissue sarcoma, a single-center, respective, case series in China. *Surgical Oncology*, *30*, 117–121. https://doi.org/10.1016/j.suronc.2019.06.004

23. Lu, P., Zhu, X. Q., Xu, Z. L., Zhou, Q., Zhang, J., & Wu, F. (2009). Increased infiltration of activated tumor-infiltrating lymphocytes after high intensity focused ultrasound ablation of human breast cancer. *Surgery*, *145*(3), 286–293. https://doi.org/10.1016/j.surg.2008.10.010

24. Wu, F., Wang, Z. B., Cao, Y. De, Chen, W. Z., Bai, J., Zou, J. Z., & Zhu, H. (2003). A randomised clinical trial of high-intensity focused ultrasound ablation for the treatment of patients with localised breast cancer. *British Journal of Cancer*, *89*(12), 2227–2233. https://doi.org/10.1038/sj.bjc.6601411

25. Wu, F., Wang, Z. B., Cao, Y. De, Zhou, Q., Zhang, Y., Xu, Z. L., & Zhu, X. Q. (2007). Expression of tumor antigens and heat-shock protein 70 in breast cancer cells after high-intensity focused ultrasound ablation. *Annals of Surgical Oncology*, *14*(3), 1237–1242. https://doi.org/10.1245/s10434-006-9275-6

26. Petitprez, F., de Reyniès, A., Keung, E. Z., Chen, T. W. W., Sun, C. M., Calderaro, J., Jeng, Y. M., Hsiao, L. P., Lacroix, L., Bougoüin, A., Moreira, M., Lacroix, G., Natario, I., Adam, J., Lucchesi, C., Laizet, Y., Toulmonde, M., Burgess, M. A., Bolejack, V., … Fridman, W.

H. (2020). B cells are associated with survival and immunotherapy response in sarcoma. *Nature*, *577*(7791), 556–560. https://doi.org/10.1038/s41586-019-1906-8

27. Smolle, M. A., Herbsthofer, L., Granegger, B., Goda, M., Brcic, I., Bergovec, M., Scheipl, S., Prietl, B., Pichler, M., Gerger, A., Rossmann, C., Riedl, J., Tomberger, M., López-García, P., El-Heliebi, A., Leithner, A., Liegl-Atzwanger, B., & Szkandera, J. (2021). T-regulatory cells predict clinical outcome in soft tissue sarcoma patients: a clinico-pathological study. *British Journal of Cancer*, *125*(5), 717–724. https://doi.org/10.1038/s41416-021-01456-0

28. Rytlewski, J., Milhem, M. M., & Monga, V. (2021). Turning 'Cold' tumors 'Hot': immunotherapies in sarcoma. *Annals of Translational Medicine*, *9*(12), 1039–1039. https://doi.org/10.21037/atm-20-6041

29. Zhang, S., Zhang, E., Long, J., Hu, Z., Peng, J., Liu, L., Tang, F., Li, L., Ouyang, Y., & Zeng, Z. (2019). Immune infiltration in renal cell carcinoma. *Cancer Science*, *110*(5), 1564–1572. https://doi.org/10.1111/cas.13996

30. Attig, S., Hennenlotter, J., Pawelec, G., Klein, G., Koch, S. D., Pircher, H., Feyerabend, S., Wernet, D., Stenzl, A., Rammensee, H. G., & Gouttefangeas, C. (2009). Simultaneous infiltration of polyfunctional effector and suppressor T cells into renal cell carcinomas. *Cancer Research*, *69*(21), 8412–8419. https://doi.org/10.1158/0008-5472.CAN-09-0852

31. Borcherding, N., Vishwakarma, A., Voigt, A. P., Bellizzi, A., Kaplan, J., Nepple, K., Salem, A. K., Jenkins, R. W., Zakharia, Y., & Zhang, W. (2021). Mapping the immune environment in clear cell renal carcinoma by single-cell genomics. *Communications Biology*, *4*(1). https://doi.org/10.1038/s42003-020-01625-6

32. de Vries-Brilland, M., Rioux-Leclercq, N., Meylan, M., Dauvé, J., Passot, C., Spirina-Menand, E., Flippot, R., Fromont, G., Gravis, G., Geoffrois, L., Chevreau, C., Rolland, F., Blanc, E., Lefort, F., Ravaud, A., Gross-Goupil, M., Escudier, B., Negrier, S., & Albiges, L. (2023). Comprehensive analyses of immune tumor microenvironment in papillary renal cell carcinoma. *Journal for ImmunoTherapy of Cancer*, *11*(11). https://doi.org/10.1136/jitc-2023-006885

33. Milner, J. J., Nguyen, H., Omilusik, K., Reina-Campos, M., Tsai, M., Toma, C., Delpoux, A., Boland, B. S., Hedrick, S. M., Chang, J. T., & Goldrath, A. W. (n.d.). *Delineation of a molecularly distinct terminally differentiated memory CD8 T cell population*. https://doi.org/10.1073/pnas.2008571117/-/DCSupplemental

34. Bos, R., & Sherman, L. A. (2010). CD4+ T-cell help in the tumor milieu is required for recruitment and cytolytic function of CD8+ T lymphocytes. *Cancer Research*, *70*(21), 8368–8377. https://doi.org/10.1158/0008-5472.CAN-10-1322

35. He, T., Hu, C., Li, S., Fan, Y., Xie, F., Sun, X., Jiang, Q., Chen, W., Jia, Y., & Li, W. (2024). The role of CD8+ T-cells in colorectal cancer immunotherapy. In *Heliyon* (Vol. 10, Issue 12). Elsevier Ltd. https://doi.org/10.1016/j.heliyon.2024.e33144

36. Tay, R. E., Richardson, E. K., & Toh, H. C. (2021). Revisiting the role of CD4+ T cells in cancer immunotherapy—new insights into old paradigms. In *Cancer Gene Therapy* (Vol. 28, Issues 1–2, pp. 5–17). Springer Nature. https://doi.org/10.1038/s41417-020-0183-x

37. Schneider, M. A., Meingassner, J. G., Lipp, M., Moore, H. D., & Rot, A. (2007). CCR7 is required for the in vivo function of CD4+ CD25 + regulatory T cells. *Journal of Experimental Medicine*, *204*(4), 735–745. https://doi.org/10.1084/jem.20061405

38. Suzuki, S., Tsuzuki, T., Saito, M., Ishii, T., Takahara, T., Satou, A., Inukai, D., Yamanaka, S., Yoshikawa, K., Ueda, R., & Ogawa, T. (2024). Regulatory T-cells activated in metastatic draining lymph nodes possibly suppress cancer immunity in cancer tissues of head and neck squamous cell cancer. *Pathology International*, *74*(6), 327–336. https://doi.org/10.1111/pin.13430

39. Qureshi, O. S., Zheng, Y., Nakamura, K., Attridge, K., Manzotti, C., Schmidt, E. M., Baker, J., Jeffery, L. E., Kaur, S., Briggs, Z., Hou, T. Z., Futter, C. E., Anderson, G., Walker, L. S. K., & Sansom, D. M. (n.d.). *Trans-Endocytosis of CD80 and CD86: A Molecular Basis for the Cell-Extrinsic Function of CTLA-4*. https://www.science.org

40. Wu, Y., Borde, M., Heissmeyer, V., Feuerer, M., Lapan, A. D., Stroud, J. C., Bates, D. L., Guo, L., Han, A., Ziegler, S. F., Mathis, D., Benoist, C., Chen, L., & Rao, A. (2006). FOXP3 Controls Regulatory T Cell Function through Cooperation with NFAT. *Cell*, *126*(2), 375–387. https://doi.org/10.1016/j.cell.2006.05.042

41. Pandiyan, P., Zheng, L., Ishihara, S., Reed, J., & Lenardo, M. J. (2007). CD4+CD25+Foxp3+ regulatory T cells induce cytokine deprivation-mediated apoptosis of effector CD4+ T cells. *Nature Immunology*, *8*(12), 1353–1362. https://doi.org/10.1038/ni1536

42. Müller, E., Christopoulos, P. F., Halder, S., Lunde, A., Beraki, K., Speth, M., Øynebråten, I., & Corthay, A. (2017). Toll-like receptor ligands and interferon-γ synergize for induction of antitumor M1 macrophages. *Frontiers in Immunology*, *8*(OCT). https://doi.org/10.3389/fimmu.2017.01383

43. Zhang, F., Wang, H., Wang, X., Jiang, G., Liu, H., Zhang, G., Wang, H., Fang, R., Bu, X., Cai, S., & Du, J. (2016). *TGF-β induces M2-like macrophage polarization via SNAIL-mediated suppression of a pro-inflammatory phenotype* (Vol. 7, Issue 32). www.impactjournals.com/oncotarget

44. Kerneur, C., Cano, C. E., & Olive, D. (2022). Major pathways involved in macrophage polarization in cancer. In *Frontiers in Immunology* (Vol. 13). Frontiers Media SA. https://doi.org/10.3389/fimmu.2022.1026954

45. Pan, Y., Yu, Y., Wang, X., & Zhang, T. (2020). Tumor-Associated Macrophages in Tumor Immunity. In *Frontiers in Immunology* (Vol. 11). Frontiers Media S.A. https://doi.org/10.3389/fimmu.2020.583084

46. Jetten, N., Verbruggen, S., Gijbels, M. J., Post, M. J., De Winther, M. P. J., & Donners, M. M. P. C. (2014). Anti-inflammatory M2, but not pro-inflammatory M1 macrophages promote angiogenesis in vivo. *Angiogenesis*, *17*(1), 109–118. https://doi.org/10.1007/s10456-013-9381-6

47. Dong, H., Strome, S. E., Salomao, D. R., Tamura, H., Hirano, F., Flies, D. B., Roche, P. C., Lu, J., Zhu, G., Tamada, K., Lennon, V. A., Cells, E., & Chen, L. (2002). Tumor-associated B7-H1 promotes T-cell apoptosis: A potential mechanism of immune evasion. *Nature Medicine*, *8*(8), 793–800. https://doi.org/10.1038/nm730

48. Freeman, G. J., Long, A. J., Iwai, Y., Bourque, K., Chernova, T., Nishimura, H., Fitz, L. J., Malenkovich, N., Okazaki, T., Byrne, M. C., Horton, H. F., Fouser, L., Carter, L., Ling, V., Bowman, M. R., Carreno, B. M., Collins, M., Wood, C. R., & Honjo, T. (2000). Engagement of the PD-1 Immunoinhibitory Receptor by a Novel B7 Family Member Leads to Negative Regulation of Lymphocyte Activation. In *J. Exp. Med* (Vol. 192, Issue 7). http://www.jem.org/cgi/content/full/192/7/1027

49. Dhatchinamoorthy, K., Colbert, J. D., & Rock, K. L. (2021). Cancer Immune Evasion Through Loss of MHC Class I Antigen Presentation. In *Frontiers in Immunology* (Vol. 12). Frontiers Media S.A. https://doi.org/10.3389/fimmu.2021.636568

50. Hu, Z., Yang, X. Y., Liu, Y., Morse, M. A., Kim Lyerly, H., Clay, T. M., & Zhong, P. (n.d.). *Release of endogenous danger signals from HIFU-treated tumor cells and their stimulatory effects on APCs*.

51. Iyer, S. S., Pulskens, W. P., Sadler, J. J., Butter, L. M., Teske, G. J., Ulland, T. K., Eisenbarth, S. C., Florquin, S., Flavell, R. A., Leemans, J. C., & Sutterwala, F. S. (n.d.). *Necrotic cells trigger a sterile inflammatory response through the Nlrp3 inflammasome*. www.pnas.org/cgi/content/full/

52. Oerlemans, M. I. F. J., Liu, J., Arslan, F., Den Ouden, K., Van Middelaar, B. J., Doevendans, P. A., & Sluijter, J. P. G. (2012). Inhibition of RIP1-dependent necrosis prevents adverse cardiac remodeling after myocardial ischemia-reperfusion in vivo. *Basic Research in Cardiology*, *107*(4). https://doi.org/10.1007/s00395-012-0270-8

53. Basu, S., Binder, R. J., Suto, R., Anderson, K. M., & Srivastava, P. K. (2000). Necrotic but not apoptotic cell death releases heat shock proteins, which deliver a partial

maturation signal to dendritic cells and activate the NF-κB pathway. In *International Immunology* (Vol. 12, Issue 11).

54. Gough, M. J., Melcher, A. A., Ahmed, A., Crittenden, M. R., Riddle, D. S., Linardakis, E., Ruchatz, A. N., Emiliusen, L. M., & Vile, R. G. (2001). Macrophages Orchestrate the Immune Response to Tumor Cell Death 1. In *CANCER RESEARCH* (Vol. 61). http://aacrjournals.org/cancerres/article-pdf/61/19/7240/2489154/ch1901007240.pdf

55. Hu, Z., Xiao, Y. Y., Liu, Y., Morse, M. A., Lyerly, H. K., Clay, T. M., & Zhong, P. (2005). Release of endogenous danger signals from HIFU-treated tumor cells and their stimulatory effects on APCs. *Biochemical and Biophysical Research Communications*, *335*(1), 124–131. https://doi.org/10.1016/j.bbrc.2005.07.071

56. Chavez, M., Silvestrini, M. T., Ingham, E. S., Fite, B. Z., Mahakian, L. M., Tam, S. M., Ilovitsh, A., Monjazeb, A. M., Murphy, W. J., Hubbard, N. E., Davis, R. R., Tepper, C. G., Borowsky, A. D., & Ferrara, K. W. (2018). Distinct immune signatures in directly treated and distant tumors result from TLR adjuvants and focal ablation. *Theranostics*, *8*(13), 3611–3628. https://doi.org/10.7150/thno.25613

57. Hu, Z., Yang, X. Y., Liu, Y., Sankin, G. N., Pua, E. C., Morse, M. A., Lyerly, H. K., Clay, T. M., & Zhong, P. (2007). Investigation of HIFU-induced anti-tumor immunity in a murine tumor model. *Journal of Translational Medicine*, *5*. https://doi.org/10.1186/1479-5876-5-34

58. Zhu, X. Q., Lu, P., Xu, Z. L., Zhou, Q., Zhang, J., Wang, Z. B., & Wu, F. (2021). Alterations in immune response profile of tumor-draining lymph nodes after high-intensity focused ultrasound ablation of breast cancer patients. *Cells*, *10*(12). https://doi.org/10.3390/cells10123346

59. D'Angelo, S. P., Mahoney, M. R., Van Tine, B. A., Atkins, J., Milhem, M. M., Jahagirdar, B. N., Antonescu, C. R., Horvath, E., Tap, W. D., Schwartz, G. K., & Streicher, H. (2018). Nivolumab with or without ipilimumab treatment for metastatic sarcoma (Alliance A091401): two open-label, non-comparative, randomised, phase 2 trials. *The Lancet Oncology*, *19*(3), 416–426. https://doi.org/10.1016/S1470-2045(18)30006-8

60. van der Graaf, W. T., Blay, J.-Y., Chawla, S. P., Kim, D.-W., Bui-Nguyen, B., Casali, P. G., Schöff ski, P., Aglietta, M., Staddon, A. P., Beppu, Y., Le Cesne, A., Gelderblom, H., Judson, I. R., Araki, N., Ouali, M., Marreaud, S., Hodge, R., Dewji, M. R., Coens, C., … Hohenberger, P. (2012). Pazopanib for metastatic soft-tissue sarcoma (PALETTE): a randomised, double-blind, placebo-controlled phase 3 trial. *Www.Thelancet.Com*, *379*, 1879–1886. https://doi.org/10.1016/S0140

61. Klaver, Y., Rijnders, M., Oostvogels, A., Wijers, R., Smid, M., Grünhagen, D., Verhoef, K., Sleijfer, S., Lamers, C., & Debets, R. (2020). Differential quantities of immune

checkpoint-expressing CD8 T cells in soft tissue sarcoma subtypes. *Journal for ImmunoTherapy of Cancer*, *8*(2). https://doi.org/10.1136/jitc-2019-000271

62. Brennan, M., Antonescu, C., Moraco, N., & Singer, S. (2014). Lessons learned from the study of 10,000 patients with soft tissue sarcoma. *Annals of Surgery*, *260*(3), 416–422. https://doi.org/10.1097/SLA.0000000000000869.Lessons

63. Katz, D., Palmerini, E., & Pollack, S. M. (2018). More Than 50 Subtypes of Soft Tissue Sarcoma: Paving the Path for Histology-Driven Treatments. *American Society of Clinical Oncology Educational Book*, *38*, 925–938. https://doi.org/10.1200/edbk_205423

64. Fletcher, C., Bridge, J., & Hogendoon, P. (2013). *WHO Classification of Tumours of Soft Tissue and Bone* (4th ed.).

65. Weiss, A. R., Chen, Y. L., Scharschmidt, T. J., Chi, Y. Y., Tian, J., Black, J. O., Davis, J. L., Fanburg-Smith, J. C., Zambrano, E., Anderson, J., Arens, R., Binitie, O., Choy, E., Davis, J. W., Hayes-Jordan, A., Kao, S. C., Kayton, M. L., Kessel, S., Lim, R., … Wang, D. (2020). Pathological response in children and adults with large unresected intermediate-grade or high-grade soft tissue sarcoma receiving preoperative chemoradiotherapy with or without pazopanib (ARST1321): a multicentre, randomised, open-label, phase 2 trial. *The Lancet Oncology*, *21*(8), 1110–1122. https://doi.org/10.1016/S1470-2045(20)30325-9

66. Chen, H., Chen, Y., Liu, H., Que, Y., Zhang, X., & Zheng, F. (2018). Integrated expression profiles analysis reveals correlations between the IL-33/ST2 axis and CD8+ T cells, regulatory T cells, and myeloid-derived suppressor cells in soft tissue sarcoma. *Frontiers in Immunology*, *9*(MAY), 1–11. https://doi.org/10.3389/fimmu.2018.01179

67. Tseng, W. W., Somaiah, N., & Engleman, E. G. (2014). Potential for immunotherapy in soft tissue sarcoma. *Human Vaccines and Immunotherapeutics*, *10*(11), 3117–3124. https://doi.org/10.4161/21645515.2014.983003

68. Chen, L., Oke, T., Siegel, N., Cojocaru, G., Tam, A. J., Blosser, R. L., Swailes, J., Ligon, J. A., Lebid, A., Morris, C., Levin, A., Rhee, D. S., Johnston, F. M., Greer, J. B., Meyer, C. F., Ladle, B. H., Thompson, E. D., Montgomery, E. A., Choi, W., … Llosa, N. J. (2020). The Immunosuppressive Niche of Soft-Tissue Sarcomas is Sustained by Tumor-Associated Macrophages and Characterized by Intratumoral Tertiary Lymphoid Structures. *Clinical Cancer Research*, *26*(15), 4018–4030. https://doi.org/10.1158/1078-0432.CCR-19-3416

69. Zhu, M., Shenasa, E., & Nielsen, T. (2020). Sarcomas: Immune biomarker expression and checkpoint inhibitor trials. *Cancer Treatment Reviews*, *91*(October), 102115. https://doi.org/10.1016/j.ctrv.2020.102115

70. Miallot, R., Galland, F., Millet, V., Blay, J. Y., & Naquet, P. (2021). Metabolic landscapes in sarcomas. *Journal of Hematology and Oncology*, *14*(1), 1–23. https://doi.org/10.1186/s13045-021-01125-y

71. Marrari, A., Bertuzzi, A., Bozzarelli, S., Gennaro, N., Giordano, L., Quagliuolo, V., De Sanctis, R., Sala, S., Balzarini, L., & Santoro, A. (2020). Activity of regorafenib in advanced pretreated soft tissue sarcoma: Results of a single-center phase II study. *Medicine*, *99*(26), e20719. https://doi.org/10.1097/MD.0000000000020719

72. Goldman, L., & Schafer, A. (2020). Malignant Tumors of Bone, Sarcomas, and Other Soft Tissue Neoplasms. In *Goldman-Cecil Medicine* (26th ed., pp. 1341–1344).

73. Pollack, S. M., Redman, M. W., Baker, K. K., Wagner, M. J., Schroeder, B. A., Loggers, E. T., Trieselmann, K., Copeland, V. C., Zhang, S., Black, G., McDonnell, S., Gregory, J., Johnson, R., Moore, R., Jones, R. L., & Cranmer, L. D. (2020). Assessment of Doxorubicin and Pembrolizumab in Patients with Advanced Anthracycline-Naive Sarcoma: A Phase 1/2 Nonrandomized Clinical Trial. *JAMA Oncology*, *6*(11), 1778–1782. https://doi.org/10.1001/jamaoncol.2020.3689

74. Meyer, M., & Seetharam, M. (2019). First-Line Therapy for Metastatic Soft Tissue Sarcoma. *Current Treatment Options in Oncology*, *20*(1). https://doi.org/10.1007/s11864-019-0606-9

75. Judson, I., Verweij, J., Gelderblom, H., Hartmann, J. T., Schöffski, P., Blay, J. Y., Kerst, J. M., Sufliarsky, J., Whelan, J., Hohenberger, P., Krarup-Hansen, A., Alcindor, T., Marreaud, S., Litière, S., Hermans, C., Fisher, C., Hogendoorn, P. C. W., Dei Tos, A. P., & Van der Graaf, W. T. A. (2014). Doxorubicin alone versus intensified doxorubicin plus ifosfamide for first-line treatment of advanced or metastatic soft-tissue sarcoma: A randomised controlled phase 3 trial. *The Lancet Oncology*, *15*(4), 415–423. https://doi.org/10.1016/S1470-2045(14)70063-4

76. Rosenberg, S. A., Tepper, J., Glatstein, E., Costa, J., Baker, A., Brennan, M., Demoss, E. V, Seipp, C., Sindelar, W. F., Sugarbaker, P., & Wesley, R. (n.d.). *The Treatment of Soft-tissue Sarcomas of the Extremities Prospective Randomized Evaluations of (1) Limb-sparing Surgery Plus Radiation Therapy Compared with Amputation and (2) the Role of Adjuvant Chemotherapy*.

77. Saxby, N. E., An, Q., & Miller, B. J. (2022). Local Recurrence of Soft Tissue Sarcoma Revisited: Is there a Role for "Selective" Radiation? *The Iowa Orthopaedic Journal*, *42*(1), 239–248.

78. Lansu, J., Bovée, J. V. M. G., Braam, P., van Boven, H., Flucke, U., Bonenkamp, J. J., Miah, A. B., Zaidi, S. H., Thway, K., Bruland, Ø. S., Baldini, E. H., Jebsen, N. L., Scholten, A. N., van den Ende, P. L. A., Krol, A. D. G., Ubbels, J. F., van der Hage, J. A., van Werkhoven, E., Klomp, H. M., … Haas, R. L. (2021). Dose Reduction of Preoperative

Radiotherapy in Myxoid Liposarcoma: A Nonrandomized Controlled Trial. *JAMA Oncology*, *7*(1), e205865–e205865. https://doi.org/10.1001/jamaoncol.2020.5865

79. Hasan, O., Nasir, M., Jessar, M., Hashimi, M., An, Q., & Miller, B. J. (2021). Is local recurrence in bone and soft tissue sarcomas just a local recurrence or does it impact the overall survival, retrospective cohort from a sarcoma referral center. *Journal of Surgical Oncology*, *124*(8), 1536–1543. https://doi.org/10.1002/jso.26663

80. D'Angelo, S. P., Richards, A. L., Conley, A. P., Woo, H. J., Dickson, M. A., Gounder, M., Kelly, C., Keohan, M. L., Movva, S., Thornton, K., Rosenbaum, E., Chi, P., Nacev, B., Chan, J. E., Slotkin, E. K., Kiesler, H., Adamson, T., Ling, L., Rao, P., … Tap, W. D. (2022). Pilot study of bempegaldesleukin in combination with nivolumab in patients with metastatic sarcoma. *Nature Communications*, *13*(1). https://doi.org/10.1038/s41467-022-30874-8

81. Tawbi, H. A., Burgess, M., Bolejack, V., Van Tine, B., Schuetze, S. M., Hu, J., D'Angelo, S., Attia, S., Riedel, R. F., Priebat, D. A., & Movva, S. (2017). Pembrolizumab in Advanced Soft Tissue and Bone Sarcomas: Results of SARC028, A Multicentre, Single arm, Phase 2 Trial. *Lancet Oncology*, *18*(11), 1493–1501. https://doi.org/10.1016/S1470-2045(17)30624-1.Pembrolizumab

82. Judge, S. J., Darrow, M. A., Thorpe, S. W., Gingrich, A. A., O'Donnell, E. F., Bellini, A. R., Sturgill, I. R., Vick, L. V., Dunai, C., Stoffel, K. M., Lyu, Y., Chen, S., Cho, M., Rebhun, R. B., Monjazeb, A. M., Murphy, W. J., & Canter, R. J. (2020). Analysis of tumor-infiltrating NK and T cells highlights IL-15 stimulation and TIGIT blockade as a combination immunotherapy strategy for soft tissue sarcomas. *Journal for ImmunoTherapy of Cancer*, *8*(2). https://doi.org/10.1136/jitc-2020-001355

83. D'Angelo, S. P., Shoushtari, A. N., Agaram, N. P., Kuk, D., Qin, L.-X., Carvajal, R. D., Dickson, M. A., Gounder, M., Keohan, M. L., Schwartz, G. K., & Tap, W. D. (2015). Prevalence of tumor infiltrating lymphocytes and PD-L1 expression in the soft tissue sarcoma microenvironment. *Human Physiology*, *46*(3), 357–365. https://doi.org/10.1016/j.humpath.2014.11.001.Prevalence

84. Dancsok, A. R., Gao, D., Lee, A. F., Steigen, S. E., Blay, J. Y., Thomas, D. M., Maki, R. G., Nielsen, T. O., & Demicco, E. G. (2020). Tumor-associated macrophages and macrophage-related immune checkpoint expression in sarcomas. *OncoImmunology*, *9*(1). https://doi.org/10.1080/2162402X.2020.1747340

85. Smolle, M. A., Herbsthofer, L., Goda, M., Granegger, B., Brcic, I., Bergovec, M., Scheipl, S., Prietl, B., El-Heliebi, A., Pichler, M., Gerger, A., Posch, F., Tomberger, M., López-García, P., Feichtinger, J., Baumgartner, C., Leithner, A., Liegl-Atzwanger, B., & Szkandera, J. (2021). Influence of tumor-infiltrating immune cells on local control rate, distant metastasis, and survival in patients with soft tissue sarcoma. *OncoImmunology*, *10*(1). https://doi.org/10.1080/2162402X.2021.1896658

86. Sorbye, S. W., Kilvaer, T., Valkov, A., Donnem, T., Smeland, E., Al-Shibli, K., Bremnes, R. M., & Busund, L. T. (2011). Prognostic impact of lymphocytes in soft tissue Sarcomas. *PLoS ONE*, *6*(1). https://doi.org/10.1371/journal.pone.0014611

87. Capitanio, U., Bensalah, K., Bex, A., Boorjian, S. A., Bray, F., Coleman, J., Gore, J. L., Sun, M., Wood, C., & Russo, P. (2019). Epidemiology of Renal Cell Carcinoma. In *European Urology* (Vol. 75, Issue 1, pp. 74–84). Elsevier B.V. https://doi.org/10.1016/j.eururo.2018.08.036

88. Pandey, N., Lanke, V., & Vinod, P. K. (2020). Network-based metabolic characterization of renal cell carcinoma. *Scientific Reports*, *10*(1). https://doi.org/10.1038/s41598-020-62853-8

89. Dudani, S., De Velasco, G., Wells, J. C., Gan, C. L., Donskov, F., Porta, C., Fraccon, A., Pasini, F., Lee, J. L., Hansen, A., Bjarnason, G. A., Beuselinck, B., Pal, S. K., Yuasa, T., Kroeger, N., Kanesvaran, R., Reaume, M. N., Canil, C., Choueiri, T. K., & Heng, D. Y. C. (2021). Evaluation of Clear Cell, Papillary, and Chromophobe Renal Cell Carcinoma Metastasis Sites and Association with Survival. *JAMA Network Open*, *4*(1). https://doi.org/10.1001/jamanetworkopen.2020.21869

90. Leibovich, B. C., Lohse, C. M., Cheville, J. C., Zaid, H. B., Boorjian, S. A., Frank, I., Thompson, R. H., & Parker, W. P. (2018). Predicting Oncologic Outcomes in Renal Cell Carcinoma After Surgery. *European Urology*, *73*(5), 772–780. https://doi.org/10.1016/j.eururo.2018.01.005

91. Tang, C., Msaouel, P., Hara, K., Choi, H., Le, V., Shah, A. Y., Wang, J., Jonasch, E., Choi, S., Nguyen, Q. nhu, Das, P., Prajapati, S., Yu, Z., Khan, K., Powell, S., Murthy, R., Sircar, K., & Tannir, N. M. (2021). Definitive radiotherapy in lieu of systemic therapy for oligometastatic renal cell carcinoma: a single-arm, single-centre, feasibility, phase 2 trial. *The Lancet Oncology*, *22*(12), 1732–1739. https://doi.org/10.1016/S1470-2045(21)00528-3

92. Dahm, P., Ergun, O., Uhlig, A., Bellut, L., Risk, M. C., Lyon, J. A., & Kunath, F. (2024). Cytoreductive nephrectomy in metastatic renal cell carcinoma. *Cochrane Database of Systematic Reviews*, *2024*(6). https://doi.org/10.1002/14651858.CD013773.pub2

93. Tourani, J. M., Pfister, C., Berdah, J. F., Benhammouda, A., Salze, P., Monnier, A., Paule, B., Guillet, P., Chretien, Y., Brewer, Y., Di Palma, M., Untereiner, M., Malaurie, E., Tadrist, Z., Pavlovitch, J. M., Hauteville, D., Mejean, A., Azagury, M., Mayeur, D., … Chastang, C. (2025). Outpatient treatment with subcutaneous interleukin-2 and interferon alfa administration in combination with fluorouracil in patients with metastatic renal cell carcinoma: results of a sequential nonrandomized phase II study. Subcutaneous Administration Propeukin Program Cooperative Group. *Journal of Clinical Oncology*, *16*(7), 2505–2513. https://doi.org/10.1200/JCO.1998.16.7.2505

94. Fyfe, G., Fisher, R. I., Rosenberg, S. A., Sznol, M., Parkinson, D. R., & Louie, A. C. (2025). Results of treatment of 255 patients with metastatic renal cell carcinoma who received high-dose recombinant interleukin-2 therapy. *Journal of Clinical Oncology*, *13*(3), 688–696. https://doi.org/10.1200/JCO.1995.13.3.688

95. Ylvie, S., Egrier, N., Hristine, C., Asset, L., Ean -Y Ves, J., Ouillard, D., Acqueline, J., Avary, S., Hevreau, C., Ean, J., Eny, P., Ousseau, M., Hierry, T., Hilip, P., Homas, T., Ursz, T., Roupe, G., & Rançais D 'i Mmunothérapie, F. (1998). The New England Journal of Medicine RECOMBINANT HUMAN INTERLEUKIN-2, RECOMBINANT HUMAN INTERFERON ALFA-2a, OR BOTH IN METASTATIC RENAL-CELL CARCINOMA A BSTRACT Background Recombinant human interleukin-2 (al. In *Apr il* (Vol. 30).

96. Tannir, N. M., Albigès, L., McDermott, D. F., Burotto, M., Choueiri, T. K., Hammers, H. J., Barthélémy, P., Plimack, E. R., Porta, C., George, S., Donskov, F., Atkins, M. B., Gurney, H., Kollmannsberger, C. K., Grimm, M. O., Barrios, C., Tomita, Y., Castellano, D., Grünwald, V., … Motzer, R. J. (2024). Nivolumab plus ipilimumab versus sunitinib for first-line treatment of advanced renal cell carcinoma: extended 8-year follow-up results of efficacy and safety from the phase III CheckMate 214 trial. *Annals of Oncology*. https://doi.org/10.1016/j.annonc.2024.07.727

97. Choueiri, T. K., Tomczak, P., Park, S. H., Venugopal, B., Ferguson, T., Symeonides, S. N., Hajek, J., Chang, Y.-H., Lee, J.-L., Sarwar, N., Haas, N. B., Gurney, H., Sawrycki, P., Mahave, M., Gross-Goupil, M., Zhang, T., Burke, J. M., Doshi, G., Melichar, B., … Powles, T. (2024). Overall Survival with Adjuvant Pembrolizumab in Renal-Cell Carcinoma. *New England Journal of Medicine*, *390*(15), 1359–1371. https://doi.org/10.1056/nejmoa2312695

98. Choueiri, T. K., Powles, T., Peltola, K., de Velasco, G., Burotto, M., Suarez, C., Ghatalia, P., Iacovelli, R., Lam, E. T., Verzoni, E., Gümüş, M., Stadler, W. M., Kollmannsberger, C., Melichar, B., Venugopal, B., Gross-Goupil, M., Poprach, A., De Santis, M., Schutz, F. A., … Rini, B. (2024). Belzutifan versus Everolimus for Advanced Renal-Cell Carcinoma. *New England Journal of Medicine*, *391*(8), 710–721. https://doi.org/10.1056/nejmoa2313906

99. Engelen, Y., Krysko, D. V., Effimova, I., Breckpot, K., Versluis, M., De Smedt, S., Lajoinie, G., & Lentacker, I. (2024). Optimizing high-intensity focused ultrasound-induced immunogenic cell-death using passive cavitation mapping as a monitoring tool. *Journal of Controlled Release*, *375*, 389–403. https://doi.org/10.1016/j.jconrel.2024.09.016

100. Kroeze, S. G. C., Daenen, L. G. M., Nijkamp, M. W., Roodhart, J. M. L., De Gast, G. C., Bosch, J. L. H. R., & Jans, J. J. M. (2012). Radio frequency ablation combined with interleukin-2 induces an antitumor immune response to renal cell carcinoma in a

murine model. *Journal of Urology*, *188*(2), 607–614. https://doi.org/10.1016/j.juro.2012.03.116

101. Ran, L. F., Xie, X. P., Xia, J. Z., Xie, F. L., Fan, Y. M., & Wu, F. (2023). T-lymphocytes from focused ultrasound ablation subsequently mediate cellular antitumor immunity after adoptive cell transfer immunotherapy. *Frontiers in Immunology*, *14*. https://doi.org/10.3389/fimmu.2023.1155229

102. Moldvai, D., Sztankovics, D., Dankó, T., Vetlényi, E., Petővári, G., Márk, Á., Patonai, A., Végső, G., Piros, L., Hosszú, Á., Pápay, J., Krencz, I., & Sebestyén, A. (2024). Tumorigenic role of tacrolimus through mTORC1/C2 activation in post-transplant renal cell carcinomas. *British Journal of Cancer*, *130*(7), 1119–1130. https://doi.org/10.1038/s41416-024-02597-8

103. Zhang, Y., Narayanan, S. P., Mannan, R., Raskind, G., Wang, X., Vats, P., Su, F., Hosseini, N., Cao, X., Kumar-Sinha, C., Ellison, S. J., Giordano, T. J., Morgan, T. M., Pitchiaya, S., Alva, A., Mehra, R., Cieslik, M., Dhanasekaran, S. M., & Chinnaiyan, A. M. (2021). Single-cell analyses of renal cell cancers reveal insights into tumor microenvironment, cell of origin, and therapy response. *Proceedings of the National Academy of Sciences*, *118*(24), e2103240118. https://doi.org/10.1073/pnas.2103240118

104. Ricketts, C. J., De Cubas, A. A., Fan, H., Smith, C. C., Lang, M., Reznik, E., Bowlby, R., Gibb, E. A., Akbani, R., Beroukhim, R., Bottaro, D. P., Choueiri, T. K., Gibbs, R. A., Godwin, A. K., Haake, S., Hakimi, A. A., Henske, E. P., Hsieh, J. J., Ho, T. H., … Mariamidze, A. (2018). The Cancer Genome Atlas Comprehensive Molecular Characterization of Renal Cell Carcinoma. *Cell Reports*, *23*(1), 313-326.e5. https://doi.org/10.1016/j.celrep.2018.03.075

105. Clark, D. J., Dhanasekaran, S. M., Petralia, F., Pan, J., Song, X., Hu, Y., da Veiga Leprevost, F., Reva, B., Lih, T. S. M., Chang, H. Y., Ma, W., Huang, C., Ricketts, C. J., Chen, L., Krek, A., Li, Y., Rykunov, D., Li, Q. K., Chen, L. S., … Zhang, H. (2019). Integrated Proteogenomic Characterization of Clear Cell Renal Cell Carcinoma. *Cell*, *179*(4), 964-983.e31. https://doi.org/10.1016/j.cell.2019.10.007

106. Meylan, M., Petitprez, F., Becht, E., Bougoüin, A., Pupier, G., Calvez, A., Giglioli, I., Verkarre, V., Lacroix, G., Verneau, J., Sun, C. M., Laurent-Puig, P., Vano, Y. A., Elaïdi, R., Méjean, A., Sanchez-Salas, R., Barret, E., Cathelineau, X., Oudard, S., … Fridman, W. H. (2022). Tertiary lymphoid structures generate and propagate anti-tumor antibody-producing plasma cells in renal cell cancer. *Immunity*, *55*(3), 527-541.e5. https://doi.org/10.1016/j.immuni.2022.02.001

107. Hiraoka, N., Ino, Y., Yamazaki-Itoh, R., Kanai, Y., Kosuge, T., & Shimada, K. (2015). Intratumoral tertiary lymphoid organ is a favourable prognosticator in patients with

pancreatic cancer. *British Journal of Cancer*, *112*(11), 1782–1790. https://doi.org/10.1038/bjc.2015.145

108. Li, H., Liu, H., Fu, H., Li, J., Xu, L., Wang, G., & Wu, H. (2021). Peritumoral Tertiary Lymphoid Structures Correlate With Protective Immunity and Improved Prognosis in Patients With Hepatocellular Carcinoma. *Frontiers in Immunology*, *12*. https://doi.org/10.3389/fimmu.2021.648812

109. R Core Team. (2024). *R: A Language and Environment for Statistical Computing* (R version 4.4.2). R Foundation for Statistical Computing. https://www.R-project.org/

110. Wickham, H., François, R., Henry, L., Müller, K., & Vaughan, D. (2023). *dplyr: A Grammar of Data Manipulation* (R package 1.1.4). https://CRAN.R-project.org/package=dplyr

111. Schauberger, P., & Walker, A. (2025). *openxlsx: Read, Write and Edit xlsx Files* (R package version 4.2.8). https://CRAN.R-project.org/package=openxlsx

112. Wickham, H., Averick, M., Bryan, J., Chang, W., McGowan, L., François, R., Grolemund, G., Hayes, A., Henry, L., Hester, J., Kuhn, M., Pedersen, T., Miller, E., Bache, S., Müller, K., Ooms, J., Robinson, D., Seidel, D., Spinu, V., … Yutani, H. (2019). Welcome to the Tidyverse. *Journal of Open Source Software*, *4*(43), 1686. https://doi.org/10.21105/joss.01686

113. Lê, S., Josse, J., Rennes, A., & Husson, F. (2008). FactoMineR: An R Package for Multivariate Analysis. In *JSS Journal of Statistical Software* (Vol. 25). http://www.jstatsoft.org/

114. Kassambara, A., & Mundt, F. (2020). *factoextra: Extract and Visualize the Results of Multivariate Data Analyses. R package version 1.0.7.999*.

115. Griswold, M., & Danaher, P. (2024). *SpatialDecon: Deconvolution of mixed cells from spatial and/or bulk gene expression data*. https://doi.org/doi:10.18129/B9.bioc.SpatialDecon

116. Danaher, P., Kim, Y., Nelson, B., Griswold, M., Yang, Z., Piazza, E., & Beechem, J. M. (2020). *Advances in mixed cell deconvolution enable quantification of cell types in spatially-resolved gene expression data*. https://doi.org/10.1101/2020.08.04.235168

117. Gu, Z., Eils, R., & Schlesner, M. (2016). Complex heatmaps reveal patterns and correlations in multidimensional genomic data. *Bioinformatics*, *32*(18), 2847–2849. https://doi.org/10.1093/bioinformatics/btw313

118. Neuwirth, E. (2022). *RColorBrewer: ColorBrewer Palettes* (R package version 1.1-3). https://CRAN.R-project.org/package=RColorBrewer

119. Ritchie, M. E., Phipson, B., Wu, D., Hu, Y., Law, C. W., Shi, W., & Smyth, G. K. (2015). Limma powers differential expression analyses for RNA-sequencing and microarray studies. *Nucleic Acids Research*, *43*(7), e47. https://doi.org/10.1093/nar/gkv007

120. Blighe, K., Rana, S., & Lewis, M. (2024). *EnhancedVolcano: Publication-ready volcano plots with enhanced colouring and labeling* (1.22.0). biocondutor. https://doi.org/10.18129/B9.bioc.EnhancedVolcano

121. Yu, G., Wang, L. G., Han, Y., & He, Q. Y. (2012). ClusterProfiler: An R package for comparing biological themes among gene clusters. *OMICS A Journal of Integrative Biology*, *16*(5), 284–287. https://doi.org/10.1089/omi.2011.0118

122. Carlson, M. (2024). *org.Hs.eg.db: Genome wide annotation for Human* (R package version 3.20.0). https://doi.org/10.18129/B9.bioc.org.Hs.eg.db

123. Langfelder, P., & Horvath, S. (2008). WGCNA: An R package for weighted correlation network analysis. *BMC Bioinformatics*, *9*. https://doi.org/10.1186/1471-2105-9-559

124. Gu, Z., Gu, L., Eils, R., Schlesner, M., & Brors, B. (2014). Circlize implements and enhances circular visualization in R. *Bioinformatics*, *30*(19), 2811–2812. https://doi.org/10.1093/bioinformatics/btu393

125. Wickham, H. (2016). *ggplot2: Elegant Graphics for Data Analysis*. Springer-Verlag New York. https://ggplot2.tidyverse.org

126. Hu, Z., Yang, X. Y., Liu, Y., Sankin, G. N., Pua, E. C., Morse, M. A., Lyerly, H. K., Clay, T. M., & Zhong, P. (2007). Investigation of HIFU-induced anti-tumor immunity in a murine tumor model. *Journal of Translational Medicine*, *5*. https://doi.org/10.1186/1479-5876-5-34

127. Eranki, A., Srinivasan, P., Ries, M., Kim, A. R., Lazarski, C. A., Rossi, C. T., Khokhlova, T. D., Wilson, E., Knoblach, S. M., Sharma, K. V., Wood, B. J., Moonen, C., Sandler, A. D., & Kim, P. C. W. (2020). High-intensity focused ultrasound (HIFU) triggers immune sensitization of refractory murine neuroblastoma to checkpoint inhibitor therapy. *Clinical Cancer Research*, *26*(5), 1152–1161. https://doi.org/10.1158/1078-0432.CCR-19-1604

128. Deng, J., Zhang, Y., Feng, J., & Wu, F. (2010). Dendritic Cells Loaded with Ultrasound-Ablated Tumour Induce in vivo Specific Antitumour Immune Responses. *Ultrasound in Medicine and Biology*, *36*(3), 441–448. https://doi.org/10.1016/j.ultrasmedbio.2009.12.004

129. Zhang, Y., Deng, J., Feng, J., & Wu, F. (2010). Enhancement of antitumor vaccine in ablated hepatocellular carcinoma by high-intensity focused ultrasound. *World Journal of Gastroenterology*, *16*(28), 3584–3591. https://doi.org/10.3748/wjg.v16.i28.3584

130. Elliott, M. R., Chekeni, F. B., Trampont, P. C., Lazarowski, E. R., Kadl, A., Walk, S. F., Park, D., Woodson, R. I., Ostankovich, M., Sharma, P., Lysiak, J. J., Harden, T. K., Leitinger, N., & Ravichandran, K. S. (2009). Nucleotides released by apoptotic cells act as a find-me signal to promote phagocytic clearance. *Nature*, *461*(7261), 282–286. https://doi.org/10.1038/nature08296

131. Chida, S., Okada, kyoji, Suzuki, N., Komori, C., & Shimada, Y. (2009). Infiltration by Macrophages and Lymphocytes in Transplantable Mouse Sarcoma after Irradiation with High-intensity Focused Ultrasound. *Anticancer Research*, *29*(10), 3877–3882.

132. Toulmonde, M., Guegan, J. P., Spalato-Ceruso, M., Peyraud, F., Kind, M., Vanhersecke, L., Le Loarer, F., Perret, R., Cantarel, C., Bellera, C., Bessede, A., & Italiano, A. (2024). Reshaping the tumor microenvironment of cold soft-tissue sarcomas with oncolytic viral therapy: a phase 2 trial of intratumoral JX-594 combined with avelumab and low-dose cyclophosphamide. In *Molecular Cancer* (Vol. 23, Issue 1). BioMed Central Ltd. https://doi.org/10.1186/s12943-024-01946-8

133. Lee, A. T. J., Chew, W., Wilding, C. P., Guljar, N., Smith, M. J., Strauss, D. C., Fisher, C., Hayes, A. J., Judson, I., Thway, K., Jones, R. L., & Huang, P. H. (2019). The adequacy of tissue microarrays in the assessment of inter- and intra-tumoural heterogeneity of infiltrating lymphocyte burden in leiomyosarcoma. *Scientific Reports*, *9*(1). https://doi.org/10.1038/s41598-019-50888-5

134. Toulmonde, M., Lucchesi, C., Verbeke, S., Crombe, A., Adam, J., Geneste, D., Chaire, V., Laroche-Clary, A., Perret, R., Bertucci, F., Bertolo, F., Bianchini, L., Dadone-Montaudie, B., Hembrough, T., Sweet, S., Kim, Y. J., Cecchi, F., Le Loarer, F., & Italiano, A. (2020). High throughput profiling of undifferentiated pleomorphic sarcomas identifies two main subgroups with distinct immune profile, clinical outcome and sensitivity to targeted therapies. *EBioMedicine*, *62*. https://doi.org/10.1016/j.ebiom.2020.103131

135. Sung, H. Y., Seung, Þ., Jung, E., Cho, H., Zhou, K., Han, J.-Y., Han, S. T., Kim, J. Il, Kim, J. K., Choi, J. Y., Yoon, S. K., Yang, J. M., Han, C. W., & Lee, Y. S. (2011). *Long-Term Outcome of High-Intensity Focused Ultrasound in Advanced Pancreatic Cancer*. www.pancreasjournal.com

136. Ma, Y., Adjemian, S., Mattarollo, S. R., Yamazaki, T., Aymeric, L., Yang, H., Portela Catani, J. P., Hannani, D., Duret, H., Steegh, K., Martins, I., Schlemmer, F., Michaud, M., Kepp, O., Sukkurwala, A. Q., Menger, L., Vacchelli, E., Droin, N., Galluzzi, L., … Kroemer, G. (2013). Anticancer chemotherapy-induced intratumoral recruitment and differentiation of antigen-presenting cells. *Immunity*, *38*(4), 729–741. https://doi.org/10.1016/j.immuni.2013.03.003

137. Wei, S., Shreiner, A. B., Takeshita, N., Chen, L., Zou, W., & Chang, A. E. (2008). Tumor-induced immune suppression of in vivo effector T-cell priming is mediated by the B7-

H1/PD-1 axis and transforming growth factor β. *Cancer Research*, *68*(13), 5432–5438. https://doi.org/10.1158/0008-5472.CAN-07-6598

138. Ma, Y., Yamazaki, T., Yang, H., Kepp, O., Galluzzi, L., Zitvogel, L., Smyth, M. J., & Kroemer, G. (2013). Tumor necrosis factor is dispensable for the success of immunogenic anticancer chemotherapy. *OncoImmunology*, *2*(6). https://doi.org/10.4161/onci.24786

139. Panagi, M., Mpekris, F., Voutouri, C., Hadjigeorgiou, A. G., Symeonidou, C., Porfyriou, E., Michael, C., Stylianou, A., Martin, J. D., Cabral, H., Constantinidou, A., & Stylianopoulos, T. (2024). Stabilizing Tumor-Resident Mast Cells Restores T-Cell Infiltration and Sensitizes Sarcomas to PD-L1 Inhibition. *Clinical Cancer Research*, *30*(11), 2582–2597. https://doi.org/10.1158/1078-0432.CCR-24-0246

140. Ahrends, T., Busselaar, J., Severson, T. M., Bąbała, N., de Vries, E., Bovens, A., Wessels, L., van Leeuwen, F., & Borst, J. (2019). CD4+ T cell help creates memory CD8+ T cells with innate and help-independent recall capacities. *Nature Communications*, *10*(1). https://doi.org/10.1038/s41467-019-13438-1

141. Principe, N., Kidman, J., Goh, S., Tilsed, C. M., Fisher, S. A., Fear, V. S., Forbes, C. A., Zemek, R. M., Chopra, A., Watson, M., Dick, I. M., Boon, L., Holt, R. A., Lake, R. A., Nowak, A. K., Lesterhuis, W. J., McDonnell, A. M., & Chee, J. (2020). Tumor Infiltrating Effector Memory Antigen-Specific CD8+ T Cells Predict Response to Immune Checkpoint Therapy. *Frontiers in Immunology*, *11*. https://doi.org/10.3389/fimmu.2020.584423

142. Sainz-Perez, A., Lim, A., Lemercier, B., & Leclerc, C. (2012). The T-cell receptor repertoire of tumor-infiltrating regulatory T lymphocytes is skewed toward public sequences. *Cancer Research*, *72*(14), 3557–3569. https://doi.org/10.1158/0008-5472.CAN-12-0277

143. Zohouri, M., Mehdipour, F., Razmkhah, M., Faghih, Z., & Ghaderi, A. (2021). CD4+CD25-FoxP3+ T cells: a distinct subset or a heterogeneous population? In *International Reviews of Immunology* (Vol. 40, Issue 4, pp. 307–316). Taylor and Francis Ltd. https://doi.org/10.1080/08830185.2020.1797005

144. Zelenay, S., Lopes-Carvalho, T., Caramalho, I., Moraes-Fontes, M. F., Rebelo, M., & Demengeot, J. (2005). *Foxp3 CD25 CD4 T cells constitute a reservoir of committed regulatory cells that regain CD25 expression upon homeostatic expansion*. www.pnas.orgcgidoi10.1073pnas.0408679102

145. Hossain, M. M., King, P., Hackett, J., Gerard, H. C., Niwinski, R., Wu, L., Van Kaer, L., Dyson, G., Gibson, H., Borowsky, A. D., & Sebzda, E. (2024). Peripheral-derived regulatory T cells contribute to tumor-mediated immune suppression in a

nonredundant manner. *Proceedings of the National Academy of Sciences of the United States of America*, *121*(36). https://doi.org/10.1073/pnas.2404916121

146. Schuster, M., Plaza-Sirvent, C., Visekruna, A., Huehn, J., & Schmitz, I. (2019). Generation of Foxp3+CD25− regulatory T-cell precursors requires c-rel and IκBNS. *Frontiers in Immunology*, *10*(JULY). https://doi.org/10.3389/fimmu.2019.01583

147. Solis-Castillo, L. A., Garcia-Romo, G. S., Diaz-Rodriguez, A., Reyes-Hernandez, D., Tellez-Rivera, E., Rosales-Garcia, V. H., Mendez-Cruz, A. R., Jimenez-Flores, J. R., Villafana-Vazquez, V. H., & Pedroza-Gonzalez, A. (2020). Tumor-infiltrating regulatory T cells, CD8/Treg ratio, and cancer stem cells are correlated with lymph node metastasis in patients with early breast cancer. *Breast Cancer*, *27*(5), 837–849. https://doi.org/10.1007/s12282-020-01079-y

148. Hu, C., Chen, B., Huang, Z., Liu, C., Ye, L., Wang, C., Tong, Y., Yang, J., & Zhao, C. (2020). Comprehensive profiling of immune-related genes in soft tissue sarcoma patients. *Journal of Translational Medicine*, *18*(1), 1–18. https://doi.org/10.1186/s12967-020-02512-8

149. Chen, M.-L., Pittet, M. J., Gorelik, L., Flavell, R. A., Weissleder, R., von Boehmer, H., & Khazaie, K. (2005). Regulatory T cells suppress tumor-specific CD8 T cell cytotoxicity through TGF-signals in vivo. In *PNAS* (Vol. 102, Issue 2). www.pnas.orgcgidoi10.1073pnas.0408197102

150. Que, Y., Xiao, W., Guan, Y. xiang, Liang, Y., Yan, S. M., Chen, H. Y., Li, Q. Q., Xu, B. S., Zhou, Z. W., & Zhang, X. (2017). PD-L1 expression is associated with FOXP3+ regulatory T-Cell infiltration of soft tissue sarcoma and poor patient prognosis. *Journal of Cancer*, *8*(11), 2018–2025. https://doi.org/10.7150/jca.18683

151. Liu, S., Lachapelle, J., Leung, S., Gao, D., Foulkes, W. D., & Nielsen, T. O. (2012). CD8+ lymphocyte infiltration is an independent favorable prognostic indicator in basal-like breast cancer. *Breast Cancer Research*, *14*(2). https://doi.org/10.1186/bcr3148

152. Jenkins, L., Jungwirth, U., Avgustinova, A., Iravani, M., Mills, A., Haider, S., Harper, J., & Isacke, C. M. (2022). Cancer-Associated Fibroblasts Suppress CD8+ T-cell Infiltration and Confer Resistance to Immune-Checkpoint Blockade. *Cancer Research*, *82*(16), 2904–2917. https://doi.org/10.1158/0008-5472.CAN-21-4141

153. Ran, L. F., Xie, X. P., Xia, J. Z., Xie, F. L., Fan, Y. M., & Wu, F. (2016). Specific antitumour immunity of HIFU-activated cytotoxic T lymphocytes after adoptive transfusion in tumour-bearing mice. *International Journal of Hyperthermia*, *32*(2), 204–210. https://doi.org/10.3109/02656736.2015.1112438

154. Chattopadhyay, S., Mehrotra, S., Chhabra, A., Hegde, U., Mukherji, B., & Chakraborty, N. G. (2006). Effect of CD4+CD25+ and CD4+CD25− T Regulatory Cells on the Generation of Cytolytic T Cell Response to a Self but Human Tumor-Associated

Epitope In Vitro. *The Journal of Immunology*, *176*(2), 984–990. https://doi.org/10.4049/jimmunol.176.2.984

155. Leveque, L., Deknuydt, F., Bioley, G., Old, L. J., Matsuzaki, J., Odunsi, K., Ayyoub, M., & Valmori, D. (2009). Interleukin 2-mediated Conversion of Ovarian Cancer-associated CD4 + Regulatory T Cells Into Proinflammatory Interleukin 17-producing Helper T Cells. In *J Immunother* (Vol. 32). http://journals.lww.com/immunotherapy-journal

156. De Leeuw, R. J., Kroeger, D. R., Kost, S. E., Chang, P. P., Webb, J. R., & Nelson, B. H. (2015). CD25 identifies a subset of CD4 FoxP3 TIL that are exhausted yet prognostically favorable in Human Ovarian cancer. *Cancer Immunology Research*, *3*(3), 245–253. https://doi.org/10.1158/2326-6066.CIR-14-0146

157. Klebanoff, C. A., Gattinoni, L., Torabi-Parizi, P., Kerstann, K., Cardones, A. R., Finkelstein, S. E., Palmer, D. C., Antony, P. A., Hwang, S. T., Rosenberg, S. A., Waldmann, T. A., & Restifo, N. P. (n.d.). *Central memory self/tumor-reactive CD8 T cells confer superior antitumor immunity compared with effector memory T cells*. www.pnas.orgcgidoi10.1073pnas.0503726102

158. Arce Vargas, F., Furness, A. J. S., Solomon, I., Joshi, K., Mekkaoui, L., Lesko, M. H., Miranda Rota, E., Dahan, R., Georgiou, A., Sledzinska, A., Ben Aissa, A., Franz, D., Werner Sunderland, M., Wong, Y. N. S., Henry, J. Y., O'Brien, T., Nicol, D., Challacombe, B., Beers, S. A., … Quezada, S. A. (2017). Fc-Optimized Anti-CD25 Depletes Tumor-Infiltrating Regulatory T Cells and Synergizes with PD-1 Blockade to Eradicate Established Tumors. *Immunity*, *46*(4), 577–586. https://doi.org/10.1016/j.immuni.2017.03.013

159. Ellis, S., Lin, E. J., & Tartar, D. (2018). Immunology of Wound Healing. In *Current Dermatology Reports* (Vol. 7, Issue 4, pp. 350–358). Current Medicine Group LLC 1. https://doi.org/10.1007/s13671-018-0234-9

160. Noah, A. C., Li, T. M., Martinez, L. M., Wada, S., Swanson, J. B., Disser, N. P., Sugg, K. B., Rodeo, S. A., Lu, T. T., Christopher, X., & Mendias, L. (2020). Adaptive and innate immune cell responses in tendons and lymph nodes after tendon injury and repair. *J Appl Physiol*, *128*, 473–482. https://doi.org/10.1152/japplphysiol.00682.2019.-Tendon

161. KATARANOVSKI, M., MAGIĆ, Z., & PEJNOVIĆ, N. (1999). Early Inflammatory Cytokine and Acute Phase Protein Response Under the Stress of Thermal Injury in Rats. *Physiology Research*, *48*.

162. Ghosh, B., Mukhopadhyay, M., & Bhattacharya, D. (2021). Biopolymer-based nanofilms for the treatment of burn wounds. In *Biopolymer-Based Nano Films: Applications in Food Packaging and Wound Healing* (pp. 311–336). Elsevier. https://doi.org/10.1016/B978-0-12-823381-8.00005-3

163. Vahidi, Y., Bagheri, M., Ghaderi, A., & Faghih, Z. (2020). CD8-positive memory T cells in tumor-draining lymph nodes of patients with breast cancer. *BMC Cancer*, *20*(1). https://doi.org/10.1186/s12885-020-6714-x

164. Manjarrez-Orduño, N., Menard, L. C., Kansal, S., Fischer, P., Kakrecha, B., Jiang, C., Cunningham, M., Greenawalt, D., Patel, V., Yang, M., Golhar, R., Carman, J. A., Lezhnin, S., Dai, H., Kayne, P. S., Suchard, S. J., Bernstein, S. H., & Nadler, S. G. (2018). Circulating T cell subpopulations correlate with immune responses at the tumor site and clinical response to PD1 inhibition in non-small cell lung cancer. *Frontiers in Immunology*, *9*(AUG). https://doi.org/10.3389/fimmu.2018.01613

165. Sckisel, G. D., Mirsoian, A., Minnar, C. M., Crittenden, M., Curti, B., Chen, J. Q., Blazar, B. R., Borowsky, A. D., Monjazeb, A. M., & Murphy, W. J. (2017). Differential phenotypes of memory CD4 and CD8 T cells in the spleen and peripheral tissues following immunostimulatory therapy. *Journal for ImmunoTherapy of Cancer*, *5*(1). https://doi.org/10.1186/s40425-017-0235-4

166. Pedroza-Gonzalez, A., Zhou, G., Vargas-Mendez, E., Boor, P. P., Mancham, S., Verhoef, C., Polak, W. G., Grünhagen, D., Pan, Q., Janssen, H. LA, Garcia-Romo, G. S., Biermann, K., Tjwa, E. T. T. L., Ijzermans, J. N. M., Kwekkeboom, J., & Sprengers, D. (2015). Tumor-infiltrating plasmacytoid dendritic cells promote immunosuppression by Tr1 cells in human liver tumors. *OncoImmunology*, *4*(6). https://doi.org/10.1080/2162402X.2015.1008355

167. Jang, J. E., Hajdu, C. H., Liot, C., Miller, G., Dustin, M. L., & Bar-Sagi, D. (2017). Crosstalk between Regulatory T Cells and Tumor-Associated Dendritic Cells Negates Anti-tumor Immunity in Pancreatic Cancer. *Cell Reports*, *20*(3), 558–571. https://doi.org/10.1016/j.celrep.2017.06.062

168. Augier, S., Ciucci, T., Luci, C., Carle, G. F., Blin-Wakkach, C., & Wakkach, A. (2010). Inflammatory Blood Monocytes Contribute to Tumor Development and Represent a Privileged Target To Improve Host Immunosurveillance. *The Journal of Immunology*, *185*(12), 7165–7173. https://doi.org/10.4049/jimmunol.0902583

169. Kostine, M., Briaire-de Bruijn, I. H., Cleven, A. H. G., Vervat, C., Corver, W. E., Schilham, M. W., Van Beelen, E., van Boven, H., Haas, R. L., Italiano, A., Cleton-Jansen, A. M., & Bovée, J. V. M. G. (2018). Increased infiltration of M2-macrophages, T-cells and PD-L1 expression in high grade leiomyosarcomas supports immunotherapeutic strategies. *OncoImmunology*, *7*(2). https://doi.org/10.1080/2162402X.2017.1386828

170. Ponzetta, A., Carriero, R., Carnevale, S., Barbagallo, M., Molgora, M., Perucchini, C., Magrini, E., Gianni, F., Kunderfranco, P., Polentarutti, N., Pasqualini, F., Di Marco, S., Supino, D., Peano, C., Cananzi, F., Colombo, P., Pilotti, S., Alomar, S. Y., Bonavita, E., … Jaillon, S. (2019). Neutrophils Driving Unconventional T Cells Mediate Resistance

against Murine Sarcomas and Selected Human Tumors. *Cell*, *178*(2), 346-360.e24. https://doi.org/10.1016/j.cell.2019.05.047

171. An, M., Yua, C., Xi, J., Reyes, J., Mao, G., Wei, W.-Z., & Liu, H. (2019). Induction of Necrotic Cell Death and Activation of STING in the Tumor Microenvironment via Cationic Silica Nanoparticles Lead to Enhanced Antitumor Immunity. *Nanoscale*, *2019-November*. https://doi.org/10.1039/x0xx00000x

172. Kuhn, S., Yang, J., & Ronchese, F. (2015). Monocyte-derived dendritic cells are essential for CD8+ T cell activation and antitumor responses after local immunotherapy. *Frontiers in Immunology*, *6*(NOV). https://doi.org/10.3389/fimmu.2015.00584

173. Nonaka, K., Saio, M., Umemura, N., Kikuchi, A., Takahashi, T., Osada, S., & Yoshida, K. (2021). Th1 polarization in the tumor microenvironment upregulates the myeloid-derived suppressor-like function of macrophages. *Cellular Immunology*, *369*. https://doi.org/10.1016/j.cellimm.2021.104437

174. Dancsok, A. R., Gao, D., Lee, A. F., Steigen, S. E., Blay, J. Y., Thomas, D. M., Maki, R. G., Nielsen, T. O., & Demicco, E. G. (2020). Tumor-associated macrophages and macrophage-related immune checkpoint expression in sarcomas. *OncoImmunology*, *9*(1). https://doi.org/10.1080/2162402X.2020.1747340

175. Muraoka, D., Seo, N., Hayashi, T., Tahara, Y., Fujii, K., Tawara, I., Miyahara, Y., Okamori, K., Yagita, H., Imoto, S., Yamaguchi, R., Komura, M., Miyano, S., Goto, M., Sawada, S. I., Asai, A., Ikeda, H., Akiyoshi, K., Harada, N., & Shiku, H. (2019). Antigen delivery targeted to tumor-associated macrophages overcomes tumor immune resistance. *Journal of Clinical Investigation*, *129*(3), 1278–1294. https://doi.org/10.1172/JCI97642

176. An, N., Wang, H., Jia, W., Jing, W., Liu, C., Zhu, H., & Yu, J. (2019). The prognostic role of circulating CD8+ T cell proliferation in patients with untreated extensive stage small cell lung cancer. *Journal of Translational Medicine*, *17*(1). https://doi.org/10.1186/s12967-019-02160-7

177. Li, F., Sun, Y., Huang, J., Xu, W., Liu, J., & Yuan, Z. (2019). CD4/CD8 + T cells, DC subsets, Foxp3, and IDO expression are predictive indictors of gastric cancer prognosis. *Cancer Medicine*, *8*(17), 7330–7344. https://doi.org/10.1002/cam4.2596

178. Dutsch-Wicherek, M. M., Szubert, S., Dziobek, K., Wisniewski, M., Lukaszewska, E., Wicherek, L., Jozwicki, W., Rokita, W., & Koper, K. (2019). Analysis of the Treg cell population in the peripheral blood of ovarian cancer patients in relation to the long-term outcomes. *Ginekologia Polska*, *90*(4), 179–184. https://doi.org/10.5603/GP.2019.0032

179. Kelany, M., Barth, T. F. E., Salem, D., & Shakweer, M. M. (2021). Prevalence and Prognostic Implications of PD-L1 Expression in Soft Tissue Sarcomas. *Pathology and Oncology Research*, *27*. https://doi.org/10.3389/pore.2021.1609804

180. Huang, Q., Wu, X., Wang, Z., Chen, X., Wang, L., Lu, Y., Xiong, D., Liu, Q., Tian, Y., Lin, H., Guo, J., Wen, S., Dong, W., Yang, X., Yuan, Y., Yue, Z., Lei, S., Wu, Q., Ran, L., … Ye, L. (2022). The primordial differentiation of tumor-specific memory CD8+ T cells as bona fide responders to PD-1/PD-L1 blockade in draining lymph nodes. *Cell*, *185*(22), 4049-4066.e25. https://doi.org/10.1016/j.cell.2022.09.020

181. Wagner, M. J., Zhang, Y., Cranmer, L. D., Loggers, E. T., Black, G., McDonnell, S., Maxwell, S., Johnson, R., Moore, R., De Viveiros, P. H., Aicher, L., Smythe, K. S., He, Q., Jones, R. L., & Pollack, S. M. (2022). A Phase 1/2 Trial Combining Avelumab and Trabectedin for Advanced Liposarcoma and Leiomyosarcoma. *Clinical Cancer Research*, *28*(11), 2306–2312. https://doi.org/10.1158/1078-0432.CCR-22-0240

182. Kim, M., Kim, Y. J., Suh, K. J., Kim, S. H., Kim, J. E., Jeong, J., Hong, J. Y., Lee, J., Lee, S. J., Oh, S. Y., Kim, J. H., Lee, G. W., Ahn, M. S., Choi, W., Choi, Y. J., Lee, T., Oum, C., Kim, J., Kim, Y. S., & Ahn, J. H. (2024). Phase 2 trial of avelumab in combination with gemcitabine in advanced leiomyosarcoma as a second-line treatment (EAGLES, Korean Cancer Study Group UN18-09). *Cancer*. https://doi.org/10.1002/cncr.35609

183. Chen, A. P., Sharon, E., O'Sullivan-Coyne, G., Moore, N., Foster, J. C., Hu, J. S., Van Tine, B. A., Conley, A. P., Read, W. L., Riedel, R. F., Burgess, M. A., Glod, J., Davis, E. J., Merriam, P., Naqash, A. R., Fino, K. K., Miller, B. L., Wilsker, D. F., Begum, A., … Doroshow, J. H. (2023). Atezolizumab for Advanced Alveolar Soft Part Sarcoma. *New England Journal of Medicine*, *389*(10), 911–921. https://doi.org/10.1056/nejmoa2303383

184. Ng, V. Y., Sahlani, M. N., Fogel, J. D., Chiu, A. K., Kallen, M. E., Davis, D., Snider, J., Regine, W., Bentzen, S. M., & Sausville, E. (2024). Results of an Integrated Phase I/II Prospective Clinical Trial (NEXIS) for Neoadjuvant Anti-PD-L1 (Durvalumab) and Anti-CTLA-4 (Tremelimumab) With Radiation for High-Risk Soft-Tissue Sarcoma of the Trunk and Extremities. *Cureus*. https://doi.org/10.7759/cureus.72119

185. Toulmonde, M., Brahmi, M., Giraud, A., Chakiba, C., Bessede, A., Kind, M., Toulza, E., Pulido, M., Albert, S., Guégan, J.-P., Cousin, S., Mathoulin-Pelissier, S., Perret, R., Croce, S., Blay, J.-Y., Ray-Coquard, I., Floquet, A., & Italiano, A. (2022). Trabectedin plus Durvalumab in Patients with Advanced Pretreated Soft Tissue Sarcoma and Ovarian Carcinoma (TRAMUNE): An Open-Label, Multicenter Phase Ib Study. *Clinical Cancer Research*, *28*(9), 1765–1772. https://doi.org/10.1158/1078-0432.CCR-21-2258

186. Kaistha, B. P., Kar, G., Dannhorn, A., Watkins, A., Opoku-Ansah, G., Ilieva, K., Mullins, S., Anderton, J., Galvani, E., Garcon, F., Lapointe, J. M., Brown, L., Hair, J., Slidel, T., Luheshi, N., Ryan, K., Hardaker, E., Dovedi, S., Kumar, R., … Eyles, J. (2024). Efficacy

and pharmacodynamic effect of anti-CD73 and anti-PD-L1 monoclonal antibodies in combination with cytotoxic therapy: observations from mouse tumor models. *Cancer Biology and Therapy*, *25*(1). https://doi.org/10.1080/15384047.2023.2296048

187. Panagi, M., Mpekris, F., Voutouri, C., Hadjigeorgiou, A. G., Symeonidou, C., Porfyriou, E., Michael, C., Stylianou, A., Martin, J. D., Cabral, H., Constantinidou, A., & Stylianopoulos, T. (2024). Stabilizing Tumor-Resident Mast Cells Restores T-Cell Infiltration and Sensitizes Sarcomas to PD-L1 Inhibition. *Clinical Cancer Research*, *30*(11), 2582–2597. https://doi.org/10.1158/1078-0432.CCR-24-0246

188. Zhou, Y., Chen, D., Qi, Y., Liu, R., Li, S., Zou, H., Lan, J., Ju, X., Jiang, J., Liang, W., Shen, Y., Pang, L., & Li, F. (2017). Evaluation of expression of cancer stem cell markers and fusion gene in synovial sarcoma: Insights into histogenesis and pathogenesis. *Oncology Reports*, *37*(6), 3351–3360. https://doi.org/10.3892/or.2017.5617

189. Liu, Y., Zugazagoitia, J., Ahmed, F. S., Henick, B. S., Gettinger, S. N., Herbst, R. S., Schalper, K. A., & Rimm, D. L. (2020). Immune cell PD-L1 colocalizes with macrophages and is associated with outcome in PD-1 pathway blockade therapy. *Clinical Cancer Research*, *26*(4), 970–977. https://doi.org/10.1158/1078-0432.CCR-19-1040

190. Noguchi, T., Ward, J. P., Gubin, M. M., Arthur, C. D., Lee, S. H., Hundal, J., Selby, M. J., Graziano, R. F., Mardis, E. R., Korman, A. J., & Schreiber, R. D. (2017). Temporally distinct PD-L1 expression by tumor and host cells contributes to immune escape. *Cancer Immunology Research*, *5*(2), 106–117. https://doi.org/10.1158/2326-6066.CIR-16-0391

191. Kowanetz, M., Zou, W., Gettinger, S. N., Koeppen, H., Kockx, M., Schmid, P., Kadel, E. E., Wistuba, I., Chaft, J., Rizvi, N. A., Spigel, D. R., Spira, A., Hirsch, F. R., Cohen, V., Smith, D., Boyd, Z., Miley, N., Flynn, S., Leveque, V., … Hegde, P. S. (2018). Differential regulation of PD-L1 expression by immune and tumor cells in NSCLC and the response to treatment with atezolizumab (anti-PD-L1). *Proceedings of the National Academy of Sciences of the United States of America*, *115*(43), E10119–E10126. https://doi.org/10.1073/pnas.1802166115

192. Schetters, S. T. T., Rodriguez, E., Kruijssen, L. J. W., Crommentuijn, M. H. W., Boon, L., Van Den Bossche, J., Den Haan, J. M. M., & Van Kooyk, Y. (2020). Monocyte-derived APCs are central to the response of PD1 checkpoint blockade and provide a therapeutic target for combination therapy. *Journal for ImmunoTherapy of Cancer*, *8*(2). https://doi.org/10.1136/jitc-2020-000588

193. Choi, Y. E., Yu, H. N., Yoon, C. H., & Bae, Y. S. (2009). Tumor-mediated down-regulation of MHC class II in DC development is attributable to the epigenetic control of the CIITA type I promoter. *European Journal of Immunology*, *39*(3), 858–868. https://doi.org/10.1002/eji.200838674

194. Johnson, D. B., Estrada, M. V., Salgado, R., Sanchez, V., Doxie, D. B., Opalenik, S. R., Vilgelm, A. E., Feld, E., Johnson, A. S., Greenplate, A. R., Sanders, M. E., Lovly, C. M., Frederick, D. T., Kelley, M. C., Richmond, A., Irish, J. M., Shyr, Y., Sullivan, R. J., Puzanov, I., … Balko, J. M. (2016). Melanoma-specific MHC-II expression represents a tumour-autonomous phenotype and predicts response to anti-PD-1/PD-L1 therapy. *Nature Communications*, *7*. https://doi.org/10.1038/ncomms10582

195. Piao, W., Li, L., Saxena, V., Iyyathurai, J., Lakhan, R., Zhang, Y., Lape, I. T., Paluskievicz, C., Hippen, K. L., Lee, Y., Silverman, E., Shirkey, M. W., Riella, L. V., Blazar, B. R., & Bromberg, J. S. (2022). PD-L1 signaling selectively regulates T cell lymphatic transendothelial migration. *Nature Communications*, *13*(1). https://doi.org/10.1038/s41467-022-29930-0

196. Castiglioni, A., Corna, G., Rigamonti, E., Basso, V., Vezzoli, M., Monno, A., Almada, A. E., Mondino, A., Wagers, A. J., Manfredi, A. A., & Rovere-Querini, P. (2015). FOXP3+ T cells recruited to sites of sterile skeletal muscle injury regulate the fate of satellite cells and guide effective tissue regeneration. *PLoS ONE*, *10*(6). https://doi.org/10.1371/journal.pone.0128094

197. Lu, H., Huang, D., Ransohoff, R. M., & Zhou, L. (2011). Acute skeletal muscle injury: CCL2 expression by both monocytes and injured muscle is required for repair. *The FASEB Journal*, *25*(10), 3344–3355. https://doi.org/10.1096/fj.10-178939

198. Pimorady-Esfahani, A., Grounds, M. D., & McMenamin, P. G. (1997). Macrophages and dendritic cells in normal and regenerating murine skeletal muscle. *Muscle and Nerve*, *20*(2), 158–166. https://doi.org/10.1002/(SICI)1097-4598(199702)20:2<158::AID-MUS4>3.0.CO;2-B

199. Martín-Broto, J., Moura, D. S., & van Tine, B. A. (2020). Facts and hopes in immunotherapy of soft-tissue sarcomas. In *Clinical Cancer Research* (Vol. 26, Issue 22, pp. 5801–5808). American Association for Cancer Research Inc. https://doi.org/10.1158/1078-0432.CCR-19-3335

200. Cruz, S. M., Sholevar, C. J., Judge, S. J., Darrow, M. A., Iranpur, K. R., Farley, L. E., Lammers, M., Razmara, A. M., Dunai, C., Gingrich, A. A., Persky, J., Mori, H., Thorpe, S. W., Monjazeb, A. M., Murphy, W. J., & Canter, R. J. (2023). Intratumoral NKp46+ natural killer cells are spatially distanced from T and MHC-I+ cells with prognostic implications in soft tissue sarcoma. *Frontiers in Immunology*, *14*. https://doi.org/10.3389/fimmu.2023.1230534

201. Rupp, L., Resag, A., Potkrajcic, V., Warm, V., Wehner, R., Jöhrens, K., Bösmüller, H., Eckert, F., & Schmitz, M. (2023). Prognostic impact of the post-treatment T cell composition and spatial organization in soft tissue sarcoma patients treated with neoadjuvant hyperthermic radio(chemo)therapy. *Frontiers in Immunology*, *14*. https://doi.org/10.3389/fimmu.2023.1185197

202. Lu, Y., Chen, D., Wang, B., Chai, W., Yan, M., Chen, Y., Zhan, Y., Yang, R., Zhou, E., Dai, S., Li, Y., Dong, R., & Zheng, B. (2024). Single-cell landscape of undifferentiated pleomorphic sarcoma. *Oncogene*, *43*(18), 1353–1368. https://doi.org/10.1038/s41388-024-03001-8

203. Penel, N., Coindre, J. M., Giraud, A., Terrier, P., Ranchere-Vince, D., Collin, F., Guellec, S. L. E., Bazille, C., Lae, M., de Pinieux, G., Ray-Coquard, I. L., Bonvalot, S., Cesne, A. L. E., Robin, Y. M., Stoeckle, E., Toulmonde, M., & Blay, J. Y. (2018). Presentation and outcome of frequent and rare sarcoma histologic subtypes: A study of 10,262 patients with localized visceral/soft tissue sarcoma managed in reference centers. *Cancer*, *124*(6), 1179–1187. https://doi.org/10.1002/cncr.31176

204. Savina, M., Le Cesne, A., Blay, J. Y., Ray-Coquard, I., Mir, O., Toulmonde, M., Cousin, S., Terrier, P., Ranchere-Vince, D., Meeus, P., Stoeckle, E., Honoré, C., Sargos, P., Sunyach, M. P., Le Péchoux, C., Giraud, A., Bellera, C., Le Loarer, F., & Italiano, A. (2017). Patterns of care and outcomes of patients with METAstatic soft tissue SARComa in a real-life setting: The METASARC observational study. *BMC Medicine*, *15*(1). https://doi.org/10.1186/s12916-017-0831-7

205. Feng, X., Tonon, L., Li, H., Darbo, E., Pleasance, E., Macagno, N., Dufresne, A., Brahmi, M., Bollard, J., Ducimetière, F., Karanian, M., Meurgey, A., Pérot, G., Valentin, T., Chibon, F., & Blay, J. Y. (2023). Comprehensive Immune Profiling Unveils a Subset of Leiomyosarcoma with “Hot” Tumor Immune Microenvironment. *Cancers*, *15*(14). https://doi.org/10.3390/cancers15143705

206. Rao, A., Barkley, D., França, G. S., & Yanai, I. (2021). Exploring tissue architecture using spatial transcriptomics. In *Nature* (Vol. 596, Issue 7871, pp. 211–220). Nature Research. https://doi.org/10.1038/s41586-021-03634-9

207. Park, Y. M., & Lin, D. C. (2023). Moving closer towards a comprehensive view of tumor biology and microarchitecture using spatial transcriptomics. In *Nature Communications* (Vol. 14, Issue 1). Nature Research. https://doi.org/10.1038/s41467-023-42960-6

208. Cilento, M. A., Sweeney, C. J., & Butler, L. M. (2024). Spatial transcriptomics in cancer research and potential clinical impact: a narrative review. In *Journal of Cancer Research and Clinical Oncology* (Vol. 150, Issue 6). Springer Science and Business Media Deutschland GmbH. https://doi.org/10.1007/s00432-024-05816-0

209. Fuller, A. M., Pruitt, H. C., Liu, Y., Irizarry-Negron, V. M., Pan, H., Song, H., DeVine, A., Katti, R. S., Devalaraja, S., Ciotti, G. E., Gonzalez, M. V., Williams, E. F., Murazzi, I., Ntekoumes, D., Skuli, N., Hakonarson, H., Zabransky, D. J., Trevino, J. G., Weeraratna, A., … Eisinger-Mathason, T. S. K. (2024). Oncogene-induced matrix reorganization controls CD8+ T cell function in the soft-tissue sarcoma microenvironment. *Journal of Clinical Investigation*, *134*(11). https://doi.org/10.1172/JCI167826

210. Kuczek, D. E., Larsen, A. M. H., Thorseth, M. L., Carretta, M., Kalvisa, A., Siersbæk, M. S., Simões, A. M. C., Roslind, A., Engelholm, L. H., Noessner, E., Donia, M., Svane, I. M., Straten, P. T., Grøntved, L., & Madsen, D. H. (2019). Collagen density regulates the activity of tumor-infiltrating T cells. *Journal for ImmunoTherapy of Cancer*, *7*(1). https://doi.org/10.1186/s40425-019-0556-6

211. Zhu, N., & Hou, J. (2020). Assessing immune infiltration and the tumor microenvironment for the diagnosis and prognosis of sarcoma. *Cancer Cell International*, *20*(1), 1–11. https://doi.org/10.1186/s12935-020-01672-3

212. Xu, S., Hu, E., Cai, Y., Xie, Z., Luo, X., Zhan, L., Tang, W., Wang, Q., Liu, B., Wang, R., Xie, W., Wu, T., Xie, L., & Yu, G. (2024). Using clusterProfiler to characterize multiomics data. *Nature Protocols*. https://doi.org/doi:10.1038/s41596-024-01020-z

213. Zhou, H., Ke, J., Liu, C., Zhu, M., Xiao, B., Wang, Q., Hou, R., Zheng, Y., Wu, Y., Zhou, X., Chen, X., & Pan, H. (2023). Potential prognostic and immunotherapeutic value of calponin 1: A pan-cancer analysis. *Frontiers in Pharmacology*, *14*. https://doi.org/10.3389/fphar.2023.1184250

214. Hu, X., Chen, M., Ruan, Q., Shi, C., Pan, J., & Luo, L. (2022). Comprehensive Analysis of PDLIM3 Expression Profile, Prognostic Value, and Correlations with Immune Infiltrates in Gastric Cancer. *Journal of Immunology Research*, *2022*. https://doi.org/10.1155/2022/2039447

215. Yang, W., Lin, L., Lu, T., Yu, H., & Zhang, S. (2024). Identification of EMT-associated prognostic features among grade II/III gliomas. *Scientific Reports*, *14*(1). https://doi.org/10.1038/s41598-024-53399-0

216. Cao, Y., Cao, W., Qiu, Y., Zhou, Y., Guo, Q., Gao, Y., & Lu, N. (2020). Oroxylin A suppresses ACTN1 expression to inactivate cancer-associated fibroblasts and restrain breast cancer metastasis. *Pharmacological Research*, *159*. https://doi.org/10.1016/j.phrs.2020.104981

217. Demirkol Canli, S. (2023). CSRP1 expression is associated with a mesenchymal, stroma-rich tumor profile and poor prognosis in colon cancer. *Turkish Journal of Medical Sciences*, *53*(6), 1678–1689. https://doi.org/10.55730/1300-0144.5736

218. Suresh, R., & Diaz, R. J. (2021). The remodelling of actin composition as a hallmark of cancer. In *Translational Oncology* (Vol. 14, Issue 6). Neoplasia Press, Inc. https://doi.org/10.1016/j.tranon.2021.101051

219. Kim, D., Cooper, J. A., & Helfman, D. M. (2024). Loss of myosin light chain kinase induces the cellular senescence associated secretory phenotype to promote breast epithelial cell migration. *Scientific Reports*, *14*(1), 25786. https://doi.org/10.1038/s41598-024-76868-y

220. Elsafadi, M., Manikandan, M., Dawud, R. A., Alajez, N. M., Hamam, R., Alfayez, M., Kassem, M., Aldahmash, A., & Mahmood, A. (2016). Transgelin is a TGFβ-inducible gene that regulates osteoblastic and adipogenic differentiation of human skeletal stem cells through actin cytoskeleston organization. *Cell Death and Disease*, *7*(8). https://doi.org/10.1038/cddis.2016.196

221. Kay, E. J., Paterson, K., Riero-Domingo, C., Sumpton, D., Däbritz, J. H. M., Tardito, S., Boldrini, C., Hernandez-Fernaud, J. R., Athineos, D., Dhayade, S., Stepanova, E., Gjerga, E., Neilson, L. J., Lilla, S., Hedley, A., Koulouras, G., McGregor, G., Jamieson, C., Johnson, R. M., … Zanivan, S. (2022). Cancer-associated fibroblasts require proline synthesis by PYCR1 for the deposition of pro-tumorigenic extracellular matrix. *Nature Metabolism*, *4*(6), 693–710. https://doi.org/10.1038/s42255-022-00582-0

222. Ludyga, N., Englert, S., Pflieger, K., Rauser, S., Braselmann, H., Walch, A., Auer, G., Höfler, H., & Aubele, M. (2013). *The impact of Cysteine-Rich Intestinal Protein 1 (CRIP1) in human breast cancer*. http://www.molecular-cancer.com/content/12/1/28

223. Nakayama, R., Nemoto, T., Takahashi, H., Ohta, T., Kawai, A., Seki, K., Yoshida, T., Toyama, Y., Ichikawa, H., & Hasegawa, T. (2007). Gene expression analysis of soft tissue sarcomas: Characterization and reclassification of malignant fibrous histiocytoma. *Modern Pathology*, *20*(7), 749–759. https://doi.org/10.1038/modpathol.3800794

224. Chen, J., Wang, J., Hart, D. A., Zhou, Z., Ackermann, P. W., & Ahmed, A. S. (2023). Complement factor D regulates collagen type I expression and fibroblast migration to enhance human tendon repair and healing outcomes. *Frontiers in Immunology*, *14*. https://doi.org/10.3389/fimmu.2023.1225957

225. Liu, Y., Li, W., Luo, J., Wu, Y., Xu, Y., Chen, T., Zhang, W., & Fu, F. (2021). Cysteine-Rich Intestinal Protein 1 Served as an Epithelial Ovarian Cancer Marker via Promoting Wnt/β -Catenin-Mediated EMT and Tumour Metastasis. *Disease Markers*, *2021*. https://doi.org/10.1155/2021/3566749

226. Cheung, A. K. L., Ko, J. M. Y., Lung, H. L., Chan, K. W., Stanbridge, E. J., Zabarovsky, E., Tokino, T., Kashima, L., Suzuki, T., Kwong, D. L. W., Chua, D., Tsao, S. W., & Lung, M. L. (2011). Cysteine-rich intestinal protein 2 (CRIP2) acts as a repressor of NF-κB-mediated proangiogenic cytokine transcription to suppress tumorigenesis and angiogenesis. *Proceedings of the National Academy of Sciences of the United States of America*, *108*(20), 8390–8395. https://doi.org/10.1073/pnas.1101747108

227. Yoshida, J., Hayashi, T., Munetsuna, E., Khaledian, B., Sueishi, F., Mizuno, M., Maeda, M., Watanabe, T., Ushida, K., Sugihara, E., Imaizumi, K., Kawada, K., Asai, N., & Shimono, Y. (2024). Adipsin-dependent adipocyte maturation induces cancer cell invasion in breast cancer. *Scientific Reports*, *14*(1). https://doi.org/10.1038/s41598-024-69476-3

228. Meyaard, L., Adema, G., Chang, C., Woolatt, E., Sutherland, G., Lanier, L., & Phillips, J. (1997). LAIR-1, a Novel Inhibitory Receptor Expressed on Human Mononuclear Leukocytes. In *Immunity* (Vol. 7). Lanier and Phillips.

229. Sum, E., Rapp, M., Dürr, H., Mazumdar, A., Romero, P. J., Trumpfheller, C., & Umaña, P. (2022). The tumor-targeted CD40 agonist CEA-CD40 promotes T cell priming via a dual mode of action by increasing antigen delivery to dendritic cells and enhancing their activation. *Journal for ImmunoTherapy of Cancer*, *10*(3). https://doi.org/10.1136/jitc-2021-003264

230. Eckfeld, K., Hesson, L., Vos, M. D., Bieche, I., Latif, F., & Clark, G. J. (2004). RASSF4/AD037 Is a Potential Ras Effector/Tumor Suppressor of the RASSF Family. In *CANCER RESEARCH* (Vol. 64). http://aacrjournals.org/cancerres/article-pdf/64/23/8688/2521289/zch02304008688.pdf

231. Crose, L. E. S., Galindo, K. A., Kephart, J. G., Chen, C., Fitamant, J., Bardeesy, N., Bentley, R. C., Galindo, R. L., Ashley Chi, J. T., & Linardic, C. M. (2014). Alveolar rhabdomyosarcoma-Associated PAX3-FOXO1 promotes tumorigenesis via Hippo pathway suppression. *Journal of Clinical Investigation*, *124*(1), 285–296. https://doi.org/10.1172/JCI67087

232. Mei, Z., Zhang, D., Hu, B., Wang, J., Shen, X., & Xiao, W. (2015). FBXO32 targets c-Myc for proteasomal degradation and inhibits c-Myc activity. *Journal of Biological Chemistry*, *290*(26), 16202–16214. https://doi.org/10.1074/jbc.M115.645978

233. Sarkozy, A., Windpassinger, C., Hudson, J., Dougan, C. F., Lecky, B., Hilton-Jones, D., Eagle, M., Charlton, R., Barresi, R., Lochmüller, H., Bushby, K., & Straub, V. (2011). Phenotypic heterogeneity in British patients with a founder mutation in the FHL1 gene. *European Journal of Human Genetics*, *19*(10), 1038–1044. https://doi.org/10.1038/ejhg.2011.84

234. Lee, H. W., Park, Y. M., Lee, S. J., Cho, H. J., Kim, D. H., Lee, J. Il, Kang, M. S., Seol, H. J., Shim, Y. M., Nam, D. H., Kim, H. H., & Joo, K. M. (2013). Alpha-smooth muscle actin (ACTA2) is required for metastatic potential of human lung adenocarcinoma. *Clinical Cancer Research*, *19*(21), 5879–5889. https://doi.org/10.1158/1078-0432.CCR-13-1181

235. Lambert, M. R., & Gussoni, E. (2023). Tropomyosin 3 (TPM3) function in skeletal muscle and in myopathy. In *Skeletal Muscle* (Vol. 13, Issue 1). BioMed Central Ltd. https://doi.org/10.1186/s13395-023-00327-x

236. Zhao, S. J., Jiang, Y. Q., Xu, N. W., Li, Q., Zhang, Q., Wang, S. Y., Li, J., Wang, Y. H., Zhang, Y. L., Jiang, S. H., Wang, Y. J., Huang, Y. J., Zhang, X. X., Tian, G. A., Zhang, C. C., Lv, Y. Y., Dai, M., Liu, F., Zhang, R., … Zhang, Z. G. (2018). SPARCL1 suppresses osteosarcoma metastasis and recruits macrophages by activation of canonical

WNT/β-catenin signaling through stabilization of the WNT-receptor complex. *Oncogene*, *37*(8), 1049–1061. https://doi.org/10.1038/onc.2017.403

237. Park, I., Han, C., Jin, S., Lee, B., Choi, H., Kwon, J. T., Kim, D., Kim, J., Lifirsu, E., Park, W. J., Park, Z. Y., Kim, D. H., & Cho, C. (2011). Myosin regulatory light chains are required to maintain the stability of myosin II and cellular integrity. *Biochemical Journal*, *434*(1), 171–180. https://doi.org/10.1042/BJ20101473

238. Du, Y. H., Jiang, X., Wang, B., Cao, J., Wang, Y., Yu, J., Wang, X. Z., & Liu, H. T. (2021). The cancer-associated fibroblasts related gene CALD1 is a prognostic biomarker and correlated with immune infiltration in bladder cancer. *Cancer Cell International*, *21*(1). https://doi.org/10.1186/s12935-021-01896-x

239. Doni, A., Stravalaci, M., Inforzato, A., Magrini, E., Mantovani, A., Garlanda, C., & Bottazzi, B. (2019). The long pentraxin PTX3 as a link between innate immunity, tissue remodeling, and cancer. In *Frontiers in Immunology* (Vol. 10, Issue APR). Frontiers Media S.A. https://doi.org/10.3389/fimmu.2019.00712

240. Chudasama, P., Renner, M., Straub, M., Mughal, S. S., Hutter, B., Kosaloglu, Z., Schweßinger, R., Scheffler, M., Alldinger, I., Schimmack, S., Persigehl, T., Kobe, C., Jäger, D., Von Kalle, C., Schirmacher, P., Beckhaus, M. K., Wolf, S., Heining, C., Gröschel, S., … Fröhling, S. (2017). Targeting fibroblast growth factor receptor 1 for treatment of soft-tissue sarcoma. *Clinical Cancer Research*, *23*(4), 962–973. https://doi.org/10.1158/1078-0432.CCR-16-0860

241. Hwang, Y. J., Lee, E. W., Song, J., Kim, H. R., Jun, Y. C., & Hwang, K. A. (2013). MafK positively regulates NF-κB activity by enhancing CBP-mediated p65 acetylation. *Scientific Reports*, *3*. https://doi.org/10.1038/srep03242

242. Han, R., Dermawan, J. K., Demicco, E. G., Ferguson, P. C., Griffin, A. M., Swanson, D., Antonescu, C. R., & Dickson, B. C. (2022). ZFP64::NCOA3 gene fusion defines a novel subset of spindle cell rhabdomyosarcoma. *Genes Chromosomes and Cancer*, *61*(11), 645–652. https://doi.org/10.1002/gcc.23052

243. Leclerc, D., Staats Pires, A. C., Guillemin, G. J., & Gilot, D. (2021). Detrimental activation of AhR pathway in cancer: an overview of therapeutic strategies. In *Current Opinion in Immunology* (Vol. 70, pp. 15–26). Elsevier Ltd. https://doi.org/10.1016/j.coi.2020.12.003

244. Elahi-Gedwillo, K. Y., Carlson, M., Zettervall, J., & Provenzano, P. P. (2019). Antifibrotic therapy disrupts stromal barriers and modulates the immune landscape in pancreatic ductal adenocarcinoma. *Cancer Research*, *79*(2), 372–386. https://doi.org/10.1158/0008-5472.CAN-18-1334

245. Zhou, Y., Tian, Q., Gao, H., Zhu, L., Zhang, Y., Zhang, C., Yang, J., & Wang, B. (2022). Immunity and Extracellular Matrix Characteristics of Breast Cancer Subtypes Based

on Identification by T Helper Cells Profiling. *Frontiers in Immunology*, *13*. https://doi.org/10.3389/fimmu.2022.859581

246. Jagroop, R., Martin, C. J., & Moorehead, R. A. (2021). Nidogen 1 regulates proliferation and migration/invasion in murine claudin-low mammary tumor cells. *Oncology Letters*, *21*(1). https://doi.org/10.3892/ol.2020.12313

247. Wu, Z., Wu, Z., Li, J., Yang, X., Wang, Y., Yu, Y., Ye, J., Xu, C., Qin, W., & Zhang, Z. (2012). MCAM is a novel metastasis marker and regulates spreading, apoptosis and invasion of ovarian cancer cells. *Tumor Biology*, *33*(5), 1619–1628. https://doi.org/10.1007/s13277-012-0417-0

248. Cui, Y., Li, Q., Li, W., Wang, Y., Lv, F., Shi, X., Tang, Z., Shen, Z., Hou, Y., Zhang, H., Mao, B., & Liu, T. (2021). NOTCH3 is a Prognostic Factor and Is Correlated With Immune Tolerance in Gastric Cancer. *Frontiers in Oncology*, *10*. https://doi.org/10.3389/fonc.2020.574937

249. Kayamori, K., Katsube, K. I., Sakamoto, K., Ohyama, Y., Hirai, H., Yukimori, A., Ohata, Y., Akashi, T., Saitoh, M., Harada, K., Harada, H., & Yamaguchi, A. (2016). Notch3 is induced in cancer-associated fibroblasts and promotes angiogenesis in oral squamous cell carcinoma. *PLoS ONE*, *11*(4). https://doi.org/10.1371/journal.pone.0154112

250. Wang, C. Y. Y., Wei, Q., Han, I., Sato, S., Ghanbari-Azarnier, R., Whetstone, H., Poon, R., Hu, J., Zheng, F., Zhang, P., Wang, W., Wunder, J. S., & Alman, B. A. (2012). Hedgehog and notch signaling regulate self-renewal of undifferentiated pleomorphic sarcomas. *Cancer Research*, *72*(4), 1013–1022. https://doi.org/10.1158/0008-5472.CAN-11-2531

251. Mosca, L., de Angelis, A., Ronchi, A., De Chiara, A., Fazioli, F., Ruosi, C., Altucci, L., Conte, M., & de Nigris, F. (2022). Sarcoma Common MHC-I Haplotype Restricts Tumor-Specific CD8+ T Cell Response. *Cancers*, *14*(14). https://doi.org/10.3390/cancers14143414

252. Armstrong, T. D., Clements, V. K., & Ostrand-Rosenberg, S. (1998). MHC Class II-Transfected Tumor Cells Directly Present Antigen to Tumor-Specific CD4+ T Lymphocytes. *The Journal of Immunology*, *160*(2), 661–666. https://doi.org/10.4049/jimmunol.160.2.661

253. Sawant, K. V., Poluri, K. M., Dutta, A. K., Sepuru, K. M., Troshkina, A., Garofalo, R. P., & Rajarathnam, K. (2016). Chemokine CXCL1 mediated neutrophil recruitment: Role of glycosaminoglycan interactions. *Scientific Reports*, *6*. https://doi.org/10.1038/srep33123

254. Mechtersheimer, G., Staudter, M., Majdic, O., Dörken, B., Moldenhauer, G., & Möller, P. (1990). Expression of HLA-A, B, C, β2-microglobulin (β2m), HLA-DR, -DP, -DQ and of

HLA-D-associated invariant chain (Ii) in soft-tissue tumors. *International Journal of Cancer*, *46*(5), 813–823. https://doi.org/10.1002/ijc.2910460512

255. Tsukahara, T., Kawaguchi, S., Torigoe, T., Asanuma, H., Nakazawa, E., Shimozawa, K., Nabeta, Y., Kimura, S., Kaya, M., Nagoya, S., Wada, T., Yamashita, T., & Sato, N. (2006). Prognostic significance of HLA class I expression in osteosarcoma defined by anti-pan HLA class I monoclonal antibody, EMR8-5. *Cancer Science*, *97*(12), 1374–1380. https://doi.org/10.1111/j.1349-7006.2006.00317.x

256. Rugh, K. M., Ashton, L. V., Schaffer, P. A., & Olver, C. S. (2024). Lymphoid Aggregates in Canine Cutaneous and Subcutaneous Sarcomas: Immunohistochemical and Gene Expression Evidence for Tertiary Lymphoid Structures. *Veterinary and Comparative Oncology*. https://doi.org/10.1111/vco.13020

257. Larsson, C., Ehinger, A., Winslow, S., Leandersson, K., Klintman, M., Dahl, L., Vallon-Christersson, J., Häkkinen, J., Hegardt, C., Manjer, J., Saal, L., Rydén, L., Malmberg, M., Borg, Å., & Loman, N. (2020). Prognostic implications of the expression levels of different immunoglobulin heavy chain-encoding RNAs in early breast cancer. *Npj Breast Cancer*, *6*(1). https://doi.org/10.1038/s41523-020-0170-2

258. Iglesia, M. D., Vincent, B. G., Parker, J. S., Hoadley, K. A., Carey, L. A., Perou, C. M., & Serody, J. S. (2014). Prognostic B-cell signatures using mRNA-seq in patients with subtype-specific breast and ovarian cancer. *Clinical Cancer Research*, *20*(14), 3818–3829. https://doi.org/10.1158/1078-0432.CCR-13-3368

259. Mei, H. E., Wirries, I., FrölichFr, D., Brisslert, M., Giesecke, C., GrünGr, J. R., Alexander, T., Schmidt, S., Luda, K., K, A. A., Engelmann, R., Scheel, T., Bokarewa, M., Perka, C., & Radbruch, A. (2015). *A unique population of IgG-expressing plasma cells lacking CD19 is enriched in human bone marrow*. https://doi.org/10.1182/blood-2014

260. Alimonti, J., Zhang, Q.-J., Gabathuler, R., Reid, G., Chen, S. S., & Jefferies, W. A. (2000). TAP expression provides a general method for improving the recognition of malignant cells in vivo. *NATURE BIOTECHNOLOGY*. http://biotech.nature.com

261. Krishnadas, D. K., Bao, L., Bai, F., Chencheri, S. C., & Lucas, K. (2014). Decitabine facilitates immune recognition of sarcoma cells by upregulating CT antigens, MHC molecules, and ICAM-1. *Tumor Biology*, *35*(6), 5753–5762. https://doi.org/10.1007/s13277-014-1764-9

262. van Niel, G., Wubbolts, R., ten Broeke, T., Buschow, S. I., Ossendorp, F. A., Melief, C. J., Raposo, G., van Balkom, B. W., & Stoorvogel, W. (2006). Dendritic Cells Regulate Exposure of MHC Class II at Their Plasma Membrane by Oligoubiquitination. *Immunity*, *25*(6), 885–894. https://doi.org/10.1016/j.immuni.2006.11.001

263. Seitz, S., Dreyer, T. F., Stange, C., Steiger, K., Bräuer, R., Scheutz, L., Multhoff, G., Weichert, W., Kiechle, M., Magdolen, V., & Bronger, H. (2022). CXCL9 inhibits tumour

growth and drives anti-PD-L1 therapy in ovarian cancer. *British Journal of Cancer*, *126*(10), 1470–1480. https://doi.org/10.1038/s41416-022-01763-0

264. Zeng, Z., Lan, T., Wei, Y., & Wei, X. (2022). CCL5/CCR5 axis in human diseases and related treatments. In *Genes and Diseases* (Vol. 9, Issue 1, pp. 12–27). Chongqing University. https://doi.org/10.1016/j.gendis.2021.08.004

265. Dangaj, D., Bruand, M., Grimm, A. J., Ronet, C., Barras, D., Duttagupta, P. A., Lanitis, E., Duraiswamy, J., Tanyi, J. L., Benencia, F., Conejo-Garcia, J., Ramay, H. R., Montone, K. T., Powell, D. J., Gimotty, P. A., Facciabene, A., Jackson, D. G., Weber, J. S., Rodig, S. J., … Coukos, G. (2019). Cooperation between Constitutive and Inducible Chemokines Enables T Cell Engraftment and Immune Attack in Solid Tumors. *Cancer Cell*, *35*(6), 885-900.e10. https://doi.org/10.1016/j.ccell.2019.05.004

266. Galpin, K. J. C., Rodriguez, G. M., Maranda, V., Cook, D. P., Macdonald, E., Murshed, H., Zhao, S., McCloskey, C. W., Chruscinski, A., Levy, G. A., Ardolino, M., & Vanderhyden, B. C. (2024). FGL2 promotes tumour growth and attenuates infiltration of activated immune cells in melanoma and ovarian cancer models. *Scientific Reports*, *14*(1). https://doi.org/10.1038/s41598-024-51217-1

267. Liu, W., Yin, H., Xie, Z., Fang, F., Chu, J., Yang, L., Huang, L., Tu, S., Cai, H., Wu, Z., Wei, A., Liu, C., Hong, Y., Tian, X., Cheng, Y., Pan, J., Wang, N., & Zhang, K. (2024). FYB1-targeted modulation of CAPG promotes AML progression. *Molecular and Cellular Biochemistry*. https://doi.org/10.1007/s11010-024-04992-4

268. Liang, Y. K., Deng, Z. K., Chen, M. T., Qiu, S. Q., Xiao, Y. S., Qi, Y. Z., Xie, Q., Wang, Z. H., Jia, S. C., Zeng, D., & Lin, H. Y. (2021). CXCL9 Is a Potential Biomarker of Immune Infiltration Associated With Favorable Prognosis in ER-Negative Breast Cancer. *Frontiers in Oncology*, *11*. https://doi.org/10.3389/fonc.2021.710286

269. Trost, M., English, L., Lemieux, S., Courcelles, M., Desjardins, M., & Thibault, P. (2009). The Phagosomal Proteome in Interferon-γ-Activated Macrophages. *Immunity*, *30*(1), 143–154. https://doi.org/10.1016/j.immuni.2008.11.006

270. Pai, C. C. S., Huang, J. T., Lu, X., Simons, D. M., Park, C., Chang, A., Tamaki, W., Liu, E., Roybal, K. T., Seagal, J., Chen, M., Hagihara, K., Wei, X. X., DuPage, M., Kwek, S. S., Oh, D. Y., Daud, A., Tsai, K. K., Wu, C., … Fong, L. (2019). Clonal Deletion of Tumor-Specific T Cells by Interferon-γ Confers Therapeutic Resistance to Combination Immune Checkpoint Blockade. *Immunity*, *50*(2), 477-492.e8. https://doi.org/10.1016/j.immuni.2019.01.006

271. Jing, Z. L., Liu, G. L., Zhou, N., Xu, D. Y., Feng, N., Lei, Y., Ma, L. L., Tang, M. S., Tong, G. H., Tang, N., & Deng, Y. J. (2024). Interferon-γ in the tumor microenvironment promotes the expression of B7H4 in colorectal cancer cells, thereby inhibiting cytotoxic T cells. *Scientific Reports*, *14*(1). https://doi.org/10.1038/s41598-024-56681-3

272. Liu, S., Han, B., Wang, R., & Fang, J. (2024). Elucidating the role of FOS in modulating the immune microenvironment through fibroblast and myeloid cell regulation in locoregional recurrent HNSCC. *Environmental Toxicology*. https://doi.org/10.1002/tox.24262

273. Duan, Z., & Luo, Y. (2021). Targeting macrophages in cancer immunotherapy. In *Signal Transduction and Targeted Therapy* (Vol. 6, Issue 1). Springer Nature. https://doi.org/10.1038/s41392-021-00506-6

274. Baron, V., Adamson, E. D., Calogero, A., Ragona, G., & Mercola, D. (2006). The transcription factor Egr1 is a direct regulator of multiple tumor suppressors including TGFβ1, PTEN, p53, and fibronectin. In *Cancer Gene Therapy* (Vol. 13, Issue 2, pp. 115–124). https://doi.org/10.1038/sj.cgt.7700896

275. Meyer, D., Seth, S., Albrecht, J., Maier, M. K., Du Pasquier, L., Ravens, I., Dreyer, L., Burger, R., Gramatzki, M., Schwinzer, R., Kremmer, E., Foerster, R., & Bernhardt, G. (2009). CD96 interaction with CD155 via its first Ig-like domain is modulated by alternative splicing or mutations in distal Ig-like domains. *Journal of Biological Chemistry*, *284*(4), 2235–2244. https://doi.org/10.1074/jbc.M807698200

276. Chan, C. J., Martinet, L., Gilfillan, S., Souza-Fonseca-Guimaraes, F., Chow, M. T., Town, L., Ritchie, D. S., Colonna, M., Andrews, D. M., & Smyth, M. J. (2014). The receptors CD96 and CD226 oppose each other in the regulation of natural killer cell functions. *Nature Immunology*, *15*(5), 431–438. https://doi.org/10.1038/ni.2850

277. Andreani, V., Ramamoorthy, S., Pandey, A., Lupar, E., Nutt, S. L., Lämmermann, T., & Grosschedl, R. (2018). Cochaperone Mzb1 is a key effector of Blimp1 in plasma cell differentiation and β1-integrin function. *Proceedings of the National Academy of Sciences of the United States of America*, *115*(41), E9630–E9639. https://doi.org/10.1073/pnas.1809739115

278. Yu, P., He, W., Zhang, Y., Hu, C., Wu, Y., Wang, Y., Bao, Z., Xia, Y., Zhang, R., Cao, M., Yuan, L., Cheng, X., & Xu, Z. (2022). SFRP4 Is a Potential Biomarker for the Prognosis and Immunotherapy for Gastric Cancer. *Journal of Oncology*, *2022*. https://doi.org/10.1155/2022/8829649

279. Mazzucchelli, R., & Durum, S. K. (2007). Interleukin-7 receptor expression: Intelligent design. In *Nature Reviews Immunology* (Vol. 7, Issue 2, pp. 144–154). https://doi.org/10.1038/nri2023

280. Yan, Y., Chen, R., Wang, X., Hu, K., Huang, L., Lu, M., & Hu, Q. (2019). CCL19 and CCR7 Expression, Signaling Pathways, and Adjuvant Functions in Viral Infection and Prevention. In *Frontiers in Cell and Developmental Biology* (Vol. 7). Frontiers Media S.A. https://doi.org/10.3389/fcell.2019.00212

281. Malhotra, P., Haslett, P., Sherry, B., Shepp, D. H., Barber, P., Abshier, J., Roy, U., & Schmidtmayerova, H. (2019). Increased Plasma Levels of the TH2 chemokine CCL18 associated with low CD4+ T cell counts in HIV-1-infected Patients with a Suppressed Viral Load. *Scientific Reports*, *9*(1). https://doi.org/10.1038/s41598-019-41588-1

282. Huang, H., Tan, M., Zheng, L., Yan, G., Li, K., Lu, D., Cui, X., He, S., Lei, D., Zhu, B., & Zhao, J. (2021). Prognostic implications of the complement protein c1q and its correlation with immune infiltrates in osteosarcoma. *OncoTargets and Therapy*, *14*, 1737–1751. https://doi.org/10.2147/OTT.S295063

283. Bulla, R., Tripodo, C., Rami, D., Ling, G. S., Agostinis, C., Guarnotta, C., Zorzet, S., Durigutto, P., Botto, M., & Tedesco, F. (2016). C1q acts in the tumour microenvironment as a cancer-promoting factor independently of complement activation. *Nature Communications*, *7*. https://doi.org/10.1038/ncomms10346

284. Chen, Y., Zhao, H., Feng, Y., Ye, Q., Hu, J., Guo, Y., & Feng, Y. (2021). Pan-Cancer Analysis of the Associations of TGFBI Expression With Prognosis and Immune Characteristics. *Frontiers in Molecular Biosciences*, *8*. https://doi.org/10.3389/fmolb.2021.745649

285. Zhang, B., Li, J., Hua, Q., Wang, H., Xu, G., Chen, J., Zhu, Y., Li, R., Liang, Q., Wang, L., Jin, M., Tang, J., Lin, Z., Zhao, L., Zhang, D., Yu, D., Ren, J., & Zhang, T. (2023). Tumor CEMIP drives immune evasion of colorectal cancer via MHC-I internalization and degradation. *Journal for ImmunoTherapy of Cancer*, *11*(1). https://doi.org/10.1136/jitc-2022-005592

286. Somers, G. R., Michael, H. O., Pienkowska, M., Shlien, A., Malkin, D., Ackerley, C., & Zielenska, M. (2010). IGF2 is highly expressed in pediatric undifferentiated sarcomas and reveals two distinct cytoplasmic trafficking patterns. *Pediatric and Developmental Pathology*, *13*(3), 169–177. https://doi.org/10.2350/09-02-0613-OA.1

287. Steigen, S. E., Schaeffer, D. F., West, R. B., & Nielsen, T. O. (2009). Expression of insulin-like growth factor 2 in mesenchymal neoplasms. *Modern Pathology*, *22*(7), 914–921. https://doi.org/10.1038/modpathol.2009.48

288. Torrejon, D. Y., Galvez, M., Abril-Rodriguez, G., Campbell, K. M., Medina, E., Vega-Crespo, A., Kalbasi, A., Comin-Anduix, B., & Ribas, A. (2023). Antitumor Immune Responses in B2M-Deficient Cancers. *Cancer Immunology Research*, *11*(12), 1642–1655. https://doi.org/10.1158/2326-6066.CIR-23-0139

289. Chen, H., Song, Y., Deng, C., Xu, Y., Xu, H., Zhu, X., Song, G., Tang, Q., & Wang, J. (2020). Comprehensive analysis of immune infiltration and gene expression for predicting survival in patients with sarcomas. *Aging*, *13*(2).

290. Xu, H., Chai, H., Chen, M., Zhu, R., Jiang, S., Liu, X., Wang, Y., Chen, J., Wei, J., Mao, Y., & Shi, Z. (2024). Single-cell RNA sequencing identifies a subtype of FN1 + tumor-

associated macrophages associated with glioma recurrence and as a biomarker for immunotherapy. *Biomarker Research*, *12*(1). https://doi.org/10.1186/s40364-024-00662-1

291. Revel, M., Sautès-Fridman, C., Fridman, W. H., & Roumenina, L. T. (2022). C1q+ macrophages: passengers or drivers of cancer progression. In *Trends in Cancer* (Vol. 8, Issue 7, pp. 517–526). Cell Press. https://doi.org/10.1016/j.trecan.2022.02.006

292. Crane, J. N., Graham, D. S., Mona, C. E., Nelson, S. D., Samiei, A., Dawson, D. W., Dry, S. M., Masri, M. G., Crompton, J. G., Benz, M. R., Czernin, J., Eilber, F. C., Graeber, T. G., Calais, J., & Federman, N. C. (2023). Fibroblast Activation Protein Expression in Sarcomas. *Sarcoma*, *2023*. https://doi.org/10.1155/2023/2480493

293. Broz, M. T., Ko, E. Y., Ishaya, K., Xiao, J., De Simone, M., Hoi, X. P., Piras, R., Gala, B., Tessaro, F. H. G., Karlstaedt, A., Orsulic, S., Lund, A. W., Chan, K. S., & Guarnerio, J. (2024). Metabolic targeting of cancer associated fibroblasts overcomes T-cell exclusion and chemoresistance in soft-tissue sarcomas. *Nature Communications*, *15*(1). https://doi.org/10.1038/s41467-024-46504-4

294. Sulsenti, R., Scialpi, G. B., Frossi, B., Botti, L., Ferri, R., Tripodi, I., Piva, A., Sangaletti, S., Pernici, D., Cancila, V., Romeo, F., Chiodoni, C., Lecis, D., Bianchi, F., Fischetti, I., Enriquez, C., Crivelli, F., Bregni, M., Renne, G., … Jachetti, E. (2024). Intracellular Osteopontin Promotes the Release of TNFα by Mast Cells to Restrain Neuroendocrine Prostate Cancer. *Cancer Immunology Research*, *12*(9), 1147–1169. https://doi.org/10.1158/2326-6066.CIR-23-0792

295. Alashkar Alhamwe, B., Ponath, V., Alhamdan, F., Dörsam, B., Landwehr, C., Linder, M., Pauck, K., Miethe, S., Garn, H., Finkernagel, F., Brichkina, A., Lauth, M., Tiwari, D. K., Buchholz, M., Bachurski, D., Elmshäuser, S., Nist, A., Stiewe, T., Pogge von Strandmann, L., … Pogge von Strandmann, E. (2024). BAG6 restricts pancreatic cancer progression by suppressing the release of IL33-presenting extracellular vesicles and the activation of mast cells. *Cellular and Molecular Immunology*, *21*(8), 918–931. https://doi.org/10.1038/s41423-024-01195-1

296. Tai, S. B., Lee, E. C. Y., Lim, B. Y., Kannan, B., Lee, J. Y., Guo, Z., Ko, T. K., Ng, C. C. Y., Teh, B. T., & Chan, J. Y. (2024). Tumor-Infiltrating Mast Cells in Angiosarcoma Correlate With Immuno-Oncology Pathways and Adverse Clinical Outcomes. *Laboratory Investigation*, *104*(3). https://doi.org/10.1016/j.labinv.2024.100323

297. Li, B., Power, M. R., & Lin, T.-J. (2006). *De novo synthesis of early growth response factor-1 is required for the full responsiveness of mast cells to produce TNF and IL-13 by IgE and antigen stimulation*. *107*, 2814–2820. https://doi.org/10.1182/blood

298. Nakae, S., Suto, H., Iikura, M., Kakurai, M., Sedgwick, J. D., Tsai, M., & Galli, S. J. (2006). Mast Cells Enhance T Cell Activation: Importance of Mast Cell Costimulatory

Molecules and Secreted TNF. *The Journal of Immunology*, *176*(4), 2238–2248. https://doi.org/10.4049/jimmunol.176.4.2238

299. Yuan, L. L., Chen, Z., Qin, J., Qin, C. J., Bian, J., Dong, R. F., Yuan, T. B., Xu, Y. T., Kong, L. Y., & Xia, Y. Z. (2022). Single-cell sequencing reveals the landscape of the tumor microenvironment in a skeletal undifferentiated pleomorphic sarcoma patient. *Frontiers in Immunology*, *13*. https://doi.org/10.3389/fimmu.2022.1019870

300. Crescioli, S., Correa, I., Ng, J., Willsmore, Z. N., Laddach, R., Chenoweth, A., Chauhan, J., Di Meo, A., Stewart, A., Kalliolia, E., Alberts, E., Adams, R., Harris, R. J., Mele, S., Pellizzari, G., Black, A. B. M., Bax, H. J., Cheung, A., Nakamura, M., … Karagiannis, S. N. (2023). B cell profiles, antibody repertoire and reactivity reveal dysregulated responses with autoimmune features in melanoma. *Nature Communications*, *14*(1). https://doi.org/10.1038/s41467-023-39042-y

301. Langfelder, P., & Horvath, S. (2012). Fast R Functions for Robust Correlations and Hierarchical Clustering. In *JSS Journal of Statistical Software* (Vol. 46). http://www.jstatsoft.org/

302. Villacis, R. A. R., Silveira, S. M., Barros-Filho, M. C., Marchi, F. A., Domingues, M. A. C., Scapulatempo-Neto, C., Aguiar, S., Lopes, A., Cunha, I. W., & Rogatto, S. R. (2014). Gene expression profiling in leiomyosarcomas and undifferentiated pleomorphic sarcomas: SRC as a new diagnostic marker. *PLoS ONE*, *9*(7). https://doi.org/10.1371/journal.pone.0102281

303. Beck, A. H., Lee, C. H., Witten, D. M., Gleason, B. C., Edris, B., Espinosa, I., Zhu, S., Li, R., Montgomery, K. D., Marinelli, R. J., Tibshirani, R., Hastie, T., Jablons, D. M., Rubin, B. P., Fletcher, C. D., West, R. B., & Van De Rijn, M. (2010). Discovery of molecular subtypes in leiomyosarcoma through integrative molecular profiling. *Oncogene*, *29*(6), 845–854. https://doi.org/10.1038/onc.2009.381

304. Mills, A. M., Beck, A. H., Montgomery, K. D., Zhu, S. X., Espinosa, I., Lee, C. H., Subramanian, S., Fletcher, C. D., Van De Rijn, M., & West, R. B. (2011). Expression of subtype-specific group 1 leiomyosarcoma markers in a wide variety of sarcomas by gene expression analysis and immunohistochemistry. *American Journal of Surgical Pathology*, *35*(4), 583–589. https://doi.org/10.1097/PAS.0b013e318211abd6

305. Hemming, M. L., Fan, C., Raut, C. P., Demetri, G. D., Armstrong, S. A., Sicinska, E., & George, S. (2020). Oncogenic gene-expression programs in leiomyosarcoma and characterization of conventional, inflammatory, and uterogenic subtypes. *Molecular Cancer Research*, *18*(9), 1302–1314. https://doi.org/10.1158/1541-7786.MCR-20-0197

306. Chen, Z., Lu, W., Garcia-Prieto, C., & Huang, P. (2007). The Warburg effect and its cancer therapeutic implications. In *Journal of Bioenergetics and Biomembranes* (Vol. 39, Issue 3, pp. 267–274). https://doi.org/10.1007/s10863-007-9086-x

307. Issaq, S. H., Teicher, B. A., & Monks, A. (2014). Bioenergetic properties of human sarcoma cells help define sensitivity to metabolic inhibitors. *Cell Cycle*, *13*(7), 1152–1161. https://doi.org/10.4161/cc.28010

308. Cancer Genome Atlas Research Network, Abeshouse, A., Adebamowo, C., Adebamowo, S. N., Akbani, R., Akeredolu, T., Ally, A., Anderson, M. L., Anur, P., Appelbaum, E. L., Armenia, J., Auman, J. T., Bailey, M. H., Baker, L., Balasundaram, M., Balu, S., Barthel, F. P., Bartlett, J., Baylin, S. B., … Zmuda, E. (2017). Comprehensive and Integrated Genomic Characterization of Adult Soft Tissue Sarcomas. *Cell*, *171*(4), 950-965.e28. https://doi.org/10.1016/j.cell.2017.10.014

309. Szeachowska, J., Dziegiel, P., Tarkowski, R., Gomuliewicz, A., Bebenek, M., Halon, A., Fortuna, K., Wojnar, A., Kornafel, J., & Matkowski, R. (2012). Therapeutic Radiation Induces Different Changes in Expression Profiles of Metallothionein (MT) mRNA, MT Protein, Ki 67 and Minichromosome Maintenance Protein 3 in Human Rectal Adenocarcinoma. *Anticancer Research*, *32*, 5291–5298.

310. Teramatsu, K., Oono, T., Oyama, K., Fujimori, N., Murakami, M., Yasumori, S., Ohno, A., Matsumoto, K., Takeno, A., Nakata, K., Nakamura, M., & Ogawa, Y. (2022). Circulating CD8+CD122+ T cells as a prognostic indicator of pancreatic cancer. *BMC Cancer*, *22*(1). https://doi.org/10.1186/s12885-022-10207-0

311. Sun, L., Jiao, A., Liu, H., Ding, R., Yuan, N., Yang, B., Zhang, C., Jia, X., Wang, G., Su, Y., Zhang, D., Shi, L., Sun, C., Zhang, A., Zhang, L., & Zhang, B. (2024). Targeting a disintegrin and metalloprotease (ADAM) 17-CD122 axis enhances CD8+ T cell effector differentiation and anti-tumor immunity. *Signal Transduction and Targeted Therapy*, *9*(1). https://doi.org/10.1038/s41392-024-01873-6

312. Ng, S. S., De Labastida Rivera, F., Yan, J., Corvino, D., Das, I., Zhang, P., Kuns, R., Chauhan, S. B., Hou, J., Li, X. Y., Frame, T. C. M., McEnroe, B. A., Moore, E., Na, J., Engel, J. A., Soon, M. S. F., Singh, B., Kueh, A. J., Herold, M. J., … Engwerda, C. R. (2020). The NK cell granule protein NKG7 regulates cytotoxic granule exocytosis and inflammation. *Nature Immunology*, *21*(10), 1205–1218. https://doi.org/10.1038/s41590-020-0758-6

313. Li, X. Y., Corvino, D., Nowlan, B., Aguilera, A. R., Ng, S. S., Braun, M., Cillo, A. R., Bald, T., Smyth, M. J., & Engwerda, C. R. (2022). NKG7 Is Required for Optimal Antitumor T-cell Immunity. *Cancer Immunology Research*, *10*(2), 154–161. https://doi.org/10.1158/2326-6066.CIR-20-0649

314. Zhang, S., Rozell, M., Verma, R. K., Albu, D. I., Califano, D., Van Valkenburgh, J., Merchant, A., Rangel-Moreno, J., Randall, T. D., Jenkins, N. A., Copeland, N. G., Liu, P., & Avram, D. (2010). Antigen-specific clonal expansion and cytolytic effector function of CD8+ T lymphocytes depend on the transcription factor Bcl11b. *Journal of Experimental Medicine*, *207*(8), 1687–1699. https://doi.org/10.1084/jem.20092136

315. Wisdom, A. J., Mowery, Y. M., Hong, C. S., Himes, J. E., Nabet, B. Y., Qin, X., Zhang, D., Chen, L., Fradin, H., Patel, R., Bassil, A. M., Muise, E. S., King, D. A., Xu, E. S., Carpenter, D. J., Kent, C. L., Smythe, K. S., Williams, N. T., Luo, L., … Kirsch, D. G. (2020). Single cell analysis reveals distinct immune landscapes in transplant and primary sarcomas that determine response or resistance to immunotherapy. *Nature Communications*, *11*(1). https://doi.org/10.1038/s41467-020-19917-0

316. Rooney, M. S., Shukla, S. A., Wu, C. J., Getz, G., & Hacohen, N. (2015). Molecular and genetic properties of tumors associated with local immune cytolytic activity. *Cell*, *160*(1–2), 48–61. https://doi.org/10.1016/j.cell.2014.12.033

317. Skelton, W., & Leslie, S. (2025, January). *Renal Angiomyolipoma*. https://www.ncbi.nlm.nih.gov/books/NBK585104/

318. Puccetti, L., Manetti, R., Parronchi, P., Piccinni, M. P., Mavilia, C., Carini, M., Romagnani, S., & Maggi, E. (2002). Role of low nuclear grading of renal carcinoma cells in the functional profile of tumor-infiltrating T cells. *International Journal of Cancer*, *98*(5), 674–681. https://doi.org/10.1002/ijc.10238

319. Knuttel, F. M., Waaijer, L., Merckel, L. G., van den Bosch, M. A. A. J., Witkamp, A. J., Deckers, R., & van Diest, P. J. (2016). Histopathology of breast cancer after magnetic resonance-guided high-intensity focused ultrasound and radiofrequency ablation. *Histopathology*, *69*(2), 250–259. https://doi.org/10.1111/his.12926

320. Medeiros, L. J., Michie, S. A., Johnson, D. E., Warnke, R. A., & Weiss, L. M. (n.d.). *An Immunoperoxidase Study of Renal Cell Carcinomas: Correlation With Nuclear Grade, Cell Type, and Histologic Pattern*.

321. Xia, J. Z., Xie, F. L., Ran, L. F., Xie, X. P., Fan, Y. M., & Wu, F. (2012). High-Intensity Focused Ultrasound Tumor Ablation Activates Autologous Tumor-Specific Cytotoxic T Lymphocytes. *Ultrasound in Medicine and Biology*, *38*(8), 1363–1371. https://doi.org/10.1016/j.ultrasmedbio.2012.03.009

322. Su, S., Liao, J., Liu, J., Huang, D., He, C., Chen, F., Yang, L. B., Wu, W., Chen, J., Lin, L., Zeng, Y., Ouyang, N., Cui, X., Yao, H., Su, F., Huang, J. D., Lieberman, J., Liu, Q., & Song, E. (2017). Blocking the recruitment of naive CD4+ T cells reverses immunosuppression in breast cancer. *Cell Research*, *27*(4), 461–482. https://doi.org/10.1038/cr.2017.34

323. Mo, Z., Liu, D., Chen, Y., Luo, J., Li, W., Liu, J., Yu, L., Huang, B., & Zhang, S. (2022). Single-cell transcriptomics reveals the role of Macrophage-Naïve CD4 + T cell interaction in the immunosuppressive microenvironment of primary liver carcinoma. *Journal of Translational Medicine*, *20*(1). https://doi.org/10.1186/s12967-022-03675-2

324. Zvirblyte, J., Nainys, J., Juzenas, S., Goda, K., Kubiliute, R., Dasevicius, D., Kincius, M., Ulys, A., Jarmalaite, S., & Mazutis, L. (2024). Single-cell transcriptional profiling of clear cell renal cell carcinoma reveals a tumor-associated endothelial tip cell

phenotype. *Communications Biology*, *7*(1). https://doi.org/10.1038/s42003-024-06478-x

325. Baldewijns, M. M., Thijssen, V. L., Van Den Eynden, G. G., Van Laere, S. J., Bluekens, A. M., Roskams, T., Van Poppel, H., De Bruïne, A. P., Griffioen, A. W., & Vermeulen, P. B. (2007). High-grade clear cell renal cell carcinoma has a higher angiogenic activity than low-grade renal cell carcinoma based on histomorphological quantification and qRT-PCR mRNA expression profile. *British Journal of Cancer*, *96*(12), 1888–1895. https://doi.org/10.1038/sj.bjc.6603796

326. Aziz, S. A., Sznol, J., Adeniran, A., Colberg, J. W., Camp, R. L., & Kluger, H. M. (2013). Vascularity of primary and metastatic renal cell carcinoma specimens. *Journal of Translational Medicine*, *11*(1). https://doi.org/10.1186/1479-5876-11-15

327. Braun, D. A., Street, K., Burke, K. P., Cookmeyer, D. L., Denize, T., Pedersen, C. B., Gohil, S. H., Schindler, N., Pomerance, L., Hirsch, L., Bakouny, Z., Hou, Y., Forman, J., Huang, T., Li, S., Cui, A., Keskin, D. B., Steinharter, J., Bouchard, G., … Wu, C. J. (2021). Progressive immune dysfunction with advancing disease stage in renal cell carcinoma. *Cancer Cell*, *39*(5), 632-648.e8. https://doi.org/10.1016/j.ccell.2021.02.013

328. Wu, Z., Zhou, J., Xiao, Y., Ming, J., Zhou, J., Dong, F., Zhou, X., Xu, Z., Zhao, X., Lei, P., & Huang, T. (2022). CD20+CD22+ADAM28+ B Cells in Tertiary Lymphoid Structures Promote Immunotherapy Response. *Frontiers in Immunology*, *13*. https://doi.org/10.3389/fimmu.2022.865596

329. Benedito, R., Roca, C., Sörensen, I., Adams, S., Gossler, A., Fruttiger, M., & Adams, R. H. (2009). The Notch Ligands Dll4 and Jagged1 Have Opposing Effects on Angiogenesis. *Cell*, *137*(6), 1124–1135. https://doi.org/10.1016/j.cell.2009.03.025

330. Leimeister, C., Schumacher, N., & Gessler, M. (2003). Expression of Notch pathway genes in the embryonic mouse metanephros suggests a role in proximal tubule development. *Gene Expression Patterns*, *3*(5), 595–598. https://doi.org/10.1016/S1567-133X(03)00114-5

331. Sjölund, J., Johansson, M., Manna, S., Norin, C., Pietras, A., Beckman, S., Nilsson, E., Ljungberg, B., & Axelson, H. (2008). Suppression of renal cell carcinoma growth by inhibition of Notch signaling in vitro and in vivo. *Journal of Clinical Investigation*, *118*(1), 217–228. https://doi.org/10.1172/JCI32086

332. Sitaram, R. T., Mallikarjuna, P., Landström, M., & Ljungberg, B. (n.d.). *Transforming growth factor-β promotes aggressiveness and invasion of clear cell renal cell carcinoma* (Vol. 7, Issue 24). www.impactjournals.com/oncotarget

333. Murray, I., & Paolini, M. (2025, January). *Histology, Kidney and Glomerulus*. https://www.ncbi.nlm.nih.gov/books/NBK554544/

334. Vorrink, S. U., & Domann, F. E. (2014). Regulatory crosstalk and interference between the and hypoxia sensing pathways at the AhR-ARNT-HIF1α signaling node. In *Chemico-Biological Interactions* (Vol. 218, pp. 82–88). Elsevier Ireland Ltd. https://doi.org/10.1016/j.cbi.2014.05.001

335. Li, S., Huang, C., Hu, G., Ma, J., Chen, Y., Zhang, J., Huang, Y., Zheng, J., Xue, W., Xu, Y., & Zhai, W. (2020). Tumor-educated B cells promote renal cancer metastasis via inducing the IL-1β/HIF-2α/Notch1 signals. *Cell Death and Disease*, *11*(3). https://doi.org/10.1038/s41419-020-2355-x

336. Chintala, S., Najrana, T., Toth, K., Cao, S., Durrani, F. A., Pili, R., & Rustum, Y. M. (2012). Prolyl hydroxylase 2 dependent and Von-Hippel-Lindau independent degradation of Hypoxia-inducible factor 1 and 2 alpha by selenium in clear cell renal cell carcinoma leads to tumor growth inhibition. *BMC Cancer*, *12*. https://doi.org/10.1186/1471-2407-12-293

337. Zhang, Z., Li, Q., Wang, F., Ma, B., Meng, Y., & Zhang, Q. (2021). Identifying Hypoxia Characteristics to Stratify Prognosis and Assess the Tumor Immune Microenvironment in Renal Cell Carcinoma. *Frontiers in Genetics*, *12*. https://doi.org/10.3389/fgene.2021.606816

338. Huang, D., Ding, Y., Luo, W. M., Bender, S., Qian, C. N., Kort, E., Zhang, Z. F., VandenBeldt, K., Duesbery, N. S., Resau, J. H., & Bin, T. T. (2008). Inhibition of MAPK kinase signaling pathways suppressed renal cell carcinoma growth and angiogenesis in vivo. *Cancer Research*, *68*(1), 81–88. https://doi.org/10.1158/0008-5472.CAN-07-5311

339. Huang, W. C., Tung, S. L., Chen, Y. L., Chen, P. M., & Chu, P. Y. (2018). IFI44L is a novel tumor suppressor in human hepatocellular carcinoma affecting cancer stemness, metastasis, and drug resistance via regulating met/Src signaling pathway. *BMC Cancer*, *18*(1). https://doi.org/10.1186/s12885-018-4529-9

340. Liu, P., Kong, X., Yi, S., Chen, Y., & Luo, W. (2024). IFIT3 accelerates the progression of head and neck squamous cell carcinoma by targeting PD-L1 to activate PI3K/AKT signaling pathway. *World Journal of Surgical Oncology*, *22*(1). https://doi.org/10.1186/s12957-023-03274-5

341. Brzostek-Racine, S., Gordon, C., Van Scoy, S., & Reich, N. C. (2011). The DNA Damage Response Induces IFN. *The Journal of Immunology*, *187*(10), 5336–5345. https://doi.org/10.4049/jimmunol.1100040

342. Zhang, X., Bobeica, M., Unger, M., Bednarz, A., Gerold, B., Patties, I., Melzer, A., & Landgraf, L. (2021). Focused ultrasound radiosensitizes human cancer cells by enhancement of DNA damage. *Strahlentherapie Und Onkologie*, *197*(8), 730–743. https://doi.org/10.1007/s00066-021-01774-5

343. Vuky, J., & Motzer, R. J. (2000). Cytokine therapy in renal cell cancer. In *Urologic Oncology* (Vol. 5).

344. Kasahara, T., Hooks, J. J., Dougherty, S. F., & Oppenheim', J. J. (1983). Interleukin 2-mediated immune interferon (IFN-gamma) production by human T cells and T cell subsets. *The Journal of Immunology*, *130*(4). http://journals.aai.org/jimmunol/article-pdf/130/4/1784/1020033/1784.pdf

345. Hoekstra, M. E., Slagter, M., Urbanus, J., Toebes, M., Slingerland, N., de Rink, I., Kluin, R. J. C., Nieuwland, M., Kerkhoven, R., Wessels, L. F. A., & Schumacher, T. N. (2024). Distinct spatiotemporal dynamics of CD8+ T cell-derived cytokines in the tumor microenvironment. *Cancer Cell*, *42*(1), 157-167.e9. https://doi.org/10.1016/j.ccell.2023.12.010

346. Matsushita, H., Hosoi, A., Ueha, S., Abe, J., Fujieda, N., Tomura, M., Maekawa, R., Matsushima, K., Ohara, O., & Kakimi, K. (2015). Cytotoxic T lymphocytes block tumor growth both by lytic activity and IFNγ-Dependent Cell-cycle arrest. *Cancer Immunology Research*, *3*(1), 26–36. https://doi.org/10.1158/2326-6066.CIR-14-0098

347. Kang, K., Park, S. H., Chen, J., Qiao, Y., Giannopoulou, E., Berg, K., Hanidu, A., Li, J., Nabozny, G., Kang, K., Park-Min, K. H., & Ivashkiv, L. B. (2017). Interferon-γ Represses M2 Gene Expression in Human Macrophages by Disassembling Enhancers Bound by the Transcription Factor MAF. *Immunity*, *47*(2), 235-250.e4. https://doi.org/10.1016/j.immuni.2017.07.017

348. Xie, C., Liu, C., Wu, B., Lin, Y., Ma, T., Xiong, H., Wang, Q., Li, Z., Ma, C., & Tu, Z. (2016). Effects of IRF1 and IFN-interaction on the M1 polarization of macrophages and its antitumor function. *International Journal of Molecular Medicine*, *38*(1), 148–160. https://doi.org/10.3892/ijmm.2016.2583

349. Langbein, L. E., El Hajjar, R., He, S., Sementino, E., Zhong, Z., Jiang, W., Leiby, B. E., Li, L., Uzzo, R. G., Testa, J. R., & Yang, H. (2022). BAP1 maintains HIF-dependent interferon beta induction to suppress tumor growth in clear cell renal cell carcinoma. *Cancer Letters*, *547*. https://doi.org/10.1016/j.canlet.2022.215885

350. Lei, X., de Groot, D. C., Welters, M. J. P., de Wit, T., Schrama, E., van Eenennaam, H., Santegoets, S. J., Oosenbrug, T., van der Veen, A., Vos, J. L., Zuur, C. L., de Miranda, N. F. C. C., Jacobs, H., van der Burg, S. H., Borst, J., & Xiao, Y. (2024). CD4+ T cells produce IFN-I to license cDC1s for induction of cytotoxic T-cell activity in human tumors. *Cellular and Molecular Immunology*, *21*(4), 374–392. https://doi.org/10.1038/s41423-024-01133-1

351. Hashimoto, H., Ueda, R., Narumi, K., Heike, Y., Yoshida, T., & Aoki, K. (2014). Type I IFN gene delivery suppresses regulatory T cells within tumors. *Cancer Gene Therapy*, *21*(12), 532–541. https://doi.org/10.1038/cgt.2014.60

352. Cao, X., Liang, Y., Hu, Z., Li, H., Yang, J., Hsu, E. J., Zhu, J., Zhou, J., & Fu, Y. X. (2021). Next generation of tumor-activating type I IFN enhances anti-tumor immune responses to overcome therapy resistance. *Nature Communications*, *12*(1). https://doi.org/10.1038/s41467-021-26112-2

353. Liu, W., Peng, J., Xiao, M., Cai, Y., Peng, B., Zhang, W., Li, J., Kang, F., Hong, Q., Liang, Q., Yan, Y., & Xu, Z. (2023). The implication of pyroptosis in cancer immunology: Current advances and prospects. In *Genes and Diseases* (Vol. 10, Issue 6, pp. 2339–2350). KeAi Communications Co. https://doi.org/10.1016/j.gendis.2022.04.019

354. He, F., He, Z., & Wang, C. (2024). A novel role of AIM2 inflammasome-mediated pyroptosis in radiofrequency ablation of hepatocellular carcinoma. *Annals of Hepatology*, *29*(6). https://doi.org/10.1016/j.aohep.2024.101532

355. Xie, Y., Chen, Z., Zhong, Q., Zheng, Z., Chen, Y., Shangguan, W., Zhang, Y., Yang, J., Zhu, D., & Xie, W. (2021). M2 macrophages secrete CXCL13 to promote renal cell carcinoma migration, invasion, and EMT. *Cancer Cell International*, *21*(1). https://doi.org/10.1186/s12935-021-02381-1

356. Chen, S., Qian, S., Zhang, L., Pan, X., Qu, F., Yu, Y., Gu, Z., Cui, X., & Shen, H. (2022). Tumor-associated macrophages promote migration and invasion via modulating IL-6/STAT3 signaling in renal cell carcinoma. *International Immunopharmacology*, *111*. https://doi.org/10.1016/j.intimp.2022.109139

357. Jorgovanovic, D., Song, M., Wang, L., & Zhang, Y. (2020). Roles of IFN-γin tumor progression and regression: A review. In *Biomarker Research* (Vol. 8, Issue 1). BioMed Central Ltd. https://doi.org/10.1186/s40364-020-00228-x

358. Liu, J., Guan, X., & Ma, X. (2005). Interferon regulatory factor 1 is an essential and direct transcriptional activator for interferon γ-induced RANTES/CCL5 expression in macrophages. *Journal of Biological Chemistry*, *280*(26), 24347–24355. https://doi.org/10.1074/jbc.M500973200

359. Dai, H., Wan, N., Zhang, S., Moore, Y., Wan, F., & Dai, Z. (2010). Cutting Edge: Programmed Death-1 Defines CD8+CD122+ T Cells as Regulatory versus Memory T Cells. *The Journal of Immunology*, *185*(2), 803–807. https://doi.org/10.4049/jimmunol.1000661

360. Hendriks, J., Gravestein, L., Tesselaar, K., van Lier, R., Schumacher, T., & Borst, J. (2000). CD27 is required for generation and long-term maintenance of T cell immunity. *Nature Immunology*.

361. Aulwurm, S., Wischhusen, J., Friese, M., Borst, J., & Weller, M. (2006). Immune stimulatory effects of CD70 override CD70-mediated immune cell apoptosis in rodent glioma models and confer long-lasting antiglioma immunity in vivo. *International Journal of Cancer*, *118*(7), 1728–1735. https://doi.org/10.1002/ijc.21544

362. Lichtenstein, L., Mattijssen, F., De Wit, N. J., Georgiadi, A., Hooiveld, G. J., Van Der Meer, R., He, Y., Qi, L., Köster, A., Tamsma, J. T., Tan, N. S., Müller, M., & Kersten, S. (2010). Angptl4 protects against severe proinflammatory effects of saturated fat by inhibiting fatty acid uptake into mesenteric lymph node macrophages. *Cell Metabolism*, *12*(6), 580–592. https://doi.org/10.1016/j.cmet.2010.11.002

363. Li, Y., Chen, S., Yang, Q., Liu, X., Zhou, W., Kang, T., Wu, W., & Ou, S. (2024). The ANGPTL4-HIF-1α loop: a critical regulator of renal interstitial fibrosis. *Journal of Translational Medicine*, *22*(1). https://doi.org/10.1186/s12967-024-05466-3

364. M H van Dierendonck, X. A., Vrieling, F., Smeehuijzen, L., Deng, L., Boogaard, J. P., Croes, C.-A., Temmerman, L., Wetzels, S., Biessen, E., Kersten, S., Stienstra, R., & by Katherine Fitzgerald, E. (2022). *Triglyceride breakdown from lipid droplets regulates the inflammatory response in macrophages*. https://doi.org/10.1073/pnas

365. Hiratsuka, S., Maru, Y., Okada, A., Seiki, M., Noda, T., & Shibuya, M. (2001). Involvement of Flt-1 Tyrosine Kinase (Vascular Endothelial Growth Factor Receptor-1) in Pathological Angiogenesis 1. In *CANCER RESEARCH* (Vol. 61). http://aacrjournals.org/cancerres/article-pdf/61/3/1207/3252010/ch030101207p.pdf

366. Wu, F., Wang, Z. B., Chen, W. Z., Wang, W., Gui, Y., Zhang, M., Zheng, G., Zhou, Y., Xu, G., Li, M., Zhang, C., Ye, H., & Feng, R. (2004). Extracorporeal high intensity focused ultrasound ablation in the treatment of 1038 patients with solid carcinomas in China: An overview. *Ultrasonics Sonochemistry*, *11*(3–4), 149–154. https://doi.org/10.1016/j.ultsonch.2004.01.011

367. Tu, H., Hu, Q., Ma, Y., Huang, J., Luo, H., Jiang, L., Zhang, S., Jiang, C., Lai, H., Liu, J., Chen, J., Guo, L., Yang, G., Xu, K., Chi, H., & Chen, H. (2024). Deciphering the tumour microenvironment of clear cell renal cell carcinoma: Prognostic insights from programmed death genes using machine learning. *Journal of Cellular and Molecular Medicine*, *28*(13). https://doi.org/10.1111/jcmm.18524

368. Wang, Y., Yan, K., Lin, J., Li, J., & Bi, J. (2021). Macrophage M2 Co-expression Factors Correlate With the Immune Microenvironment and Predict Outcome of Renal Clear Cell Carcinoma. *Frontiers in Genetics*, *12*. https://doi.org/10.3389/fgene.2021.615655

369. Chen, F. W., Wu, Y. L., Cheng, C. C., Hsiao, Y. W., Chi, J. Y., Hung, L. Y., Chang, C. P., Lai, M. D., & Wang, J. M. (2024). Inactivation of pentraxin 3 suppresses M2-like macrophage activity and immunosuppression in colon cancer. *Journal of Biomedical Science*, *31*(1). https://doi.org/10.1186/s12929-023-00991-7

370. Cai, Q., Que, Y., & Zhang, X. (2024). Neoadjuvant immunotherapy in the evolving landscape of sarcoma treatment. In *Journal for immunotherapy of cancer* (Vol. 12, Issue 11). https://doi.org/10.1136/jitc-2024-010074

371. Pilavaki, P., Panagi, M., Arifi, S., Jones, R. L., Stylianopoulos, T., & Constantinidou, A. (2023). Exploring the landscape of immunotherapy approaches in sarcomas. In *Frontiers in Oncology* (Vol. 12). Frontiers Media S.A. https://doi.org/10.3389/fonc.2022.1069963

372. Martín-Broto, J., Moura, D. S., & van Tine, B. A. (2020). Facts and hopes in immunotherapy of soft-tissue sarcomas. In *Clinical Cancer Research* (Vol. 26, Issue 22, pp. 5801–5808). American Association for Cancer Research Inc. https://doi.org/10.1158/1078-0432.CCR-19-3335

# Supplementary Figures

Oxford Radcliffe Biobank
NDCLS, Level 4, Academic Block
University of Oxford
John Radcliffe Hospital, Headley Way
Headington Oxford OX3 9DU

T +44 (0) 1865 220550
E orbmanager@ndcls.ox.ac.uk

Dr. Paul Lyon

13/08/2024

Department of Radiology, Churchill Hospital

Re Biobank reference **24/A082**

Dear Dr Lyon

**Pilot Tissue to Characterise Immune Response to HIFU Treatment in Renal Cancer**

I am writing to inform you that the above named project is approved under the Oxford Radcliffe Biobank (ORB) research tissue bank ethics, reference 19/SC/0173. Please find attached a copy of the ORB approval letter from NRES Committee South Central – Oxford C as confirmation of this approval.
The favourable ethical opinion applies to this research project conducted in the UK using the material supplied by the tissue bank, provided that the release of material complies with the attached NRES conditions. Also attached is your finalised OCHRe application form with the ORB/OCHRe Terms and Conditions as an appendix (note in particular sections 3.3, 3.4 and 3.11).
Please note that this approval applies to this specific research project only. Any further work or deviation from the project as outlined in the application form would require further committee review and approval. Examples of changes that would require further review would include sharing the samples with other researchers or performing a different test or assay.
We ask that any publication or presentation that is based (in whole or in part) on materials obtained via the Oxford Centre for Histopathology Research (OCHRe) or ORB will include the following standard acknowledgement: "We acknowledge the contribution to this study made by the Oxford Centre for Histopathology Research and the Oxford Radcliffe Biobank, which are funded by the University of Oxford, the Oxford CRUK Cancer centre, and the NIHR CRN Thames Valley network." You should provide to ORB a copy of any publication(s) based on work derived from the material provided.
NOTE FOR ACCESS TO THE DIAGNOSTIC ARCHIVE: only recent cases from the diagnostic archive are held in Oxford, the rest have to be recalled from the off-site archive (CellNass) and we recover these costs from researchers. Due to our limited storage capacity in OCHRe, any specimens recalled from CellNass may be returned to them at any point after 12 weeks of a batch being completed and collected by the research team. Any repeat requests will incur recall charges again.
Please note it is your responsibility to ensure you destroy all remaining human tissue at the end of the project, or return it to us. Failure to do this is a breach of the Human Tissue Act and the terms of the University of Oxford's Human Tissue Authority licence. All staff working with human tissue must complete HTA training (this is accessed from the MRC Regulatory Support Centre Learning Management System: https://byglearning.com/mrcrsc-lms/login/index.php).

Yours sincerely

;

David Maldonado-Perez
ORB Collections Governance Manager

Supplementary Figure 2.1: Ethical approval letter from Oxford Radcliffe Biobank for the use of renal cell carcinoma tissue within this study.

Oxford Radcliffe Biobank
NDCLS, Level 4, Academic Block
University of Oxford
John Radcliffe Hospital, Headley Way
Headington Oxford OX3 9DU

T +44 (0) 1865 220550
E orbmanager@ndcls.ox.ac.uk

Dr. Paul LYONS

08/02/2022

Department of Radiology,
Churchill Hospital
Oxford University Hospitals

Re Biobank reference **22/A020**

Dear Dr Lyons

**SarcAblate: A pilot study in HIFU ablation of soft tissue sarcoma**

I am writing to inform you that the above named project is approved under the Oxford Radcliffe Biobank (ORB) research tissue bank ethics, reference 19/SC/0173. Please find attached a copy of the ORB approval letter from NRES Committee South Central – Oxford C as confirmation of this approval.

The favourable ethical opinion applies to this research project conducted in the UK using the material supplied by the tissue bank, provided that the release of material complies with the attached NRES conditions. Also attached is your finalised OCHRe application form with the ORB/OCHRe Terms and Conditions as an appendix (note in particular sections 3.3, 3.4 and 3.11).

Please note that this approval applies to this specific research project only. Any further work or deviation from the project as outlined in the application form would require further committee review and approval. Examples of changes that would require further review would include sharing the samples with other researchers or performing a different test or assay.

We ask that any publication or presentation that is based (in whole or in part) on materials obtained via the Oxford Centre for Histopathology Research (OCHRe) or ORB will include the following standard acknowledgement: "We acknowledge the contribution to this study made by the Oxford Centre for Histopathology Research and the Oxford Radcliffe Biobank, which are funded by the University of Oxford, the Oxford CRUK Cancer centre, the NIHR Oxford Biomedical Research Centre (BRC) (Molecular Diagnostics Theme/Multimodal Pathology Subtheme and the NIHR CRN Thames Valley network." You should provide to ORB a copy of any publication(s) based on work derived from the material provided.

NOTE FOR ACCESS TO THE DIAGNOSTIC ARCHIVE: only recent cases from the diagnostic archive are held in Oxford, the rest have to be recalled from the off-site archive (CellNass) and we recover these costs from researchers. Due to our limited storage capacity in OCHRe, any specimens recalled from CellNass may be returned to them at any point after 12 weeks of a batch being completed and collected by the research team. Any repeat requests will incur recall charges again.

Please note it is your responsibility to ensure you destroy all remaining human tissue at the end of the project, or return it to us. Failure to do this is a breach of the Human Tissue Act and the terms of the University of Oxford's Human Tissue Authority licence. All staff working with human tissue must complete HTA training (this is accessed from the MRC Regulatory Support Centre Learning Management System: https://byglearning.com/mrcrsc-lms/login/index.php).

Yours sincerely

Supplementary Figure 2.2: Ethical approval letter from Oxford Radcliffe Biobank for the use of soft tissue sarcoma tissue within this study.

COPY for information only,
OCHRe ref: 24/A082

NHS
Health Research Authority

**South Central - Oxford C Research Ethics Committee**
Level 3, Block B
Whitefriars Building
Lewins Mead
Bristol
BS1 2NT
Telephone: 0207 1048 045

07 May 2019

Dr Stephanie G Jones
University of Oxford
Nuffield Department of Surgical Sciences
Level 6, John Radcliffe Hospital
Oxford
OX3 9DU

Dear Dr Jones

| | |
|---|---|
| **Title of the Research Tissue Bank:** | **Oxford Radcliffe Biobank** |
| **REC reference:** | **19/SC/0173** |
| **Designated Individual:** | **Dr Brian Shine** |
| **IRAS project ID:** | **262470** |

The Research Ethics Committee reviewed the above application at the meeting held on 29 March 2019. Thank you for attending to discuss the application.

We plan to publish your research summary wording for the Research Tissue Bank on the HRA website, together with your contact details. Publication will be no earlier than three months from the date of this favourable opinion letter. The expectation is that this information will be published for all Research Tissue Banks that receive an ethical opinion but should you wish to provide a substitute contact point, wish to make a request to defer, or require further information, please contact hra.studyregistration@nhs.net outlining the reasons for your request. Under very limited circumstances (e.g. for student research which has received an unfavourable opinion), it may be possible to grant an exemption to the publication of the research summary for the tissue bank

**Ethical opinion**

The members of the Committee present gave a favourable ethical opinion of the above research tissue bank on the basis described in the application form and supporting documentation, subject to the conditions specified below.

The Committee has also confirmed that the favourable ethical opinion applies to all research projects conducted in the UK using tissue or data supplied by the tissue bank, provided that the release of the tissue or data complies with the attached conditions. It will not be necessary for these researchers to make project-based applications for ethical approval. They will be deemed to have ethical approval from this committee. You should provide the researcher with a copy of this letter as confirmation of this. The Committee should be notified of all projects receiving tissue and data from the tissue bank by means of an annual report.

This application was for the renewal of a Research Tissue Bank application. The previous REC Reference number for this application was 09/H0606/5+5.

COPY for information only,
OCHRe ref: 23/A035

NHS
Health Research Authority

**Conditions of the favourable opinion**

The favourable opinion is subject to the following conditions being met prior to the start of the Research Tissue Bank.

1. The Committee requested that the PIS and CF were made consistent on the point of feedback of results.

**You should notify the REC once all conditions have been met (except for site approvals from host organisations) and provide copies of any revised documentation with updated version numbers. Revised documents should be submitted to the REC electronically from IRAS. The REC will acknowledge receipt and provide a final list of the approved documentation for the Research Tissue Bank, which can be made available to host organisations to facilitate their permission for the Research Tissue Bank. Failure to provide the final versions to the REC may cause delay in obtaining permissions.**

**Research governance**

Under the UK Policy Framework for Health and Social Care Research, there is no requirement for NHS research permission for the establishment of research tissue banks in the NHS. Applications to NHS R&D offices through IRAS are not required as all NHS organisations are expected to have included management review in the process of establishing the research tissue bank.

Research permission is also not required by collaborators at tissue collection centres (TCCs) who provide tissue or data under the terms of a supply agreement between the organisation and the research tissue bank. TCCs are not research sites for the purposes of the RGF.

Research tissue bank managers are advised to provide R&D offices at all TCCs with a copy of the REC application for information, together with a copy of the favourable opinion letter when available. All TCCs should be listed in Part C of the REC application.

NHS researchers undertaking specific research projects using tissue or data supplied by the research tissue bank must apply for permission to R&D offices at all organisations where the research is conducted, whether or not the research tissue bank has ethical approval.

Site-specific assessment (SSA) is not a requirement for ethical review of research tissue banks.

**Registration of Research Tissue Banks**

It is a condition of the ethical approval that all Research Tissue Banks are registered on the UK Clinical Research Collaboration (UKCRC) Tissue Directory. The Research Tissue Bank should be registered no later than 6 weeks after the date of this favourable ethical opinion letter or 6 weeks after the Research Tissue Bank holds tissue with the intention to provide for research purposes. Please use the following link to register the Research Tissue Bank on the UKCRC Directory: https://directory.biobankinguk.org/Register/Biobank Registration is defined as having added details of the types of tissue samples held in the tissue bank.

COPY for information only,
OCHRe ref: 23/A035

NHS
Health Research Authority

There is no requirement to separately notify the REC but you should do so at the earliest opportunity e.g. when submitting an amendment or when submitting an annual progress report. We will monitor the registration details as part of the annual progress reporting process.

[redacted]

COPY for information only,
OCHRe ref: 23/A035

NHS
Health Research Authority

[redacted]

**Duration of ethical opinion**

The favourable opinion has been renewed for five years from the end of the previous five year period provided that you comply with the standard conditions of ethical approval for Research Tissue Banks set out in the attached document. You are advised to study the conditions carefully. The opinion may be renewed for a further period of up to five years on receipt of a fresh application. It is suggested that the fresh application is made 3-5 months before the 5 years expires, to ensure continuous approval for the research tissue bank.

**Research Tissue Bank Renewals**

The previous five year period ran from 11 December 2013 to 11 December 2018. This Research Tissue Bank may be renewed for further periods of five years at a time by following the process described in the above paragraph. This Research Tissue Bank may be renewed for further periods of five years at a time by following the process described in the above paragraph.

COPY for information only,
OCHRe ref: 23/A035

NHS
Health Research Authority

**Approved documents**

The documents reviewed and approved at the meeting were:

| *Document* | *Version* | *Date* |
|---|---|---|
| Covering letter on headed paper [Cover letter] | | 11 March 2019 |
| Human Tissue Authority licence [HTA licence] | | 17 November 2017 |
| IRAS Checklist XML [Checklist_13032019] | | 13 March 2019 |
| Other [Protocol Annex 1 collection leads] | 4 | 26 February 2019 |
| Other [Protocol Annex 2 Ethically approved collections] | 2 | 26 February 2019 |
| Other [Protocol Annex 3 Projects currently supported by ORB] | 2 | 27 February 2019 |
| Other [Protocol Annex 4 Pathway for verification and feedback incidental findings] | 2 | 03 March 2017 |
| Other [Protocol Annex 5 Collection centres] | 4 | 27 February 2019 |
| Other [Protocol Annex 6 ORB UTrust SLA] | n/a | 16 April 2012 |
| Other [Protocol Annex 10 CV Clare Verrill] | n/a | 27 February 2019 |
| Other [Protocol Annex 11 Casablanca questionnaire] | 1 | 04 January 2010 |
| Other [ORB poster Healthy volunteers] | 3 | 05 February 2019 |
| Other [ORB Privacy notice website wording] | 1 | 12 September 2018 |
| Other [Annual report for 2017 activity] | 1 | 06 August 2018 |
| Other [Sponsor letter of approval] | n/a | 12 March 2019 |
| Other [Sponsor insurance certificate] | n/a | 04 September 2018 |
| Other [Protocol Annex 7 MTA template] | n/a | 11 March 2019 |
| Other [Protocol Annex 10 CV Stephanie Jones] | n/a | 08 August 2019 |
| Other [Access policy ORB] | 4 | 11 March 2019 |
| Participant consent form [OUH consent form 1] | 04/13 | 01 April 2013 |
| Participant consent form [OUH consent form 3] | 10/13 | 01 October 2013 |
| Participant consent form [ORB Consent form adult clinically relevant genomics] | 5 | 05 February 2019 |
| Participant consent form [ORB Consent form general] | 5 | 05 February 2019 |
| Participant consent form [ORB consent form Healthy volunteers] | 3 | 05 February 2019 |
| Participant consent form [ORB Assent Child clinically relevant genomics] | 2 | 05 February 2019 |
| Participant consent form [ORB Proctoscope Consent form] | 2 | 05 February 2019 |
| Participant information sheet (PIS) [ORB Proctoscope PIS] | 2 | 05 February 2019 |
| Participant information sheet (PIS) [ORB PIS general] | 4 | 05 February 2019 |
| Participant information sheet (PIS) [ORB PIS Child 0-7 clinically relevant genomics] | 2 | 05 February 2019 |
| Participant information sheet (PIS) [OUH NHS tissue for research leaflet] | none | 24 October 2013 |
| Participant information sheet (PIS) [ORB PIS Child 8-11 clinically relevant genomics] | | 05 February 2019 |
| Participant information sheet (PIS) [ORB PIS Child 12-15 clinically | 3 | 05 February 2019 |

COPY for information only,
OCHRe ref: 23/A035

NHS
Health Research Authority

| | | |
|---|---|---|
| relevant genomics] | | |
| Participant information sheet (PIS) [ORB PIS clinically relevant genomics] | 4 | 05 February 2019 |
| Participant information sheet (PIS) [ORB PIS Healthy volunteers] | 3 | 05 February 2019 |
| Participant information sheet (PIS) [ORB PIS Child 8-11 clinically relevant genomics] | 2 | 05 February 2019 |
| Protocol for management of the tissue bank [ORB Protocol v8.0] | 8 | 07 March 2019 |
| REC Application Form [RTB_Form_13032019] | | 13 March 2019 |
| Relative consent form [OUH consent form 2] | 9/13 | 01 September 2013 |
| Relative consent form [ORB Consent form Parental clinically relevant genomics] | 5 | 05 February 2019 |
| Relative information sheet [ORB PIS Parental clinically relevant genomics] | 4 | 05 February 2019 |
| Summary of research programme(s) [ORB Research programme] | 1 | 27 February 2019 |

**Licence from the Human Tissue Authority**

Thank you for providing a copy of the above licence.

**Membership of the Committee**

The members of the Ethics Committee who were present at the meeting are listed on the attached sheet.

**Statement of compliance**

The Committee is constituted in accordance with the Governance Arrangements for Research Ethics Committees and complies fully with the Standard Operating Procedures for Research Ethics Committees in the UK.

**After ethical review**

Reporting requirements

The attached standard conditions give detailed guidance on reporting requirements for research tissue banks with a favourable opinion, including:

- Notifying substantial amendments
- Submitting Annual Progress reports

The HRA website also provides guidance on these topics, which is updated in the light of changes in reporting requirements or procedures.

**User Feedback**

The Health Research Authority is continually striving to provide a high quality service to all applicants and sponsors. You are invited to give your view of the service you have received and the application procedure. If you wish to make your views known please use the feedback form

COPY for information only,
OCHRe ref: 23/A035

NHS
Health Research Authority

available on the HRA website:
http://www.hra.nhs.uk/about-the-hra/governance/quality-assurance/

**HRA Learning**

We are pleased to welcome researchers and research staff to our HRA Learning Events and online learning opportunities– see details at:
https://www.hra.nhs.uk/planning-and-improving-research/learning/

| 19/SC/0173 | Please quote this number on all correspondence |
|---|---|

Yours sincerely

PP

**Mrs Susan Lousada**
**Chair**

E-mail: nrescommittee.southcentral-oxfordc@nhs.net

*Enclosures:* *List of names and professions of members who were present at the meeting and those who submitted written comments*

*Standard approval conditions*

*Copy to:* *Dr Brian Shine, University of Oxford*

COPY for information only,
OCHRe ref: 23/A035

NHS
Health Research Authority

**South Central - Oxford C Research Ethics Committee**

**Attendance at Committee meeting on 29 March 2019**

**Committee Members:**

| *Name* | *Profession* | *Present* | *Notes* |
|---|---|---|---|
| Dr Leonard Brookes | Consultant to the Pharmaceutical Industry | Yes | |
| Mr David Carpenter | Retired Social Scientist | Yes | |
| Dr Linda Cartwright | Retired Consultant Epidemiologist | Yes | |
| Dr Ben Caswell | Accountant | Yes | |
| Mrs Rebekah Howe | Farmer | No | |
| Mrs Vivienne Laurie | Barrister | Yes | |
| Mrs Susan Lousada | Company Director (Property) & Non-legal member of first-tier tax tribunal | Yes | |
| Mr Barry Muir | NHS Management Consultant (Retired) | Yes | |
| Dr Lee Potiphar | Lecturer in Adult Nursing (Evidence Based Practice) | Yes | |
| Ms Anna Rathmell | Medical Manager - GI | Yes | |
| Dr Pamela Susan Ross | GP Principal | Yes | |
| Dr Sabeena Sharma | Consultant Anaesthetist | Yes | |
| Ms Kayleigh Stanbury | Trial Coordinator and Developmental Assessor | No | |

**Also in attendance:**

| *Name* | *Position (or reason for attending)* |
|---|---|
| Miss Charlotte Ferris | REC Manager |

NHS
Health Research Authority
South Central - Oxford C Research Ethics Committee
Level 3, Block B
Whitefriars Building
Lewins Mead
Bristol
BS1 2NT

Telephone: 0207 104 8210

06 June 2019

Dr Stephanie G Jones
University of Oxford
Nuffield Department of Surgical Sciences
Level 6, John Radcliffe Hospital
Oxford
OX3 9DU

Dear Dr Jones

**Title of the Database:** **Oxford Radcliffe Biobank**
**Designated Individual:** **Dr Brian Shine**
**REC reference:** **19/SC/0173**
**IRAS project ID:** **262470**

Thank you for your letter of 17 May 2019. I can confirm the REC has received the documents listed below and that these comply with the approval conditions detailed in our letter dated 12 April 2019.

**Documents received**

The documents received were as follows:

| *Document* | *Version* | *Date* |
|---|---|---|
| IRAS Checklist XML [Checklist_17052019] | | 17 May 2019 |
| Participant information sheet (PIS) [ORB PIS Healthy volunteers] | 4 | 17 May 2019 |

**Approved documents**

The final list of approved documentation for the study is therefore as follows:

| *Document* | *Version* | *Date* |
|---|---|---|
| Covering letter on headed paper [Cover letter] | | 11 March 2019 |
| Human Tissue Authority licence [HTA licence] | | 17 November 2017 |
| IRAS Checklist XML [Checklist_13032019] | | 13 March 2019 |
| IRAS Checklist XML [Checklist_17052019] | | 17 May 2019 |

| | | |
|---|---|---|
| Other [Protocol Annex 1 collection leads] | 4 | 26 February 2019 |
| Other [Protocol Annex 2 Ethically approved collections] | 2 | 26 February 2019 |
| Other [Protocol Annex 3 Projects currently supported by ORB] | 2 | 27 February 2019 |
| Other [Protocol Annex 4 Pathway for verification and feedback incidental findings] | 2 | 03 March 2017 |
| Other [Protocol Annex 5 Collection centres] | 4 | 27 February 2019 |
| Other [Protocol Annex 6 ORB UTrust SLA] | n/a | 16 April 2012 |
| Other [Protocol Annex 10 CV Clare Verrill] | n/a | 27 February 2019 |
| Other [Protocol Annex 11 Casablanca questionnaire] | 1 | 04 January 2010 |
| Other [ORB poster Healthy volunteers] | 3 | 05 February 2019 |
| Other [ORB Privacy notice website wording] | 1 | 12 September 2018 |
| Other [Annual report for 2017 activity] | 1 | 06 August 2018 |
| Other [Sponsor letter of approval] | n/a | 12 March 2019 |
| Other [Sponsor insurance certificate] | n/a | 04 September 2018 |
| Other [Protocol Annex 7 MTA template] | n/a | 11 March 2019 |
| Other [Protocol Annex 10 CV Stephanie Jones] | n/a | 08 August 2019 |
| Other [Access policy ORB] | 4 | 11 March 2019 |
| Participant consent form [OUH consent form 1] | 04/13 | 01 April 2013 |
| Participant consent form [OUH consent form 3] | 10/13 | 01 October 2013 |
| Participant consent form [ORB Consent form adult clinically relevant genomics] | 5 | 05 February 2019 |
| Participant consent form [ORB Consent form general] | 5 | 05 February 2019 |
| Participant consent form [ORB consent form Healthy volunteers] | 3 | 05 February 2019 |
| Participant consent form [ORB Assent Child clinically relevant genomics] | 2 | 05 February 2019 |
| Participant consent form [ORB Proctoscope Consent form] | 2 | 05 February 2019 |
| Participant information sheet (PIS) [ORB Proctoscope PIS] | 2 | 05 February 2019 |
| Participant information sheet (PIS) [ORB PIS general] | 4 | 05 February 2019 |
| Participant information sheet (PIS) [ORB PIS Child 0-7 clinically relevant genomics] | 2 | 05 February 2019 |
| Participant information sheet (PIS) [OUH NHS tissue for research leaflet] | none | 24 October 2013 |
| Participant information sheet (PIS) [ORB PIS Child 8-11 clinically relevant genomics] | | 05 February 2019 |
| Participant information sheet (PIS) [ORB PIS Child 12-15 clinically relevant genomics] | 3 | 05 February 2019 |
| Participant information sheet (PIS) [ORB PIS clinically relevant genomics] | 4 | 05 February 2019 |
| Participant information sheet (PIS) [ORB PIS Child 8-11 clinically relevant genomics] | 2 | 05 February 2019 |
| Participant information sheet (PIS) [ORB PIS Healthy volunteers] | 4 | 17 May 2019 |
| Protocol for management of the tissue bank [ORB Protocol v8.0] | 8 | 07 March 2019 |
| REC Application Form [RTB_Form_13032019] | | 13 March 2019 |
| Relative consent form [OUH consent form 2] | 9/13 | 01 September 2013 |
| Relative consent form [ORB Consent form Parental clinically | 5 | 05 February 2019 |

| | | |
|---|---|---|
| relevant genomics] | | |
| Relative information sheet [ORB PIS Parental clinically relevant genomics] | 4 | 05 February 2019 |
| Summary of research programme(s) [ORB Research programme] | 1 | 27 February 2019 |

| | |
|---|---|
| **19/SC/0173** | **Please quote this number on all correspondence** |

Yours sincerely

**Mrs Stacey Bamford**
**Approvals Administrator**

E-mail: nrescommittee.southcentral-oxfordc@nhs.net

*Copy to:* *Dr Brian Shine, University of Oxford*

Health Research Authority

**South Central - Oxford C Research Ethics Committee**
Level 3, Block B
Whitefriars Building
Lewins Mead
Bristol
BS1 2NT

Telephone: 0207 104 8241

18 February 2020

Dr Stephanie G Jones
University of Oxford
Nuffield Department of Surgical Sciences
Level 6, John Radcliffe Hospital
Oxford
OX3 9DU

Dear Dr Jones

| | |
|---|---|
| **Title of the Research Tissue Bank:** | **Oxford Radcliffe Biobank** |
| **REC reference:** | **19/SC/0173** |
| **Designated Individual:** | **Dr Brian Shine ((Organisation name not set))** |
| **Amendment number:** | **SA01** |
| **Amendment date:** | **07 January 2020** |
| **IRAS project ID:** | **262470** |

The above amendment was reviewed at the meeting of the Sub-Committee held on 07 February 2020.

**Ethical Opinion**

The members of the Committee present gave a favourable ethical opinion of the amendment on the basis described in the notice of amendment form and supporting documentation.

**Approved Documents**

The documents reviewed and approved at the meeting were:

| *Document* | *Version* | *Date* |
|---|---|---|
| Covering letter on headed paper [ORB amendment cover letter 2020_AM01] | | 14 January 2020 |
| Notice of Substantial Amendment (RTBs) [AmendmentFormRTB_ReadyForSubmission] | SA01 | 07 January 2020 |
| Other [CTRG support letter] | | 15 January 2020 |
| Other [HOLMES study Enrolment CRF version 1] | 1.0 | 07 January 2020 |
| Participant information sheet (PIS) [ORB PIS general] | 5 (Clean + Tracked) | 07 January 2020 |
| Protocol for management of the tissue bank [Oxford Radcliffe Biobank Protocol] | 9.0 (Clean + Tracked) | 07 January 2020 |

**Membership of the Committee**

The members of the Ethics Committee who were present at the meeting are listed on the attached sheet.

**Statement of compliance**

The Committee is constituted in accordance with the Governance Arrangements for Research Ethics Committees and complies fully with the Standard Operating Procedures for Research Ethics Committees in the UK.

**HRA Learning**

We are pleased to welcome researchers and research staff to our HRA Learning Events and online learning opportunities– see details at:
https://www.hra.nhs.uk/planning-and-improving-research/learning/

| 19/SC/0173 | Please quote this number on all correspondence |
|---|---|

Yours sincerely

PP
**Dr Lee Potiphar**
**Chair**

E-mail: oxfordc.rec@hra.nhs.uk

*Enclosures:* *List of names and professions of members who were present at the meeting and those who submitted written comments*

*Copy to:* *Dr Brian Shine ((Organisation name not set)), University of Oxford*

**South Central - Oxford C Research Ethics Committee**

**Attendance at Sub-Committee of the REC meeting on 07 February 2020**

**Committee Members:**

| *Name* | *Profession* | *Present* | *Notes* |
|---|---|---|---|
| Mrs Vivienne Laurie (Vice Chair and Meeting Chair) | Barrister | Yes | |
| Dr Lee Potiphar | Senior Lecturer in Adult Nursing and Senior Tutor | Yes | |

**Also in Attendance:**

| *Name* | *Position (or reason for attending)* |
|---|---|
| Miss Charlotte Ferris | Approvals Officer |

Health Research Authority

**South Central - Oxford C Research Ethics Committee**
Level 3, Block B
Whitefriars Building
Lewins Mead
Bristol
BS1 2NT

Telephone: 0207 104 8241

27 April 2020_Revised 06 May 2020

Prof Clare Verrill
University of Oxford
Nuffield Department of Surgical Sciences
Level 6, John Radcliffe Hospital
Oxford
OX3 9DU

Dear Prof Verrill

| | |
|---|---|
| **Title of the Research Tissue Bank:** | **Oxford Radcliffe Biobank** |
| **REC reference:** | **19/SC/0173** |
| **Designated Individual:** | **Dr Brian Shine ((Organisation name not set))** |
| **Amendment number:** | **SA2** |
| **Amendment date:** | **16 April 2020** |
| **IRAS project ID:** | **262470** |

The above amendment was reviewed at the meeting of the Committee held on 20 April 2020. Thank you for attending to discuss the amendment.

**Ethical Opinion**

The members of the Committee present gave a favourable ethical opinion of the amendment on the basis described in the notice of amendment form and supporting documentation.

**Mental Capacity Act 2005**

I confirm that the Committee has approved this research project for the purposes of the Mental Capacity Act 2005. The Committee is satisfied that the requirements of section 31 of the Act will be met in relation to research carried out as part of this project on, or in relation to, a person who lacks capacity to consent to taking part in the project.

**Approved Documents**

The documents reviewed and approved at the meeting were:

| *Document* | *Version* | *Date* |
|---|---|---|
| Covering letter on headed paper [ORB amendment cover letter 2020_AM02] | | 16 April 2020 |
| Covering letter on headed paper [ORB amendment response to REC letter 2020_AM02] | | 24 April 2020 |

| | | |
|---|---|---|
| Notice of Substantial Amendment (RTBs) [AmendmentFormRTB_SA2 ReadyForSubmission] | SA2 | 16 April 2020 |
| Other [ORB Email Healthy Volunteers COVID] | 1 | 11 April 2020 |
| Other [Annex 5 Collection centres] | 5 | 14 April 2020 |
| Other [Appendix 16 Feedback of research grade findings] | 1 | 14 April 2020 |
| Other [CTRG support letter] | | 16 April 2020 |
| Other [FullDataSetRtbForm with ORB SA2] | | |
| Other [ORB Poster Healthy Volunteers COVID] | 1 | 06 April 2020 |
| Other [Guidance for Consultees from DoH] | | |
| Other [MCIP health-workers-guide] | | |
| Other [MCIP-Guide_for_Family_Friends_Unpaid_Carers] | | |
| Other [ORB CLN-009 extracts for REC reference] | | |
| Other [ORB Consultee Declaration Form v1] | 1 | 22 April 2020 |
| Other [ORB Nominated Consultee Information Sheet] | 1 (Clean + Tracked) | 22 April 2020 |
| Other [ORB Personal Consultee Information Sheet] | 1 (Clean + Tracked) | 23 April 2020 |
| Other [20A049 Text for research test results] | | |
| Other [ORB website Consultee information] | 1 | 23 April 2020 |
| Other [Study questionnaire saliva-based SARS-CoV2 20A049] | 1.0 | 23 April 2020 |
| Participant information sheet (PIS) [ORB PIS GEN Recovered capacity v6.1] | 6.1 | 16 April 2020 |
| Participant information sheet (PIS) [ORB PIS clinically relevant genomics v5] | 5 (Clean + Tracked) | 23 April 2020 |
| Participant information sheet (PIS) [ORB PIS general] | 6 (Clean + Tracked) | 23 April 2020 |
| Protocol for management of the tissue bank [Oxford Radcliffe Biobank Protocol ] | 10.0 | 23 April 2020 |
| Relative information sheet [ORB PIS clinically relevant genomics v5] | 5 (Clean + Tracked) | 16 April 2020 |
| Relative information sheet [ORB PIS general_v6] | 6 (Clean + Tracked) | 16 April 2020 |

**Membership of the Committee**

The members of the Ethics Committee who were present at the meeting are listed on the attached sheet.

**Statement of Compliance**

The Committee is constituted in accordance with the Governance Arrangements for Research Ethics Committees and complies fully with the Standard Operating Procedures for Research Ethics Committees in the UK.

**HRA Learning**

We are pleased to welcome researchers and research staff to our HRA Learning Events and online learning opportunities– see details at:
https://www.hra.nhs.uk/planning-and-improving-research/learning/

| | |
|---|---|
| **19/SC/0173** | **Please quote this number on all correspondence** |

Yours sincerely

**South Central - Oxford C Research Ethics Committee**

**Attendance at Committee meeting on 20 April 2020**

**Committee Members:**

| *Name* | *Profession* | *Present* | *Notes* |
|---|---|---|---|
| Dr Leonard Brookes | Consultant to the Pharmaceutical Industry | Yes | |
| Dr Linda Cartwright (Alternate Vice Chair) | Retired Consultant Epidemiologist | Yes | |
| Mrs Vivienne Laurie (Vice Chair) | Barrister | Yes | |
| Dr Lee Potiphar (Chair) | Senior Lecturer in Adult Nursing and Senior Tutor | Yes | |
| Dr Pamela Susan Ross | GP Principal | Yes | |
| Mr Barjinder Sahota | Solicitor Advocate | Yes | |
| Dr David Scott | Lecturer | Yes | |

**Also in Attendance:**

| *Name* | *Position (or reason for attending)* |
|---|---|
| Miss Charlotte Ferris | Approvals Officer |
| Mrs Maeve Ip Groot Bluemink | Approvals Specialist |

**COPY for information only,**
**OCHRe ref: 23/A035**

PP
**Dr Lee Potiphar**
**Chair**

E-mail: oxfordc.rec@hra.nhs.uk

*Enclosures:* *List of names and professions of members who were present at the meeting and those who submitted written comments*

*Copy to:* *Dr Brian Shine ((Organisation name not set)), University of Oxford*



*Supplementary Figure 2.3: Research Ethics Committee letter*

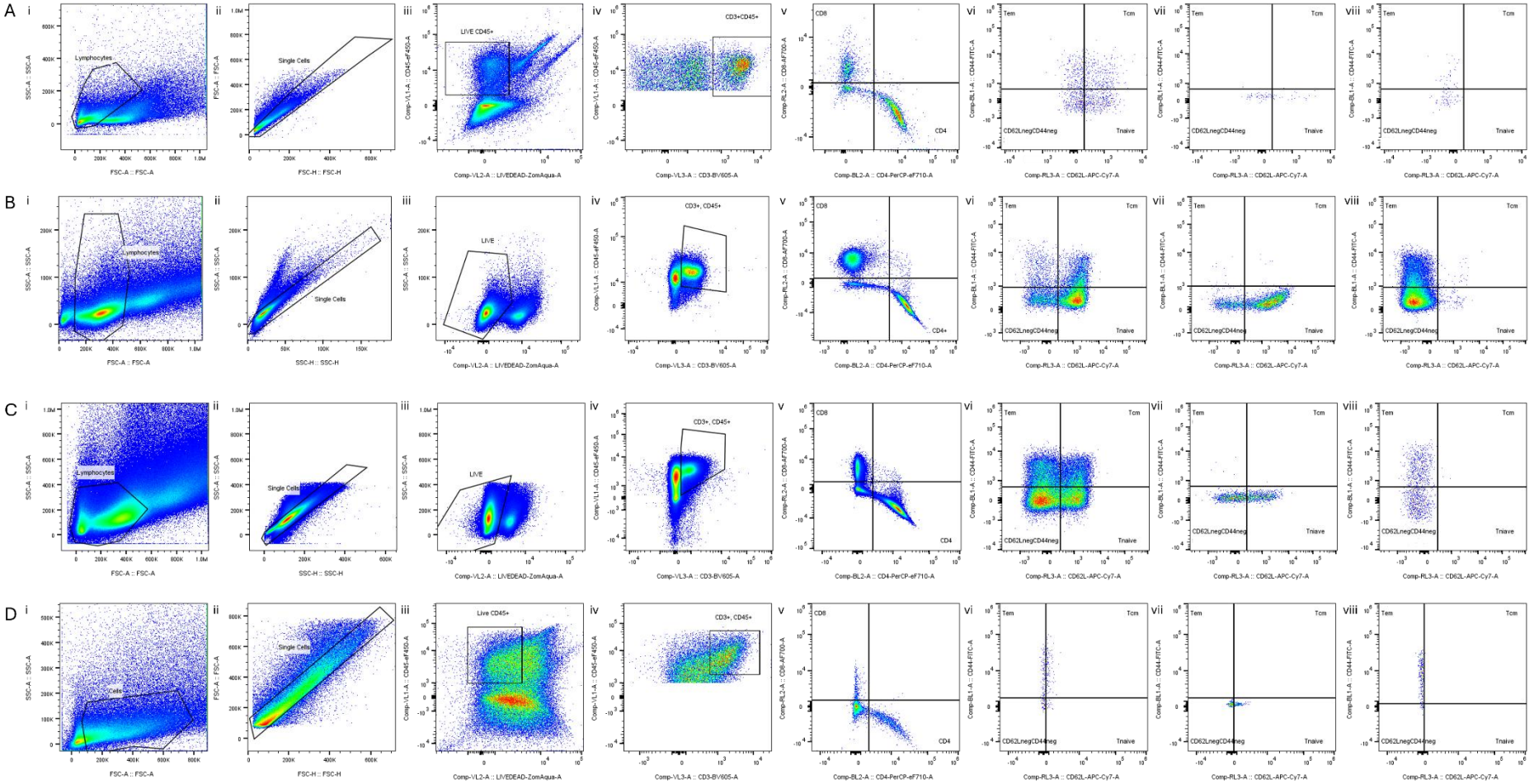
A
B
C
D
i
ii
iii
iv
v
vi
vii
viii
Lymphocytes
Single Cells
LIVE CD45+
LIVE
CD3+CD45+
CD3+, CD45+
CD8
CD4
CD4+
Tem
Tcm
Tnaive
CD62LnegCD44neg
FSC-A :: FSC-A
SSC-A :: SSC-A
FSC-H :: FSC-H
SSC-H :: SSC-H
Comp-VL2-A :: LIVEDEAD-ZomAqua-A
Comp-VL1-A :: CD45-eF450-A
Comp-VL3-A :: CD3-BV605-A
Comp-RL2-A :: CD8-AF700-A
Comp-RL2-A :: CD4-PerCP-eF710-A
Comp-BL1-A :: CD44-FITC-A
Comp-RL3-A :: CD62L-APC-Cy7-A

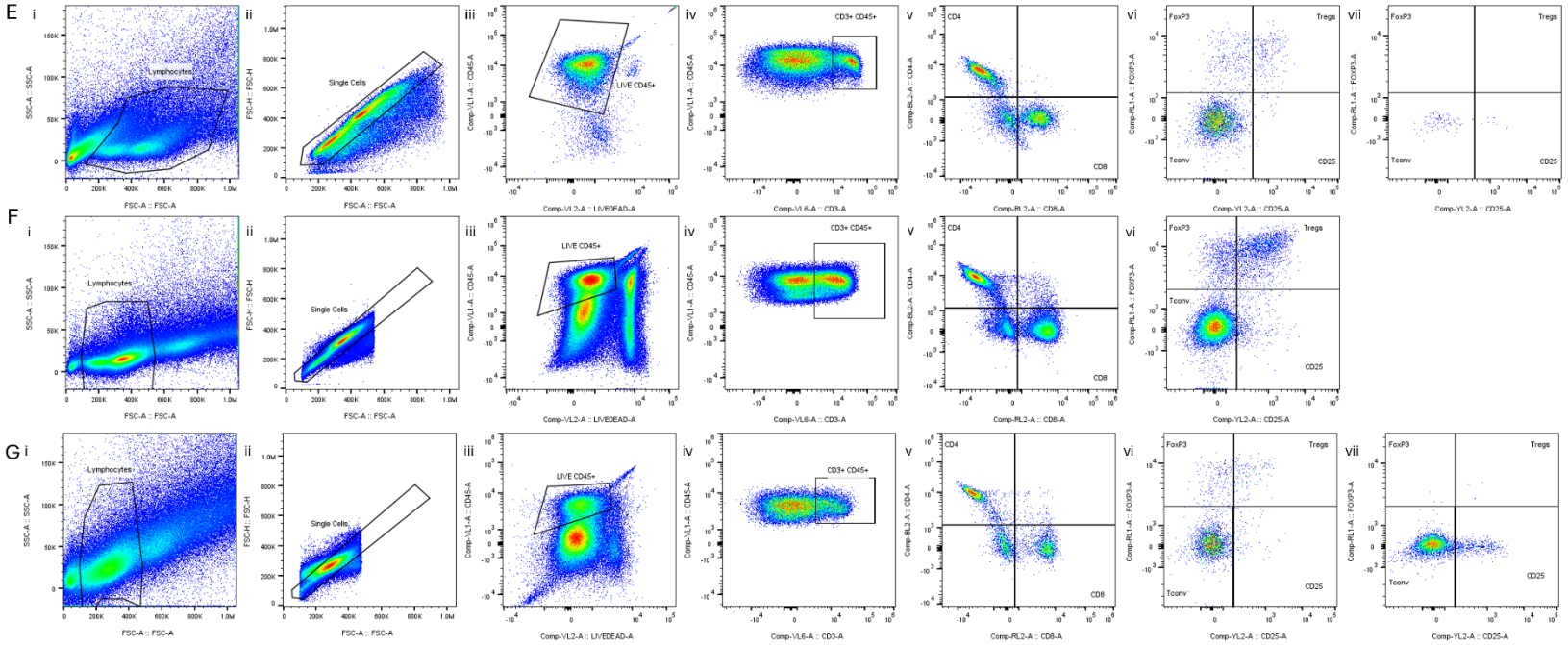


Supplementary Figure 3.1: Flow cytometry gating strategy for the assessment of T cell subpopulations in (A, E) blood, (B, F) lymph nodes, (C, G) spleen and (D) tumour from MCA205 growth pilot with 5 x $10^5$ cell seeding density experiment. CD8 subpopulations are shown in A-D, with gating of (i) size selection based on forward and side scatter, (ii) single cells, (iii) live CD45 cells, (iv) CD3+CD45+ T cells, (v) CD4 and CD8 T cell selection, (vi) CD8 T cell subpopulations including CD62L-CD44- T cells, T effector cells (Tem, CD62L-CD44T central memory cells (Tcm, CD62L+CD44+), naïve T cells (Tnaïve , CD62L+CD44), (vii) CD44 fluorescence-minus-one (FMO) for population differentiation, (viii) CD62L fluorescence-minus-one (FMO) for population differentiation. CD4 subpopulations are shown in E-G with gating of (i) size selection based on forward and side scatter, (ii) single cells, (iii) live CD45 cells, (iv) CD3+CD45+ T cells, (v) CD4 and CD8 T cell selection, (vi) CD4 T cell subpopulations including CD4+CD25-FoxP3+ T cells, CD4+CD25+FoxP3- T cells, CD4+ regulatory T cells (Tregs, CD4+CD25+FoxP3+), and conventional CD4 T cells (Tconvs, CD4+CD25-FoxP3-), (vii) FoxP3 fluorescence-minus-one (FMO) for population differentiation.

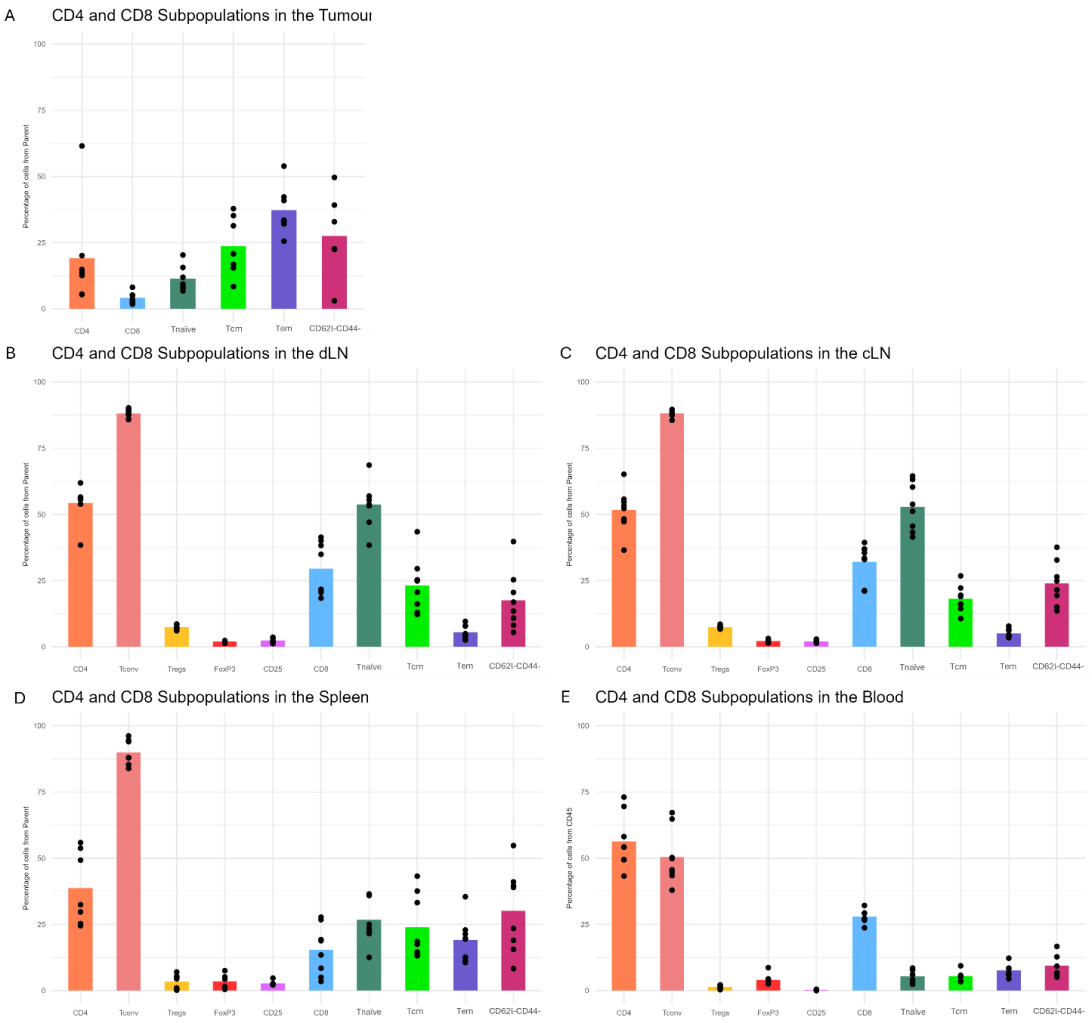


Supplementary Figure 3.2: Representation of proportion of CD8 and CD4 T cells and subpopulations as a percentage of CD3+ T cells from flow cytometry analysis of (A) tumour (n = 7), (B) draining lymph nodes (dLN, n = 8), (C) contralateral lymph nodes (cLN, n = 8), (D) spleen (n = 7), and blood (CD4 n = 8, CD8 n = 6). From MCA205 growth pilot with 5 x $10^5$ cell seeding density experiment. Blood had reduced replicated due to CD3 stain being poor in 2 samples, tumour and spleen had reduced replicates due to issue with acquisition. (Orange) CD4 T cells, (Salmon) CD4 T cells (Tconvs, CD4+CD25-FoxP3-), (Yellow) CD4+ regulatory T cells (Tregs, CD4+CD25+FoxP3+), (Red) CD4+CD25-FoxP3+ T cells, (purple) CD4+CD25+FoxP3- T cells. (Blue) CD8 T cells, (Dark green) CD8+ naïve T cells (Tnaïve, CD62L+CD44-), (Light green) T central memory cells (Tcm, CD62L+CD44+), (Dark purple) CD8+ T effector cells (Tem, CD62L-CD44+), (Magenta) CD8+CD62L-CD44- T cells.

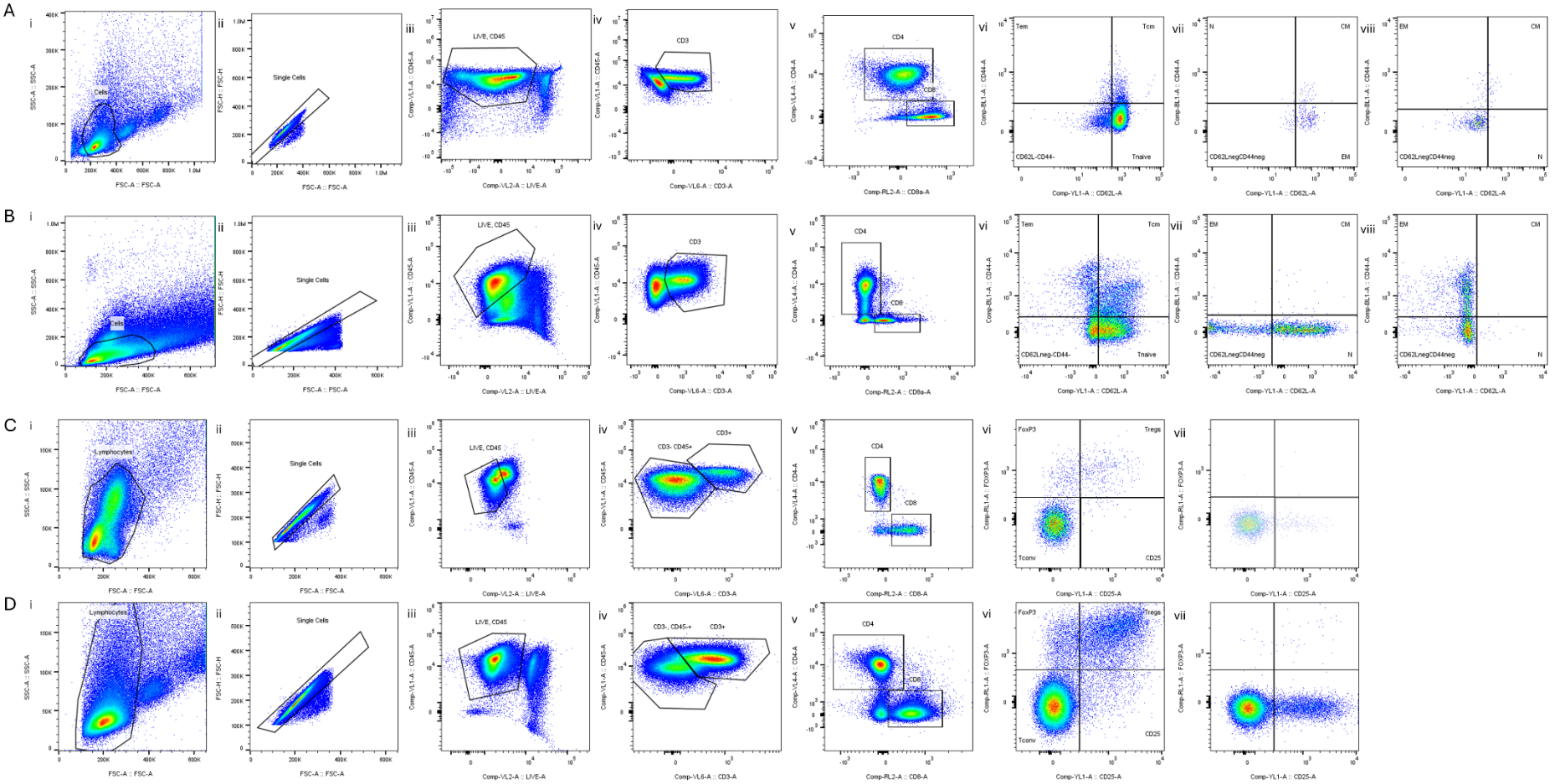
A
B
C
D
Cells
Lymphocytes
Single Cells
LIVE, CD45
CD3
CD3- CD45+
CD3+
CD4
CD8
Tem
Tcm
Tnaive
CM
EM
N
FoxP3
Tregs
Tconv
CD25
CD62L-CD44-
CD62LnegCD44neg
FSC-A :: FSC-A
SSC-A :: SSC-A
FSC-H :: FSC-H
Comp-VL1-A :: CD45-A
Comp-VL2-A :: LIVE-A
Comp-VL6-A :: CD3-A
Comp-VL4-A :: CD4-A
Comp-RL2-A :: CD8a-A
Comp-BL1-A :: CD44-A
Comp-YL1-A :: CD62L-A
Comp-RL1-A :: FOXP3-A
Comp-YL1-A :: CD25-A

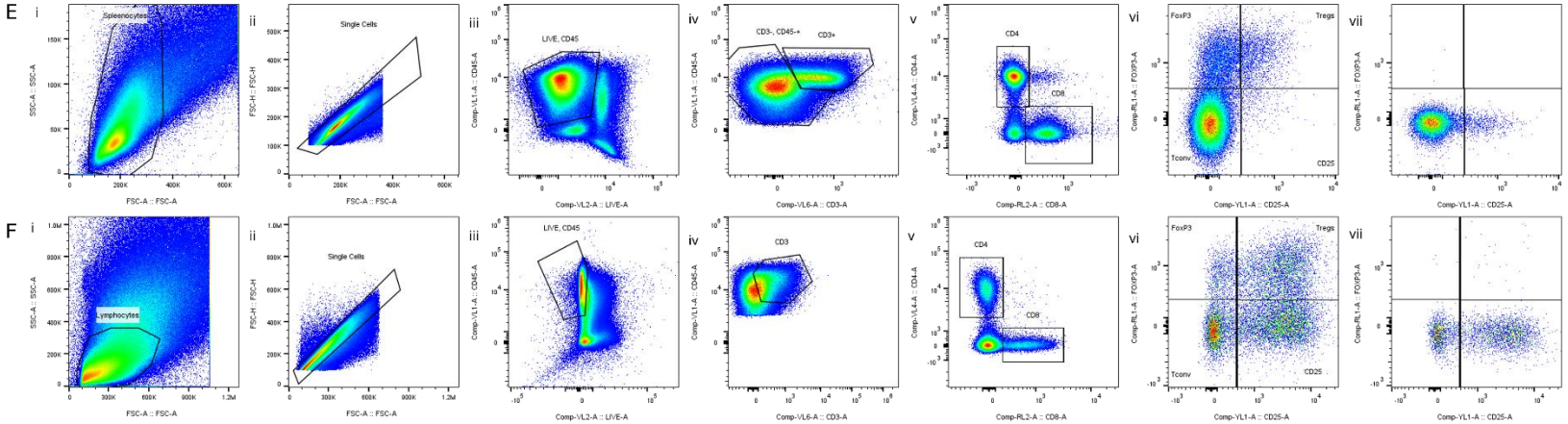


Supplementary Figure 3.3: Flow cytometry gating strategy for the assessment of T cell subpopulations in (A, D) lymph nodes, and (B, E) spleen, (C) blood, and (F) tumour of MCA205 growth pilot with lower cell seeding density experiment. Groups included non-tumour bearing control, 1 x $10^5$, 2 x $10^5$. CD8 subpopulations are shown in A-B, with gating of (i) size selection based on forward and side scatter, (ii) single cells, (iii) live CD45 cells, (iv) CD3+CD45+ T cells, (v) CD4 and CD8 T cell selection, (vi) CD8 T cell subpopulations including CD62L-CD44- T cells, T effector cells (Tem, CD62L-CD44T central memory cells (Tcm, CD62L+CD44+), naïve T cells (Tnaïve , CD62L+CD44-), (vii) CD44 fluorescence-minus-one (FMO) for population differentiation, (viii) CD62L fluorescence-minus-one (FMO) for population differentiation. CD4 subpopulations are shown in C-F with gating of (i) size selection based on forward and side scatter, (ii) single cells, (iii) live CD45 cells, (iv) CD3+CD45+ T cells, (v) CD4 and CD8 T cell selection, (vi) CD4 T cell subpopulations including CD4+CD25-FoxP3+ T cells, CD4+CD25+FoxP3- T cells, CD4+ regulatory T cells (Tregs, CD4+CD25+FoxP3+), and conventional CD4 T cells (Tconvs, CD4+CD25-FoxP3-), (vii) FoxP3 fluorescence-minus-one (FMO) for population differentiation.

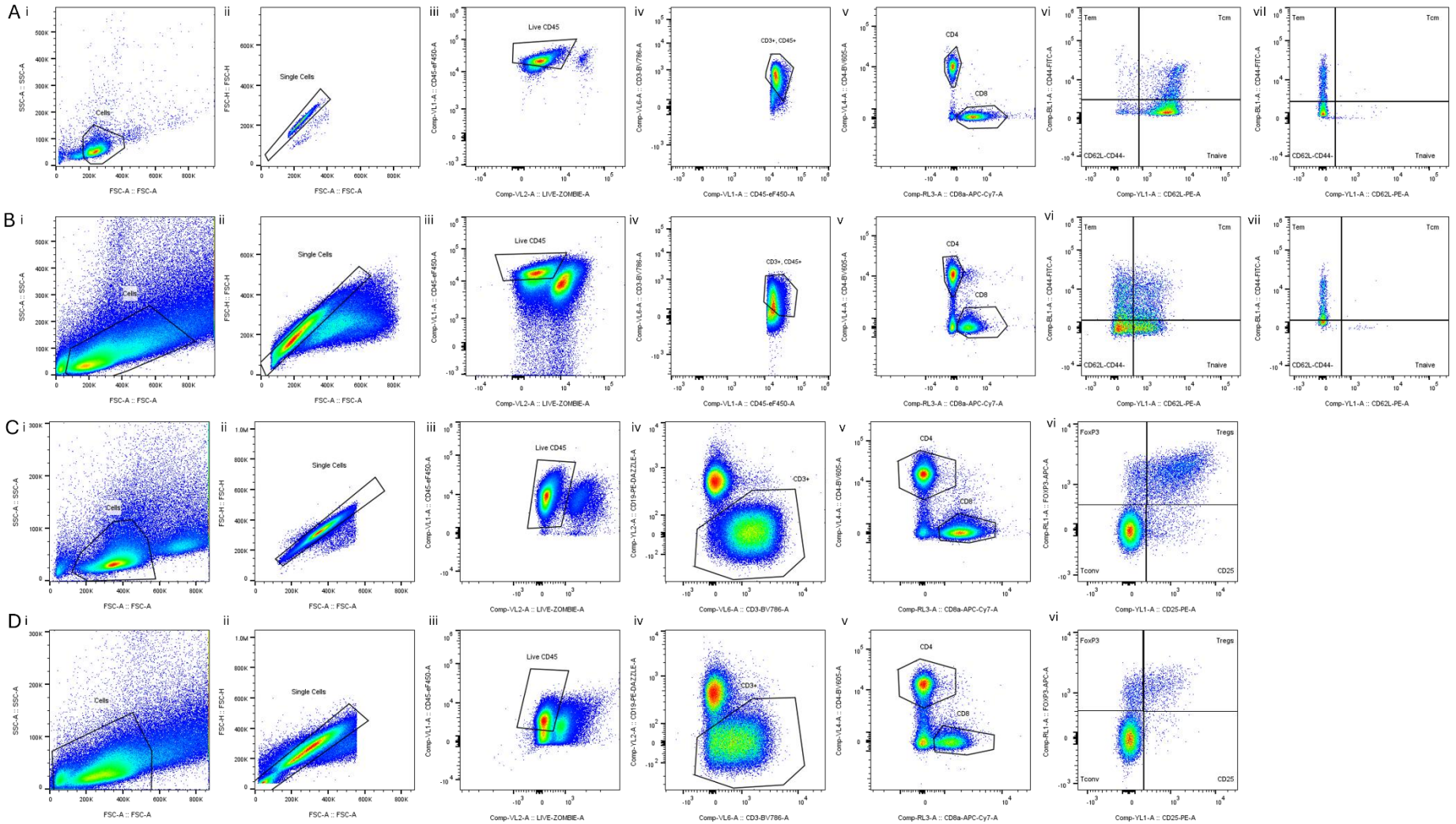


Supplementary Figure 3.4: Flow cytometry gating strategy for the assessment of T cell subpopulations in (A, C) lymph nodes, and (B, C) spleen of HIFU treated MCA205 induced fibrosarcoma. CD8 subpopulations are shown in A-B, with gating of (i) size selection based on forward and side scatter, (ii) single cells, (iii) live CD45 cells, (iv) CD3+CD45+ T cells, (v) CD4 and CD8 T cell selection, (vi) CD8 T cell subpopulations including CD62L-CD44- T cells, T effector cells (Tem, CD62L-CD44T central memory cells (Tcm, CD62L+CD44+), naïve T cells (Tnaïve, CD62L+CD44-), (vii) CD62L fluorescence-minus-one (FMO) for population differentiation. CD4 subpopulations are shown in C-D with gating of (i) size selection based on forward and side scatter, (ii) single cells, (iii) live CD45 cells, (iv) CD3+CD45+ T cells and CD19+ B cells, (v) CD4 and CD8 T cell selection from CD3+ T cells, (vi) CD4 T cell subpopulations including CD4+CD25-FoxP3+ T cells, CD4+CD25+FoxP3- T cells, CD4+ regulatory T cells (Tregs, CD4+CD25+FoxP3+), and conventional CD4 T cells (Tconvs, CD4+CD25-FoxP3-.

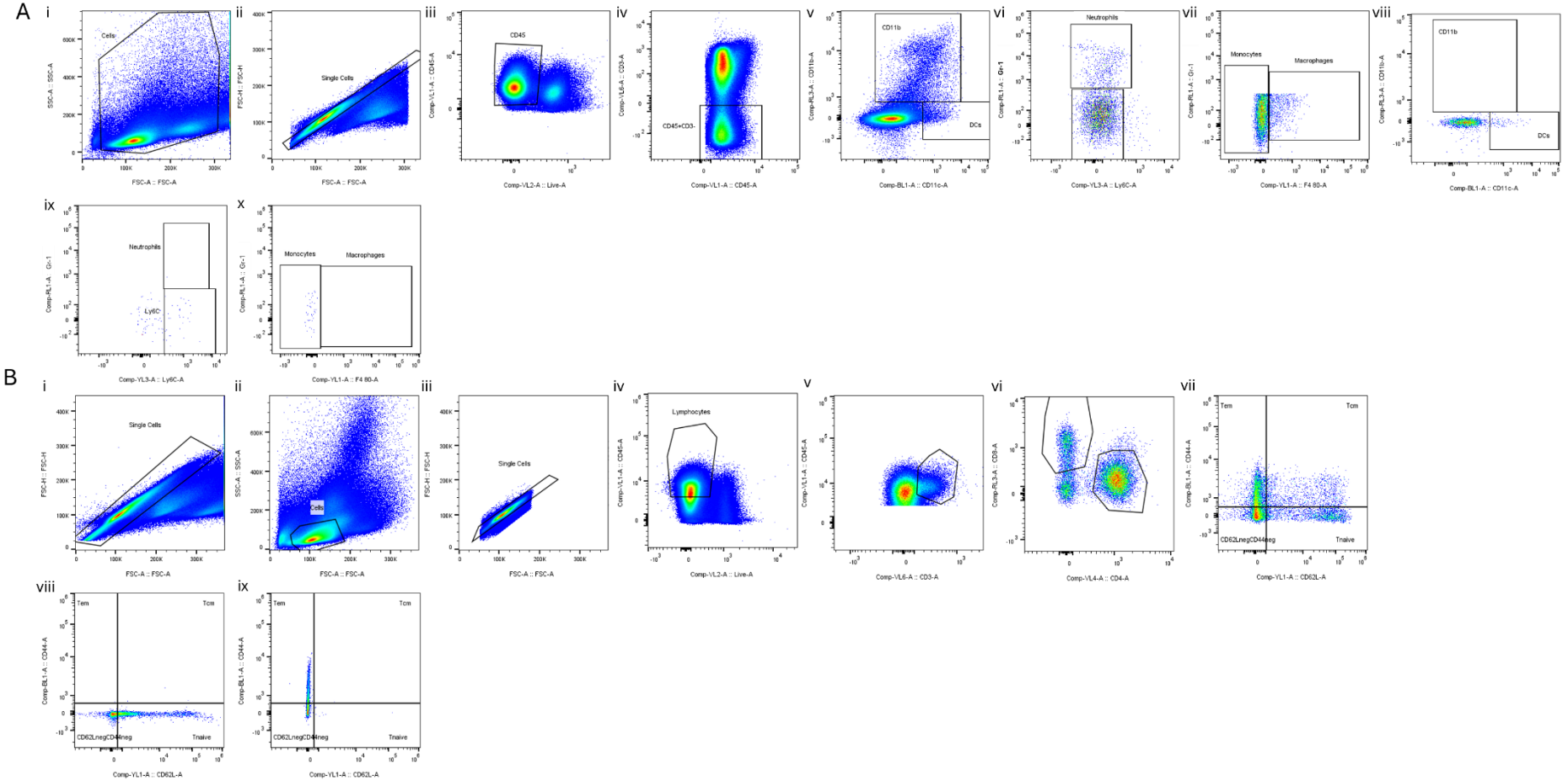
A
i
Cells
SSC-A :: SSC-A
FSC-A :: FSC-A
ii
Single Cells
FSC-H :: FSC-H
FSC-A :: FSC-A
iii
CD45
Comp-VL2-A :: Live-A
iv
CD45+CD3-
Comp-VL1-A :: CD45-A
Comp-VL6-A :: CD3-A
v
CD11b
DCs
Comp-BL1-A :: CD11c-A
Comp-BL3-A :: CD11b-A
vi
Neutrophils
Comp-YL3-A :: Ly6C-A
Comp-RL1-A :: Gr-1
vii
Monocytes
Macrophages
Comp-YL1-A :: F4 80-A
viii
CD11b
DCs
ix
Neutrophils
Ly6C
x
Monocytes
Macrophages
B
i
Single Cells
ii
Cells
iii
Single Cells
iv
Lymphocytes
v
vi
vii
Tem
Tcm
CD62LnegCD44neg
Tnaive
viii
ix

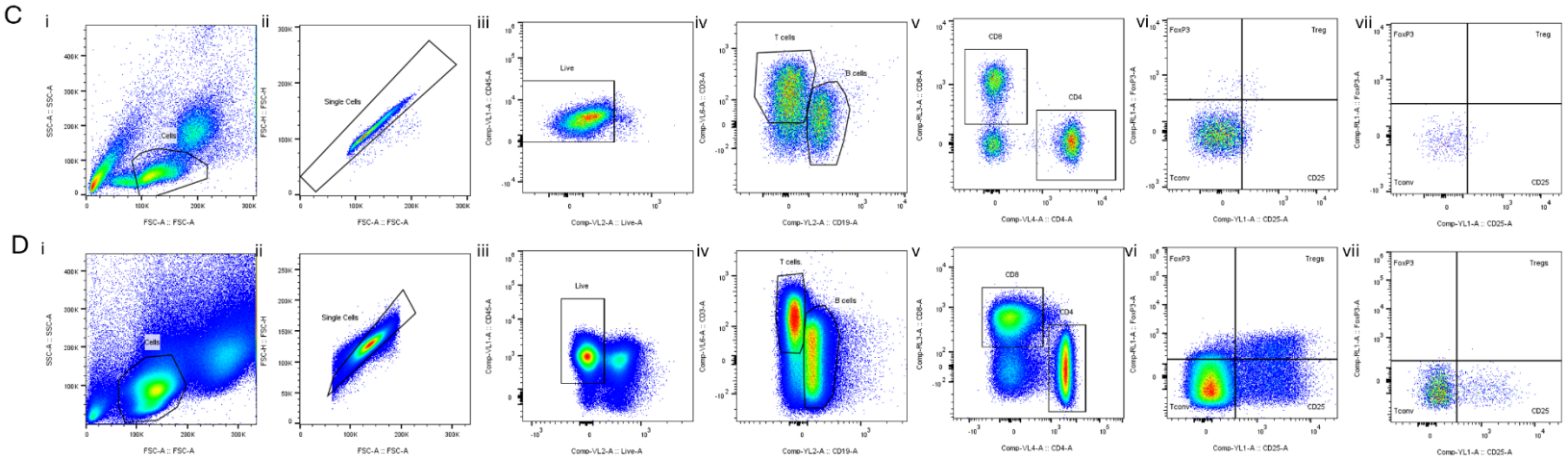


Supplementary Figure 3.5: Flow cytometry gating strategy for the assessment of (A) Myeloid and (B-D) T cell subpopulations in (A, D) lymph nodes, (C) blood and (B) spleen of HIFU treated MCA205 induced fibrosarcoma. (A) Myeloid populations gated by (i) size selection based on forward and side scatter, (ii) single cells, (iii) live CD45 cells, (iv) CD3-CD45+ cells, (v) dendritic cells (DCs, CD45+CD3-CD11b-CD11c+), and CD11b cells for further selection including (vi) neutrophils (CD45+CD3-CD11b+CD11c-Gr1+) and Ly8C+ cells for further selection including (vii) F4/80 for selection of monocytes (CD45+CD3-CD11b+CD11c-Gr1-Ly6C+F4/80-) and macrophages (CD45+CD3-CD11b+CD11c-Gr1-Ly6C+F4/80+), (viii) CD11b fluorescence-minus-one (FMO) for population differentiation, (ix) Ly6G fluorescence-minus-one (FMO) for population differentiation, (x) F4/80 fluorescence-minus-one (FMO) for population differentiation. CD8 subpopulations for spleen (B) with gating of (i) single cells (ii) size selection based on forward and side scatter, (iii) single cells, (iv) live CD45 cells, (v) CD3+CD45+ T cells, (vi) CD4 and CD8 T cell selection, (vii) CD8 T cell subpopulations including CD62L-CD44- T cells, T effector cells (Tem, CD62L-CD44T central memory cells (Tcm, CD62L+CD44+), naïve T cells (Tnaïve , CD62L+CD44-), (viii) CD44 fluorescence-minus-one (FMO) for population differentiation, ) (ix) CD62L fluorescence-minus-one (FMO) for population differentiation. CD4 subpopulations (C and D) with gating of (i) size selection based on forward and side scatter, (ii) single cells, (iii) live CD45 cells, (iv) CD3+CD45+ T cells and CD19+ B cells, (v) CD4 and CD8 T cell selection from CD3+ T cells, (vi) CD4 T cell subpopulations including CD4+CD25-FoxP3+ T cells, CD4+CD25+FoxP3- T cells, CD4+ regulatory T cells (Tregs, CD4+CD25+FoxP3+), and conventional CD4 T cells (Tconvs, CD4+CD25-FoxP3-), (vii) FoxP3 fluorescence-minus-one (FMO) for population differentiation.

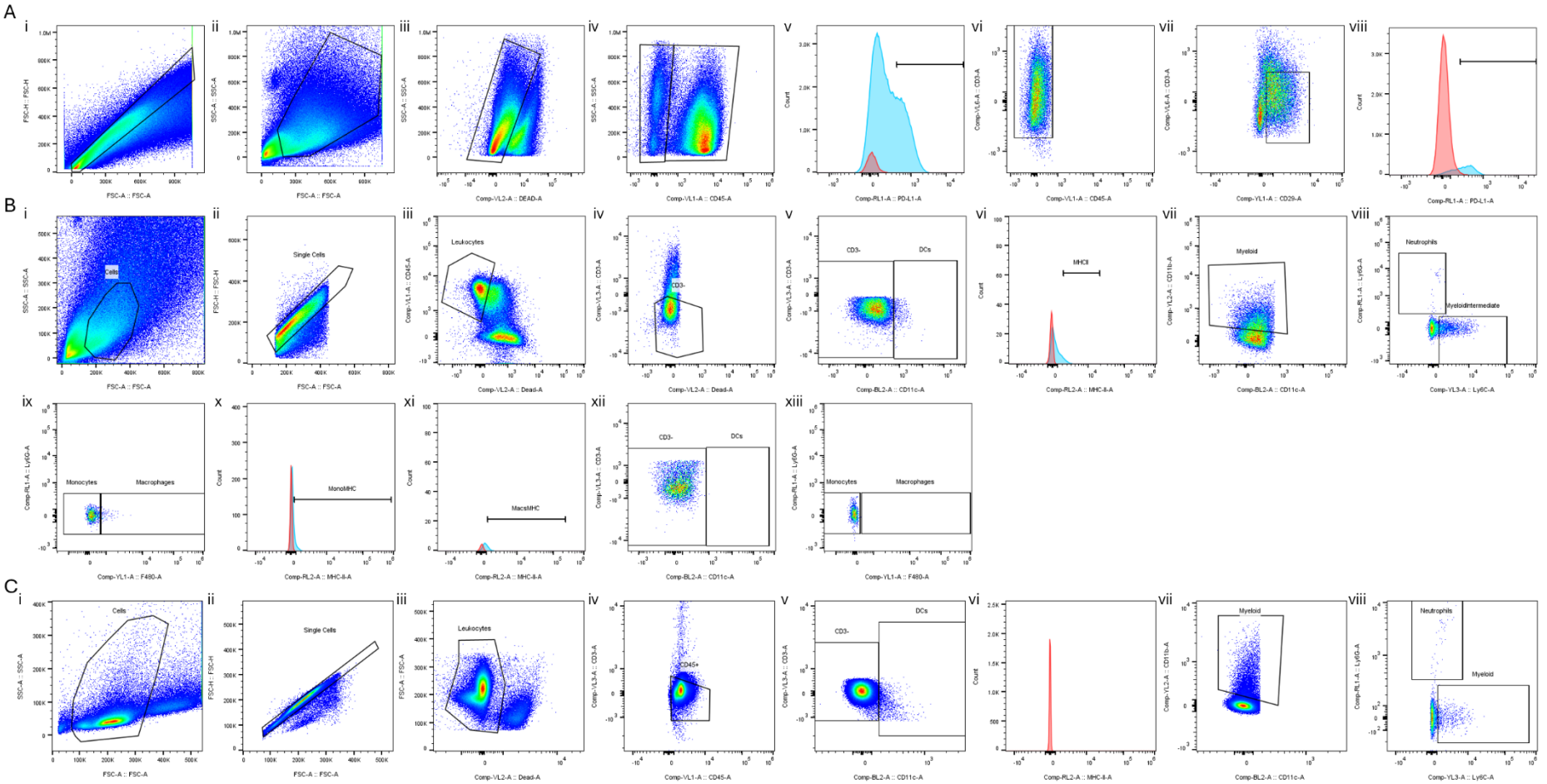
A
i
ii
iii
iv
v
vi
vii
viii
B
i
ii
iii
iv
v
vi
vii
viii
ix
x
xi
xii
xiii
C
i
ii
iii
iv
v
vi
vii
viii
Cells
Single Cells
Leukocytes
CD3-
DCs
MHCII
Myeloid
Neutrophils
MyeloidIntermediate
Monocytes
Macrophages
Mono\MHC
Macs\MHC
CD45+

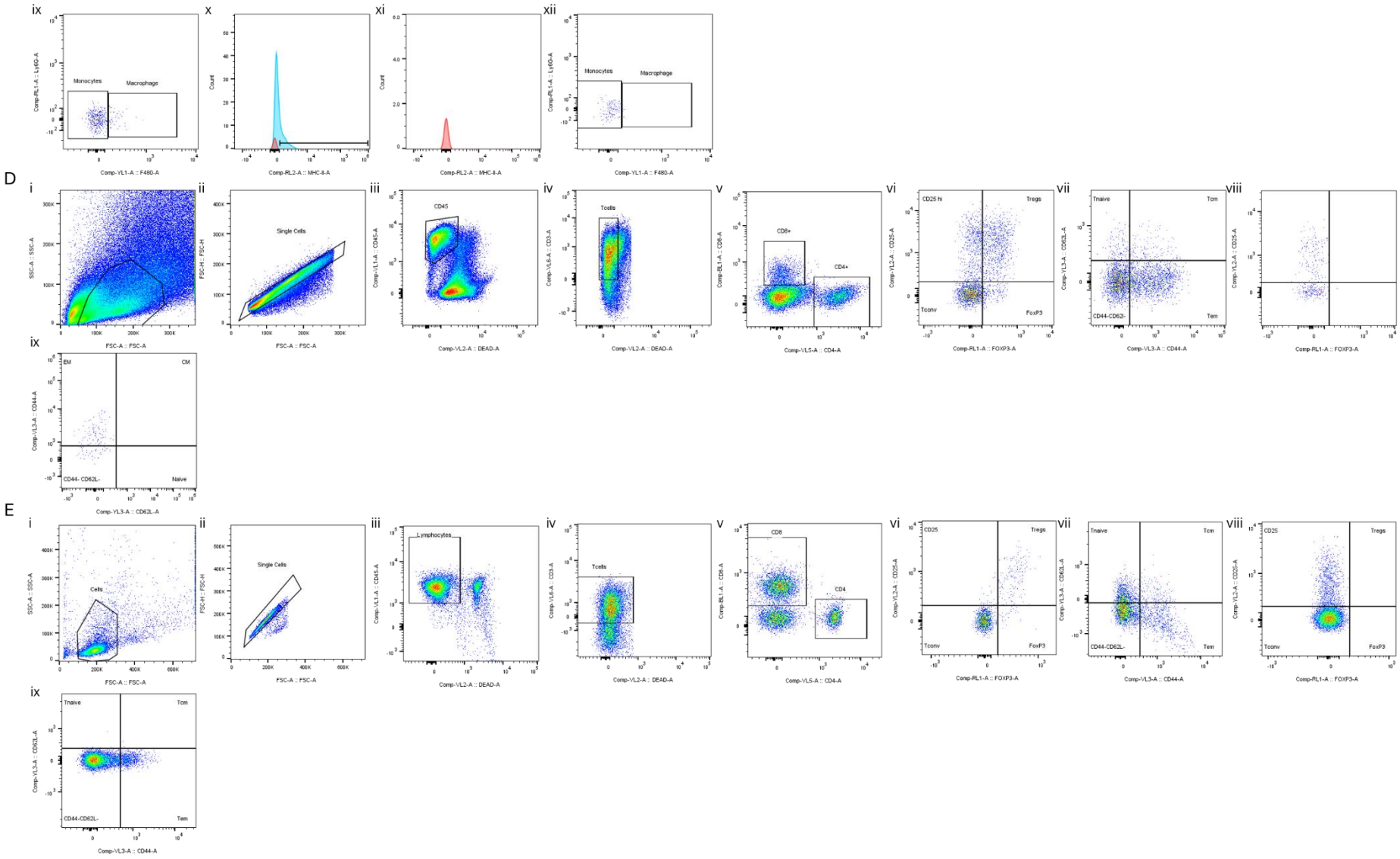
ix
Monocytes
Macrophage
Comp-RL1-A :: Ly6G-A
Comp-YL1-A :: F480-A
x
Count
Comp-RL2-A :: MHC-II-A
xi
Count
Comp-RL2-A :: MHC-II-A
xii
Monocytes
Macrophage
Comp-RL1-A :: Ly6G-A
Comp-YL1-A :: F480-A
D
i
SSC-A :: SSC-A
FSC-A :: FSC-A
ii
Single Cells
FSC-H :: FSC-H
FSC-A :: FSC-A
iii
CD45
Comp-VL1-A :: CD45-A
Comp-VL2-A :: DEAD-A
iv
Tcells
Comp-VL6-A :: CD3-A
Comp-VL2-A :: DEAD-A
v
CD8+
CD4+
Comp-BL1-A :: CD8-A
Comp-VL5-A :: CD4-A
vi
CD25 hi
Tregs
Tconv
FoxP3
Comp-YL3-A :: CD25-A
Comp-RL1-A :: FOXP3-A
vii
Tnaive
Tcm
CD44-CD62L-
Tem
Comp-YL3-A :: CD62L-A
Comp-VL3-A :: CD44-A
viii
Comp-YL2-A :: CD25-A
Comp-RL1-A :: FOXP3-A
ix
EM
CM
CD44- CD62L-
Naive
Comp-VL3-A :: CD44-A
Comp-YL3-A :: CD62L-A
E
i
Cells
SSC-A :: SSC-A
FSC-A :: FSC-A
ii
Single Cells
FSC-H :: FSC-H
FSC-A :: FSC-A
iii
Lymphocytes
Comp-VL1-A :: CD45-A
Comp-VL2-A :: DEAD-A
iv
Tcells
Comp-VL6-A :: CD3-A
Comp-VL2-A :: DEAD-A
v
CD8
CD4
Comp-BL1-A :: CD8-A
Comp-VL5-A :: CD4-A
vi
CD25
Tregs
Tconv
FoxP3
Comp-YL3-A :: CD25-A
Comp-RL1-A :: FOXP3-A
vii
Tnaive
Tcm
CD44-CD62L-
Tem
Comp-YL3-A :: CD62L-A
Comp-VL3-A :: CD44-A
viii
CD25
Tregs
Tconv
FoxP3
Comp-YL3-A :: CD25-A
Comp-RL1-A :: FOXP3-A
ix
Tnaive
Tcm
CD44-CD62L-
Tem
Comp-YL3-A :: CD62L-A
Comp-VL3-A :: CD44-A

Supplementary Figure 3.6: Flow cytometry gating strategy for the assessment of (A) PD-L1+ selection of cancer cells and CD45+ leukocytes for assessment of tumours treated with HIFU and PD-L1 immunotherapy, (i) Myeloid and (B-E) T cell subpopulations in (A, E) lymph nodes, (B, D) blood and (C) spleen of HIFU treated MCA205 induced fibrosarcoma by (i) single cells, (ii) size selection based on forward and side scatter, (iii) live cells, (iv) CD45 selection for differentiation of immune cells from cancer cells, (v) PD-L1 selection of CD45+ cells (blue) compared to fluorescence-minus-one (red), (vi) selection of CD45-CD3-cancer cells, (vii) CD29+ cancer cells, (viii) PD-L1+ cells (blue) compared to FMO (red) control. Myeloid populations of (B) tumour tissue and (C) lymph nodes gated by (i) size selection based on forward and side scatter, (ii) single cells, (iii) live CD45 cells, (iv) CD3-CD45+ cells, (v) dendritic cells (DCs, CD45+CD3-CD11b-CD11c+), and CD11c- cells for further selection including (vi) MHC-II+ DCs (blue) compared to fluorescence-minus-one control (FMO, red), (vii) CD11b+CD11c- myeloid cells, (viii) neutrophils (CD45+CD3-CD11b+CD11c-Gr1+) and Ly8C+ cells for further selection including (ix) F4/80 for selection of monocytes (CD45+CD3-CD11b+CD11c-Gr1-Ly6C+F4/80-) and macrophages (CD45+CD3-CD11b+CD11c-Gr1-Ly6C+F4/80+), (x) MHC-II expression on monocytes (blue) based on fluorescence-minus-one control (FMO, red), (xi) MHC-II expression on macrophages (blue) based on fluorescence-minus-one control (FMO, red). For tumour (B), (xii) CD11c fluorescence-minus-one (FMO) for population differentiation, (xiii) F4/80 fluorescence-minus-one (FMO) for population differentiation, or lymph nodes (C) (xii) F4/80 fluorescence-minus-one (FMO) for population differentiation. T cell subpopulations for (D) tumour tissue and (E) lymph nodes with gating of (i) size selection based on forward and side scatter, (ii) single cells, (iii) live CD45 cells, (iv) CD3+CD45+ T cells, (v) CD4 and CD8 T cell selection, (vi) CD4 T cell subpopulations from CD4 gate including CD4+CD25-FoxP3+ T cells, CD4+CD25+FoxP3- T cells, CD4+ regulatory T cells (Tregs, CD4+CD25+FoxP3+), and conventional CD4 T cells (Tconvs, CD4+CD25-FoxP3-), (vi) CD8 T cell subpopulations from CD8 population including CD62L-CD44- T cells, T effector cells (Tem, CD62L-CD44T central memory cells (Tcm, CD62L+CD44+), naïve T cells (Tnaïve , CD62L+CD44-), (viii) FoxP3 fluorescence-minus-one (FMO) for population differentiation, (ix) CD62L fluorescence-minus-one (FMO) for population differentiatio.

| Gene | logFC | adjPVal | Gene | logFC | adjPVal | Gene | logFC | adjPVal |
|---|---|---|---|---|---|---|---|---|
| ACTG2 | -6.28 | 1.33E-24 | CALD1 | -1.98 | 6.12E-08 | CRIP2 | 1.73 | 2.78E-06 |
| CNN1 | -4.86 | 1.33E-24 | CSRP2 | -1.61 | 6.12E-08 | PLXND1 | 1.29 | 2.81E-06 |
| MYH11 | -4.55 | 7.41E-23 | TSPY1 | 1.70 | 6.39E-08 | DVL1 | 0.99 | 2.84E-06 |
| MYLK | -5.10 | 2.27E-21 | TMEM30B | -1.13 | 6.8E-08 | ING1 | 1.05 | 2.86E-06 |
| CSRP1 | -3.79 | 1.42E-17 | PLS3 | -1.68 | 6.84E-08 | ADAP1 | 1.43 | 2.94E-06 |
| MYL9 | -4.25 | 2.82E-17 | NUDT3 | 1.16 | 9.91E-08 | UGCG | 1.83 | 3.14E-06 |
| SBSPON | -2.39 | 3.25E-16 | RASSF3 | -1.32 | 1.56E-07 | CASQ2 | -1.49 | 3.14E-06 |
| TAGLN | -3.95 | 7.61E-16 | ITPR1 | -1.19 | 1.61E-07 | DDX4 | -1.73 | 3.2E-06 |
| SYNPO2 | -3.01 | 8.3E-15 | TCEAL4 | -1.58 | 1.98E-07 | LTBP1 | -1.47 | 3.81E-06 |
| LMOD1 | -2.27 | 3.76E-14 | AKAP1 | -1.33 | 2.24E-07 | MACF1 | -1.35 | 3.81E-06 |
| TPM2 | -3.31 | 5.04E-14 | PPP1R14A | -1.23 | 2.82E-07 | ITIH5 | -1.23 | 4.06E-06 |
| ACTN1 | -2.66 | 2.86E-13 | PFKP | -1.49 | 3.2E-07 | PRPF4B | 1.26 | 4.16E-06 |
| ACTA2 | -4.43 | 7.45E-13 | LDOC1 | -1.78 | 3.2E-07 | TUBB6 | -1.29 | 4.18E-06 |
| SORBS1 | -2.25 | 1.29E-12 | IRAG1 | -1.37 | 3.23E-07 | ACTN4 | -1.17 | 4.18E-06 |
| TPM1 | -3.42 | 3.5E-12 | WDR1 | -1.37 | 3.26E-07 | DPYSL3 | -1.47 | 4.37E-06 |
| AOC3 | -1.84 | 6.85E-12 | ZNF432 | 2.11 | 3.42E-07 | SERTM2 | -2.12 | 4.63E-06 |
| SLMAP | -1.90 | 1.37E-11 | PDK3 | -1.28 | 3.8E-07 | POU1F1 | 1.29 | 4.84E-06 |
| SELENOM | -1.83 | 1.52E-11 | DPYD | 1.12 | 4.15E-07 | CT47A10 | 2.56 | 5.14E-06 |
| PPP1R12B | -2.42 | 6.2E-11 | C11orf96 | -2.14 | 4.15E-07 | CKMT2 | -1.04 | 5.14E-06 |
| MCAM | -2.30 | 6.2E-11 | SYNM | -1.78 | 5.19E-07 | IP6K2 | 0.95 | 5.29E-06 |
| SPECC1 | -2.12 | 6.2E-11 | CA3 | -1.58 | 6E-07 | CFD | 1.27 | 5.45E-06 |
| RASL12 | -1.99 | 9.7E-11 | ALCAM | -1.11 | 6.01E-07 | TAF8 | 0.93 | 5.55E-06 |
| SREBF1 | 2.89 | 1.22E-10 | PLCG1 | 1.33 | 6.6E-07 | CEBPB | 2.22 | 6.11E-06 |
| MAOB | -1.68 | 2.02E-10 | SH3D19 | -1.51 | 7.42E-07 | H2BC4 | 1.42 | 6.3E-06 |
| NID1 | -1.88 | 2.21E-10 | PI15 | -1.45 | 7.7E-07 | FMOD | -1.28 | 6.3E-06 |
| PDLIM3 | -2.35 | 5.86E-10 | CAV2 | -1.24 | 7.7E-07 | ACTC1 | -2.66 | 6.55E-06 |
| FBXO32 | -1.95 | 9.04E-10 | ACTRT1 | -1.13 | 8.89E-07 | TUB | -1.56 | 6.55E-06 |
| HSPB6 | -2.36 | 1.04E-09 | KCNH2 | -1.08 | 8.89E-07 | H2BC7 | 1.47 | 7.09E-06 |
| ALDH1B1 | -1.83 | 1.82E-09 | ASB2 | -1.46 | 9.88E-07 | TNFAIP1 | -1.35 | 7.32E-06 |
| MYOCD | -2.32 | 1.82E-09 | PDK4 | -1.87 | 1.01E-06 | CD163L1 | 1.29 | 7.37E-06 |
| CHRDL1 | -1.88 | 2.65E-09 | MARCKS | 2.30 | 1.03E-06 | LARGE1 | -0.83 | 7.7E-06 |
| GSN | -2.15 | 3.24E-09 | CD9 | -1.67 | 1.03E-06 | RAB9B | -1.19 | 7.72E-06 |
| ACOT1 | -1.30 | 3.24E-09 | LPP | -1.57 | 1.04E-06 | MAFK | 1.87 | 7.78E-06 |
| CFL2 | -1.41 | 3.31E-09 | KHDRBS3 | -1.04 | 1.04E-06 | NIBAN1 | -1.31 | 7.89E-06 |
| DSTN | -2.40 | 4.52E-09 | EPN1 | 1.44 | 1.09E-06 | HSPB8 | -1.61 | 7.91E-06 |
| FERMT2 | -1.68 | 6.12E-09 | MYADM | -1.13 | 1.09E-06 | TSNAX | -1.63 | 8.45E-06 |
| PALLD | -1.97 | 8.68E-09 | PDLIM5 | -1.23 | 1.1E-06 | FEM1B | -0.95 | 8.52E-06 |
| CDC42EP3 | -1.52 | 9.71E-09 | IL17B | -1.10 | 1.29E-06 | KLHL23 | -1.14 | 8.57E-06 |
| CLU | -2.32 | 1.2E-08 | RBM26 | 1.15 | 1.35E-06 | CGGBP1 | 2.13 | 9.15E-06 |
| PAK3 | -1.69 | 1.47E-08 | MAP3K20 | -1.24 | 1.35E-06 | DAPK1 | 1.14 | 9.15E-06 |
| SPARCL1 | -2.67 | 2.03E-08 | LDHB | -1.30 | 1.58E-06 | ODF2L | 0.93 | 9.15E-06 |
| ACOT2 | -1.24 | 2.29E-08 | FHL1 | -2.11 | 1.63E-06 | PBX1 | -1.24 | 9.15E-06 |
| SLC25A37 | 1.30 | 2.74E-08 | SPANXN5 | -1.17 | 1.63E-06 | TCEAL1 | -1.01 | 9.15E-06 |
| KCNMB1 | -1.48 | 3.56E-08 | CD40 | 1.41 | 2.26E-06 | MERTK | 1.12 | 9.39E-06 |
| VCL | -1.53 | 3.63E-08 | CRIP1 | 1.92 | 2.36E-06 | ZC3HC1 | -1.09 | 9.4E-06 |
| PCP4 | -2.88 | 4.69E-08 | C3orf38 | 1.87 | 2.36E-06 | HSD17B4 | 1.30 | 9.98E-06 |
| FLNA | -2.42 | 5.04E-08 | PDLIM7 | -1.26 | 2.36E-06 | SLC9A8 | 1.00 | 9.98E-06 |
| MGST3 | -1.48 | 5.43E-08 | VGLL3 | 2.33 | 2.38E-06 | NTF3 | -0.92 | 1E-05 |
| MAMDC2 | -1.37 | 5.48E-08 | SPEG | -1.32 | 2.61E-06 | FILIP1L | -1.17 | 1.03E-05 |
| PPP2R1A | 2.52 | 5.52E-08 | LUC7L | 1.24 | 2.69E-06 | MYOC | -1.21 | 1.07E-05 |

Supplementary Figure 4.1: Top 150 genes differentially expressed between all ROIs identified comparing the UPS and LMS samples.

| Gene | logFC | adjPVal | Gene | logFC | adjPVal | Gene | logFC | adjPVal |
|---|---|---|---|---|---|---|---|---|
| ACTG2 | -6.28 | 1.33E-24 | CALD1 | -1.98 | 6.12E-08 | CRIP2 | 1.73 | 2.78E-06 |
| CNN1 | -4.86 | 1.33E-24 | CSRP2 | -1.61 | 6.12E-08 | PLXND1 | 1.29 | 2.81E-06 |
| MYH11 | -4.55 | 7.41E-23 | TSPY1 | 1.70 | 6.39E-08 | DVL1 | 0.99 | 2.84E-06 |
| MYLK | -5.10 | 2.27E-21 | TMEM30B | -1.13 | 6.8E-08 | ING1 | 1.05 | 2.86E-06 |
| CSRP1 | -3.79 | 1.42E-17 | PLS3 | -1.68 | 6.84E-08 | ADAP1 | 1.43 | 2.94E-06 |
| MYL9 | -4.25 | 2.82E-17 | NUDT3 | 1.16 | 9.91E-08 | UGCG | 1.83 | 3.14E-06 |
| SBSPON | -2.39 | 3.25E-16 | RASSF3 | -1.32 | 1.56E-07 | CASQ2 | -1.49 | 3.14E-06 |
| TAGLN | -3.95 | 7.61E-16 | ITPR1 | -1.19 | 1.61E-07 | DDX4 | -1.73 | 3.2E-06 |
| SYNPO2 | -3.01 | 8.3E-15 | TCEAL4 | -1.58 | 1.98E-07 | LTBP1 | -1.47 | 3.81E-06 |
| LMOD1 | -2.27 | 3.76E-14 | AKAP1 | -1.33 | 2.24E-07 | MACF1 | -1.35 | 3.81E-06 |
| TPM2 | -3.31 | 5.04E-14 | PPP1R14A | -1.23 | 2.82E-07 | ITIH5 | -1.23 | 4.06E-06 |
| ACTN1 | -2.66 | 2.86E-13 | PFKP | -1.49 | 3.2E-07 | PRPF4B | 1.26 | 4.16E-06 |
| ACTA2 | -4.43 | 7.45E-13 | LDOC1 | -1.78 | 3.2E-07 | TUBB6 | -1.29 | 4.18E-06 |
| SORBS1 | -2.25 | 1.29E-12 | IRAG1 | -1.37 | 3.23E-07 | ACTN4 | -1.17 | 4.18E-06 |
| TPM1 | -3.42 | 3.5E-12 | WDR1 | -1.37 | 3.26E-07 | DPYSL3 | -1.47 | 4.37E-06 |
| AOC3 | -1.84 | 6.85E-12 | ZNF432 | 2.11 | 3.42E-07 | SERTM2 | -2.12 | 4.63E-06 |
| SLMAP | -1.90 | 1.37E-11 | PDK3 | -1.28 | 3.8E-07 | POU1F1 | 1.29 | 4.84E-06 |
| SELENOM | -1.83 | 1.52E-11 | DPYD | 1.12 | 4.15E-07 | CT47A10 | 2.56 | 5.14E-06 |
| PPP1R12B | -2.42 | 6.2E-11 | C11orf96 | -2.14 | 4.15E-07 | CKMT2 | -1.04 | 5.14E-06 |
| MCAM | -2.30 | 6.2E-11 | SYNM | -1.78 | 5.19E-07 | IP6K2 | 0.95 | 5.29E-06 |
| SPECC1 | -2.12 | 6.2E-11 | CA3 | -1.58 | 6E-07 | CFD | 1.27 | 5.45E-06 |
| RASL12 | -1.99 | 9.7E-11 | ALCAM | -1.11 | 6.01E-07 | TAF8 | 0.93 | 5.55E-06 |
| SREBF1 | 2.89 | 1.22E-10 | PLCG1 | 1.33 | 6.6E-07 | CEBPB | 2.22 | 6.11E-06 |
| MAOB | -1.68 | 2.02E-10 | SH3D19 | -1.51 | 7.42E-07 | H2BC4 | 1.42 | 6.3E-06 |
| NID1 | -1.88 | 2.21E-10 | PI15 | -1.45 | 7.7E-07 | FMOD | -1.28 | 6.3E-06 |
| PDLIM3 | -2.35 | 5.86E-10 | CAV2 | -1.24 | 7.7E-07 | ACTC1 | -2.66 | 6.55E-06 |
| FBXO32 | -1.95 | 9.04E-10 | ACTRT1 | -1.13 | 8.89E-07 | TUB | -1.56 | 6.55E-06 |
| HSPB6 | -2.36 | 1.04E-09 | KCNH2 | -1.08 | 8.89E-07 | H2BC7 | 1.47 | 7.09E-06 |
| ALDH1B1 | -1.83 | 1.82E-09 | ASB2 | -1.46 | 9.88E-07 | TNFAIP1 | -1.35 | 7.32E-06 |
| MYOCD | -2.32 | 1.82E-09 | PDK4 | -1.87 | 1.01E-06 | CD163L1 | 1.29 | 7.37E-06 |
| CHRDL1 | -1.88 | 2.65E-09 | MARCKS | 2.30 | 1.03E-06 | LARGE1 | -0.83 | 7.7E-06 |
| GSN | -2.15 | 3.24E-09 | CD9 | -1.67 | 1.03E-06 | RAB9B | -1.19 | 7.72E-06 |
| ACOT1 | -1.30 | 3.24E-09 | LPP | -1.57 | 1.04E-06 | MAFK | 1.87 | 7.78E-06 |
| CFL2 | -1.41 | 3.31E-09 | KHDRBS3 | -1.04 | 1.04E-06 | NIBAN1 | -1.31 | 7.89E-06 |
| DSTN | -2.40 | 4.52E-09 | EPN1 | 1.44 | 1.09E-06 | HSPB8 | -1.61 | 7.91E-06 |
| FERMT2 | -1.68 | 6.12E-09 | MYADM | -1.13 | 1.09E-06 | TSNAX | -1.63 | 8.45E-06 |
| PALLD | -1.97 | 8.68E-09 | PDLIM5 | -1.23 | 1.1E-06 | FEM1B | -0.95 | 8.52E-06 |
| CDC42EP3 | -1.52 | 9.71E-09 | IL17B | -1.10 | 1.29E-06 | KLHL23 | -1.14 | 8.57E-06 |
| CLU | -2.32 | 1.2E-08 | RBM26 | 1.15 | 1.35E-06 | CGGBP1 | 2.13 | 9.15E-06 |
| PAK3 | -1.69 | 1.47E-08 | MAP3K20 | -1.24 | 1.35E-06 | DAPK1 | 1.14 | 9.15E-06 |
| SPARCL1 | -2.67 | 2.03E-08 | LDHB | -1.30 | 1.58E-06 | ODF2L | 0.93 | 9.15E-06 |
| ACOT2 | -1.24 | 2.29E-08 | FHL1 | -2.11 | 1.63E-06 | PBX1 | -1.24 | 9.15E-06 |
| SLC25A37 | 1.30 | 2.74E-08 | SPANXN5 | -1.17 | 1.63E-06 | TCEAL1 | -1.01 | 9.15E-06 |
| KCNMB1 | -1.48 | 3.56E-08 | CD40 | 1.41 | 2.26E-06 | MERTK | 1.12 | 9.39E-06 |
| VCL | -1.53 | 3.63E-08 | CRIP1 | 1.92 | 2.36E-06 | ZC3HC1 | -1.09 | 9.4E-06 |
| PCP4 | -2.88 | 4.69E-08 | C3orf38 | 1.87 | 2.36E-06 | HSD17B4 | 1.30 | 9.98E-06 |
| FLNA | -2.42 | 5.04E-08 | PDLIM7 | -1.26 | 2.36E-06 | SLC9A8 | 1.00 | 9.98E-06 |
| MGST3 | -1.48 | 5.43E-08 | VGLL3 | 2.33 | 2.38E-06 | NTF3 | -0.92 | 1E-05 |
| MAMDC2 | -1.37 | 5.48E-08 | SPEG | -1.32 | 2.61E-06 | FILIP1L | -1.17 | 1.03E-05 |
| PPP2R1A | 2.52 | 5.52E-08 | LUC7L | 1.24 | 2.69E-06 | MYOC | -1.21 | 1.07E-05 |

Supplementary Figure 4.2: Top 150 genes differentially expressed within the tumour border ROIs identified comparing the UPS and LMS samples.

| Gene | logFC | adjPVal | Gene | logFC | adjPVal | Gene | logFC | adjPVal |
|---|---|---|---|---|---|---|---|---|
| CNN1 | -5.43 | 9.14E-21 | TCEAL4 | -1.76 | 1.07E-08 | FLNA | -2.47 | 4.01E-07 |
| MYLK | -5.83 | 1.69E-20 | ITM2C | -2.37 | 1.47E-08 | MAOB | -1.75 | 4.11E-07 |
| ACTG2 | -6.90 | 8.98E-20 | CGGBP1 | 2.85 | 1.64E-08 | SLC25A37 | 1.39 | 4.11E-07 |
| MYH11 | -5.16 | 2.11E-19 | VCL | -1.77 | 1.69E-08 | LDOC1 | -2.07 | 4.21E-07 |
| TPM1 | -3.98 | 1.99E-17 | MXRA8 | 2.24 | 1.69E-08 | ITIH5 | -1.43 | 4.25E-07 |
| ACTA2 | -5.00 | 4.46E-17 | PCP4 | -3.45 | 2.07E-08 | KCNH2 | -1.13 | 4.95E-07 |
| SYNPO2 | -3.58 | 1.28E-16 | MARCKS | 2.83 | 2.08E-08 | NUDT3 | 1.37 | 4.95E-07 |
| SPARCL1 | -3.45 | 1.39E-16 | CDC42EP3 | -1.78 | 2.4E-08 | LDHB | -1.59 | 5.09E-07 |
| MYL9 | -4.81 | 2.12E-16 | ALDH1B1 | -2.12 | 2.48E-08 | TUT7 | 1.08 | 5.17E-07 |
| TAGLN | -4.32 | 2.48E-15 | KHDRBS3 | -1.13 | 3.1E-08 | CBFB | 1.42 | 5.17E-07 |
| CSRP1 | -4.17 | 1.27E-14 | PLXDC2 | 1.51 | 3.17E-08 | WDR1 | -1.60 | 5.42E-07 |
| TPM2 | -3.73 | 1.27E-14 | PTX3 | 2.75 | 3.18E-08 | STAB1 | 2.29 | 5.57E-07 |
| ACTN1 | -3.17 | 3.26E-14 | SYNM | -2.25 | 4.14E-08 | CRIP2 | 2.14 | 5.71E-07 |
| MCAM | -2.86 | 6.46E-14 | FBXO32 | -2.14 | 4.47E-08 | MAP3K20 | -1.38 | 5.75E-07 |
| NID1 | -2.30 | 6.46E-14 | CAV2 | -1.43 | 5.55E-08 | HTR1F | 1.66 | 6.02E-07 |
| RASL12 | -2.38 | 4.94E-13 | FERMT2 | -1.71 | 6.1E-08 | EPN1 | 1.74 | 6.02E-07 |
| AOC3 | -2.27 | 7.78E-13 | DNM1 | 1.80 | 6.1E-08 | STPG2 | 1.72 | 6.13E-07 |
| PDLIM3 | -2.72 | 1.11E-12 | CSRP2 | -1.82 | 6.11E-08 | PLCG1 | 1.58 | 6.18E-07 |
| SBSPON | -2.63 | 1.11E-12 | ITPR1 | -1.46 | 6.52E-08 | AKAP1 | -1.42 | 6.71E-07 |
| ZNF432 | 2.78 | 1.61E-12 | ANKRD30A | 2.27 | 6.68E-08 | PXDC1 | 1.54 | 7.04E-07 |
| GSN | -2.75 | 2.34E-12 | CA3 | -1.86 | 8.6E-08 | CLU | -2.32 | 7.05E-07 |
| PPP1R12B | -2.95 | 2.73E-12 | CRYAB | -2.17 | 8.77E-08 | GABRE | 1.49 | 7.12E-07 |
| CHRDL1 | -2.11 | 3.78E-12 | CD40 | 1.60 | 8.77E-08 | CSE1L | 1.30 | 7.28E-07 |
| LMOD1 | -2.44 | 4.77E-12 | COL5A1 | 3.90 | 8.87E-08 | NIBAN1 | -1.55 | 7.44E-07 |
| FHL1 | -2.58 | 5.1E-12 | RHOBTB3 | 1.99 | 8.98E-08 | PLXND1 | 1.53 | 8.03E-07 |
| SORBS1 | -2.68 | 5.55E-12 | MGST3 | -1.71 | 9.22E-08 | IRAG1 | -1.58 | 8.8E-07 |
| TNXB | 2.35 | 5.55E-12 | POU1F1 | 1.70 | 1.04E-07 | FMOD | -1.54 | 8.97E-07 |
| SREBF1 | 3.52 | 5.55E-12 | PDK4 | -2.17 | 1.07E-07 | IL17B | -1.27 | 9.42E-07 |
| SPECC1 | -2.65 | 8.16E-12 | RASSF3 | -1.63 | 1.12E-07 | PCOLCE | 2.09 | 9.42E-07 |
| DES | -3.57 | 9.66E-12 | MAMDC2 | -1.49 | 1.12E-07 | EPHX2 | -1.08 | 1.03E-06 |
| PPP2R1A | 3.26 | 1.28E-11 | ACOT2 | -1.33 | 1.3E-07 | KCNMB1 | -1.64 | 1.06E-06 |
| SLMAP | -2.15 | 1.33E-11 | TGFBI | 3.62 | 1.33E-07 | FEM1B | -1.11 | 1.06E-06 |
| ACTC1 | -3.29 | 6.37E-11 | DPM1 | 1.55 | 1.34E-07 | DAB2 | 2.45 | 1.08E-06 |
| SELENOM | -1.96 | 8.98E-11 | SIT1 | 1.24 | 1.57E-07 | PLS3 | -1.75 | 1.12E-06 |
| VGLL3 | 3.02 | 1.19E-10 | HSPB8 | -1.98 | 1.6E-07 | PI15 | -1.66 | 1.12E-06 |
| PFKP | -1.87 | 3.06E-10 | CHMP2B | 1.49 | 1.6E-07 | ZNF836 | 1.31 | 1.12E-06 |
| CFL2 | -1.66 | 4.13E-10 | ADAP1 | 1.81 | 1.82E-07 | PIGL | 1.47 | 1.12E-06 |
| ACTA1 | -2.83 | 4.55E-10 | CT47A10 | 3.25 | 2.02E-07 | IGFBP7 | -2.02 | 1.15E-06 |
| C3orf38 | 2.55 | 4.77E-10 | VASN | 1.91 | 2.16E-07 | MACO1 | 1.21 | 1.19E-06 |
| PALLD | -2.31 | 5.13E-10 | A2M | -2.61 | 2.18E-07 | FGF2 | 1.97 | 1.22E-06 |
| DSTN | -2.74 | 5.91E-10 | DAPK1 | 1.39 | 2.69E-07 | HSPB7 | -1.25 | 1.25E-06 |
| ZNF841 | 2.42 | 7.37E-10 | FBN1 | 1.74 | 2.81E-07 | ZNF287 | 1.22 | 1.25E-06 |
| MAFK | 2.29 | 8.7E-10 | SERPINE2 | 2.72 | 2.81E-07 | COL27A1 | 1.10 | 1.38E-06 |
| MYOCD | -2.72 | 1.93E-09 | CAV1 | -1.67 | 3.17E-07 | UNC5C | 1.59 | 1.38E-06 |
| CASQ2 | -1.87 | 4.42E-09 | UBAP1L | -1.22 | 3.2E-07 | SERTM2 | -2.63 | 1.45E-06 |
| ACOT1 | -1.49 | 6.43E-09 | SPEG | -1.54 | 3.22E-07 | LAIR1 | 1.40 | 1.56E-06 |
| CALD1 | -2.33 | 7.37E-09 | ASB2 | -1.81 | 3.55E-07 | DVL1 | 1.16 | 1.58E-06 |
| C11orf96 | -2.58 | 9.68E-09 | SLC9A8 | 1.20 | 3.6E-07 | ALCAM | -1.30 | 1.64E-06 |
| HSPB6 | -2.58 | 9.91E-09 | KIFC3 | 1.26 | 3.77E-07 | LPP | -1.82 | 1.8E-06 |
| PAK3 | -2.01 | 1.07E-08 | SLC35C2 | 1.00 | 3.86E-07 | PDLIM5 | -1.30 | 1.8E-06 |

Supplementary Figure 4.3: Top 150 genes differentially expressed within the central tumour ROIs identified comparing the UPS and LMS samples.

| Gene | logFC | adjPVal |
|---|---|---|
| TRBC1 | 1.41 | 1.9E-05 |
| FYB1 | 0.70 | 0.001744 |
| LIMD2 | 0.83 | 0.001744 |
| HLA-DPB1 | 1.19 | 0.001744 |
| GIMAP4 | 0.64 | 0.001922 |
| IL32 | 1.09 | 0.001922 |
| HLA-DPA1 | 1.42 | 0.001922 |
| LYZ | 1.58 | 0.001922 |
| GIMAP7 | 0.60 | 0.004206 |
| HLA-DQB1 | 1.29 | 0.004237 |
| HLA-E | 1.09 | 0.004968 |
| FGL2 | 0.63 | 0.005511 |
| STAT1 | 1.03 | 0.005511 |
| ITGAL | 0.53 | 0.005531 |
| HLA-F | 0.70 | 0.005531 |
| CCL5 | 0.71 | 0.005531 |
| HLA-DRA | 1.09 | 0.005531 |
| HLA-DRB1 | 1.45 | 0.005531 |
| LCP1 | 1.06 | 0.006787 |
| HLA-DQA1 | 0.93 | 0.006947 |
| ARHGDIB | 0.63 | 0.0071 |
| LCP2 | 0.77 | 0.007386 |
| PECAM1 | 0.63 | 0.007976 |
| GBP5 | 0.84 | 0.007976 |
| IGHG1 | 2.00 | 0.008133 |
| COTL1 | 0.84 | 0.00853 |
| CCND2 | 0.52 | 0.008901 |
| TRIM22 | 0.69 | 0.008938 |
| PTPRC | 0.76 | 0.008938 |
| CXCL9 | 1.48 | 0.008938 |
| UBD | 0.58 | 0.010431 |
| SEMA4D | 0.51 | 0.011742 |
| IGKC | 2.30 | 0.012112 |
| KLRG1 | 0.52 | 0.012217 |
| CD74 | 1.72 | 0.012635 |
| CD2 | 0.59 | 0.01359 |
| LAP3 | 0.66 | 0.01359 |
| IGHG4 | 2.17 | 0.013706 |
| C1S | 0.88 | 0.017317 |
| IGHG3 | 2.10 | 0.017317 |
| CD3E | 0.57 | 0.020687 |
| TRAC | 0.53 | 0.021586 |
| HLA-DMA | 0.83 | 0.022261 |
| IGHG2 | 2.03 | 0.023034 |
| GMFG | 0.55 | 0.023377 |
| CYBA | 0.71 | 0.049227 |

Supplementary Figure 4.4: All differentially expressed genes comparing areas of high immune infiltration to areas of low immune infiltration within the LMS tumour subtype.

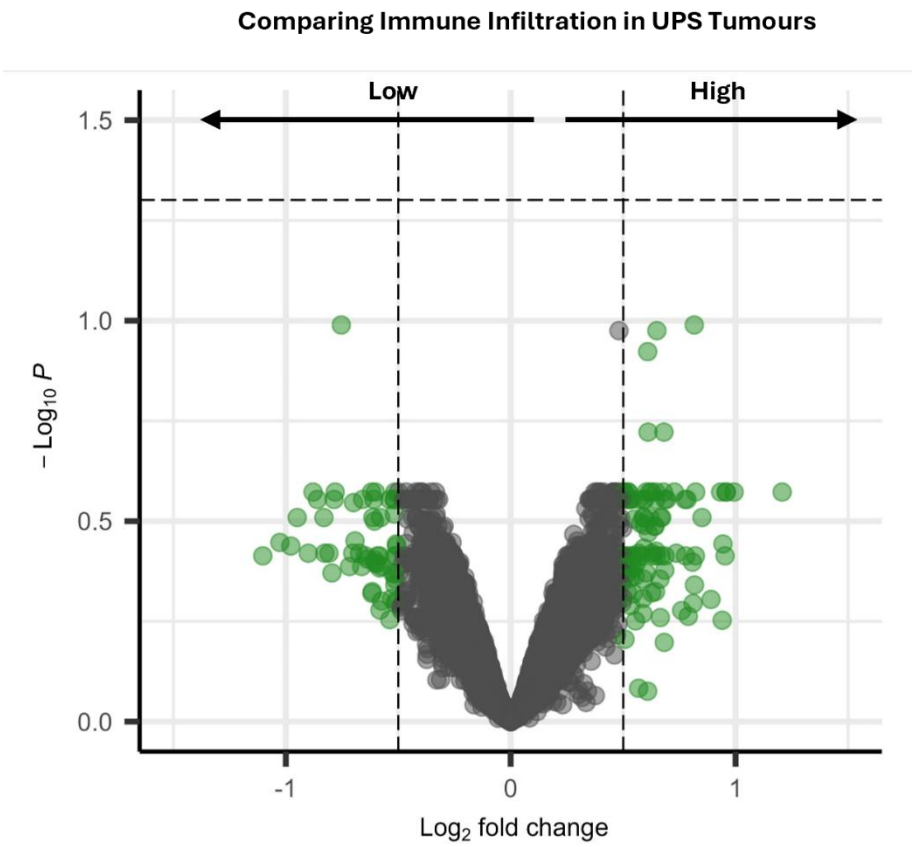


Supplementary Figure 4.5: Comparing areas of different infiltration within PMS tumours type assessed by immunofluorescence during ROI selection. Volcano plots showing differential expressed genes within comparing (left) low infiltration and (right) high infiltration with log2 FC indicates the relative expression level changes for each gene compared to each other with P adj = 0.05 significance level. Pathway analyses upregulated differentially expressed genes from (B) highly infiltrated LMS ROIs, Padj value of 0.5. Green points represent genes that were expressed above the fold change threshold but were not above the Padj value and genes represented in black were not statistically different between the variables being described.

| Gene | logFC | adjPVal | Gene | logFC | adjPVal | Gene | logFC | adjPVal |
|---|---|---|---|---|---|---|---|---|
| TNNT3 | -3.23 | 2.7E-07 | FCN1 | -1.27 | 1.46E-05 | CD3E | -1.05 | 7.16E-05 |
| TTN | -2.89 | 6.99E-07 | ITGAL | -1.22 | 1.65E-05 | HOMER3 | 1.05 | 7.16E-05 |
| RND3 | 1.62 | 9.59E-07 | PTPRK | 1.27 | 1.7E-05 | DNTTIP1 | 1.01 | 7.21E-05 |
| PPP2R1A | 1.96 | 9.59E-07 | CD2 | -1.25 | 1.87E-05 | DDAH2 | 1.23 | 7.21E-05 |
| LLGL1 | 1.66 | 1.57E-06 | PMP22 | 1.38 | 1.87E-05 | GABRE | 1.13 | 7.4E-05 |
| MYH1 | -2.82 | 2.03E-06 | ITPKB | -1.24 | 1.91E-05 | IL7R | -1.79 | 7.6E-05 |
| TRBC1 | -1.99 | 2.06E-06 | ATP8A1 | -1.28 | 2.14E-05 | HEG1 | 1.18 | 7.68E-05 |
| CKM | -2.39 | 3.5E-06 | PIM2 | -1.62 | 2.18E-05 | HLA-B | 1.85 | 7.91E-05 |
| SFRP2 | -1.75 | 3.5E-06 | PYHIN1 | -1.07 | 2.22E-05 | TUBA1C | 1.49 | 8.08E-05 |
| PTX3 | 3.01 | 3.5E-06 | TUBB2A | 1.25 | 2.22E-05 | SAA2 | -1.22 | 8.09E-05 |
| CDKN1B | -1.48 | 3.53E-06 | PXDC1 | 1.37 | 2.22E-05 | FAM50A | 0.97 | 8.09E-05 |
| CT47A10 | 2.02 | 3.53E-06 | CYTIP | -1.61 | 2.67E-05 | CTSA | 1.65 | 8.09E-05 |
| USP22 | 1.21 | 3.67E-06 | TNFAIP3 | -1.21 | 2.67E-05 | IL2RB | -1.07 | 8.31E-05 |
| ACTA2 | -2.10 | 3.68E-06 | COPS3 | 1.48 | 2.67E-05 | SCARB2 | 1.19 | 8.42E-05 |
| TNNC2 | -2.63 | 3.81E-06 | B4GALT5 | 1.70 | 2.78E-05 | JAK3 | -1.14 | 8.56E-05 |
| TRAC | -1.56 | 3.81E-06 | TNNI2 | -1.90 | 2.85E-05 | CCDC88B | -1.03 | 8.56E-05 |
| DBNDD2 | 1.63 | 3.81E-06 | TSC22D3 | -1.18 | 2.87E-05 | EBNA1BP2 | 1.04 | 8.56E-05 |
| MFAP2 | 1.89 | 3.81E-06 | RRAD | -2.12 | 3.18E-05 | RESF1 | -1.16 | 8.6E-05 |
| FOS | -2.27 | 3.82E-06 | DAB2 | 1.07 | 3.18E-05 | CD69 | -1.41 | 8.74E-05 |
| ACTN2 | -1.64 | 3.82E-06 | PLTP | 1.43 | 3.49E-05 | KLRK1 | -1.20 | 9.05E-05 |
| MZB1 | -1.54 | 3.82E-06 | CRIP2 | 1.32 | 3.75E-05 | BTG2 | -1.38 | 9.62E-05 |
| CCL5 | -1.54 | 3.82E-06 | RASAL3 | -1.08 | 3.78E-05 | NKG7 | -0.94 | 9.62E-05 |
| CXCR4 | -1.40 | 3.82E-06 | COLGALT1 | 1.11 | 3.82E-05 | FGF2 | 1.57 | 9.63E-05 |
| ANGPTL2 | 1.37 | 3.82E-06 | ALDH3A2 | 1.29 | 4.25E-05 | PSTPIP1 | -1.22 | 0.000103 |
| ANKRD30A | 1.93 | 3.82E-06 | SYTL1 | -1.13 | 4.32E-05 | SREBF1 | 1.43 | 0.000107 |
| ARHGEF1 | -1.32 | 5E-06 | PIK3CD | -1.05 | 4.32E-05 | NR4A1 | -1.16 | 0.000108 |
| CGGBP1 | 1.51 | 5.23E-06 | OLFML2A | 1.57 | 4.35E-05 | DPM1 | 1.12 | 0.000108 |
| RAC2 | -1.50 | 5.44E-06 | FBN2 | 1.35 | 4.83E-05 | POLD2 | 1.23 | 0.000109 |
| TPM1 | -1.51 | 5.74E-06 | MAFK | 1.53 | 5.1E-05 | TNNC1 | -1.04 | 0.000109 |
| RPS27 | -1.16 | 5.74E-06 | DDX24 | 0.98 | 5.22E-05 | ADD3 | -0.84 | 0.00011 |
| MGP | -1.88 | 6.08E-06 | TNXB | 1.71 | 5.27E-05 | TBRG4 | 1.04 | 0.00011 |
| TCAP | -2.42 | 6.42E-06 | PTPRCAP | -1.47 | 5.29E-05 | MYBL2 | 1.88 | 0.000114 |
| CORO1A | -1.37 | 6.42E-06 | KANK2 | 1.32 | 5.29E-05 | VPS37A | 1.18 | 0.000129 |
| PEMT | 1.33 | 6.83E-06 | ARFGEF2 | 1.14 | 5.47E-05 | LUM | -2.02 | 0.000132 |
| GPR183 | -1.29 | 7.04E-06 | CHMP2B | 1.42 | 5.7E-05 | EIF3B | 0.98 | 0.000132 |
| EPHB2 | 1.24 | 7.04E-06 | PRKCH | -1.13 | 5.92E-05 | PFDN4 | 1.14 | 0.000132 |
| CDK4 | 1.23 | 7.27E-06 | MEX3D | 0.98 | 5.97E-05 | SEMA4D | -1.13 | 0.000144 |
| MPRIP | 1.33 | 7.92E-06 | ALKBH5 | 1.26 | 5.98E-05 | ARHGAP45 | -1.23 | 0.000148 |
| CRYAB | -1.72 | 8.41E-06 | IER3IP1 | 1.32 | 5.98E-05 | SLC35C2 | 1.10 | 0.000151 |
| ACTA1 | -2.63 | 8.53E-06 | CD27 | -1.04 | 6.02E-05 | MORF4L2 | 0.99 | 0.000152 |
| MMP14 | 2.08 | 1.08E-05 | PKD1 | 1.16 | 6.02E-05 | ARHGAP15 | -1.00 | 0.000153 |
| TNC | 1.93 | 1.13E-05 | VIM | 1.20 | 6.02E-05 | PSMA7 | 1.26 | 0.000153 |
| PTPRC | -1.37 | 1.16E-05 | SPC24 | 1.30 | 6.29E-05 | ZNF841 | 1.52 | 0.000153 |
| UBE2C | 2.19 | 1.16E-05 | SIK1 | -1.13 | 6.38E-05 | DBN1 | 1.11 | 0.000161 |
| MYL1 | -2.11 | 1.17E-05 | C3orf38 | 1.49 | 6.4E-05 | GNLY | -1.37 | 0.000163 |
| THBS4 | -1.77 | 1.22E-05 | H1-3 | -1.36 | 6.45E-05 | LMNA | 1.01 | 0.000163 |
| PEDS1 | 1.20 | 1.22E-05 | RGS16 | -1.53 | 6.61E-05 | CDC42EP4 | 1.11 | 0.000163 |
| UBE2S | 1.42 | 1.25E-05 | CST7 | -1.11 | 6.61E-05 | ADCY3 | 1.17 | 0.000163 |
| FCMR | -1.29 | 1.39E-05 | NR2F1 | 1.27 | 6.61E-05 | TAF13 | 1.20 | 0.000163 |
| FAM20C | 1.54 | 1.41E-05 | KDELR2 | 1.39 | 6.64E-05 | EGR1 | -1.37 | 0.000164 |

Supplementary Figure 4.6: Top 150 genes differentially expressed comparing the transcriptomic profile at the tumour border to areas outside the tumour border in the UPS tumour type.

| Gene | logFC | adjPVal | Gene | logFC | adjPVal | Gene | logFC | adjPVal |
|---|---|---|---|---|---|---|---|---|
| IGF2 | 1.58 | 2.13E-05 | RAP2B | 0.58 | 0.008809 | NR1H3 | 0.82 | 0.018528 |
| HLA-DQA1 | 1.49 | 0.000224 | LUC7L3 | -0.69 | 0.008846 | FAM20A | 0.60 | 0.019765 |
| B2M | 1.22 | 0.000309 | CPVL | 0.70 | 0.00908 | SQOR | 0.64 | 0.019967 |
| LGALS3 | 1.01 | 0.000426 | IRF1 | 0.81 | 0.00908 | DNASE2 | 0.68 | 0.019967 |
| SERPINF1 | 1.08 | 0.000426 | LAMB1 | 0.75 | 0.009318 | ANGPTL2 | 0.57 | 0.021953 |
| IRF8 | 0.94 | 0.000495 | H2BC9 | 0.70 | 0.009665 | C1QC | 1.35 | 0.021989 |
| ADAMDEC1 | 1.04 | 0.000495 | FCER1G | 0.90 | 0.009754 | CST3 | 1.07 | 0.02224 |
| CGGBP1 | -1.00 | 0.000584 | CTSC | 0.87 | 0.010391 | FCGRT | 0.97 | 0.022521 |
| TPP1 | 0.84 | 0.001157 | IGKC | 3.23 | 0.010787 | EVI2B | 0.54 | 0.022552 |
| SRGN | 0.96 | 0.001157 | DHRS7 | 0.71 | 0.010946 | ACTN1 | 0.57 | 0.023454 |
| GBP2 | 0.96 | 0.001582 | CLEC14A | 0.80 | 0.010946 | APOBEC3C | 0.69 | 0.023454 |
| CTSH | 0.85 | 0.001676 | ATOX1 | 0.67 | 0.011424 | CTSB | 0.99 | 0.023454 |
| ENPP2 | 0.93 | 0.001757 | PLVAP | 0.67 | 0.011581 | CCDC13 | -1.00 | 0.025686 |
| ALDH2 | 0.81 | 0.001879 | NPIPA1 | -0.65 | 0.011729 | ST14 | 0.61 | 0.025686 |
| CAPG | 0.98 | 0.001879 | ECHDC2 | -0.66 | 0.011825 | PRKCH | 0.62 | 0.025686 |
| NPC2 | 0.88 | 0.002553 | IGHG3 | 2.71 | 0.011825 | SGPL1 | 0.64 | 0.025686 |
| PLTP | 0.97 | 0.002747 | KRTAP5-8 | -0.90 | 0.012427 | CXCL16 | 0.72 | 0.025686 |
| HLA-DQB1 | 1.22 | 0.002894 | PDHA2 | -0.92 | 0.012433 | IFI16 | 0.50 | 0.025867 |
| HLA-DRA | 1.28 | 0.002894 | HLA-B | 1.12 | 0.012433 | ZNF346 | -0.64 | 0.026043 |
| IGHG4 | 2.98 | 0.002894 | LYZ | 1.52 | 0.012433 | TTC19 | -0.64 | 0.026043 |
| NCKAP1L | 0.74 | 0.003044 | SLC5A10 | -0.73 | 0.012671 | CD68 | 0.98 | 0.026043 |
| TNFSF10 | 0.76 | 0.003044 | LCP1 | 0.89 | 0.012671 | IFI30 | 1.01 | 0.026043 |
| LILRB4 | 0.85 | 0.003044 | TMEM176B | 1.04 | 0.012671 | ZNF614 | -0.82 | 0.02697 |
| H3C7 | 0.94 | 0.003044 | CYBA | 0.72 | 0.013072 | EPC1 | -0.59 | 0.02697 |
| RARRES1 | 1.00 | 0.003044 | HLA-DMB | 0.75 | 0.013072 | SREBF1 | -0.76 | 0.027236 |
| TYROBP | 0.94 | 0.003144 | GBP4 | 0.58 | 0.013144 | CIITA | 0.62 | 0.027236 |
| IFITM3 | 0.76 | 0.003228 | SLCO2B1 | 0.85 | 0.013399 | MPRIP | -0.56 | 0.028055 |
| IL32 | 0.81 | 0.003228 | SAMHD1 | 0.78 | 0.013536 | ARL6IP5 | 0.62 | 0.028055 |
| ASAH1 | 1.02 | 0.003228 | WARS1 | 0.85 | 0.013536 | MZT2B | -0.89 | 0.028175 |
| IGHG1 | 2.31 | 0.003228 | CD4 | 0.96 | 0.013724 | TRAC | 0.62 | 0.028175 |
| SDCBP | 0.76 | 0.003838 | ZNF654 | -0.75 | 0.013957 | FXYD5 | 0.66 | 0.028289 |
| CTSS | 1.30 | 0.003838 | RNASEH2B | 0.57 | 0.013957 | HLA-DQA2 | 0.84 | 0.028768 |
| USP22 | -0.60 | 0.004097 | JCHAIN | 1.12 | 0.013957 | CRKL | -0.66 | 0.030186 |
| TMEM176A | 0.78 | 0.004097 | DHRS1 | -0.82 | 0.014335 | LAP3 | 0.79 | 0.03043 |
| GIMAP4 | 0.80 | 0.004097 | ABRACL | 0.58 | 0.014335 | SDC3 | 0.62 | 0.03133 |
| ITM2B | 1.05 | 0.004289 | TSPAN14 | 0.59 | 0.014454 | ALDH1A1 | 0.61 | 0.031341 |
| APOC2 | 0.93 | 0.004909 | TTC33 | -0.66 | 0.015301 | RPS13 | 0.54 | 0.031738 |
| A2M | 1.25 | 0.004909 | SYNGR2 | 0.81 | 0.015301 | C1R | 0.60 | 0.032365 |
| HLA-DRB1 | 1.44 | 0.004909 | TYMP | 0.92 | 0.015301 | ETS1 | 0.60 | 0.03267 |
| APOE | 1.48 | 0.004909 | CDH5 | 0.77 | 0.015796 | CSF2RB | 0.53 | 0.032795 |
| IGLL5 | 2.04 | 0.004909 | HLA-DMA | 0.91 | 0.015796 | TNFRSF1B | 0.52 | 0.033114 |
| LSP1 | 0.85 | 0.005344 | IFITM1 | 0.68 | 0.017789 | TBC1D13 | -0.56 | 0.033437 |
| IGHA1 | 2.12 | 0.005656 | SIGLEC10 | 0.68 | 0.018028 | FPR3 | 0.60 | 0.033713 |
| HLA-DPB1 | 1.22 | 0.005807 | COTL1 | 0.71 | 0.018028 | CMTM6 | 0.56 | 0.033766 |
| PECAM1 | 0.98 | 0.006129 | LMO2 | 0.58 | 0.018066 | SH3GLB1 | 0.58 | 0.034392 |
| PNN | -0.62 | 0.006191 | HLA-DOA | 0.77 | 0.018066 | IDH1 | 0.60 | 0.03681 |
| LY96 | 0.67 | 0.006479 | PDGFRA | 0.86 | 0.018066 | STPG2 | -1.00 | 0.037791 |
| SECTM1 | 0.71 | 0.006479 | CD14 | 1.02 | 0.018066 | EIF3E | 0.52 | 0.037867 |
| APOC1 | 1.62 | 0.007017 | GBP5 | 0.81 | 0.018293 | BCL3 | 0.56 | 0.037867 |
| IGHG2 | 2.55 | 0.007936 | FLNA | -0.53 | 0.01843 | BMERB1 | -0.70 | 0.03895 |

Supplementary Figure 4.7: Top 150 differentially expressed genes comparing the transcriptomic profile at the tumour border to central tumour in the UPS tumour type.

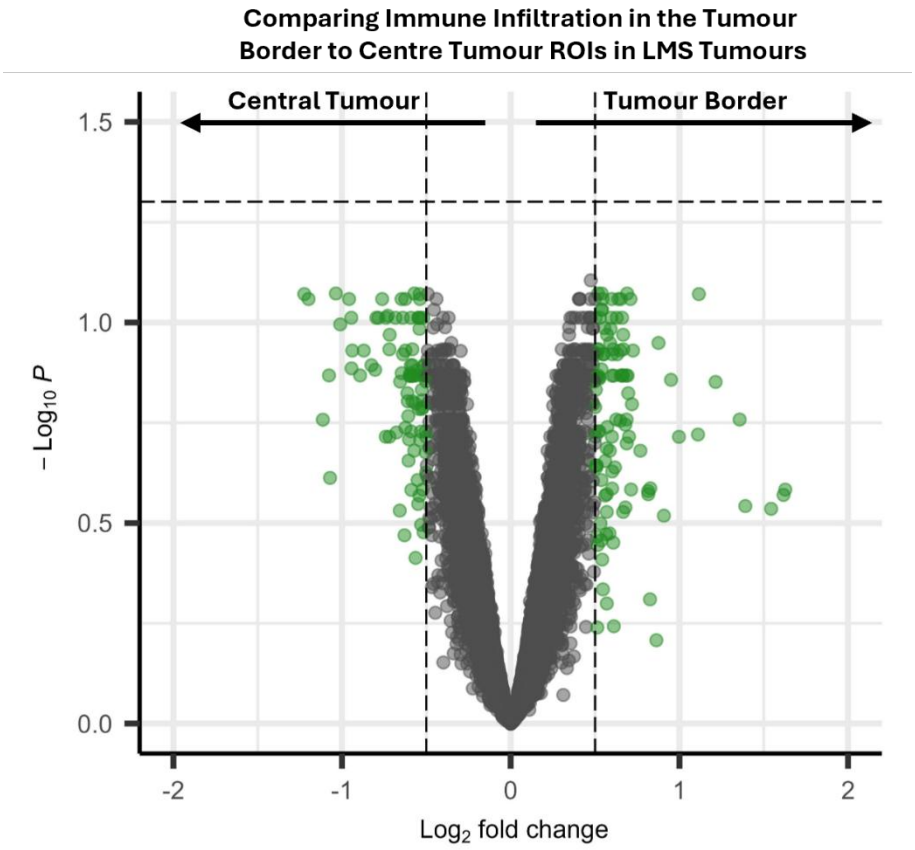


Supplementary Figure 4.8: Comparing the transcriptomic profile of highly infiltrated ROIs at the tumour border to central tumour in the UPS tumour type assessed by immunofluorescence during ROI selection. (A) Volcano plots showing differential expressed genes comparing (left) central tumour and (right) the tumour border, log2 FC indicates the relative expression level changes for each gene compared to each other with P adj = 0.5 significance level. (B) pathway analyses of upregulated differentially expressed genes from regions inside the tumour border when compared to central tumour, with a Padj value of 0.5. Green points represent genes that were expressed above the fold change threshold but were not above the Padj value and genes represented in black were not statistically different between the variables being described.

| Gene | logFC | adjPVal |
|---|---|---|
| SUPT7L | 3.03406 | 1.04E-11 |
| SERTM2 | -2.64492 | 4.99E-09 |
| C4orf46 | -2.96878 | 1.43E-08 |
| GAGE10 | -2.39509 | 6.3E-08 |
| ACTG2 | -2.69904 | 1.15E-07 |
| IGHG3 | -2.52705 | 1.53E-07 |
| RPS4Y1 | 2.570554 | 0.00022 |
| IFI6 | -1.80722 | 0.002025 |
| SPDYE5 | -1.8728 | 0.002753 |
| IGHG2 | -2.00194 | 0.002753 |
| KRTAP5-8 | -1.6506 | 0.003091 |
| FOXD4L5 | -1.73133 | 0.003222 |
| VIM | 1.919108 | 0.004392 |
| ZNF616 | -1.61649 | 0.005494 |
| PCP4 | -2.17757 | 0.006974 |
| FCF1 | -2.34254 | 0.007724 |
| HLA-DRB1 | 1.735754 | 0.007724 |
| FLNA | -1.80662 | 0.007724 |
| IGHG1 | -1.97222 | 0.011021 |
| CXCL9 | 2.049263 | 0.011021 |
| FABP4 | -1.95077 | 0.01133 |
| CACNB3 | -1.37136 | 0.013223 |
| TLE6 | -1.35298 | 0.013223 |
| CD8A | -1.90567 | 0.013223 |
| KRT8 | -1.49408 | 0.013223 |
| USP17L3 | -2.09314 | 0.015322 |
| RBBP7 | -2.03097 | 0.015322 |
| LMO3 | -1.47156 | 0.015953 |
| PRMT8 | -1.7327 | 0.015953 |
| PRPS2 | -2.00281 | 0.015953 |
| DACT3 | -1.44223 | 0.015953 |
| ACTC1 | -2.16883 | 0.015953 |
| TCEA2 | -1.43821 | 0.016524 |
| REV3L | -1.41587 | 0.023381 |
| SLAMF6 | -1.2841 | 0.024372 |
| BHMT2 | -1.33438 | 0.024372 |
| TUFM | -1.43139 | 0.026578 |
| GLRX | -1.57813 | 0.027033 |
| E2F1 | -1.73066 | 0.035652 |
| CKB | -2.00154 | 0.036969 |
| GADD45B | -1.57504 | 0.037135 |
| IGHM | 1.973901 | 0.037135 |
| CD320 | -1.54415 | 0.037135 |
| IFI44L | -1.40469 | 0.037135 |
| MCRIP2 | -1.48355 | 0.037135 |
| KLHL23 | -1.36456 | 0.037135 |
| BCKDHB | -1.17045 | 0.037135 |
| COL1A1 | 1.942705 | 0.037897 |
| EIF1AX | -1.85651 | 0.037897 |
| TMEM158 | -1.05028 | 0.040145 |
| DFFA | -1.13641 | 0.040145 |
| PIM3 | -1.13196 | 0.046694 |
| JUNB | -1.92037 | 0.046797 |
| CRYAB | 1.896581 | 0.046797 |
| SYF2 | -1.35573 | 0.047031 |
| PPDPF | -1.82807 | 0.047031 |
| LNX2 | -1.17822 | 0.048524 |
| TNFRSF21 | -1.45785 | 0.04928 |

Supplementary Figure 4.9: All differentially expressed genes comparing the transcriptomic profile of CD45+CD8+ T cells from segmented ROIs in LMS tumour comparing tumour border to central tumour.